

# Author Index

Aakeröy, Christer .....	10.03.07	Anfinrud, P. ....	T-P049	Beavers, Christine.....	13.14.06
Aakeröy, Christer.....	10.03.16	Anokhina, E. ....	M-P098	Beavers, Christine.....	M-P164
Aakeröy, Christer.....	13.02.07	Antipin, Mikhail .....	10.02.03	Becker, B. ....	T-P156
Aakeröy, Christer.....	SP01.03	Antipin, Mikhail .....	T-P177	Becker, Donald .....	01.01.04
Aakeröy, Christer.....	T-P127	Appleby, Todd.....	M-P034	Becker, Joseph W.....	T-P090
Aakeröy, Christer.....	T-P135	Appleby, Todd.....	04.01.03	Becker, M. ....	T-P025
Abagyan, Ruben .....	T-P094	Arabshahi, Abolfazl.....	13.06.08	Bedzyk, Michael.....	T-P007
Abalos, Gil .....	S-P095	Arasappan, Ashok.....	S-P163	Begley, Tadhg P.....	01.01.05
Abashidze, Mariam .....	M-P076	Arai, M. ....	13.15.05	Begley, Tadhg P.....	S-P157
Abdul Salam, Abdul Ajees.....	S-P129	Arai, M. ....	M-P002	Begley, Tadhg P.....	T-P078
Abdullah, James .....	S-P051	Arakaki, Tracy .....	T-P071	Beglova, Natalia .....	T-P056
Abdullah, James.....	S-P105	Aranda, Roman.....	T-P091	Begum, Anjuman.....	M-P056
Abendroth, Jan.....	01.05.04	Arjunan, Palaniappa .....	T-P020	Bell, Jessica .....	01.06.02
Abendroth, Jan.....	M-P168	Arleth, Lise.....	13.13.04	Bell, Jessica.....	T-P069
Adachi, Hiroaki.....	S-P177	Arola, T.M. ....	T-P185	Bella, Jordi .....	AW.01.04
Adachi, Hiroaki.....	S-P179	Arrowsmith, Cheryl.....	T-P096	Bellamy, Henry .....	11.01.01
Adams, E.J. ....	01.06.08	Arvai, Andrew.....	T-P138	Bellen, Hugo .....	S-P161
Adams, Michael W.W. ....	S-P185	Asahara, Haruichi .....	M-P146	Bellon, Anne .....	S-P095
Adams, Paul .....	01.02.06	Asaithamby, Aroumougame .....	M-P218	Ben Jelloul, Marouane.....	01.02.05
Afonine, Pavel .....	01.02.06	Ashton, Alun .....	M-P158	Bender, Steve .....	04.01.02
Agarwal, Rakhi.....	S-P187	Askins, Janine .....	01.06.02	Benn, Rich.....	T-P039
Agbandje-McKenna, Mavis .....	AW.03.02	Askins, Janine .....	T-P069	Bennett, Brad .....	TR.01.09
Agbandje-McKenna, Mavis .....	S-P007	Asojo, Oluwatoyin.....	T-P057	Bennett, Frank.....	S-P163
Agbandje-McKenna, Mavis .....	S-P009	Athay, Russ .....	S-P113	Benning, Matthew .....	M-P036
Agbandje-McKenna, Mavis .....	S-P011	Athay, Russ .....	M-P024	Benning, Matthew .....	T-P156
Agbandje-McKenna, Mavis .....	M-P140	Auperin, Thierry .....	M-P046	Bensen, Daniel.....	S-P113
Agbandje-McKenna, Mavis. ....	M-P142	Austin, Brian.....	01.01.03	Benson, Ronald.....	T-P173
Ahmed, Misonara .....	M-P212	Avdeev, Maxim.....	M-P118	Beraldo, Heloisa .....	S-P039
Aich, Sanjukta.....	T-P054	Avvakumov, G. ....	T-P026	Berard, Daniel.....	T-P101
Aizawa, K.....	M-P002	Babson, Victor.....	13.07.08	Berejnov, Viatcheslav .....	S-P107
Aizawa, Kazuya.....	13.15.05	Bache, Chris.....	10.02.01	Berejnov, Viatcheslav .....	T-P047
Akana, Julie.....	S-P167	Bader, Martin W.....	01.01.07	Berejnov, Viatcheslav .....	T-P178
Akella, Radha.....	M-P032	Badger, John.....	S-P113	Berg, Russ .....	13.10.02
Akella, Radha.....	M-P048	Badger, John.....	M-P024	Berghuis, Albert.....	13.10.04
Akgun, B. ....	09.01.03	Baek, Ji-Hye.....	T-P134	Berghuis, Albert.....	S-P063
Ali, Maruf.....	T-P207	Baettig, Oliver.....	S-P063	Bergmann, Ernst .....	13.10.02
Alkire, Randy.....	S-P191	Bagautdinov, Bagautdin .....	T-P066	Bergmann, Ernst .....	T-P010
Alkire, Randy.....	T-P031	Baharev, Vladimir.....	10.02.09	Berk, N.F. ....	AW.02.10
Allaire, Marc .....	01.04.04	Bai, Yun.....	M-P046	Berman, Helen M. ....	AW.01.01
Allaire, Marc .....	T-P043	Baker, Susan.....	T-P112	Berman, L.E. ....	T-P025
Allen, Karen N.....	T-P032	Baker, Timothy .....	S-P011	Bernstein, Herbert J. ....	S-P083
Allewell, Norma .....	S-P123	Balch, Alan.....	13.14.06	Bernstein, Herbert J. ....	M-P156
Almendarez Camarillo, A.....	09.03.01	Balch, Alan.....	M-P164	Bernstein, Herbert J. ....	WK.02.01
Almer, Jon .....	13.09.08	Bale, Shridhar .....	T-P078	Bernstein, Joel.....	10.03.01
Almo, Steve.....	S-P167	Ballentine, Gregory .....	09.01.04	Berntson, Alec.....	T-P043
Almrud, Jeffrey.....	T-P004	Ban, Nenad.....	01.03.04	Berntsson, Ronnie.....	S-P075
Alsaied, O.A.....	T-P178	Ban, Nenad.....	01.03.05	Bertozzi, Carolyn.....	S-P017
Alvarado, Johnjeff .....	13.14.01	Banchs, Christian .....	01.04.02	Beyer, Brian M.....	S-P163
Amaro-Luis, Juan Manuel .....	10.02.07	Bansal, Amitabh.....	13.11.02	Bhatt, Deepa.....	AW.03.02
Amaya, Maria F. ....	01.01.07	Barbazon, Danielle .....	S-P141	Bian, Chuanbing .....	S-P071
Ambing, Eileen.....	M-P074	Barbosa, J.A.R.G. ....	01.07.04	Bian, Chuanbing .....	T-P213
Amulele, George.....	05.01.04	Bargassa, Monireh.....	T-P068	Bilcer, Geoffrey .....	M-P038
An, K. ....	13.09.07	Barretto, Naina.....	T-P112	Bilderback, Don.....	T-P014
Anantharamaiah, G.M.....	S-P129	Batista, Alzir .....	S-P039	Billinge, Simon .....	S-P031
Anderson, Carly S. ....	10.01.03	Batra, Vinod .....	T-P072	Billinge, Simon .....	T-P009
Anderson, Daniel.....	T-P219	Battaile, Kevin .....	T-P037	Bingman, Craig.....	13.06.08
Anderson, I.S. ....	13.09.01	Battaile, Kevin .....	T-P170	Binkowski, T. Andrew.....	S-P219
Anderson, Jack.....	T-P089	Bau, Robert .....	TR.01.01	Birrell, Geoff.....	S-P131
Anderson, Ross.....	M-P076	Baucom, Albion.....	M-P146	Bitto, Eduard.....	13.06.08
Anderson, Spencer.....	T-P033	Bauer, Cary .....	M-P036	Blacklow, Stephen C. ....	T-P056
Anderson, Spencer.....	T-P049	Beamer, Lesa.....	S-P151	Blakeley, Mathew .....	TR.01.07
Andi, Babak .....	M-P184	Beard, William.....	T-P072	Blanchard, Didier.....	13.01.03
Andreasen, Peter.....	S-P071	Beasley, A.G.....	10.03.02	Blomqvist, Ingvar.....	13.10.01
Andrykovitch, M. ....	S-P143	Beaton, Stephen A. ....	10.03.13	Blount, Kenneth.....	04.01.06

# Author Index

Blundell, David.....	09.03.03	Bu, Xianhui.....	13.12.04	Chakoumakos, B.C.....	M-P088
Blundell, Tom.....	01.02.02	Bu, Xianhui.....	T-P183	Chambers, Henry.....	M-P152
Boczek, Tomasz.....	S-P087	Bucar, Dejan-Kresimir.....	T-P147	Chamorro Perez, Eva.....	05.01.05
Bogdanova, Natalia.....	M-P042	Buchanan, Susan.....	T-P207	Chandra, Dhanesh.....	13.09.03
Bogen, Stephane L.....	S-P163	Buchmeier, Michael.....	01.01.08	Chandrasekhar, K.....	T-P020
Boker, Alexander.....	09.03.04	Buchmeier, Michael.....	T-P132	Chang, Changsoo.....	S-P051
Bollag, Gideon.....	M-P030	Buckley, Thomas.....	M-P126	Chang, Changsoo.....	S-P105
Bolotovskiy, Robert.....	S-P199	Buckner, Fred.....	T-P071	Chang, Changsoo.....	S-P191
Bolotovskiy, Robert.....	T-P095	Bueno, Marta.....	T-P166	Chang, Changsoo.....	M-P066
Bonander, Nicklas.....	S-P075	Bujacz, Grzegorz.....	01.07.02	Chang, Chia-Hao.....	01.07.03
Bond, Marcus.....	13.07.01	Bunick, Gerard.....	TR.01.08	Chang, Chung-I.....	01.06.06
Bond, Marcus.....	SP.01.02	Buono, R.....	T-P027	Chang, Geoffrey.....	T-P201
Bonhoure, Fabien.....	M-P012	Burgin, Alex.....	M-P134	Chang, Jessie.....	S-P149
Bonny, Christophe.....	T-P130	Burgin, Alex.....	T-P104	Chang, Jessie.....	S-P185
Borek, Dominika.....	01.06.06	Burley, Stephen.....	AW.01.06	Chang, Shu-Huey.....	S-P185
Borek, Dominika.....	11.01.06	Burrows, Lori L.....	S-P093	Chao, Ti-Chun.....	T-P062
Borek, Dominika.....	M-P070	Burrows, Lori L.....	S-P155	Chapman, Martin D.....	S-P193
Borek, Dominika.....	T-P221	Burse, Evan.....	13.06.06	Chapman, Steve.....	M-P076
Borek, Dominika.....	T-P223	Burse, Evan.....	M-P084	Chartron, Justin.....	S-P017
Borhan, Babak.....	S-P165	Burse, Evan.....	M-P186	Chatake, Toshiyuki.....	M-P008
Borisova, Svetlana.....	S-P013	Burse, Evan.....	M-P198	Chatterjee, A.....	01.01.05
Borisova, Svetlana.....	M-P126	Burton, Dennis R.....	T-P075	Chavali, Krishna.....	10.02.02
Borkowski, Lauren.....	13.12.01	Bushnell, David.....	01.03.02	Cheetham, Anthony K.....	13.13.06
Born, Timothy L.....	T-P154	Buslaps, Thomas.....	13.09.06	Chelliah, Yogarany.....	01.06.06
Borovinskaya, Maria A.....	01.03.01	Busse, Armin.....	13.15.04	Chen, Bo-Tsang.....	S-P133
Bosch, Eric.....	10.03.12	Butcher, Ray.....	13.07.01	Chen, Chun-Jung.....	T-P019
Bösecke, Peter.....	09.03.01	Butcher, Ray.....	SP.01.02	Chen, David.....	M-P218
Bosshard, H.....	13.07.06	Butler, Paul.....	09.03.06	Chen, Hsin-Yi.....	S-P133
Botos, Istvan.....	01.06.02	Butler, Paul.....	T-P005	Chen, Huifen.....	M-P026
Bott, Richard.....	T-P114	Bychkov, Eugene.....	M-P104	Chen, Huiyi.....	S-P017
Bouzida, Djamel.....	T-P136	Cabantous, Stephanie.....	T-P187	Chen, Huizhong.....	M-P210
Bowman, Robert.....	13.01.04	Caffrey, Martin.....	T-P197	Chen, Kevin.....	S-P163
Brady, R. Leo.....	T-P073	Cahill, Christopher.....	13.12.01	Chen, Lan.....	T-P183
Brammer, Lee.....	TR.01.04	Calero, Guillermo.....	S-P085	Chen, Liqing.....	M-P220
Brandao-Neto, Jose.....	M-P158	Camargo, Ademir.....	10.02.04	Chen, Liqing.....	T-P213
Brayer, Gary.....	M-P056	Cambon, Olivier.....	13.03.02	Chen, Lirong.....	S-P185
Breton, Gary W.....	10.01.03	Camin, Bettina.....	13.09.06	Chen, Lirong.....	M-P210
Breton, Gary W.....	T-P167	Campana, Charles.....	13.02.02	Chen, Lu.....	M-P214
Bricogne, Gerard.....	01.05.02	Campbell, Branton J.....	M-P106	Chen, Xi.....	S-P067
Briggs, Peter.....	T-P085	Caparon, Mike.....	T-P124	Chen, Xiaojia.....	M-P114
Brinks, Hendrick W.....	13.01.01	Capel, Malcolm.....	T-P045	Chen, Yu-Sheng.....	T-P023
Brinks, Hendrik W.....	13.01.03	Carlile, Candice.....	T-P052	Chen, Zhongguo.....	S-P213
Brister, Keith.....	11.01.02	Carlucci-Dayton, M.....	T-P027	Chen, Zhongzhou.....	S-P059
Brittain, W.J.....	09.01.03	Carmen, Peter.....	13.06.07	Cheney, Wayne.....	M-P034
Brock, Carolyn P.....	10.01.02	Carney, Jill.....	S-P099	Cheng, Hui-Chun.....	S-P133
Brock, Carolyn P.....	13.02.06	Carpenter, Gene.....	13.12.03	Cheng, Lin.....	13.05.02
Brockhauser, Sandor.....	13.07.05	Carrell, H.L.....	TR.01.08	Cheng, Yi-Sheng.....	T-P060
Broderick, Joan.....	M-P166	Carroll, Kate.....	S-P017	Cherezov, Vadim.....	T-P197
Brooks, Cory.....	M-P126	Carrall, Patrick.....	13.14.03	Cherney, Maia.....	T-P010
Brooun, Alexei.....	S-P125	Carrondo, Maria.....	01.07.01	Cheung, J.....	M-P054
Brostromer, Erik.....	M-P058	Carter, Charles.....	T-P099	Chew, Guanhan.....	S-P215
Brouillette, Christie.....	M-P194	Caruthers, Jonathan.....	T-P071	Chien, Wen-Ming.....	13.09.03
Brouillette, Wayne.....	M-P194	Castagna, Jean-Charles.....	13.15.04	Childers, Seth W.....	13.11.04
Broutin, Isabelle.....	M-P012	Castilho, Marcelo.....	10.02.04	Chinte, Unmesh.....	11.01.02
Brown, C. Kent.....	T-P108	Castro-Colin, M.....	M-P098	Chiorini, J.A.....	M-P142
Brown, C. Kent.....	T-P076	Catalano, Jeffrey.....	T-P007	Chipot, Christophe.....	09.04.05
Brown, D.W.....	13.09.07	Catanzariti, Ann-Maree.....	01.07.05	Chiu, Thang.....	AW.03.05
Brown, Eric.....	AW.03.03	Cate, Jamie H.D.....	01.03.01	Chiu, Wah.....	AW.01.05
Brown, Rhoderick E.....	T-P094	Cecchini, Gary.....	T-P205	Chmaissem, Omar.....	M-P116
Bruckmann, Chiara.....	M-P076	Cerasoli, Douglas.....	M-P224	Cho, Ki Joon.....	13.15.07
Bruno Julia C.....	10.02.07	Cerione, Richard.....	S-P085	Cho, Uhn Soo.....	01.01.07
Brunzelle, Joseph.....	T-P148	Cerniglia, C.E.....	M-P210	Chokhawala, Harshal.....	S-P067
Bruono, R.....	13.07.06	Cervin, Maggie.....	T-P114	Choo, H.....	13.09.07
Brusau, E.V.....	T-P181	Chainok, Kittipong.....	M-P162	Chooback, Lilian.....	M-P180

# Author Index

Chrencik, Jill .....	S-P125	Court, Donald.....	01.01.03	Deivanayagam, Champion.....	M-P194
Christendat, Dinesh .....	S-P115	Cousido, Alexandra .....	S-P223	Delbaere, Louis.....	13.10.01
Chruszcz, Maksymilian.....	T-P008	Cowan, M.....	13.07.06	Delbaere, Louis.....	13.10.02
Chruszcz, Maksymilian.....	T-P097	Crane, Brian R. ....	T-P078	Delbaere, Louis.....	T-P038
Chruszcz, Maksymilian.....	T-P122	Cremades, Nunilo.....	T-P166	Delbaere, Louis.....	T-P044
Chruszcz, Maksymilian.....	T-P223	Criswell, Angela .....	T-P095	Delbaere, Louis.....	T-P046
Chrzas, John.....	13.07.09	Croteau, Nathalie.....	01.04.04	Delbaere, Louis.....	T-P054
Chrzas, John.....	13.07.08	Crow, Lowell .....	T-P160	Delbaere, Louis.....	T-P080
Chu, Chen-Hsi .....	S-P135	Cruite, J. ....	S-P095	Delgado, Jose Miguel, Q.....	10.02.07
Chu, Yong.....	13.11.08	Crundwell, Guy .....	13.07.01	DeLong, Hugh C. ....	13.14.04
Chuang, Woei-Jer .....	01.07.03	Crundwell, Guy .....	SP01.02	DeLucas, Larry .....	M-P194
Chung, Jae Woo.....	T-P137	Cudney, Bob.....	S-P201	DeMartino, Julie .....	T-P090
Ciloy, Jose Martin.....	M-P132	Cuff, Marianne E. ....	S-P191	Demirors, Mehmet.....	09.03.02
Cipriani, Florent.....	13.07.05	Cuff, Marianne E. ....	T-P110	Deng, Junpeng .....	01.05.04
Clarke, Tony.....	T-P073	Culnane, Lance .....	13.01.01	Deng, Lu.....	T-P065
Classen, Scott.....	T-P055	Cutfield, John .....	T-P012	Dera, Pzremek.....	05.01.04
Clausen, Bjorn .....	13.03.04	Cutfield, Sue.....	T-P012	Derewenda, Urszula .....	T-P215
Clausen, Bjorn .....	13.09.07	Cygler, M. ....	T-P120	Derewenda, Zygmunt.....	S-P087
Clausen, Henrik .....	T-P023	Cymborowski, Marcin .....	11.01.06	Derewenda, Zygmunt.....	T-P215
Clayton, Gina.....	T-P209	Cymborowski, Marcin .....	S-P051	Deschamps, Jeffrey.....	M-P108
Clearfield, Abraham.....	S-P031	Cymborowski, Marcin .....	T-P008	Desgreniers, Serge .....	13.10.08
Clearfield, Abraham.....	T-P111	Cymborowski, Marcin .....	T-P097	Desigan, Kumaran .....	M-P226
Clogston, Jeffrey .....	T-P197	Cymborowski, Marcin .....	T-P122	Desper, John.....	10.03.16
Coates, Leighton.....	TR.01.05	Cymborowski, Marcin .....	T-P223	Desper, John.....	13.02.07
Coates, Leighton.....	TR.01.08	D'Amico, Kevin L.....	T-P174	Desper, John.....	SP01.03
Coates, Leighton.....	TR.01.09	Dabrowski, Bogdan.....	M-P116	Desper, John.....	T-P127
Cobb, Melanie.....	T-P102	Daha, Mohamed .....	01.05.03	Desper, John.....	T-P135
Cody, Vivian.....	S-P189	Dai, Pengcheng.....	M-P100	DeTitta, George.....	13.06.03
Cohen, Aina.....	13.15.04	Dai, Shaodong.....	01.01.01	DeTitta, George.....	T-P071
Cohen, Aina.....	M-P160	Dai, Xiaoping.....	T-P042	Devarapalli, Satish.....	T-P039
Cohen, David.....	S-P207	Daka, Philiias .....	10.03.06	Devasamudram, T.....	M-P038
Cohen, Serge X.....	01.02.05	Daley, Margaret E.....	01.01.07	Devlin, Karl Ian .....	T-P040
Cohen, Seth.....	13.12.02	Danel, Franck.....	13.10.03	Devos, Juliette.....	M-P178
Colabroy, Keri L. ....	T-P078	Daniels, Lee M.....	13.05.01	Dey, Barna.....	T-P075
Colaneri, Michael .....	T-P179	Daniels, Lee M.....	T-P173	Dhe-Paganon, S. ....	T-P026
Colburn, Nancy.....	T-P050	Dar, Imran .....	T-P130	di Michiel, Marco .....	11.01.05
Colella, Roberto.....	13.11.07	Darakev, Georgi.....	M-P156	di Michiel, Marco .....	13.09.06
Collart, Frank.....	M-P066	Das, J. ....	T-P028	Diawara, Y.....	T-P156
Collart, Frank .....	T-P068	Dauter, Zbigniew .....	01.05.01	Diaz de Delgado, Graciela .....	10.02.07
Collart, Frank .....	T-P126	David, S.A.....	13.09.07	Dickerson, Tobin.....	S-P079
Collins, Craig .....	10.03.05	Davidson, A.R.....	S-P097	Dillard, Bret.....	T-P193
Collins, Paul.....	M-P024	Davies, David.....	01.06.02	DiMarco, John .....	04.01.01
Collins, Paul.....	S-P113	Davies, David.....	AW.03.05	DiMarco, John .....	10.02.10
Colman, Roberta F.....	AW.03.04	Davies, David.....	T-P069	DiMattia, Michael.....	S-P009
Connors, Rebecca .....	T-P073	Davis, Jamaine.....	S-P119	DiMattia, Michael.....	M-P142
Cook, Mike .....	T-P014	Davlieva, Milya .....	T-P018	Ding, Yili .....	04.01.03
Cook, Paul F.....	M-P184	Dawson, Eric.....	T-P205	Dmowski, Wojtek .....	13.03.06
Cooper, David.....	S-P087	Day, Catherine .....	T-P012	Dobson, Allison J.....	10.01.07
Cooper, David.....	T-P215	de Jersey, John .....	S-P131	Dodds, Peter N.....	01.07.05
Cooper, Priscilla.....	M-P218	de Jonge, Martin .....	13.11.08	Doi, Masaaki.....	S-P179
Cooper, Priscilla.....	T-P138	De la Mora, Eugenio .....	T-P082	Domsic, John .....	S-P171
Cope, Elizabeth.....	13.03.05	De la Mora, Teresa.....	M-P138	Donaldson, L.....	S-P097
Copeland, Daniel .....	S-P159	De Lill, Daniel .....	13.12.01	Dong, Huaze .....	T-P107
Copeland, Daniel .....	M-P180	De Lurgio, Patrick .....	T-P031	Donnelly, Adam .....	10.01.07
Cork, Carl.....	T-P051	Deacon, Ashley .....	M-P062	Donnelly, Mark.....	13.06.02
Cornaby, Sterling .....	T-P014	Deacon, Ashley .....	M-P074	Donner, W. ....	M-P098
Cornell, Kenneth.....	S-P145	Deal, Kennon .....	10.01.07	Dooley, Helen .....	T-P067
Cosgrove, Daniel .....	T-P152	Dealwis, Chris.....	TR.01.09	Dormitzer, Philip.....	T-P061
Cote, Valentina.....	10.02.07	DeCarlo, Sacha.....	01.03.03	Dorn, Harry .....	13.14.06
Cotelesage, Julien .....	T-P038	deGroot, A. Willem .....	09.03.02	Dorn, Harry .....	M-P164
Cotelesage, Julien .....	13.10.01	Degtyareva, Olga .....	M-P114	Dosch, Helmut.....	09.01.05
Cotton, F. Albert.....	13.14.05	Degtyareva, Valentina .....	05.01.02	Doudeva, Lucy, G.....	T-P064
Coulton, James W.....	01.04.04	Dehez, Francois .....	09.04.05	Doudeva, Lyudmila .....	T-P060
Coureux, Pierre-Damien .....	13.14.02	Deisenhofer, Johann .....	01.06.06	Dove, Martin.....	13.03.02

# Author Index

Dove, Martin.....	13.03.05	Elmore, Brad.....	T-P048	Fitzgerald, Paula M.D. ....	AW.01.02
Drake, Stephen D.....	10.03.15	Elser, Veit.....	13.0804	Fitzgerald, Paula M.D. ....	M-P028
Drake, Stephen D.....	T-P121	Elsliger, Marc.....	M-P062	Fitzsimmons, M.R. ....	AW.02.08
Drennan, Catherine.....	M-P166	Engström, Sven.....	01.04.03	Flajnik, Martin .....	T-P067
Du, P. ....	13.11.06	Engström, Sven.....	T-P195	Fleming, Christopher.....	M-P224
Duax, William.....	S-P117	Enright, Gary.....	13.02.08	Fodje, Michel.....	13.10.02
Duax, William L. ....	M-P052	Erlacher, Kurt.....	M-P050	Fong, Desiree.....	13.10.04
Dufour, Catherine.....	AW.02.09	Esaki, Nobuyoshi.....	S-P137	Forouhar, Farhad.....	M-P076
Duggan, Erika.....	S-P105	Esaki, Nobuyoshi.....	S-P139	Fossdal, Anita.....	13.01.03
Duke, Elizabeth.....	M-P158	Escorihuela, Inmaculada.....	T-P115	Foster, Mark D. ....	AW.02.03
Duke, Norma E.C. ....	S-P191	Esser, Lothar.....	01.04.10	Foster, Mark D. ....	09.01.03
Duke, Norma E.C. ....	T-P031	Esser, Lothar.....	T-P191	Fowler, Frank.....	T-P129
Duke, Norma E.C. ....	T-P126	Esser, Lothar.....	T-P207	Frampton, Chris.....	13.11.03
Dumas, John.....	T-P079	Evans, Gwyndaf.....	M-P158	Frankel, Ken.....	T-P055
Dumesnil, Karine.....	AW.02.09	Evans, John.....	13.03.02	Frankel, Ken.....	T-P168
Dunaway-Mariano, Debra.....	T-P032	Evans, Phil.....	M-P144	Fransen, Martijn.....	S-P053
Dunny, Gary.....	T-P108	Evans, Stephen.....	S-P013	Frappier, Lori.....	T-P096
Duntun, Pete.....	M-P160	Evans, Stephen.....	M-P126	Frey, Perry.....	13.06.08
Durst, R. ....	T-P156	Evdokimova, Elena.....	S-P061	Fritsky, Igor.....	T-P149
Duxbury, Phillip M.....	T-P009	Evdokimova, Elena.....	M-P078	Froelich, Jamie.....	M-P040
Duzen, Jill.....	S-P189	Evdokimova, Elena.....	M-P080	Fronczek, Frank.....	T-P015
Dyakonenko, Viktoriya.....	T-P125	Evdokimova, Elena.....	T-P008	Fujimoto, Y.....	T-P164
Dzakula, Zeljko.....	T-P101	Evdokimova, Elena.....	T-P100	Fujita, Makoto.....	10.03.14
Ealick, Steven E.....	01.01.05	Ezersky, Alexanfra.....	M-P080	Fuller, Watson.....	09.03.03
Ealick, Steven E.....	S-P157	Fait, James.....	13.07.08	Furey, William.....	T-P020
Ealick, Steven E.....	S-P195	Fait, James.....	13.07.09	Furey, William.....	T-P105
Ealick, Steven E.....	T-P021	Falus, Péter.....	09.01.05	Furnham, Nicholas.....	01.02.02
Ealick, Steven E.....	T-P045	Falvello, Larry R.....	T-P115	Gajhede, Michael.....	T-P077
Ealick, Steven E.....	T-P078	Falvello, Larry R.....	T-P117	Gajhede, Michael.....	T-P130
Earhart, Cathleen.....	M-P124	Fan, Li.....	T-P138	Galella, Michael.....	04.01.01
Earhart, Cathleen.....	T-P076	Fan, Lixin.....	13.11.06	Galvão-Botton, L.M.P.....	01.07.04
Earhart, Cathleen.....	T-P108	Fan, Zi Peng.....	13.14.02	Gambino, Leah.....	S-P117
Earnest, Thomas.....	T-P051	Fang, Ying.....	S-P013	Gambino, Leah.....	M-P052
Eaton, William.....	AW.03.05	Farah, C.S.....	01.07.04	Gan, Jianhua.....	01.01.03
Ebata, K.....	M-P002	Farrell, Kevin.....	S-P207	Gan, Jianhua.....	S-P143
Ebata, Kazuhiro.....	13.15.05	Fasulo, Meg E.....	SP.01.03	Ganshaw, Grant.....	T-P114
Ebata, Toshiobu.....	M-P004	Fedorov, Alexander.....	S-P167	Gao, Hong.....	S-P017
Echeverria, G.....	T-P181	Fedorov, Elena.....	S-P167	Gao, Qi.....	13.05.03
Eckert, Juergen.....	S-P027	Fee, James.....	S-P089	Gao, Yan.....	13.01.05
Eddins, Michael.....	T-P052	Felcher, Gian P.....	09.01.05	Garavito, R. Michael.....	01.04.09
Edmonds, L.....	S-P097	Feldman, Anna.....	M-P044	Garcia, K.C.....	01.06.08
Edwards, Aled.....	S-P061	Feng, Pingyun.....	13.12.04	Garcia-Reynaldos, Paula X.....	T-P109
Edwards, Aled.....	M-P078	Feng, Xu.....	M-P228	Gary, Brayer.....	13.06.04
Edwards, Aled.....	M-P080	Feng, Z.....	13.09.07	Gates, Stacy.....	M-P112
Edwards, Aled.....	T-P008	Fenter, Paul.....	T-P007	Geiger, James H.....	S-P165
Edwards, Aled.....	T-P096	Ferguson-Miller, Shelagh.....	01.04.09	Genick, Ulrich K.....	13.14.02
Edwards, Aled.....	T-P100	Fernandez-Baca, J.A.....	13.09.04	Genis, Caroli.....	S-P007
Edwards, Carol.....	M-P224	Fernandez-Baca, J.A.....	M-P100	Georgiadis, Millie.....	T-P106
Egami, Takeshi.....	13.03.06	Fernandez, Marisa.....	M-P128	Georgiev, Ivan.....	T-P133
Egami, Takeshi.....	13.13.01	Ferrara, Joseph.....	S-P199	Gerbauer, Damara.....	T-P074
Egorova, Olga.....	S-P061	Ferrara, Joseph.....	T-P173	Gerlt, John.....	S-P167
Egorova, Olga.....	M-P080	Ferraro, Dan.....	AW.03.03	Ghetu, Alexandru.....	13.10.05
Eisenberg, David.....	01.05.06	Ferrence, Gregory.....	13.07.01	Ghosh, Anita.....	13.14.01
Eisenberg, David.....	S-P087	Ferrence, Gregory.....	SP.01.02	Ghosh, Arun.....	M-P038
Eisenberg, David.....	T-P219	Ferrence, Gregory.....	S-P019	Ghosh, Joydeep.....	T-P124
Elam, Jeffrey.....	09.01.04	Fieramosca, Joseh.....	M-P116	Gibson, David.....	AW.03.03
Elberry, Maria.....	01.04.10	Finkelstein, Kenneth D.....	13.11.07	Gibson, J.M.....	13.11.06
Elder, John H.....	T-P030	Fischetti, Robert.....	T-P039	Gidaspov, Alexander.....	10.02.09
Ellena, Javier.....	10.02.04	Fischmann, Thierry.....	S-P163	Giefers, Hubertus.....	T-P157
Ellena, Javier.....	S-P039	Fish, Sarah.....	M-P040	Gilbert, E.P.....	S-P021
Ellena, Javier.....	M-P170	Fisher, Andrew.....	S-P067	Gillilan, Richard.....	T-P014
Ellena, Javier.....	M-P174	Fisher, Carl.....	T-P056	Gindhart, Amy.....	S-P043
Ellena, Javier.....	T-P181	Fisher, S. Zoe.....	AW.03.02	Ginell, Steve.....	TR.01.07
Ellis, Jeffrey G.....	01.07.05	Fisher, S. Zoe.....	S-P007	Ginell, Steve.....	S-P191

# Author Index

GINELL, Steve.....	S-P223	GU, J.....	S-P061	HASE, Toshiharu .....	M-P148
GLASS, Colin W. ....	05.01.03	GU, Y.....	S-P143	HASEGAWA, Kazuya .....	11.01.04
GLAZER, Richard .....	S-P053	GU, Zu-Yi .....	T-P076	HASEGAWA, Kazuya .....	13.07.07
GLEASON, William .....	T-P089	GU, Zu-Yi .....	T-P108	HASEGAWA, Tomokazu .....	S-P109
GLUSKER, Jenny.....	TR.01.08	GUAN, Hong-Hsiang.....	T-P019	HASEMANN, Charles .....	M-P026
GODERIS, Bart .....	13.11.01	GUAN, Rongjin.....	M-P128	HASSON, Miriam .....	13.14.01
GODZIK, A. ....	M-P062	GUANGA, Gerald.....	T-P118	HATZOS, Cathy.....	13.06.02
GODZIK, Adam.....	M-P064	GUDDAT, Luke .....	S-P131	HAUBACK, Bjorn C. ....	13.01.01
GOLDIE, Hughes .....	T-P038	GUENAT, Silvie.....	T-P130	HAUBACK, Bjorn C. ....	13.01.03
GOLDIE, Hughes .....	T-P046	GUENGERICH, F. Peter .....	S-P169	HAUNG, Xiaojing.....	13.08.04
GOLDIE, Hughes .....	T-P080	GULDE, Stacey .....	13.06.03	HAUPTMAN, Herbert A. ....	01.02.03
GOLDMAN, Adrian .....	M-P082	GULICK, Andrew.....	S-P099	HAUPTMAN, Herbert A. ....	TR.01.11
GOLDSCHMIDT, Lukasz.....	S-P087	GUNCAR, Gregor .....	01.07.05	HAUSSLER, Wolfgang.....	09.04.02
GOLDSMITH, Elizabeth.....	S-P221	GUO, Fei.....	M-P154	HAZEMANN, Isabelle.....	TR.01.07
GOLDSMITH, Elizabeth.....	M-P032	GUO, Hwai-Chen.....	M-P206	HAZEMANN, Isabelle.....	S-P223
GOLDSMITH, Elizabeth.....	M-P048	GUO, Liang .....	13.11.04	HAZRA, Saugata .....	S-P065
GOLDSMITH, Elizabeth.....	M-P200	GUO, Yi .....	01.06.05	HE, Bob.....	13.11.03
GOLDSMITH, Elizabeth.....	T-P102	GUO, Zhuyan .....	S-P163	HEASLET, Holly .....	01.04.08
GOMEZ, Kamila.....	T-P052	GURDA-WHITAKER, Brittney .....	S-P011	HEASLET, Holly .....	T-P030
GONCHAROV, Alexander.....	05.01.01	GURDA-WHITAKER, Brittney .....	M-P140	HEDFAK, Kristina.....	01.04.01
GONCZY, John.....	13.07.09	GURDA-WHITAKER, Brittney .....	M-P142	HEIKINHEIMO, Pirkko .....	M-P082
GONZALEZ, Ana.....	M-P160	GUSTCHINA, Alla.....	S-P073	HELLER, William.....	09.02.03
GOODWIN, Andrew .....	13.03.02	GUSTCHINA, Alla.....	S-P193	HELLER, William.....	09.02.07
GOODWIN, Andrew .....	13.03.05	GUZEI, Ilia A. ....	10.01.08	HEMINGWAY, Janet.....	M-P220
GOODWIN, Kristie .....	T-P106	GUZZO, C.R.....	01.07.04	HEMLEY, Russell J.....	05.01.01
GOOSSENS, D.J.....	10.03.02	HABEL, Jeff .....	S-P185	HEMLEY, Russell J.....	M-P114
GORDON, Euan.....	T-P162	HACKERT, Marvin.....	T-P004	HENDERSON, Wesley .....	13.14.04
GORNICKI, Piotr.....	M-P202	HADZI, Dusan.....	S-P027	HENDRICKSON, W.A. ....	M-P054
GOSHE, Andrew .....	09.02.02	HAERTLEIN, Michael .....	TR.01.07	HENNING, Robert W.....	T-P033
GOSU, Ramachandraiah .....	T-P076	HAGEN, Wilfred.....	01.07.01	HENNING, Robert W.....	T-P049
GOTO, Masaru .....	S-P137	HAINES, Julien.....	13.03.02	HENRY, Charles S. ....	T-P199
GOU, Shaohua.....	T-P107	HALL, Pamela.....	01.06.02	HERMANN, Thomas .....	04.01.06
GOUGOUTAS, Jack.....	04.01.01	HALL, Pamela.....	T-P069	HERMANN, Thomas .....	M-P040
GOUGOUTAS, Jack.....	10.02.10	HALLER, Kenneth.....	10.02.08	HERMEL-DAVIDOCK, Theresa.....	09.03.02
GOURDON, Pontus .....	S-P075	HALLER, Kenneth.....	S-P029	HERMOSO, Juan .....	S-P181
GOVINDASAMY, Lakshmanan.....	S-P007	HALLER, Kenneth.....	M-P162	HERMOSO, Juan .....	T-P166
GOVINDASAMY, Lakshmanan.....	S-P009	HALLER, Kenneth.....	T-P139	HERNANDEZ-GUZMAN, F. ....	P103
GOVINDASAMY, Lakshmanan.....	S-P011	HALLER, Kenneth.....	T-P141	HERNÁNDEZ-ORTEGA, Simón .....	10.03.10
GOVINDASAMY, Lakshmanan.....	S-P171	HALLER, Kenneth.....	T-P145	HERNANDEZ-ORTEGA, Simón .....	T-P109
GOVINDASAMY, Lakshmanan.....	M-P142	HALLIN, Emil.....	13.10.02	HERNÁNDEZ-ORTEGA, Simón .....	T-P155
GRABER, Tim .....	T-P023	HALLORAN, Zachary .....	T-P104	HÉROUX, Annie.....	13.07.06
GRABER, Tim .....	T-P033	HALPER, Sara.....	13.12.02	HÉROUX, Annie.....	T-P013
GRABER, Tim .....	T-P049	HAMILTON, Tamara D. ....	T-P147	HEROUX, Luke .....	T-P160
GRABOWSKI, Marek.....	13.06.05	HAMILTON, William .....	T-P005	HERR, J.C.....	T-P122
GRANT, Alan .....	M-P158	HAN, Qing .....	04.01.06	HERRERA, N.....	T-P185
GRANT, L. ....	S-P005	HAN, Qing .....	M-P040	HERRON, S.R. ....	S-P005
GRANT, Stephan .....	T-P136	HAN, Seungil.....	M-P218	HEWAT, Alan W.....	13.09.02
GREEN, Mark .....	T-P105	HANAOKA, Fumio .....	T-P138	HIETSCHOLD, Michael.....	M-P094
GREGORYANZ, Eugene .....	05.01.01	HANNA, Yuan.....	T-P060	HIGASHIURA, Akifumi .....	13.15.01
GREGORYANZ, Eugene .....	05.01.05	HANNAN, Bruce .....	T-P160	HIGGINS, Tom.....	13.07.01
GREINER, E.R. ....	S-P005	HANSON, Leif.....	11.01.02	HIGGINS, Tom.....	SP01.02
GRELEWSKA, Katarzyna .....	S-P087	HANSON, Leif.....	TR.01.08	HILL, Christopher P. ....	01.01.02
GREVELIS, Harris.....	M-P012	HANSON, Leif.....	M-P010	HILL, Darryl .....	T-P073
GRIZOT, Sylvestre .....	T-P207	HAO, Quan .....	13.08.02	HILLS, Tanya .....	M-P152
GROB, Patricia .....	01.03.03	HAO, Quan .....	M-P130	HIRAI, Mitsuhiro .....	09.04.04
GROCE, Stephanie.....	M-P192	HAO, X. ....	10.01.02	HIROSE, Raita.....	13.07.07
GROCHULSKI, Pawel.....	13.10.01	HARDER, D.....	T-P025	HIROTSU, Ken.....	S-P137
GROCHULSKI, Pawel.....	13.10.02	HARDIE, Michael .....	10.03.09	HIROTSU, Ken.....	S-P139
GRODSKY, Neil .....	T-P136	HARDING, Mic .....	M-P158	HISER, Carrie .....	01.04.09
GRONDONA, Brandi P. ....	M-P030	HARRINGTON, Daniel .....	13.15.04	HITOMI, Chiharu .....	M-P218
GROS, Piet.....	01.05.03	HARRINGTON, Daniel .....	M-P160	HJELM, Rex .....	13.13.02
GROSSE-KUNSTLEVE, Ralf .....	01.02.06	HART, Mary Kate.....	T-P059	HJERRILD, Kathryn.....	T-P104
GROSSIE, David .....	T-P175	HART, John P. ....	T-P217	HNATH, Eric .....	M-P018
GRUNER, Sol M. ....	M-P130	HARTMAN, Mike.....	13.01.04	HO, Winny .....	M-P208

# Author Index

Hodges, Jason .....	T-P160	Hughes, Stephen .....	S-P103	Jenkins, Hilary A. ....	10.03.13
Hodgson, K.O. ....	M-P062	Huizinga, Eric .....	01.05.03	Jenni, Simon.....	01.03.04
Hoeffner, Ed.....	M-P138	Hulbert, S. ....	T-P025	Jenni, Simon.....	01.03.05
Hoelt, Rebecca.....	M-P192	Hultgren, Scott .....	T-P124	Jensen, Anne-Marie L. ....	01.05.05
Hofrichter, James .....	AW.03.05	Humphreys, John.....	S-P221	Jensen, Craig M. ....	13.01.01
Hol, Wim.....	01.05.04	Humphreys, John.....	M-P048	Jensen, Craig M. ....	13.01.03
Hol, Wim.....	M-P168	Hung, Li-Wei .....	13.06.06	Jensen, Jordan .....	T-P136
Hol, Wim.....	T-P071	Hung, Li-Wei .....	M-P084	Jerry, Alexandratos .....	S-P073
Holden, Lauren .....	M-P218	Hung, Li-Wei .....	M-P186	Jeyakanthan, Jeyaraman.....	M-P122
Holliday, Jason.....	S-P101	Hung, Li-Wei .....	M-P198	Jha, K.N.....	T-P122
Hollis, Thomas.....	S-P183	Hunt, John F. ....	S-P211	Ji, X.....	S-P143
Holman, K. Travis .....	10.03.15	Hunt, John F. ....	01.0106	Ji, Xinhua .....	01.01.03
Holman, K. Travis .....	13.12.06	Hunter, Allen .....	13.07.01	Jia, Zongchao .....	01.07.06
Holman, K. Travis .....	T-P121	Hunter, Allen .....	SP.01.02	Jia, Zongchao .....	S-P033
Holman, K. Travis .....	T-P131	Huq, Ashfia .....	13.09.03	Jiao, Xuesong.....	T-P158
Holmes, Margaret.....	T-P071	Hura, Greg.....	T-P055	Jin, Zhongmin .....	13.07.09
Holowaty, Melissa .....	T-P096	Huseby, Medora.....	M-P124	Jin, Zhongmin .....	13.07.08
Holton, James.....	T-P168	Hussain, Azhar .....	M-P038	Jitsumori, Keiji.....	S-P139
Holton, James.....	T-P176	Hussain, Mahmood, M.....	S-P129	Joachimiak, Andrzej .....	13.06.02
Hong, Lin .....	M-P038	Husseini, Naji.....	11.01.03	Joachimiak, Andrzej .....	TR.01.07
Hong, Xia.....	S-P059	Husseini, Naji.....	T-P178	Joachimiak, Andrzej .....	S-P051
Hong, Zhi .....	M-P034	Hwang, Jiyoung .....	13.10.04	Joachimiak, Andrzej .....	S-P105
Honkimaki, Veijo.....	11.01.05	Hwang, Son-Jong .....	13.01.04	Joachimiak, Andrzej .....	S-P191
Hooper, Alan .....	T-P048	Hyacinth, Marilise .....	10.03.04	Joachimiak, Andrzej .....	S-P219
Hope, Håkon .....	13.02.01	Ignatchenko, Alexander.....	M-P078	Joachimiak, Andrzej .....	S-P223
Hopper, S.L. ....	M-P210	Ikubo, S. ....	13.13.07	Joachimiak, Andrzej .....	M-P066
Horanyi, Peter .....	T-P193	Ikeda, K. ....	13.01.06	Joachimiak, Andrzej .....	M-P068
Horjales, Eduardo .....	T-P082	Ilavsky, Jan .....	T-P001	Joachimiak, Andrzej .....	M-P070
Horton, Linda.....	13.09.05	Imabayashi, Fumie .....	T-P054	Joachimiak, Andrzej .....	M-P202
Houde, Christian .....	T-P022	Inaka, Koji.....	13.15.01	Joachimiak, Andrzej .....	T-P068
Houde, Christian .....	T-P024	Inaka, Koji.....	S-P209	Joachimiak, Andrzej .....	T-P100
Howard, Andy.....	13.07.09	Inaka, Koji.....	M-P132	Joachimiak, Andrzej .....	T-P110
Howell, Elizabeth .....	TR.01.09	Inaka, Koji.....	T-P006	Joachimiak, Andrzej .....	T-P116
Howell, P. Lynne.....	AW.03.04	Ingram, Richard .....	S-P163	Joachimiak, Andrzej .....	T-P126
Howell, P. Lynne.....	S-P093	Inoue, Tsuyoshi .....	S-P177	Joachimiak, Andrzej .....	T-P142
Howell, P. Lynne.....	S-P097	Inoue, Tsuyoshi .....	S-P179	Joachimiak, Andrzej .....	T-P221
Howell, P. Lynne.....	S-P145	Ipsen, Henrik .....	T-P077	Joachimiak, Grazyna .....	13.06.02
Howell, P. Lynne.....	S-P155	Irimpan, Mathews.....	T-P114	Joachimiak, Grazyna .....	M-P202
Howell, P. Lynne.....	M-P188	Isaac Cerceau Neta, Augusta .....	13.09.06	Jogl, Gerwald .....	S-P153
Hsaio, Nai-Wan.....	S-P133	Ishii, Yoshinobu .....	13.09.04	Johanson, Urban .....	01.04.01
Hsiao, Chwan-Deng .....	01.07.03	Ishikawa, Takuya .....	M-P008	Johmoto, Kohei.....	T-P153
Hsiao, Chwan-Deng .....	13.15.06	Iversen, Bo .....	T-P023	Johnson, Bryan .....	S-P077
Hsiao, Chwan-Deng .....	S-P127	Iverson, Tina.....	T-P205	Johnson, Eric.....	T-P089
Hsiao, Yu-Shan .....	S-P153	Iwai, Shigenori.....	T-P138	Johnson, John E. ....	09.02.04
Hsinchin, Huang .....	T-P060	Jaakola, Veli-Pekka.....	M-P082	Johnson, John E. ....	13.08.07
Hsu, Che-Hsiung .....	S-P127	Jabarullahan, J. ....	S-P035	Johnson, John E. ....	S-P213
Huai, Qing.....	T-P213	Jackson, Edward A. ....	13.02.04	Johnson, Louise .....	M-P158
Huang, Cheng-Yang .....	01.07.03	Jacobsen, Chris .....	13.0804	Johnson, William .....	T-P004
Huang, Cheng-Yang .....	S-P127	Jada, Srinivasa .....	10.02.01	Jones, Charles .....	M-P178
Huang, Chung-Yu.....	T-P062	Jain, Anubhav.....	T-P043	Joosten, Krista.....	01.02.05
Huang, Haimei.....	T-P062	Jakoncic, Jean .....	11.01.05	Jordan, Frank.....	T-P020
Huang, Mingdong.....	S-P071	Jakoncic, Jean .....	T-P043	Jorgensen, James.....	M-P116
Huang, Mingdong.....	T-P213	Jambon, Albert.....	05.01.05	Jorgensen, James.....	M-P118
Huang, Qingzhen.....	M-P100	James, Manley .....	T-P074	Jorgensen, Rene .....	01.06.07
Huang, Xiaoying .....	13.12.05	James, Michael .....	T-P010	Joseph, Jeremiah .....	01.01.08
Huang, Ying .....	T-P140	Janda, Kim .....	S-P079	Joseph, Jeremiah .....	T-P132
Huang, Zixian .....	S-P071	Janssen, Bert.....	01.05.03	Joseph-Horne, Tim .....	T-P073
Hubbard, C.....	13.09.07	Jao, Edwin.....	S-P163	Jouanneau, Yves.....	11.01.05
Huc, Ivan .....	13.05.01	Jaroszewski, Lukasz .....	M-P064	Judas, Nenad .....	T-P143
Huddler, Donald P.....	T-P154	Jaskolski, Mariusz .....	01.07.02	Juhas, Pavol.....	T-P009
Huether, Robert.....	S-P117	Jaskolski, Mariusz .....	S-P073	Julian, Maureen M.....	M-P110
Huether, Robert.....	M-P052	Jayaraman, Seetharaman.....	M-P076	Juo, Z.S.....	01.06.08
Huffman, John C.....	13.07.02	Jayaraman, Seetharaman.....	T-P083	Jurgenson, C.T. ....	01.01.05
Huffman, Kianosh L.....	13.07.02	Jeffery, Constance.....	T-P211	Justice, Ryan S. ....	T-P001

# Author Index

Kaduk, James.....	S-P045	Kim, Youngchang.....	S-P191	Kreger, Allison.....	M-P168
Kaercher, Joerg.....	T-P172	Kim, Youngchang.....	M-P066	Kreusch, Andreas.....	T-P070
Kagan, O.....	S-P061	Kim, Youngchang.....	T-P116	Kridel, Steve.....	S-P069
Kalinin, Yevgeniy.....	11.01.03	Kimberlin, Christopher.....	S-P095	Krishnamurthy, N.....	M-P222
Kalinin, Yevgeniy.....	S-P107	Kimura, T.....	M-P100	Krishnan, Navasona.....	01.01.04
Kaminski, Heinz.....	13.09.06	King, Danny.....	09.03.02	Kristensen, Ole.....	T-P077
Kanack, Alex T.....	T-P094	Kinnibrugh, Tiffany.....	10.02.03	Kristensen, Ole.....	T-P130
Kanagalaghata, Rajashankar.....	T-P045	Kirby, B.J.....	AW.02.08	Krivolapov, Dmitry.....	10.02.09
Kaneko, Syuzo.....	T-P074	Kirillova, Olga.....	13.06.05	Kronenberg, M.....	01.06.01
Kang, Seong A.....	T-P078	Kirkwood, Kevin.....	13.06.04	Krueger, Susan.....	AW.02.05
Kang, You-Na.....	S-P195	Kirz, Janos.....	13.08.04	Krumm, Brian.....	01.05.04
Kania, Robert.....	04.01.02	Kishida, Hiroyuki.....	S-P147	Krupka, Heike.....	M-P030
Kantardjieff, Katherine.....	13.07.01	Kitagawa, Susumu.....	10.03.08	Ku, Shao-Yang.....	S-P145
Kantardjieff, Katherine.....	SP.01.01	Kitajima, Masato.....	M-P132	Ku, Shao-Yang.....	S-P155
Kantardjieff, Katherine.....	SP.01.02	Kitano, Hiroshi.....	S-P179	Kubelka, Jan.....	AW.03.05
Kantardjieff, Katherine.....	S-P003	Kiyayagi, Ryoji.....	M-P116	Kudritska, Marina.....	S-P061
Kantardjieff, Katherine.....	S-P005	Kjellbom, Per.....	01.04.01	Kudritska, Marina.....	M-P080
Kantardjieff, Katherine.....	S-P015	Klemmer, Kent.....	T-P080	Kudritska, Marina.....	T-P100
Kaplan, Craig.....	01.03.02	Klevit, Rachel E.....	01.01.07	Kuhl, Tonya.....	AW.02.06
Kapustina, Maryna.....	T-P099	Klinman, Judith.....	S-P077	Kuhlmann, Marion.....	09.03.01
Karen, Pavel.....	S-P049	Klock, Heath.....	M-P074	Kuhn, Peter.....	01.01.08
Kasaian, Marion.....	T-P079	Klooster, Wim T.....	T-P011	Kuhn, Peter.....	S-P125
Kashii, Masafumi.....	S-P177	Kmetko, Jan.....	11.01.03	Kuhn, Peter.....	T-P132
Kashii, Masafumi.....	S-P179	Knapp, James.....	13.08.03	Kuk, Jane.....	T-P128
Kastrup, Jette Sandholm.....	T-P130	Kobayashi, Tomoyuki.....	S-P209	Kulleck, James.....	13.01.04
Kataeva, Irina.....	S-P149	Kobayashi, Tomoyuki.....	T-P006	Kumalah, Sayon.....	13.12.06
Katagiri, Kazuo.....	SP.01.04	Kobayashi, Yoichiro.....	M-P004	Kumar, Abhinav.....	M-P030
Kato, Mitsuyasu.....	T-P006	Kobayashi, Yoshiko.....	M-P132	Kumar, D.....	13.11.06
Kato, S.....	13.01.06	Kobe, Bostjan.....	01.07.05	Kumar, Saikatendu.....	01.01.08
Katz, Amy.....	TR.01.08	Koch, Michel H. J.....	09.02.05	Kumar, Saikatendu.....	T-P132
Kaufmann, Gunnar.....	S-P079	Koclega, K.....	T-P008	Kumar, T.K.S.....	M-P154
Kaufmann, Kristian.....	T-P205	Kodama, K.....	13.13.07	Kumar, V.....	01.06.01
Kaviratne, Anthony.....	M-P198	Koelsch, Gerald.....	M-P038	Kumaran, Desigan.....	T-P081
Kaviratne, Anthony.....	M-P186	Koesma, Eric.....	T-P070	Kumaran, Desigan.....	T-P144
Kawano, Takeharu.....	M-P150	Koetzle, Thomas.....	S-P027	Kumasaka, Takashi.....	13.07.07
Kazmierczak, Michael.....	11.01.01	Kokozay, Vladimir.....	T-P119	Kunishima, Naoki.....	T-P066
Keefe, Lisa J.....	T-P037	Kokozay, Vladimir.....	T-P123	Kunishima, Naoki.....	T-P164
Keefe, Lisa J.....	T-P170	Kokozay, Vladimir.....	T-P125	Kunishima, Naoki.....	T-P189
Keen, David.....	13.03.05	Kolatkhar, Anand.....	S-P125	Kuntz, Douglas A.....	S-P091
Keen, David.....	13.03.02	Komoto, Junichi.....	S-P173	Kuo - Chiang, Hsia.....	T-P060
Keiski, Carrie-Lynn.....	S-P093	Kong, Deyuan.....	T-P111	Kuramitsu, Seiki.....	M-P122
Kelley, Brian.....	04.01.05	Konnert, John.....	M-P108	Kurihara, Kazuo.....	13.15.05
Kent, Helen.....	M-P144	Koo, Jason.....	AW.03.04	Kurihara, Kazuo.....	M-P002
Kent, Michael.....	AW.02.04	Koo, Jason.....	S-P155	Kurihara, Kazuo.....	M-P008
Ketcha, Daniel.....	T-P175	Kornberg, Roger.....	01.03.02	Kurihara, Tatsuo.....	S-P137
Khan, Javed.....	T-P092	Korolev, Sergey.....	S-P001	Kurihara, Tatsuo.....	S-P139
Khazins, David.....	M-P036	Koroleva, Olga.....	S-P001	Kurusu, Genji.....	M-P148
Khazins, David.....	T-P156	Korostelev, Andrei.....	M-P146	Kuroishi, Chizu.....	M-P122
Khoja, Hamid.....	T-P018	Korotkov, Konstantin.....	01.05.04	Kuroishi, Chizu.....	T-P189
Khursigara, Cezar M.....	01.04.04	Koss, John W.....	T-P174	Kuroki, Ryota.....	M-P008
Ki, Wooseok.....	13.12.05	Kostek, Seth.....	01.03.03	Kusaka, Katsuhiro.....	13.15.05
Kickhoefer, Valerie.....	T-P219	Kottar, Andreas.....	13.09.06	Kusaka, Katsuhiro.....	M-P002
Kim, Chae Un.....	M-P130	Kourinov, Igor.....	T-P016	Kuspa, M.K.....	T-P185
Kim, Chang-Yub.....	M-P186	Kourinov, Igor.....	T-P021	Kusunoki, Masami.....	M-P148
Kim, Chang-Yub.....	M-P198	Kourinov, Igor.....	T-P045	Kutilek, Victoria.....	T-P030
Kim, Dorothy.....	S-P211	Kovaleva, E.G.....	S-P057	Kuzmenko, Ivan.....	AW.02.04
Kim, Hidong.....	S-P217	Kovari, Ladislau.....	S-P197	Kwak, Seung-Yeop.....	T-P137
Kim, Jin kwang.....	13.15.07	Kovari, Ladislau.....	M-P196	Kwong, Peter D.....	T-P002
Kim, Kyung Hyun.....	13.15.07	Kozasa, Tohru.....	M-P150	Kwong, Peter D.....	T-P075
Kim, Kyung-Nam.....	M-P190	Kozlowski, Briana.....	T-P108	Kycia, Stefan.....	13.10.09
Kim, Myung Hee.....	T-P215	Krachodnok, Samroeng.....	T-P145	Laco, Gary.....	S-P073
Kim, Sang Bok.....	13.12.03	Kraus, Michelle.....	S-P125	Ladner, Jane.....	S-P141
Kim, Sun Hwa.....	13.15.07	Krause, Kurt L.....	T-P012	Lai, R.H.....	S-P003
Kim, Youngchang.....	13.06.02	Krause, Kurt L.....	T-P018	Lai, Yi-Ju.....	S-P135

# Author Index

Lainer, L.L.....	01.06.08	Levy, H.....	M-P142	Longenecker, Kenton.....	04.01.04
Laivenieks, Maris.....	T-P038	Lewis, Sarah.....	13.11.02	Longo, Antonella.....	T-P118
Lakshminarasimhan, D.....	M-P226	Li, Chia-Lung.....	T-P060	Longtin, Joseph.....	T-P018
Lam, Sonia Y.....	S-P175	Li, Chia-Lung.....	T-P064	Love, L.J.....	M-P088
LaMarra, S.....	T-P025	Li, Chunmin.....	13.06.04	Love, Robert.....	T-P136
Lamzin, Victor.....	01.02.05	Li, Chunmin.....	M-P056	Lovell, Scott.....	T-P104
Lamzin, Victor.....	T-P093	Li, Hongmin.....	01.06.05	Lovering, Andrew.....	13.10.03
Lancaster, Laura.....	M-P146	Li, Hui.....	13.06.02	Lovey, Raymond G.....	S-P163
Landes, Brian.....	09.03.02	Li, Hui.....	M-P066	Low, Harry.....	T-P150
Landes, Steven.....	09.03.02	Li, Hui.....	T-P126	Lowe, Jan.....	T-P150
Lane, Michael.....	M-P140	Li, Huiying.....	M-P208	Lowther, Todd.....	S-P069
Langan, Paul.....	TR.01.05	Li, Jing.....	13.12.05	Lu, Hailong.....	10.02.05
Langan, Paul.....	TR.01.08	Li, Lian-Chao.....	T-P152	Lu, Kun.....	13.11.04
Langan, Paul.....	TR.01.09	Li, Meng.....	M-P166	Luecke, Hartmut.....	01.04.07
Langley, Ries.....	T-P065	Li, Mi.....	S-P073	Luecke, Hartmut.....	M-P034
Langs, David A.....	TR.01.11	Li, Mi.....	S-P193	Luecke, Hartmut.....	T-P084
LaRonde-LeBlanc, Nicole.....	T-P050	Li, Rongbao.....	M-P228	Luecke, Hartmut.....	T-P203
Larsen, Jørgen N.....	T-P077	Li, X.....	09.01.03	Luft, Joseph.....	13.06.03
Lauher, Joseph.....	10.03.03	Li, Xin.....	01.07.06	Luna, V. Mitch.....	S-P089
Lauher, Joseph.....	T-P129	Li, Xinmin.....	TR.01.08	Lund, Kaare.....	T-P077
Laurberg, Martin.....	M-P146	Li, Xuefa.....	09.01.01	Lundy, Matt.....	M-P072
Lauricella, Angela.....	13.06.03	Li, Y.....	S-P143	Lunin, Volodia.....	S-P223
Lavie, Arnon.....	S-P065	Li, Ying.....	T-P136	Luo, Bing-Hao.....	T-P034
Lavin, Martin.....	S-P131	Li, Yongdong.....	T-P213	Lurio, Lawrence.....	13.11.02
Lazarski, Krzysztof.....	S-P191	Li, Youli.....	09.02.06	Lurio, Laurence.....	T-P158
Lazicki, Amy.....	05.01.06	Li, Z. Jane.....	10.03.18	Luu, Tien Hung.....	M-P094
Le Magueres, Pierre.....	M-P018	Li, Zhi-Pan.....	AW.02.08	Lynch, D.....	T-P025
Le Trong, Isolde.....	T-P071	Li, Zhong.....	01.06.05	Lynch, Ed.....	T-P045
Leary, Julie.....	S-P017	Li, Zhong.....	T-P129	Lynn, David G.....	13.11.04
Lee, Allen.....	01.04.05	Liang, Yan.....	13.11.04	Lynn, Gary.....	T-P005
Lee, Byeongdu.....	09.01.04	Lieberman, Raquel L.....	01.04.06	Lynn, Gary.....	09.02.07
Lee, Byeongdu.....	09.03.05	Lima, Enju.....	13.08.04	Lynn, J.W.....	M-P100
Lee, Byeongdu.....	WK.03.02	Lin, Laura.....	T-P079	Lyssenko, Konstantin.....	T-P177
Lee, Chi-Shen.....	M-P102	Lin, Li-ying.....	T-P088	Lyu, Ping-Chiang.....	S-P133
Lee, Chi-Shen.....	13.15.02	Lin, Ying-Chuan.....	T-P030	Mace, Peter.....	T-P012
Lee, Dong Ryeol.....	09.01.01	Lind, Cora.....	S-P043	MacGillivray, Leonard R.....	10.03.17
Lee, Dong Ryeol.....	09.01.03	Lind, Cora.....	M-P112	MacGillivray, Leonard R.....	T-P133
Lee, Jeffrey E.....	M-P188	Lipkowski, Janusz.....	T-P113	MacGillivray, Leonard R.....	T-P147
Lee, Jeffrey E.....	T-P059	Lipscomb, John.....	S-P057	Mackenzie, F.....	T-P026
Lee, John.....	T-P031	Lipscomb, John.....	M-P192	MacPherson, Iain.....	M-P204
Lee, Kelly.....	09.02.04	Litchev, Vassil.....	M-P156	MacDonald, David.....	T-P089
Lee, Kwang-Hoon.....	T-P134	Litteer, Brian.....	S-P053	Madden, M.E.....	M-P088
Lee, Seung-Jae.....	S-P221	Littrell, Kenneth.....	S-P025	Madden, Tim.....	T-P031
Lee, Seung-Jae.....	T-P102	Litvinov, Igor.....	10.02.09	Madegowda, Mahendra.....	T-P083
Lee, Shao-Chen.....	13.15.06	Liu, A.....	S-P097	Madhavan, Vidya.....	T-P211
Lee, Shao-Chen.....	T-P019	Liu, Chun-Feng.....	M-P038	Madhavapeddi, Prashanti.....	S-P221
Lee, Suk-Hee.....	T-P106	Liu, Jyung-Hung.....	13.15.06	Madison, Vincent.....	S-P163
Lee, Thomas.....	M-P042	Liu, Peng.....	13.11.04	Mahendrasingam, A.....	09.03.03
Lee, Woo Cheol.....	T-P036	Liu, Xiaobo.....	01.06.07	Maier, Timm.....	01.03.04
Leger, Jean-Michel.....	13.05.01	Liu, Zhi-Jie.....	S-P149	Maier, Timm.....	01.03.05
Lehtinen, Duane A.....	S-P183	Liu, Zhi-Jie.....	S-P185	Maigret, Bernard.....	09.04.05
Lehtiö, Lari.....	M-P082	Liu, Zhi-Jie.....	M-P210	Majeed, Shahzad.....	T-P002
Lei, Hui.....	M-P038	Liu, Zhi-Jie.....	T-P193	Majewski, Jaroslaw.....	AW.02.06
Lei, Ning.....	T-P033	Liub, Chia-Jyi.....	M-P102	Majkrzak, Charles F.....	AW.02.01
Leibundgut, Marc.....	01.03.04	Liv, James Zhi-Jie.....	S-P117	Major, János.....	09.01.05
Lekin, Tim.....	M-P186	Llusar, Rosa M.....	T-P115	Makarov, Oleg.....	T-P039
Lekin, Timothy P.....	M-P198	Lo, Chieh-Tsung.....	09.03.05	Makharashvili, Nodar.....	S-P001
Lenardo, Michael.....	M-P212	Lo, Samuel M-F.....	10.02.06	Mäki, Seija.....	M-P082
Lenhard, A.....	T-P025	Loewen, Roderick.....	T-P041	Maklashina, Elena.....	T-P205
Lesley, Scott.....	M-P062	Loizou, Elena.....	09.03.06	Malakhova, Margarita L.....	T-P094
Lesley, Scott.....	M-P074	Lokanath, Neratur K.....	T-P189	Malchiodi, Emilio.....	M-P128
Lesley, Scott.....	T-P070	Loll, Patrick J.....	T-P199	Malcolm, Bruce.....	S-P163
Letts, James.....	S-P013	Long, Fei.....	T-P087	Malinina, Lucy.....	T-P094
Levin, Elena.....	T-P091	Long, Robert.....	10.02.03	Malkowski, Michael.....	13.06.03

# Author Index

Malley, Mary.....	04.01.01	McRee, Duncan .....	S-P113	Moffat, Keith.....	T-P128
Malvar, Thomas .....	M-P042	McRee, Duncan .....	M-P024	Moffatt, B. ....	M-P188
Mandel, Corey .....	T-P074	McSweeney, Sean.....	13.07.05	Moiseeva, Natalia.....	01.04.04
Manghnani, Murli.....	05.01.04	McTigue, Michele .....	04.01.02	Molitsky, Michael.....	T-P031
Mangin, Philippe .....	AW.02.09	Medina, Milagros .....	S-P181	Møller, Jesper V. ....	01.05.05
Manivannan, V.....	M-P120	Medved, Sergei.....	M-P036	Montanez, P.....	T-P025
Manley, James.....	M-P046	Medved, Sergei.....	T-P156	Montelione, Gaetano T.....	M-P076
Mao, Ho-kwang.....	05.01.01	Mee, Jenny .....	S-P079	Moody, D.B.....	01.06.01
Mao, Ho-kwang.....	M-P114	Meehan, Edward.....	M-P220	Moon, J.-W.....	M-P088
Mao, Qilong .....	S-P117	Meehl, Mike.....	T-P124	Moon, Jin Ho .....	M-P198
Mao, Qilong .....	M-P052	Mehta, Sunil.....	S-P161	Morais Cabral, Joao.....	T-P209
Marino, John .....	S-P141	Meigs, George.....	T-P176	Morales-Morales, David .....	10.03.10
Mariuzza, Roy.....	M-P128	Meiler, Jens .....	T-P205	Mori, Toshiyuki .....	01.01.09
Mariuzza, Roy.....	T-P065	Meilleur, Flora .....	TR.01.07	Mori, Yusuke.....	S-P177
Markham, George.....	S-P173	Meilleur, Flora .....	M-P016	Mori, Yusuke.....	S-P179
Marple, Larry .....	13.05.04	Mengin-Lecreulx, D.....	01.06.06	Morii, Yukio .....	13.15.05
Marquette, Kimberly .....	T-P079	Meno, Kåre .....	T-P077	Morii, Yukio .....	M-P002
Marschand, Lyle .....	T-P158	Mercer, Darren D.W.....	10.03.13	Morisco, Laura L.....	T-P174
Martin, Kenneth L. ....	10.01.03	Meron, M. ....	T-P049	Morosin, Bruno.....	M-P118
Martin, Kenneth L. ....	T-P167	Merrill, A. Rod.....	01.06.07	Moroz, Yura .....	T-P149
Martin, Philip .....	S-P197	Merritt, Ethan A. ....	01.02.01	Morris, Garrett .....	T-P030
Martin, Philip .....	M-P196	Merritt, Ethan A. ....	T-P071	Mosko, Rollan.....	M-P072
Martinez, Jorge .....	M-P196	Mesecar, Andrew .....	T-P112	Moss, S.C. ....	M-P098
Martinez Vargas, Sergio .....	T-P155	Meyer, C.R. ....	S-P005	Mosyak, Lidia .....	T-P079
Martínez-Júlvez, Marta .....	S-P181	Mezouar, Mohamed .....	05.01.05	Motohara, Moritoshi.....	S-P209
Martínez-Júlvez, Marta .....	T-P166	Miao, Huijie .....	13.08.04	Moua, Y. ....	T-P185
Marx, A.....	M-P120	Miao, Jianwei (John).....	01.03.06	Mough, Scott T. ....	10.03.15
Masci, Paul.....	S-P131	Michalska, Karolina .....	01.07.02	Mourad, Walid .....	01.06.05
Massey, Bridgette .....	10.01.07	Mickley, Mandel.....	M-P072	Mowat, Chris .....	M-P076
Mathes, Erika.....	S-P165	Mihara, Hisaaki.....	S-P137	Moy, Shiu .....	M-P066
Mathews, Irimpan.....	M-P074	Milinda, A.M.....	M-P098	Moy, Shiu .....	M-P070
Mathews, Irimpan.....	M-P160	Miller, Chad .....	AW.02.06	Moy, Shiu.....	T-P142
Matias, Pedro .....	01.07.01	Miller, Echo.....	13.06.07	Moy, Shiu F. ....	M-P068
Matkovic-Calogovic, D. ....	T-P143	Miller, Edward.....	S-P011	Moy, Shiu F. ....	T-P221
Matsumura, Hiroyoshi.....	S-P177	Miller, H.P. ....	09.02.06	Mueller, Peter .....	13.02.03
Matsumura, Hiroyoshi.....	S-P179	Miller, K.W.....	T-P028	Mueser, Timothy .....	M-P010
Matsushita, Osamu .....	13.08.06	Miller, Maria .....	S-P205	Mueser, Timothy .....	M-P178
Matsushita, Osamu .....	M-P136	Miller, Russ .....	T-P105	Muir, J. Lewis .....	T-P037
Matsushita, Osamu .....	T-P017	Miller, Samuel I. ....	01.01.07	Muir, J. Lewis .....	T-P170
Matta, Cherif.....	T-P171	Millers, Emma-Karin .....	S-P131	Mukherjee, Tathagata .....	T-P078
Matte, A.....	T-P120	Milochova, Mariana .....	M-P104	Mulichak, Anne .....	01.04.09
Maul, Robert .....	S-P189	Min, Xiaoshan.....	M-P032	Mulichak, Anne .....	T-P037
Maxey, Evan R.....	13.09.03	Minor, Wladek .....	11.01.06	Mulichak, Anne .....	T-P170
May, Andrew.....	S-P207	Minor, Wladek .....	13.06.05	Müller-Buschbaum, Peter .....	09.01.05
May, Andrew.....	T-P168	Minor, Wladek .....	S-P051	Mulligan, Rory.....	T-P068
Mazock, Gloria .....	T-P211	Minor, Wladek .....	T-P008	Mulligan, Rory.....	T-P142
McCleverty, Clare.....	T-P070	Minor, Wladek .....	T-P097	Murai, Ryota .....	S-P177
McConnell, Patrick.....	M-P026	Minor, Wladek .....	T-P122	Murakami, Satoshi.....	S-P177
McCoy, Jason .....	13.06.08	Minor, Wladek .....	T-P223	Murakami, Satoshi.....	S-P179
McDonald, Heather .....	M-P194	Mironova, Ekaterina.....	10.02.09	Muramatsu, Hisashi.....	S-P137
McGeorge, Garry.....	13.05.03	Mishra, Vinod, K. ....	S-P129	Murillo, Carlos A. ....	13.14.05
McIntyre, Garry J. ....	T-P011	Misra, Saurav .....	T-P040	Murphy, Drew .....	13.12.02
McKenna, Robert .....	AW.03.02	Mitchell, Dan .....	01.05.04	Murphy, Michael .....	M-P204
McKenna, Robert .....	S-P007	Mitev, Kostadin Z. ....	S-P083	Murphy, Paul.....	M-P168
McKenna, Robert .....	S-P009	Mitev, Kostadin Z. ....	M-P156	Murshudov, N.N. ....	T-P087
McKenna, Robert .....	S-P011	Mitschler, Andre .....	TR.01.07	Murthy, Krishna, H.M. ....	S-P129
McKenna, Robert .....	S-P171	Mitschler, Andre .....	S-P223	Mustyamikov, Marat .....	TR.01.09
McKenna, Robert .....	M-P140	Mixon, Mark .....	M-P134	Muthusubramanian, S. ....	M-P120
McKenna, Robert .....	M-P142	Miyahara, Ikuko.....	S-P137	Muzyczka, Nicholas .....	S-P009
McKenzie, Kathleen.....	S-P079	Miyahara, Ikuko.....	S-P139	Muzyczka, Nicholas .....	S-P011
McMullen, Donald F. ....	13.07.02	Miyatake, Hideyuki.....	S-P109	Muzyczka, Nicholas .....	M-P140
McNulty, I. ....	13.11.06	Moffat, Keith.....	T-P033	Muzyczka, Nicholas .....	M-P142
McPherson, Alexander.....	13.08.01	Moffat, Keith.....	T-P035	Myers, Michael P. ....	T-P140
McPherson, Alexander.....	S-P201	Moffat, Keith.....	T-P049	Myers, Joseph, Jr.....	S-P163

# Author Index

Myles, Dean.....	09.02.07	Nocek, Bogi.....	T-P100	Pace, Jim.....	S-P189
Myles, Dean.....	TR.01.07	Nöchel, Ulrich.....	09.03.01	Page, Katharine.....	13.13.06
Myles, Dean.....	TR.01.10	Nodes, Beverly.....	T-P136	Page, Malcolm.....	13.10.03
Nabel, Gary J.....	T-P075	Nogales, Eva.....	01.03.03	Pahl, R.....	T-P049
Naciri, Jawad.....	M-P108	Noinaj, Nicholas.....	S-P081	Pahl, Reinhard.....	13.08.03
Nagata, Koji.....	T-P036	Nolan, W.....	T-P025	Pahl, Reinhard.....	T-P033
Nagem, R.A.P.....	01.07.04	Nolan, W.....	T-P027	Pahl, Reinhard.....	T-P035
Nagy, Kathryn.....	T-P007	Noll, Bruce C.....	10.01.04	Painter, G.....	01.06.01
Naides, Matthew.....	11.01.03	Noller, Harry.....	M-P146	Pal, Gour.....	S-P033
Nakagawa, Atsushi.....	13.15.01	Nollert, Peter.....	M-P134	Palcic, Monica.....	S-P013
Nakamori, Y.....	13.01.06	Nonomiya, Jim.....	T-P136	Palmer, Cynthia.....	04.01.02
Nakamura, Tai.....	T-P006	Nossal, Nancy.....	M-P178	Palmer, David.....	T-P044
Nakamura, Yumiko.....	13.01.03	Nyblom, Maria.....	T-P162	Palmer, Kenneth.....	01.01.09
Nakata, Shinya.....	S-P177	O'Keefe, Steve.....	T-P090	Palosz, Bogdan.....	13.03.03
Nakayama, Masato.....	M-P148	O'Neill, Jim.....	T-P051	Pan, Junhua.....	T-P086
Nam, Hyun-Joo.....	M-P140	Oganov, Artem R.....	05.01.03	Panjikar, Santosh.....	T-P093
Nan, Jie.....	M-P058	Ogata, Craig.....	T-P045	Papiz, Miroslav Z.....	T-P197
Nan, Jie.....	M-P060	Oh, Byung-Ha.....	T-P134	Papoular, R.J.....	13.13.05
Napolitano, Hamilton.....	10.02.04	Oh, Seung-Ick.....	M-P190	Park, Changyong.....	T-P007
Narayanan, Suresh.....	09.01.01	Ohashi, Yuji.....	T-P153	Park, Eun Young.....	M-P190
Narayanan, Suresh.....	13.11.02	Ohhara, Takashi.....	13.15.05	Park, Sam-Yong.....	S-P147
Narayanan, Theyencheri.....	09.03.03	Ohhara, Takashi.....	M-P002	Park, Sung Soo.....	13.15.07
Narda, G.E.....	T-P181	Ohlendorf, Douglas.....	M-P124	Parker, Lauren.....	M-P144
Nascimento, Fábio.....	S-P039	Ohlendorf, Douglas.....	M-P192	Parker, W. Larry.....	13.05.03
Nassef, Hany.....	T-P168	Ohlendorf, Douglas.....	T-P076	Parkin, Sean.....	10.01.02
Neder, Reinhard.....	13.13.03	Ohlendorf, Douglas.....	T-P108	Parkin, Sean.....	13.02.06
Needleman, D. J.....	09.02.06	Ohnishi, Yuki.....	M-P004	Parris, Kevin.....	T-P079
Neidle, Stephen.....	AW.01.03	Ohnishi, Yuki.....	M-P006	Parthasarathy, Venkataram.....	T-P093
Nemeria, Natalia.....	T-P020	Ohnishi, Yuki.....	M-P008	Parton, Mark.....	09.03.03
Nesterov, Dmytro.....	T-P123	Ohren, Jeffrey.....	M-P026	Passerini, Stefano.....	13.14.04
Nesterova, Oksana.....	T-P119	Ojala, C.R.....	T-P185	Pasupulati, L.....	T-P105
Nettles, James.....	04.01.05	Ojala, W.H.....	T-P185	Patapoutian, Ardem.....	T-P070
Neuman, Benjamin.....	01.01.08	Ojeda-Lopez, M.A.....	09.02.06	Patel, Dinshaw J.....	T-P094
Neuman, Benjamin.....	T-P132	Okazaki, Nobuo.....	13.07.07	Patel, Rajen.....	09.03.02
Neutze, Richard.....	01.04.01	Olesen, Claus.....	01.05.05	Patel, Sangita B.....	T-P090
Neutze, Richard.....	01.04.03	Ollmann Sapphire, Erica.....	S-P095	Paterson, D. J.....	13.11.06
Neutze, Richard.....	S-P075	Olmstead, Marilyn M.....	13.14.06	Pathuri, Puja.....	T-P084
Neutze, Richard.....	T-P162	Olmstead, Marilyn M.....	M-P164	Patrick, Brian O.....	13.02.06
Neutze, Richard.....	T-P195	Omi, Rie.....	S-P137	Pavlovsky, Alexander.....	M-P026
Newhouse, Yvonne.....	13.08.05	Omi, Rie.....	S-P139	Pawelek, Peter D.....	01.04.04
Newman, E.M.....	T-P026	Onoprienko, O.....	S-P061	Pearson, Arwen.....	S-P077
Ng, Seik Weng.....	T-P139	Orimo, S.....	13.01.06	Pearson, Arwen.....	M-P138
Ng-Thow-Hing, Christopher.....	01.04.04	Orpen, Guy.....	10.03.11	Pearson, Arwen.....	T-P048
Ni, Lisheng.....	S-P067	Ortiz de Montellano, Paul.....	M-P208	Pearson, Wayne.....	05.01.07
Nibbe, Caroline.....	T-P089	Orwenyo, Jared N.....	S-P007	Pedelacq, Jean-Denis.....	T-P187
Nicholls, A.....	M-P020	Osborn, James.....	10.03.05	Pedersen, Lars.....	T-P072
Nickel, Bert.....	09.04.01	Oshige, Masahiko.....	T-P106	Peiris, Suhithi.....	05.01.07
Nicol, Malcolm.....	T-P157	Osipiuk, Jerzy.....	S-P191	Peisach, Jack.....	T-P179
Niemeyer, T.J.....	T-P095	Osipiuk, Jerzy.....	M-P066	Pell, Lisa.....	S-P097
Nienaber, Kurt.....	T-P044	Osipiuk, Jerzy.....	T-P068	Pelletier, Dale.....	TR.01.10
Niesman, Michael.....	04.01.02	Osipiuk, Jerzy.....	T-P221	Pellin, Michael.....	09.01.04
Niimura, Nobuo.....	13.15.05	Ostyk-Narbutt, Jerzy.....	T-P113	Peltier, Tracy.....	09.03.02
Niimura, Nobuo.....	TR.01.03	Otwinowski, Zbyszek.....	11.01.06	Pemble, Charles.....	S-P069
Niimura, Nobuo.....	M-P002	Otwinowski, Zbyszek.....	13.06.05	Peñacoba, José Ignacio.....	T-P117
Niimura, Nobuo.....	M-P004	Otwinowski, Zbyszek.....	M-P070	Penczek, Pawel.....	01.03.03
Niimura, Nobuo.....	M-P006	Otwinowski, Zbyszek.....	T-P008	Pennycocock-Brown, Micha.....	M-P080
Niimura, Nobuo.....	M-P008	Otwinowski, Zbyszek.....	T-P097	Peregrina, José Ramón.....	S-P181
Nikitina, Vitalina.....	T-P125	Otwinowski, Zbyszek.....	T-P221	Perez-Salas, Ursula.....	T-P005
Nilsson, Bo.....	01.05.03	Otwinowski, Zbyszek.....	T-P223	Perrakis, Anastassis.....	01.02.05
Nilsson-Ekdahl, Kristina.....	01.05.03	Ouyang, X.....	S-P005	Perrotta, Anthony J.....	M-P090
Nishida, Clinton.....	M-P208	Ouyang, Xiang.....	S-P015	Perry, John.....	M-P218
Nissen, Poul.....	01.05.05	Ozeki, Tomoji.....	13.15.05	Peters-Libeu, Clare.....	13.08.05
Njoroge, F. George.....	S-P163	Ozeki, Tomoji.....	M-P002	Petersen, Hanna.....	T-P010
Noble, Schroeder M.....	T-P154	O, Keefe, Barry R.....	01.01.09	Peterson, Matthew.....	10.03.19

# Author Index

Petkowski, J.J.....	T-P008	Prongay, Andrew J.....	S-P163	Richardson, James.....	M-P116
Petrache, Horia.....	09.04.03	Protashevitch, Irina.....	M-P194	Richter-Addo, George.....	13.05.02
Petrova, Tatiana.....	S-P223	Proteasa, Georghe.....	M-P196	Richter-Addo, George.....	S-P159
Petrova, Tatiana.....	T-P110	Pruett, Pam.....	M-P194	Richter-Addo, George.....	M-P180
Petrukhina, Marina A.....	13.02.04	Pu, Lin.....	10.03.04	Rifkin, Jeffrey.....	T-P041
Petrusenko, Svitlana.....	T-P119	Punte, G.....	T-P181	Rijssenbeek, Job.....	13.01.05
Pflugrath, James.....	S-P199	Puntharod, Ratchadaporn.....	T-P141	Ringwall, Andy.....	13.15.04
Pflugrath, James.....	T-P095	Purdy, Michael.....	01.04.02	Ripmeester, John.....	10.02.05
Phan, Jason.....	T-P098	Puttick, Jennifer.....	13.10.01	Ripmeester, John.....	13.02.08
Phelps, T.J.....	M-P088	Puttick, Jennifer.....	T-P046	Risal, Dipesh.....	T-P101
Phenix, Chris.....	T-P044	Pynn, Roger.....	AW.02.11	Riscoe, Michael.....	S-P145
Phillips, George.....	13.06.08	Pyzalla, Anke.....	13.09.06	Roach, Claudia.....	01.05.04
Phillips, George.....	T-P091	Qian, Kun.....	T-P043	Robbins, David.....	M-P072
Phillips, John D.....	01.01.02	Qin, Ling.....	01.04.09	Roberts, Mary F.....	S-P203
Phillips, Matt.....	S-P085	Qu, Zhican.....	M-P228	Robertson, Ian.....	13.01.01
Philominathan, Sagaya T.L.....	13.08.06	Quartey, Pearl.....	13.06.02	Robinson, H.....	13.07.06
Philominathan, Sagaya T.L.....	M-P136	Quartey, Pearl.....	T-P116	Robinson, H.....	T-P013
Philominathan, Sagaya T.L.....	T-P017	Quint, Patrick.....	S-P171	Robinson, H.....	T-P027
Phothikanith, Auphatham.....	10.02.08	Quiocho, Florante.....	S-P161	Rodgers, David.....	S-P081
Piccoli, Paula.....	S-P027	Raaijmakers, Hans.....	01.05.03	Rodrigues, Cláudia.....	S-P039
Pichardo, John.....	S-P163	Rabedeau, Thomas.....	13.15.04	Rodriguez, Angela.....	T-P217
Pichaud, Franck.....	S-P161	Radfar, Ramin.....	S-P101	Rogers, Claude.....	S-P079
Pickart, Cecile.....	T-P052	Radhakannan, T.....	13.06.06	Rome, Leonard.....	T-P219
Pickett, Warren.....	05.01.06	Radhakannan, T.....	M-P186	Roos, Anja.....	01.05.03
Pinayev, I.....	T-P025	Rädler, Joachim.....	09.04.01	Rose, David R.....	S-P091
Pingali, Sai Venkatesh.....	13.11.04	Rae, A. David.....	S-P029	Rose, John.....	13.07.08
Pinkerton, Alan.....	10.01.06	Raghavan, Aravinda.....	13.11.02	Rose, John.....	13.07.09
Pinkerton, Alan.....	11.01.02	Rajalingam, D.....	M-P154	Rose, John.....	S-P149
Pinkerton, Alan.....	S-P027	Rajashankar, Kanagalaghatta.....	T-P016	Rose, John.....	S-P185
Pinkerton, Alan.....	T-P171	Rajeswaran, Manju.....	T-P169	Rose, John.....	M-P210
Pinkett, Heather.....	01.04.05	Rakowsky, G.....	T-P025	Rose, John.....	T-P193
Pinkner, Jerry.....	T-P124	Ramamoorthy, S.....	T-P025	Rose, Natisha.....	S-P013
Pinko, Christopher.....	04.01.02	Ramaswamy, S.....	AW.03.03	Rose, Robert.....	T-P118
Pinkowska, Malgorzata.....	S-P087	Ramirez, Laura.....	13.07.01	Rosenbaum, Gerd.....	11.01.01
Pitt, Mark.....	13.01.01	Ramirez, Laura.....	SP.01.02	Rosenbaum, Gerd.....	T-P025
Pletnev, Vladimir.....	S-P117	Ranganathan, Senthil.....	M-P228	Rosenbaum, Gerd.....	S-P191
Pletnev, Vladimir.....	M-P052	Ranson, Hilary.....	M-P220	Rosenfeld, Robin.....	S-P113
Podjarny, Alberto.....	TR.01.07	Rao, Zihe.....	01.07.08	Rosenfeld, Robin.....	M-P024
Podjarny, Alberto.....	S-P223	Rath, Nigam.....	M-P120	Rosenzweig, Amy C.....	01.04.06
Polder, N.....	S-P005	Rathbone, Dan.....	10.02.01	Roshchin, Igor V.....	AW.02.08
Pomés, Anna.....	S-P193	Ratia, Kiira.....	T-P112	Rotella, Frank J.....	S-P191
Ponticelli, Sarah.....	S-P189	Ratna, Banahalli.....	M-P108	Rotella, Frank J.....	T-P031
Porcar, Lionel.....	09.03.06	Ravelli, Raimond.....	13.07.05	Rotella, Frank J.....	T-P142
Porcar, Lionel.....	T-P005	Raviv, U.....	09.02.06	Roth, Lauren.....	S-P123
Post, Kai.....	M-P134	Rawn, C.J.....	M-P088	Roth, Stephan Volkher.....	09.03.01
Potter, Philip.....	M-P224	Raynor, J.....	T-P008	Roy, S.....	AW.02.08
Potter, Stephen.....	T-P105	Recht, Michael.....	S-P125	Royer, William.....	13.08.03
Poulos, Thomas.....	M-P208	Reddy, Vijay.....	S-P213	Rozycki, Jan.....	S-P073
Poulsen, Rasmus.....	T-P023	Redinbo, Matthew.....	M-P224	Ruan, Shengyang.....	T-P033
Powell, Ben.....	M-P030	Rees, Douglas.....	01.04.05	Rubin, Harvey.....	S-P119
Powell, Douglas R.....	13.05.02	Reger, Albert.....	S-P099	Ruble, John.....	11.01.02
Pozzi, C.G.....	T-P181	Regni, Catherine.....	S-P151	Rudiño-Piñera, Enrique.....	T-P082
Prabakaran, P.....	S-P143	Reich, Christian.....	09.04.01	Ruf, Michael.....	05.01.08
Prasad, Lata.....	13.10.01	Reimers, Walter.....	13.09.06	Ruf, Michael.....	T-P172
Prasad, Lata.....	T-P038	Reingold, Jeffrey.....	13.12.03	Ruiz, Federico.....	TR.01.07
Prasad, Lata.....	T-P054	Ren, Y.....	M-P100	Ruiz-Pérez, Catalina.....	T-P151
Prasad, Lata.....	T-P080	Ren, Zhong.....	M-P014	Rupp, Bernhard.....	13.06.07
Pravica, Michael.....	T-P157	Repo, Heidi.....	M-P082	Rupp, Bernhard.....	S-P005
Preece, Geoff.....	M-P158	Resines, Alvaro.....	T-P082	Rush, John.....	13.01.04
Prive, Gilbert G.....	13.10.05	Rewolinski, David.....	04.01.02	Russell, Thomas P.....	09.01.02
Prive, Gilbert G.....	M-P214	Reyes, Christopher L.....	T-P201	Russell, Thomas P.....	AW.02.02
Proffen, Thomas.....	13.03.01	Rezacova, Pavlina.....	M-P070	Ruth, Ronald.....	T-P041
Proffen, Thomas.....	13.03.04	Rheinstadter, Maikel.....	09.04.02	Ruzicka, Frank.....	13.06.08
Proffen, Thomas.....	13.13.07	Richardson, James.....	13.09.03	Rydel, Timothy.....	M-P042

# Author Index

Ryu, Eui Kyung .....	13.15.07	Schadler, Linda .....	13.11.02	Sheldrick, George M. ....	10.01.05
Sabat, Michal .....	10.03.04	Schaefer, Dale W. ....	13.11.05	Shen, Qun .....	13.11.07
Sabini, Elisabetta .....	S-P065	Schaefer, Dale W. ....	T-P001	Shen, Qun .....	13.11.08
Sacchettini, James .....	01.06.04	Schäfer, Frank .....	T-P024	Sheng, Yi .....	T-P096
Saenger, Wolfram .....	TR.01.06	Schall, Constance .....	11.01.02	Sheridan, Dean .....	T-P104
Safinya, C.R. ....	09.02.06	Schall, Constance .....	M-P010	Sheu, Hwo Shuenn .....	13.15.02
Safranek, James .....	13.15.04	Scheidt, W. Robert .....	10.01.04	Shevchenko, Denys .....	T-P125
Safro, Mark .....	M-P044	Schlievert, Patrick .....	T-P076	Shi, Dashuang .....	S-P123
Sagineedu, Sreenivasa .....	10.02.01	Schmidt, Burkhard .....	05.01.05	Shi, Ke .....	M-P124
Sahinidis, Nick .....	M-P172	Schmidt, Gudrun .....	09.03.06	Shi, Ke .....	T-P108
Said, Meriem .....	13.06.03	Schneider, D.K. ....	13.07.06	Shi, Yang .....	S-P059
Saigo, Kaoru .....	T-P036	Schneider, D.K. ....	T-P025	Shibata, Fujiko .....	M-P132
Saikatendu, Kumar .....	T-P112	Schneider, D.K. ....	T-P027	Shiloach, Jossi .....	01.06.02
Saito, Chie .....	T-P006	Schoenborn, Benno .....	TR.01.05	Shilton, Brian .....	13.10.07
Sakon, Joshua .....	13.08.06	Schoenborn, Benno .....	TR.01.08	Shim, Jae Hoon .....	M-P034
Sakon, Joshua .....	M-P136	Schoenborn, Benno .....	TR.01.09	Shimizu, K. ....	T-P164
Sakon, Joshua .....	M-P154	Schramm, Andrew .....	S-P151	Shimizu, Nobutaka .....	11.01.04
Sakon, Joshua .....	T-P017	Schroer, Christian .....	09.03.01	Shin, Hye Jung .....	13.15.07
Sala, Kadsada .....	T-P139	Schubert, Heidi L. ....	01.01.02	Shin, Jeong Sheop .....	M-P190
Sala, Raphael .....	T-P114	Schuermann, Jonathan .....	T-P217	Shinozaki, Shinichi .....	T-P006
Saldajeno, Mae .....	T-P114	Schuller, Ivan K. ....	AW.02.08	Shiro, Yoshitugu .....	M-P122
Salditt, Tim .....	09.04.02	Schultheiss, Nate .....	10.03.16	Shishkin, Oleg .....	T-P119
Salditt, Tim .....	09.04.07	Schultz, Arthur .....	TR.01.02	Shishkin, Oleg .....	T-P125
Salloum, Rogério .....	M-P170	Schultz, Arthur .....	S-P027	Short, Simine .....	M-P118
Samara, George .....	M-P118	Schulze, Steffen .....	M-P094	Shpeizer, Boris G. ....	S-P031
Sampaleanu, Lili .....	S-P155	Schwalbe, Carl .....	10.02.01	Shultis, David .....	01.04.02
Sancho, Javier .....	T-P166	Schwarzenbacher, Robert .....	M-P064	Shumilin, I.A. ....	T-P122
Sanders, B.L. ....	T-P185	Scott, Benjamin .....	T-P127	Shvelidze, Jane .....	T-P089
Sanders, David .....	13.14.01	Scott, Lawrence T. ....	13.02.04	Siddons, Peter David .....	11.01.05
Sanders, Laurie .....	S-P189	Scott, William .....	M-P146	Sides, Cynthia .....	M-P136
Sandkvist, Maria .....	M-P168	Sebolt-Leopold, Judith .....	M-P026	Siegler, M.A. ....	10.01.02
Sandy, Alec .....	09.01.01	Sedov, Vladislav .....	M-P036	Sievers, Stuart .....	T-P219
Sandy, Alec .....	T-P158	Sedov, Vladislav .....	T-P156	Silvaggi, Nicholas R. ....	T-P032
Sanloup, Chrysteale .....	05.01.01	Segal, David .....	01.06.02	Silverman, David .....	AW.03.02
Sanloup, Chrysteale .....	05.01.05	Segal, David .....	T-P069	Silverman, David .....	S-P171
Sano, Satoshi .....	S-P209	Segall, Mark L. ....	AW.03.04	Silvernail, Nathan J. ....	10.01.04
Santarsiero, Bernard .....	T-P112	Segelke, Brent W. ....	M-P186	Simonsen, Klaus .....	M-P040
Santhanam, Arti .....	T-P050	Segelke, Brent W. ....	M-P198	Singh, Divya .....	T-P005
Santos-Jr, Sauli .....	M-P174	Seifert, Soenke .....	09.01.04	Singh, Sasha .....	S-P115
Sapphire, Erica Ollmann .....	T-P059	Sekar, Mariappan .....	05.01.04	Singh-Wilmot, Marvadeen .....	M-P176
Saravanan, S. ....	M-P120	Serrano-Becerra, J.M. ....	10.03.10	Sinha, Sunil .....	AW.02.08
Saridakis, Vivian .....	T-P096	Seshadri, Ram .....	13.13.06	Sinha, Sunil .....	AW.02.12
Sarkari, Feroz .....	T-P096	Sessions, Richard .....	T-P073	Siu, Karen, K.W. ....	M-P188
Sartbaeva, Asel .....	S-P031	Seto, Nina .....	S-P013	Sivaraman, J. ....	T-P120
Sasaki, Katsunari .....	T-P173	Settembre, Ethan C. ....	S-P157	Skarina, Tatiana .....	S-P061
Sasaki, Takatomo .....	S-P177	Sevryugina, Yulia .....	13.02.04	Skarina, Tatiana .....	M-P078
Sasaki, Takatomo .....	S-P179	Sexe, H.M. ....	T-P185	Skarina, Tatiana .....	M-P080
Satija, Sushil .....	AW.02.04	Seybold, Paul .....	T-P175	Skarina, Tatiana .....	T-P008
Sato, Masaru .....	13.15.01	Seydel, Tilo .....	09.04.02	Skaritka, J. ....	T-P025
Sato, Masaru .....	S-P209	Shaftan, T. ....	T-P025	Skelton, Brian .....	T-P123
Sato, Masaru .....	T-P006	Shah, Binal .....	11.01.02	Skillman, A.G. ....	M-P020
Savchenko, Alexei .....	S-P061	Shah, Binal .....	M-P010	Skinner, J. ....	13.07.06
Savchenko, Alexei .....	M-P078	Shah, Naimesh .....	T-P105	Skinner, J. ....	T-P027
Savchenko, Alexei .....	M-P080	Shah, Neil .....	M-P210	Smicja, J.M. ....	T-P185
Savchenko, Alexei .....	T-P008	Shah, Niket .....	S-P091	Smith, Alexander .....	M-P172
Savchenko, Alexei .....	T-P100	Shamoto, S. ....	13.13.07	Smith, Bradley .....	M-P024
Sawatzki, Juergen .....	13.11.03	Shankaranarayanan, Aruna .....	M-P150	Smith, C. ....	S-P005
Sawaya, Michael .....	01.05.06	Shanmugasundararaj, S. ....	T-P028	Smith, Craig .....	T-P124
Saxena, A.M. ....	13.07.06	Shapiro, David .....	13.0804	Smith, David W. ....	T-P174
Saxena, A.M. ....	T-P025	Sharma, Anish .....	S-P063	Smith, Donna .....	10.01.01
Saxena, A.M. ....	T-P027	Sharma, Brahma D. ....	13.02.09	Smith, Janet .....	T-P039
Sayre, David .....	13.0804	Sharma, Nandini .....	M-P028	Smith, Jennifer .....	13.06.03
Scalettar, Richard .....	05.01.06	Shea-McCarthy, G. ....	T-P027	Smith, Michelle .....	13.02.07
Scapin, Giovanna .....	T-P090	Shek, Fanny L-Y. ....	10.02.06	Smith, Michelle .....	T-P135

# Author Index

Smith, Ward .....	T-P039	Stout, C. David.....	01.04.08	Swigart, Dwight.....	13.12.03
Smits, Calum.....	T-P012	Stout, C. David.....	S-P017	Swider-Lyons, Karen E. ....	13.03.06
Snell, Edward.....	11.01.01	Stout, C. David.....	S-P089	Swierczynski, Dariusz.....	T-P113
Snell, Edward.....	S-P189	Stout, C. David.....	T-P030	Szalay, Paul .....	13.07.01
Snijder, Arjan .....	01.04.03	Straka, Derek.....	T-P089	Szalay, Paul .....	SP01.02
Snijder, Arjan .....	S-P075	Stribeck, Norbert.....	09.03.01	Szebenyi, Doletha.....	T-P029
Snijder, Arjan .....	T-P195	Strong, Michael.....	01.05.06	Szebenyi, Tom .....	T-P014
Soares, A.....	13.07.06	Struble, Evi.....	S-P141	Szymanski, Michal .....	S-P111
Soares, A.....	T-P027	Struzhkin, Viktor V. ....	M-P114	Tabler, Elizabeth .....	S-P019
Soares, Alexei .....	S-P159	Strych, Ulrich.....	T-P018	Tabuchi, Akira.....	T-P152
Soares, Alexei .....	T-P013	Strynadka, Natalie .....	13.10.02	Taguchi, T.....	13.13.07
Sochor, Matthew.....	S-P215	Strynadka, Natalie .....	13.10.03	Tainer, John .....	M-P216
Sodroski, Joseph G. ....	T-P075	Strynadka, Natalie .....	M-P152	Tainer, John .....	M-P218
Sokolov, Anatoliy N. ....	10.03.17	Sturchio, Neil.....	T-P007	Tainer, John.....	T-P055
Soler, Tatiana.....	T-P115	Sturman, Eric.....	M-P042	Tainer, John.....	T-P138
Soler, Tatiana.....	T-P117	Su, Xiao-Dong .....	01.07.07	Tainer, John.....	T-P168
Soltis, Michael .....	13.07.03	Su, Xiao-Dong .....	M-P058	Takahashi, Sachiko .....	13.15.01
Soltis, Michael .....	M-P160	Su, Xiao-Dong .....	M-P060	Takahashi, Sachiko .....	S-P209
Soltis, Michael .....	T-P114	Subramaniam, E. ....	M-P226	Takano, Kazufumi .....	S-P177
Somphon, Weenawan.....	S-P029	Subramaniam, E. ....	T-P083	Takano, Kazufumi .....	S-P179
Son, Seung Uk .....	13.12.03	Subramaniam, E. ....	T-P146	Takano, Y.....	M-P002
Song, Hyun Kyu .....	M-P190	Subramanian, Vanitha.....	01.0108	Takeshita, Daijiro.....	T-P036
Sorby, Magnus H. ....	13.01.03	Subramanian, Vanitha.....	T-P132	Takeuchi, Michiyo .....	M-P132
Sørensen, Thomas L. ....	01.05.05	Subramanyam, S.....	M-P226	Takusagawa, Fusao.....	S-P173
Soriano, Erika V. ....	S-P157	Subramanyam, S.....	T-P083	Tam, Amy.....	T-P079
Spangfort, Michael D. ....	T-P077	Subramanyam, S.....	T-P146	Tamada, Taro.....	M-P008
Spedding, Lindsey .....	10.01.07	Sufrin, J. ....	M-P188	Tame, R. H. Jeremy .....	S-P147
Spillmann, Christopher.....	M-P108	Sugahara, Matsuaki .....	T-P164	Tan, Xiang-Yang .....	T-P079
Springer, Timothy A. ....	T-P034	Sugahara, Matsuaki .....	T-P189	Tanabe, T. ....	T-P025
Sprung, Michael.....	09.01.01	Sugimori, Kaoru .....	M-P132	Tanaka, Hiroaki.....	13.15.01
Sprung, Michael.....	T-P158	Sugiyama, Shigeru.....	13.15.01	Tanaka, Hiroaki.....	S-P209
Spude, J.M.....	T-P185	Sugiyama, Shigeru.....	S-P209	Tanaka, Hiroaki.....	T-P006
Srajer, Vukica.....	13.08.03	Sugiyama, Shigeru.....	M-P132	Tanaka, Ichiro .....	13.15.05
Srajer, Vukica.....	T-P033	Suits, Michael .....	S-P033	Tanaka, Ichiro .....	M-P002
Srajer, Vukica.....	T-P035	Sukumar, Narayanasami .....	T-P045	Tanaka, Ichiro .....	M-P004
Srajer, Vukica.....	T-P049	Sul, Soon-Hee.....	M-P200	Tanaka, Ichiro .....	M-P006
Srinivasan, C.....	S-P005	Sulic, Martin.....	13.01.01	Tanaka, Ichiro .....	M-P008
St. Geme, Joseph .....	S-P111	Sumby, Christopher .....	10.03.09	Tanaka, Isao .....	01.02.04
Stanfield, Robyn .....	T-P067	Sun, Mingchi.....	S-P067	Tanaka, Tetsuo .....	13.15.01
Stanslas, Johnson .....	10.02.01	Sun, Peter .....	T-P063	Tanaka, Tetsuo .....	S-P209
Stash, Adam .....	10.01.06	Sun, Yixin.....	M-P206	Tanaka, Tetsuo .....	T-P006
Stec, Boguslaw .....	S-P203	Sun, Yuh-Ju .....	01.07.03	Tang, Jordan.....	M-P038
Stepanov, Sergey.....	T-P039	Sun, Yuh-Ju .....	S-P127	Tanner, John .....	01.01.04
Stephenson, Gregory .....	10.02.02	Sun, Yuh-Ju .....	S-P133	Tanokura, Masaru .....	T-P036
Sterling, Craig .....	S-P217	Sun, Yuh-Ju .....	S-P135	Tao, Xiao .....	T-P092
Stevens, Edwin D. ....	10.01.03	Sun, Yuh-Ju .....	T-P062	Tao, Yizhi Jane.....	T-P086
Stevens, Edwin D. ....	T-P167	Sung, Herman, H-Y. ....	10.02.06	Tarek, Mounir .....	09.04.05
Stevens, Malcolm .....	10.02.01	Sung, Herman, H-Y. ....	M-P162	Tari, Les.....	S-P113
Stevens, Raymond .....	01.01.08	Sunita, S. ....	T-P120	Tatur, Jadwiga .....	01.07.01
Stevens, Raymond.....	T-P132	Surian, Jean.....	10.03.05	Taylor, Alex.....	T-P217
Stevens, Raymond.....	T-P112	Sutter, Jon.....	T-P101	Tchistiakov, Lioudmila.....	T-P079
Stewart, Andrew .....	13.08.04	Sutton, Mark .....	S-P189	te Velthuis, Suzanne G.E. ....	09.01.05
Stewart, Lance .....	S-P217	Suzuki, Mamoru .....	13.15.01	Tecele, Haile .....	M-P026
Stewart, Lance .....	M-P134	Suzuki, Yoshihisa.....	M-P030	Teh, Trazel.....	01.07.05
Stewart, Lance .....	T-P104	Svergun, Dmitri .....	09.02.01	Teixeira, Leticia .....	S-P039
Stieglitz, Kimberly A.....	SP01.04	Swaathi, J. ....	T-P120	Tennakoon, Sanka.....	T-P018
Stieglitz, Kimberly A.....	S-P203	Swaminathan, S. ....	S-P187	Terwilliger, Thomas C. ....	M-P084
Stogios, Peter J.....	M-P214	Swaminathan, S. ....	M-P222	Terwilliger, Thomas C. ....	M-P186
Stoica, Alexandru D. ....	13.09.08	Swaminathan, S. ....	T-P081	Terwilliger, Thomas C. ....	M-P198
Stojanoff, Vivian .....	11.01.05	Swaminathan, S. ....	T-P144	Terwilliger, Thomas C. ....	T-P187
Stojanoff, Vivian.....	T-P043	Sweet, Robert M. ....	13.07.06	Terzyan, Simon .....	T-P148
Stojkovic, Emina .....	T-P128	Sweet, Robert M. ....	WK.02.01	Tesmer, John .....	M-P150
Stokes, Harold T. ....	M-P106	Sweet, Robert M. ....	T-P013	Tesmer, Valerie.....	M-P150
Stone, Anne.....	T-P018	Sweet, Robert M. ....	T-P027	Tetreault, Steve .....	T-P022

# Author Index

Tetreault, Steve .....	T-P024	Turley, Stewart .....	01.05.04	Wachter, G.....	T-P156
Teyton, L. ....	01.06.01	Tworowski, Dmitry .....	M-P044	Wadsten, Pia.....	01.04.03
Thanuja, M. Rabiathul.....	S-P035	Tyagi, Rajiv .....	T-P081	Wadsten, Pia.....	T-P195
Thayer, Max .....	13.06.03	Udachin, Konstantin.....	10.02.05	Wagner, Armin.....	M-P158
Theis-Broehl, Katharina.....	AW.02.07	Udachin, Konstantin.....	T-P113	Walchli, John.....	M-P134
Theodoro, Jahyr .....	10.02.04	Udovic, Boris .....	M-P096	Waldo, Geoffrey S. ....	T-P187
Thibault, Pierre .....	13.08.04	Udovic, Terrence J. ....	13.01.02	Walker, J.R. ....	T-P026
Thiyagarajan, Pappanan .....	09.03.05	Udovic, Terrence J. ....	13.01.04	Walkiewicz, Katarzyna.....	S-P111
Thiyagarajan, Pappanan .....	13.11.02	Uekusa, Hidehiro.....	T-P153	Wall, Dan.....	M-P040
Thiyagarajan, Pappannan.....	13.11.04	Ueno, Go .....	11.01.04	Walsh, Jace.....	13.06.07
Thompson, James .....	T-P090	Ueno, Go .....	13.07.07	Wan, Fengyi .....	M-P212
Thorne, Robert.....	11.01.03	Ugono, Onome .....	10.03.15	Wand, Yujun.....	M-P220
Thorne, Robert.....	S-P107	Ugono, Onome .....	T-P131	Wang, Bi-Cheng .....	11.01.02
Thorne, Robert.....	S-P215	Ugur, G. ....	09.01.03	Wang, Bi-Cheng .....	13.07.09
Thorne, Robert.....	T-P047	Umland, Timothy.....	S-P117	Wang, Bi-Cheng .....	13.07.08
Thorne, Robert.....	T-P178	Umland, Timthy.....	M-P052	Wang, Bi-Cheng .....	S-P117
Thorsted, Peter B. ....	T-P077	Unik, John .....	T-P045	Wang, Bi-Cheng .....	S-P149
Tiede, David.....	09.02.02	Unzai, Satoru.....	S-P147	Wang, Bi-Cheng .....	S-P185
Tieman, Brian .....	T-P158	Urakhchin, Alex.....	T-P039	Wang, Bi-Cheng .....	M-P210
Tikhonov, George .....	09.01.04	Urban, Volker.....	09.02.07	Wang, Bi-Cheng.....	T-P193
Timofeeva, Tatiana .....	10.02.03	Üstündag, Ersan.....	13.03.04	Wang, Chia-Hui.....	13.15.06
Tjian, Robert .....	01.03.03	Vaezeslami, Soheila.....	S-P165	Wang, Ching-I.....	01.07.05
Toba, Samuel.....	T-P101	Vagin, A.A.....	T-P087	Wang, Dong .....	01.03.02
Todorov, Georgi.....	S-P083	Vajda, Stefan .....	09.01.04	Wang, J. ....	09.01.03
Tomanicek, Stephen .....	M-P010	Vakharia, Vikram.....	T-P086	Wang, Jia-huai.....	01.06.03
Tomás, Milagros .....	T-P115	Valderrama, Brenda.....	T-P082	Wang, Jin.....	09.01.01
Tomás, Milagros .....	T-P117	Valdés-Martínez, Jesús.....	10.03.10	Wang, Jun.....	T-P021
Tomasiak, Thomas.....	T-P205	Valdes-Martínez, Jesús.....	T-P109	Wang, Jun.....	T-P045
Tomczyk, Nancy.....	09.01.04	Valdés-Martínez, Jesús.....	T-P155	Wang, Limin .....	01.06.05
Tong, Harry .....	T-P033	van der Woerd, Mark.....	11.01.01	Wang, Liwei.....	M-P212
Tong, Liang .....	S-P153	Van Voorhis, Wesley.....	T-P071	Wang, Ming-Fang.....	M-P102
Tong, Liang .....	M-P046	Van Zandt, Michael .....	S-P223	Wang, Peng .....	13.11.05
Tong, Liang .....	M-P076	Vasileiou, Chrysoula.....	S-P165	Wang, Tao.....	T-P058
Tong, Liang .....	T-P074	Vaughan, David E.W. ....	M-P090	Wang, X.-L.....	13.09.07
Tong, Liang .....	T-P092	Vaughn, Shae .....	10.01.07	Wang, Xiaoping .....	13.14.05
Topalianb, Suzanne.....	T-P065	Veatch, Christina.....	13.06.03	Wang, Xu.....	01.06.07
Toperverg, Boris P. ....	AW.02.07	Vederas, John .....	T-P010	Wang, Xun-Li .....	13.09.08
Tor, Yitzhak .....	04.01.06	Venkatraman, Srikanth .....	S-P163	Wang, Yeming.....	M-P206
Torbett, Bruce E. ....	T-P030	Venturini, Eugene .....	M-P118	Wang, Yi.....	01.04.01
Tomroth-Horsefield, S.....	01.04.01	Verlinde, Christophe.....	T-P071	Wang, Yi-Ting.....	T-P064
Toscano, Rubén A.....	T-P155	Vethantham, Vasupradha.....	T-P074	Wang, Yimin .....	M-P228
Trakhanov, Sergei.....	M-P146	Vey, Jessica.....	M-P166	Wang, Yuchang.....	05.01.04
Treacy, M.M.J. ....	13.11.06	Viccaro, P.J. ....	T-P023	Warfel, J.M.....	S-P005
Treptow, Werner .....	09.04.05	Viccaro, P.J. ....	T-P049	Warkentin, Matt .....	T-P047
Trehwella, Jill.....	13.15.03	Vickrey, John.....	M-P196	Warkentin, Matt .....	T-P178
Tripp, Brian .....	S-P007	Vinson, Paige .....	M-P022	Wasserman, Stephen R.....	T-P174
Tropea, Joseph .....	01.01.03	Viola, Jean Pascal .....	T-P022	Watanabe, G. ....	S-P005
Tropea, Joseph .....	T-P098	Viola, Jean-Pascal.....	T-P024	Waterman, Michael .....	S-P169
Trulove, Paul.....	13.14.04	Viola, Robert.....	13.06.07	Watts, Kevin T.....	M-P138
Tsai, James .....	M-P030	Virji, Mumtaz.....	T-P073	Waugh, David .....	01.01.03
Tsai, Jia-Yin.....	S-P133	Vitali, Jacqueline.....	T-P179	Waugh, David .....	T-P098
Tsai, Jia-Yin.....	T-P062	Vittal, J.J. ....	T-P011	Weaver, Suzanne.....	S-P207
Tsai, Kuang-Lei .....	01.07.03	Vo, Vong .....	M-P094	Weber, Patricia C. ....	S-P163
Tsai, May .....	AW.03.04	Voehler, Markus.....	S-P169	Weeks, Charles M.....	01.02.03
Tsirelson, Vladimir .....	10.01.06	Vogeley, Lutz .....	01.04.07	Weeks, Charles M.....	M-P052
Tsuruta, Hiro .....	09.02.04	Vogeley, Lutz .....	M-P034	Weeks, Charles M.....	T-P105
Tsutakawa, Susan.....	T-P055	Vogeley, Lutz .....	T-P203	Wei, Qun.....	01.07.06
Tu, Chingkuang .....	AW.03.02	Volkart, Lour .....	13.06.02	Weinreb, Violetta .....	T-P099
Tu, Chingkuang .....	S-P171	Volkart, Lour .....	M-P202	Weisgraber, Karl .....	13.08.05
Tuchman, Mendel.....	S-P123	von Groll, Uritza.....	T-P024	Weiss, Kevin .....	09.02.07
Tucker, Matthew .....	13.03.02	Vorndran, Tom .....	M-P072	Weiss, Kevin .....	TR.01.10
Tucker, Matthew .....	13.03.05	Vorobiev, Alexei.....	09.01.05	Weiss, Manfred.....	T-P093
Tucker, Paul .....	T-P093	Vorobiev, Sergey M.....	M-P076	Weiss, Thomas M. ....	T-P003
Turk, Dusan.....	T-P097	Vourloumis, Dionisios.....	M-P040	Welberry, T.R. ....	10.03.02

# Author Index

Wells, Stephen.....	13.03.02	Woodruff, Theresa L.....	M-P186	Yamano, Akihito.....	S-P109
Wennerberg, Goran.....	13.02.07	Wooley, J. ....	M-P062	Yamashita, Masahiro.....	M-P004
Wesolowski, David.....	T-P007	Wooliscroft, Richard.....	M-P158	Yan, Chunhong.....	M-P026
West, Ann.....	S-P159	Worcester, David.....	WK.03.01	Yan, H.....	S-P143
West, Ann.....	M-P180	Wu, Ruiying.....	S-P051	Yan, Shunqi.....	04.01.03
West, Ann.....	M-P184	Wu, D. ....	01.06.01	Yan, Xiaodong.....	S-P011
Westbrook, John.....	AW.01.02	Wu, Dedong.....	13.05.03	Yanez, Marissa.....	01.05.04
Westferro, F. ....	T-P049	Wu, Dedong.....	10.03.05	Yang, Cheng.....	S-P199
Westover, Ken.....	01.03.02	Wu, Edward.....	S-P103	Yang, Cheng.....	T-P048
Weyler, Walter.....	T-P114	Wu, Hao.....	M-P212	Yang, Hua.....	S-P149
Wheeler, Kraig.....	10.03.06	Wu, Huey-Nan.....	S-P127	Yang, In Seok.....	13.15.07
Whetstine, Johnathan.....	S-P059	Wu, Jim.....	M-P034	Yang, Jian.....	M-P166
Whitaker, Britteny.....	S-P009	Wu, Ming-Chen.....	13.15.02	Yang, Jin Kuk.....	M-P212
Whitcomb, David.....	T-P169	Wu, Nan.....	T-P171	Yang, Ling.....	13.09.08
White, Robert H.....	S-P195	Wu, Ruying.....	13.06.02	Yang, Pin.....	M-P118
White, Tommi.....	01.01.04	Wu, Shuya.....	S-P161	Yang, Wanjuan.....	T-P085
Whited, Gregg.....	T-P114	Wu, Ruiying.....	M-P066	Yang, Wei-Jen.....	T-P064
Whitehead, Christopher.....	M-P026	Wu, Ruiying.....	M-P068	Yang, Xiaochun.....	T-P045
Whitman, Chris.....	T-P004	Wu, Ruiying.....	M-P202	Yang, Xiaojing.....	T-P128
Wickersham, John.....	04.01.02	Wu, Ruiying.....	T-P110	Yannone, Steve.....	M-P218
Widmer, Hans.....	S-P125	Wu, Ruiying.....	T-P221	Yao, Min.....	01.02.04
Wiener, Michael.....	01.04.02	Wu, Wen-guey.....	13.15.06	Yao, Nanhua.....	04.01.03
Wiesner, U.....	13.11.06	Wu, Wen-guey.....	T-P019	Yao, Nanhua.....	S-P163
Wignall, George.....	09.02.07	Wünschmann, Sabina.....	S-P193	Yao, Nanhua.....	M-P034
Wilbanks, Sigurd.....	T-P012	Wuthrich, K.....	M-P062	Ye, F.....	M-P100
Wilhelm, James.....	T-P079	Wyatt, Richard T.....	T-P075	Ye, Qilu.....	01.07.06
Wilke, Mark.....	M-P152	Xia, Di.....	01.04.10	Ye, Xiaoming.....	S-P071
Williams, Ian D.....	10.02.06	Xia, Di.....	T-P191	Yeager, Mark.....	01.04.08
Williams, Ian D.....	M-P162	Xia, Jiarong.....	SP.01.04	Yeary, L. W.....	M-P088
Williamson, Anthony.....	S-P095	Xiang, Shi-Hua.....	T-P075	Yedidi, Ravikiran.....	M-P196
Willis, Michael.....	M-P072	Xiao, Tsan.....	T-P034	Yennawar, Hemant.....	M-P090
Wilmot, Carrie.....	AW.03.01	Xiao, Xianghui.....	13.11.08	Yennawar, Hemant.....	T-P152
Wilmot, Carrie.....	S-P077	Xiong, Bing.....	13.10.04	Yennawar, Neela.....	T-P152
Wilmot, Carrie.....	M-P138	Xiong, Wen-Cheng.....	M-P228	Yeo, Hye-Jeong.....	S-P111
Wilmot, Carrie.....	T-P048	Xu, Hao.....	S-P149	Yeung, Rachel C.Y.....	S-P175
Wilson, Ian.....	01.06.01	Xu, Hao.....	S-P185	Yi, Yong.....	S-P207
Wilson, Ian.....	13.06.01	Xu, Hongliang.....	01.02.03	Yim, Hyun.....	AW.02.04
Wilson, Ian.....	S-P079	Xu, Hongliang.....	TR.01.11	Yin, Jiang.....	T-P010
Wilson, Ian.....	M-P062	Xu, Hongliang.....	T-P105	Yip, Patrick.....	AW.03.04
Wilson, Ian.....	T-P042	Xu, Jian.....	M-P018	Yip, Patrick.....	S-P093
Wilson, Ian.....	T-P067	Xu, Jian.....	M-P072	Yip, Patrick.....	S-P145
Wilson, L.....	09.02.06	Xu, Linda.....	M-P078	Yoder, Derek.....	T-P039
Wilson, Samuel.....	T-P072	Xu, Linda.....	M-P080	Yoder, Joshua.....	T-P061
Wilson, William W.....	T-P199	Xu, Ling.....	T-P075	Yokaichiya, Fabiano.....	T-P043
Winans, Randall E.....	09.01.04	Xu, Nan.....	13.05.02	Yokochi, Alex.....	13.05.04
Winans, Randall E.....	09.03.05	Xu, Rui-Ming.....	T-P140	Yokoyama, Shigeyuki.....	M-P122
Wind, Troels.....	S-P071	Xu, Shenglan.....	T-P039	Yokoyama, Takeshi.....	S-P111
Winter, Graeme.....	13.07.04	Xu, Wenqing.....	01.01.07	Yongliang, Chen.....	T-P060
Winter, Roland.....	09.04.06	Xu, X.....	T-P008	Yoo, Choong-Shik.....	05.01.06
Withers, Stephen.....	M-P056	Xu, X.....	S-P061	Young, Victor.....	13.14.04
Wlodawer, Alexander.....	01.01.09	Xu, Zhen.....	T-P040	Yu, Bomina.....	01.01.06
Wlodawer, Alexander.....	S-P073	Xue, S.....	T-P026	Yu, Chang-An.....	01.04.10
Wlodawer, Alexander.....	S-P193	Yagi, Daichi.....	M-P006	Yu, Chang-An.....	T-P191
Wlodawer, Alexander.....	T-P050	Yakovenko, Andrey.....	10.02.03	Yu, Chi-Li.....	AW.03.03
Wlodek, Stanislaw.....	M-P020	Yakunin, Alexandre.....	M-P080	Yu, Linda.....	01.04.10
Wöhri, Annemarie.....	01.04.03	Yamada, N.....	13.13.07	Yu, Minmin.....	13.06.06
Wöhri, Annemarie.....	T-P195	Yamada, Taro.....	S-P173	Yu, Minmin.....	M-P198
Wolberger, Cynthia.....	T-P052	Yamagata, Atsushi.....	M-P216	Yu, Minmin.....	M-P186
Wolberger, Cynthia.....	T-P058	Yamaguchi, Mutsuo.....	01.04.08	Yu, Rongmin.....	13.14.05
Wolfley, Jennifer.....	13.06.03	Yamamoto, Masaki.....	11.01.04	Yu, Xiaolin.....	S-P123
Wong, Andrew.....	01.07.06	Yamamoto, Masaki.....	13.07.07	Yu, Zhihao.....	M-P182
Wong, C.-H.....	01.06.01	Yamanaka, Ari.....	T-P006	Yuan, Cai.....	S-P071
Wong, Kam-Bo.....	S-P175	Yamanaka, Mari.....	13.15.01	Yuan, Cai.....	T-P213
Woo, W.....	13.09.07	Yamanaka, Mari.....	S-P209	Yuan, Hanna, S.....	T-P064

# Author Index

Zabel, Hartmut .....	AW.02.07	Zhurova, Elizabeth .....	S-P027
Zacharias, Annette .....	T-P024	Zhurova, Elizabeth .....	T-P171
Zahran, Zaki .....	M-P180	Zimmerman, M.D.....	T-P008
Zajonc, D.M. ....	01.06.01	Ziolkowska, Natasza .....	01.01.09
Zakharov, Lev N. ....	S-P031	Zitvogel, E.....	T-P025
Zaller, Dennis .....	T-P090	Zolotukhin, Sergei .....	S-P009
Zang, Jangye .....	S-P059	Zolotukhin, Sergei .....	S-P011
Zavalij, Peter .....	13.02.05	Zolotukhin, Sergei .....	M-P140
Zawadzki, Michal .....	S-P087	Zolotukhin, Sergei .....	M-P142
Zeikus, J. Gregory .....	T-P038	Zon, Jerzy .....	T-P111
Zeller, Matthias .....	13.07.01	Zuo, Xiaobing .....	09.02.02
Zeller, Matthias .....	SP01.02	Zwart, Peter .....	01.02.06
Zenno, Shuhei .....	T-P036		
Zhang, Chao .....	M-P030		
Zhang, Erli .....	M-P026		
Zhang, Gongyi .....	S-P059		
Zhang, Hailong .....	T-P074		
Zhang, Hong-Zhong .....	M-P152		
Zhang, Jianmin .....	T-P010		
Zhang, Kam Y.J. ....	M-P030		
Zhang, RongGuang .....	S-P191		
Zhang, RongGuang .....	M-P066		
Zhang, RongGuang .....	M-P068		
Zhang, RongGuang .....	M-P202		
Zhang, RongGuang .....	T-P142		
Zhang, Rumin .....	S-P163		
Zhang, Xi .....	01.04.09		
Zhang, Xiangbin .....	T-P058		
Zhang, Xuejun .....	T-P148		
Zhang, Yang .....	T-P078		
Zhang, Zhan .....	T-P007		
Zhao, Bin .....	S-P169		
Zhao, Fang .....	04.01.06		
Zhao, Gengxiang .....	S-P071		
Zhao, Min .....	S-P149		
Zhao, Min .....	S-P185		
Zhao, Qiang .....	04.01.06		
Zhao, Qiang .....	M-P040		
Zhao, Qinliang .....	13.14.05		
Zhao, Yiwei .....	01.06.05		
Zheng, H. ....	S-P061		
Zheng, Heping .....	13.06.05		
Zheng, Heping .....	T-P122		
Zheng, Lixin .....	M-P212		
Zheng, Nanfeng .....	13.12.04		
Zhenxing, H. ....	T-P120		
Zhong, Zhong .....	11.01.05		
Zhonghao, Shi .....	T-P060		
Zhou, Jing .....	M-P220		
Zhou, Min .....	13.06.02		
Zhou, Tianjun .....	S-P221		
Zhou, Tianjun .....	M-P048		
Zhou, Tongqing .....	T-P002		
Zhou, Tongqing .....	T-P075		
Zhou, Yong .....	01.02.04		
Zhu, Charles .....	01.01.09		
Zhu, Guangyu .....	T-P148		
Zhu, Haibin .....	T-P107		
Zhu, Jilian .....	05.01.04		
Zhu, Xueyong .....	S-P079		
Zhuravleva, Marina .....	T-P063		
Zhurov, Vladimir .....	10.01.06		
Zhurov, Vladimir .....	T-P171		
Zhurova, Elizabeth .....	10.01.06		

# Keyword Index

PI-PI INTERACTIONS .....	THIOSEMICABAZONES .....	H-BONDING .....	T-P109
(BETA/ALPHA) 8-BARREL.....	D-RIBULOSE 5-PHOSPHATE 3-EPIMERASE .....	ENOLASE SUPERFAMILY .....	S-P167
1,2,3-SELENADIAZOLES .....	SELENADIAZOLES .....	STRUCUTRE OF SELENADIAZOLES .....	M-P120
1,3,5-TRIAZINE DERIVATIVES .....	TETRAZOLO[1,5-A]-1,3,5-TRIAZINES .....	X-RAY STRUCTURE .....	10.02.09
2,3-DIOXYGENASE.....	TDO .....	TRYPTOPHAN .....	M-P076
2-(DIMETHYLAMINO)ETHANOL.....	HETEROTRIMETALLIC.....	COPPER .....	T-P123
2-MERCAPTOTHIAZOLINE.....	QUANTUM MECHANICS.....	SMALL MOLECULES .....	M-P170
2D CRYSTALS.....	MEMBRANES .....	RAFTS .....	WK.03.01
3C.....	INHIBITOR.....	PICORNAVIRUS .....	T-P010
3TC.....	HUMAN DEOXYCYTIDINE KINASE.....	L-NUCLEOSIDE ANALOG .....	S-P065
5' TO 3' EXONUCLEASE.....	PROTEIN:DNA COMPLEX .....	BACTERIOPHAGE T4 RNASE H.....	M-P178
6-OH BUSPIRONE.....	CRYSTALS .....	SOLID FORMS .....	13.05.03
A LARGE SINGLE CRYSTAL.....	BETA-LACTOGLOBULIN.....	NEUTRON PROTEIN CR.....	M-P006
A-ATPASE.....	SUBUNIT E .....	STATOR ARCHITECTURE.....	T-P189
A. SUCCINICIPRODUCENS .....	COORDINATION OF DIVALENT METAL.....	PEPCK .....	T-P038
A. THALIANA .....	NUCLEOSIDASE.....	SPECIFICITY .....	M-P188
A2(WO4)3.....	PXRD .....	NTE .....	S-P043
A2M3O12.....	NTE .....	HIGH-PRESSURE .....	M-P112
AB INITIO METHODS .....	SMALL-ANGLE SCATTERING .....	RIGID BODY REFINEMENT .....	09.02.01
AB-INITIO STRUCTURE SOLUTION .....	PAIR DISTRIBUTION FUNCTION .....	PDF.....	T-P009
ABC ATPASE .....	DNA REPAIR.....		S-P001
ABC TRANSPORTER .....	MEMBRANE PROTEIN .....		01.04.05
ABC TRANSPORTER .....	MULTIDRUG RESISTANCE .....	MEMBRANE PROTEIN .....	T-P201
ABSORPTION .....	CORRECTION .....	HEAVY METALS .....	M-P174
ABSORPTION CORRECTION.....	MACROMOLECULES.....	PHASING.....	T-P016
ABSORPTION CORRECTIONS .....	DATA PROCESSING .....	SCALING.....	10.01.05
ACETYLTRANSFERASE.....	ENZYME MECHANISM.....	ANTIBIOTIC RESISTANCE .....	S-P063
ACID-BASE CATALYSIS .....	OXYGEN ACTIVATION.....	DIOXYGENASE.....	S-P057
ACTINIDE .....	COORDINATION POLYMER.....	LANTHANIDE.....	13.12.01
ACTIVATION.....	COPPER ENZYMES.....	OXYGEN .....	S-P077
ACYLPHOSPHATASE.....	STABILITY.....	CATALYSIS .....	S-P175
ACYLTRANSFERASE.....	SGNH HYDROLASE.....		T-P114
ADAPTOR COMPLEXES .....	CELL TRAFFICKING.....		M-P144
ADENO-ASSOCIATED VIRUS.....	ENDOSOMAL PROCESS .....	PARVOVIRUS.....	M-P140
ADENO-ASSOCIATED VIRUS.....	GENE THERAPY .....	CRYO-ELECTRON MICROSCOPY.....	S-P011
ADENO-ASSOCIATED VIRUS 5.....	GENE THERAPY .....	PARVOVIRIDAE.....	M-P142
ADENOSINE PHOSPHOSULFATE.....	IRON SULFUR CLUSTER .....	FE K-EDGE MAD .....	S-P017
ADENOSYLCOBALAMIN.....	TUBERCULOSIS.....	HELIX-BUNDLE.....	M-P198
ADENYLATE FORMING ENZYMES.....	CONFORMATION CHANGE .....		S-P099
ADENYLOSUCCINATE LYASE.....	ENZYMATIC MECHANISM.....	CLASS II FUMARASE SUPERFA .....	AW.03.04
ADHESION .....	COILED COIL .....		T-P073
ADP-RIBOSYLATION.....	EUKARYOTIC ELONGATION FACTOR 2 .....	BACTERIAL TOXINS.....	01.06.07
ADVANCED REFINEMENT .....	PROBLEM STRUCTURES.....	WHOLE MOLECULE DISORDER.....	13.02.02
AGING.....	CANCER .....	DNA REPAIR.....	M-P218
ALANATE.....	HYDROGEN STORAGE .....	MICROSTRUCTURE .....	13.01.01
ALIPHATICS DICARBOXILATES BRIDG .....	HYBRID FRAMEWORKS .....	LANTHANIDE CARBOXYLATES .....	T-P181
ALKB.....	DNA REPAIR.....	IRON DIOXYGENASE .....	01.01.06
ALLANTOATE-AMIDOHYDROLASE.....	PURINE CATABOLISM.....	PSI.....	S-P187
ALLERGEN.....	ASPARTIC PROTEASE.....	ANTIBODY .....	S-P193
ALLERGY .....	ANTIBODY BINDING.....	HOUSE DUST MITE .....	T-P077
ALLOSTERY.....	MAP KINASE.....	DOCKING.....	M-P048
ALPHA SCREEN.....	PROTEIN COMPLEX.....		T-P193
ALPHA-AMINOADIPATE PATHWAY.....	SACCHAROMYCES CEREVISIAE.....	SACCHAROPINE REDUCTASE .....	M-P184
ALPO .....	SODALITE.....	ALUMINOPHOSPATE .....	M-P090
ALUMINOPHOSPATE.....	ALPO .....	SODALITE.....	M-P090
ALZHEIMER'S.....	BACE .....	BETA SECRETASE.....	M-P038
AMINO TERMINAL FRAGMENT.....	ANTI-UPAR ANTIBODY.....	UROKINASE RECEPTOR.....	T-P213
AMINOACYL-TRNA SYNTHETASES .....	TRNA .....	RNA-PROTEIN INTERACTIONS .....	M-P044
AMPICILLIN RESISTANCE.....	PATHOGENICITY ISLAND .....	ENTEROTOXIN .....	T-P076
AMYLOID PEPTIDES .....	SELF-ASSEMBLED NANOSTRUCTURES .....	SMALL ANGLE SCATTERING .....	13.11.04
AMYLOIDOSIS.....	DRUG DELIVERY .....		13.08.06
ANABAENA .....	SENSORY .....	RHODOPSIN .....	T-P203
ANALYSIS.....	STATISTICAL .....	DATA.....	13.06.05

# Keyword Index

ANDROGRAPHOLIDE .....	BLOCKING GROUPS .....	CONFORMATION .....	10.02.01
ANESTHETICS .....	CRYSTAL STRUCTURE .....	PROTEIN KINASE C .....	T-P028
ANISOTROPY .....	REFINEMENT .....		01.05.06
ANOMALOUS .....	POWDER .....	SYNCHROTRON .....	M-P098
ANTHRAX .....	NAD+ SYNTHETASE .....	ANTIBACTERIAL TARGET .....	M-P194
ANTI-UPAR ANTIBODY .....	UROKINASE RECEPTOR .....	AMINO TERMINAL FRAGMENT .....	T-P213
ANTIBACTERIAL TARGET .....	ANTHRAX .....	NAD+ SYNTHETASE .....	M-P194
ANTIBIOTIC .....	PENICILLIN .....	PEPTIDOGLYCAN .....	13.10.03
ANTIBIOTIC RESISTANCE .....	ACETYLTRANSFERASE .....	ENZYME MECHANISM .....	S-P063
ANTIBIOTIC RESISTANCE .....	DRUG DESIGN .....	KINASE .....	13.10.04
ANTIBIOTIC RESISTANCE .....	STAPHYLOCOCCUS AUREUS .....	BETA-LACTAM .....	M-P152
ANTIBIOTICS .....	CRYSTAL STRUCTURE .....	PENICILLIN BINDING PROTEIN .....	S-P147
ANTIBIOTICS .....	RYBOSOME .....	TRANSLOCATION .....	01.03.01
ANTIBODY .....	ALLERGEN .....	ASPARTIC PROTEASE .....	S-P193
ANTIBODY .....	RECEPTOR .....	IL-13 .....	T-P079
ANTIBODY .....	SHARK .....	NEW ANTIGEN RECEPTOR .....	T-P067
ANTIBODY BINDING .....	HOUSE DUST MITE .....	ALLERGY .....	T-P077
ANTICORROSION .....	NEUTRON REFLECTIVITY .....	X-RAY SMALL ANGLE SCATTERING .....	13.11.05
ANTIVIRAL ACTIVITY .....	DOMAIN SWAPPING .....	LECTIN .....	01.01.09
APOFLAVODOXIN .....	HELICOBACTER PYLORI .....	FMN .....	T-P166
APOLIPOPROTEIN A-I .....	SAD .....	UNKNOWN FUNCTION .....	T-P122
APOPTOSIS .....	BAD .....	BCL-XL .....	T-P134
APOPTOSIS .....	DED .....	FLIP .....	M-P212
APPL1 .....	RAB5 EFFECTOR .....	BAR AND PH DOMAIN .....	T-P148
APS .....	PROTEIN CRYSTALLOGRAPHY .....	SYNCHROTRON .....	T-P039
APS .....	SYNCHROTRON .....	BEAMLINE .....	T-P045
APS KINASE .....	CHEMOLITHOTROPHIC .....	ATP SULFURYLASE .....	M-P182
AQUAPORIN .....	MEMBRANE PROTEIN .....	X-RAY CRYSTALLOGRAPHY .....	01.04.01
ARGE GENE .....	DEACETYLASE .....	ARGININE BIOSYNTHESIS .....	S-P123
ARGININE BIOSYNTHESIS .....	ARGE GENE .....	DEACETYLASE .....	S-P123
AROMATICITY .....	REACTION REGIOSELECTIVITY .....	PYRROLE .....	T-P175
AROMATICITY .....	SMALL-MOLECULE .....	LOW-TEMPERATURE .....	T-P167
ARSENIC VANADATE .....	OPEN-FRAMEWORK .....	HYDROTHERMAL SYNTHESIS .....	T-P145
AS-TE GLASSES .....	NEUTRON AND X-RAY DIFFR .....	CHEMICAL DISORDER .....	M-P104
ASPARTIC ENDOPROTEASE .....	AUTOPROTEOLYSIS .....		T-P068
ASPARTIC PROTEASE .....	ANTIBODY .....	ALLERGEN .....	S-P193
ASSEMBLY .....	COORDINATION POLYMER .....		T-P107
ASSEMBLY .....	SELENIUM SAD .....	DEBLOCKING AMINOPEPTIDASE .....	S-P051
ASSMBLY .....	ELECTRON CRYOMICROSCOPY .....	MACROMOLECULE .....	AW.01.05
ATHEROSCLEROSIS .....	HIGH DENSITY LIPOPROTEINS .....	HELICAL STRUCTURE .....	S-P129
ATP SULFURYLASE .....	APS KINASE .....	CHEMOLITHOTROPHIC .....	M-P182
ATPASE .....	HEXAMER .....	SECRETION .....	M-P216
ATPASE .....	SECA .....	PROTEIN TRANSLOCATION .....	S-P211
AUTOMATED DATA COLLECTION .....	MAIL-IN DATA COLLECTION .....	SPRING-8 .....	13.07.07
AUTOMATED MODEL BUILDING .....	SOFTWARE .....	MACROMOLECULAR CRYSTALLOGRAPHY .....	T-P097
AUTOMATED MODEL BUILDING .....	STRUCTURE DETERMINATION .....	MULTIPLE CONFORMERS .....	01.02.02
AUTOMATED PHASING .....	HIGH THROUGHPUT .....	PARALLEL COMPUTING .....	01.02.03
AUTOMATED REFINEMENT .....	LAFIRE .....	HIGH-THROUGHPUT .....	01.02.04
AUTOMATED STRUCTURE DETERMIN .....	AUTOMATION .....	SOFTWARE PIPELINE .....	T-P093
AUTOMATIC MODEL BUILDING .....			01.02.05
AUTOMATIC STRUCTURE SOLUTION .....	BENCHTOP DIFFRACTOMETER .....		T-P173
AUTOMATION .....	CRYSTAL IMAGING .....		M-P018
AUTOMATION .....	CRYSTALLISATION .....	SCREENING M- .....	P082
AUTOMATION .....	CRYSTALLIZATION .....	ROBOT .....	M-P072
AUTOMATION .....	CRYSTALLIZATION .....	SOFTWARE .....	M-P022
AUTOMATION .....	DATA COLLECTION STRATEGY .....	CRYSTAL RANKING .....	T-P095
AUTOMATION .....	HIGH THROUGHPUT .....	REMOTE ACCESS .....	13.07.04
AUTOMATION .....	IMAGING ROBOT .....	PROTEIN CRYSTALLOGRAPHY .....	M-P058
AUTOMATION .....	IN VITRO .....	PROTEIN EXPRESSION .....	M-P084
AUTOMATION .....	MOLECULAR REPLACEMENT .....		T-P087
AUTOMATION .....	PYTHON .....	FRAGMENT SCREENING .....	M-P024
AUTOMATION .....	RE-CENTERING .....	OFFLINE DATA COLLECTION .....	T-P176
AUTOMATION .....	REMOTE ACCESS .....	SYNCHROTRON .....	13.07.09
AUTOMATION .....	SGX-CAT .....	BEAMLINE .....	T-P174

# Keyword Index

AUTOMATION.....	SOFTWARE PIPELINE.....	AUTOMATED STRUCTURE DETERMINATION.....	T-P093
AUTOMATION.....	STRUCTURAL GENOMICS.....	HIGH THROUGHPUT.....	M-P062
AUTOMATION.....	SYNCHROTRON.....	PROTEIN CRYSTALLOGRAPHY.....	13.10.02
AUTOMATION.....	SYNCHROTRON FACILITY.....	MACROMOLECULAR CRYSTALLOGRAPHY.....	T-P037
AUTOMATION PROTEIN CRYST SITTING DROP.....			M-P012
AUTOMATION TECHNIQUES.....	X-RAY CRYSTALLOGRAPHY.....	BEALMINE.....	T-P043
AUTOMOUNTER.....	MARCOMOLECULAR CRYSTALLOGRAPHY.....	SCREENING.....	T-P027
AUTOMOUNTER, CRYOGENIC.....	SYNCHROTRON RADIATION.....	REMOTE DATA COLLECTION.....	13.07.06
AUTOPROCESSING.....	N-O ACYL SHIFT.....	AUTOPROTEOLYSIS.....	M-P206
AUTOPROTEOLYSIS.....	ASPARTIC ENDOPROTEASE.....		T-P068
AUTOPROTEOLYSIS.....	AUTOPROCESSING.....	N-O ACYL SHIFT.....	M-P206
AUTOPROTEOLYSIS.....	PRECURSOR ACTIVATION.....	INTERMEDIATE STRUCTURE.....	13.15.07
AXIAL METHIONINE.....	COPPER NITRITE REDUCTASE.....	TYPE-1 COPPER.....	M-P204
AZOREDUCTASE.....	FMN.....	CRYSTAL.....	M-P210
B. SUBTILIS.....	NRDI PROTEIN.....	CRYSTAL STRUCTURE.....	M-P068
B4C.....	XRD.....	RAMAN SPECTROSCOPY.....	05.01.04
BA3.....	NANODISC.....	MEMBRANE PROTEIN.....	S-P089
BACE.....	BETA SECRETASE.....	ALZHEIMER'S.....	M-P038
BACILLUS ANTHRACIS.....	"TIM, CBS".....	IMP DEHYDROGENASE.....	M-P202
BACTERIA.....	CYTOKINESIS.....	DYNAMIN.....	T-P150
BACTERIAL PATHOGENESIS.....	PROTEIN INHIBITOR.....	PROTEIN-PROTEIN INTERACTIONS.....	T-P124
BACTERIAL PATHOGENESIS.....	TWO-PARTNER SECRETION.....	OUTER MEMBRANE CRYSTALLIZATION.....	S-P111
BACTERIAL TOXINS.....	ADP-RIBOSYLATION.....	EUKARYOTIC ELONGATION FACTOR 2.....	01.06.07
BACTERIOPHAGE LAMBDA.....			S-P097
BACTERIOPHAGE T4 RNASE H.....	5' TO 3' EXONUCLEASE.....	PROTEIN:DNA COMPLEX.....	M-P178
BAD.....	BCL-XL.....	APOPTOSIS.....	T-P134
BAR AND PH DOMAIN.....	APPL1.....	RAB5 EFFECTOR.....	T-P148
BARREL.....	PROLINE DEHYDROGENASE.....	REACTIVE OXYGEN SPECIES.....	01.01.04
BCL-XL.....	APOPTOSIS.....	BAD.....	T-P134
BEALMINE.....	AUTOMATION TECHNIQUES.....	X-RAY CRYSTALLOGRAPHY.....	T-P043
BEAM HEATING.....	CRYOCOOLING.....	THERMAL IMAGING.....	11.01.01
BEAM LINE.....	SYNCHROTRON RADIATION.....	MICROCRYSTALS.....	13.15.04
BEAMLINE.....	APS.....	SYNCHROTRON.....	T-P045
BEAMLINE.....	AUTOMATION.....	SGX-CAT.....	T-P174
BEAMLINE.....	MACROMOLECULAR.....	SYNCHROTRON.....	13.10.01
BEAMLINE.....	PROTEIN CRYSTALLOGRAPHY.....	SAXS.....	T-P055
BEAMLINE AUTOMATION.....	SYNCHROTRON RADIATION.....		T-P051
BEAMLINE.....	SYNCHROTRON RADIATION.....	UNDULATOR.....	T-P025
BENCHTOP DIFFRACTOMETER.....	AUTOMATIC STRUCTURE SOLUTION.....		T-P173
BENZYLIDENEANILINE.....	PHENYLHYDRAZONE.....	ISOSTRUCTURAL.....	T-P185
BETA SECRETASE.....	ALZHEIMER'S.....	BACE.....	M-P038
BETA-LACTAM.....	ANTIBIOTIC RESISTANCE.....	STAPHYLOCOCCUS AUREUS.....	M-P152
BETA-LACTOGLOBULIN.....	NEUTRON PROTEIN CR.....	A LARGE SINGLE CRYSTAL.....	M-P006
BICARBONATE.....	CARBONIC ANHYDRASE.....	ZINC ENZYME.....	M-P122
BICELLE.....	LIPID PHASE.....		T-P005
BILAYER MEMBRANE.....	VESICLE FORMATION.....	SAXS.....	T-P003
BINDING.....	STABILITY.....		T-P017
BIO-MEMBRANES.....	NEUTRON REFLECTOMETRY.....	GRAZING INCIDENCE X-RAY DIFF.....	AW.02.06
BIOENERGETICS.....	RHODOBACTER SPHAEROIDES.....	MEMBRANE PROTEIN.....	01.04.10
BIOINFORMATICS.....	FINGERPRINT.....	SHORT CHAIN OXIDOREDUCTASE.....	S-P117
BIOLOGICAL CRYSTALLOGRAPHY.....	NEUTON TOF DIFFRACTOMETER.....	SIMULATION OF TOF DIFFRACTION DATA.....	M-P002
BIOLOGICAL LABS.....	SCIENTIFIC LAB MANAGEMENT.....	COST ANALYSIS.....	S-P035
BIOLOGICAL MACROMOLECULE.....	PROTEIN CRYSTALLOGRAPHY.....	STRUCTURAL BIOLOGY.....	M-P036
BIOLOGICAL MACROMOLECULES.....	HYDROGEN BONDING.....	COLLAGEN.....	AW.01.04
BIOMACROMOLECULAR CRYSTALLIZ.....	OPTIMIZATION.....	CRYSTAL GROWTH APPARATUS DESIGN.....	T-P022
BIOPARTICLE.....	BLOCK COPOLYMER.....	GISAXS.....	WK.03.02
BIOSYNTHESIS.....	CONFORMATIONAL.....	HEME.....	01.01.02
BIOSYNTHESIS.....	MAGNETITE.....	NANOPARTICLE.....	M-P088
BIOTERRORISM.....	SMALLPOX.....	DRUG DESIGN.....	T-P098
BIOTINALATION.....	CRYSTAL STRUCTURES.....	LIGAND BINDING.....	T-P066
BISUBSTRATE INHIBITOR.....	MAP2K.....	PHOSPHORYLATION KINETICS.....	S-P221
BLOCK COPOLYMER.....	GISAXS.....	BIOPARTICLE.....	WK.03.02
BLOCK COPOLYMER NANOSTRUCTU.....	COPOLYMER MICRODOMAINS.....	ION INFLUENCE.....	AW.02.02
BLOCK COPOLYMERS.....	POLYMER NANOCOMPOSITES.....	PHASE BEHAVIOR.....	09.03.05

# Keyword Index

BLOCKING GROUPS .....	CONFORMATION .....	ANDROGRAPHOLIDE .....	10.02.01
BLOOD GROUPS .....	H-ANTIGENS .....	GLYCOSYLTRANSFERASE .....	S-P013
BONE RESORPTION .....	INTEGRIN .....	PROTEIN KINASE .....	M-P228
BOWL-SHAPED POLYARENES .....	DISORDER .....	X-RAY CRYSTALLOGRAPHY .....	13.02.04
BRCT REPEAT .....	PHOSPHOPEPTIDE RECOGNITION .....	PROTEIN-PROTEIN INTERACTION .....	S-P205
BUERGER AWARD .....	MMCIF .....		AW.01.02
BUILDING BLOCK .....	H-BONDING .....	COPPER (II) .....	T-P155
BULK METALLIC GLASS .....	PDF .....	INTERNAL STRAIN .....	13.03.04
C2A .....	SYNAPTOTAGMIN .....	COPPER BINDING .....	M-P154
C3 .....	IMMUNITY .....	COMPLEMENT .....	01.05.03
CALCINEURIN .....	MOLECULAR RECOGNITION .....	CALMODULIN .....	01.07.06
CALCIUM -BOUND STRUCTURE .....	METASTASIS .....	S100A4 .....	T-P084
CALCIUM ACTIVATION .....	PEP CK .....	TRYPSIN .....	T-P080
CALCIUM BINDING .....	COLLAGENASE .....		M-P136
CALCIUM PUMP .....	MEMBRANE PROTEIN .....	P-TYPE ATPASE .....	01.05.05
CALIX[4]RESORCINARENE .....			T-P131
CALMODULIN .....	CALCINEURIN .....	MOLECULAR RECOGNITION .....	01.07.06
CANADIAN LIGHT SOURCE .....	SMALL ANGLE SCATTERING .....	PROTEIN STRUCTURE .....	13.10.07
CANCER .....	DNA REPAIR .....	AGING .....	M-P218
CANCER .....	INHIBITORS .....	GLYCOSYLATION .....	S-P091
CAPILLARIES .....	TEMPERATURE .....	DIFFRACTION .....	S-P053
CAPILLARY OPTICS .....	MICROBEAM .....	MIROCRYSTALLOGRAPHY .....	T-P014
CARBON DIOXIDE .....	PCK .....	E. COLI .....	T-P046
CARBON NANOTUBES .....	SMALL-ANGLE SCATTERING .....	NANOCOMPOSITES .....	T-P001
CARBON REPELLER .....	RELATIVISTIC REHYBRIDIZATION .....	DIAMOND NUCLEATION .....	M-P096
CARBONIC ANHYDRASE .....	PROTON TRANSFER .....	SOLVENT NETWORK .....	AW.03.02
CARBONIC ANHYDRASE .....	SULFONAMIDE .....		S-P007
CARBONIC ANHYDRASE .....	ZINC ENZYME .....	BICARBONATE .....	M-P122
CARBONYL-ETHER INTERACTION .....	SALACIA CHINENSIS LINN .....	SUPRAMOLECULAR STRUCTURE .....	10.02.08
CARBOXYLESTERASE .....	ORGANOPHOPHATES .....	NERVE AGENTS .....	M-P224
CARBOYLATES .....	SILVER COMPLEXES .....	COORDINATION CHEMISTRY .....	T-P169
CARNITNE ACYLTRANSFERASE .....			S-P153
CATALYSIS .....	ACYLPHOSPHATASE .....	STABILITY .....	S-P175
CATALYSTS .....	FERROELCTRICS .....	DIFFRACTION .....	13.03.06
CATALYTIC ANTIBODY .....	COCAINE ABUSE .....	REACTION PATHWAY .....	S-P079
CATALYTIC MECHANISM .....	SAM SYNTHETASE .....	S-ADENOSYLMETHIONINE SYNTHETASE .....	S-P173
CAVITAND LIGANDS .....	COORDINATION POLYMER .....	METALLO-SUPRAMOLECULAR ASSEMBLY .....	10.03.09
CCD .....	X-RAY PHOTON CORRELATION SP .....	DETECTOR .....	T-P158
CCD-SYSTEM .....	SOFTWARE .....	HIGH-PRESSURE .....	05.01.08
CDC42 .....	SIGNAL TRANSDUCTION .....	GTPASE .....	S-P085
CDSE/ZNS .....	NANO PARTICLES .....	PAIR DISTRIBUTION FUNCTION .....	13.13.03
CELL SURFACE RETENTATION .....	SURFACE PLASMON RESONANCE .....	HEPARAN SULFATE .....	T-P019
CELL TRAFFICKING .....	ADAPTOR COMPLEXES .....		M-P144
CELL WALL LOOSENING .....	PLANT PROTEIN .....	EXPANSIN .....	T-P152
CELL-FREE EXPRESSION SYSTEM .....	PROTEIN SYNTHESIS .....	CRYSTALLOGRAPHY & NMR .....	T-P024
CELLULAR RETINOIC ACID BINDING P .....	INTRACELLULAR LIPID BINDING .....	RETINOIC ACID .....	S-P165
CENTROSYMMETRIC .....	SMALL MOLECULE .....	PHASING .....	M-P172
CH .....	PROTEIN FOLDING .....		M-P052
CHAIN-LENGTH SELECTIVITY .....	FATTY ACID SYNTHASE .....	THIOESTERASE .....	S-P069
CHALCOGENIDE .....	THERMOELECTRIC MATERIALS .....	IN2SN4BI6SE16 .....	M-P102
CHALCOGENIDE TETRAHEDRAL CLUST. .....	SUPERLATTICES .....	HYBRID MATERIALS .....	13.12.04
CHAPERONE .....	TRANSPORT .....	TELOMERASE .....	S-P103
CHARGE DENSITY DISTRIBUTION .....	PEROVSKITE-TYPE HYDRIDES .....	MEM/RIETVELD ANALYSIS .....	13.01.06
CHARGE-DENSITY .....	ELECTROSTATIC-POTENTIAL .....	X-RAY-DIFFRACTION .....	T-P171
CHARGE-DENSITY .....	HIGH-PRESSURE-STRUCTURE .....	TOPOLOGICAL-ANALYSIS .....	10.01.06
CHEMICAL DISORDER .....	AS-TE GLASSES .....	NEUTRON AND X-RAY DIFFRACTION .....	M-P104
CHEMICAL REACTION .....	SINGLE CRYSTAL .....	CRYSTAL STRUCTURE .....	13.14.05
CHEMOLITHOTROPHIC .....	ATP SULFURYLASE .....	APS KINASE .....	M-P182
CHIMERIC PROTEIN .....	CRY PROTEIN .....	INSECTICIDAL PROTEIN .....	M-P042
CHIP .....	U-BOX LIGASE .....	SYMMETRIC HOMODIMER .....	T-P040
CHOLESTERYL ESTER .....	ENOLASE .....	INHIBITION .....	S-P101
CHROMIUM .....	SAD .....	PHASING .....	S-P199
CHROMIUM RADIATION .....	IN-HOUSE PHASING .....	DUAL-WAVELENGTH .....	T-P012
CIF .....	PUBLICATION .....	MANUSCRIPT .....	10.01.08

# Keyword Index

CIF.....	VALIDATION.....	DICTIONARY.....	S-P083
CLAMP LOADING.....	TRANSLESION SYNTHESIS.....	POLYMERASE.....	S-P189
CLASS II FUMARASE SUPERFAMILY.....	ADENYLOSUCCINATE LYASE.....	ENZYMATIC MECHANISM.....	AW.03.04
CLATHRATE.....	HYDRATE.....	NATURAL.....	10.02.05
CLOSED-SHELL INTERACTIONS.....	SILVER(I).....	N-DONOR LIGANDS.....	10.03.13
CLUSTERS.....	METALS.....		M-P176
CMP.....	TWO ROSSMANN DOMAINS.....	SIALLYLTRANSFERASE.....	S-P067
CNMS.....	NANOSCIENCE.....	NANOPHASE MATERIALS SCIENCES.....	13.09.05
CO-CRYSTALS.....	HYDROGEN BOND.....	GRAPH SET.....	10.03.01
CO-CRYSTALS.....	HYDROGEN BONDING.....	PHARMACEUTICAL.....	10.03.05
CO-CRYSTALS.....	MOLECULAR RECOGNITION.....	HYDROGEN BONDS.....	10.03.07
COA-BINDING.....	P. FURIOSUS.....	STRUCTURAL GENOMICS.....	S-P185
COBRA CARDIOTOXIN.....	GLYCOSPHINGOLIPID.....	MEMBRANE INSERTION.....	13.15.06
COCAINE ABUSE.....	REACTION PATHWAY.....	CATALYTIC ANTIBODY.....	S-P079
COCRYSTAL.....	SUPRAMOLECULAR STRUCTURE.....	SUBSTRUCTURES.....	T-P139
COCRYSTALLIZATION.....	X-RAY CRYSTALLOGRAPHY.....	DITOPIC LIGANDS.....	T-P135
COCRYSTALS.....	CRYSTAL PACKING TENDENCIES.....	SUPRAMOLECULAR CHEMISTRY.....	10.03.06
COENZYME SPECIFICITY.....	FNR.....	ENZYME.....	S-P181
COFE HOMOLOG.....	HOMOLOG OF F420-0:γ-GLUTAMYL.....	NOVEL FOLD.....	T-P100
COHERENCE.....	ERL.....	SYNCHROTRON SOURCE.....	T-P029
COHERENT DIFFRACTION.....	NANOPARTICLE.....	PHASE RETRIEVAL.....	13.11.08
COHERENT DIFFRACTION IMAGING.....	X-RAY MICROSCOPY.....		13.0804
COILED COIL.....	ADHESION.....		T-P073
COILED-COIL.....	NEURONAL MIGRATION.....	PROTEIN STRUCTURE.....	T-P215
COLICIN.....	H-N-N MOTIF.....		T-P060
COLLABORATION.....	INSTRUMENTATION.....	INFORMATICS.....	13.07.02
COLLAGEN.....	BIOLOGICAL MACROMOLECULES.....	HYDROGEN BONDING.....	AW.01.04
COLLAGENASE.....	CALCIUM BINDING.....		M-P136
COLLECTIVE MEMBRANE DYNAMICS.....	DISPERSION RELATIONS.....	INELASTIC NEUTRON SCATTERING.....	09.04.02
COLLOIDS.....	SMALL ANGLE X-RAY SCATTERING.....	PROTEINS.....	09.02.05
COLOSSAL MAGNETO RESISTANCE.....	SYNTHORIZING MULTIMETALLIC P.....	CORE-SHELL, NANOPARTICLE.....	M-P094
COMPLEMENT.....	C3.....	IMMUNITY.....	01.05.03
COMPLEX.....	RAP.....	LDLR.....	T-P056
COMPLEX.....	UBIQUITINATION.....	DEUBIQUITINATION.....	T-P026
COMPLEX STRUCTURE.....	SUPERANTIGEN.....	MHC CLASS II.....	M-P128
CONFORMATION.....	ANDROGRAPHOLIDE.....	BLOCKING GROUPS.....	10.02.01
CONFORMATION CHANGE.....		ADENYLATE FORMING ENZYMES.....	S-P099
CONFORMATIONAL.....	HEME.....	BIOSYNTHESIS.....	01.01.02
CONFORMATIONAL CHANGE.....	MG++ATP.....	MOLECULAR DYNAMICS.....	T-P099
CONTROL OF MOTION SWITCH.....	ELECTRON TRANSFER.....	MEMBRANE PROTEIN.....	T-P191
COORDINATION.....	SELF-ASSEMBLY.....	CRYSTAL ENGINEERING.....	10.03.12
COORDINATION CHEMISTRY.....	CARBOYLATES.....	SILVER COMPLEXES.....	T-P169
COORDINATION CHEMISTRY.....	SUPRAMOLECULAR ASSEMBLIES.....	CRYSTAL ENGINEERING.....	T-P133
COORDINATION COMPLEX.....	TOTAL SCATTERING.....		13.05.04
COORDINATION NETWORK.....	ORGANOMETALLOLIGAND.....	QUINONE.....	13.12.03
COORDINATION OF DIVALENT METAL.....	PEPCK.....	A. SUCCINICIPRODUCENS.....	T-P038
COORDINATION POLYMER.....	ASSEMBLY.....		T-P107
COORDINATION POLYMER.....	LANTHANIDE.....	ACTINIDE.....	13.12.01
COORDINATION POLYMER.....	METALLO-SUPRAMOLECULAR ASS.....	CAVITAND LIGANDS.....	10.03.09
COORDINATION POLYMERS.....			13.12.06
COORDINATION POLYMERS.....	POROUS CRYSTALS.....	DYNAMIC STRUCTURES.....	10.03.08
COPOLYMER MICRODOMAINS.....	ION INFLUENCE.....	BLOCK COPOLYMER NANOSTRUCTURES.....	AW.02.02
COPPER.....	2-(DIMETHYLAMINO)ETHANOL.....	HETEROTRIMETALLIC.....	T-P123
COPPER.....	ETHYLENEDIAMINE.....	POLYMER.....	T-P119
COPPER.....	HETEROMETALLIC COMPLEXES.....	REINECKE ANION.....	T-P125
COPPER.....	MEMBRANE PROTEIN.....	METALLOENZYME.....	01.04.06
COPPER.....	TUTTON SALT.....	ESEEM.....	T-P179
COPPER (II).....	BUILDING BLOCK.....	H-BONDING.....	T-P155
COPPER BINDING.....	C2A.....	SYNAPTOTAGMIN.....	M-P154
COPPER ENZYMES.....	OXYGEN.....	ACTIVATION.....	S-P077
COPPER NITRITE REDUCTASE.....	TYPE-1 COPPER.....	AXIAL METHIONINE.....	M-P204
CORE-SHELL, NANOPARTICLE.....	COLOSSAL MAGNETO RESISTANCE.....	SYNTHORIZING MULTIMETALLIC PERVSKITE.....	M-P094
CORE FACILITY.....	UNDERGRADUATE.....	REMOTE ACCESS.....	S-P015
CORRECTION.....	HEAVY METALS.....	ABSORPTION.....	M-P174

# Keyword Index

COST ANALYSIS.....	BIOLOGICAL LABS .....	SCIENTIFIC LAB MANAGEMENT .....	S-P035
COUNTER-DIFFUSION .....	GEL-TUBE.....	MICROGRAVITY.....	S-P209
CREEP DAMAGE .....	TOMOGRAPHY .....	SYNCHROTRON X-RAY .....	13.09.06
CROSS-LINKED HEME.....	HEME P460.....	SULFUR SAD .....	T-P048
CRY PROTEIN.....	INSECTICIDAL PROTEIN.....	CHIMERIC PROTEIN .....	M-P042
CRYO CONDITION.....	CRYOPROTECTANT OPTIMIZATION.....	HIGH-THROUGHPUT .....	13.06.06
CRYO-ELECTRON MICROSCOPY.....	ADENO-ASSOCIATED VIRUS.....	GENE THERAPY .....	S-P011
CRYO-ELECTRON MICROSCOPY.....	TRANSCRIPTION.....	MACROMOLECULAR COMPLEXES.....	01.03.03
CRYOCOOLING .....	THERMAL IMAGING.....	BEAM HEATING .....	11.01.01
CRYOPROTECTANT.....	CRYSTALLIZATION .....	OPTIMIZATION .....	S-P061
CRYOPROTECTANT OPTIMIZATION.....	HIGH-THROUGHPUT .....	CRYO CONDITION.....	13.06.06
CRYOPROTECTION.....	PHASING.....	HIGH PRESSURE CRYOCOOLING.....	M-P130
CRYSTAL.....	AZOREDUCTASE.....	FMN .....	M-P210
CRYSTAL.....	STRUCTURE .....	RIBOSOME .....	M-P146
CRYSTAL ENGINEERING .....	COORDINATION .....	SELF-ASSEMBLY.....	10.03.12
CRYSTAL ENGINEERING .....	COORDINATION CHEMISTRY .....	SUPRAMOLECULAR ASSEMBLIES.....	T-P133
CRYSTAL ENGINEERING .....	NON-CENTROSYMMETRIC.....	ORGANIC SOLID STATE .....	10.03.10
CRYSTAL ENGINEERING .....	PHOSPHONIC ACID .....	CRYSTAL STRUCTURE .....	T-P111
CRYSTAL ENGINEERING .....	POLYMORPHISM.....	REACTIVITY.....	10.03.19
CRYSTAL ENGINEERING .....	SEMICONDUCTORS.....	HYDROGEN BONDING .....	10.03.17
CRYSTAL ENGINEERING .....	SPACE GROUPS.....	HYDROGEN BONDS .....	10.03.03
CRYSTAL GROWTH .....	METAL-CONTAINING ARCHITECTUR.....	DITOPIC BUILDING BLOCKS.....	T-P143
CRYSTAL GROWTH APPARATUS DESIGN.....	BIOMACROMOLECULAR CRYSTAL.....	OPTIMIZATION .....	T-P022
CRYSTAL HARVESTING .....	ROBOTIC CRYSTAL HARVESTING .....	CRYSTAL MOUNTING.....	13.06.07
CRYSTAL IMAGING .....	AUTOMATION.....		M-P018
CRYSTAL MANIPULATION.....	PROTEIN CRYSTALLOGRAPHY.....	SMALL MOLECULE CRYSTALLOGRAPHY.....	S-P215
CRYSTAL MOUNTING.....	CRYSTAL HARVESTING .....	ROBOTIC CRYSTAL HARVESTING .....	13.06.07
CRYSTAL PACKING.....	POLYMORPHISM.....	MODULATED SUPERSTRUCTURES .....	10.01.02
CRYSTAL PACKING TENDENCIES .....	SUPRAMOLECULAR CHEMISTRY .....	COCRYSTALS .....	10.03.06
CRYSTAL RANKING.....	AUTOMATION.....	DATA COLLECTION STRATEGY .....	T-P095
CRYSTAL STRUCTURE .....	B. SUBTILIS.....	NRDI PROTEIN.....	M-P068
CRYSTAL STRUCTURE .....	CHEMICAL REACTION .....	SINGLE CRYSTAL.....	13.14.05
CRYSTAL STRUCTURE .....	CRYSTAL ENGINEERING .....	PHOSPHONIC ACID.....	T-P111
CRYSTAL STRUCTURE .....	DEHALOGENASE.....	INTERMEDIATE.....	S-P139
CRYSTAL STRUCTURE .....	DISORDER .....	OD STRUCTURE.....	13.02.05
CRYSTAL STRUCTURE .....	LIPID.....	CYTOCHROME C OXIDASE.....	01.04.09
CRYSTAL STRUCTURE .....	PENICILLIN BINDING PROTEIN.....	ANTIBIOTICS .....	S-P147
CRYSTAL STRUCTURE .....	PROTEIN KINASE C.....	ANESTHETICS .....	T-P028
CRYSTAL STRUCTURE .....	REDUCTASE.....	NADP-DEPENDENT.....	S-P137
CRYSTAL STRUCTURE .....	SHIKIMATE DEHYDROGENASE.....		S-P143
CRYSTAL STRUCTURE .....	SPHINGOMYELINASE.....	HEMOLYSIS .....	M-P124
CRYSTAL STRUCTURE PREDICTION.....	HIGH PRESSURE.....	NOVEL STRUCTURES .....	05.01.03
CRYSTAL STRUCTURES.....	LIGAND BINDING.....	BIOTINALATION .....	T-P066
CRYSTAL SYNTHESIS .....	INORGANIC SOLID-STATE CHEMI.....	SUPRAMOLECULAR CRYSTALLOGRAPHY.....	10.03.11
CRYSTALLINE COMPLEX.....	STABILITY .....	DRUG FORM.....	10.03.18
CRYSTALLISATION .....	SCREENING .....	AUTOMATION.....	M-P082
CRYSTALLISATION .....	STRAIN-INDUCED .....	POLY (LACTIC ACID).....	09.03.03
CRYSTALLIZATION.....	HYPERACIDS.....	UNUSUAL STOICHIOMETRY .....	04.01.01
CRYSTALLIZATION.....	MEMBRANE PROTEIN .....	VIRIAL COEFFICIENT.....	T-P199
CRYSTALLIZATION.....	MICROFLUIDIC.....	PARALLEL.....	S-P207
CRYSTALLIZATION.....	OPTIMIZATION .....	CRYOPROTECTANT.....	S-P061
CRYSTALLIZATION.....	OPTIMIZATION .....	MACROMOLECULE.....	13.06.03
CRYSTALLIZATION.....	PLATE.....	SBS.....	S-P217
CRYSTALLIZATION.....	POLYMER .....	SAXS .....	09.03.01
CRYSTALLIZATION.....	PROTEIN .....	DATABASE .....	T-P008
CRYSTALLIZATION.....	PROTEIN .....	LATTICE.....	S-P201
CRYSTALLIZATION.....	ROBOT .....	AUTOMATION.....	M-P072
CRYSTALLIZATION.....	SCREEN DESIGN .....	DATABASE .....	13.06.04
CRYSTALLIZATION.....	SOFTWARE.....	AUTOMATION.....	M-P022
CRYSTALLIZATION.....	SURFACE ENTROPY.....	MUTAGENESIS .....	S-P087
CRYSTALLIZATION.....	TRANSYDROGENASE.....	MEMBRANE PROTEIN .....	01.04.08
CRYSTALLIZATION CONDITON.....	DATABASE .....	PREDICTION.....	M-P132
CRYSTALLIZATION PHASE DIAGRAM.....	NEUTRON DIFFRACTION .....	LARGE SINGLE CRYSTAL.....	M-P004
CRYSTALLIZATION SCREENS.....	OPTIMIZATION .....	MEMBRANE PROTEINS.....	M-P078

# Keyword Index

CRYSTALLOGRAPHIC MODELLING.....	HIGH-PRESSURE STRUCTURES .....	STRUCTURE-PHYSICAL PROPERTIES RELATI.....	05.01.02
CRYSTALLOGRAPHY.....	INSULIN .....	NEUTRON.....	M-P008
CRYSTALLOGRAPHY.....	LIGAND.....		04.01.05
CRYSTALLOGRAPHY.....	SYNCHROTRON .....	MACROMOLECULAR .....	T-P033
CRYSTALLOGRAPHY.....	UNDULATOR .....	X-RAY SOURCE .....	T-P041
CRYSTALLOGRAPHY & NMR.....	CELL-FREE EXPRESSION SYSTEM.....	PROTEIN SYNTHESIS.....	T-P024
CRYSTALS.....	SOLID FORMS .....	6-OH BUSPIRONE.....	13.05.03
CSTF.....	RNA PROCESSING .....		M-P046
CYBERINSTRUMENTATION.....	REMOTE ACCESS.....	STARBURSTT .....	13.07.01
CYBERINSTRUMENTATION.....	TEACHING.....	STARBURSTT .....	SP.01.02
CYCLIC PEPTIDE .....	UROKINASE.....	INHIBITOR .....	S-P071
CYCLODEXTRIN.....	WXR.....	FE-SEM.....	T-P137
CYCLODEXTRINS .....	HYDROGEN BONDING .....	PHOTOSYSTEM II.....	TR.01.06
CYP158A2 .....	FERROUS-DIOXYGEN.....	PROTON TRANSFER .....	S-P169
CYSTIC FIBROSIS .....	PARVOVIRIDAE.....	GENE THERAPY .....	S-P009
CYTOCHROME C OXIDASE.....	CRYSTAL STRUCTURE .....	LIPID.....	01.04.09
CYTOKINESIS .....	DYNAMIN.....	BACTERIA.....	T-P150
D-RIBULOSE 5-PHOSPHATE 3-EPIMERA.....	ENOLASE SUPERFAMILY .....	(BETA/ALPHA) 8-BARREL.....	S-P167
D-XYLOSE ISOMERASE .....	NEUTRON DIFFRACTION .....	TIME-OF-FLIGHT NEUTRONS .....	TR.01.08
DAMAGE DNA.....	XPB .....	HELICASE.....	T-P138
DATA.....	ANALYSIS.....	STATISTICAL.....	13.06.05
DATA ANALYSIS.....	ERROR MODEL.....	RADIATION DAMAGE.....	11.01.06
DATA COLLECTION PIPELINE.....	KAPPA GONIOMETRY .....	MULTI-PASS STRATEGY .....	13.07.05
DATA COLLECTION STRATEGY .....	CRYSTAL RANKING.....	AUTOMATION.....	T-P095
DATA PROCESSING.....	SCALING.....	ABSORPTION CORRECTIONS .....	10.01.05
DATA STANDARD .....	DATA STORAGE.....	SOFTWARE.....	WK.02.01
DATA STORAGE.....	SOFTWARE.....	DATA STANDARD .....	WK.02.01
DATABASE.....	CRYSTALLIZATION .....	PROTEIN .....	T-P008
DATABASE.....	CRYSTALLIZATION .....	SCREEN DESIGN .....	13.06.04
DATABASE.....	PREDICTION.....	CRYSTALLIZATION CONDITIOIN.....	M-P132
DATABASE.....	REMOTE DATA COLLECTION.....	HIGH THROUGHPUT .....	T-P172
DATABASES.....	PROTEIN CRYSTALLOGRAPHY.....	SOFTWARE.....	T-P085
DEACETYLASE .....	ARGININE BIOSYNTHESIS .....	ARGE GENE.....	S-P123
DEBLOCKING AMINOPEPTIDASE.....	ASSEMBLY.....	SELENIUM SAD.....	S-P051
DED.....	FLIP.....	APOPTOSIS.....	M-P212
DEFORMATION .....	IN-SITU .....	POLYETHYLENE.....	09.03.02
DEHALOGENASE.....	INTERMEDIATE.....	CRYSTAL STRUCTURE.....	S-P139
DEMETHYLASE .....	JMJC.....	HISTONE.....	S-P059
DEOXYRIBONUCLEOTIDE.....	RIBONUCLEOTIDE REDUCTASE.....	DNA REPAIR .....	S-P119
DETECTOR.....	CCD.....	X-RAY PHOTON CORRELATION SPECTROSCO.....	T-P158
DETECTOR.....	NEUTRON .....		T-P160
DEUBIQUITINATION.....	COMPLEX.....	UBIQUITINATION .....	T-P026
DHDPS .....	MOSA.....		T-P044
DIAMOND NUCLEATION .....	CARBON REPELLER .....	RELATIVISTIC REHYBRIDIZATION.....	M-P096
DIBLOCK COPOLYMERS .....	GISAXS.....	POLYMER BRUSHES.....	09.01.03
DICER.....	RIBONUCLEASE III.....	DSRNA PROCESSING.....	01.01.03
DICTIONARY.....	CIF.....	VALIDATION.....	S-P083
DIFFICULT STRUCTURE.....	SEMI-AUTOMATIC SOLUTION.....	HKL-2000-PH.....	T-P223
DIFFICULT STRUCTURES .....	TWINNING.....	PSEUDOSYMMETRY .....	01.05.01
DIFFRACTION.....	CAPILLARIES.....	TEMPERATURE .....	S-P053
DIFFRACTION.....	CATALYSTS.....	FERROELCTRICS .....	13.03.06
DIFFRACTION.....	NEUTRON .....	SINGLE CRYSTAL.....	T-P011
DIFFRACTION.....	SYNCHROTRON .....	MATERIALS SCIENCE .....	13.10.09
DIFFRACTION ANALYSIS .....	PLUTONIUM.....		10.01.01
DIFFRACTOMETER.....	REAL-TIME .....	NEUTRON.....	13.09.02
DIFFUSE.....	GRAZING INCIDENCE.....	OFF-SPECULAR .....	AW.02.12
DIFFUSE SCATTERING.....	DISORDER.....		13.02.08
DIFFUSE SCATTERING.....	DISORDER.....	POLYMORPHISM .....	10.03.02
DIFFUSE SCATTERING.....	SAXS.....	LIPOPROTEIN .....	13.08.05
DIHYDROFOLATE REDUCTASE.....	NEUTRON DIFFRACTION .....	ULTRAHIGH RESOLUTION .....	TR.01.09
DIMERIC STRUCTURE.....	PYROCOCCUS HORIKOSHII OT3.....	PEPTIDYL-TRNA HYDROLASE.....	T-P164
DIMERIZATION.....	PROTEIN-PROTEIN INTERACTIONS .....	TRANSCRIPTION FACTOR.....	M-P214
DIOXYGENASE .....	ACID-BASE CATALYSIS .....	OXYGEN ACTIVATION.....	S-P057
DIOXYGENASE.....	ENZYME MECHANISM.....	QUINOLINATE BIOSYNTHESIS.....	T-P078

# Keyword Index

DIPEPTIDYL PEPTIDASE .....	DRUG DESIGN .....	04.01.04
DIPHTHERIA TOXIN .....	ENZYME TRANSLOCATION .....	NEUTRON REFLECTIVITY .....
DIPYRRIN .....	METALLOLIGAND .....	MOF .....
DIRECT METHODS .....	MACROMOLECULAR STRUCTURE .....	NEUTRON DIFFRACTION .....
DIRECT METHODS .....	SHAKE-AND-BAKE .....	SUBSTRUCTURE DETERMINATION .....
DISORDER .....	DIFFUSE SCATTERING .....	13.02.08
DISORDER .....	GEORGE LUCAS .....	TWIN .....
DISORDER .....	OD STRUCTURE .....	CRYSTAL STRUCTURE .....
DISORDER .....	PAIR DISTRIBUTION FUNCTION .....	TOTAL SCATTERING .....
DISORDER .....	PHASE TRANSITION .....	TWINNING .....
DISORDER .....	POLYMORPHISM .....	DIFFUSE SCATTERING .....
DISORDER .....	REFINEMENT .....	SHELXL .....
DISORDER .....	TIME OR SPACE .....	MOSAICS .....
DISORDER .....	TWIN .....	PHASE TRANSITION .....
DISORDER .....	WHOLE-MOLECULE DISORDER .....	IMPURITIES .....
DISORDER .....	X-RAY CRYSTALLOGRAPHY .....	BOWL-SHAPED POLYARENES .....
DISPERSION RELATIONS .....	INELASTIC NEUTRON SCATTERING .....	COLLECTIVE MEMBRANE DYNAMICS .....
DISPLACEMENT PARAMETERS .....	JAHN-TELLER EFFECT .....	PACKING EFFECTS .....
DISTORTION .....	SHORT-RANGE ORDER .....	PHASE TRANSITION .....
DISULFIDE BOND .....	X-RAY IRRADIATION .....	REDUCTIVE UNFOLDING PATHWAY .....
DITOPIC BUILDING BLOCKS .....	CRYSTAL GROWTH .....	METAL-CONTAINING ARCHITECTURES .....
DITOPIC LIGANDS .....	COCRYSTALLIZATION .....	X-RAY CRYSTALLOGRAPHY .....
DNA .....	PDX-1 .....	HOMEODOMAIN .....
DNA .....	PROTEINS .....	X-RAY SCATTERING .....
DNA POLYMERASE BETA .....	MUTAGENESIS .....	T-P072
DNA REPAIR .....	ABC ATPASE .....	S-P001
DNA REPAIR .....	AGING .....	CANCER .....
DNA REPAIR .....	DEOXYRIBONUCLEOTIDE .....	RIBONUCLEOTIDE REDUCTASE .....
DNA REPAIR .....	IRON DIOXYGENASE .....	ALKB .....
DNA REPLICATION RESTART .....	PRIB .....	PRIMOSOME .....
DOCKING .....	ALLOSTERY .....	MAP KINASE .....
DOCKING .....	KINASE .....	LIPINSKY .....
DOCKING .....	SCORING .....	INHIBITOR .....
DOMAIN SWAPPING .....	LECTIN .....	ANTIVIRAL ACTIVITY .....
DROP PINNING .....	HIGH-THROUGHPUT CRYSTALLIZA .....	EVAPORATION RATE .....
DRUG .....	KINASE .....	INHIBITOR .....
DRUG DELIVERY .....	AMYLOIDOSIS .....	13.08.06
DRUG DESIGN .....	BIOTERRORISM .....	SMALLPOX .....
DRUG DESIGN .....	DIPEPTIDYL PEPTIDASE .....	04.01.04
DRUG DESIGN .....	HCV PROTEASE .....	INHIBITORS .....
DRUG DESIGN .....	KINASE .....	ANTIBIOTIC RESISTANCE .....
DRUG DESIGN .....	PROTEAE INHIBITORS .....	WIDE OPEN HIV-I PROTEASE .....
DRUG FORM .....	CRYSTALLINE COMPLEX .....	STABILITY .....
DRUG RESISTANCE .....	HIV .....	MUTATION .....
DRUG-DNA .....	QUADRUPLEX .....	AW.01.03
DSRNA PROCESSING .....	DICER .....	RIBONUCLEASE III .....
DUAL WAVELENGTH ANOMALOUS DIF .....	TREHALOSE 6-PHOSPHATE PHOSP .....	HAD HYDROLASE FAMILY .....
DUAL-WAVELENGTH .....	CHROMIUM RADIATION .....	IN-HOUSE PHASING .....
DYNAMIC STRUCTURES .....	COORDINATION POLYMERS .....	POROUS CRYSTALS .....
DYNAMICS .....	POLYMER NANOCOMPOSITES .....	STRUCTURE .....
DYNAMICS .....	REVERSE MONTE CARLO .....	PAIR DISTRIBUTION FUNCTION .....
DYNAMIN .....	BACTERIA .....	CYTOKINESIS .....
E. COLI .....	CARBON DIOXIDE .....	PCK .....
E1 COMPONENT .....	THIAMIN DIPHOSPHATE .....	PYRUVATE DEHYDROGENASE .....
E2 .....	UBIQUITIN .....	UBC13 .....
EBOLA VIRUS .....	NEUTRALIZING ANTIBODY .....	$\nu\lambda_x$ LIGHT CHAIN .....
EDUCATION .....	MATERIALS SCIENCE .....	M-P110
EDUCATION .....	TRAINING .....	POLICY .....
EDUCATION .....	TUTORIAL .....	SOFTWARE .....
ELASTOMER .....	MUSCLE .....	LIQUID CRYSTAL .....
ELECTRIC FIELD .....	ORIENTATION KINETICS .....	SAXS .....
ELECTRON CRYOMICROSCOPY .....	MACROMOLECULE .....	ASSEMBLY .....
ELECTRON MICROSCOPY .....	VIRUS STRUCTURE .....	13.08.07
ELECTRON TRANSFER .....	FERREDOXIN .....	THIOREDOXIN .....

# Keyword Index

ELECTRON TRANSFER.....	MEMBRANE PROTEIN .....	CONTROL OF MOTION SWITCH.....	T-P191
ELECTRON TRANSFER COMPLEX .....	PLANT ENZYME.....		M-P148
ELECTROSTATIC-POTENTIAL.....	X-RAY-DIFFRACTION.....	CHARGE-DENSITY .....	T-P171
ENDOHEDRAL.....	FULLERENE.....		13.14.06
ENDOHEDRAL.....	NON-IPR .....	FULLERENE.....	M-P164
ENDOSOMAL PROCESS.....	PARVOVIRUS.....	ADENO-ASSOCIATED VIRUS.....	M-P140
ENOLASE.....	INHIBITION .....	CHOLESTERYL ESTER.....	S-P101
ENOLASE SUPERFAMILY.....	(BETA/ALPHA) 8-BARREL.....	D-RIBULOSE 5-PHOSPHATE 3-EPIMERASE .....	S-P167
ENTEROTOXIN .....	AMPICILLIN RESISTANCE.....	PATHOGENICITY ISLAND.....	T-P076
ENVELOPE.....	PHASING.....	SAXS .....	13.08.02
ENZYMATIC MECHANISM.....	CLASS II FUMARASE SUPERFAMILY.....	ADENYLOSUCCINATE LYASE.....	AW.03.04
ENZYMATIC MECHANISM.....	QUASI-LAUE.....	PROTONATION .....	M-P016
ENZYME.....	COENZYME SPECIFICITY .....	FNR.....	S-P181
ENZYME MECHANISM.....	ANTIBIOTIC RESISTANCE .....	ACETYLTRANSFERASE .....	S-P063
ENZYME MECHANISM.....	IMP CYCLOHYDROLASE.....	PURO.....	S-P195
ENZYME MECHANISM.....	QUINOLINATE BIOSYNTHESIS.....	DIOXYGENASE .....	T-P078
ENZYME MECHANISM.....	QUINOLINATE SYNTHASE.....	NAD BIOSYNTHESIS .....	S-P157
ENZYME MECHANISM KINETICS .....	STRUCTURE-FUNCTION RELATION .....	METALLOENZYMES.....	M-P192
ENZYME TRANSLOCATION.....	NEUTRON REFLECTIVITY.....	DIPHThERIA TOXIN.....	AW.02.04
ENZYME-INTERMEDIATE COMPLEX.....	PROCESSIVITY .....	PHOSHOHEXOMUTASE.....	S-P151
ENZYMOLGY.....	HELIUM COOLING .....	SUBATOMIC RESOLUTION .....	S-P223
ENZYMOLGY.....	NEUTRON DIFFRACTION .....	X-RAY SUBATOMIC RESOLUTION .....	TR.01.07
ERL.....	SYNCHROTRON SOURCE.....	COHERENCE .....	T-P029
ERROR MODEL.....	RADIATION DAMAGE.....	DATA ANALYSIS.....	11.01.06
ESCHERICHIA COLI O157:H7.....	IRON ACQUISITION.....	HEME OXYGENASE.....	S-P033
ESEEM .....	COPPER .....	TUTTON SALT.....	T-P179
ETHYLENEDIAMINE.....	POLYMER .....	COPPER .....	T-P119
EUKARYOTIC ELONGATION FACTOR 2 .....	BACTERIAL TOXINS.....	ADP-RIBOSYLATION.....	01.06.07
EUKARYOTIC PATHOGENS.....	PYRIMIDINE BIOSYNTHESIS.....	STRUCTURAL GENOMICS.....	T-P071
EVAPORATION RATE.....	DROP PINNING.....	HIGH-THROUGHPUT CRYSTALLIZATION .....	S-P107
EXCHANGE BIAS.....	POLARIZED NEUTRON REFLECTOMETRY .....		AW.02.08
EXOCYST.....	VESICLE TRAFFICKING.....	SEC15 .....	S-P161
EXOPOLYPHOSPHATASE.....	POLYPHOSPHATE .....	PHOSPHOTRANSFERASE .....	13.14.01
EXOPOLYSACCHARIDE.....	EXPORT .....	PSEUDOMONAS AERUGINOSA.....	S-P093
EXPANSIN.....	CELL WALL LOOSENING .....	PLANT PROTEIN .....	T-P152
EXPERIMENTAL CHARGE DENSITY.....	SINGLE CRYSTAL.....	NEUTRON DIFFRACTION .....	S-P027
EXPLOSIVES.....	HIGH PRESSURE.....	SYNCHROTRON RADIATION .....	T-P157
EXPORT.....	PSEUDOMONAS AERUGINOSA .....	EXOPOLYSACCHARIDE.....	S-P093
EXTENSIVE DISORDER .....	SMALL- MOLECULE.....	LOW TEMPERATURE.....	10.01.03
EXTREME CONDITIONS.....	SYNCHROTRON .....	X-RAY DIFFRACTION.....	13.10.08
FATTY ACID SYNTHASE.....	MULTIFUNCTIONAL ENZYME.....	STRUCTURE .....	01.03.04
FATTY ACID SYNTHASE.....	THIOESTERASE.....	CHAIN-LENGTH SELECTIVITY.....	S-P069
FATTY ACID SYNTHESIS .....	MACROMOLECULAR ASSEMBLY .....	INTERMEDIATE RESOLUTION.....	01.03.05
FE K-EDGE MAD.....	ADENOSINE PHOSPHOSULFATE.....	IRON SULFUR CLUSTER .....	S-P017
FE-SEM .....	CYCLODEXTRIN.....	WXRD .....	T-P137
FERREDOXIN .....	THIOREDOXIN.....	ELECTRON TRANSFER.....	01.01.01
FERRICHROME.....	HETEROCOMPLEX.....	OUTER MEMBRANE TRANSPORTER .....	01.04.04
FERRITIN .....	IRON STORAGE .....	THERMOSTABILITY .....	01.07.01
FERROELCTRICS .....	DIFFRACTION.....	CATALYSTS.....	13.03.06
FERROUS-DIOXYGEN.....	PROTON TRANSFER .....	CYP158A2 .....	S-P169
FICTION.....	POETRY .....	MOVIES.....	T-P015
FINGERPRINT.....	SHORT CHAIN OXIDOREDUCTASE .....	BIOINFORMATICS .....	S-P117
FIRST-PRINCIPLES CALCULATIONS .....	HYDROGEN STORAGE .....	NEUTRON SCATTERING .....	13.01.02
FLAP ENDONUCLEASE-1 .....	NEUTRON DIFFRACTION .....	FLASH-COOLING.....	M-P010
FLASH FREEZING.....	VITRIFICATION.....	PLUNGE COOLING.....	T-P047
FLASH-COOLING.....	FLAP ENDONUCLEASE-1 .....	NEUTRON DIFFRACTION .....	M-P010
FLAVOPROTEIN .....	TRP REPRESSOR.....		T-P116
FLIP.....	APOPTOSIS.....	DED.....	M-P212
FLOCK HOUSE VIRUS.....	VIRUS MATURATION.....	VIRUS ASSEMBLY .....	S-P213
FLUCTUATION X-RAY MICROSCOPY.....	MEDIUM ANGE ORDER.....	NONCRYSTALLINE.....	13.11.06
FMN .....	APOFLAVODOXIN .....	HELICOBACTER PYLORI.....	T-P166
FMN .....	CRYSTAL.....	AZOREDUCTASE .....	M-P210
FNR.....	ENZYME.....	COENZYME SPECIFICITY .....	S-P181
FOCUSING.....	SMALL-ANGLE SCATTERING .....	RESOLUTION .....	S-P025

# Keyword Index

FOLDING.....	LARGE SMALL-MOLECULE .....	SYNTHETIC DBLE-HELIX.....	13.05.01
FORCE FIELD .....	SHAPE .....	LIGAND.....	M-P020
FORKHEAD PROTEIN.....	INTERLEUKIN ENHANCER BINDING.....	WINGED HELIX.....	01.07.03
FRACTIONAL CRYSTALLIZATION.....	WHOLE-MOLECULE DISORDER .....	SOLID-STATE COMPOUND.....	13.02.06
FRAGMENT BASED DRUG DISCOVERY.....	KINASES AND ONCOLOGY .....	STRUCTURE GUIDED DRUG DISCOVERY.....	AW.01.06
FRAGMENT SCREENING .....	AUTOMATION.....	PYTHON.....	M-P024
FREE INTERFACE DIFFUSION .....	HOMOSERINE TRANSUCCINYLAASE.....	METHIONINE BIOSYNTHESIS .....	T-P154
FREE INTERFACE DIFFUSION.....	MICROFLUIDICS.....		T-P168
FULLERENE.....	ENDOHEDRAL.....		13.14.06
FULLERENE.....	ENDOHEDRAL.....	NON-IPR.....	M-P164
FUNCTION ANALYSIS.....	STRUCTURAL GENOMICS.....	PROTEIN SURFACE ANALYSIS .....	S-P219
FUNCTIONAL STUDIES .....	MEMBRANE PROTEIN .....		T-P162
FUNCTIONALIZED CAVITANDS.....	SUPRAMOLECULAR ASSEMBLY .....	HOST-GUEST .....	10.03.16
FUSION PROTEIN.....	X-RAY CRYSTALLOGRAPHY.....	GREEN FLUORESCENT PROTEIN .....	T-P187
GAG .....	HIV .....	PROTEASE.....	S-P197
GANGLIOSIDE.....	GLYCOSPHINGOLIPID.....	RAFT .....	09.04.04
GATING .....	STRUCTURAL.....	ION CHANNEL.....	T-P209
GEL-TUBE .....	MICROGRAVITY.....	COUNTER-DIFFUSION.....	S-P209
GENE SYNTHESIS.....	PROTEIN DESIGN.....	SOFTWARE.....	M-P134
GENE THERAPY .....	CRYO-ELECTRON MICROSCOPY.....	ADENO-ASSOCIATED VIRUS.....	S-P011
GENE THERAPY .....	CYSTIC FIBROSIS.....	PARVOVIRIDAE.....	S-P009
GENE THERAPY.....	PARVOVIRIDAE.....	ADENO-ASSOCIATED VIRUS 5 .....	M-P142
GEORGE LUCAS.....	TWIN .....	DISORDER .....	13.14.03
GISAXS.....	BIOPARTICLE .....	BLOCK COPOLYMER .....	WK.03.02
GISAXS.....	POLYMER BRUSHES.....	DIBLOCK COPOLYMERS .....	09.01.03
GISAXS.....	SIZE-SELECTED CLUSTERS.....	MODEL NANOCATALYSTS.....	09.01.04
GLUTATHIONE S-TRANSFERASE.....	INSECTICIDE RESISTANCE .....	MALARIA VECTOR .....	M-P220
GLYCOLIPID TRANSFER PROTEIN.....	GLYCOSPHINGOLIPIDS .....	STRUCTURE OF INTERMOLECULAR INTERAC .....	T-P094
GLYCOSPHINGOLIPID .....	MEMBRANE INSERTION.....	COBRA CARDIOTOXIN.....	13.15.06
GLYCOSPHINGOLIPID .....	RAFT.....	GANGLIOSIDE.....	09.04.04
GLYCOSPHINGOLIPIDS.....	STRUCTURE OF INTERMOLECULAR.....	GLYCOLIPID TRANSFER PROTEIN.....	T-P094
GLYCOSYLATION.....	CANCER.....	INHIBITORS .....	S-P091
GLYCOSYLTRANSFERASE.....	BLOOD GROUPS.....	H-ANTIGENS .....	S-P013
GLYOXYLASE.....	VICINAL OXYGEN CHELATE.....	STRUCTURAL GENOMICS.....	T-P126
GP120.....	HIV-1.....	NEUTRALIZING ANTIBODY .....	T-P075
GPI ANCHOR.....	RECEPTOR BINDING .....	PORE-FORMING TOXIN.....	M-P126
GRAPH SET .....	CO-CRYSTALS.....	HYDROGEN BOND.....	10.03.01
GRAZING INCIDENCE.....	OFF-SPECULAR.....	DIFFUSE.....	AW.02.12
GRAZING INCIDENCE SCATTERING .....	SPIN ECHO.....		09.01.05
GRAZING INCIDENCE X-RAY DIFFRACT.....	BIO-MEMBRANES .....	NEUTRON REFLECTOMETRY .....	AW.02.06
GREEN FLUORESCENT PROTEIN .....	FUSION PROTEIN.....	X-RAY CRYSTALLOGRAPHY.....	T-P187
GTP-DEPENDENT.....	X-RAY STRUCTURE .....	PCK .....	T-P054
GTPASE.....	CDC42.....	SIGNAL TRANSDUCTION .....	S-P085
H-ANTIGENS .....	GLYCOSYLTRANSFERASE.....	BLOOD GROUPS .....	S-P013
H-BONDING.....	COPPER (II).....	BUILDING BLOCK.....	T-P155
H-N-N MOTIF.....	COLICIN .....		T-P060
HAD HYDROLASE FAMILY .....	DUAL WAVELENGTH ANOMALOUS .....	TREHALOSE 6-PHOSPHATE PHOSPHATASE .....	M-P222
HALOALKANOIC ACID DEHALOGENAS .....	PHOSPHOTRANSFERASE CHEM.....	PROTEIN GLYCOSYLATION.....	T-P032
HCV .....	POLYMERASE.....	INHIBITOR.....	04.01.03
HCV PROTEASE.....	INHIBITORS .....	DRUG DESIGN .....	S-P163
HEAVY METALS .....	ABSORPTION.....	CORRECTION.....	M-P174
HELICAL STRUCTURE.....	ATHEROSCLEROSIS.....	HIGH DENSITY LIPOPROTEINS .....	S-P129
HELICASE.....	DAMAGE DNA .....	XPB.....	T-P138
HELICOBACTER PYLORI .....	FMN .....	APOFLAVODOXIN.....	T-P166
HELICOBACTER PYLORI.....	INORGANIC PYROPHOSPHATASE.....		T-P062
HELICOBACTER PYLORI.....	NEW FOLD.....		S-P133
HELICOBACTER PYLORI.....	TRIOSEPHOSPHATE ISOMERASE.....		S-P135
HELIUM.....	RADIATION DAMAGE.....		11.01.02
HELIUM COOLING .....	SUBATOMIC RESOLUTION.....	ENZYMOLOGY.....	S-P223
HELIX-BUNDLE.....	ADENOSYLCOBALAMIN.....	TUBERCULOSIS .....	M-P198
HEME .....	BIOSYNTHESIS.....	CONFORMATIONAL .....	01.01.02
HEME NITROSYL THIOLATE.....	POOR QUALITY DATA.....	HETEROGENEOUS READTION.....	13.05.02
HEME OXYGENASE.....	ESCHERICHIA COLI O157:H7 .....	IRON ACQUISITION .....	S-P033
HEME P460 .....	SULFUR SAD .....	CROSS-LINKED HEME.....	T-P048

# Keyword Index

HEME SYSTEM .....	SUPRAMOLECULAR STRUCTURE .....	OCTAETHYLPORPHYRIN .....	T-P141
HEMOLYSIS .....	CRYSTAL STRUCTURE .....	SPHINGOMYELINASE .....	M-P124
HEPARAN SULFATE .....	CELL SURFACE RETENTION .....	SURFACE PLASMON RESONANCE .....	T-P019
HETEROCOMPLEX .....	OUTER MEMBRANE TRANSPORTER .....	FERRICHROME .....	01.04.04
HETEROGENEOUS READTION .....	HEME NITROSYL THIOLATE .....	POOR QUALITY DATA .....	13.05.02
HETEROMETALLIC COMPLEXES .....	REINECKE ANION .....	COPPER .....	T-P125
HETEROTRIMETALLIC .....	COPPER .....	2-(DIMETHYLAMINO)ETHANOL .....	T-P123
HEXAMER .....	SECRETION .....	ATPASE .....	M-P216
HEXAMER .....	STRUCTURAL GENOMICS .....	SALMONELLA TYPHIMURIUM .....	T-P110
HI P/LOW T NEUTRON/DIELECTRIC ME .....	PEROVSKITE STRUCTURES .....	PHASE TRANSITIONS & STRUCTURES .....	M-P118
HIGH DENSITY LIPOPROTEINS .....	HELICAL STRUCTURE .....	ATHEROSCLEROSIS .....	S-P129
HIGH ENERGY .....	PHASING .....	RADIATION DAMAGE .....	11.01.05
HIGH ENERGY .....	RADIATION DAMAGE .....	SYNCHROTRON RADIATION .....	11.01.04
HIGH PRESSURE .....	LITHIUM NITRIDE .....	LITHIUM OXIDE .....	05.01.06
HIGH PRESSURE .....	NEUTRON POWDER DIFFRACTION .....	PEROVSKITE .....	M-P116
HIGH PRESSURE .....	NOVEL STRUCTURES .....	CRYSTAL STRUCTURE PREDICTION .....	05.01.03
HIGH PRESSURE .....	SILANE .....	SYNCHROTRON X-RAY DIFFRACTION .....	M-P114
HIGH PRESSURE .....	SYNCHROTRON RADIATION .....	EXPLOSIVES .....	T-P157
HIGH PRESSURE CRYOCOOLING .....	CRYOPROTECTION .....	PHASING .....	M-P130
HIGH QUALITY PROTEIN CRYSTAL .....	SPACE EXPERIMENT .....	MICROGRAVITY CRYSTAL GROWTH .....	T-P006
HIGH SPEED .....	TIME RESOLVED .....	X-RAY DETECTOR .....	T-P156
HIGH THROUGHPUT .....	AUTOMATION .....	STRUCTURAL GENOMICS .....	M-P062
HIGH THROUGHPUT .....	DATABASE .....	REMOTE DATA COLLECTION .....	T-P172
HIGH THROUGHPUT .....	PARALLEL COMPUTING .....	AUTOMATED PHASING .....	01.02.03
HIGH THROUGHPUT .....	REMOTE ACCESS .....	AUTOMATION .....	13.07.04
HIGH THROUGHPUT METHODOLOGIES .....	PROTEOMICS .....	STRUCTURAL GENOMICS .....	13.06.01
HIGH THROUGHPUT METHODS .....	MOLECULAR REPLACEMENT .....	STRUCTURAL GENOMICS .....	M-P064
HIGH-PRESSURE .....	A2M3O12 .....	NTE .....	M-P112
HIGH-PRESSURE .....	SYNCHROTRON .....	RDX .....	05.01.07
HIGH-PRESSURE .....	XENON .....	SILICA .....	05.01.05
HIGH-PRESSURE STRUCTURES .....	STRUCTURE-PHYSICAL PROPERTIE .....	CRYSTALLOGRAPHIC MODELLING .....	05.01.02
HIGH-THROUGHPUT .....	AUTOMATED REFINEMENT .....	LAFIRE .....	01.02.04
HIGH-THROUGHPUT .....	CRYO CONDITION .....	CRYOPROTECTANT OPTIMIZATION .....	13.06.06
HIGH-THROUGHPUT .....	NMR STRUCTURES .....	MOLECULAR REPLACEMENT .....	T-P103
HIGH-THROUGHPUT CRYSTALLIZATION .....	EVAPORATION RATE .....	DROP PINNING .....	S-P107
HIGH-THROUGHPUT SCREENING .....	INHIBITOR DISCOVERY .....	INHIBITOR STRUCTURAL ANALYSIS .....	M-P056
HIGH-PRESSURE .....	CCD-SYSTEM .....	SOFTWARE .....	05.01.08
HIGH-PRESSURE-STRUCTURE .....	TOPOLOGICAL-ANALYSIS .....	CHARGE-DENSITY .....	10.01.06
HISTIDINE .....	ZINC PHOSPHITE .....	METAL ORGANIC FRAMEWORK .....	T-P183
HISTIDINE KINASE .....	STUCTURAL GENOMICS .....	TWO-COMPONENET SIGNALING .....	M-P054
HISTONE .....	DEMETHYLASE .....	JMJC .....	S-P059
HIV .....	MUTATION .....	DRUG RESISTANCE .....	T-P030
HIV .....	PROTEASE .....	GAG .....	S-P197
HIV-1 .....	NEUTRALIZING ANTIBODY .....	GP120 .....	T-P075
HKL-2000-PH .....	DIFFICULT STRUCTURE .....	SEMI-AUTOMATIC SOLUTION .....	T-P223
HOLMIUM PHASING .....	METHIONINE RECYCLING .....	PROTEIN CRYSTALLOGRAPHY .....	S-P145
HOMEODOMAIN .....	DNA .....	PDX-1 .....	T-P118
HOMOLOG OF F420-0:γ-GLUTAMYL LI .....	NOVEL FOLD .....	COFE HOMOLOG .....	T-P100
HOMOSERINE TRANSSUCCINYLAASE .....	METHIONINE BIOSYNTHESIS .....	FREE INTERFACE DIFFUSION .....	T-P154
HOOKWORM .....	VACCINE .....	IMMUNITY .....	T-P057
HOST GEST CHEMISTRY .....	SOLID STATE POLYMERIZATION .....	POLYDIACETYLENES .....	T-P129
HOST-GUEST .....	FUNCTIONALIZED CAVITANDS .....	SUPRAMOLECULAR ASSEMBLY .....	10.03.16
HOST-PATHOGEN INTERACTION .....	PLANT DISEASE RESISTANCE .....	SAD PHASING .....	01.07.05
HOUSE DUST MITE .....	ALLERGY .....	ANTIBODY BINDING .....	T-P077
HTLV PROTEASE .....			S-P073
HTP EXPRESSION, PURIFICATION .....	METHOD DEVELOPMENT .....	STRUCTURE GEMONICS .....	13.06.02
HUMAN DEOXYCYTIDINE KINASE .....	L-NUCLEOSIDE ANALOG .....	3TC .....	S-P065
HYBRID FRAMEWORKS .....	LANTHANIDE CARBOXYLATES .....	ALIPHATICS DICARBOXYLATES BRIDGING .....	T-P181
HYBRID II-VI SEMICONDUCTOR .....	NANOSTRUCTURE .....	QUANTUM CONFINEMENT EFFECT .....	13.12.05
HYBRID MATERIALS .....	CHALCOGENIDE TETRAHEDRAL .....	SUPERLATTICES .....	13.12.04
HYDRATE .....	HYDROPHOBIC .....	MOLECULAR INCLUSION .....	T-P113
HYDRATE .....	NATURAL .....	CLATHRATE .....	10.02.05
HYDROGELS .....	SHEAR-SANS .....	PEO-LAPONITE .....	09.03.06
HYDROGEN .....	POWDER NEUTRON DIFFRACTION .....	SYNCHROTRON POWDER X-RAY DIFF .....	13.01.03

# Keyword Index

HYDROGEN AND HYDRATION.....	NEUTRON PROTEIN CR.....	SPALLATION NEUTRON SOURCE.....	TR.01.03
HYDROGEN BOND.....	GRAPH SET.....	CO-CRYSTALS.....	10.03.01
HYDROGEN BONDING.....	COLLAGEN.....	BIOLOGICAL MACROMOLECULES.....	AW.01.04
HYDROGEN BONDING.....	CRYSTAL ENGINEERING.....	SEMICONDUCTORS.....	10.03.17
HYDROGEN BONDING.....	PHARMACEUTICAL.....	CO-CRYSTALS.....	10.03.05
HYDROGEN BONDING.....	PHOTOSYSTEM II.....	CYCLODEXTRINS.....	TR.01.06
HYDROGEN BONDING.....	SUPRAMOLECULAR CHEMISTRY.....	SELF RECOGNITION.....	T-P117
HYDROGEN BONDS.....	CO-CRYSTALS.....	MOLECULAR RECOGNITION.....	10.03.07
HYDROGEN BONDS.....	CRYSTAL ENGINEERING.....	SPACE GROUPS.....	10.03.03
HYDROGEN STORAGE.....	MICROSTRUCTURE.....	ALANATE.....	13.01.01
HYDROGEN STORAGE.....	NEUTRON SCATTERING.....	FIRST-PRINCIPLES CALCULATIONS.....	13.01.02
HYDROGEN STORAGE MATERIAL.....	NEUTRON SCATTERING.....	POWDER DIFFRACTION.....	13.09.03
HYDROGEN STORAGE MATERIALS.....	IN-SITU SYNCHROTRON DIFF.....	NEUTRON DIFFRACTION.....	13.01.05
HYDROPHOBIC.....	MOLECULAR INCLUSION.....	HYDRATE.....	T-P113
HYDROPHOBIC CORE.....	MUTATIONAL STUDY.....	THYMIDYLATE.....	M-P074
HYDROTHERMAL CRYSTALLIZATION.....	PHARMACEUTICAL.....	NEUTRON DIFFRACTION.....	10.02.06
HYDROTHERMAL SYNTHESIS.....	ARSENIC VANADATE.....	OPEN-FRAMEWORK.....	T-P145
HYDROTHERMAL SYNTHESIS.....	SUPRAMOLECULAR STRUCTURE.....	ORGANIC-INORGANIC HYBRID.....	M-P162
HYPERACIDS.....	UNUSUAL STOICHIOMETRY.....	CRYSTALLIZATION.....	04.01.01
HYPOTHETICAL PROTEIN.....	YAEQ.....	XANTHOMONAS AXONOPODIS PV. CITRI.....	01.07.04
H-BONDING.....	PI-PI INTERACTIONS.....	THIOSEMICABAZONES.....	T-P109
IG-LIKE V- AND C2-SET DOMAINS.....	SIGLEC-5.....	INTERDOMAIN DISULFIDE.....	T-P063
IL-13.....	ANTIBODY.....	RECEPTOR.....	T-P079
IMAGING ROBOT.....	PROTEIN CRYSTALLOGRAPHY.....	AUTOMATION.....	M-P058
IMGCIF.....	NEXUS.....	XML.....	M-P156
IMIDAZOLONEPROPIONASE.....	STRUCTURAL GENOMICS.....	TIM BARREL.....	T-P081
IMMUNE SYSTEM.....	NATURAL KILLER CELLS.....	VIRAL ANTIGEN.....	01.06.08
IMMUNITY.....	COMPLEMENT.....	C3.....	01.05.03
IMMUNITY.....	HOOKWORM.....	VACCINE.....	T-P057
IMP CYCLOHYDROLASE.....	PURO.....	ENZYME MECHANISM.....	S-P195
IMP DEHYDROGENASE.....	BACILLUS ANTHRACIS.....	TIM, CBS.....	M-P202
IMPURITIES.....	DISORDER.....	WHOLE-MOLECULE DISORDER.....	13.02.01
IN VITRO.....	PROTEIN EXPRESSION.....	AUTOMATION.....	M-P084
IN-HOUSE PHASING.....	DUAL-WAVELENGTH.....	CHROMIUM RADIATION.....	T-P012
IN-SITU.....	POLYETHYLENE.....	DEFORMATION.....	09.03.02
IN-SITU.....	TRANSFORMATION.....	TIME RESOLVED.....	13.09.08
IN-SITU SYNCHROTRON DIFFRACTION.....	NEUTRON DIFFRACTION.....	HYDROGEN STORAGE MATERIALS.....	13.01.05
IN-SITU TIME-RESOLVED TEST.....	THERMAL STRESS & TEMPERATUR.....	NEUTRON DIFFRACTION.....	13.09.07
IN2SN4BI6SE16.....	CHALCOGENIDE.....	THERMOELECTRIC MATERIALS.....	M-P102
INDUSTRIAL USE.....	NEW DIFFRACTOMETER IN J-PARC.....	MACROMOLECULAR CRYSTALLOGRAPHY.....	13.15.05
INELASTIC NEUTRON SCATTERING.....	COLLECTIVE MEMBRANE DYNAM.....	DISPERSION RELATIONS.....	09.04.02
INELASTIC SCATTERING.....	MEMBRANE PROTEINS.....	MD SIMULATIONS.....	09.04.05
INFORMATICS.....	COLLABORATION.....	INSTRUMENTATION.....	13.07.02
INFORMATION MANAGEMENT SYSTEM.....	LIMS.....	STRUCTURAL GENOMICS.....	M-P060
INHIBITION.....	CHOLESTERYL ESTER.....	ENOLASE.....	S-P101
INHIBITOR.....	CYCLIC PEPTIDE.....	UROKINASE.....	S-P071
INHIBITOR.....	DOCKING.....	SCORING.....	SP.01.04
INHIBITOR.....	DRUG.....	KINASE.....	04.01.02
INHIBITOR.....	HCV.....	POLYMERASE.....	04.01.03
INHIBITOR.....	PICORNAVIRUS.....	3C.....	T-P010
INHIBITOR BINDING.....	MAP KINASE.....		M-P032
INHIBITOR DISCOVERY.....	INHIBITOR STRUCTURAL ANALYSIS.....	HIGH-THROUGHPUT SCREENING.....	M-P056
INHIBITOR STRUCTURAL ANALYSIS.....	HIGH-THROUGHPUT SCREENING.....	INHIBITOR DISCOVERY.....	M-P056
INHIBITORS.....	DRUG DESIGN.....	HCV PROTEASE.....	S-P163
INHIBITORS.....	GLYCOSYLATION.....	CANCER.....	S-P091
INHIBITORY ACTIVITY.....	LEISHMANIASIS.....		10.02.04
INHIBITORY MECHANISM.....	REACTIVE CENTER LOOP.....	SERPIN.....	M-P200
INNATE IMMUNITY.....	LEUCINE RICH REPEAT.....	TOLL-LIKE RECEPTOR.....	T-P069
INNATE IMMUNITY.....	TOLL-LIKE RECEPTOR.....	LEUCINE RICH REPEAT.....	01.06.02
INORGANIC PYROPHOSPHATASE.....	HELICOBACTER PYLORI.....		T-P062
INORGANIC SOLID-STATE CHEMISTRY.....	SUPRAMOLECULAR CRYSTALLOG.....	CRYSTAL SYNTHESIS.....	10.03.11
INOSITOL.....	PROTEIN FOLDING.....	PHOSPHATASE.....	S-P203
INSECTICIDAL PROTEIN.....	CHIMERIC PROTEIN.....	CRY PROTEIN.....	M-P042
INSECTICIDE RESISTANCE.....	MALARIA VECTOR.....	GLUTATHIONE S-TRANSFERASE.....	M-P220

# Keyword Index

INSTRUMENTATION .....	INFORMATICS .....	COLLABORATION .....	13.07.02
INSTRUMENTATION .....	SMALL ANGLE SCATTERING .....	SANS .....	S-P021
INSULIN .....	NEUTRON .....	CRYSTALLOGRAPHY .....	M-P008
INTEGRAL MEMBRANE PROTEIN .....	PROTEIN MOBILITY .....	REDOX CHEMISTRY .....	T-P205
INTEGRAL MEMBRANE PROTEIN .....	TRANSDUCER .....	PHOTORECEPTOR .....	01.04.07
INTEGRIN .....	PROTEIN KINASE .....	BONE RESORPTION .....	M-P228
INTEGRIN .....	THROMBOCYTOPENIA .....	PLATELET .....	T-P034
INTERDOMAIN DISULFIDE .....	IG-LIKE V- AND C2-SET DOMAINS .....	SIGLEC-5 .....	T-P063
INTERFACE .....	STRUCTURE .....	SCATTERING .....	T-P007
INTERLEUKIN ENHANCER BINDING FA .....	WINGED HELIX .....	FORKHEAD PROTEIN .....	01.07.03
INTERMEDIATE .....	CRYSTAL STRUCTURE .....	DEHALOGENASE .....	S-P139
INTERMEDIATE RESOLUTION .....	FATTY ACID SYNTHESIS .....	MACROMOLECULAR ASSEMBLY .....	01.03.05
INTERMEDIATE STRUCTURE .....	AUTOPROTEOLYSIS .....	PRECURSOR ACTIVATION .....	13.15.07
INTERNAL STRAIN .....	BULK METALLIC GLASS .....	PDF .....	13.03.04
INTRACELLULAR LIPID BINDING PROTE .....	RETINOIC ACID .....	CELLULAR RETINOIC ACID BINDING PROTEIN .....	S-P165
INVERSION .....	NEUTRONS .....	REFLECTION .....	AW.02.10
IODINE DERIVATIVE .....	VAPORIZING IODINE LABELING .....	SAD PHASING .....	S-P109
ION CHANNEL .....	GATING .....	STRUCTURAL .....	T-P209
ION INFLUENCE .....	BLOCK COPOLYMER NANOSTRUCT .....	COPOLYMER MICRODOMAINS .....	AW.02.02
ION-LIPID INTERACTIONS .....	MEMBRANE STRUCTURE .....	VAN DER WAALS FORCES .....	09.04.03
IRON .....	TONB .....	OUTER MEMBRANE .....	T-P207
IRON ACQUISITION .....	HEME OXYGENASE .....	ESCHERICHIA COLI O157:H7 .....	S-P033
IRON DIOXYGENASE .....	ALKB .....	DNA REPAIR .....	01.0106
IRON STORAGE .....	THERMOSTABILITY .....	FERRITIN .....	01.07.01
IRON SULFUR CLUSTER .....	FE K-EDGE MAD .....	ADENOSINE PHOSPHOSULFATE .....	S-P017
ISOASPARTYL PEPTIDASE .....	TASPASE .....	L-ASPARAGINASE .....	01.07.02
ISOSTRUCTURAL .....	BENZYLIDENEANILINE .....	PHENYLHYDRAZONE .....	T-P185
ISOTOPE LABELING .....	MACROMOLECULAR COMPLEX .....	SMALL ANGLE SCATTERING .....	09.02.07
JAHN-TELLER EFFECT .....	PACKING EFFECTS .....	DISPLACEMENT PARAMETERS .....	T-P115
JMJC .....	HISTONE .....	DEMETHYLASE .....	S-P059
KAPPA GONIOMETRY .....	MULTI-PASS STRATEGY .....	DATA COLLECTION PIPELINE .....	13.07.05
KINASE .....	ANTIBIOTIC RESISTANCE .....	DRUG DESIGN .....	13.10.04
KINASE .....	INHIBITOR .....	DRUG .....	04.01.02
KINASE .....	LIPINSKY .....	DOCKING .....	T-P089
KINASE .....	PKC .....	.....	T-P136
KINASE .....	PROTEIN:PROTEIN COMPLEX .....	SPECIFICITY .....	T-P090
KINASE .....	PSI .....	PYROPHOSPHATE .....	T-P146
KINASE .....	PYK2 .....	SCAFFOLD .....	M-P030
KINASE DOMAIN .....	OSR1 .....	STE20P .....	T-P102
KINASES AND ONCOLOGY .....	STRUCTURE GUIDED DRUG DISCO .....	FRAGMENT BASED DRUG DISCOVERY .....	AW.01.06
KINETICS .....	PROTEIN FOLDING .....	VILLIN .....	AW.03.05
L-ASPARAGINASE .....	ISOASPARTYL PEPTIDASE .....	TASPASE .....	01.07.02
L-NUCLEOSIDE ANALOG .....	3TC .....	HUMAN DEOXYCYTIDINE KINASE .....	S-P065
LACCASSE .....	REDOX .....	.....	T-P082
LACTATE DEHYDROGENASE .....	UNDERGRADUATE LABORATORY .....	SYNCHROTRON DATA COLLECTION .....	S-P003
LACTATE DEHYDROGENASE .....	UNDERGRADUATE LABORATORY .....	SYNCHROTRON DATA COLLECTION .....	S-P005
LAFIRE .....	HIGH-THROUGHPUT .....	AUTOMATED REFINEMENT .....	01.02.04
LANTHANIDE .....	ACTINIDE .....	COORDINATION POLYMER .....	13.12.01
LANTHANIDE CARBOXYLATES .....	ALIPHATICS DICARBOXYLATES BRI .....	HYBRID FRAMEWORKS .....	T-P181
LARGE SINGLE CRYSTAL .....	CRYSTALIZATION PHASE DIAGRA .....	NEUTRON DIFFRACTION .....	M-P004
LARGE SMALL-MOLECULE .....	SYNTHETIC DBLE-HELIX .....	FOLDING .....	13.05.01
LASER PROCESSING .....	PULSED UV LASER SOFT ABLATION .....	PROTEIN CRYSTAL .....	S-P179
LATTICE .....	CRYSTALLIZATION .....	PROTEIN .....	S-P201
LAUE .....	NEUTRON .....	SOFTWARE .....	M-P014
LAUE .....	UNDULATOR .....	TIME-RESOLVED .....	T-P049
LDLR .....	COMPLEX .....	RAP .....	T-P056
LECTIN .....	ANTIVIRAL ACTIVITY .....	DOMAIN SWAPPING .....	01.01.09
LEISHMANIASIS .....	INHIBITORY ACTIVITY .....	.....	10.02.04
LEUCINE RICH REPEAT .....	INNATE IMMUNITY .....	TOLL-LIKE RECEPTOR .....	01.06.02
LEUCINE RICH REPEAT .....	TOLL-LIKE RECEPTOR .....	INNATE IMMUNITY .....	T-P069
LIGAND .....	CRYSTALLOGRAPHY .....	.....	04.01.05
LIGAND .....	FORCE FIELD .....	SHAPE .....	M-P020
LIGAND .....	MANGANESE .....	MYOGLOBIN .....	M-P180
LIGAND BINDING .....	BIOTINALATION .....	CRYSTAL STRUCTURES .....	T-P066

# Keyword Index

LIGAND SCREEN .....	PROTEIN CRYSTALLIZATION .....	METABOLITES.....	M-P080
LIGHT HARVESTING COMPLEX 2 .....	MEMBRANE PROTEIN .....	LIPIDIC CUBIC PHASE .....	T-P197
LIMS .....	STRUCTURAL GENOMICS.....	INFORMATION MANAGEMENT SYSTEM .....	M-P060
LIPID.....	CYTOCHROME C OXIDASE .....	CRYSTAL STRUCTURE .....	01.04.09
LIPID BILAYER .....	MEMBRANE PROTEIN .....	NEUTRON REFLECTOMETRY .....	AW.02.05
LIPID MESOPHASE TRANSITIONS.....	PRESSURE JUMP TECHNIQUE.....	SAXS .....	09.04.06
LIPID PHASE.....	BICELLE .....		T-P005
LIPID PHASE TRANSITIONS.....	RHODOBACTER SPHAEROIDES .....	SPONGE PHASE.....	01.04.03
LIPIDIC CUBIC PHASE .....	LIGHT HARVESTING COMPLEX 2 .....	MEMBRANE PROTEIN .....	T-P197
LIPINSKY .....	DOCKING.....	KINASE.....	T-P089
LIPOPROTEIN.....	DIFFUSE SCATTERING.....	SAXS .....	13.08.05
LIQUID CRYSTAL.....	ELASTOMER.....	MUSCLE.....	M-P108
LIQUID INTERFACES.....	NANOPARTICLES.....		09.01.02
LIQUID PHASE.....	RHODOBACTER SPHAEROIDES .....	PROTEIN CRYSTALLIZATION .....	T-P195
LITHIUM NITRIDE .....	LITHIUM OXIDE .....	HIGH PRESSURE .....	05.01.06
LITHIUM OXIDE.....	HIGH PRESSURE.....	LITHIUM NITRIDE.....	05.01.06
LOCAL STRUCTURE.....	NANO-SCALE STRUCTURE.....	PAIR DENSITY FUNCTION.....	13.13.01
LOW TEMPERATURE.....	EXTENSIVE DISORDER .....	SMALL- MOLECULE.....	10.01.03
LOW TEMPERATURE.....	SINGLE CRYSTAL X-RDAY DIFFRAC.....	SYNCHROTRON RADIATION .....	T-P023
LOW-TEMPERATURE .....	AROMATICITY .....	SMALL-MOLECULE.....	T-P167
MACROMOLECULAR.....	CRYSTALLOGRAPHY .....	SYNCHROTRON.....	T-P033
MACROMOLECULAR.....	SYNCHROTRON .....	BEAMLINE .....	13.10.01
MACROMOLECULAR ASSEMBLY .....	INTERMEDIATE RESOLUTION.....	FATTY ACID SYNTHESIS.....	01.03.05
MACROMOLECULAR COMPLEX.....	SMALL ANGLE SCATTERING .....	ISOTOPE LABELING .....	09.02.07
MACROMOLECULAR COMPLEXES.....	CRYO-ELECTRON MICROSCOPY.....	TRANSCRIPTION .....	01.03.03
MACROMOLECULAR CRYSTALLOGRA.....	AUTOMATED MODEL BUILDING.....	SOFTWARE.....	T-P097
MACROMOLECULAR CRYSTALLOGRA.....	AUTOMATION .....	SYNCHROTRON FACILITY .....	T-P037
MACROMOLECULAR CRYSTALLOGRA.....	INDUSTRIAL USE.....	NEW DIFFRACTOMETER IN J-PARC.....	13.15.05
MACROMOLECULAR CRYSTALLOGRA.....	MAD PHASING.....	MICROFOCUS .....	M-P158
MACROMOLECULAR CRYSTALLOGRAPHY.....		ROBOTICS.. REMOTE DATA COLLECTION.....	T-P170
MACROMOLECULAR STRUCTURE.....	NEUTRON DIFFRACTION .....	DIRECT METHODS .....	TR.01.11
MACROMOLECULE.....	ASSMBLY.....	ELECTRON CRYOMICROSCOPY .....	AW.01.05
MACROMOLECULE.....	CRYSTALLIZATION .....	OPTIMIZATION .....	13.06.03
MACROMOLECULE.....	STRUCTURE REFINEMENT .....	PHENIX.....	01.02.06
MACROMOLECULES.....	PHASING.....	ABSORPTION CORRECTION.....	T-P016
MACROMOLECULES.....	USER FACILITIES .....	SYNCHROTRON RADIATION .....	S-P191
MAD .....	SAD.....	STRATEGY.....	T-P042
MAD PHASING.....	MICROFOCUS.....	MACROMOLECULAR CRYSTALLOGRAPHY.....	M-P158
MAD PHASING.....	STRUCTURAL GENOMICS.....	THERMOTOGA MARITIMA .....	T-P083
MAGNETIC ORDER IN CUFeO2.....	STRUCTURE TRANSITION.....	NEUTRON & X-RAY DIFFRACTION.....	M-P100
MAGNETISM.....	SUPERLATTICE.....	RARE EARTH.....	AW.02.09
MAGNETITE .....	NANOPARTICLE .....	BIOSYNTHESIS.....	M-P088
MAIL-IN DATA COLLECTION .....	SPRING-8.....	AUTOMATED DATA COLLECTION .....	13.07.07
MALARIA VECTOR .....	GLUTATHIONE S-TRANSFERASE.....	INSECTICIDE RESISTANCE.....	M-P220
MANGANESE .....	MYOGLOBIN .....	LIGAND.....	M-P180
MANGANESE SUPEROXIDE DISMUTASE.....			S-P171
MANUSCRIPT.....	CIF.....	PUBLICATION .....	10.01.08
MAP KINASE .....	DOCKING.....	ALLOSTERY.....	M-P048
MAP KINASE .....	INHIBITOR BINDING.....		M-P032
MAP2K.....	PHOSPHORYLATION KINETICS.....	BISUBSTRATE INHIBITOR .....	S-P221
MARCOMOLECULAR CRYSTALLOGRA.....	SCREENING .....	AUTOMOUNTER .....	T-P027
MATERIALS .....	NEUTRON SCATTERING.....	TIME-DEPENDENCE .....	13.09.01
MATERIALS SCIENCE .....	DIFFRACTION .....	SYNCHROTRON.....	13.10.09
MATERIALS SCIENCE .....	EDUCATION.....		M-P110
MAXIMUM ENTROPY .....	PAIR DISTIBUTION FUNCTION .....	POWDER DIFFRACTION.....	13.13.05
MCSG .....	TOPRIM DOMAIN.....	METAL BINDING .....	M-P070
MD SIMULATIONS.....	INELASTIC SCATTERING.....	MEMBRANE PROTEINS.....	09.04.05
MEDIUM ANGE ORDER.....	NONCRYSTALLINE.....	FLUCTUATION X-RAY MICROSCOPY.....	13.11.06
MELANOMA.....	T CELL STIMULATION .....	TUMOR ANTIGEN.....	T-P065
MEM/RIETVELD ANALYSIS .....	CHARGE DENSITY DISTRIBUTION .....	PEROVSKITE-TYPE HYDRIDES .....	13.01.06
MEMBRANE .....	REFLECTIVITY .....	MICROSCOPY .....	09.04.01
MEMBRANE INSERTION.....	COBRA CARDIOTOXIN.....	GLYCOSPHINGOLIPID .....	13.15.06
MEMBRANE PROTEIN .....	ABC TRANSPORTER .....		01.04.05
MEMBRANE PROTEIN.....	ABC TRANSPORTER .....	MULTIDRUG RESISTANCE.....	T-P201

# Keyword Index

MEMBRANE PROTEIN.....	BA3.....	NANODISC.....	S-P089
MEMBRANE PROTEIN.....	BIOENERGETICS.....	RHODOBACTER SPHAEROIDES.....	01.04.10
MEMBRANE PROTEIN.....	CONTROL OF MOTION SWITCH.....	ELECTRON TRANSFER.....	T-P191
MEMBRANE PROTEIN.....	CRYSTALLIZATION.....	TRANSHYDROGENASE.....	01.04.08
MEMBRANE PROTEIN.....	FUNCTIONAL STUDIES.....		T-P162
MEMBRANE PROTEIN.....	LIPIDIC CUBIC PHASE.....	LIGHT HARVESTING COMPLEX 2.....	T-P197
MEMBRANE PROTEIN.....	METALLOENZYME.....	COPPER.....	01.04.06
MEMBRANE PROTEIN.....	NEUTRON REFLECTOMETRY.....	LIPID BILAYER.....	AW.02.05
MEMBRANE PROTEIN.....	P-TYPE ATPASE.....	CALCIUM PUMP.....	01.05.05
MEMBRANE PROTEIN.....	STRUCTURE.....	PROTEORHODOPSIN.....	S-P075
MEMBRANE PROTEIN.....	VIRIAL COEFFICIENT.....	CRYSTALLIZATION.....	T-P199
MEMBRANE PROTEIN.....	X-RAY CRYSTALLOGRAPHY.....	AQUAPORIN.....	01.04.01
MEMBRANE PROTEIN STRUCTURE.....	MEMBRANE TRANSPORT.....	PROTEIN COMPLEX.....	01.04.02
MEMBRANE PROTEINS.....	CRYSTALLIZATION SCREENS.....	OPTIMIZATION.....	M-P078
MEMBRANE PROTEINS.....	MD SIMULATIONS.....	INELASTIC SCATTERING.....	09.04.05
MEMBRANE PROTEINS.....	TOXIN.....	PATHOGEN.....	M-P168
MEMBRANE STRUCTURE.....	VAN DER WAALS FORCES.....	ION-LIPID INTERACTIONS.....	09.04.03
MEMBRANE TRANSPORT.....	PROTEIN COMPLEX.....	MEMBRANE PROTEIN STRUCTURE.....	01.04.02
MEMBRANES.....	RAFTS.....	2D CRYSTALS.....	WK.03.01
MEOMYCIN.....	NEOMYCIN DERIVATIVE.....	RNA.....	04.01.06
METABOLITES.....	LIGAND SCREEN.....	PROTEIN CRYSTALLIZATION.....	M-P080
METAL BINDING.....	MCSG.....	TOPRIM DOMAIN.....	M-P070
METAL HYDRIDES.....	NUCLEAR MAGNETIC RESONANCE.....	NEUTRON SCATTERING.....	13.01.04
METAL ORGANIC FRAMEWORK.....	HISTIDINE.....	ZINC PHOSPHITE.....	T-P183
METAL OXIDE.....	THERMODECOMPOSITION.....	NANOPARTICLE.....	13.15.02
METAL-CONTAINING ARHITECTURES.....	DITOPIC BUILDING BLOCKS.....	CRYSTAL GROWTH.....	T-P143
METAL-ORGANIC FRAMEWORKS.....	SOLID STATE SYNTHESIS.....	[2+2]-PHOTODIMERISATION.....	T-P147
METALLO-B-LACTAMASE.....	PRE-MRNA PROCESSING.....	POLYADENYLATION.....	T-P074
METALLO-SUPRAMOLECULAR ASSEM.....	CAVITAND LIGANDS.....	COORDINATION POLYMER.....	10.03.09
METALLOENZYME.....	COPPER.....	MEMBRANE PROTEIN.....	01.04.06
METALLOENZYMES.....	ENZYME MECHANISM KINETICS.....	STRUCTURE-FUNCTION RELATIONSHIPS.....	M-P192
METALLOLIGAND.....	MOF.....	DIPYRRIN.....	13.12.02
METALS.....	CLUSTERS.....		M-P176
METASTASIS.....	S100A4.....	CALCIUM - BOUND STRUCTURE.....	T-P084
METHIONINE BIOSYNTHESIS.....	FREE INTERFACE DIFFUSION.....	HOMOSERINE TRANSUCCINYLAASE.....	T-P154
METHIONINE RECYCLING.....	PROTEIN CRYSTALLOGRAPHY.....	HOLMIUM PHASING.....	S-P145
METHOD DEVELOPMENT.....	STRUCTURE GEMONICS.....	HTP EXPRESSION, PURIFICATION& CRYSTAL.....	13.06.02
METNASE.....	SET.....	TRANSPOSASE.....	T-P106
MG++ATP.....	MOLECULAR DYNAMICS.....	CONFORMATIONAL CHANGE.....	T-P099
MHC.....	SUPERANTIGEN.....	TCR.....	01.06.05
MHC CLASS II.....	COMPLEX STRUCTURE.....	SUPERANTIGEN.....	M-P128
MICROBEAM.....	MIROCRYSTALLOGRAPHY.....	CAPILLARY OPTICS.....	T-P014
MICROCRYSTALS.....	BEAM LINE.....	SYNCHROTRON RADIATION.....	13.15.04
MICROFLUIDIC.....	PARALLEL.....	CRYSTALLIZATION.....	S-P207
MICROFLUIDICS.....	FREE INTERFACE DIFFUSION.....		T-P168
MICROFOCUS.....	MACROMOLECULAR CRYSTALLO.....	MAD PHASING.....	M-P158
MICROGRAVITY.....	COUNTER-DIFFUSION.....	GEL-TUBE.....	S-P209
MICROGRAVITY CRYSTAL GROWTH.....	HIGH QUALITY PROTEIN CRYSTAL.....	SPACE EXPERIMENT.....	T-P006
MICROHETEROGENEITY.....	PYP.....	SIGNAL TRANSDUCTION.....	13.14.02
MICROSCOPY.....	MEMBRANE.....	REFLECTIVITY.....	09.04.01
MICROSTRUCTURE.....	ALANATE.....	HYDROGEN STORAGE.....	13.01.01
MICROTUBULE.....	PROTEIN-LIPID COMPLEXES.....	SMALL ANGLE SCATTERING.....	09.02.06
MIROCRYSTALLOGRAPHY.....	CAPILLARY OPTICS.....	MICROBEAM.....	T-P014
MMCIF.....	BUERGER AWARD.....		AW.01.02
MOCN.....	MOLECULAR MAGNETISM.....	SUPRAMOLECULAR.....	T-P151
MODEL NANOCATALYSTS.....	GISAXS.....	SIZE-SELECTED CLUSTERS.....	09.01.04
MODULATED SUPERSTRUCTURES.....	CRYSTAL PACKING.....	POLYMORPHISM.....	10.01.02
MOF.....	DIPYRRIN.....	METALLOLIGAND.....	13.12.02
MOLECUAR RECOGNITION.....	HYDROGEN BONDS.....	CO-CRYSTALS.....	10.03.07
MOLECULAR ASSOCIATION.....	MOLYBDOPTERIN BIOSYNTHESIS P.....	PRASEODYMIUM DECAHYDRATE.....	M-P226
MOLECULAR DYNAMICS.....	CONFORMATIONAL CHANGE.....	MG++ATP.....	T-P099
MOLECULAR INCLUSION.....	HYDRATE.....	HYDROPHOBIC.....	T-P113
MOLECULAR MAGNETISM.....	SUPRAMOLECULAR.....	MOCN.....	T-P151
MOLECULAR RECOGNITION.....	CALMODULIN.....	CALCINEURIN.....	01.07.06

# Keyword Index

MOLECULAR REPLACEMENT.....	AUTOMATION.....	T-P087
MOLECULAR REPLACEMENT.....	HIGH-THROUGHPUT.....	NMR STRUCTURES.....
MOLECULAR REPLACEMENT.....	STRUCTURAL GENOMICS.....	HIGH THROUGHPUT METHODS.....
MOLYBDOPTERIN BIOSYNTHESIS PROT.	PRASEODYMIUM DECAHYDRATE.....	MOLECULAR ASSOCIATION.....
MOSA.....	DHDPS.....	T-P044
MOSAICS.....	DISORDER.....	TIME OR SPACE.....
MOVIES.....	FICTION.....	POETRY.....
MULTI-PASS STRATEGY.....	DATA COLLECTION PIPELINE.....	KAPPA GONIOMETRY.....
MULTIDRUG RESISTANCE.....	MEMBRANE PROTEIN.....	ABC TRANSPORTER.....
MULTIFUNCTIONAL ENZYME.....	STRUCTURE.....	FATTY ACID SYNTHASE.....
MULTILAYERS.....	NEUTRON.....	REFLECTOMETRY.....
MULTIPLE CONFORMERS.....	AUTOMATED MODEL BUILDING.....	STRUCTURE DETERMINATION.....
MULTIVARIATE LIKELIHOOD FUNCTIO..	SMART DATA COLLECTION.....	RADIATION DAMAGE.....
MUSCLE.....	LIQUID CRYSTAL.....	ELASTOMER.....
MUTAGENESIS.....	CRYSTALLIZATION.....	SURFACE ENTROPY.....
MUTAGENESIS.....	DNA POLYMERASE BETA.....	T-P072
MUTATION.....	DRUG RESISTANCE.....	HIV.....
MUTATIONAL STUDY.....	THYMIDYLATE.....	HYDROPHOBIC CORE.....
MYCOBACTERIUM TUBERCULOSIS.....	RHDANESE HOMOLOGY DOMAIN.....	SULFURTRANSFERASE.....
MYOGLOBIN.....	LIGAND.....	MANGANESE.....
MYOGLOBIN.....	NITRIC OXIDE.....	NITROSYL.....
MYOGLOBIN.....	TIME-RESOLVED CRYSTALLOGRA.....	REFINEMENT METHODS.....
N-DONOR LIGANDS.....	CLOSED-SHELL INTERACTIONS.....	SILVER(I).....
N-O ACYL SHIFT.....	AUTOPROTEOLYSIS.....	AUTOPROCESSING.....
NAD BIOSYTHESIS.....	ENZYME MECHANISM.....	QUINOLINATE SYNTHASE.....
NAD+ SYNTHETASE.....	ANTIBACTERIAL TARGET.....	ANTHRAX.....
NADP-DEPENDENT.....	CRYSTAL STRUCTURE.....	REDUCTASE.....
NAMPT.....	PHOSPHORIBOSYLTRANSFERASE.....	STRUCTURE.....
NANO PARTICLES.....	PAIR DISTRIBUTION FUNCTION.....	CDSE/ZNS.....
NANO-SCALE STRUCTURE.....	PAIR DENSITY FUNCTION.....	LOCAL STRUCTURE.....
NANOCAPSULE.....	VAULT.....	RIBONUCLEOPROTEIN.....
NANOCOMPOSITES.....	CARBON NANOTUBES.....	SMALL-ANGLE SCATTERING.....
NANOCRYSTALS.....	NEUTRONS.....	SIC DIAMOND.....
NANOCSCALE.....	SURFACE.....	VIRUSES.....
NANODISC.....	MEMBRANE PROTEIN.....	BA3.....
NANOMAGNETISM.....	POLARIZED NEUTRON SCATTERING.....	NANOSTRUCTURES.....
NANOMATERIALS.....	NEUTRON SCATTERING.....	PAIR DISTRIBUTION FUNCTION.....
NANOPARTICLE.....	BIOSYNTHESIS.....	MAGNETITE.....
NANOPARTICLE.....	METAL OXIDE.....	THERMODECOMPOSITION.....
NANOPARTICLE.....	PARTICLE FORM FACTOR.....	PDF.....
NANOPARTICLE.....	PHASE RETRIEVAL.....	COHERENT DIFFRACTION.....
NANOPARTICLES.....	LIQUID INTERFACES.....	09.01.02
NANOPHASE MATERIALS SCIENCES.....	CNMS.....	NANOSCIENCE.....
NANOSCIENCE.....	NANOPHASE MATERIALS SCIENCES.....	CNMS.....
NANOSTAR.....	PROTEIN.....	SAXS.....
NANOSTRUCTURE.....	QUANTUM CONFINEMENT EFFECT.....	HYBRID II-VI SEMICONDUCTOR.....
NANOSTRUCTURES.....	NANOMAGNETISM.....	POLARIZED NEUTRON SCATTERING.....
NATURAL.....	CLATHRATE.....	HYDRATE.....
NATURAL KILLER CELLS.....	VIRAL ANTIGEN.....	IMMUNE SYSTEM.....
NATURAL PRODUCTS.....	SESQUITERPENE LACTONES.....	VENEZUELAN ANDES.....
NEGATIVE THERMAL EXPANSION.....	NEUTRON TOTAL SCATTERING.....	RMC.....
NEOMYCIN DERIVATIVE.....	RNA.....	MEOMYCIN.....
NERVE AGENTS.....	CARBOXYLESTERASE.....	ORGANOPHOPHATES.....
NEUROLYSIN.....	SPECIFICITY.....	THIMET OLIGOPEPTIDASE.....
NEURONAL MIGRATION.....	PROTEIN STRUCTURE.....	COILED-COIL.....
NEUTON TOF DIFFRACTOMETER.....	SIMULATION OF TOF DIFFRACTION.....	BIOLOGICAL CRYSTALLOGRAPHY.....
NEUTRALIZING ANTIBODY.....	GP120.....	HIV-1.....
NEUTRALIZING ANTIBODY.....	V <sub>λ</sub> LIGHT CHAIN.....	EBOLA VIRUS.....
NEUTRON.....	CRYSTALLOGRAPHY.....	INSULIN.....
NEUTRON.....	DETECTOR.....	T-P160
NEUTRON.....	DIFFRACTOMETER.....	REAL-TIME.....
NEUTRON.....	PROTEIN.....	TR.01.10
NEUTRON.....	REFLECTOMETRY.....	MULTILAYERS.....
NEUTRON.....	SINGLE CRYSTAL.....	DIFFRACTION.....

# Keyword Index

NEUTRON.....	SOFTWARE.....	LAUE.....	M-P014
NEUTRON & X-RAY DIFFRACTION.....	MAGNETIC ORDER IN CUFeO2.....	STRUCTURE TRANSITION.....	M-P100
NEUTRON AND X-RAY DIFFRACTION.....	CHEMICAL DISORDER.....	AS-TE GLASSES.....	M-P104
NEUTRON DIFFRACTION.....	DIRECT METHODS.....	MACROMOLECULAR STRUCTURE.....	TR.01.11
NEUTRON DIFFRACTION.....	EXPERIMENTAL CHARGE DENSITY.....	SINGLE CRYSTAL.....	S-P027
NEUTRON DIFFRACTION.....	FLASH-COOLING.....	FLAP ENDONUCLEASE-1.....	M-P010
NEUTRON DIFFRACTION.....	HYDROGEN STORAGE MATERIALS.....	IN-SITU SYNCHROTRON DIFFRACTION.....	13.01.05
NEUTRON DIFFRACTION.....	HYDROTHERMAL CRYSTALLIZATI.....	PHARMACEUTICAL.....	10.02.06
NEUTRON DIFFRACTION.....	IN-SITU TIME-RESOLVED TEST.....	THERMAL STRESS AND TEMPERATURE.....	13.09.07
NEUTRON DIFFRACTION.....	LARGE SINGLE CRYSTAL.....	CRYSTALLIZATION PHASE DIAGRAM.....	M-P004
NEUTRON DIFFRACTION.....	SUPRAMOLECULAR CHEMISTRY.....	STRUCTURAL BIOLOGY.....	TR.01.04
NEUTRON DIFFRACTION.....	TIME-OF-FLIGHT NEUTRONS.....	D-XYLOSE ISOMERASE.....	TR.01.08
NEUTRON DIFFRACTION.....	ULTRAHIGH RESOLUTION.....	DIHYDROFOLATE REDUCTASE.....	TR.01.09
NEUTRON DIFFRACTION.....	X-RAY SUBATOMIC RESOLUTION.....	ENZYMOLGY.....	TR.01.07
NEUTRON POWDER DIFFRACTION.....	PEROVSKITE.....	HIGH PRESSURE.....	M-P116
NEUTRON PROTEIN CRYSTALLOG.....	A LARGE SINGLE CRYSTAL.....	BETA-LACTOGLOBULIN.....	M-P006
NEUTRON PROTEIN CRYSTALLOG.....	SPALLATION NEUTRON SOURCE.....	HYDROGEN AND HYDRATION.....	TR.01.03
NEUTRON REFLECTIVITY.....	DIPHThERIA TOXIN.....	ENZYME TRANSLOCATION.....	AW.02.04
NEUTRON REFLECTIVITY.....	X-RAY SMALL ANGLE SCATTERING.....	ANTICORROSION.....	13.11.05
NEUTRON REFLECTOMETRY.....	GRAZING INCIDENCE X-RAY DIFFR.....	BIO-MEMBRANES.....	AW.02.06
NEUTRON REFLECTOMETRY.....	LIPID BILAYER.....	MEMBRANE PROTEIN.....	AW.02.05
NEUTRON REFLECTOMETRY.....	NEUTRON SCATTERING.....	NEUTRON SPIN ECHO.....	AW.02.11
NEUTRON REFLECTOMETRY.....	POLYMERS.....		AW.02.03
NEUTRON SCATTERING.....	FIRST-PRINCIPLES CALCULATIONS.....	HYDROGEN STORAGE.....	13.01.02
NEUTRON SCATTERING.....	METAL HYDRIDES.....	NUCLEAR MAGNETIC RESONANCE.....	13.01.04
NEUTRON SCATTERING.....	NEUTRON SPIN ECHO.....	NEUTRON REFLECTOMETRY.....	AW.02.11
NEUTRON SCATTERING.....	PAIR DISTRIBUTION FUNCTION.....	NANOMATERIALS.....	13.13.06
NEUTRON SCATTERING.....	POWDER DIFFRACTION.....	HYDROGEN STORAGE MATERIAL.....	13.09.03
NEUTRON SCATTERING.....	SMALL-ANGLE SCATTERING.....	SYSTEMS BIOLOGY.....	09.02.03
NEUTRON SCATTERING.....	TIME-DEPENDENCE.....	MATERIALS.....	13.09.01
NEUTRON SCATTERING.....	TIME-RESOLVED STUDIES.....	POWDER DIFFRACTION.....	13.09.04
NEUTRON SPIN ECHO.....	NEUTRON REFLECTOMETRY.....	NEUTRON SCATTERING.....	AW.02.11
NEUTRON TOTAL SCATTERING.....	RMC.....	NEGATIVE THERMAL EXPANSION.....	13.03.02
NEUTRONS.....	REFLECTION.....	INVERSION.....	AW.02.10
NEUTRONS.....	SIC DIAMOND.....	NANOCRYSTALS.....	13.03.03
NEW ANTIGEN RECEPTOR.....	ANTIBODY.....	SHARK.....	T-P067
NEW DIFFRACTOMETER IN J-PARC.....	MACROMOLECULAR CRYSTALLO.....	INDUSTRIAL USE.....	13.15.05
NEW FOLD.....	HELICOBACTER PYLORI.....		S-P133
NEXUS.....	XML.....	IMGCIF.....	M-P156
NITRIC OXIDE.....	NITROSYL.....	MYOGLOBIN.....	S-P159
NITROSYL.....	MYOGLOBIN.....	NITRIC OXIDE.....	S-P159
NMR STRUCTURES.....	MOLECULAR REPLACEMENT.....	HIGH-THROUGHPUT.....	T-P103
NON-CENTROSYMMETRIC.....	ORGANIC SOLID STATE.....	CRYSTAL ENGINEERING.....	10.03.10
NON-CRYSTALLOGRAPHIC SYMMETRY.....	STRUCTURAL PROTEIN.....	SPORULATION.....	T-P221
NON-IPR.....	FULLERENE.....	ENDOHEDRAL.....	M-P164
NONCRYSTALLINE.....	FLUCTUATION X-RAY MICROSCOPY.....	MEDIUM ANGE ORDER.....	13.11.06
NOVEL FOLD.....	COFE HOMOLOG.....	HOMOLOG OF F420-0:Å-GLUTAMYL LIGASE.....	T-P100
NOVEL FOLD.....	SARS CORONAVIRUS.....	STRUCTURE-FUNCTION RELATIONSHIPS.....	01.0108
NOVEL FOLD.....	SARS CORONAVIRUS.....	STRUCTURE-FUNCTION RELATIONSHIPS.....	T-P132
NOVEL STRUCTURES.....	CRYSTAL STRUCTURE PREDICTION.....	HIGH PRESSURE.....	05.01.03
NOVEL TOPOLOGY.....	PROTEIN-PRIMING.....	POLYMERASE.....	T-P086
NRDI PROTEIN.....	CRYSTAL STRUCTURE.....	B. SUBTILIS.....	M-P068
NTE.....	A2(WO4)3.....	PXRD.....	S-P043
NTE.....	HIGH-PRESSURE.....	A2M3O12.....	M-P112
NUCLEAR MAGNETIC RESONANCE.....	NEUTRON SCATTERING.....	METAL HYDRIDES.....	13.01.04
NUCLEASE.....	RNASE III.....		T-P036
NUCLEOSIDASE.....	SPECIFICITY.....	A. THALIANA.....	M-P188
NUDIX FAMILY.....	STRUCTURAL GENOMICS.....		S-P105
OCTAETHYLPORPHYRIN.....	HEME SYSTEM.....	SUPRAMOLECULAR STRUCTURE.....	T-P141
OD STRUCTURE.....	CRYSTAL STRUCTURE.....	DISORDER.....	13.02.05
OFF-SPECULAR.....	DIFFUSE.....	GRAZING INCIDENCE.....	AW.02.12
OFFLINE DATA COLLECTION.....	AUTOMATION.....	RE-CENTERING.....	T-P176
ONCOGENE.....	TRANSCRIPTION FACTOR.....		13.10.05
OPEN-FRAMEWORK.....	HYDROTHERMAL SYNTHESIS.....	ARSENIC VANADATE.....	T-P145

# Keyword Index

OPTIMIZATION	CRYOPROTECTANT	CRYSTALLIZATION	S-P061
OPTIMIZATION	CR GROWTH APPARATUS DESIGN	BIOMACROMOLECULAR CRYSTALLIZATION	T-P022
OPTIMIZATION	MACROMOLECULE	CRYSTALLIZATION	13.06.03
OPTIMIZATION	MEMBRANE PROTEINS	CRYSTALLIZATION SCREENS	M-P078
ORGANIC SOLID STATE	CRYSTAL ENGINEERING	NON-CENTROSYMMETRIC	10.03.10
ORGANIC-INORGANIC HYBRID	HYDROTHERMAL SYNTHESIS	SUPRAMOLECULAR STRUCTURE	M-P162
ORGANOMETALLOLIGAND	QUINONE	COORDINATION NETWORK	13.12.03
ORGANOPHOPHATES	NERVE AGENTS	CARBOXYLESTERASE	M-P224
ORIENTATION KINETICS	SAXS	ELECTRIC FIELD	09.03.04
OSR1	STE20P	KINASE DOMAIN	T-P102
OUTER MEMBRANE	IRON	TONB	T-P207
OUTER MEMBRANE CRYSTALLIZATION	BACTERIAL PATHOGENESIS	TWO-PARTNER SECRETION	S-P111
OUTER MEMBRANE TRANSPORTER	FERRICHROME	HETEROCOMPLEX	01.04.04
OXYGEN	ACTIVATION	COPPER ENZYMES	S-P077
OXYGEN ACTIVATION	DIOXYGENASE	ACID-BASE CATALYSIS	S-P057
P-TYPE ATPASE	CALCIUM PUMP	MEMBRANE PROTEIN	01.05.05
P. FURIOSUS	STRUCTURAL GENOMICS	COA-BINDING	S-P185
P450 STRUCTURE	X-RAY STRUCTURE DETERMINAT	THERMOPHILIC HEMOPROTEINS	M-P208
PACKING EFFECTS	DISPLACEMENT PARAMETERS	JAHN-TELLER EFFECT	T-P115
PAIR DENSITY FUNCTION	LOCAL STRUCTURE	NANO-SCALE STRUCTURE	13.13.01
PAIR DISTRIBUTION FUNCTION	POWDER DIFFRACTION	MAXIMUM ENTROPY	13.13.05
PAIR DISTRIBUTION FUNCTION	CDSE/ZNS	NANO PARTICLES	13.13.03
PAIR DISTRIBUTION FUNCTION	DYNAMICS	REVERSE MONTE CARLO	13.03.05
PAIR DISTRIBUTION FUNCTION	NANOMATERIALS	NEUTRON SCATTERING	13.13.06
PAIR DISTRIBUTION FUNCTION	PDF	AB-INITIO STRUCTURE SOLUTION	T-P009
PAIR DISTRIBUTION FUNCTION	TOTAL SCATTERING	DISORDER	13.03.01
PARALLEL	CRYSTALLIZATION	MICROFLUIDIC	S-P207
PARALLEL COMPUTING	AUTOMATED PHASING	HIGH THROUGHPUT	01.02.03
PARTICLE FORM FACTOR	PDF	NANOPARTICLE	13.13.07
PARVOVIRIDAE	ADENO-ASSOCIATED VIRUS 5	GENE THERAPY	M-P142
PARVOVIRIDAE	GENE THERAPY	CYSTIC FIBROSIS	S-P009
PARVOVIRUS	ADENO-ASSOCIATED VIRUS	ENDOSOMAL PROCESS	M-P140
PATHOGEN	MEMBRANE PROTEINS	TOXIN	M-P168
PATHOGENICITY ISLAND	ENTEROTOXIN	AMPICILLIN RESISTANCE	T-P076
PCK	E. COLI	CARBON DIOXIDE	T-P046
PCK	GTP-DEPENDENT	X-RAY STRUCTURE	T-P054
PDF	AB-INITIO STRUCTURE SOLUTION	PAIR DISTRIBUTION FUNCTION	T-P009
PDF	INTERNAL STRAIN	BULK METALLIC GLASS	13.03.04
PDF	NANOPARTICLE	PARTICLE FORM FACTOR	13.13.07
PDF METHOD	SUPERMIRCOPOROUS MATERIALS		S-P031
PDX-1	HOMEODOMAIN	DNA	T-P118
PENICILLIN	PEPTIDOGLYCAN	ANTIBIOTIC	13.10.03
PENICILLIN BINDING PROTEIN	ANTIBIOTICS	CRYSTAL STRUCTURE	S-P147
PEO-LAPONITE	HYDROGELS	SHEAR-SANS	09.03.06
PEPCK	TRYPSIN	CALCIUM ACTIVATION	T-P080
PEPCK	A. SUCCINICIPRODUCENS	COORDINATION OF DIVALENT METAL	T-P038
PEPTIDE DEFORMYLASE	STRUCTURE COMPARISONS	STRUCTURE BASED DRUG DESIGN	M-P028
PEPTIDOGLYCAN	ANTIBIOTIC	PENICILLIN	13.10.03
PEPTIDYL-TRNA HYDROLASE	DIMERIC STRUCTURE	PYROCOCBUS HORIKOSHII OT3	T-P164
PEROVSKITE	HIGH PRESSURE	NEUTRON POWDER DIFFRACTION	M-P116
PEROVSKITE STRUCTURES	PHASE TRANSITIONS & STRUCTUR	HI P/LOW T NEUTRON/DIELECTRIC MEAS	M-P118
PEROVSKITE-TYPE HYDRIDES	MEM/RIETVELD ANALYSIS	CHARGE DENSITY DISTRIBUTION	13.01.06
PHARMACEUTICAL	CO-CRYSTALS	HYDROGEN BONDING	10.03.05
PHARMACEUTICAL	NEUTRON DIFFRACTION	HYDROTHERMAL CRYSTALLIZATION	10.02.06
PHASE BEHAVIOR	BLOCK COPOLYMERS	POLYMER NANOCOMPOSITES	09.03.05
PHASE DETERMINATION	RESONANT SCATTERING	THREE-BEAM DIFFRACTION	13.11.07
PHASE RETRIEVAL	COHERENT DIFFRACTION	NANOPARTICLE	13.11.08
PHASE TRANSITION	DISORDER	TWIN	S-P029
PHASE TRANSITION	DISTORTION	SHORT-RANGE ORDER	M-P106
PHASE TRANSITION	TWINNING	DISORDER	13.14.04
PHASE TRANSITIONS & STRUCTURES	HI P/LOW T NEUTRON/DIELECTRIC	PEROVSKITE STRUCTURES	M-P118
PHASING	ABSORPTION CORRECTION	MACROMOLECULES	T-P016
PHASING	CENTROSYMMETRIC	SMALL MOLECULE	M-P172
PHASING	CHROMIUM	SAD	S-P199

# Keyword Index

PHASING.....	HIGH PRESSURE CRYOCOOLING .....	CRYOPROTECTION.....	M-P130
PHASING.....	RADIATION DAMAGE.....	HIGH ENERGY .....	11.01.05
PHASING.....	SARS.....	PROTEASE.....	T-P112
PHASING.....	SAXS.....	ENVELOPE.....	13.08.02
PHENIX.....	MACROMOLECULE.....	STRUCTURE REFINEMENT.....	01.02.06
PHENYLHYDRAZONE.....	ISOSTRUCTURAL.....	BENZYLIDENEANILINE.....	T-P185
PHEROMONE.....	REPRESSOR.....		T-P108
PHOQ/PHOP.....	TWO-COMPONENT SYSTEM.....	TRANS-MEMBRANE SIGNALING.....	01.01.07
PHOSHOHEXOMUTASE.....	ENZYME-INTERMEDIATE COMPLEX.....	PROCESSIVITY.....	S-P151
PHOSPHATASE.....	INOSITOL.....	PROTEIN FOLDING.....	S-P203
PHOSPHONIC ACID.....	CRYSTAL STRUCTURE.....	CRYSTAL ENGINEERING.....	T-P111
PHOSHOPEPTIDE RECOGNITION.....	PROTEIN-PROTEIN INTERACTION.....	BRCT REPEAT.....	S-P205
PHOSPHORIBOSYLTRANSFERASE.....	STRUCTURE.....	NAMPT.....	T-P058
PHOSPHORYLASE.....	PYROPHOSPHORYLASE.....	STRUCTURAL GENOMICS.....	13.06.08
PHOSPHORYLATION KINETICS.....	BISUBSTRATE INHIBITOR.....	MAP2K.....	S-P221
PHOSPHOTRANSFERASE.....	EXOPOLYPHOSPHATASE.....	POLYPHOSPHATE.....	13.14.01
PHOSPHOTRANSFERASE CHEMISTRY.....	PROTEIN GLYCOSYLATION.....	HALOALKANOIC ACID DEHALOGENASE.....	T-P032
PHOTOCHROMISM.....	SOLID STATE REACTION.....	UNSTABLE STRUCTURE.....	T-P153
PHOTOCRYSTALLOGRAPHY.....	SELF-ASSEMBLY.....	PHOTOREACTIONS.....	10.03.14
PHOTOREACTIONS.....	PHOTOCRYSTALLOGRAPHY.....	SELF-ASSEMBLY.....	10.03.14
PHOTORECEPTOR.....	INTEGRAL MEMBRANE PROTEIN.....	TRANSDUCER.....	01.04.07
PHOTORECEPTOR.....	PHYTOCHROME.....		T-P128
PHOTOSYSTEM II.....	CYCLODEXTRINS.....	HYDROGEN BONDING.....	TR.01.06
PHYTOCHROME.....	PHOTORECEPTOR.....		T-P128
PICORNAVIRUS.....	3C.....	INHIBITOR.....	T-P010
PKC.....	KINASE.....		T-P136
PLANT DISEASE RESISTANCE.....	SAD PHASING.....	HOST-PATHOGEN INTERACTION.....	01.07.05
PLANT ENZYME.....	ELECTRON TRANSFER COMPLEX.....		M-P148
PLANT PROTEIN.....	EXPANSIN.....	CELL WALL LOOSENING.....	T-P152
PLASMIN.....	TEXTILININ.....	SNAKE VENOM.....	S-P131
PLATE.....	SBS.....	CRYSTALLIZATION.....	S-P217
PLATELET.....	INTEGRIN.....	THROMBOCYTOPENIA.....	T-P034
PLUNGE COOLING.....	FLASH FREEZING.....	VITRIFICATION.....	T-P047
PLUTONIUM.....	DIFFRACTION ANALYSIS.....		10.01.01
POETRY.....	MOVIES.....	FICTION.....	T-P015
POLARIZED NEUTRON REFLECTOMETRY.....		EXCHANGE BIAS.....	AW.02.08
POLARIZED NEUTRON SCATTERING.....	NANOSTRUCTURES.....	NANOMAGNETISM.....	AW.02.07
POLICY.....	EDUCATION.....	TRAINING.....	SP.01.01
POLY (LACTIC ACID).....	CRYSTALLISATION.....	STRAIN-INDUCED.....	09.03.03
POLYADENYLATION.....	METALLO-B-LACTAMASE.....	PRE-MRNA PROCESSING.....	T-P074
POLYDIACETYLENES.....	HOST GUEST CHEMISTRY.....	SOLID STATE POLYMERIZATION.....	T-P129
POLYETHYLENE.....	DEFORMATION.....	IN-SITU.....	09.03.02
POLYFUNCTIONAL.....	TETRANUCLEAR COMPLEX.....		T-P149
POLYMER.....	COPPER.....	ETHYLENEDIAMINE.....	T-P119
POLYMER.....	SAXS.....	CRYSTALLIZATION.....	09.03.01
POLYMER BRUSHES.....	DIBLOCK COPOLYMERS.....	GISAXS.....	09.01.03
POLYMER CRYSTALLIZATION.....	SAXS.....		13.11.01
POLYMER NANOCOMPOSITES.....	PHASE BEHAVIOR.....	BLOCK COPOLYMERS.....	09.03.05
POLYMER NANOCOMPOSITES.....	STRUCTURE.....	DYNAMICS.....	13.11.02
POLYMERASE.....	CLAMP LOADING.....	TRANSLESION SYNTHESIS.....	S-P189
POLYMERASE.....	INHIBITOR.....	HCV.....	04.01.03
POLYMERASE.....	NOVEL TOPOLOGY.....	PROTEIN-PRIMING.....	T-P086
POLYMERASE.....	RHINOVIRUS.....	RNA.....	M-P034
POLYMERS.....	NEUTRON REFLECTOMETRY.....		AW.02.03
POLYMORPHISM.....	DIFFUSE SCATTERING.....	DISORDER.....	10.03.02
POLYMORPHISM.....	MODULATED SUPERSTRUCTURES.....	CRYSTAL PACKING.....	10.01.02
POLYMORPHISM.....	REACTIVITY.....	CRYSTAL ENGINEERING.....	10.03.19
POLYPHOSPHATE.....	PHOSPHOTRANSFERASE.....	EXOPOLYPHOSPHATASE.....	13.14.01
POOR QUALITY DATA.....	HETEROGENEOUS READTION.....	HEME NITROSYL THIOLATE.....	13.05.02
PORE-FORMING TOXIN.....	GPI ANCHOR.....	RECEPTOR BINDING.....	M-P126
POROUS CRYSTALS.....	DYNAMIC STRUCTURES.....	COORDINATION POLYMERS.....	10.03.08
PORPHYRIN.....	TWINNING.....		10.01.04
POWDER.....	RIETVELD.....	TETRAFLUOROBORATE.....	S-P045
POWDER.....	SYNCHROTRON.....	ANOMALOUS.....	M-P098

# Keyword Index

POWDER DIFFRACTION.....	HYDROGEN STORAGE MATERIAL.....	NEUTRON SCATTERING.....	13.09.03
POWDER DIFFRACTION.....	MAXIMUM ENTROPY.....	PAIR DISTRIBUTION FUNCTION.....	13.13.05
POWDER DIFFRACTION.....	NEUTRON SCATTERING.....	TIME-RESOLVED STUDIES.....	13.09.04
POWDER DIFFRACTION.....	VIBRATIONAL CIRCULAR DICHROI.....	SIMULATED ANNEALING.....	10.02.02
POWDER NEUTRON DIFFRACTION.....	SYNCHROTRON POWDER X-RAY.....	HYDROGEN.....	13.01.03
PRASEODYMIUM DECAHYDRATE.....	MOLECULAR ASSOCIATION.....	MOLYBDOPTERIN BIOSYNTHESIS PROTEIN.....	M-P226
PRE-MRNA PROCESSING.....	POLYADENYLATION.....	METALLO-B-LACTAMASE.....	T-P074
PRECURSOR ACTIVATION.....	INTERMEDIATE STRUCTURE.....	AUTOPROTEOLYSIS.....	13.15.07
PREDICTION.....	CRYSTALLIZATION CONDITIOIN.....	DATABASE.....	M-P132
PRESSURE JUMP TECHNIQUE.....	SAXS.....	LIPID MESOPHASE TRANSITIONS.....	09.04.06
PRIB.....	PRIMOSOME.....	DNA REPLICATION RESTART.....	S-P127
PRIMOSOME.....	DNA REPLICATION RESTART.....	PRIB.....	S-P127
PROBLEM STRUCTURES.....	WHOLE MOLECULE DISORDER.....	ADVANCED REFINEMENT.....	13.02.02
PROCESSIVITY.....	PHOSHOHEXOMUTASE.....	ENZYME-INTERMEDIATE COMPLEX.....	S-P151
PROLINE DEHYDROGENASE.....	REACTIVE OXYGEN SPECIES.....	BARREL.....	01.01.04
PROPARGYLIC ALCOHOLS.....	SYNERGY OF INTERACTIONS.....	SUPRAMOLECULAR ASSEMBLIES.....	10.03.04
PROTEAE INHIBITORS.....	WIDE OPEN HIV-I PROTEASE.....	DRUG DESIGN.....	M-P196
PROTEASE.....	GAG.....	HIV.....	S-P197
PROTEASE.....	PHASING.....	SARS.....	T-P112
PROTEIN.....	DATABASE.....	CRYSTALLIZATION.....	T-P008
PROTEIN.....	LATTICE.....	CRYSTALLIZATION.....	S-P201
PROTEIN.....	NEUTRON.....		TR.01.10
PROTEIN.....	SAXS.....	NANOSTAR.....	M-P050
PROTEIN ALLOSTERY.....	TIME-RESOLVED CRYSTALLOGRAPHY.....		13.08.03
PROTEIN COMPLEX.....	ALPHA SCREEN.....		T-P193
PROTEIN COMPLEX.....	MEMBRANE PROTEIN STRUCTURE.....	MEMBRANE TRANSPORT.....	01.04.02
PROTEIN CRYSTAL.....	LASER PROCESSING.....	PULSED UV LASER SOFT ABLATION (PULSA).....	S-P179
PROTEIN CRYSTAL STRUCTURE.....	SAM RADICAL.....	PYRUVATE-FORMATE LYASE ACTIVASE.....	M-P166
PROTEIN CRYSTALLIZATION.....	LIQUID PHASE.....	RHODOBACTER SPHAEROIDES (RCSPH).....	T-P195
PROTEIN CRYSTALLIZATION.....	METABOLITES.....	LIGAND SCREEN.....	M-P080
PROTEIN CRYSTALLOGRAPHY.....	AUTOMATION.....	IMAGING ROBOT.....	M-P058
PROTEIN CRYSTALLOGRAPHY.....	AUTOMATION.....	SYNCHROTRON.....	13.10.02
PROTEIN CRYSTALLOGRAPHY.....	HOLMIUM PHASING.....	METHIONINE RECYCLING.....	S-P145
PROTEIN CRYSTALLOGRAPHY.....	SAXS.....	BEAMLINE.....	T-P055
PROTEIN CRYSTALLOGRAPHY.....	SMALL MOLECULE CRYSTALLOGR.....	CRYSTAL MANIPULATION.....	S-P215
PROTEIN CRYSTALLOGRAPHY.....	SOFTWARE.....	DATABASES.....	T-P085
PROTEIN CRYSTALLOGRAPHY.....	STRUCTURAL BIOLOGY.....	BIOLOGICAL MACROMOLECULE.....	M-P036
PROTEIN CRYSTALLOGRAPHY.....	SYNCHROTRON.....	APS.....	T-P039
PROTEIN DESIGN.....	SOFTWARE.....	GENE SYNTHESIS.....	M-P134
PROTEIN EVOLUTION.....	SUPERFAMILY.....	TAUTOMERASE.....	T-P004
PROTEIN EXPRESSION.....	AUTOMATION.....	IN VITRO.....	M-P084
PROTEIN FOLDING.....	CH.....		M-P052
PROTEIN FOLDING.....	PHOSPHATASE.....	INOSITOL.....	S-P203
PROTEIN FOLDING.....	VILLIN.....	KINETICS.....	AW.03.05
PROTEIN GLYCOSYLATION.....	HALOALKANOIC ACID DEHALOGE.....	PHOSPHOTRANSFERASE CHEMISTRY.....	T-P032
PROTEIN INHIBITOR.....	PROTEIN-PROTEIN INTERACTIONS.....	BACTERIAL PATHOGENESIS.....	T-P124
PROTEIN KINASE.....	BONE RESORPTION.....	INTEGRIN.....	M-P228
PROTEIN KINASE C.....	ANESTHETICS.....	CRYSTAL STRUCTURE.....	T-P028
PROTEIN MOBILITY.....	REDOX CHEMISTRY.....	INTEGRAL MEMBRANE PROTEIN.....	T-P205
PROTEIN PRECIPITATION POINT.....	ROBOTIC CRYSTALLIZATION.....		T-P002
PROTEIN RNA INTERACTION.....			S-P141
PROTEIN STRUCTURE.....	CANADIAN LIGHT SOURCE.....	SMALL ANGLE SCATTERING.....	13.10.07
PROTEIN STRUCTURE.....	COILED-COIL.....	NEURONAL MIGRATION.....	T-P215
PROTEIN SURFACE ANALYSIS.....	FUNCTION ANALYSIS.....	STRUCTURAL GENOMICS.....	S-P219
PROTEIN SYNTHESIS.....	CRYSTALLOGRAPHY & NMR.....	CELL-FREE EXPRESSION SYSTEM.....	T-P024
PROTEIN TRANSLOCATION.....	ATPASE.....	SECA.....	S-P211
PROTEIN TYROSINE PHOSPHATASE.....	STRUCTURAL GENOMICS.....	PSI-II.....	T-P144
PROTEIN-LIPID COMPLEXES.....	SMALL ANGLE SCATTERING.....	MICROTUBULE.....	09.02.06
PROTEIN-PRIMING.....	POLYMERASE.....	NOVEL TOPOLOGY.....	T-P086
PROTEIN-PROTEIN INTERACTION.....	BRCT REPEAT.....	PHOSPHOPEPTIDE RECOGNITION.....	S-P205
PROTEIN-PROTEIN INTERACTIONS.....	BACTERIAL PATHOGENESIS.....	PROTEIN INHIBITOR.....	T-P124
PROTEIN-PROTEIN INTERACTIONS.....	TRANSCRIPTION FACTOR.....	DIMERIZATION.....	M-P214
PROTEIN:DNA COMPLEX.....	BACTERIOPHAGE T4 RNASE H.....	5' TO 3' EXONUCLEASE.....	M-P178
PROTEIN:PROTEIN COMPLEX.....	SPECIFICITY.....	KINASE.....	T-P090

# Keyword Index

PROTEINS.....	COLLOIDS.....	SMALL ANGLE X-RAY SCATTERING.....	09.02.05
PROTEINS.....	X-RAY SCATTERING.....	DNA.....	09.02.02
PROTEINS IN SOLUTION.....	STRUCTURE.....	SMALL-ANGLE SCATTERING.....	13.13.04
PROTEOMICS.....	STRUCTURAL GENOMICS.....	HIGH THROUGHPUT METHODOLOGIES.....	13.06.01
PROTEORHODOPSIN.....	MEMBRANE PROTEIN.....	STRUCTURE.....	S-P075
PROTON TRANSFER.....	CYP158A2.....	FERROUS-DIOXYGEN.....	S-P169
PROTON TRANSFER.....	SOLVENT NETWORK.....	CARBONIC ANHYDRASE.....	AW.03.02
PROTONATION.....	ENZYMATIC MECHANISM.....	QUASI-LAUE.....	M-P016
PSEUDOMAS AEURGINOSA.....	TYPE 4 PILUS.....	TPR DOMAIN.....	S-P155
PSEUDOMONAS AERUGINOSA.....	EXOPOLYSACCHARIDE.....	EXPORT.....	S-P093
PSEUDOSYMMETRY.....	DIFFICULT STRUCTURES.....	TWINNING.....	01.05.01
PSEUDOSYMMETRY.....	SOD1.....	TWINNING.....	T-P217
PSEUDOURIDINE SYNTHASE.....	RRNA MODIFICATION.....		T-P120
PSI.....	ALLANTOATE-AMIDOHYDROLASE.....	PURINE CATABOLISM.....	S-P187
PSI.....	PYROPHOSPHATE.....	KINASE.....	T-P146
PSI-II.....	PROTEIN TYROSINE PHOSPHATASE.....	STRUCTURAL GENOMICS.....	T-P144
PUBLICATION.....	MANUSCRIPT.....	CIF.....	10.01.08
PULSED NEUTRON DIFFRACTION.....	SINGLE CRYSTAL.....		TR.01.02
PULSED UV LASER SOFT ABLATION.....	PROTEIN CRYSTAL.....	LASER PROCESSING.....	S-P179
PURINE CATABOLISM.....	PSI.....	ALLANTOATE-AMIDOHYDROLASE.....	S-P187
PURO.....	ENZYME MECHANISM.....	IMP CYCLOHYDROLASE.....	S-P195
PXRD.....	NTE.....	A2(WO4)3.....	S-P043
PYK2.....	SCAFFOLD.....	KINASE.....	M-P030
PYP.....	SIGNAL TRANSDUCTION.....	MICROHETEROGENEITY.....	13.14.02
PYRIMIDINE BIOSYNTHESIS.....	STRUCTURAL GENOMICS.....	EUKARYOTIC PATHOGENS.....	T-P071
PYROCOCCLUS HORIKOSHII OT3.....	PEPTIDYL-TRNA HYDROLASE.....	DIMERIC STRUCTURE.....	T-P164
PYROPHOSPHATE.....	KINASE.....	PSI.....	T-P146
PYROPHOSPHORYLASE.....	STRUCTURAL GENOMICS.....	PHOSPHORYLASE.....	13.06.08
PYRROLE.....	AROMATICITY.....	REACTION REGIOSELECTIVITY.....	T-P175
PYRUVATE DEHYDROGENASE.....	E1 COMPONENT.....	THIAMIN DIPHOSPHATE.....	T-P020
PYRUVATE-FORMATE LYASE ACTIVASE.....	PROTEIN CRYSTAL STRUCTURE.....	SAM RADICAL.....	M-P166
PYTHON.....	FRAGMENT SCREENING.....	AUTOMATION.....	M-P024
QUADRUPLEX.....	DRUG-DNA.....		AW.01.03
QUANTUM CONFINEMENT EFFECT.....	HYBRID II-VI SEMICONDUCTOR.....	NANOSTRUCTURE.....	13.12.05
QUANTUM MECHANICS.....	SMALL MOLECULES.....	2-MERCAPTOTHIAZOLINE.....	M-P170
QUASI-LAUE.....	PROTONATION.....	ENZYMATIC MECHANISM.....	M-P016
QUINOLINATE BIOSYNTHESIS.....	DIOXYGENASE.....	ENZYME MECHANISM.....	T-P078
QUINOLINATE SYNTHASE.....	NAD BIOSYNTHESIS.....	ENZYME MECHANISM.....	S-P157
QUINONE.....	COORDINATION NETWORK.....	ORGANOMETALLOLIGAND.....	13.12.03
QUINOPROTEIN.....	REDOX ENZYME.....	SINGLE CRYSTAL MICROSPECTROPHOTOMET.....	M-P138
RAB5 EFFECTOR.....	BAR AND PH DOMAIN.....	APPL1.....	T-P148
RADIATION DAMAGE.....			11.01.03
RADIATION DAMAGE.....	DATA ANALYSIS.....	ERROR MODEL.....	11.01.06
RADIATION DAMAGE.....	HELIUM.....		11.01.02
RADIATION DAMAGE.....	HIGH ENERGY.....	PHASING.....	11.01.05
RADIATION DAMAGE.....	MULTIVARIATE LIKELIHOOD FUNC.....	SMART DATA COLLECTION.....	01.05.02
RADIATION DAMAGE.....	SYNCHROTRON RADIATION.....	HIGH ENERGY.....	11.01.04
RAFT.....	GANGLIOSIDE.....	GLYCOSPHINGOLIPID.....	09.04.04
RAFTS.....	2D CRYSTALS.....	MEMBRANES.....	WK.03.01
RAMAN.....	SCREENING.....	XRD.....	13.11.03
RAMAN SPECTROSCOPY.....	B4C.....	XRD.....	05.01.04
RAP.....	LDLR.....	COMPLEX.....	T-P056
RARE EARTH.....	MAGNETISM.....	SUPERLATTICE.....	AW.02.09
RDX.....	HIGH-PRESSURE.....	SYNCHROTRON.....	05.01.07
RE-CENTERING.....	OFFLINE DATA COLLECTION.....	AUTOMATION.....	T-P176
REACTION PATHWAY.....	CATALYTIC ANTIBODY.....	COCAINE ABUSE.....	S-P079
REACTION REGIOSELECTIVITY.....	PYRROLE.....	AROMATICITY.....	T-P175
REACTIVE CENTER LOOP.....	SERPIN.....	INHIBITORY MECHANISM.....	M-P200
REACTIVE OXYGEN SPECIES.....	BARREL.....	PROLINE DEHYDROGENASE.....	01.01.04
REACTIVITY.....	CRYSTAL ENGINEERING.....	POLYMORPHISM.....	10.03.19
REAL-TIME.....	NEUTRON.....	DIFFRACTOMETER.....	13.09.02
REARRANGEMENT.....	ROTAVIRUS.....	VP5* ANTIGEN DOMAIN.....	T-P061
RECEPTOR.....	IL-13.....	ANTIBODY.....	T-P079
RECEPTOR.....	SIGNALING.....	TUMORIGENESIS.....	S-P125

# Keyword Index

RECEPTOR BINDING .....	PORE-FORMING TOXIN .....	GPI ANCHOR .....	M-P126
REDOX .....	LACCASSE .....		T-P082
REDOX CHEMISTRY .....	INTEGRAL MEMBRANE PROTEIN .....	PROTEIN MOBILITY .....	T-P205
REDOX ENZYME .....	SINGLE CRYSTAL MICROSPECTROPHOTOMETRY .....	QUINOPROTEIN .....	M-P138
REDOX ENZYMES .....	SINGLE CRYSTAL SPECTROSCOPY .....	TIME-RESOLVED CRYSTALLOGRAPHY .....	AW.03.01
REDUCTASE .....	NADP-DEPENDENT .....	CRYSTAL STRUCTURE .....	S-P137
REDUCTIVE UNFOLDING PATHWAY .....	DISULFIDE BOND .....	X-RAY IRRADIATION .....	T-P021
REFINEMENT .....			01.02.01
REFINEMENT .....	ANISOTROPY .....		01.05.06
REFINEMENT .....	SHELXL .....	DISORDER .....	13.02.03
REFINEMENT METHODS .....	MYOGLOBIN .....	TIME-RESOLVED CRYSTALLOGRAPHY .....	T-P091
REFLECTION .....	INVERSION .....	NEUTRONS .....	AW.02.10
REFLECTIVITY .....	MICROSCOPY .....	MEMBRANE .....	09.04.01
REFLECTOMETRY .....	MULTILAYERS .....	NEUTRON .....	AW.02.01
REINECKE ANION .....	COPPER .....	HETEROMETALLIC COMPLEXES .....	T-P125
RELATIVISTIC REHYBRIDIZATION .....	DIAMOND NUCLEATION .....	CARBON REPELLER .....	M-P096
REMOTE ACCESS .....	AUTOMATION .....	HIGH THROUGHPUT .....	13.07.04
REMOTE ACCESS .....	CORE FACILITY .....	UNDERGRADUATE .....	S-P015
REMOTE ACCESS .....	STARBURST .....	CYBERINSTRUMENTATION .....	13.07.01
REMOTE ACCESS .....	SYNCHROTRON .....	AUTOMATION .....	13.07.09
REMOTE ACCESS .....	UNDULATOR .....	SYNCHROTRON .....	M-P160
REMOTE DATA COLLECTION .....	AUTOMOUNTER, CRYOGENIC .....	SYNCHROTRON RADIATION .....	13.07.06
REMOTE DATA COLLECTION .....	HIGH THROUGHPUT .....	DATABASE .....	T-P172
REMOTE DATA COLLECTION .....	MACROMOLECULAR CRYSTALLO .....	ROBOTICS .....	T-P170
REMOTE DATA COLLECTION .....	SER-CAT .....		13.07.08
REPRESSOR .....	PHEROMONE .....		T-P108
RESOLUTION .....	FOCUSING .....	SMALL-ANGLE SCATTERING .....	S-P025
RESONANT SCATTERING .....	THREE-BEAM DIFFRACTION .....	PHASE DETERMINATION .....	13.11.07
RESORCINARENES .....	SELF-ASSEMBLY .....	SUPRAMOLECULAR .....	10.03.15
RETINOIC ACID .....	CELLULAR RETINOIC ACID BINDIN .....	INTRACELLULAR LIPID BINDING PROTEINS .....	S-P165
REVERSE MONTE CARLO .....	PAIR DISTRIBUTION FUNCTION .....	DYNAMICS .....	13.03.05
RHINOVIRUS .....	RNA .....	POLYMERASE .....	M-P034
RHODANESE HOMOLOGY DOMAIN .....	SULFURTRANSFERASE .....	MYCOBACTERIUM TUBERCULOSIS .....	M-P186
RHODOBACTER SPHAEROIDES .....	MEMBRANE PROTEIN .....	BIOENERGETICS .....	01.04.10
RHODOBACTER SPHAEROIDES (RCSPH) .....	PROTEIN CRYSTALLIZATION .....	LIQUID PHASE .....	T-P195
RHODOBACTER SPHAEROIDES (RCSPH) .....	SPONGE PHASE .....	LIPID PHASE TRANSITIONS .....	01.04.03
RHODOPSIN .....	ANABAENA .....	SENSORY .....	T-P203
RIBONUCLEASE III .....	DSRNA PROCESSING .....	DICER .....	01.01.03
RIBONUCLEOPROTEIN .....	NANOCAPSULE .....	VAULT .....	T-P219
RIBONUCLEOTIDE REDUCTASE .....	DNA REPAIR .....	DEOXYRIBONUCLEOTIDE .....	S-P119
RIBOSOME .....	CRYSTAL .....	STRUCTURE .....	M-P146
RIBOSOME .....	TRANSLOCATION .....	ANTIBIOTICS .....	01.03.01
RIESKE DIOXYGENASE .....			AW.03.03
RIETVELD .....	TETRAFLUOROBORATE .....	POWDER .....	S-P045
RIGID BODY REFINEMENT .....	AB INITIO METHODS .....	SMALL-ANGLE SCATTERING .....	09.02.01
RMC .....	NEGATIVE THERMAL EXPANSION .....	NEUTRON TOTAL SCATTERING .....	13.03.02
RNA .....	MEOMYCIN .....	NEOMYCIN DERIVATIVE .....	04.01.06
RNA .....	POLYMERASE .....	RHINOVIRUS .....	M-P034
RNA EDITING .....	TROPICAL DISEASE .....	TYPE II SECRETION .....	01.05.04
RNA POLYMERASE .....	TRANSCRIPTION .....		01.03.02
RNA PROCESSING .....	CSTF .....		M-P046
RNA-PROTEIN INTERACTIONS .....	AMINOACYL-TRNA SYNTHETASES .....	TRNA .....	M-P044
RNASE III .....	NUCLEASE .....		T-P036
ROBOT .....	AUTOMATION .....	CRYSTALLIZATION .....	M-P072
ROBOTIC CRYSTAL HARVESTING .....	CRYSTAL MOUNTING .....	CRYSTAL HARVESTING .....	13.06.07
ROBOTIC CRYSTALLIZATION .....	PROTEIN PRECIPITATION POINT .....		T-P002
ROBOTICS .....	REMOTE DATA COLLECTION .....	MACROMOLECULAR CRYSTALLOGRAPHY .....	T-P170
ROBOTICS .....	SPARSE-MATRIX APPROACH .....		T-P018
ROTAVIRUS .....	VP5* ANTIGEN DOMAIN .....	REARRANGEMENT .....	T-P061
RRNA MODIFICATION .....	PSEUDOURIDINE SYNTHASE .....		T-P120
S-ADENOSYLMETHIONINE SYNTHETA .....	CATALYTIC MECHANISM .....	SAM SYNTHETASE .....	S-P173
S100A4 .....	CALCIUM -BOUND STRUCTURE .....	METASTASIS .....	T-P084
SACCHAROMYCES CEREVISIAE .....	SACCHAROPINE REDUCTASE .....	ALPHA-AMINOADIPATE PATHWAY .....	M-P184
SACCHAROPINE REDUCTASE .....	ALPHA-AMINOADIPATE PATHWAY .....	SACCHAROMYCES CEREVISIAE .....	M-P184

# Keyword Index

SAD.....	PHASING.....	CHROMIUM.....	S-P199
SAD.....	STRATEGY.....	MAD.....	T-P042
SAD.....	UNKNOWN FUNCTION.....	APOLIPOPROTEIN A-I.....	T-P122
SAD PHASING.....	HOST-PATHOGEN INTERACTION.....	PLANT DISEASE RESISTANCE.....	01.07.05
SAD PHASING.....	IODINE DERIVATIVE.....	VAPORIZING IODINE LABELING.....	S-P109
SALACIA CHINENSIS LINN.....	SUPRAMOLECULAR STRUCTURE.....	CARBONYL-ETHER INTERACTION.....	10.02.08
SALMONELLA TYPHIMURIUM.....	HEXAMER.....	STRUCTURAL GENOMICS.....	T-P110
SAM RADICAL.....	PYRUVATE-FORMATE LYASE ACTIV.....	PROTEIN CRYSTAL STRUCTURE.....	M-P166
SAM SYNTHETASE.....	S-ADENOSYLMETHIONINE SYNTH.....	CATALYTIC MECHANISM.....	S-P173
SANS.....	INSTRUMENTATION.....	SMALL ANGLE SCATTERING.....	S-P021
SARS.....	PROTEASE.....	PHASING.....	T-P112
SARS CORONAVIRUS.....	STRUCTURE-FUNCTION RELATION.....	NOVEL FOLD.....	01.0108
SARS CORONAVIRUS.....	STRUCTURE-FUNCTION RELATION.....	NOVEL FOLD.....	T-P132
SAXS.....	BEAMLINE.....	PROTEIN CRYSTALLOGRAPHY.....	T-P055
SAXS.....	BILAYER MEMBRANE.....	VESICLE FORMATION.....	T-P003
SAXS.....	CRYSTALLIZATION.....	POLYMER.....	09.03.01
SAXS.....	ELECTRIC FIELD.....	ORIENTATION KINETICS.....	09.03.04
SAXS.....	ENVELOPE.....	PHASING.....	13.08.02
SAXS.....	LIPID MESOPHASE TRANSITIONS.....	PRESSURE JUMP TECHNIQUE.....	09.04.06
SAXS.....	LIPOPROTEIN.....	DIFFUSE SCATTERING.....	13.08.05
SAXS.....	NANOSTAR.....	PROTEIN.....	M-P050
SAXS.....	POLYMER CRYSTALLIZATION.....		13.11.01
SBS.....	CRYSTALLIZATION.....	PLATE.....	S-P217
SCAFFOLD.....	KINASE.....	PYK2.....	M-P030
SCAFFOLDING.....	SH3.....	SIGNALING.....	T-P130
SCALING.....	ABSORPTION CORRECTIONS.....	DATA PROCESSING.....	10.01.05
SCATTERING.....	INTERFACE.....	STRUCTURE.....	T-P007
SCIENTIFIC LAB MANAGEMENT.....	COST ANALYSIS.....	BIOLOGICAL LABS.....	S-P035
SCORING.....	INHIBITOR.....	DOCKING.....	SP01.04
SCREEN DESIGN.....	DATABASE.....	CRYSTALLIZATION.....	13.06.04
SCREENING.....	AUTOMATION.....	CRYSTALLISATION.....	M-P082
SCREENING.....	AUTOMOUNTER.....	MARCOMOLECULAR CRYSTALLOGRAPHY.....	T-P027
SCREENING.....	XRD.....	RAMAN.....	13.11.03
SEC15.....	EXOCYST.....	VESICLE TRAFFICKING.....	S-P161
SECA.....	PROTEIN TRANSLOCATION.....	ATPASE.....	S-P211
SECRETION.....	ATPASE.....	HEXAMER.....	M-P216
SELENADIAZOLES.....	STRUCUTRE OF SELENADIAZOLES.....	1,2,3-SELENADIAZOLES.....	M-P120
SELENIUM SAD.....	DEBLOCKING AMINOPEPTIDASE.....	ASSEMBLY.....	S-P051
SELF RECOGNITION.....	HYDROGEN BONDING.....	SUPRAMOLECULAR CHEMISTRY.....	T-P117
SELF-ASSEMBLED NANOSTRUCTURES.....	SMALL ANGLE SCATTERING.....	AMYLOID PEPTIDES.....	13.11.04
SELF-ASSEMBLY.....	CRYSTAL ENGINEERING.....	COORDINATION.....	10.03.12
SELF-ASSEMBLY.....	PHOTOREACTIONS.....	PHOTOCYRSTALLOGRAPHY.....	10.03.14
SELF-ASSEMBLY.....	SUPRAMOLECULAR.....	RESORCINARENES.....	10.03.15
SEMI-AUTOMATIC SOLUTION.....	HKL-2000-PH.....	DIFFICULT STRUCTURE.....	T-P223
SEMICONDUCTORS.....	HYDROGEN BONDING.....	CRYSTAL ENGINEERING.....	10.03.17
SENSORY.....	RHODOPSIN.....	ANABAENA.....	T-P203
SER-CAT.....	REMOTE DATA COLLECTION.....		13.07.08
SERPIN.....	INHIBITORY MECHANISM.....	REACTIVE CENTER LOOP.....	M-P200
SERVICE CRYSTALLOGRAPHY.....	STRCTURE DETERMINATION.....	SYNCHROTRON RADIATION.....	T-P013
SESQUITERPENE LACTONES.....	VENEZUELAN ANDES.....	NATURAL PRODUCTS.....	10.02.07
SET.....	TRANSPOSASE.....	METNASE.....	T-P106
SGNH HYDROLASE.....	ACYLTRANSFERASE.....		T-P114
SGX-CAT.....	BEAMLINE.....	AUTOMATION.....	T-P174
SH3.....	SIGNALING.....	SCAFFOLDING.....	T-P130
SHAKE-AND-BAKE.....	SUBSTRUCTURE DETERMINATION.....	DIRECT METHODS.....	T-P105
SHAPE.....	LIGAND.....	FORCE FIELD.....	M-P020
SHARK.....	NEW ANTIGEN RECEPTOR.....	ANTIBODY.....	T-P067
SHEAR-SANS.....	PEO-LAPONITE.....	HYDROGELS.....	09.03.06
SHELXL.....	DISORDER.....	REFINEMENT.....	13.02.03
SHIKIMATE DEHYDROGENASE.....	CRYSTAL STRUCTURE.....		S-P143
SHORT CHAIN OXIDOREDUATSE.....	BIOINFORMATICS.....	FINGERPRINT.....	S-P117
SHORT-RANGE ORDER.....	PHASE TRANSITION.....	DISTORTION.....	M-P106
SHUTTER.....	SYNCHROTRON.....	TIMING.....	T-P031
SIALYLTRANSFERASE.....	CMP.....	TWO ROSSMANN DOMAINS.....	S-P067

# Keyword Index

SIC DIAMOND.....	NANOCRYSTALS.....	NEUTRONS.....	13.03.03
SIGLEC-5.....	INTERDOMAIN DISULFIDE.....	IG-LIKE V- AND C2-SET DOMAINS.....	T-P063
SIGNAL TRANSDUCTION.....	GTPASE.....	CDC42.....	S-P085
SIGNAL TRANSDUCTION.....	MICROHETEROGENEITY.....	PYP.....	13.14.02
SIGNALING.....	SCAFFOLDING.....	SH3.....	T-P130
SIGNALING.....	TUMORIGENESIS.....	RECEPTOR.....	S-P125
SILANE.....	SYNCHROTRON X-RAY DIFFRACT.....	HIGH PRESSURE.....	M-P114
SILICA.....	HIGH-PRESSURE.....	XENON.....	05.01.05
SILVER COMPLEXES.....	COORDINATION CHEMISTRY.....	CARBOYLATES.....	T-P169
SILVER(I).....	N-DONOR LIGANDS.....	CLOSED-SHELL INTERACTIONS.....	10.03.13
SIMULATED ANNEALING.....	POWDER DIFFRACTION.....	VIBRATIONAL CIRCULAR DICHROISM.....	10.02.02
SIMULATION OF TOF DIFFRACTION DA.....	BIOLOGICAL CRYSTALLOGRAPHY.....	NEUTON TOF DIFFRACTOMETER.....	M-P002
SINGLE CRYSTAL.....	CRYSTAL STRUCTURE.....	CHEMICAL REACTION.....	13.14.05
SINGLE CRYSTAL.....	DIFFRACTION.....	NEUTRON.....	T-P011
SINGLE CRYSTAL.....	NEUTRON DIFFRACTION.....	EXPERIMENTAL CHARGE DENSITY.....	S-P027
SINGLE CRYSTAL.....	PULSED NEUTRON DIFFRACTION.....		TR.01.02
SINGLE CRYSTAL MICROSPECTROPHO.....	QUINOPROTEIN.....	REDOX ENZYME.....	M-P138
SINGLE CRYSTAL SPECTROSCOPY.....	TIME-RESOLVED CRYSTALLOGRA.....	REDOX ENZYMES.....	AW.03.01
SINGLE CRYSTAL STRUCTURES.....	TAXOL.....	SOLID STATE.....	10.02.10
SINGLE CRYSTAL X-RDAY DIFFRACTION.....	SYNCHROTRON RADIATION.....	LOW TEMPERATURE.....	T-P023
SIZE-SELECTED CLUSTERS.....	MODEL NANOCATALYSTS.....	GISAXS.....	09.01.04
SMALL ANGLE SCATTERING.....	AMYLOID PEPTIDES.....	SELF-ASSEMBLED NANOSTRUCTURES.....	13.11.04
SMALL ANGLE SCATTERING.....	ISOTOPE LABELING.....	MACROMOLECULAR COMPLEX.....	09.02.07
SMALL ANGLE SCATTERING.....	MICROTUBULE.....	PROTEIN-LIPID COMPLEXES.....	09.02.06
SMALL ANGLE SCATTERING.....	PROTEIN STRUCTURE.....	CANADIAN LIGHT SOURCE.....	13.10.07
SMALL ANGLE SCATTERING.....	SANS.....	INSTRUMENTATION.....	S-P021
SMALL ANGLE X-RAY SCATTERING.....	PROTEINS.....	COLLOIDS.....	09.02.05
SMALL MOLECULE.....	PHASING.....	CENTROSYMMETRIC.....	M-P172
SMALL MOLECULE.....	UNDERGRADUATE RESEARCH.....		10.01.07
SMALL MOLECULE CRYSTALLOGRA.....	CRYSTAL MANIPULATION.....	PROTEIN CRYSTALLOGRAPHY.....	S-P215
SMALL MOLECULES.....	2-MERCAPTOTHIAZOLINE.....	QUANTUM MECHANICS.....	M-P170
SMALL- MOLECULE.....	LOW TEMPERATURE.....	EXTENSIVE DISORDER.....	10.01.03
SMALL-ANGLE SCATTERING.....	NANOCOMPOSITES.....	CARBON NANOTUBES.....	T-P001
SMALL-ANGLE SCATTERING.....	PROTEINS IN SOLUTION.....	STRUCTURE.....	13.13.04
SMALL-ANGLE SCATTERING.....	RESOLUTION.....	FOCUSING.....	S-P025
SMALL-ANGLE SCATTERING.....	RIGID BODY REFINEMENT.....	AB INITIO METHODS.....	09.02.01
SMALL-ANGLE SCATTERING.....	SYSTEMS BIOLOGY.....	NEUTRON SCATTERING.....	09.02.03
SMALL-MOLECULE.....	LOW-TEMPERATURE.....	AROMATICITY.....	T-P167
SMALLPOX.....	DRUG DESIGN.....	BIOTERRORISM.....	T-P098
SMART DATA COLLECTION.....	RADIATION DAMAGE.....	MULTIVARIATE LIKELIHOOD FUNCTIONS.....	01.05.02
SNAKE VENOM.....	PLASMIN.....	TEXTILININ.....	S-P131
SOD1.....	TWINNING.....	PSEUDOSYMMETRY.....	T-P217
SODALITE.....	ALUMINOPHOSPATE.....	ALPO.....	M-P090
SOFTWARE.....	AUTOMATION.....	CRYSTALLIZATION.....	M-P022
SOFTWARE.....	DATA STANDARD.....	DATA STORAGE.....	WK.02.01
SOFTWARE.....	DATABASES.....	PROTEIN CRYSTALLOGRAPHY.....	T-P085
SOFTWARE.....	EDUCATION.....	TUTORIAL.....	S-P019
SOFTWARE.....	GENE SYNTHESIS.....	PROTEIN DESIGN.....	M-P134
SOFTWARE.....	HIGH-PRESSURE.....	CCD-SYSTEM.....	05.01.08
SOFTWARE.....	LAUE.....	NEUTRON.....	M-P014
SOFTWARE.....	MACROMOLECULAR CRYSTALLO.....	AUTOMATED MODEL BUILDING.....	T-P097
SOFTWARE PIPELINE.....	AUTOMATED STRUCTURE DETERMINATION.....	AUTOMATION.....	T-P093
SOLID FORMS.....	6-OH BUSPIRONE.....	CRYSTALS.....	13.05.03
SOLID STATE.....	SINGLE CRYSTAL STRUCTURES.....	TAXOL.....	10.02.10
SOLID STATE POLYMERIZATION.....	POLYDIACETYLENES.....	HOST GEST CHEMISTRY.....	T-P129
SOLID STATE REACTION.....	UNSTABLE STRUCTURE.....	PHOTOCHROMISM.....	T-P153
SOLID STATE SYNTHESIS.....	[2+2]-PHOTODIMERISATION.....	METAL-ORGANIC FRAMEWORKS.....	T-P147
SOLID-STATE COMPOUND.....	FRACTIONAL CRYSTALLIZATION.....	WHOLE-MOLECULE DISORDER.....	13.02.06
SOLUTION STIRRING.....	TEMPERATURE.....	SUPERSATURATION.....	S-P177
SOLVENT NETWORK.....	CARBONIC ANHYDRASE.....	PROTON TRANSFER.....	AW.03.02
SPACE EXPERIMENT.....	MICROGRAVITY CRYSTAL GROWTH.....	HIGH QUALITY PROTEIN CRYSTAL.....	T-P006
SPACE GROUPS.....	HYDROGEN BONDS.....	CRYSTAL ENGINEERING.....	10.03.03
SPALLATION NEUTRON SOURCE.....	HYDROGEN AND HYDRATION.....	NEUTRON PROTEIN CRYSTALLOGRAPHY.....	TR.01.03
SPARSE-MATRIX APPROACH.....	ROBOTICS.....		T-P018

# Keyword Index

SPECIFICITY .....	A. THALIANA.....	NUCLEOSIDASE.....	M-P188
SPECIFICITY .....	KINASE.....	PROTEIN:PROTEIN COMPLEX .....	T-P090
SPECIFICITY .....	THIMET OLIGOPEPTIDASE .....	NEUROLYSIN .....	S-P081
SPECTROPHOTOMETRY .....	SYNCHROTRON RAD INSTRUMEN.....	TIME-RESOLVED CR.....	T-P035
SPHINGOMYELINASE.....	HEMOLYSIS .....	CRYSTAL STRUCTURE .....	M-P124
SPIN ECHO .....	GRAZING INCIDENCE SCATTERING.....		09.01.05
SPONGE PHASE.....	LIPID PHASE TRANSITIONS.....	RHODOBACTER SPHAEROIDES (RCSPH).....	01.04.03
SPORULATION .....	NON-CRYSTALLOGRAPHIC SYMM.....	STRUCTURAL PROTEIN .....	T-P221
SPRING-8.....	AUTOMATED DATA COLLECTION.....	MAIL-IN DATA COLLECTION .....	13.07.07
STABILITY .....	BINDING .....		T-P017
STABILITY .....	CATALYSIS .....	ACYLPHOSPHATASE.....	S-P175
STABILITY .....	DRUG FORM .....	CRYSTALLINE COMPLEX .....	10.03.18
STAPHYLOCOCCUS AUREUS.....	BETA-LACTAM .....	ANTIBIOTIC RESISTANCE.....	M-P152
STARBURSTT .....	CYBERINSTRUMENTATION.....	REMOTE ACCESS.....	13.07.01
STARBURSTT .....	CYBERINSTRUMENTATION.....	TEACHING .....	SP.01.02
STATISTICAL .....	DATA .....	ANALYSIS.....	13.06.05
STATOR ARCHITECTURE.....	A-ATPASE.....	SUBUNIT E .....	T-P189
STE20P .....	KINASE DOMAIN .....	OSR1 .....	T-P102
STRAIN-INDUCED .....	POLY (LACTIC ACID) .....	CRYSTALLISATION.....	09.03.03
STRATEGY.....	MAD.....	SAD.....	T-P042
STRUCUTURE DETERMINATION.....	SYNCHROTRON RADIATION.....	SERVICE CRYSTALLOGRAPHY .....	T-P013
STRUCTURAL .....	ION CHANNEL .....	GATING .....	T-P209
STRUCTURAL BIOLOGY.....	BIOLOGICAL MACROMOLECULE.....	PROTEIN CRYSTALLOGRAPHY.....	M-P036
STRUCTURAL BIOLOGY.....	NEUTRON DIFFRACTION .....	SUPRAMOLECULAR CHEMISTRY .....	TR.01.04
STRUCTURAL GENOMICS.....	COA-BINDING.....	P. FURIOSUS.....	S-P185
STRUCTURAL GENOMICS.....	EUKARYOTIC PATHOGENS.....	PYRIMIDINE BIOSYNTHESIS .....	T-P071
STRUCTURAL GENOMICS.....	GLYOXYLASE.....	VICINAL OXYGEN CHELATE .....	T-P126
STRUCTURAL GENOMICS.....	HIGH THROUGHPUT.....	AUTOMATION.....	M-P062
STRUCTURAL GENOMICS.....	HIGH THROUGHPUT METHODOLOGIES.....	PROTEOMICS .....	13.06.01
STRUCTURAL GENOMICS.....	HIGH THROUGHPUT METHODS.....	MOLECULAR REPLACEMENT .....	M-P064
STRUCTURAL GENOMICS.....	INFORMATION MANAGEMENT SYSTEM .....	LIMS .....	M-P060
STRUCTURAL GENOMICS.....	NUDIX FAMILY .....		S-P105
STRUCTURAL GENOMICS.....	PHOSPHORYLASE .....	PYROPHOSPHORYLASE.....	13.06.08
STRUCTURAL GENOMICS.....	PROTEIN SURFACE ANALYSIS.....	FUNCTION ANALYSIS.....	S-P219
STRUCTURAL GENOMICS.....	PSI-II .....	PROTEIN TYROSINE PHOSPHATASE .....	T-P144
STRUCTURAL GENOMICS.....	SALMONELLA TYPHIMURIUM.....	HEXAMER.....	T-P110
STRUCTURAL GENOMICS.....	SYNCHROTRON RADIATION.....	TRANSCRIPTIONAL REGULATOR.....	T-P142
STRUCTURAL GENOMICS.....	THERMOTOGA MARITIMA .....	MAD PHASING.....	T-P083
STRUCTURAL GENOMICS.....	TIM BARREL .....	IMIDAZOLONEPROPIONASE .....	T-P081
STRUCTURAL PROTEIN .....	SPORULATION .....	NON-CRYSTALLOGRAPHIC SYMMETRY .....	T-P221
STRUCTURE .....	DYNAMICS.....	POLYMER NANOCOMPOSITES.....	13.11.02
STRUCTURE .....	FATTY ACID SYNTHASE.....	MULTIFUNCTIONAL ENZYME.....	01.03.04
STRUCTURE .....	NAMPT.....	PHOSPHORIBOSYLTRANSFERASE .....	T-P058
STRUCTURE .....	PROTEORHODOPSIN .....	MEMBRANE PROTEIN .....	S-P075
STRUCTURE .....	RIBOSOME .....	CRYSTAL .....	M-P146
STRUCTURE .....	SCATTERING .....	INTERFACE.....	T-P007
STRUCTURE.....	SMALL-ANGLE SCATTERING .....	STRUCTURE IN SOLUTION.....	13.13.04
STRUCTURE BASED DRUG DESIGN.....	PEPTIDE DEFORMYLASE .....	STRUCTURE COMPARISONS.....	M-P028
STRUCTURE COMPARISONS.....	STRUCTURE BASED DRUG DESIGN.....	PEPTIDE DEFORMYLASE.....	M-P028
STRUCTURE DETERMINATION.....	MULTIPLE CONFORMERS .....	AUTOMATED MODEL BUILDING .....	01.02.02
STRUCTURE GEMONICS.....	HTP EXPRESSION, PURIFICATION .....	METHOD DEVELOPMENT.....	13.06.02
STRUCTURE GUIDED DRUG DISCOVERY.....	FRAGMENT BASED DRUG DISCOVE.....	KINASES AND ONCOLOGY.....	AW.01.06
STRUCTURE OF INTERMOLECULAR IN .....	GLYCOLIPID TRANSFER PROTEIN.....	GLYCOSPHINGOLIPIDS .....	T-P094
STRUCTURE REFINEMENT .....	PHENIX.....	MACROMOLECULE.....	01.02.06
STRUCTURE TRANSITION .....	NEUTRON & X-RAY DIFFRACTION.....	MAGNETIC ORDER IN CUFeO2.....	M-P100
STRUCTURE-FUNCTION RELATIONSHIPS.....	METALLOENZYMES.....	ENZYME MECHANISM KINETICS .....	M-P192
STRUCTURE-FUNCTION RELATIONSHIPS.....	NOVEL FOLD.....	SARS CORONAVIRUS.....	01.01.08
STRUCTURE-FUNCTION RELATIONSHIPS.....	NOVEL FOLD.....	SARS CORONAVIRUS.....	T-P132
STRUCTURE-PHYSICAL PROPERTIES .....	CRYSTALLOGRAPHIC MODELLING.....	HIGH-PRESSURE STRUCTURES .....	05.01.02
STRUCUTRE OF SELENADIAZOLES .....	1,2,3-SELENADIAZOLES .....	SELENADIAZOLES.....	M-P120
STUCTURAL GENOMICS.....	TWO-COMPONENT SIGNALING .....	HISTIDINE KINASE .....	M-P054
SUBATOMIC RESOLUTION .....	ENZYMOMOLOGY .....	HELIUM COOLING .....	S-P223
SUBSTRUCTURE DETERMINATION .....	DIRECT METHODS .....	SHAKE-AND-BAKE.....	T-P105
SUBSTRUCTURES .....	COCRYSTAL.....	SUPRAMOLECULAR STRUCTURE .....	T-P139

# Keyword Index

SUBUNIT E.....	STATOR ARCHITECTURE.....	A-ATPASE.....	T-P189
SULFONAMIDE.....	CARBONIC ANHYDRASE.....		S-P007
SULFUR SAD.....	CROSS-LINKED HEME.....	HEME P460.....	T-P048
SULFURTRANSFERASE.....	MYCOBACTERIUM TUBERCULOSIS.....	RHODANESE HOMOLOGY DOMAIN.....	M-P186
SUPERANTIGEN.....	MHC CLASS II.....	COMPLEX STRUCTURE.....	M-P128
SUPERANTIGEN.....	TCR.....	MHC.....	01.06.05
SUPERFAMILY.....	TAUTOMERASE.....	PROTEIN EVOLUTION.....	T-P004
SUPERLATTICE.....	RARE EARTH.....	MAGNETISM.....	AW.02.09
SUPERLATTICES.....	HYBRID MATERIALS.....	CHALCOGENIDE TETRAHEDRAL CLUSTERS.....	13.12.04
SUPERMIRROPOROUS MATERIALS.....	PDF METHOD.....		S-P031
SUPERSATURATION.....	SOLUTION STIRRING.....	TEMPERATURE.....	S-P177
SUPRAMOLECULAR.....			T-P121
SUPRAMOLECULAR.....	MOCN.....	MOLECULAR MAGNETISM.....	T-P151
SUPRAMOLECULAR.....	RESORCINARENES.....	SELF-ASSEMBLY.....	10.03.15
SUPRAMOLECULAR ASSEMBIES.....	CRYSTAL ENGINEERING.....	COORDINATION CHEMISTRY.....	T-P133
SUPRAMOLECULAR ASSEMBLIES.....	PROPARGYLIC ALCOHOLS.....	SYNERGY OF INTERACTIONS.....	10.03.04
SUPRAMOLECULAR ASSEMBLY.....	HOST-GUEST.....	FUNCTIONALIZED CAVITANDS.....	10.03.16
SUPRAMOLECULAR CHEMISTRY.....	COCRYSTALS.....	CRYSTAL PACKING TENDENCIES.....	10.03.06
SUPRAMOLECULAR CHEMISTRY.....	SELF RECOGNITION.....	HYDROGEN BONDING.....	T-P117
SUPRAMOLECULAR CHEMISTRY.....	STRUCTURAL BIOLOGY.....	NEUTRON DIFFRACTION.....	TR.01.04
SUPRAMOLECULAR CRYSTALLOGRA.....	CRYSTAL SYNTHESIS.....	INORGANIC SOLID-STATE CHEMISTRY.....	10.03.11
SUPRAMOLECULAR STRUCTURE.....	CARBONYL-ETHER INTERACTION.....	SALACIA CHINENSIS LINN.....	10.02.08
SUPRAMOLECULAR STRUCTURE.....	OCTAETHYLPORPHYRIN.....	HEME SYSTEM.....	T-P141
SUPRAMOLECULAR STRUCTURE.....	ORGANIC-INORGANIC HYBRID.....	HYDROTHERMAL SYNTHESIS.....	M-P162
SUPRAMOLECULAR STRUCTURE.....	SUBSTRUCTURES.....	COCRYSTAL.....	T-P139
SURFACE.....	VIRUSES.....	NANOSCALE.....	13.08.01
SURFACE ENTROPY.....	MUTAGENESIS.....	CRYSTALLIZATION.....	S-P087
SURFACE PLASMON RESONANCE.....	HEPARAN SULFATE.....	CELL SURFACE RETENTION.....	T-P019
SYMMETRIC HOMODIMER.....	CHIP.....	U-BOX LIGASE.....	T-P040
SYNAPTOTAGMIN.....	COPPER BINDING.....	C2A.....	M-P154
SYNCHROTRON.....	ANOMALOUS.....	POWDER.....	M-P098
SYNCHROTRON.....	APS.....	PROTEIN CRYSTALLOGRAPHY.....	T-P039
SYNCHROTRON.....	AUTOMATION.....	REMOTE ACCESS.....	13.07.09
SYNCHROTRON.....	BEAMLINE.....	APS.....	T-P045
SYNCHROTRON.....	BEAMLINE.....	MACROMOLECULAR.....	13.10.01
SYNCHROTRON.....	MACROMOLECULAR.....	CRYSTALLOGRAPHY.....	T-P033
SYNCHROTRON.....	MATERIALS SCIENCE.....	DIFFRACTION.....	13.10.09
SYNCHROTRON.....	PROTEIN CRYSTALLOGRAPHY.....	AUTOMATION.....	13.10.02
SYNCHROTRON.....	RDX.....	HIGH-PRESSURE.....	05.01.07
SYNCHROTRON.....	REMOTE ACCESS.....	UNDULATOR.....	M-P160
SYNCHROTRON.....	TIMING.....	SHUTTER.....	T-P031
SYNCHROTRON.....	X-RAY DIFFRACTION.....	EXTREME CONDITIONS.....	13.10.08
SYNCHROTRON DATA COLLECTION.....	LACTATE DEHYDROGENASE.....	UNDERGRADUATE LABORATORY.....	S-P003
SYNCHROTRON DATA COLLECTION.....	LACTATE DEHYDROGENASE.....	UNDERGRADUATE LABORATORY.....	S-P005
SYNCHROTRON FACILITY.....	MACROMOLECULAR CRYSTALLOG.....	AUTOMATION.....	T-P037
SYNCHROTRON POWDER X-RAY DIFFRACTION.....		HYDROGEN POWDER NEUTRON DIFFRACTION.....	13.01.03
SYNCHROTRON RADIATION.....	BEAMLINE AUTOMATION.....		T-P051
SYNCHROTRON RADIATION.....	EXPLOSIVES.....	HIGH PRESSURE.....	T-P157
SYNCHROTRON RADIATION.....	HIGH ENERGY.....	RADIATION DAMAGE.....	11.01.04
SYNCHROTRON RADIATION.....	LOW TEMPERATURE.....	SINGLE CRYSTAL X-RDAY DIFFRACTION.....	T-P023
SYNCHROTRON RADIATION.....	MACROMOLECULES.....	USER FACILITIES.....	S-P191
SYNCHROTRON RADIATION.....	MICROCRYSTALS.....	BEAM LINE.....	13.15.04
SYNCHROTRON RADIATION.....	REMOTE DATA COLLECTION.....	AUTOMOUNTER, CRYOGENIC.....	13.07.06
SYNCHROTRON RADIATION.....	SERVICE CRYSTALLOGRAPHY.....	STRCUTURE DETERMINATION.....	T-P013
SYNCHROTRON RADIATION.....	TRANSCRIPTIONAL REGULATOR.....	STRUCTURAL GENOMICS.....	T-P142
SYNCHROTRON RADIATION.....	UNDULATOR.....	BEAMLINE.....	T-P025
SYNCHROTRON RADIATION INSTRUM.....	TIME-RESOLVED CRYSTALLOG.....	SPECTROPHOTOMETRY.....	T-P035
SYNCHROTRON SOURCE.....	COHERENCE.....	ERL.....	T-P029
SYNCHROTRON X-RAY.....	CREEP DAMAGE.....	TOMOGRAPHY.....	13.09.06
SYNCHROTRON X-RAY DIFFRACTION.....	HIGH PRESSURE.....	SILANE.....	M-P114
SYNERGY OF INTERACTIONS.....	SUPRAMOLECULAR ASSEMBLIES.....	PROPARGYLIC ALCOHOLS.....	10.03.04
SYNTHERIZING MULTIMETALLIC PERV.....	CORE -SHELL, NANOPARTICLE.....	COLOSSAL MAGNETO RESISTANCE.....	M-P094
SYNTHETIC DBLE-HELIX.....	FOLDING.....	LARGE SMALL-MOLECULE.....	13.05.01
SYSTEMS BIOLOGY.....	NEUTRON SCATTERING.....	SMALL-ANGLE SCATTERING.....	09.02.03

# Keyword Index

T CELL STIMULATION .....	TUMOR ANTIGEN .....	MELANOMA .....	T-P065
TASPASE .....	L-ASPARAGINASE .....	ISOASPARTYL PEPTIDASE .....	01.07.02
TAUTOMERASE .....	PROTEIN EVOLUTION .....	SUPERFAMILY .....	T-P004
TAXOL .....	SOLID STATE .....	SINGLE CRYSTAL STRUCTURES .....	10.02.10
TCR .....	MHC .....	SUPERANTIGEN .....	01.06.05
TDO .....	TRYPTOPHAN .....	2,3-DIOXYGENASE .....	M-P076
TEACHING .....	STARBURST .....	CYBERINSTRUMENTATION .....	SP.01.02
TELOMERASE .....	CHAPERONE .....	TRANSPORT .....	S-P103
TEMPERATURE .....	DIFFRACTION .....	CAPILLARIES .....	S-P053
TEMPERATURE .....	SUPERSATURATION .....	SOLUTION STIRRING .....	S-P177
TETRAFLUOROBORATE .....	POWDER .....	RIETVELD .....	S-P045
TETRANUCLEAR COMPLEX .....	POLYFUNCTIONAL .....		T-P149
TETRAZOLO[1,5-A]-1,3,5-TRIAZINES .....	X-RAY STRUCTURE .....	1,3,5-TRIAZINE DERIVATIVES .....	10.02.09
TEXTILININ .....	SNAKE VENOM .....	PLASMIN .....	S-P131
THERMAL IMAGING .....	BEAM HEATING .....	CRYOCOOLING .....	11.01.01
THERMAL STRESS AND TEMPERATURE .....	NEUTRON DIFFRACTION .....	IN-SITU TIME-RESOLVED TEST .....	13.09.07
THERMODECOMPOSITION .....	NANOPARTICLE .....	METAL OXIDE .....	13.15.02
THERMOELECTRIC MATERIALS .....	IN2SN4BI6SE16 .....	CHALCOGENIDE .....	M-P102
THERMOPHILIC HEMOPROTEINS .....	P450 STRUCTURE .....	X-RAY STRUCTURE DETERMINATION .....	M-P208
THERMOSTABILITY .....	FERRITIN .....	IRON STORAGE .....	01.07.01
THERMOTOGA MARITIMA .....	MAD PHASING .....	STRUCTURAL GENOMICS .....	T-P083
THIAMIN BIOSYNTHESIS .....	THIAZOLE .....	YEAST .....	01.01.05
THIAMIN DIPHOSPHATE .....	PYRUVATE DEHYDROGENASE .....	E1 COMPONENT .....	T-P020
THIAZOLE .....	YEAST .....	THIAMIN BIOSYNTHESIS .....	01.01.05
THIMET OLIGOPEPTIDASE .....	NEUROLYSIN .....	SPECIFICITY .....	S-P081
THIOESTERASE .....	CHAIN-LENGTH SELECTIVITY .....	FATTY ACID SYNTHASE .....	S-P069
THIOREDOXIN .....	ELECTRON TRANSFER .....	FERREDOXIN .....	01.01.01
THIOSEMICABAZONES .....	H-BONDING .....	PI-PI INTERACTIONS .....	T-P109
THREE-BEAM DIFFRACTION .....	PHASE DETERMINATION .....	RESONANT SCATTERING .....	13.11.07
THROMBOCYTOPENIA .....	PLATELET .....	INTEGRIN .....	T-P034
THYMIDYLATE .....	HYDROPHOBIC CORE .....	MUTATIONAL STUDY .....	M-P074
TIM BARREL .....	IMIDAZOLONEPROPIONASE .....	STRUCTURAL GENOMICS .....	T-P081
TIM, CBS .....	IMP DEHYDROGENASE .....	BACILLUS ANTHRACIS .....	M-P202
TIME OR SPACE .....	MOSAICS .....	DISORDER .....	13.02.09
TIME RESOLVED .....	IN-SITU .....	TRANSFORMATION .....	13.09.08
TIME RESOLVED .....	X-RAY DETECTOR .....	HIGH SPEED .....	T-P156
TIME-DEPENDENCE .....	MATERIALS .....	NEUTRON SCATTERING .....	13.09.01
TIME-OF-FLIGHT NEUTRONS .....	D-XYLOSE ISOMERASE .....	NEUTRON DIFFRACTION .....	TR.01.08
TIME-RESOLVED .....	LAUE .....	UNDULATOR .....	T-P049
TIME-RESOLVED CRYSTALLOGRAPHY .....	PROTEIN ALLOSTERY .....		13.08.03
TIME-RESOLVED CRYSTALLOGRAPHY .....	REDOX ENZYMES .....	SINGLE CRYSTAL SPECTROSCOPY .....	AW.03.01
TIME-RESOLVED CRYSTALLOGRAPHY .....	REFINEMENT METHODS .....	MYOGLOBIN .....	T-P091
TIME-RESOLVED CRYSTALLOGRAPHY .....	SPECTROPHOTOMETRY .....	SYNCHROTRON RADIATION INSTRUMENTAT .....	T-P035
TIME-RESOLVED STUDIES .....	POWDER DIFFRACTION .....	NEUTRON SCATTERING .....	13.09.04
TIMING .....	SHUTTER .....	SYNCHROTRON .....	T-P031
TOLL-LIKE RECEPTOR .....	INNATE IMMUNITY .....	LEUCINE RICH REPEAT .....	T-P069
TOLL-LIKE RECEPTOR .....	LEUCINE RICH REPEAT .....	INNATE IMMUNITY .....	01.06.02
TOMOGRAPHY .....	SYNCHROTRON X-RAY .....	CREEP DAMAGE .....	13.09.06
TONB .....	OUTER MEMBRANE .....	IRON .....	T-P207
TOPOLOGICAL-ANALYSIS .....	CHARGE-DENSITY .....	HIGH-PRESSURE-STRUCTURE .....	10.01.06
TOPRIM DOMAIN .....	METAL BINDING .....	MCSG .....	M-P070
TOTAL SCATTERING .....	COORDINATION COMPLEX .....		13.05.04
TOTAL SCATTERING .....	DISORDER .....	PAIR DISTRIBUTION FUNCTION .....	13.03.01
TOXIN .....	PATHOGEN .....	MEMBRANE PROTEINS .....	M-P168
TPR DOMAIN .....	PSEUDOMAS AEURGINOSA .....	TYPE 4 PILUS .....	S-P155
TRAINING .....	POLICY .....	EDUCATION .....	SP.01.01
TRANS-MEMBRANE SIGNALING .....	PHOQ/PHOP .....	TWO-COMPONENT SYSTEM .....	01.01.07
TRANSCRIPTION .....	MACROMOLECULAR COMPLEXES .....	CRYO-ELECTRON MICROSCOPY .....	01.03.03
TRANSCRIPTION .....	RNA POLYMERASE .....		01.03.02
TRANSCRIPTION FACTOR .....	DIMERIZATION .....	PROTEIN-PROTEIN INTERACTIONS .....	M-P214
TRANSCRIPTION FACTOR .....	ONCOGENE .....		13.10.05
TRANSCRIPTIONAL REGULATOR .....	STRUCTURAL GENOMICS .....	SYNCHROTRON RADIATION .....	T-P142
TRANSDUCER .....	PHOTORECEPTOR .....	INTEGRAL MEMBRANE PROTEIN .....	01.04.07
TRANSFORMATION .....	TIME RESOLVED .....	IN-SITU .....	13.09.08

# Keyword Index

TRANSHYDROGENASE.....	MEMBRANE PROTEIN .....	CRYSTALLIZATION.....	01.04.08
TRANSLATION SYNTHESIS.....	POLYMERASE .....	CLAMP LOADING.....	S-P189
TRANSLOCATION.....	ANTIBIOTICS.....	RIBOSOME .....	01.03.01
TRANSPORT.....	TELOMERASE.....	CHAPERONE .....	S-P103
TRANSPOSASE.....	METNASE.....	SET.....	T-P106
TREHALOSE 6-PHOSPHATE PHOSPHATA.....	HAD HYDROLASE FAMILY .....	DUAL WAVELENGTH ANOMALOUS DIFFR.....	M-P222
TRIOSEPHOSPHATE ISOMERASE .....	HELICOBACTER PYLORI.....		S-P135
TRNA.....	RNA-PROTEIN INTERACTIONS .....	AMINOACYL-TRNA SYNTHETASES .....	M-P044
TROPICAL DISEASE.....	TYPE II SECRETION .....	RNA EDITING .....	01.05.04
TRP REPRESSOR.....	FLAVOPROTEIN.....		T-P116
TRYPSIN.....	CALCIUM ACTIVATION .....	PEP CK.....	T-P080
TRYPTOPHAN .....	2,3-DIOXYGENASE.....	TDO.....	M-P076
TUBERCULOSIS .....	HELIX-BUNDLE.....	ADENOSYLCOBALAMIN.....	M-P198
TUMOR ANTIGEN.....	MELANOMA.....	T CELL STIMULATION .....	T-P065
TUMORIGENESIS.....	RECEPTOR.....	SIGNALING.....	S-P125
TUTORIAL.....	SOFTWARE.....	EDUCATION.....	S-P019
TUTTON SALT .....	ESEEM.....	COPPER .....	T-P179
TWIN .....	DISORDER .....	GEORGE LUCAS.....	13.14.03
TWIN .....	PHASE TRANSITION .....	DISORDER.....	S-P029
TWINNING .....	DISORDER .....	PHASE TRANSITION .....	13.14.04
TWINNING .....	PORPHYRIN.....		10.01.04
TWINNING.....	PSEUDOSYMMETRY.....	DIFFICULT STRUCTURES .....	01.05.01
TWINNING.....	PSEUDOSYMMETRY.....	SOD1.....	T-P217
TWO ROSSMANN DOMAINS.....	SIALYLTRANSFERASE.....	CMP.....	S-P067
TWO-COMPONENT SIGNALING .....	HISTIDINE KINASE.....	STRUCTURAL GENOMICS .....	M-P054
TWO-COMPONENT SYSTEM.....	TRANS-MEMBRANE SIGNALING .....	PHOQ/PHOP.....	01.01.07
TWO-PARTNER SECRETION .....	OUTER MEMBRANE CRYSTALLIZA.....	BACTERIAL PATHOGENESIS .....	S-P111
TYPE 4 PILUS.....	TPR DOMAIN.....	PSEUDOMAS AEURGINOSA .....	S-P155
TYPE II SECRETION .....	RNA EDITING .....	TROPICAL DISEASE.....	01.05.04
TYPE-1 COPPER.....	AXIAL METHIONINE .....	COPPER NITRITE REDUCTASE .....	M-P204
U-BOX LIGASE .....	SYMMETRIC HOMODIMER.....	CHIP.....	T-P040
UBC13.....	E2.....	UBIQUITIN .....	T-P052
UBIQUITIN .....	UBC13.....	E2.....	T-P052
UBIQUITINATION .....	DEUBIQUITINATION.....	COMPLEX.....	T-P026
ULTRAHIGH RESOLUTION.....	DIHYDROFOLATE REDUCTASE .....	NEUTRON DIFFRACTION .....	TR.01.09
UNDERGRADUATE.....	REMOTE ACCESS.....	CORE FACILITY.....	S-P015
UNDERGRADUATE LABORATORY .....	SYNCHROTRON DATA COLLECTION.....	LACTATE DEHYDROGENASE .....	S-P003
UNDERGRADUATE LABORATORY .....	SYNCHROTRON DATA COLLECTION.....	LACTATE DEHYDROGENASE .....	S-P005
UNDERGRADUATE RESEARCH.....	SMALL MOLECULE.....		10.01.07
UNDULATOR.....	BEAMLINE .....	SYNCHROTRON RADIATION .....	T-P025
UNDULATOR.....	SYNCHROTRON .....	REMOTE ACCESS.....	M-P160
UNDULATOR.....	TIME-RESOLVED.....	LAUE.....	T-P049
UNDULATOR.....	X-RAY SOURCE .....	CRYSTALLOGRAPHY.....	T-P041
UNKNOWN FUNCTION.....	APOLIPOPROTEIN A-I.....	SAD.....	T-P122
UNSTABLE STRUCTURE.....	PHOTOCHROMISM.....	SOLID STATE REACTION .....	T-P153
UNUSUAL STOICHIOMETRY.....	CRYSTALLIZATION.....	HYPERACIDS .....	04.01.01
UROKINASE.....	INHIBITOR.....	CYCLIC PEPTIDE .....	S-P071
UROKINASE RECEPTOR .....	AMINO TERMINAL FRAGMENT.....	ANTI-UPAR ANTIBODY .....	T-P213
USER FACILITIES.....	SYNCHROTRON RADIATION.....	MACROMOLECULES .....	S-P191
$\nu_{\lambda}$ LIGHT CHAIN.....	EBOLA VIRUS.....	NEUTRALIZING ANTIBODY .....	T-P059
VACCINE.....	IMMUNITY .....	HOOKWORM.....	T-P057
VALIDATION.....	DICTIONARY .....	CIF.....	S-P083
VAN DER WAALS FORCES.....	ION-LIPID INTERACTIONS .....	MEMBRANE STRUCTURE.....	09.04.03
VAPORIZING IODINE LABELING .....	SAD PHASING .....	IODINE DERIVATIVE.....	S-P109
VAULT.....	RIBONUCLEOPROTEIN.....	NANOCAPSULE.....	T-P219
VENEZUELAN ANDES .....	NATURAL PRODUCTS .....	SESQUITERPENE LACTONES.....	10.02.07
VESICLE FORMATION.....	SAXS.....	BILAYER MEMBRANE.....	T-P003
VESICLE TRAFFICKING .....	SEC15.....	EXOCYST.....	S-P161
VIBRATIONAL CIRCULAR DICHROISM .....	SIMMULATED ANNEALING .....	POWDER DIFFRACTION.....	10.02.02
VICINAL OXYGEN CHELATE .....	STRUCTURAL GENOMICS.....	GLYOXYLASE.....	T-P126
VILLIN.....	KINETICS .....	PROTEIN FOLDING .....	AW.03.05
VIRAL ANTIGEN.....	IMMUNE SYSTEM .....	NATURAL KILLER CELLS.....	01.06.08
VIRIAL COEFFICIENT.....	CRYSTALLIZATION.....	MEMBRANE PROTEIN.....	T-P199
VIRUS ASSEMBLY .....	FLOCK HOUSE VIRUS .....	VIRUS MATURATION .....	S-P213

# Keyword Index

VIRUS ASSEMBLY .....	VIRUS PARTICLE DYNAMICS.....	VIRUS MATURATION .....	09.02.04
VIRUS MATURATION .....	VIRUS ASSEMBLY .....	FLOCK HOUSE VIRUS.....	S-P213
VIRUS MATURATION .....	VIRUS ASSEMBLY .....	VIRUS PARTICLE DYNAMICS .....	09.02.04
VIRUS PARTICLE DYNAMICS.....	VIRUS MATURATION.....	VIRUS ASSEMBLY .....	09.02.04
VIRUS STRUCTURE .....	ELECTRON MICROSCOPY .....		13.08.07
VIRUSES.....	NANOCSCALE.....	SURFACE .....	13.08.01
VITRIFICATION .....	PLUNGE COOLING.....	FLASH FREEZING.....	T-P047
VP5* ANTIGEN DOMAIN.....	REARRANGEMENT.....	ROTAVIRUS.....	T-P061
WHOLE MOLECULE DISORDER.....	ADVANCED REFINEMENT.....	PROBLEM STRUCTURES .....	13.02.02
WHOLE-MOLECULE DISORDER.....	IMPURITIES.....	DISORDER.....	13.02.01
WHOLE-MOLECULE DISORDER.....	SOLID-STATE COMPOUND.....	FRACTIONAL CRYSTALLIZATION .....	13.02.06
WIDE OPEN HIV-1 PROTEASE.....	DRUG DESIGN.....	PROTEASE INHIBITORS.....	M-P196
WINGED HELIX.....	FORKHEAD PROTEIN.....	INTERLEUKIN ENHANCER BINDING FACTOR.....	01.07.03
WXR.....	FE-SEM.....	CYCLODEXTRIN.....	T-P137
X-RAY CRYSTALLOGRAPHY.....	AQUAPORIN.....	MEMBRANE PROTEIN.....	01.04.01
X-RAY CRYSTALLOGRAPHY.....	BEALMINE.....	AUTOMATION TECHNIQUES.....	T-P043
X-RAY CRYSTALLOGRAPHY.....	BOWL-SHAPED POLYARENES .....	DISORDER.....	13.02.04
X-RAY CRYSTALLOGRAPHY.....	DITOPIC LIGANDS.....	COCRYSTALLIZATION.....	T-P135
X-RAY CRYSTALLOGRAPHY.....	GREEN FLUORESCENT PROTEIN.....	FUSION PROTEIN.....	T-P187
X-RAY DETECTOR.....	HIGH SPEED.....	TIME RESOLVED.....	T-P156
X-RAY DIFFRACTION.....	EXTREME CONDITIONS.....	SYNCHROTRON.....	13.10.08
X-RAY IRRADIATION.....	REDUCTIVE UNFOLDING PATHWAY.....	DISULFIDE BOND.....	T-P021
X-RAY MICROSCOPY.....	COHERENT DIFFRACTION IMAGING.....		13.08.04
X-RAY PHOTON CORRELATION SPECTROSCOPY.....		DETECTOR . CCD.....	T-P158
X-RAY SCATTERING.....	DNA.....	PROTEINS.....	09.02.02
X-RAY SMALL ANGLE SCATTERING.....	ANTICORROSION .....	NEUTRON REFLECTIVITY .....	13.11.05
X-RAY SOURCE.....	CRYSTALLOGRAPHY .....	UNDULATOR.....	T-P041
X-RAY STRUCTURE.....	1,3,5-TRIAZINE DERIVATIVES.....	TETRAZOLO[1,5-A]-1,3,5-TRIAZINES.....	10.02.09
X-RAY STRUCTURE.....	PCK.....	GTP-DEPENDENT .....	T-P054
X-RAY STRUCTURE DETERMINATION.....	THERMOPHILIC HEMOPROTEINS .....	P450 STRUCTURE .....	M-P208
X-RAY SUBATOMIC RESOLUTION .....	ENZYMOLGY.....	NEUTRON DIFFRACTION.....	TR.01.07
X-RAY-DIFFRACTION.....	CHARGE-DENSITY .....	ELECTROSTATIC-POTENTIAL.....	T-P171
XANTHOMONAS AXONOPODIS PV. CITRI.....	HYPOTHETICAL PROTEIN.....	YAEQ.....	01.07.04
XENON .....	SILICA.....	HIGH-PRESSURE.....	05.01.05
XML.....	IMGCIF.....	NEXUS.....	M-P156
XPB.....	HELICASE.....	DAMAGE DNA.....	T-P138
XRD .....	RAMAN .....	SCREENING.....	13.11.03
XRD .....	RAMAN SPECTROSCOPY.....	B4C.....	05.01.04
YAEQ.....	XANTHOMONAS AXONOPODIS PV. ...	HYPOTHETICAL PROTEIN .....	01.07.04
YEAST.....	THIAMIN BIOSYNTHESIS .....	THIAZOLE .....	01.01.05
ZINC ENZYME .....	BICARBONATE .....	CARBONIC ANHYDRASE.....	M-P122
ZINC PHOSPHITE .....	METAL ORGANIC FRAMEWORK .....	HISTIDINE.....	T-P183
[2+2]-PHOTODIMERISATION.....	METAL-ORGANIC FRAMEWORKS .....	SOLID STATE SYNTHESIS.....	T-P147

## 01.01 New Structures

**01.01.01 Catch the Precious Moments of Reduction of Disulfide by FeS Cluster: Structures of Ferredoxin:Thioredoxin Reductase at Different Intermediate States.** Shaodong Dai, Howard Hughes Medical Inst., Integrated Dept. of Immunology, National Jewish Medical and Research Ctr., Denver, CO 80206.

The ferredoxin:thioredoxin reductase (FTR) belongs to a novel family of disulfide reductases. It uniquely utilizes a [4Fe-4S] cluster to catalyze the reduction of active-site disulfide bonds of thioredoxins. This enables the photosynthetic organisms to switch between anabolic and catabolic pathways to prevent futile cycling. We have solved the crystal structures of NEM modified FTR, which is an analog of the one-electron-reduced reaction intermediate, and FTR in a two-electron-reduced state to 1.7 and 1.9 Å resolution respectively. The NEM-FTR structure for the first time reveals that the [4Fe-4S] cluster is coordinated by five cysteine ligands and the less accessible active-site cysteine 87 is ligated to the unique Fe of the [4Fe-4S] center, which explains the reason why the redox potential of NEM-FTR comparing with resting FTR is decreased more than 650 mV. We also determined the structures of FTR complexed with its electron transfer partners, thioredoxin and ferredoxin. The complex between ferredoxin and FTR positions the [2Fe-2S] cluster of ferredoxin suitably for electron transfer to the [4Fe-4S] center of FTR. The structure of FTR and thioredoxin complex elucidates molecular interaction between these two proteins and demonstrates the changes upon formation of intermolecular disulfide bond. Based on the structural information together with spectroscopic data, a novel reaction mechanism is proposed.

**01.01.02 Enzyme Flexibility is the Key to Cyclizing a Linear Tetrapyrrole.** Heidi L. Schubert, John D. Phillips, Christopher P. Hill, Dept. of Biochemistry, Univ. of Utah, Salt Lake City, 84112.

Uroporphyrinogen III synthase, U3S, the fourth enzyme in the porphyrin biosynthetic pathway, catalyzes cyclization of the linear tetrapyrrole, hydroxymethylbilane, to the macrocyclic uroporphyrinogen III, which is used in several different pathways to form heme, siroheme, chlorophyll, F<sub>430</sub>, and vitamin B<sub>12</sub>. U3S activity is essential in all organisms, and decreased activity in humans leads to the autosomal recessive disorder congenital erythropoietic porphyria. We have solved nine unique apo-structures and two product-bound complexes of U3S (two human structures and nine from the



*Thermus thermophilus* HB8 sequence) at 1.6-2.4 Å resolutions. The proteins' two domains are connected by a non-conserved β-ladder which enables a large degree of conformational flexibility. The highly complex catalytic mechanism requires multiple nucleophilic attacks to initiate hydroxyl loss, C-C bond formation followed by an additional C-C bond breakage and subsequent formation. Very few conserved amino acids flank the active site, and the two invariant residues are distant from the uroporphyrinogen III product suggesting that the linear tetrapyrrole substrate may be recognized by an alternate region of the active site prior to cyclization.

**01.01.03 The Mechanism of Double-Stranded RNA Processing by Ribonuclease III: How Dicer Dices.** X. Ji, J.H. Gan, J.E. Tropea, B.P. Austin, D.L. Court, D.S. Waugh, Center for Cancer Research, National Cancer Inst., NIH, Frederick, MD 21702.

Members of the Ribonuclease III (RNase III) family are double-stranded (ds) RNA-specific endoribonucleases, characterized by a

signature motif in their active centers and a two-base 3' overhang in their products. While Dicer, which produces small interfering RNAs, is currently the focus of intense interest, the structurally simpler bacterial RNase III serves as a paradigm for the entire family. Recently, we reported the crystal structure of RNase III in complex with product of RNA processing, the first catalytic complex observed for the RNase III family (Gan, Tropea, Austin, Court, Waugh, and Ji, *Cell* 124:355-366). The structure reveals a wealth of information about the mechanism of dsRNA hydrolysis which can be extrapolated to other RNase III family members. Here, we present novel structural data demonstrating the involvement of two metal ions in catalysis. In light of the crystal structure of Dicer from *Giardia intestinalis* (MacRae, Zhou, Li, Repic, Brooks, Cande, Adams, and Doudna, *Science* 311:195-198) and that of a PAZ domain in complex with dsRNA (Ma, Ye, and Patel, *Nature* 429:318-322), the catalytic mechanism of Dicer is being elucidated.

**01.01.04 First Structure of a Monofunctional Proline Dehydrogenase Involved in Reactive Oxygen Species Generation.** Tommi A. White, Navasona Krishnan, Donald F. Becker, John J. Tanner, Depts. of Biochemistry and Chemistry, Univ. of Missouri-Columbia, Columbia, MO 65211.

Nature recycles proline by converting it to glutamate. This 4-electron oxidation process is catalyzed by the sequential actions of two enzymes, the flavoprotein proline dehydrogenase (PRODH) and the NAD-dependent enzyme Δ<sup>1</sup>-pyrroline-5-carboxylate dehydrogenase. Human PRODH is part of the p53 signaling pathway and up-regulation of PRODH in lung, renal, and colon carcinoma cells has been shown to generate reactive oxygen species (ROS) and induce cell death by apoptosis. Also, mutations in PRODH have been linked to increased schizophrenia susceptibility. The molecular mechanism of ROS generation by PRODH and the molecular consequences of schizophrenia-linked mutations have been poorly understood due to a lack of biochemical and structural information for human PRODH, which is a mitochondrial inner membrane protein. We used bioinformatics analysis to show that PRODH homologs exist in Gram-positive bacteria and then targeted PRODH from *Thermus thermophilus* (TtPRODH) for structure determination and biochemical study. TtPRODH was crystallized in the presence of MPD and the detergent n-octyl β-D-glucopyranoside. The structure was solved to 2.0 Å resolution using SAD phasing from a selenomethionyl derivative combined with two-fold NCS averaging. The structure reveals a unique β<sub>8</sub>α<sub>8</sub> barrel with the FAD bound at the carboxyl terminal end of the strands of the barrel. Unexpectedly, the FAD isoalloxazine is highly solvent exposed, which contrasts the highly buried FAD bound to PRODH domain of bifunctional Proline Utilization A (PutA). Biochemical studies showed that TtPRODH, like human PRODH, generates proline-dependent ROS. Our structure suggests that the solvent exposed active site of TtPRODH underlies the observed ROS production by this enzyme.

**01.01.05 Structural Insights into the Function of the Thiamin Biosynthetic Enzyme Thi4 from *Saccharomyces cerevisiae*.** C.T. Jurgenson, A. Chatterjee, T.P. Begley, S.E. Ealick, Dept. of Chemistry and Chemical Biology, Baker Lab, Cornell Univ., Ithaca, NY 14853.

The structure of thiazole synthase (Thi4) from *Saccharomyces cerevisiae* has been solved by molecular replacement to 1.8 Å resolution. Thi4 exists as an octamer with one dimer in the asymmetric unit. The structure has the bound molecule adenosine diphosphate 5-(β-ethyl)-4-methyl-thiazole-2-carboxylic acid (AHZ), which has been characterized by NMR and ESI-MS. The overall fold resembles that

of a flavoenzyme and displays a characteristic dinucleotide binding domain, suggesting that a dinucleotide precursor such as NAD<sup>+</sup> or FAD is the substrate for this enzyme. A cis-proline (Pro121) is located after the second  $\beta$ -strand of the dinucleotide binding fold and is believed to be involved in release of the small molecule for further catalysis upon isomerization through a cyclophilin known to bind to Thi4. The product that is present when Thi4 is overexpressed in bacteria and has been shown to react with 4-amino-5-hydroxymethyl-2-methylpyrimidine (HMP-PP) through the enzyme Thi6 to give thiamin phosphate. The evidence presented here allows for the unequivocal assignment of Thi4 as being responsible for thiazole biosynthesis in yeast, as well as the reaction pathway utilized in yeast to biosynthesize thiamin phosphate.

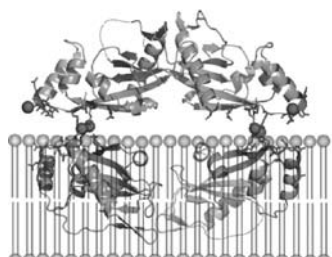
**01.01.06 Crystal Structures of Catalytic Complexes of the Oxidative DNA/RNA Repair Enzyme AlkB.** B. Yu, J.F. Hunt, Dept. of Biological Sciences, Columbia Univ., New York, NY 10027.

The most widely used chemotherapeutic drugs for the treatment of cancer are alkylating agents that create DNA lesions resulting in cell death. However, the efficacy of these agents is limited by their cytotoxicity to healthy tissues, and a number of serious side-effects are associated with their use. While endogenous DNA repair mechanisms help protect healthy cells, they also lead to drug resistance. AlkB is a protein whose role in DNA repair has only recently been elucidated. Identified as a member of the 2-oxoglutarate-Fe(II)-dependent digoxylase superfamily, AlkB directly converts Sn2-alkylated DNA and RNA bases back into their original form. We have determined crystal structures of substrate and product complexes of *E. coli* AlkB at resolutions from 1.5 to 2.3 Å. Whereas the dioxygenase core matches that in other superfamily members, a unique subdomain holds methylated trinucleotide substrates into the active site through contacts to the polynucleotide backbone. Exposing crystals of the anaerobic Michaelis complex to air yields slow but substantial oxidation of 2-oxoglutarate that is inefficiently coupled to nucleotide oxidation. Ongoing work describing the binding of different nucleotide substrates will be presented.



**01.01.07 Crystal Structures of the PhoQ Sensor Domain Suggest a Novel Mechanism for Signal Transduction Across Cell Membranes.** U.S. Cho, M. W. Bader, M.F. Amaya, M.E. Daley, R.E. Klevit, S.I. Miller, W. Xu, Dept. of Biological Structure, Microbiology, Biochemistry, Medicine and Genome Sciences, Univ. of Washington, Seattle, WA 98195.

Many bacterial histidine kinases respond to environmental stimuli by transducing a signal from an extracytosolic domain to a cytosolic catalytic domain. PhoQ is a transmembrane sensor histidine kinase that functions to promote bacterial virulence for animals and plants by regulating resistance to antimicrobial peptides. PhoQ is repressed by divalent cations and activated by antimicrobial peptides. The crystal structure of *Salmonella* PhoQ sensor domain, in the Ca<sup>2+</sup>-bound state, reveals a highly negatively charged surface of the PhoQ sensor domain



that is in close proximity to the inner membrane. This surface binds at least three metal ions to neutralize charge repulsion between PhoQ and the membrane. The crystal structure of PhoQ sensor domain, in the Ca<sup>2+</sup>-free state, exhibits a dramatic dimerization interface change. Our crystallographic, NMR and mutagenesis results suggest that charge repulsion from the membrane initiates a dimerization interface change which promotes signal transduction by bringing the transmembrane helices in closer proximity.

**01.01.08 Is There a Preponderance of Novel Folds in the SARS Coronavirus Proteome?** Jeremiah S. Joseph, Kumar S. Saikatendu, Vanitha Subramanian, Benjamin W. Neuman, Michael J. Buchmeier, Raymond C. Stevens, Peter Kuhn, Depts. of Cell Biology and Molecular Biology, The Scripps Research Institute, 10550 N. Torrey Pines Rd, La Jolla, CA, 92122 USA.

The SARS coronavirus has a ~29.7kb genome with 14 ORFs yielding ~28 mature proteins, many with very low sequence similarity to other proteins. Several NMR and crystal structures of full length viral proteins and/or their constituent domains have been determined by us and others. We observe that even at the structural level, SARS-CoV proteins appear to comprise of a significant number of new folds. To date, out of the 10 proteins with available 3-D structural information (ADRP and PLP domains of nsp3, nsp5, nsp7, nsp8, nsp9, nsp10, sars2, sars7a, N-terminal domain of sars9a), five contain new folds. These novel structures allow us to model and understand structure-function relationships in several new families of proteins, including those in other pathogenic coronaviruses affecting humans. As more structures of the SARS-CoV proteome and those of other viruses are structurally characterized, it will also be interesting to see if the preponderance of uncommon folds is unique to coronaviruses or true of viruses in general. This study was supported by NIAID/NIH Contract #HHSN 266200400058C "Functional & Structural Proteomics of the SARS-CoV".

**01.01.09 Domain-swapped Structure of an Antiviral Protein Griffithsin.** Alexander Wlodawer<sup>1</sup>, Natasza Ziolkowska<sup>1</sup>, Charles Zhu<sup>2</sup>, Toshiyuki Mori<sup>2</sup>, Kenneth Palmer<sup>3</sup>, Barry R. O'Keefe<sup>2</sup>, <sup>1</sup>Macromolecular Crystallography Laboratory, <sup>2</sup>Molecular Targets Development Program, CCR, NCI, Frederick, MD 21702; <sup>3</sup>Large Scale Biologics Corp., Vacaville, CA 95688.

Crystal structure of griffithsin, an antiviral lectin from the red alga *Griffithsia* sp., was solved by SAD and refined at 1.3 Å resolution. Griffithsin molecules form a domain-swapped dimer, in which two  $\beta$ -strands of one molecule complete a  $\beta$ -prism consisting of three four-stranded sheets, with an approximate three-fold axis, of another molecule (and vice versa). The structure of each monomer bears close resemblance to other mannose- and galactose-specific lectins such as jacalin or heltuba, but its dimeric structure is unique. High-resolution structures of complexes of griffithsin with mannose and N-acetylglucosamine defined the location of the carbohydrate-binding sites, some of which are not present in other lectins. Griffithsin has been reported to display picomolar activity against HIV-1, inhibition over 1000-fold better than previously reported for jacalin and other monosaccharide-specific lectins. The presence of multiple binding sites may explain the high-specificity binding of mannose-containing oligosaccharides to griffithsin, the basis of its remarkable activity against viruses that cause diseases such as AIDS and SARS.

## 01.02 Computational Methods

### 01.02.01 Protein Structure as a Blurred Snapshot – Dynamic Information from a Static Experiment. Ethan A Merritt, Dept of Biochemistry, Univ. of Washington, Seattle, WA 98195.

A crystal structure is usually thought of as static information, i.e. it is a snapshot of a protein at rest. But the distribution of thermal parameters in a well-refined structure can be strongly indicative of dynamic motions and allowed flexibility. This distribution of  $B_{iso}$  or  $U^{ij}$  terms can be modeled as arising from TLS (Translation/Libration/Screw) rigid-body vibrational motion. A one-group TLS model can approximate the vibration of an entire protein molecule within the crystal lattice. More complex TLS models are broadly applicable to describe inter-domain and other internal vibrational modes of proteins. Use of multi-group TLS models in crystallographic refinement can improve  $R$  and  $R_{free}$  significantly compared to conventional models. This is a strong hint that the flexibility described by the model is truly present in the protein.

We have developed an analysis tool, *TLsMD*, that generates optimal multi-group TLS models. These may be used to analyze the presence and physical significance of TLS motion in existing structures, to guide additional crystallographic refinement, or to generate target models of protein flexibility for use in computational protein-protein or protein-ligand docking. The analysis is applicable to protein structures at any resolution. <http://skuld.bmsc.washington.edu/~tksmd>

### 01.02.02 Explorations in Conformational Space: Revealing Inaccuracy and Heterogeneity in Crystal Structures. N. Furnham, T.L. Blundell, Dept. of Biochemistry, Cambridge Univ., Cambridge, UK.

It still remains a challenge to produce reliable high quality models of proteins from medium and low resolution crystals, despite significant progress in developing model building and refinement techniques for structure determination by X-ray crystallography. This is primarily due to the difficulty in adequately exploring the large and complex energy landscape and determining the set of conformers that best describes the experimental data. We have developed and applied a restraint based conformational search engine called *RAPPER* to this problem, using electron density as a restraint in the building process. By coupling this with traditional molecular dynamics/simulated annealing techniques we can explore unconnected local minima in the energy landscape. Thus we generate ensembles of solutions where all the members are equally compatible with original experimental data. Depending on how the models are generated this may either reflect the experimental uncertainty or also the spatial heterogeneity or dynamics. This has been applied to both high and medium resolution data and most recently to low resolution data. We have shown that there can be significant heterogeneity in protein structures. Ignoring this can lead to overestimation of the accuracy of crystallographic models.

### 01.02.03 Adapting *BnP* for Different Computing Environments. C.M. Weeks<sup>a</sup>, S.A. Potter<sup>a</sup>, N. Shah<sup>a</sup>, H. Xu<sup>a</sup>, M.L. Green<sup>b</sup>, R. Miller<sup>b</sup>, L. Pasupulati<sup>c</sup>, W. Furey<sup>c</sup>, <sup>a</sup>Hauptman-Woodward Inst., Buffalo, NY, <sup>b</sup>Center for Comp. Res., SUNY at Buffalo. <sup>c</sup>VA Med. Center, Pittsburgh PA & Dept. Pharmacol., U. Pittsburgh.

*BnP* is a protein-phasing package that provides a convenient pathway from intensity data to an interpretable electron-density map [1]. This pathway includes substructure determination using the powerful statistical minimal function, heavy-atom refinement, protein phasing, density modification, and skeletonization. Scripts can be created and executed automatically for chain tracing, graphical visualization, and

refinement by external downstream programs.

*BnP* was first developed with a graphical user interface (GUI) that is written in Java and is suitable for both manual and semi-automatic operation. Recently, an option has been added that allows startup from a command line, thereby permitting a higher degree of automation and bypassing the GUI altogether. In addition, a new interface has been developed in PHP. This interface allows users to run *BnP* from a web browser, supports remote computation, and has the capability of distributing multiple parallel jobs over a computational grid. *BnP* is available at <http://www.hwi.buffalo.edu/BnP/>. This work was supported by NIH grant EBO02057 & NSF ACI-0204918.

[1] C. M. Weeks *et al.* (2002). *Z. Kristallogr.* 217, 686-693.

### 01.02.04 Automated Refinement for Protein Crystallography. Min Yao, Yong Zhou, Isao Tanaka, Graduate School of life Science, Hokkaido Univ., Sapporo, 060-0810, Japan.

During refinement process of protein crystal structures, manual intervention is usually required in the multiple rounds including linking and/or extending the fragments of the initial model and fitting ill-matched residues using computer graphics software. Such manual modification is both consuming time and requiring a great deal of expertise in crystallography. For realizing the manual-intervention-free refinement, we have developed a new automatic refinement software package, *LAFIRE* ([http://altair.sci.hokudai.ac.jp/g6/Research/Lafire\\_English.html](http://altair.sci.hokudai.ac.jp/g6/Research/Lafire_English.html)). This software was designed to perform the whole process of protein structural refinement automatically with the refinement programs *CNS* or *REFMAC5* from an initial model that can be approximate, fragmentary or even only main chain. By using *LAFIRE*, a fully or semi-automatic refinement process can be realized within a few hours or days. The overall strategies and methods used in *LAFIRE* for model completing and fitting will be presented.

### 01.02.05 Enhancing the Capabilities of *ARP/wARP*. Serge X. Cohen, Krista Joosten, Marouane Ben Jelloul, Victor Lamzin, Anastassis Perrakis, Molecular Carcinogenesis, NKI, Plesmanlaan 121, Amsterdam 1066CX, NL.

As automated protein model building procedures (such as implemented in *ARP/wARP*, *Resolve* or *MAID*) are able to build partial initial models with minimum user intervention, manual interactive building is gradually shifted towards the end of the process. Hence it is a natural trend for automatic building development to spend more effort towards providing a more complete model.

First we propose a new algorithm to estimate the posterior probability of a given amino acid (characterised by its observed topology) to be one of the 20 amino-acid types. These probabilities are then compared to the protein sequences present in the crystal to assign sequence to the present fragments. This Bayesian approach enables us to dock even shorter fragments.

If NCS is present in the crystal, we use docked fragments to derive the NCS operators which are in turn used to perform cross-completion of the different copies. This step has to be done carefully to avoid introducing bias when the NCS is genuinely broken in the structure.

Finally, we propose an algorithm using both electron density and prior knowledge of protein main chain structure to extend main chain fragments at their ends and to build loops between fragments already docked in sequence.

These algorithms are implemented in the new version of *ARP/wARP*, and enable this version to trace more complete models even at lower diffraction resolution.

**01.02.06 Automated Structure Refinement in PHENIX: Recent Advances and New Algorithms.** Pavel V. Afonine, Ralf W. Grosse-Kunstleve, Peter H. Zwart, Paul D. Adams, Lawrence Berkeley National Laboratory, One Cyclotron Rd, Berkeley, CA 94720.

The advent of new computational technologies (hardware and software) makes it possible to rethink the algorithms for crystallographic structure refinement and to increase the level of automation. The ongoing development of structure refinement tools in the PHENIX project [1,2] has lead to a comprehensive suite of algorithms covering a variety of refinement scenarios. A robust bulk solvent correction with anisotropic scaling, rigid body refinement with a large convergence radius, refinement of individual atomic coordinates and atomic displacement parameters (ADPs) using gradient-driven minimization, grouped ADP refinement, simulated annealing, and NCS restraints are readily available. All optimization steps, including bulk solvent modeling and scaling, can be performed using a variety of least-squares and maximum-likelihood target functions. Under active development is the generalization of ADP refinement combining isotropic, anisotropic, grouped and TLS algorithms in a uniform framework suitable for integration of automated decision making to determine the best parameterization. We have also implemented automatic twinning detection and the development of suitable target functions is under way. Robustness of the PHENIX refinement tools was tested by automatic re-refinement of all models in the Protein Data Bank (PDB) for which unambiguous experimental data and cross validation flags are available.

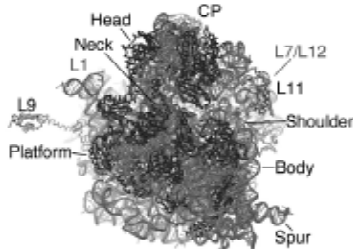
[1] Adams PD, Gopal K, Grosse-Kunstleve RW, Hung L-W, Ioerger TR, McCoy AJ, Moriarty NW, Pai RK, Read RJ, Romo TD, Sacchettini JC, Sauter NK, Storz LC, Terwilliger TC: Recent developments in the PHENIX software for automated crystallographic structure determination. *J. Synchrotron Rad.* 2004, 11:53-55.  
[2] Afonine PV, Grosse-Kunstleve RW, Adams PD: The Phenix refinement framework. CCP4 newsletter, July 2005; Contribution 8.

## 01.03 Large Macromolecular Assemblies

**01.03.01 Structures of the Bacterial Ribosome at 3.5 Å Resolution: Apo-Ribosome and Complexes with Translocation Inhibitors.** Maria A. Borovinskaya, Jamie H.D. Cate, Physical Biosciences Div., Lawrence Berkeley National Laboratory, Berkeley, CA 94720.

Protein biosynthesis occurs on the ribosome in all forms of life. Ribosomes are large ribonucleoprotein complexes composed of a RNA functional core enhanced by ribosomal proteins. Ribosomes translate information encoded in mRNA into proteins in a sophisticated GTP-driven process involving tRNAs and various factors. The molecular mechanism of ribosomal action is not yet fully understood.

Here we describe two structures of the intact bacterial ribosome from *Escherichia coli* determined to a resolution of 3.5 Å by X-ray crystallography [BS Schuwirth et al, *Science* 310, 827 (2005)]. These structures provide a detailed view of the interface between small and large ribosomal subunits and the conformation of the peptidyl transferase center in the context of the intact ribosome. In these structures we observe swiveling of the head of the small subunit that, coupled to the ratchet-like motion observed previously, suggests a mechanism for translocation: the coordinated movement of mRNA and tRNAs on the ribosome following peptide bond formation.



Recently, we have determined structures of the *E.coli* ribosome in complexes with several antibiotics that inhibit translocation. These structures provide new insights into the mechanism of translocation.

**01.03.02 Mechanism of RNA Synthesis: Understanding Nucleotide Addition and Selectivity in Multi-subunit RNA Polymerases.** David Bushnell, Dong Wang, Craig Kaplan, Ken Westover, Roger Kornberg, Structural Biology, Stanford Univ., Stanford, CA 94305.

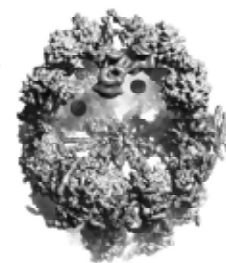
Multisubunit RNA polymerases range in size from 4 subunits to more than 18 subunits, with total mass greater than half a megadalton. Until recently structural information on the mechanism of RNA synthesis has been limited to single subunit RNA polymerases, with the assumption that the multi-subunit polymerases were similar. Structural studies of RNA polymerase II (12 subunits, 514 kDal) now reveal a basis of nucleotide entry and selectivity in multi-subunit RNA polymerases very different from that observed in single subunit enzymes.

**01.03.03 Conformational Variability in Eukaryotic Transcription Complexes Revealed by Cryo-Electron Microscopy Studies.** Grob, P.<sup>1</sup>, Kostek, S.<sup>1</sup>, DeCarlo, S.<sup>1,3</sup>, Tjian, R.<sup>1,3</sup>, Penczek, P.<sup>4</sup>, Nogales, E.<sup>1,2,3</sup>, Molecular and Cell Biology Dept., Univ. of California, Berkeley, CA, <sup>2</sup>Physical Biosciences Div., Lawrence Berkeley National Lab, Berkeley, CA, <sup>3</sup>Howard Hughes Medical Inst., Molecular & Cell Biology Dept., Univ. of California, Berkeley, CA, <sup>4</sup>Univ. of Texas – Houston Medical School, Dept. of Biochemistry & Molecular Biology, Houston, TX.

The multi-subunit transcription factor TFIID and RNA Polymerase II are essential elements of the transcription machinery in eukaryotes. We adopted the cryo-electron microscopy and single particle approach to obtain 3D reconstructions of the endogenous human complexes in solution. Additionally we obtained the associated 3D variance maps as well as covariance information. The localization and the amplitude of the variations have given us a novel insight into the dynamics of these complex molecular machines. For human TFIID this strategy has shown that several domains of the complex moved in a concerted manner that reshaped the putative DNA-binding cavities. In human RNA Polymerase II we have identified a more complex set of variable regions that can be interpreted based on the crystallographic structures available for the yeast enzyme.

**01.03.04 Architecture of a Fungal Fatty Acid Synthase: A 2.6 MDa Molecular Assembly Line.** S. Jenni, M. Leibundgut, T. Maier, N. Ban, Inst. of Molecular Biology and Biophysics, Swiss Federal Inst. of Technology (ETH Zurich), Switzerland.

Fungal  $\alpha_6\beta_6$  heterododecameric fatty acid synthase harbors all catalytic domains required for *de novo* fatty acid synthesis. We crystallized *Thermomyces lanuginosus* fatty acid synthase and derived a 5 Å resolution x-ray crystallographic electron density map, which allowed fitting of homologous enzymes that catalyze the individual reaction steps [1]. The catalytic domains are embedded into well-defined structural features, which serve as a matrix and define the architecture of the huge assembly. The synthesis is compartmentalized in two large reaction chambers, each containing three sets of active sites and three flexible acyl carrier proteins that transfer substrates between the catalytic domains. This architectural solution differs considerably from the mammalian enzyme [2], which catalyzes the same conserved reaction pathway but evolved as a homodimer.



References:

- [1] S. Jenni, M. Leibundgut, T. Maier, N. Ban (2006). Architecture of a Fungal Fatty Acid Synthase at 5 Å Resolution. *Science*, in press.
- [2] T. Maier, S. Jenni, N. Ban (2006). Architecture of Mammalian Fatty Acid Synthase at 4.5 Å Resolution. *Science*, in press.

**01.03.05 The Domain Architecture of Mammalian Fatty Acid Synthase at 4.5Å Resolution.** Timm Maier, Simon Jenni, Nenad Ban, IMB, ETH Zurich, Switzerland.

Fatty acids are central building blocks of life; they serve as energy storage compounds and messenger molecules. Synthesis of fatty acids is an essential process for most organisms, which is carried out in a conserved cyclic pathway of multiple enzymatic reactions. While in bacteria and plants all these reactions are catalyzed by individual, monofunctional enzymes, large multifunctional enzymes for fatty acid synthesis have evolved in most other eukaryotes. The homodimeric mammalian fatty acid synthase is one of the most complex cellular multienzymes in that each 270 kDa polypeptide chain carries all seven functional domains required for fatty acid synthesis. We have calculated a 4.5 Å resolution X-ray crystallographic map of porcine fatty acid synthase, which is a paradigm for all mammalian fatty acid synthases, and placed structures of homologues of all individual catalytic domains responsible for the cyclic elongation of fatty acid chains into the electron density. The positioning of domains reveals the complex architecture of the multienzyme forming an intertwined dimer with two lateral reaction chambers. Considerable distances between active sites and conformational differences between the reaction chambers demonstrate that mobility of the acyl carrier protein and general flexibility of the multi-enzyme must accompany handover of the reaction intermediates during the reaction cycle.

**01.03.06 3D Coherent Diffraction Microscopy and its Applications in Structural Biology.** Jianwei Miao, Dept. of Physics and Astronomy, California NanoSystems Inst., Univ. of California, Los Angeles, CA 90095, [miao@physics.ucla.edu](mailto:miao@physics.ucla.edu).

When a coherent diffraction pattern is sampled at a spacing sufficiently finer than the Bragg peak frequency, the phase information is encoded inside the diffraction pattern and can be directly retrieved by using an iterative process. In a combination of this oversampling method with coherent X-rays or electrons, a novel form of microscopy, *i.e.* lensless imaging, has recently been developed to image biological systems. In this talk, I will present the principle of this microscope, discuss some applications in structural biology, and illustrate the future opportunities with X-ray free electron lasers.

References:

- D. Shapiro, P. Thibault, T. Beetz, V. Elser, M. Howells, C. Jacobsen, J. Kirz, E. Lima, H. Miao, A. M. Neiman, D. Sayre, "Biological imaging by soft x-ray diffraction microscopy," *Proceedings of the National Academy of Science* 102 (43), 15343-15346 (2005).
- J. Miao, H. N. Chapman, J. Kirz, D. Sayre, K. O. Hodgson, "Taking X-ray Diffraction to the Limit: Macromolecular Structures from Femtosecond X-ray Pulses and Diffraction Microscopy of Cells with Synchrotron Radiation", *Annu. Rev. Biophys. Biomol. Struct.* 33, 157-176 (2004).
- J. Miao, K. O. Hodgson, T. Ishikawa, C. A. Larabell, M. A. LeGros, Y. Nishino, "Imaging Whole *Escherichia Coli* Bacteria by Using Single Particle X-ray Diffraction", *Proc. Natl. Acad. Sci. USA* 100, 110-112 (2003).
- J. Miao, K. O. Hodgson, D. Sayre, "A New Approach to 3-D Structures of Biomolecules Utilizing Single Molecule Diffraction Images", *Proc. Natl. Acad. Sci. USA* 98, 6641-6645 (2001).

## 01.04 Membrane Protein Structures

**01.04.01 Structural Mechanism of Plant Aquaporin Gating.** Susanna Tomroth-Horsefield, Yi Wang, Kristina Hedfalk, Urban Johanson, Per Kjellbom, Richard Neutze, Dept. of Chemical & Biological Engineering, Molecular Biotechnology, Chalmers Univ. of Technology, Lundberg Laboratory, Gothenburg, SWEDEN.

Aquaporins (AQP) are membrane water channels that play a critical role in controlling the water content of the cell. They are widely distributed in all kingdoms of life; from bacteria to yeast, plants and humans. They facilitate the rapid transport of water in response to osmotic gradients. In plants cells, the cell wall allows for the maintaining of a large osmotic gradient between the cell interior and exterior. This results in turgor pressure and is crucial for many aspects of plant physiology. To counteract fluctuations in the water supply, land plants have evolved to regulate all aquaporins which lie within the plasma membrane. One of the most abundant proteins in the spinach leaf plasma membrane is the aquaporin SoPIP2;1, previously known as PM28A. It is regulated by phosphorylation of two highly conserved serines and by pH involving protonation of a conserved histidine. Both events close the water channel in response to drought stress (phosphorylation) or low pH in the cytosol during for example flooding (protonation).

We have solved the structure of SoPIP2;1 to 2.1 Å resolution. This is the first high resolution structure of a plant aquaporin as well as of a regulated aquaporin and reveals SoPIP2;1 captured in a closed conformation. We have also solved the structure of SoPIP2;1 in an open conformation at 3.9 Å and have performed molecular dynamics simulations of the initial events governing gating. From these results we have proposed a detailed mechanism for how SoPIP2;1 is regulated by phosphorylation and pH.

**01.04.02 Structure of the Outer Membrane Cobalamin Transporter BtuB Complexed with TonB.** D.D. Shultz<sup>1</sup>, M.D. Purdy<sup>1</sup>, C.N. Banchs<sup>2</sup>, M.C. Wiener<sup>1,2</sup>, <sup>1</sup>Dept. of Molecular Physiology and Biological Physics, <sup>2</sup>Interdisciplinary Graduate Program in Biophysics, Univ. of Virginia, Charlottesville, VA 22908.

Import of scarce organometallic substrates across the outer membrane of Gram-negative bacteria is carried out by a multi-protein active transport system. An inner membrane protein complex, utilizing the proton-motive force (pmf), couples to substrate-specific outer membrane transporters to drive transport across the outer membrane. The coupling protein in this system is TonB. A detailed molecular mechanism of TonB-dependent outer membrane transport remains unknown. We formed and crystallized a complex of the outer membrane cobalamin transporter BtuB and a carboxy-terminal domain of TonB (in the presence of cyanocobalamin substrate). Crystals of the complex (spacegroup P2<sub>1</sub>2<sub>1</sub>2<sub>1</sub> [a= 74.3Å, b=82.4Å, c=122.6Å]) diffract to 2.1 Å resolution. The structure of the complex was solved by molecular replacement using a BtuB search model. The structure will be presented and discussed.

This work is supported by NIH grant DK59999. D.D.S. is supported by an NIH Training Grant in Pharmacological Science T32 GM00Z055. Data were collected at Southeastern Regional Collaborative Access Team (SER-CAT) beamline 22-ID at the Advanced Photon Source, Argonne National Laboratory.

**01.04.03 Membrane Protein Crystallization in Bicontinuous Lipid Systems.** Pia Wadsten, Annemarie Wöhri, Arjan Snijder, Richard Neutze, Sven Engström, Dept. of Chemical and Biological Engineering, Chalmers Univ. of Technology, Gothenburg 412 96, Sweden.

In 1996, a new concept for membrane protein crystallization in the

cubic phase was introduced. The method has been successful for proteins with small hydrophilic domains where a phase change, from a curved bilayer to a flat bilayer plays an important role in the crystallization process. The cubic phase is stiff and time consuming to handle. The phase also puts restrictions on the hydrophilic parts of the protein due to limited aqueous domain size. The method however yielded crystals from two photosynthetic reaction centers (RC) with larger hydrophilic domains as a result from the transformation cubic phase-to-liquid phase. Simulating the crystallization conditions in a small angle X-ray setup we conclude that the cubic phase in the RC case forms a sponge phase, which can be visualized as a 'melted' cubic phase. The presence of this phase should play the same role as the lamellar phase for smaller proteins, but with larger aqueous pores for the accommodation of RCs hydrophilic domain. Here we introduce a new method using the sponge phase directly in a hanging drop setup. Crystals of RC from *Rhodobacter sphaeroides*, diffracting to 2.1 Å, were obtained and the practical advantages of the sponge phase make it a potent tool for protein crystallization.

**01.04.04 Crystal Structure of TonB in Complex with FhuA, E. coli Outer Membrane Receptor.** M. Allaire, N. Moiseeva, National Synchrotron Light Source, Brookhaven National Laboratory, Upton, NY, 11973, P.D. Pawelek, N. Croteau, C. Ng-Thow-Hing, C.M. Khursigara, J. Coulton, Dept. of Microbiology and Immunology, McGill Univ., Montréal, Québec, H3A 2B4 Canada.

The cytoplasmic membrane protein TonB spans the periplasm of the Gram-negative cell envelope, contacts cognate outer membrane receptors, and facilitates siderophore transport. The outer membrane receptor FhuA mediates TonB-dependent import of ferrichrome. We report the 3.3 angstrom resolution crystal structure of the TonB-FhuA complex from *Escherichia coli*. Initial phases were obtained from molecular replacement using the FhuA structure alone. Electron density corresponding to TonB and the FhuA Ton box is observed. The Ton box forms an inter-protein  $\beta$  sheet with TonB via strand exchange. The stable inter-protein  $\beta$  sheet orients the highly conserved TonB residue Arg<sup>166</sup> to form multiple contacts with the FhuA cork domain. The TonB-FhuA structure reflects an ensemble poised to transport ferrichrome. We propose a mechanism whereby conformational changes are propagated through TonB Arg<sup>166</sup> to FhuA and disruption of the central  $\beta$  sheet of the FhuA cork domain promotes siderophore transport across the outer membrane.

**01.04.05 Structural Studies of an ABC Transporter.** H.W. Pinkett, A.T. Lee, D.C. Rees, Chemistry/HHMI, California Inst. of Technology, Pasadena, CA 91125.

ABC transporters form a family of importer and exporter proteins that use ATP hydrolysis to pump substrates across the membrane against a concentration gradient. They are minimally composed of four domains, with two transmembrane domains (TMDs) and two ATP binding cassettes (ABCs) located in the cytoplasm. The TMDs form a pathway to translocate substrates across the lipid bilayer. While diverse with respect to physiological function, ABC transporters are characterized by two highly conserved cytoplasmic ATP binding cassettes that contain critical sequence motifs for binding and hydrolysis of ATP. The ATP binding cassettes serve as the motor, coupling the energy of ATP binding and hydrolysis to transmembrane transport. In addition, most bacterial ABC transporters also utilize a periplasmic binding protein (PBP) to deliver the substrate to the TMD domains. We have determined the three dimensional structure to 2.4 Å of a bacterial ABC transporter homologous to the vitamin B<sup>12</sup> ABC transporter, BtuCD.

Insights into the mechanism of substrate translocation by ABC transporters provided by this structure will be discussed.

**01.04.06 Crystal Structure of Particulate Methane Monooxygenase.** Raquel L. Lieberman, Amy C. Rosenzweig, Dept. of Biochemistry, Molecular Biology & Cell Biology & Dept. of Chemistry, Northwestern Univ., Evanston, IL 60208.

Particulate methane monooxygenase (pMMO) is a three-subunit integral membrane metalloenzyme that converts methane to methanol. Although pMMO is the predominant methane oxidation catalyst in nature, it has proved difficult to isolate, and the literature addressing details of its structure and active site composition has been mired in controversy for longer than a decade. Knowledge of how pMMO activates the inert methane C-H bond is of fundamental chemical interest, and could lead to development of new synthetic catalysts that could impact the use of methane (natural gas) as an alternative energy source.

We have determined the 2.8 Å resolution structure of pMMO from *Methylococcus capsulatus* (Bath). The enzyme is a 300 kDa trimer with an  $\alpha_3\beta_3\gamma_3$  polypeptide arrangement. Two metal centers, modeled as mononuclear copper and dinuclear copper, are located in soluble regions of each pmoB subunit, which resembles cytochrome *c* oxidase subunit II. A third metal center, occupied by zinc in the crystal, is located within the membrane. The structure provides significant new insight into the molecular details of biological methane oxidation and lays the foundation for future directed biochemical and mechanistic studies of pMMO.

**01.04.07 Structures of a Cyanobacterial Photoreceptor and its Soluble Transducer.** Hartmut Luecke, Depts. of Biochem., Biophysics & Computer Science, Univ. of California, Irvine, CA 92697, hudel@uci.edu, <http://bass.bio.uci.edu/~hudel/>

The Cubic Lipid Phase (CLP) method for membrane protein crystallization has been refined to allow large-scale screening of various membrane proteins. Various parameters (CLP lipid, water content, bilayer lipid additive, pH, ionic strength, precipitating agent etc.) can be varied. Several distinct seven-transmembrane proteins have been crystallized and their structures determined.

Sensory Rhodopsin (SR): Atomic resolution structures of a phototaxis receptor in haloarchaea, the first sensory member of the widespread microbial rhodopsin family, have yielded insights into spectral tuning and the interaction face with its membrane-embedded transducer. Spectral differences between the sensory rhodopsin and light-driven proton pump bacteriorhodopsin depend largely on the repositioning of a conserved arginine residue in the chromophore-binding pocket. Information from the structures combined with biophysical and biochemical analysis have established a model for receptor activation and signal relay involving light-induced helix tilting in the receptor transmitted to the transducer by lateral transmembrane helix-helix interactions.

*Anabaena* SR (ASR): Most recently, the structure of a sensory rhodopsin from the cyanobacterium *Anabaena* has been determined to 1.9 Å resolution. This represents the first bacterial rhodopsin structure. In comparison to the archaeal rhodopsins BR and SR there are many striking rearrangements and shifts in hydrogen bonding patterns and hydration on both the extracellular and the cytoplasmic half of the receptor. Also, the cytoplasmic face, which is thought to interact with the soluble transducer, is structurally well-defined and very different from that of the archaeal rhodopsins. The structure of the soluble transducer of this photoreceptor (ASRT) has also been determined - it forms a C4 tetramer with a new fold.

**01.04.08 Experiments Toward Crystallization of Transhydrogenase.** C.D. Stout<sup>1</sup>, M. Yamaguchi<sup>1</sup>, H.A. Heaslet<sup>1</sup>, M. Yeager<sup>2</sup>, <sup>1</sup>Depts. of Molecular Biology<sup>1</sup>, and Cell Biology<sup>2</sup>, The Scripps Research Institute, La Jolla, CA.

Transhydrogenase (TH) is essential enzyme in mitochondria that couples hydride transfer between NAD(H) and NADP(H), bound to extramembranous domains, to proton translocation through a membrane-intercalated domain. It is the only respiratory membrane component lacking structural data for an intact complex. The mechanism for transducing binding energy into conformational change and proton translocation is unknown, but TH resembles ATP synthase in that the proton gradient is utilized for chemical bond formation in the absence of net redox. The *E. coli* enzyme is a 200 kD homodimer of gene products, the *alpha* subunit containing the NAD(H) binding domain and four trans-membrane helices, and the *beta* subunit, containing the NADP(H) binding domain and nine TM helices. Together, the 13 TM helices comprise the proton channel of each monomer. The approach to crystallization of TH is combining expression methods, mutagenesis, His-tag design, and detergent solubilization, with biochemical methods, activity assays, and electron microscopy. The results are integrated to assess TH monodispersity and conformational homogeneity for 2D and 3D crystallization screening. Observations and progress with these experiments will be reported.

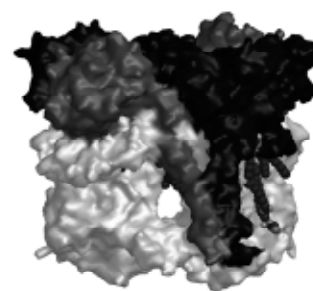
**01.04.09 The 2.0 Å Structure of a Bacterial Cytochrome *c* Oxidase: Evidence for the Conservation of Lipid Binding Sites.** Ling Qin<sup>1</sup>, Carrie Hiser<sup>1</sup>, Xi Zhang<sup>1</sup>, Anne Mulichak<sup>2</sup>, R. Michael Garavito<sup>1</sup>, Shelagh Ferguson-Miller<sup>1</sup>, <sup>1</sup>Dept. of Biochemistry, Michigan State Univ., East Lansing, MI, <sup>2</sup>IMCA-CAT, APS, Argonne National Laboratory, Argonne, IL.

Crystals of the two subunit catalytic core of cytochrome *c* oxidase (CcO) from *Rhodobacter sphaeroides* were obtained with isotropic x-ray diffraction to 2.0 Å resolution, by using an expression construct designed to eliminate molecular inhomogeneity and an optimized purification protocol. Interesting features of this structure include identification of a Cd<sup>2+</sup> inhibitory site, confirmation of an unusual covalent linkage between sidechain rings of a tyrosine and histidine close to the active site, and resolution of many waters, including the distinctive chain in the D-proton uptake pathway similar to that found in the four subunit holoenzyme. A number of alkyl chains of membrane lipids or detergents are observed in the structure, some with well-defined maltoside head groups. Comparison of CcO crystal structures from different sources reveals that alkyl chain positions of membrane lipids and detergent substitutes are conserved, indicating the mode and unexpected specificity of lipid binding sites on membrane proteins, as well as the ability of certain detergent molecules to mimic lipid binding. (supported by NIH GM26916; HFSP RG315/2000-M; MTTC-CSB-CTA 085P1000817; NIH P01GM57323)

**01.04.10 The bc1 Complex from *Rhodobacter Sphaeroides* at 2.85 Å Resolution.** Lothar Esser<sup>1</sup>, Maria Elberry<sup>2</sup>, Chang-An Yu<sup>2</sup>, Linda Yu<sup>2</sup>, Di Xia<sup>1</sup>, <sup>1</sup>National Institutes of Health, National Cancer Inst., Bethesda, MD 20892, <sup>2</sup>Dept. of Biochemistry and Molecular Biology, Oklahoma State Univ., Stillwater, OK 74078.

Proton-translocating quinol/quinone oxido-reductases are membrane embedded protein complexes (bc1) that play a central role in the ATP production of the majority of organisms. The structures of mutant *Rhodobacter Sphaeroides* bc1 inhibited by stigmatellin (1) and stigmatellin and antimycin (2) have been determined. These crystals are monoclinic (C2) with cell dimensions of a=353.4Å, b=147.1Å, c=162.3Å, β=104.5° and diffract between 2.85 and 3.10 Å. The structures were

solved by MR using a dimeric model of beef bc1. The asymmetric unit contains three dimers of cyt b, cyt c1 and ISP with clearly visible density for the respective inhibitors. However, there was no density for subunit IV. Δ-Sub IV *R.S.* bc1 crystals are triclinic and contain two independent dimers. The appearance of interpretable electron density for *R.S.*-specific sequences as well as lipid and detergent molecules proved the solution to be correct. The difficulties in crystallizing this membrane protein, the function of the longer bacterial sequences and the role of the lipids will be discussed. The current best model (1) containing 42,192 atoms refined to R(cryst) = 0.24 and R(free) = 0.28.



## 01.05 Difficult Structures

**01.05.01 How to Make the Structure Difficult.** Z. Dauter, Synchrotron Radiation Research Section, MCL, NCI, Argonne National Laboratory, Argonne, IL 60439.

Classification of a particular structure as easy or difficult is very subjective, since its solution might be an easy task for one investigator and a difficult one for another. Taking as a criterion the time and effort spent on structure solution, the most difficult of all was the structure of hemoglobin, solved by Perutz through an effort that took 20 years. That structure would nowadays probably require no more than a few hours and a personal computer. Obviously, the most difficult structures are those that have never been successfully solved, but they are very rarely publicized. The factors contributing to the total "difficulty" depend on diffraction properties of the crystals, peculiarities of molecular packing, availability of appropriate software, the experience of investigators, and, last but not least, a measure of good luck. The most serious difficulties may reside in various steps of the whole procedure; some macromolecules are difficult to crystallize, some cannot be derivatized, and some crystals display atypical diffraction properties such as twinning or pseudosymmetry. If these factors are not understood and properly dealt with, difficulties arise. Various examples of different kinds of such problems will be presented and discussed.

**01.05.02 On-going Developments Aimed at Improving the Success Rate of Challenging Structure Determinations.** G. Brignone, Global Phasing Ltd., Sheraton House, Castle Park, Cambridge CB3 0AX, UK.

The pursuit of high throughput in structure determination has stimulated an unprecedented level of coordinated effort between developers of instruments and of software towards increasing degrees of automation in the determination of macromolecular crystal structures. Some of its concrete achievements, such as the automated screening of large numbers of crystals, are already contributing valuable help to investigators wanting to tackle challenging projects.

This talk will describe a number of further on-going developments, all based on (or guided by) improved statistical analyses of the reality of experiments and of data, which are specifically aimed at providing greater help still to such projects. They include the design and on-line monitoring of experiments (smart data collection), and the systematic use of unmerged data, together with new likelihood functions based on them, to accommodate the effects of radiation damage in scaling, in phasing from weak signals, and in structure refinement.

**01.05.03 Conformational Complexity of Complement Component C3.** Bert J.C. Janssen<sup>1</sup>, Eric G. Huizinga<sup>1</sup>, Hans C.A. Raaijmakers<sup>1</sup>, Anja Roos<sup>2</sup>, Mohamed R. Daha<sup>2</sup>, Kristina Nilsson-Ekdahl<sup>3,4</sup>, Bo Nilsson<sup>3</sup>, Piet Gros<sup>1</sup>, <sup>1</sup>Crystal & Structural Chemistry, Bijvoet Center for Biomolecular Research, Utrecht Univ., The Netherlands, <sup>2</sup>Dept. of Nephrology, Leiden Univ. Medical Center, The Netherlands, <sup>3</sup>Dept. of Clinical Immunology, Univ. Hospital, Uppsala, Sweden, <sup>4</sup>Dept. of Chemistry & Biomedical Sciences, Univ. of Kalmar, Sweden.

The mammalian complement system plays a key role in innate and adaptive immunity. The activation of its central component C3 (1,641 residues), results in inflammation and elimination of self and non-self targets. Recently we solved the structures of native C3 and its major proteolytic fragment C3c. First, C3c, purified from outdated human plasma, was solved by SIRAS and MAD phasing. Multi-crystal averaging using nine partial masks was required to obtain an interpretable electron-density map. Second, C3, purified from fresh human plasma, was solved by molecular replacement. Initial positioning of C3c or any of its fragments was unsuccessful. However, the  $\alpha 6$ - $\alpha 6$  barrel structure of C3d (18% of C3) was positioned correctly and gradually the domains of C3c could be placed. The structures show that C3 consist of thirteen domains, of which nine were unpredicted and that the central core consists of eight structural homologous domains. Large and surprising structural rearrangements are observed in going from C3 to C3c, indicating an unprecedented, conformation-dependent mechanism of activation and deactivation of C3.

**01.05.04 Molecular Machines, Tropical Pathogens and Difficult Structures.** Wim Hol<sup>1</sup>, Junpeng Deng, Jan Abendroth, Konstantin Korotkov, Marissa Yanez, Claudia Roach, Brian Krumm, Stewart Turley, Dept. of Biochemistry, HHMI, Univ. of Washington, Seattle, WA.

The “Type 2 Secretion System” (T2SS) from *Vibrio cholerae* and enterotoxigenic *E. coli* (ETEC) is responsible for secreting proteins like cholera toxin (CT) and heat-labile enterotoxin (LT). The T2SS consists of ~ 14 different proteins, and spans the inner and outer membrane. We have expressed many components of the T2SS including soluble proteins, integral membrane proteins and multi-protein complexes. Six crystal structures have been elucidated which gives initial insight into the architecture of the inner membrane subcomplex.

The editosome is essential for Trypanosomatids, which are causative agents of sleeping sickness, Chagas’ disease and leishmaniasis. For several mitochondrial proteins the pre-mRNA needs to be edited substantially. The editing information is encoded in numerous small “guide RNAs” which are used by the “editosome” to create a mature messenger. The editosome consists of over a dozen different proteins. High-resolution structures of editosome RNA-editing Ligase 1 and TUTase 2 provide the first three-dimensional insights into this complex machinery.

A summary will be given of the surprisingly many hurdles which needed to be overcome to solve quite a few of these structures.

**01.05.05 Rational Approaches in Structure Determination of Membrane Proteins.** P. Nissen, J. P. Morth, B.P. Pedersen, T. L. Sorensen, Dept. Molecular Biology, Univ. Aarhus, Gustav Wieds Vej 10C, DK - 8000 Aarhus C, Denmark.

Implementation of high-throughput methods in protein crystallography ranging from cloning, expression and purification of targets, to crystallization, datacollection, phasing and model building is gradually spreading into the crystallographic community. However difficult, yet highly important targets in the life sciences, such as membrane proteins and large complexes, do not readily fit into this pipeline, and

present large challenges at all stages of the structure determination process, crystallization not the least (1). Determination of such structures thus calls for highly dedicated efforts and unique solutions. The use of selenomethionine MAD/SAD phasing will not be possible for membrane proteins isolated from native tissue or advanced expression systems, and “classical” heavy-metal derivatives must be applied in such cases. This is particularly challenging when applied to small, fragile crystals with weak diffraction properties. However, the aforementioned development of the available technologies combined with data mining of the growing data base offer specific opportunities to design rational and efficient experimental strategies in crystallization and phasing of membrane proteins (2).

1. Sorensen TL, Olesen C, Jensen AM, Moller JV, Nissen P (2006). Crystals of sarcoplasmic reticulum Ca(2+)-ATPase. *J Biotechnol.* epub ahead of print.
2. Morth JP, Sorensen TL, Nissen P. Membrane’s eleven: heavy-atom derivatives of membrane protein crystals. *Submitted*

**01.05.06 Overcoming Severe Diffraction Anisotropy in Crystallographic Refinement.** Michael R. Sawaya, Michael Strong, David Eisenberg, Univ. of California, Los Angeles, CA 90095.

Diffraction anisotropy is characteristic of most macromolecular crystals used for structure determination. Moderate anisotropy can be satisfactorily modeled by anisotropic scaling factors such as those applied by REFMAC or CNS; however, such modeling has proven insufficient for 3 severe cases reported here. In the most severe case (rv2430c-rv2431c), 2.2 Å resolution is observed near the  $a^*$  and  $c^*$  cell axes, but only 3.2 Å resolution near the  $b^*$  axis. Refinement stalled at  $R_{\text{work}}=32\%$  and  $R_{\text{free}}=36\%$ , and model building was impeded by the lack of interpretable features in the electron density map. The R factors improved after eliminating poorly measured reflections falling outside the bounds of an ellipsoid, rather than the usual sphere. However, the density remained featureless. This problem was finally reasoned to be the side effect of the anisotropic scaling algorithm in which isotropy is effected in  $F_{\text{obs}}$  not only by dampening the resolution falloff in weak diffracting direction(s), but also enhancing the falloff in the strong diffracting direction(s). That is, anisotropic scaling imposed an artificially high overall Wilson B factor. Subsequent application of a negative, isotropic B factor, facilitated model building efforts, leading to  $R_{\text{work}}=24.8\%$ ,  $R_{\text{free}}=31.3\%$ .

## 01.06 Proteins Involved in Host Immune Systems and Pathogen Interactions

**01.06.01 Structural Basis of Lipid Antigen Presentation by CD1.** I.A. Wilson, D.M. Zajonc, D. Wu, G. Painter, V. Kumar, M. Kronenberg, D.B. Moody, C.-H. Wong, L. Teyton, The Scripps Research Institute, La Jolla, CA.

The human CD1 family of cell surface receptors, CD1a to CD1d, presents a variety of lipid antigens to CD1-restricted T cell receptors (TCRs) in order to elicit a specific immune response against invading pathogens, or to carry out immuno-regulatory functions. Many classes of lipid antigens have been identified including self-antigens, such as glycerolipids and sphingolipids, as well as foreign lipids, such as phosphatidylinositol mannosides (PIMs), mycolates, phosphoisoprenoids, small hydrophobic molecules and lipopeptides. To elucidate how such structurally diverse antigens can be presented by a limited number of CD1 receptors, we have determined multiple CD1-lipid structures. Structural differences among the CD1 binding grooves confer antigen binding specificity. All ligands bind with their lipid tails buried within the hydrophobic CD1 binding groove, whereas

their diverse headgroups are exposed for TCR recognition at the CD1 surface. Whereas only a few specific polar interactions are observed between the glycolipid headgroups bound to either CD1a or CD1b, a specific hydrogen bond network is found in CD1d, which orients and stabilizes different classes of CD1d ligands, such as the highly stimulatory  $\alpha$ -GalCer.

**01.06.02 The Molecular Structure of the Toll-like Receptor 3 Ligand-binding Domain.** David Davies, J.K. Bell, I. Botos, P.R. Hall, J. Askins, J. Shiloach, D.M. Segal, NIDDK and NCI, National Institutes of Health, Bethesda, MD 20892-0560.

Innate immunity provides the first line of defense against pathogen attack. Pathogen associated molecular signatures are recognized by the Toll-like receptors which then initiate a rapid host response. The TLRs, of which there are ten human homologs, are of ancient lineage and are germline encoded. We describe the structure of the ectodomain of the first of these TLRs. The molecule forms a large horseshoe consisting of 23 leucine rich repeats together with N- and C-terminal domains. There are 11 N-linked glycans together with two inserts. These results are discussed in terms of potential binding sites for dsRNA, the ligand for TLR3, and models for the mechanism of action.

This work supported by NIDDK and NCI intramural funding, and by a NIAID Biodefense Award.

**01.06.03 Structure and Bi-functionality of Dscam Headpiece: One Stone for Two Birds.** Jia-huai Wang, Dana-Farber Cancer Inst., Harvard Medical School.

Dscam is a highly diverse cell surface receptor expressed in the nervous system as well as the immune system of insects. Mutually exclusive splicing of exons arranged in three clusters results in extensive sequence variability in three immunoglobulin-like ecto-domains. It has been proposed that homophilic and heterophilic interactions involving thousands of Dscam isoforms provide recognition specificity for neuronal wiring and immune responses. X-ray structures of the N-terminal four Ig-like domains of two different Dscam isoforms have been determined, both encompassing variable domains D2 and D3. Both isoforms assume a horseshoe configuration. The most variable residues of D2 and D3 constitute two independent surface-epitopes presented as unique structural elements at opposite faces of the horseshoe. Epitope I is engaged in homophilic dimer formation, involving symmetric, antiparallel pairing of identical peptide segments within D2<sup>A</sup>/D2<sup>B</sup> and D3<sup>A</sup>/D3<sup>B</sup> interfaces. This suggests an exclusive homophilic interactions of Dscam isoforms. In contrast, epitope II does not contribute to homophilic interactions and is likely involved in heterophilic recognition.

**01.06.04 TB Drug Discovery: Addressing Issues of Persistence and Resistance.** James Sacchettini, Center for Structural Biology, Dept. of Biochemistry and Biophysics, College Station, TX.

*Mycobacterium tuberculosis* infections are responsible for one in four avoidable adult deaths in developing countries. While there are a number of effective drugs available for treating tuberculosis (TB), current strategies are greatly complicated by the long chemotherapy treatment that lasts several months, which is required to eliminate persistent bacteria. In addition, widespread patient non-compliance has contributed to the emergence of multidrug-resistant (MDR) and extensively drug resistant (XDR) TB strains. There is a clear need for fast acting drugs that are capable of eliminating an infection in just a few weeks.

Our lab work, in conjunction with the TB Structural Genomics Consortium, has focused on the identification of new drug targets for per-

sistent infections. Our long range goal is to identify lead compounds that are fast acting and would simplify chemotherapy regimens. A significant step forward has been our recent collaborative discovery of several new targets essential for maintaining the persistent infection. High throughput library screens, virtual screens and structure-based inhibitor design techniques are now being applied to the discovery of new lead compound against these promising targets.

**01.06.05 Crystal Structure of a Complete Ternary Complex Between a TCR, Superantigen, and Peptide/MHC Molecule.** Hongmin Li<sup>1,2</sup>, Limin Wang<sup>1</sup>, Yiwei Zhao<sup>1</sup>, Zhong Li<sup>1</sup>, Yi Guo<sup>1</sup>, David M. Kranz<sup>3</sup>, Walid Mourad<sup>4</sup> <sup>1</sup>Wadsworth Center, NYSDOH, <sup>2</sup>Dept. of Biomedical Sciences, Univ. at Albany, Albany, NY 12208, <sup>3</sup>Dept. of Biochemistry, Univ. of Illinois, Urbana, IL 61801, <sup>4</sup>Univ. de Montréal, Montréal, Québec, H2X 1P1, Canada.

Superantigens (SAGs) are potent T cell stimulators generally produced by viruses and bacteria. Here we present the 2.4Å crystal structure of a SAG *Mycobacterium arthritidis* mitogen (MAM) in complex with its two receptors, TCR 2C and HLA-DR1/HA molecules. The structure of the TCR/MAM/MHC complex is, to our knowledge, the first 3D structure of a complete ternary complex between TCR, SAG, and MHC. The structure showed that the binding geometry of the MAM/MHC binary complex is preserved in the ternary complex. MAM predominantly binds the TCR  $\beta$  chain. The *most striking finding* is that MAM directly interacts with the TCR  $\alpha$  chain. The contacts include both van der Waals contacts and specific hydrogen bonds. Large conformational change of the TCR V $\alpha$  CDR3 loop was also observed. This very novel finding that a SAG can directly interact with the TCR  $\alpha$  chain makes a significant extension from the earlier definition of SAG, a hallmark of which is the TCR V $\beta$ -restriction. Our finding has led us to hypothesize that the TCR  $\alpha$  chain plays a critical role in MAM recognition.

**01.06.06 Structure of Tracheal Cytotoxin in Complex With a Heterodimeric Pattern-Recognition Receptor.** Chung-I Chang,<sup>1,2</sup> Yagarany Chelliah,<sup>1,2</sup> Dominika Borek,<sup>2</sup> Dominique Mengin-Lecreulx,<sup>3</sup> Johann Deisenhofer<sup>1,2</sup>, <sup>1</sup>Howard Hughes Medical Institute and <sup>2</sup>Dept. of Biochemistry, Univ. of Texas Southwestern Medical Center, Dallas, TX 75390, <sup>3</sup>Inst. de Biochimie et Biophysique Moléculaire et Cellulaire, Centre National de la Recherche Scientifique, Univ. de Paris-Sud, 91405 Orsay, France.

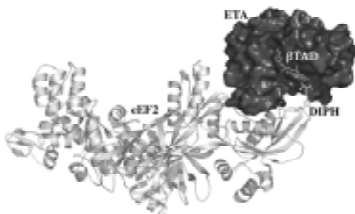
Tracheal cytotoxin (TCT), a naturally occurring fragment of Gram-negative peptidoglycan, is a potent elicitor of innate immune responses in *Drosophila*. It induces the heterodimerization of its recognition receptors, the peptidoglycan recognition proteins (PGRPs) LCa and LCx, which activates the immune deficiency (Imd) pathway. The crystal structure at 2.1 Å resolution of TCT complexed with the ectodomains of PGRP-LCa and PGRP-LCx shows that TCT is bound to and presented by the LCx ectodomain for recognition by the LCa ectodomain; the latter lacks a canonical peptidoglycan-docking groove conserved in other PGRPs. The interface revealed in atomic detail between TCT and the receptor complex highlights the importance of the anhydro-containing disaccharide in bridging the two ectodomains together and the critical role of diaminopimelic acid (DAP) as the specificity determinant for PGRP interaction.

**01.06.07 Closing the Lid on the Mono-ADP-ribosylating Reaction Mechanism by Bacterial Toxins.** R. Jorgensen, X. Wang, X. Liu, R. Merrill, Molecular and Cellular Biology, Univ. of Guelph, Guelph, ON N1G 2W1 Canada.

The bacteria causing diphtheria, cholera and other human diseases secrete mono-ADP-ribosylating toxins that modify proteins in the target host eukaryotic cell. Recently, we have solved four 3 Å crystal structures of a catalytically active complex of the enzyme domain of Exotoxin A (ETA) and its substrate, elongation factor 2 (eEF2), which have led to a breakthrough in the understanding of the reaction mechanism of this family of deadly toxins. The target residue in eEF2, a modified histidine, diphthamide, spans across a cleft in the complex and faces the two phosphates of the NAD<sup>+</sup> analogue, βTAD. This suggests that the diphthamide is involved in NAD<sup>+</sup> cleavage and is interacting with the proposed oxacarbenium intermediate during the nucleophilic substitution reaction. Notably, the βTAD phosphates mimic the phosphate backbone of two highly conserved nucleotides in the 18S rRNA, thereby achieving universal recognition of eEF2 by ETA. In addition, we have new data showing that there are catalytic residues located within an active-site loop of the toxin. We propose that this loop is in an open conformation in the protein complex structures and during transition-state closes in on the active site partly as a cover for solvents and partly to help stabilize the oxacarbenium ion.

**01.06.08 Crystal Structure of m157, A Viral Antigen that Directly Engages Ly49 Natural Killer (NK) Cell Receptors.** Z.S. Juo, E.J. Adams, L.L. Lanier, K.C. Garcia, HHMI/Stanford Univ., Stanford, CA 94305.

NK cells provide a first line of defense against infections. They display both activating and inhibitory receptors on their surface to survey the expression level of major histocompatibility complex (MHC) class I molecules and other antigens of the target cells. Persistent viruses, such as cytomegalovirus (CMV), have developed specific mechanisms to evade immune response by the NK cells. We report here the 2.0 Å crystal structure of m157, a decoy protein produced by mouse CMV that is currently the only known viral antigen that directly engages both activating and inhibitory Ly49 receptors of murine NK cells. Although morphologically resembling the canonical MHC class I molecule, m157 deviates from the MHC structures more than other known homologues. One striking feature of m157 is that the helices on the top of platform are positioned closely to each other, leaving no room for peptide presentation. One section of a helix is unwound in a manner strikingly similar to the murine non-classical MHC T22. Since m157 lacks beta-2 microglobulin, which normally associates with mammalian MHC, m157 relies on an extended helix bridging the alpha1/alpha2 platform and the alpha3 stem in order to enforce a tight packing that results in an overall more compact molecule. We predict that m157 will engage with the Ly49 NK cell receptors in a manner different from that by canonical MHC molecules, and discuss companion cellular and functional data probing this interaction.



## 01.07 International Macromolecular Crystallographic Advances

**01.07.01 Three-dimensional Structure of a Ferritin from the Hyperthermophilic Archaeon and Anaerobe *Pyrococcus furiosus*.** P.M. Matias<sup>a</sup>, J. Tatur<sup>b</sup>, M.A. Carrondo<sup>a</sup>, W.R. Hagen<sup>b</sup>, <sup>a</sup>Inst. de Tecnologia Química e Biológica, Oeiras, Portugal, <sup>b</sup>Dept. of Biotechnology, Delft Univ. of Technology, Delft, The Netherlands.

*P. furiosus* is a marine, strictly anaerobic, fermentative, hyperthermophilic archaeon with an optimal growth temperature of 100°C. A putative ferritin gene was cloned and overexpressed in *E. coli*, and the purified protein was identified as an active ferritin, forming a 24-meric structure that can incorporate up to 2700 iron ions into a superparamagnetic core when incubated with Fe(II) under air. This protein exhibits the highest thermostability known among ferritins: its activity is fully retained after incubation at 100°C for 8 hours or autoclaving at 120°C for 20 minutes. Orthorhombic crystals of PfFtn were obtained in space group C222<sub>1</sub>, with cell dimensions a=258.1, b=340.1 and c=266.5 Å, and 1 1/2 24-meric clusters in the asymmetric unit. Diffraction data to 2.75 Å resolution from a flash frozen crystal was collected at ESRF beamline BM14. The structure was solved by the molecular replacement method and refined to R=0.209 and R<sub>free</sub>=0.258.



We thank the ESRF BM14 staff for technical support with the data collection and EMBL Grenoble for travel and accommodation support under the EU I3 Project IA-SFS.

**01.07.02 Plant L-asparaginase and its Relation to Human and Bacterial Cousins.** M. Jaskolski<sup>ab</sup>, K. Michalska<sup>a</sup>, G. Bujacz<sup>bc</sup>, <sup>a</sup>Dept. of Crystallography, A. Mickiewicz Univ., Poznan, Poland; <sup>b</sup>Center for Biocrystallographic Res., IBCh, Pol. Acad. Sci., Poznan, Poland; <sup>c</sup>Faculty of Biotech. & Food Sci., Technical Univ. of Lodz, Poland.

L-Asparaginases hydrolyze the β-amide bond of asparagine, releasing aspartate and ammonia. In plants, asparaginases are essential in nitrogen circulation, which uses L-asparagine as the main vehicle. *E. coli* expresses a protein (EcAIII) with sequence similarity to the plant enzymes. We have shown that EcAIII and its lupine counterpart (LIA) are more active as isoaspartyl aminopeptidases. This dual activity is crucial in seeds for removal of β-aspartyl aberrations during storage and for quick nitrogen release during germination. The crystal structure of LIA confirms the classification of plant asparaginases in the family of Ntn-hydrolases. The α- and β-subunits of the mature (αβ)<sub>2</sub> enzyme arise from autoproteolysis of a precursor protein. The T193 nucleophile at the N-terminus of subunit β is part of an active site that is similar to that of EcAIII. A Cl<sup>-</sup> ion marks the position of the α-carboxylate group of the L-aspartyl substrate/product. An Na<sup>+</sup>-binding loop is necessary for proper positioning of the components of the active site. LIA is structurally similar to threonine aspartase and provides clues about Na<sup>+</sup> and Cl<sup>-</sup> binding by this leukemia-related enzyme.

**01.07.03 Crystal Structure of the Human FOXK1a/DNA Complex and Its Implications on the Diverse Binding Specificity of Winged Helix/forkhead Proteins.** C.-D. Hsiao<sup>‡</sup>, K.-L. Tsai<sup>‡</sup>, C.-Y. Huang<sup>‡</sup>, C.-H. Chang<sup>‡</sup>, Y.-J. Sun<sup>§</sup>, W.-J. Chuang<sup>‡</sup>, <sup>‡</sup>Inst. of Molecular Biology, Academia Sinica, Taipei, Taiwan, ROC, <sup>§</sup>Inst. of Bioinformatics & Structural Biology, National Tsing Hua Univ., Hsinchu, Taiwan, ROC, <sup>¶</sup>Dept. of Biochemistry, National Cheng Kung Univ. College of Medicine, Tainan, Taiwan.

Interleukin enhancer binding factor (ILF) is a human transcription factor and a new member of the winged helix/forkhead family. ILF can bind to purine-rich regulatory motifs such as the human T-cell leukemia virus long terminal region (HILV-1 LTR) and the interleukin-2

(IL-2) promoter. Here we report the 2.4 Å crystal structure of two DNA-binding domain of ILF (FOXK1a) binding to a 16-base pair DNA duplex containing promoter sequence. Electrophoretic mobility shift assay (EMSA) studies demonstrate that two ILF-DBD molecules bind to DNA in a cooperative manner. In addition to the recognition helix recognizes the core sequences through the major groove, the structure shows that wing 1 interacts with minor groove of DNA, and the H2-H3 loop region makes ionic bonds to the phosphate group resulting in affect the recognition of DNA. The structure also reveals that the presence of the C-terminal  $\alpha$ -helix in place of a typical wing 2 in a member of this family results in an alteration of the orientation of the C-terminal basic residues (RKRPR) in binding to DNA outside the core sequence. These results provide a new insight into that how the DNA-binding specificities of winged helix/forkhead proteins may be regulated by their less conserved regions.

**01.07.04 The Crystal Structure of YaeQ from *Xanthomonas axonopodis* pv. *Citri*.** J.A.R.G. Barbosa<sup>1</sup>, C.R. Guzzo<sup>2</sup>, R.A.P. Nagem<sup>3</sup>, L.M.P. Galvão-Botton<sup>2</sup>, C.S. Farah<sup>2</sup>, <sup>1</sup>Laboratório Nacional de Luz Síncrotron, Campinas, SP, Brazil, <sup>2</sup>Univ. de São Paulo, São Paulo, SP, Brazil, <sup>3</sup>Univ. Federal de Minas Gerais, Belo Horizonte, MG, Brazil.

*Xanthomonas axonopodis* pv. *citri* (Xac) YaeQ (XAC2396) is a member of a hypothetical proteins' family conserved in several gram negative pathogens. This protein was been cloned, expressed, purified and crystallized. Initial trials to get heavy atoms derivatives were unsuccessful, leading to the expression, purification and crystallization of recombinant YaeQ containing selenomethionine for MAD experiments. The crystals of space group P2<sub>1</sub> diffracted up to 1.9 Å resolution at a synchrotron source. The unit cell parameters are a = 39.75, b = 91.88, c = 48.03 Å and  $\beta$  = 108.37°. The MAD data was used with SHELXD and autoSHARP to solve the crystal structure, which has two molecules in the asymmetric unit. The YaeQ structure reveals a novel protein fold characterized by a helix located inside an incomplete  $\beta$ -barrel. This barrel is open in one side where the internal helix is slightly exposed. The conserved residues are clustered on two loops located on the top of the barrel and on the exposed face of the central helix. Analysis of the YaeQ structure may provide leads through which information regarding its function may be gained.

**01.07.05 Structural Basis of Plant Disease Resistance in Flax against Flax Rust.** B. Kobe<sup>1</sup>, C.I. Wang<sup>1</sup>, G. Guncar<sup>1</sup>, T. Teh<sup>1</sup>, A.-M. Catanzariti<sup>2</sup>, J.G. Ellis<sup>2</sup>, P.N. Dodds<sup>2</sup>, <sup>1</sup>SMMS/IMB, Univ. of Queensland, Brisbane, <sup>2</sup>Plant Industry, CSIRO, Canberra, Australia.

In plants, the innate immune response involves the recognition of pathogen "avirulence" (Avr) proteins by plant resistance (R) proteins. We have focused on the flax-flax rust fungus interaction as a model system to understand the molecular basis of plant disease resistance. In flax, the L5, L6 and L7 resistance proteins recognise the pathogen AvrL567 proteins. AvrL567 proteins from different flax rust strains exhibit different recognition specificities by the corresponding resistance proteins. Yeast-two-hybrid assays suggest direct protein interactions between the R and Avr proteins. We crystallized two different Avr proteins with differing specificities. The structures were solved using SAD phasing on a home X-ray source, with the anomalous signal contributed by bound Co<sup>2+</sup> ions. The proteins have a novel  $\beta$ -barrel fold, explain the specificity of recognition of flax R proteins and suggest possible functions for the Avr proteins in the fungus. The two major topics of discussion will include: (i) implications of using Co<sup>2+</sup> ions for SAD phasing on a home X-ray source, and (ii) implications for understanding the molecular basis and evolution of plant disease resistance pathways.

**01.07.06 When Crystal Structure Does Not Seem to Depict Physiologically Relevant Conformation - A Novel Calmodulin**

**Conformation in Calmodulin and Calcineurin-Peptide Complex.** Zongchao Jia, Qilu Ye, Xin Li, Andrew Wong, Qun Wei, Biochemistry, Queen's Univ., 18 Stuart St., Kingston ONT., K7L 3N6, CANADA.

Calcineurin is a calmodulin-binding protein in brain and the only serine/threonine protein phosphatase under the control of Ca<sup>2+</sup>/calmodulin (CaM) which plays a critical role in coupling Ca<sup>2+</sup> signals to cellular responses. CaM up-regulates the phosphatase activity of calcineurin by binding to CaM-binding domain (CBD) of calcineurin subunit A. We have determined crystal structures of CaM bound to a CBD peptide in two forms and different space groups. The first one is a chimeric construct containing CaM and the CBD peptide covalently fused through a glycine linker; the second form is a conventional complex structure between CaM and the peptide obtained through co-crystallization. Unexpectedly, both structures display an intimate homodimer, in which CaM possesses a native-like extended conformation and the CBD peptide shows  $\infty$ N-helical structure. The N-terminal lobe from one CaM and the C-terminal lobe from the second molecule form a combined binding site to trap the peptide. Thus the dimer provides two binding sites, each of which is reminiscent of the fully collapsed conformation of CaM commonly observed in complex with, for example, MLCK peptide. The interaction between the peptide and CaM is highly specific and similar to MLCK. However, the novel CaM binding conformation is "deemed" physiologically irrelevant because the full-length calcineurin and CaM forms 1:1 complex as observed in early studies and because of the fact that CaM-peptide construct exists predominantly as a monomer in solution. It is thus extremely intriguing that three independent crystal structures obtained from different constructs and under different conditions persistently reveal a physiologically "irrelevant" conformation. Investigating the cause of this unique observation would be interesting and informative.

**01.07.07 A Medium-scale, High-efficiency and Low-cost Platform for Structural Genomics Studies.** Xiao-Dong Su<sup>a</sup>, <sup>a</sup>College of Life Sciences, Peking Univ., Beijing 100871, China.

A platform for structural studies using Beckman Coulter Biomek FX and self-made automation systems has been set up at Peking University, the platform has a capacity to process about 2000 genes per year. So far, more than 470 *B. subtilis* and 1200 *S. mutans* genes, and hundreds of other genes, including human were selected as targets. More than 40 independent structures have been determined, among them, 11 are of novel structures by the criterion <30% sequence identity with known structures. More than 10 structures were determined *ab initio* by SAD/MAD phasing. We have adapted the genomic approaches in a moderately funded lab, and this adaptation has greatly improved the production of protein structures. Our goal is to solve a protein structure at an average cost of USD 10K.

As part of the platform, a low-cost, in-house developed, imaging robot for SBS crystallization plate has been constructed. It can scan a microplate in one to six minutes and a web-based crystallization database system has been developed, enabling users to follow their crystallization experiments from a web browser. The basic ideas for our system are simplicity, robustness and low-cost. The software consists of a controlling interface and an Image Management system, integrated with our in-house developed lab information management (LIMS).

**01.07.08 Structural Insights into SARS Coronavirus Proteins.** Zihao Rao, Tsinghua Univ., Inst. of Biophysics, CAS Joint Research Group for Structural Biology, Beijing, 100084 China.

Zihao Rao's group has been active in SARS basic research since the 2003 global outbreak, and was the first to determine the crystal structure of a key replicase protein encoded by the SARS coronavirus (SARS-CoV) – the main protease or M<sup>pro</sup> – and its complex with an inhibitor. His group has since made a number of important break-

throughs in SARS research, major achievements include: wide spectrum inhibitor design targeting coronavirus M<sup>pro</sup>; the elucidation of the autocleavage mechanism of coronavirus M<sup>pro</sup>; the structures of the spike (S) protein fusion cores from SARS-CoV and MHV; the structure of the super-complex between two SARS non-structural proteins, nsp7 and nsp8; the dodecamer structure of the SARS non-structural protein nsp10; and the hexamer structure of the MHV non-structural protein nsp15, an endoribonuclease. With more than 18 protein and complex structures from SARS-CoV and related coronaviruses to date, Zihe Rao's group has provided important structural insights into coronavirus replication/transcription.

## 04.01 Structural Biology in Industry

**04.01.01 Nature's Sometimes Indifference to Stoichiometry in Assembling Crystal Structures – Hypersalts.** J.D. DiMarco, M.A. Galella, M.F. Malley, J.Z. Gougoutas, Solid State Chemistry, Bristol-Myers Squibb Pharmaceutical Research Inst., Princeton, NJ 08543.

Crystallization usually is regarded as a means of isolating one chemical component from a mixture (perhaps in combination with the solvent or an additional chemical component introduced by design). However, our results, and a survey of the ~350,000 crystal structures in the Cambridge Crystallographic Database, bear testimony to Nature's ability to assemble surprising combinations of chemical components into well-ordered three dimensional crystals, which in fact represent a failed separation. We present several examples of Hyperacidsalts: homogeneous crystal structures which contain an excess of the acid component (e.g. a pentahydrochloride of trimethylamine). In several other instances, solvates of a base are crystallographically isostructural with some salts of the base, resulting in crystalline solid solutions of variable stoichiometry.

**04.01.02 Differing Protein Conformations used in the Design of VEGFR2 Kinase Inhibitors.** Michele McTigue, Steve Bender, Robert Kania, Michael Niesman, Cynthia Palmer, Christopher Pinko, David Rewolinski, John Wickersham, Structural Biology, Pfizer Global Research and Development, Dr., San Diego, CA 92121.

Vascular endothelial growth factor (VEGF) and its receptor (VEGFR2), expressed primarily on endothelial cells, are recognized as the key initiators of most of the important signaling cascades that promote angiogenesis. Unwanted angiogenesis plays a fundamental role in the pathophysiology of ocular diseases and cancer, among many other diseases. X-ray crystal structures of VEGFR2 kinase in the apo form and in complex with diverse inhibitors reveal distinct protein conformations. In two conformations most of the kinase activation loop is disordered. One inhibitor-bound conformation shows the entire activation loop to be well-ordered and the beginning of the loop to be in the "DFG-out" conformation. An iterative structure-based drug design process employed these multiple conformations to transform a poorly selective inhibitor series that binds to the "open" kinase conformation to a much more potent and selective series that binds to the "DFG-out" conformation. Compounds resulting from this effort are currently in clinical trials: AG-013736 (Phase 2 Oncology) targeting multiple types of solid tumors and AG-013958 (Phase 1/2 Ophthalmology) targeting neovascular age-related macular degeneration (AMD).

**04.01.03 Targeting the HCV RNA Polymerase: Study of Two Types of Non Nucleoside Analogs that Inhibit HCV Replication by Binding In-and-Outside of the Catalytic Site.** Nanhua Yao, Todd Appleby, Shunqi Yan, Yili Ding, Valeant Pharmaceuticals International, Costa Mesa, CA.

Hepatitis C virus (HCV) nonstructural protein 5B (NS5B) is an RNA-dependent RNA polymerase that is essential for the viral replication. It is a valid target for anti-HCV therapy. High-throughput screening identifies two novel series of HCV RNA polymerase inhibitors. X-ray crystallographic study reveals two different binding sites. Subsequent study uncovers two different mechanisms of action. One analog, bound near the center of polymerase close to the catalytic site, interferes with the primer binding. Another analog, bound within a narrow cleft in the "thumb" domain on the surface, is an allosteric inhibitor. It locks the polymerase conformation and perturbs fluctuation within polymerase sub-domains. Structure-activity relationships (SAR) studies are carried out for both series as well.

**04.01.04 Crystal Structures of DPP-IV Exhibit Flexible Accommodation of Peptidase-selective Inhibitors.** Kenton Longenecker, Structural Biology, Abbott Laboratories, Abbott Park, IL 60064.

Dipeptidyl peptidase IV belongs to a family of serine peptidases, and due to its indirect role in regulation of human plasma glucose levels, DPP-IV has become an attractive pharmaceutical target for diabetes therapy. To elucidate details of the active site for structure-based drug design, we crystallized a native source preparation of DPP-IV isolated from rat kidney, and determined its three-dimensional structure using X-ray diffraction techniques. With high similarity to structures of human DPP-IV, the active site architecture provides important details for the design of inhibitory compounds, and structures of inhibitor-protein complexes offer detailed insight to three-dimensional structure-activity relationships that include accommodating protein movement. Structural information aided drug candidate discovery at Abbott Laboratories and examples will be presented in this case study.

**04.01.05 Automated Validation of Ligand Fitness Using "Difference of Difference" Analysis.** Brian Kelley, James Nettles, OpenEye Scientific, 3600 Cerrillos Rd., Suite 1107, Santa Fe, NM 87507.

Current techniques that are used to fit ligands within unoccupied electron density of protein complexes range from manually fitting rigid conformers by eye to automated fitting with conformational flexibility. The techniques for validating these poses primarily rely upon choosing a low energy conformer, and/or selection of a biologically feasible binding mode. Subsequent refinement of the complex is biased by the initial pose selection.

We propose an automated validation technique to be used prior or post refinement. Given multiple poses, it ranks them by Fourier difference analysis in the proposed active site. The efficacy of our "difference of difference" method is illustrated with examples of difficult ligands or low resolution data. Our method provides a quantitative measure of ligand fitness based upon the diffraction data as well as the protein interaction scoring of the model.

**04.01.06 Molecular Recognition of RNA by Neomycin and a Restricted Neomycin Derivative.** Qiang Zhao, Fang Zhao\*, Kenneth F. Blount\*, Qing Han, Yitzhak Tor\*, Thomas Hermann\*, Anadys Pharmaceuticals, Inc. 3115 Merryfield Row, San Diego, CA 92121, \*Dept of Chem & Biochem, UCSD, La Jolla, CA 92093.

Aminoglycoside antibiotics bind to ribosomal RNA at the decoding site and interfere with the accuracy of protein synthesis, ultimately leading to bacterial cell death. We have determined the three-dimensional structure of decoding-site RNA (19 residues) complexes of the aminoglycoside antibiotic neomycin and a conformationally restricted analogue. Both complexes crystallized in space group P212121 with cell dimensions of a=b= 50 Å, and c=145 Å. The structures were

solved by molecular replacement at 3 Å resolution.

The intramolecular 2,-5, cross-link introduced into the restricted natural product is compatible with binding. Comparison of the structures reveals the sensitivity of aminoglycoside target recognition toward even slight modifications to the architecture of the ligand. While most key interactions are undisturbed by the modification, two hydrogen bonding contacts are abolished. Neomycin binds to the decoding-site RNA in the same conformation and at the same site as the structurally similar paromomycin. Unexpectedly, a secondary binding site was discovered for both neomycin and the restricted derivative.

Help in data collection by personnel of the APS beamstation 14 is acknowledged.

## 05.01 Non-Ambient Crystallography

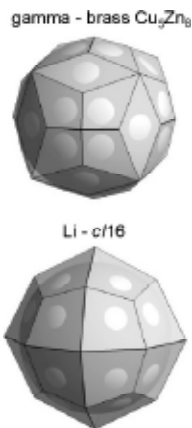
**05.01.01 Phase Diagram of Nitrogen at High Pressures and Temperatures.** Eugene Gregoryanz, Chrystele Sanloup, Alexander Goncharov, Russell Hemley, Ho-kwang Mao, School of Physics, Univ. of Edinburgh, Mayfield St., Edinburgh EH9 3JZ, UK.

The evolution of molecular solids under pressure constitutes an important problem in condensed matter physics. Under compression, delocalization of electronic shells and eventual molecular dissociation is expected, leading to the formation of a framework or closed packed structures. However, this process may not necessarily be simple and direct, because of large barriers of transformation between states with different types of bonding and molecular structures with various types of orientational order, including possible associated and charge transfer intermediate states.

We report the discovery of a new class of molecular phases of solid nitrogen at high pressures and temperatures by Raman scattering, infrared and optical absorption, and powder synchrotron x-ray diffraction. The most remarkable is a new phase theta which is characterized by strong intermolecular interactions and infrared vibron absorption and can be reached within the wide pressure range at temperatures above 550 K. A second phase iota is diatomic with orientationally equivalent molecules. Both phases can be quenched to room temperature and are observed over a wide P-T range from 20 to 100 GPa and 30 to 1000 K. The results suggest a major revision of the phase relations of nitrogen at high pressures and temperatures.

**05.01.02 Crystal Structure of High-pressure Phases in Simple Metals: View from the Reciprocal Space.** Valentina F. Degtyareva, Inst. of Solid State Physics, Russian Academy of Sciences, Chernogolovka, Moscow region, 142432 Russia.

Recent high-pressure studies on simple metals yielded transitions from close-packed high-symmetry structures (like *fcc*, *bcc* and *hcp*) to complex, low-symmetry structures. Underlying physical reasons can be understood by Fermi sphere – Brillouin zone interactions (FS-BZ) within the nearly-free-electron model. Crystal structure energy is lowered by formation of the energy gap at BZ boundaries lying close to the Fermi level. The classical example of a crystal structure stabilized by FS-BZ effects is a Hume-Rothery gamma-brass phase  $\text{Cu}_3\text{Zn}_8$  with 36-faced BZ polyhedron accommodating well the FS and filled by electron states to ~93% (upper figure). Similar Hume-Rothery effect is a characteristic of high-pressure structures of alkali metals as *Li-c/16* [1] and related structures of heavy



alkalis. The BZ polyhedron of *Li-c/16* consists of 24 planes in contact with the FS and is filled by electron states to ~89% (lower figure). A program BRIZ is developed to visualize the FS-BZ configurations [2]. Several complex structures in *sp* metals at ambient and high pressure are considered with the electron contribution as a dominant part of the crystal structure energy.

This research is supported by Russian Foundation for Basic Research under the grant 04-02-17343.

[1] Hanfland M, Syassen K, Christensen NE, Novikov DL, Nature 408, 174 (2000). [2] Smirnova I.S., Degtyareva V.F., *BRIZ – a program for the FS-BZ visualization*, Institute of Solid State Physics, Russian Academy of Sciences (2005).

**05.01.03 High Pressure Phases of  $\text{CaCO}_3$ , S and H Obtained by USPEX.** Colin W. Glass\*, Artem R. Oganov, Lab. of Crystallography, ETH Zürich, Wolfgang-Pauli-Str. 10, 8093 Zurich, CH, cglass@student.ethz.ch.

Recently we have developed a very efficient and reliable method for crystal structure prediction [1,2], merging an evolutionary algorithm with *in initio* total-energy calculations. Relying purely on theoretical knowledge and being thus independent from experiment, this method allows prediction of the most stable crystal structure at any given *P-T* conditions. Simultaneously it finds a large number of competitive metastable structures and gives an insight into the structural chemistry of the compound.

Focus here is on the results from USPEX on  $\text{CaCO}_3$ , S and H at high pressure. For  $\text{CaCO}_3$  we have discovered new stable structures between 42 and 137 GPa and above 137 GPa [3]. For S competitive metastable and a new stable structure around 5 GPa will be presented. In the case of H we show results from runs at 600 GPa, where contrary to conventional wisdom we have found only molecular structures.

[1] Glass C.W, Oganov A.R., Hansen N. (2006). USPEX: evolutionary crystal structure prediction

[2] Oganov A.R., Glass C.W. (2006). Crystal structure prediction using *ab initio* evolutionary techniques: principles and applications. Submitted.

[3] Oganov A.R., Glass C.W., Ono S. (2006). High-pressure phases of  $\text{CaCO}_3$ : crystal structure prediction and experiment. *Earth Planet. Sci. Lett.* **241**, 95-103.

**05.01.04 Crystal Structure, Equation of State and Pressure-Induced Phase/Distortional Transition(s) in  $\text{B}_4\text{C}$ : *In-situ* Synchrotron XRD and Raman Study to 60 GPa.** Murli H. Manghnani<sup>1</sup>, George Amulele<sup>1</sup>, Jilian Zhu<sup>1</sup>, Pzremek Dera<sup>2</sup>, Yuchang Wang<sup>1</sup>, Mariappan Sekar<sup>1</sup>, <sup>1</sup>Univ. of Hawaii, Hawaii Inst. of Geophysics & Planology, <sup>2</sup>Geophysical Laboratory, Carnegie Inst. of Washington.

Synchrotron X-ray diffraction (XRD) and Raman spectroscopy measurements have been carried out on  $\text{B}_4\text{C}$  in a diamond-anvil cell to 60 GPa. These results, in conjunction with single-crystal XRD at ambient conditions and high-pressure ultrasonic measurements, are compared with shock wave data in order to understand the compression behavior, establish the equations of state, and explain the observed poor ballistic performance.

Whereas the powder XRD data indicate no easily detectable discontinuous changes within the studied pressure range, the Raman spectroscopy, electrical conductivity measurements, and shock wave data suggest a more complex behavior. Motivated by this discrepancy, a detailed strain/stress analysis based on the peak profile broadening was performed, revealing two regions of discontinuous strain change, which cannot be explained by the transformations of pressure transmitting medium. These changes can be tentatively associated with electronic transformations and changes in bonding. Preliminary results from the electrical resistivity and optical measurements support this interpretation.

**05.01.05 Reactivity of Xe with Silica at High Pressures and Temperatures.** C. Sanloup<sup>1</sup>, B. Schmidt<sup>2</sup>, E. Chamorro Perrez<sup>3</sup>, A. Jambon<sup>1</sup>, E. Gregoryanz<sup>4</sup>, M. Mezouar<sup>5</sup>, <sup>1</sup>Univ. Pierre et Marie Curie-Paris, France, <sup>2</sup>Goettingen Univ., Germany, <sup>3</sup>CSEC, Univ. of Edinburgh, UK, <sup>4</sup>ESRF, Grenoble, France.

The rare gases are widely used as geochemical tracers assuming they are volatile and chemically inert. Xenon isotopes are used to date the formation of the atmosphere, and the age of the Earth. Argon isotopes are used as tracers of mantle mixing/dynamics. However, normally inert rare gases have shown to be not that inert starting in 1962, with the synthesis of xenon salts (1). The chemistry of Xe now extends to O, C, N, S, and halogens (2). Several Kr compounds are known (3), few Ar compounds have also been synthesized and bonding with C and Si is predicted (4).

We show that at high temperatures and pressures, the normally unreactive xenon can bond covalently with oxygen in quartz (5), displacing silicon atoms in the crystal lattice. This suggests that xenon could exist in stores of quartz that lie deep inside the Earth's crust, a possibility that would normally escape notice because xenon diffuses out almost immediately at surface conditions. This result provides an answer to the long standing "missing Xe" problem, *i.e.* the deficiency of the atmosphere in xenon compared to other rare gases. This result also opens the way to rare gases chemistry.

(1) Bartlett, Proc. Chem. Soc., 27, 218, 1962. (2) Pettersen et al., Eur. J. Inorg. Chem., 505, 729, 1999. (3) Khriachtchev, J. Am. Chem. Soc., 125, 6876, 2003. (4) Cohen et al., J. Chem. Physics, 119, 6415, 2003. (5) Sanloup et al., Science, 310, 1174, 2005.

**05.01.06 Structure and Stability of Low-Z Ionic Solids at High Pressure.** A. Lazicki<sup>1,2</sup>, C.S. Yoo<sup>1</sup>, W. Pickett<sup>2</sup>, R. Scalettar<sup>2</sup>, <sup>1</sup>Lawrence Livermore Nat'l Lab, Livermore, CA, <sup>2</sup>Univ. of California, Davis, CA.

We explore pressure-induced phase transitions in a class of highly ionic low-Z compounds with simple structures using synchrotron x-ray diffraction and spectroscopy in diamond anvil cells and with electronic structure calculations. Results for Li<sub>3</sub>N and Li<sub>2</sub>O reveal some original and unexpected properties and provide a better general understanding of this class of closed-shell materials, and of their hydrogen-containing analogs NH<sub>3</sub> and H<sub>2</sub>O. Li<sub>3</sub>N has a hexagonal to cubic structural transition at 40 GPa, accompanied by a volume collapse and electronic band-gap widening. The new phase is stable to over 200 GPa, and the N<sup>3-</sup> ions (isovalent to neon) retain their ionic character. Like neon, the compressibility and metallization pressure are very high. Li<sub>2</sub>O, which is structurally and electronically similar to high pressure ice, undergoes a cubic-orthorhombic transition at 50 GPa, with a 100% increase in bulk modulus. Considered with the known behavior of alkali sulfides, the present results for Li<sub>2</sub>O indicate a systematic high-pressure behavior of all alkali chalcogenides, including non-molecular ice at ultra-high pressure.

Supported by the LDRD-04-ERD-020 and PDRP programs at LLNL, U.S. DOE Contract No. W-7405-ENG-48 and by the SSAAP, grant No. 01-06NA26204.

**05.01.07 The Molecular Structure of RDX at High Pressure.** Wayne H. Pearson<sup>1</sup>, Suhithi M. Peiris<sup>2</sup>, <sup>1</sup>Chemistry Dept., US Naval Academy, Annapolis, MD, <sup>2</sup>Indian Head Div., Naval Surface Warfare Center, Indian Head, MD.

RDX, 1,3,5-trinitrohexahydro-1,3,5-triazine, is an explosive material used for military applications. We have undertaken a study of the crystal structure of RDX to determine how the geometry of the molecule changes in high-pressure environments. Data were collected at Cornell University's synchrotron source (CHESS) with crystals loaded in Merrill-Bassett type DACs at various pressures. Omega scans of 4° were performed at different chi settings on a two-circle goniometer.

The images were recorded on a MARS 3450 image-plate detector and the resulting data were indexed and integrated using DPS/Mosflm. Full structural analyses of the data were performed using SHELX. Significant changes in bond lengths, angular distortions and ring puckering are evident at 1.5 GPa when compared to the ambient pressure structure. The 2 and 3.5 GPa data appear to reveal the existence of two separate phases, indicating that the phase transition previously seen at 3.8 GPa may start occurring at lower pressure.

**05.01.08 Advanced Processing of High-Pressure Data from CCD Detector System.** Michael Ruf, Bruker AXS Inc., Madison, WI.

A major challenge in the field of High Pressure crystallography is the acquisition of sufficient quality data for a successful structure determination especially for low symmetry samples. The volume of reciprocal space accessible for X-ray examination is constrained by the shape and size of the Diamond Anvil cell used and mostly determined by its opening angle. In addition the acquired data suffer from absorption effects from the Diamond Anvils, high background and Beryllium powder diffraction as well as overlapping of sample reflections with those from the diamonds used in the experiment.

The advantages of using CCD detectors in the field of high-pressure single-crystal structure determination have been well recognized in recent years. Modern 3- and 4-axes goniometers equipped with a CCD detector allow the acquisition of virtually all accessible data. These diffraction systems are very sensitive and fast with highly automated software for strategy planning, data acquisition and data processing.

This presentation will focus on recent advances in software development which help tackling the problems with data acquired in high-pressure experiments as outlined above. We will present new algorithms for data integration for simultaneous processing and deconvolution of reflections from the sample and the diamond reflections.

## 09.01 Grazing Incidence for Nanoscience and Biotechnology

**09.01.01 Developing A Dedicated Grazing-Incidence Small-Angle X-ray Scattering Beamline at the APS.** Xuefa Li, Michael Sprung, Suresh Narayanan, Alec Sandy, Dong Ryeol Lee, Jin Wang, APS, Argonne National Lab, Argonne, IL.

As an increasingly important structural-characterization technique, grazing-incidence small-angle scattering (GISAXS) finds vast applications in nanostructures and nanocomposites at surfaces and interfaces for *in situ* and real-time studies.

To meet the strong demand from the nanoscience community, a dedicated GISAXS beamline has been designed and constructed as a part of the 8-ID-E beam line at the Advanced Photon Source (APS). Taking advantages of x-ray beam from an undulator, this beamline is designed with both simplicity and flexibility in mind to achieve high resolutions in both reciprocal and real spaces as well as high temporal resolution in measurement. The simplicity comes from a fixed photon energy of 7.4 KeV with a stable upstream slit arrangement to ensure a high throughput user operation. The flexibility comes from the many aspects: four-circle diffractometer-based sample holder for freedoms and precision of sample manipulations, and, various sample environments. More specifically, the samples can be situated in an integrated vacuum chamber on a high-precision heating and cooling stage. The sample chamber can also be isolated from the beamline to allow solvent flows and to accommodate other mechanical systems such as *in situ* dip-coating devices. In this presentation, the details of this dedicated beamline will be discussed along with scientific highlights from the first group of the experiments performed at the beamline.

**09.01.02 Self-assembly and Cross-linking of Nanoparticles at Liquid-liquid Interfaces.** Thomas P. Russell, Polymer Science and Engineering Dept., Univ. of Massachusetts, Amherst, MA 01003.

The fabrication of functional nanostructured materials for sensing, encapsulation and delivery requires practical approaches to self-assembly on multiple length scales and the synthesis of tough yet permeable structures. Here, ligand-stabilized nanoparticles assembled into three-dimensional constructs at fluid-fluid interfaces driven by the reduction in interfacial energy were investigated. Studies on the dynamics of the nanoparticles and the self-assembled structures formed at the interface, using fluorescence photobleaching methods and *in-situ* grazing incidence small angle x-ray scattering (GISAXS), suggest a liquid-like behavior and ordering at the interfaces. Cross-linking of the nanoparticle assembly using functional ligands, affords robust membranes that maintain their integrity even when they are removed from the interface. These composite membranes, nanometers in thickness, are elastic yet permeable and have potential applications involving controlled permeability and diffusion. The assembly of virus and other biological complexes at fluid interfaces was also investigated where interfacial assembly rendered an easy route to direct and assemble the bioparticles into 2-D and 3-D constructs with hierarchical ordering. These assemblies enable the potential use of the bioparticles as a natural supramolecular building block to obtain materials with well-defined bio-functionalities.

In collaboration with: Yao Lin, Alexander Böker, Habib Skaff, Jinbo He, Kevin Sill, Todd Emrick, A. D. Dinsmore (Univ. of Massachusetts Amherst), Su Long, Qian Wang (Univ. South Carolina)

**09.01.03 Internal and Interface Structure in Diblock Copolymer Brushes.** M.D. Foster<sup>1</sup>, B. Akgun<sup>1</sup>, G. Ugru<sup>1</sup>, W.J. Brittain<sup>1</sup>, X. Li<sup>2</sup>, D.R. Lee<sup>2</sup>, J. Wang<sup>2</sup>, <sup>1</sup>Maurice Morton Inst. of Polymer Science, Univ. of Akron, Akron, OH 44325, <sup>2</sup>Experimental Facilities Div., Argonne National Laboratory, Argonne, IL 60439.

Internal and surface structure of polystyrene-*b*-polyacrylate diblock copolymer brushes have been studied using grazing-incidence small-angle X-ray scattering (GISAXS) and atomic force microscopy (AFM). Polystyrene-*b*-polyacrylate or polyacrylate-*b*-polystyrene brushes were synthesized using atom transfer radical polymerization. Poly (methylacrylate) or poly(*n*-butyl acrylate) is used as the acrylate block. Each as-deposited diblock brush shows an internal lateral structure with a spacing comparable to the thickness of the top layer of the brush on the order of 10 nm. After a brush is treated with a solvent which is a good or theta solvent for the bottom block and poor solvent for the top block, Bragg rods appear in GISAXS pattern. The lateral spacing corresponding to the Bragg rods is on the order of the total thickness of the brush. This lateral correlation is also detected by the power spectral density analysis of the AFM measurements of the samples' surfaces using tapping mode imaging. The Bragg rods disappear upon heating to 80 °C and this behavior does not depend on which polyacrylate block was used.

**09.01.04 GISAXS Studies of Gold and Platinum Nanoparticles Formed by Atomic Cluster Deposition.** S. Vajda<sup>1,2</sup>, R.E. Winans<sup>1,3</sup>, G.E. Ballentine<sup>1</sup>, J.W. Elam<sup>4</sup>, B. Lee<sup>3</sup>, M.J. Pellin<sup>3</sup>, S. Seifert<sup>3</sup>, G.Y. Tikhonov<sup>1</sup>, N.A. Tomczyk<sup>1</sup>, <sup>1</sup>Chemistry Div., <sup>2</sup>Center for Nanoscale Materials, <sup>3</sup>Experimental Facility Div., <sup>4</sup>Energy Systems Div., <sup>5</sup>Materials Science Div., Argonne National Laboratory, Argonne, IL.

GISAXS is a powerful tool for the determination of the size and shape of nanoparticles dispersed on surfaces or embedded into thin films. It allows for real-time monitoring of the evolution of particle size and shape with temperature and to study the kinetics of particle aggregation under vacuum conditions or when exposed to reactive gases. We

have used this technique for the characterization of sub-nm to several nm size platinum and gold particles produced by deposition of atomic metal clusters from molecular beams on technologically relevant oxide surfaces. These studies made it possible to monitor cluster isomerization, to follow aggregation of clusters into larger nanoparticles with various shapes, to identify cluster-support combinations for potential use e.g. in catalysis oriented research, as well as the characterization of ultrathin oxide films used as supports.

This work and use of APS was supported by the U.S. Department of Energy, Office of Basic Energy Sciences, Division of Chemical Sciences, Geosciences, and Biosciences under contract number W-31-109-ENG-38.

**09.01.05 Spin Echo Resolved Grazing Incidence Neutron Scattering.** Suzanne G.E. te Velthuis, Péter Falus, Gian P. Felcher, Materials Science Div., Argonne National Laboratory, Argonne IL, Alexei Vorobiev, János Major, Helmut Dosch, Max Planck Institut für Metallforschung, Stuttgart, Germany, Peter Müller-Buschbaum, Technische Univ. München, Garching, Germany.

Conventionally the spin-echo technique is used to encode energy transfer in neutron inelastic scattering experiments. However, spin-echo may encode the neutron momentum transfer, allowing the probing of large length scale structures without the need of a tight neutron beam collimation and resulting intensity loss. This concept has recently been successfully utilized for small angle scattering experiments in transmission geometry as well as scattering in the grazing incidence geometry at a reflectometer (EVA, Institut Laue-Langevin, Grenoble) equipped with neutron resonance spin echo circuits as well as appropriate neutron spin rotators. The tests included the measurement in transmission geometry of suspensions of polystyrene balls (1500 Å radius) as well as anodized aluminum oxide 2D gratings, as well as the measurement in reflection geometry of the characteristic lengths of assemblies of polystyrene droplets dewetted from a silicon surface. The results are guiding the design of an instrument for the Spallation Neutron Source capable of studying the structure and working of biological membranes.

## 09.02 Bio-Macromolecular Assemblies

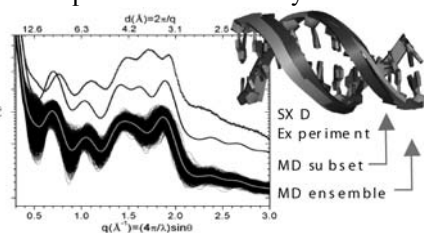
**09.02.01 Structural Studies of Macromolecular Complexes in Solution by Small-Angle X-ray and Neutron Scattering.** D.I. Svergun, European Molecular Biology Laboratory, Hamburg Outstation c/o DESY, Notkestr. 85, D22603 Hamburg, Germany, Inst. of Crystallography, Russian Academy of Sciences, Leninsky pr. 59, 117333 Moscow.

Small-angle scattering of X-rays and neutrons (SAS) is an increasingly important tool for the study of biological macromolecules in solution. The method allows one to study low resolution (1-2nm) structure of native particles, from individual proteins to large macromolecular complexes and also to analyse structural responses to variations in external conditions. Recent progress in instrumentation and data analysis (1) significantly enhanced resolution and reliability of structural models provided by the technique. Advanced methods to analyze X-ray and neutron scattering data from solutions of biological macromolecules will be presented including (i) *ab initio* low resolution shape and domain structure determination; (ii) modeling of quaternary structure by rigid body refinement; (iii) specific deuteration combined with contrast variation in neutron scattering to study multi-component complexes; (iv) quantitative analysis of equilibrium mixtures. Practical applications of the methods will be illustrated by recent examples.

Koch, M. H. J., Vachette, P. & Svergun, D. I. (2003) *Quart. Rev. Biophys.* 36, 147–227.

**09.02.02 X-ray Diffraction “Fingerprints” of Biomolecular Structure and Dynamics in Solution.** D.M. Tiede, X. Zuo, A.J. Goshe, Chemistry Div., Argonne National Lab, Argonne, IL, 60439.

Advances in synchrotron X-ray scattering techniques offer new opportunities for characterization of biomolecular structure and dynamics in non-crystalline media that build upon crystallographic, NMR, and molecular dynamics (MD) databases, but are applied to conditions relevant to in-situ function. Advances include extension to the high-angle domain where measurements can be routinely made to a spatial resolution of 1 Å, and the development of coordinate-based analyses that allows scattering data to be analyzed in terms of detailed coordinate models for structure and dynamics. Solution X-ray diffraction (SXD) “fingerprint” patterns provide a 1D summary of 3D structure. Peak positions and linewidths are found to provide direct measures of structure and configurational dispersion, respectively. We have found that experimental SXD patterns can be used as benchmarks to discriminate between crystallographic, NMR, and MD models for solution state protein and DNA structures, and to “refine” coordinate models to fit solution state data. Comparisons to MD simulation for A-tract (polyA-polyT) DNA reveal shortcomings in the underlying force fields that skew simulated ensembles toward B-form conformers.



Work performed at sectors 11 and 12 Advanced Photon Source. Support DOE contract W-31-109-ENG-38.

**09.02.03 Visualizing Protein-Protein and Protein-Nucleic Acid Interactions by Small-angle Scattering.** William T. Heller, Center for Structural Molecular Biology and Chemical Sciences Div., Oak Ridge National Laboratory, Oak Ridge, TN 37831.

In the post-genomics era, the focus of attention in structural biology has expanded from studies of the structure-function relation of single biological macromolecules in isolation to investigations of the interactions that exist among the systems of proteins and nucleic acids that are responsible for higher-order biological processes. Small-angle scattering is poised to play a significant role in structurally characterizing these macromolecular complexes and understanding the dynamic processes involved in the interactions between the subunits. Advances in modeling structures from small-angle scattering data have provided a means for the user to visualize both the structures of the subunits and complexes and the conformational changes that occur upon complex formation and the binding of ligands. A brief overview of the efforts at Oak Ridge National Laboratory will be presented with examples of the application of these methods to the study of protein-protein and protein-nucleic acid interactions.

This work was supported by the Office of Biological and Environmental Research of the U. S. Department of Energy project KP1101010, under contract No. DE-AC05-00OR22725 with Oak Ridge National Laboratory, managed and operated by UT-Batelle, LLC.

**09.02.04 Virus Particle Maturation followed by SAX.** John E. Johnson, Kelly Lee, Hiro Tsuruta, The Scripps Research Institute, 10550 N. Torrey Pines Rd, La Jolla, CA.

The complex protein capsids of many viruses exhibit dramatic reorganizations at critical stages in their life-cycle. Here, time-resolved solution X-ray scattering was used to investigate two stages of dynamic, large-scale conformational maturation steps of the 420 subunit, 13 MDa, icosahedrally symmetric HK97 bacteriophage capsid. The first transition

was triggered by lowering the pH to 4. The analysis demonstrated that the population shift from Prohead-II to Expansion Intermediate I, EI-I (60 Å larger than Prohead-II) occurs in minutes, but does not reveal the time required for individual transitions that occur stochastically. Any intermediate forms that may be traversed during this conversion are unstable and do not constitute an appreciable population of the ensemble of particles. The second stage studied is the maturation from E-I to the final mature form triggered by raising the pH to 7. This transition is dependent on chemical cross-link formation between subunits. Like the first transition, no intermediates were found indicating that a quorum of cross-links needs to form before the transition occurs and then it proceeds without detectable intermediates.

**09.02.05 The Role of SAXS in the Study of Non-crystalline Biological Systems.** Michel H. J. Koch, European Molecular Biology Laboratory, Hamburg Outstation, Notkestrasse 85, Hamburg, 22603 GERMANY.

The progress in the study of non-crystalline systems by X-ray scattering and closely related imaging techniques, made possible by advances in synchrotron radiation sources and instrumentation, will be reviewed. A brief introduction to the techniques will be followed by the presentation of a range of applications to problems in fundamental and applied research in biochemistry and biophysics as well as in food and pharmaceutical technology.

**09.02.06 Nanotubular Structures of Microtubule-Spermine and Microtubule-Lipid Complexes.** Y. Li, D.J. Needleman, U. Raviv, M.A. Ojeda-Lopez, H.P. Miller, L. Wilson, C.R. Safinya, Materials Research Lab, Materials Dept., Physics Dept., Dept. of Molecular, Cellular, and Developmental Biology, Biomolecular Science and Engineering Program, Univ. of California, Santa Barbara, CA 93106.

Two distinct supramolecular assemblies of microtubules (MT) in the presence of spermine and cationic lipids membranes were revealed using small angle x-ray diffraction and electron microscopy. The MT-spermine complex is characterized as a columnar phase of inverted tubules, in which the orientation of the tubulin units was switched from inside out. The transformation of normal MT to the inverted tubules is induced by a novel phase transition driven by a discrete conformational change in the constituent tubulin subunit. In MT-membrane complexes, two new structures were observed. Depending on conditions, lipid vesicles either adsorb onto the microtubule, forming a ‘beads on a rod’ structure, or coat the microtubule to form a sheath. Tubulin rings can then coat the external lipid bilayer to form a multi-shell tubular structure with a tubulin-lipid-tubulin radial profile. Kinetic experiments were conducted to shed light on the mechanism of hierarchical complex formation. Research supported by NIH GM-59288, NSF DMR-0503347, CTS-0404444.

**09.02.07 The Center for Structural Molecular Biology (CSMB) at Oak Ridge National Laboratory (ORNL).** V.S. Urban<sup>1</sup>, W.T. Heller<sup>1</sup>, G.W. Lynn<sup>1</sup>, G.D. Wignall<sup>2</sup>, K. Weiss<sup>1</sup>, D.A.A. Myles<sup>1</sup>, <sup>1</sup>Chemical Sciences Div. and <sup>2</sup>Condensed Matter Sciences Div., ORNL, Oak Ridge, TN 37831.

The CSMB at ORNL is developing facilities and techniques for the characterization and analysis of biological systems at the High Flux Isotope Reactor (HFIR) and the Spallation Neutron Source (SNS). The cornerstone of the effort is a small angle neutron scattering instrument (Bio-SANS) currently under construction at HFIR that will be dedicated to the analysis of the structure, function and dynamics of complex biological systems. In support of this program, we are de-

veloping advanced computational tools for neutron analysis and modeling, alongside a supporting biophysical characterization and X-ray scattering infrastructure. Specifically, we established a Bio-Deuteration Laboratory for *in vivo* production of H/D labeled macromolecules that will permit selected parts of macromolecular structures to be highlighted and analyzed *in situ* using neutron scattering. These new facilities will make ORNL a world-leading scientific center and user facility for neutron-based studies of bio-molecular structure and function.

Sponsored by the Office of Biological and Environmental Research, U.S. Department of Energy, under contract No. DE-AC05-00OR22725 with Oak Ridge National Laboratory, managed and operated by UT-Battelle, LLC.

## 09.03 Polymer Science & Technology

### 09.03.01 Structure Evolution and Gradients in Oriented Polymer Parts Studied by Scattering Methods Using Synchrotron Radiation.

N. Stribeck, S.V. Roth, P. Bösecke, C. Schroer, A. Al-mendarez Camarillo, M. Kuhlmann, U. Nöchel, Dept. of Chemistry, Inst. TMC, Univ. of Hamburg, Hamburg, Germany.

In the field of semicrystalline polymer parts structure evolution during crystallization and melting as well as the spatial variation of nanoscale structure is studied. We develop and apply advanced Fourier-transform methods (multidimensional chord distribution function analysis (CDF), SAXS tomography) and investigate nanostructure evolution *in-situ* in order to understand its mechanisms. Our samples are commercial grades from different polymers (PE, PP, PVDF).

We focus on samples with fiber symmetry because we require complete reciprocal space data recorded fast. For the study of the interaction between nanostructure formation and crystallization a time-resolution of 1 s appears to be sufficient. Our data collected so far indicate that a dominant mechanism of quiescent polymer crystallization is a random crowding (random car parking process). SAXS tomography is demonstrated in a study of the inner structure of an injection moulded PE rod. The spatial resolution of 80  $\mu\text{m}$  must be enhanced for the investigation of real fibers.

We acknowledge HASYLAB, Hamburg (BW4) and ESRF, Grenoble (ID02) for provision of synchrotron radiation facilities. Financial support by the Deutsche Forschungsgemeinschaft (DFG STR501/4-1) is gratefully acknowledged.

### 09.03.02 Deformation Mechanisms of Polyethylene via *in-situ* X-ray Scattering.

Brian G. Landes, Theresa J. Hermel-Davidock\*, Willem DeGroot\*, Mehmet Demirors\*, Rajen Patel\*, Tracy Peltier\*, Danny King\*, Steven Weigand\*\*, The Dow Chemical Co., Midland, MI 48667, \*The Dow Chemical Co., Freeport, TX, 77541, \*\*DND-CAT, APS/ANL, Argonne, IL 60439.

Changes in the microstructure of ethylene based copolymers can be used to modify and enhance their mechanical performance. However, polyethylene films exhibiting very different performance may not be differentiated by standard tensile test methods. Alternative methods that link morphology and mechanical response need to be found. In this study the mechanical performance of select polyethylene polymers were examined. Wide-angle and small-angle x-ray scattering data were collected *in-situ* during tensile testing to understand the mechanical response of semicrystalline polyethylene polymers. A comparison of continuous stretch, and stop/hold experiments was performed. These studies reveal that the method of experimental interrogation has a direct impact on the morphological response, and thus the performance, in these systems. Methods for reduction of these large volume data sets will also be reviewed.

This work was performed at the DuPont-Northwestern-Dow Collaborative Access Team (DND-CAT) Synchrotron Research Center located at Sector 5 of the Advanced

Photon Source. DND-CAT is supported by the E.I. DuPont de Nemours & Co., The Dow Chemical Company, the U.S. National Science Foundation through Grant DMR-9304725 and the State of Illinois through the Department of Commerce and the Board of Higher Education Grant IBHE HECA NWU 96. Use of the Advanced Photon Source was supported by the U. S. Department of Energy, Office of Science, Office of Basic Energy Sciences, under Contract No. W-31-109-Eng-38.

### 09.03.03 *In-situ* Studies of Strain-induced Crystallisation of Poly (lactic acid) During Fast Uniaxial Deformation.

A. Mahendrasingam\*, DJ Blundell\*, M Parton\*, W Fuller\*, T Narayanan\*, \*School of Physical and Geographical Sciences, Keele Univ., Keele, Staffordshire, ST5 5BG, UK, \*ESRF, Grenoble, France.

Recently, there is rapidly growing industrial interest in producing biodegradable polymers as alternatives to the conventional polymer materials produced from petrochemicals. Poly (lactic acid) (PLA) is attracting particular attention by industry because it can be derived from renewable natural resources such as corn starch and sugar cane.

Our recent studies shows that:

At temperatures less than 100°C, the onset of crystallisation is close to the point where the deformation has ceased. Subsequent crystallisation follows a first order kinetics. This behaviour is similar to that we have observed in our previous studies of PET during the very fast uniaxial deformation.

WAXS pattern recorded after annealing shows intermediate layer lines which is consistent with the  $\alpha$ -form with a 10<sub>1</sub> helix. However, prior to annealing the separation of the layer lines indicates a different helical configuration.

In this paper further studies on the effect of draw temperatures, draw rates and small amounts of poly (D-lactide) on strain-induced crystallisation during the uniaxial deformation of PLA using *in-situ* time-resolved x-ray diffraction techniques at the ESRF will be discussed.

### 09.03.04 Electric Field Induced Effects on the Microdomains in Concentrated Block Copolymer Solutions.

Alexander Böker, Physikalische Chemie II, Univ. Bayreuth, 95440 Bayreuth, Germany.

We investigate the electric field induced orientation of diblock copolymer microdomains in concentrated solutions using Synchrotron SAXS. Recently, we have identified rotation of grains and nucleation and growth as the two governing mechanisms during microdomain orientation.<sup>1,2</sup> Moreover, the dependence of the reorientation kinetics on the dielectric contrast of the blocks, the defect density as well as the electric field strength was investigated.<sup>3,4</sup> More recently, the effect of the electric field on the polymer chains and on the block copolymer phase behavior has been studied. In this talk, we will show SAXS experiments elucidating the mechanisms and kinetics of block copolymer microdomain alignment. In addition, we will demonstrate the distinct influence of the electric field on the microphase, resulting in chain stretching and even phase mixing at sufficiently high field strengths.

#### References

- (1) Böker, A.; Elbs, H.; Hänsel, H.; Knoll, A.; Ludwigs, S.; Zettl, H.; Urban, V.; Abetz, V.; Müller, A. H. E.; Krausch, G. *Phys. Rev. Lett.* 2002, 89, 135501-135504.
- (2) Böker, A.; Elbs, H.; Hänsel, H.; Knoll, A.; Ludwigs, S.; Zettl, H.; Zvelindovsky, A. V.; Sevink, G. J. A.; Urban, V.; Abetz, V.; Müller, A. H. E.; Krausch, G. *Macromolecules* 2003, 36, 8078-8087.
- (3) Böker, A.; Schmidt, K.; Knoll, A.; Zettl, H.; Hänsel, H.; Urban, V.; Abetz, V.; Krausch, G. *Polymer* 2006, 47, 849-857.
- (4) Schmidt, K.; Böker, A.; Zettl, H.; Schubert, F.; Hänsel, H.; Fischer, F.; Weiss, T. M.; Abetz, V.; Zvelindovsky, A. V.; Sevink, G. J. A.; Krausch, G. *Langmuir* 2005, 21, 11974.

**09.03.05 Phase Behavior of Nanoparticle/Diblock Copolymer Composites.** P. Thiyagarajan<sup>1</sup>, Chieh-Tsung Lo<sup>2</sup>, Byeongdu Lee<sup>2</sup>, Randall E. Winans<sup>2,3</sup>, <sup>1</sup>IPNS, <sup>2</sup>XFD, APS, <sup>3</sup>Chemistry Div., Argonne National Laboratory, Argonne, IL.

Our research is focused on developing techniques to organize nanoparticles in 2D arrays by using self-assembled copolymers as templates. Our method involves the synthesis of nanoparticles covalently attached to a polymer that can selectively sequester into one domain of diblock copolymers. We investigated the effect of fillers on the phase behavior of polymer nanocomposites composed of polystyrene-*b*-poly(2-vinylpyridine) (PS-PVP) and thiol terminated PS stabilized Au nanoparticles in *d*-toluene at semidilute concentration. We observe that the morphologies of the neat and nanoparticle containing polymer solutions strongly depend on the copolymer composition, polymer molecular weight, filler loading and temperature. Comparison of the phase diagrams of the neat and nanoparticle loaded polymer solutions as a function of temperature shows dramatic shifts in the order-disorder and order-order transition temperatures. This dramatic effect can be understood by a model wherein the added nanoparticles that sequester in the preferred PS domains lead to an increase in the interfacial curvature and hence the nanostructure of the composite. Knowledge gained from these studies on the effects of nanoparticle loading and temperature on the phase behavior of the polymer nanocomposites will be critical to tailor the physical properties of these novel nanocomposites for various applications.

This work supported by the LDRD and benefited by the use of APS and IPNS funded by DOE-BES under contract #W-31-109-ENG-38.

**09.03.06 Dynamic Responses in Nanocomposite Hydrogels.** Elena Loizou<sup>1,2</sup>, Paul Butler<sup>2</sup>, Lionel Porcar<sup>2,3</sup>, Gudrun Schmidt<sup>1</sup>, <sup>1</sup>Louisiana State Univ., Baton Rouge, LA, 70803, <sup>2</sup>National Institute of Standards and Technology, Gaithersburg, MD, 20899, <sup>3</sup>Univ. of Maryland, College Park, MD, 20742.

In recent years, polymer-clay nanocomposites are generating tremendous interest as materials with novel properties both in solution and in bulk. Several studies have tried to understand, control, and exploit the structure of nanocomposites, their interactions, and their shear-induced structural changes. Many physical properties depend on the structural changes in the nanometer level, such as the orientation of the anisotropic clay within the nanocomposite, which can be greatly affected by shear flow. The ability to alter properties to the desired application by controlling the nanoscopic structure can optimize the material's performance for a variety of applications. Here we report on a study of polyethylene oxide - clay hydrogels with different polymer molecular weights. We explore the structural changes that occur at various length scales in response to a shear field by means of rheology, small angle neutron scattering and microscopy. The polymer chain length and the cross-linking between the clay platelets, allow us to explore the effects of bridging on structure and dynamical responses.

## 09.04 Membranes and Membrane Proteins

**09.04.01 Structure and Fluidity of Solid-supported Membranes.** Bert Nickel, Christian Reich, Joachim Rädler, Dept. für Physik, Ludwig-Maximilians-Univ. München, Geschwister-Scholl-Platz 1, München, 80539 GERMANY.

In this talk, I will present a comprehensive approach to study solid supported membranes. The experiments are based on a microfluidics chamber embedding a flat substrate. Fluorescence microscopy and synchrotron reflectivity experiments have been performed at the same samples to study simultaneously the structure and fluidity of solid supported membranes on silicon oxide, on polyelectrolyte (multi-)layers, and on thermoplastics. Furthermore, we have used this setup to develop new strategies of tethering membranes to surfaces and to study lipid mixtures.

**09.04.02 Using Neutron Spectroscopy to Study Collective Dynamics of Biological and Model Membrane System.** Maikel C. Rheinstädter<sup>1</sup>, Wolfgang Häußler<sup>2</sup>, Tilo Seydel<sup>1</sup>, Tim Salditt<sup>3</sup>, <sup>1</sup>Inst.Laue-Langevin, BP 156, 38042 Grenoble, France, <sup>2</sup>FRM-II, Technische Univ. München, 85747 Garching, Germany, <sup>3</sup>Inst. für Röntgenphysik, Friedrich-Hund Platz 1, 37077 Göttingen, Germany.

Only recently, it has become possible to study collective dynamics of planar lipid bilayers using neutron spectroscopy techniques [1]. We determined the dispersion relations of the coherent fast picosecond density fluctuations on nearest neighbor distances of the phospholipid acyl chains in the gel and in the fluid phases of a DMPC bilayer. By combining different neutron scattering techniques, namely three-axis, backscattering and spin-echo spectroscopy, we present measurements of short and long wavelength collective fluctuations in phospholipid model membranes in a large range in momentum and energy transfer, covering time scales from about 0.1ps to almost 1 $\mu$ s and length scales from 3 $\text{\AA}$  to about 0.1 $\mu$ m [1-3]. From smectic hydrodynamic theory, the long wavelength dispersion relations, as shown in the Figure, give direct access to the elasticity parameters of the membranes in the fluid phase (30 °C) [3].

[1] M.C. Rheinstädter et al., Phys. Rev. Lett. 93, 108107 (2004).

[2] Maikel C. Rheinstädter et al., Phys. Rev. E 71, 061908 (2005).

[3] M.C. Rheinstädter, Wolfgang Häußler, Tim Salditt, submitted.

**09.04.03 Salt Screening of Lipid Membrane Interactions Measured by Small-Angle X-ray Scattering.** Horia I. Petrache, Dept. of Physics, Indiana Univ., Purdue Univ., Indianapolis, IN 46202.

Challenging accepted models of macromolecular interactions, lipid lamellar phases swell when immersed in monovalent salt solutions. Moreover, typical of a Hofmeister series, Br salts swell lipid multilayers more than Cl salts, offering an excellent opportunity to investigate long-standing questions of ionic specificity. We show experimentally that swelling is a superposition of ion-specific electrostatic repulsion, more pronounced for Br than for Cl, and non-specific weakening of the van der Waals (vdW) attraction. Negligible in low salt, weakening of vdW forces becomes significant by the time electrostatic forces vanish, resulting in a smooth monotonic swelling curve with no apparent distinction between low and high salt concentration regimes. We show that salt does not alter membrane structure or bending rigidity, eliminating the possibility that repulsive fluctuation forces change with salt. The combination of ion-specific binding and non-specific ionic screening of low-frequency fluctuations explains salt effects on lipid membrane interactions, and by extension, explains specific (Hof-

meister) effects at macromolecular interfaces between low and high dielectric. By weakening vdW attractions, salt increases energy barriers to membrane contact, possibly affecting cellular communication and biological signaling.

**09.04.04 Structural and Functional Properties of Glycosphingolipid-containing Mixture as a Model Raft.** M. Hirai, Dept. of Physics, Gunma Univ., Maebashi 371-8510, Japan.

So-called rafts or glycosphingolipids (GSLs) signaling microdomains in plasma membrane are now attracting a huge interest in cell biology since they are assumed to act as a molecular device for membrane-associated events such as signal transmission, cell adhesion and so on. Gangliosides, major components of GSLs, are acidic lipids composed of a ceramide linked to an oligosaccharide chain containing one or more sialic acid residues, which are rich in central nervous system. Functionality of the GSLs microdomains is assumed to be closely related to the peculiar features both in ceramide and oligosaccharide portions which can form complex hydrogen bonding networks. A recent spectroscopic study suggests that amyloid  $\beta$  proteins ( $A\beta$ ) interact strongly with gangliosides to promote the structural transition of  $A\beta$  from helix to sheet that result in the seeds of amyloid fibrils. By using synchrotron radiation (SR) X-ray and neutron scattering techniques, we have clarified several notable characteristics of the aggregated structures of ganglioside micelles and ganglioside-containing vesicles, and also the interaction between those aggregates and model ligands such as cholera toxin B-subunit and amyloid protein. The functionality of ganglioside aggregates clarified by using the scattering techniques will be shown.

**09.04.05 Investigation of Membrane Proteins Dynamics from MD Simulations. Connection to Inelastic Scattering Techniques.** M. Tarek, B. Maigret, C. Chipot, F. Dehez, W. Treptow. Equipe de Dynamique des Assemblages Membranaires, UMR 7565, CNRS- Univ. Henri-Poincaré, Nancy, FRANCE.

Function of membranes and membrane proteins depend on their dynamics and relaxation behavior. These may be in principle probed using -neutron and x-ray- scattering techniques, yet, inelastic data on membrane proteins are very scarce, and still difficult to interpret. In the past we have shown that, combined with experiments, Molecular Dynamics (MD) simulations are able of providing exquisite details about the dynamics of membranes, that of globular proteins and of their associated hydration-water (1). We use here state of the art simulation techniques to perform *in silico* (inelastic and elastic) neutron and x-ray scattering measurements on membrane proteins. We will discuss in particular the appropriate experimental conditions allowing to extract the maximum information from scattering techniques as well as the expected insight from such measurements.

(1) Tarek M. and Tobias D. J. *Biophys. J.* 79: 3244-3257 (2000). Tarek M.; Tobias D.J.; Chen H-S. and Klein M.L. *Phys. Rev. Lett.* 87, 238202 (2001) Tarek M. and Tobias D.J. *Phys. Rev. Lett.* 89, 275501 (2002) Tarek M.; Neumann D. A. and Tobias D.J. *Chem. Phys* 292, 435-443 (2003)

**09.04.06 The Kinetics and Mechanisms of Pressure-jump Induced Phase Transitions in Lyotropic Lipid Systems.** Roland Winter, Dept. of Chemistry, Univ. of Dortmund, Otto-Hahn Str. 6, D-44227 Dortmund, Germany.

The kinetic and structural aspects of lamellar to inverse bicontinuous cubic phase transitions have been investigated in various lipid systems, such as monoolein (MO). Transitions in both the forward and reverse directions were achieved by means of fast pressure-jumps and

the subsequent structures monitored using time-resolved X-ray diffraction. The data obtained are analyzed with reference to established models, such as for biological cell fusion. Lamellar to non-lamellar lipid phase transitions are primarily determined by the bilayer physical properties, but also by protein-lipid interactions. Hence, we also studied the effect of protein incorporation into the nanochannel structures of MO on the structure and phase transition kinetics of the system. Hydrostatic pressure has been used as a physical parameter for studying the dynamics of lyotropic lipid mesophase transformations and for the fundamental understanding of protein-membrane interactions in intracellular events, but also because high pressure is an important feature of certain natural membrane environments and because the high pressure phase behavior of biomolecules is of biotechnological interest, such as for baroenzymology.

**09.04.07 Perspectives in the Structure and Collective Dynamics of Multi-component Membranes.** Tim Salditt, Univ. of Göttingen, Germany.

We review recent X-ray and neutron experiments on membranes with an emphasis on oriented lipid bilayers. We address the current status and future perspectives, including sample preparation, sources, instrumentation, and data analysis. Where and to which extent can these methods contribute to the understanding of multi-component membranes? What are the present and future challenges, and how do these techniques compare to other methods.

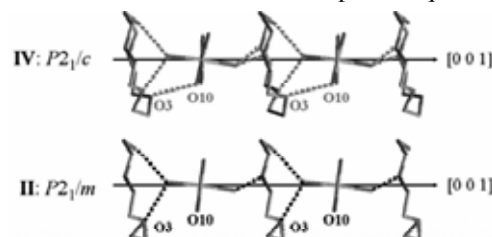
## 10.01 Applications of Crystal Growth and Low-Temperature Techniques

**10.01.01 Methods for Containing Radioactive Materials for Diffraction Analysis.** D.M. Smith, Los Alamos National Laboratory, Los Alamos, NM 87544.

Plutonium compounds present a challenge for diffraction analysis because they must be contained for analysis due to their radioactivity and toxicity. This talk will discuss different methods for containing plutonium and other radioactive elements for crystal diffraction, powder diffraction and SEM analysis.

**10.01.02  $[\text{Ni}(\text{H}_2\text{O})_6](\text{NO}_3)_2 \cdot (15\text{-crown-5}) \cdot 2\text{H}_2\text{O}$ : An Uncommon Polymorphic System.** M.A. Siegler, X. Hao, S. Parkin, C. P. Brock, Dept. of Chemistry, Univ. of Kentucky, Lexington KY, 40506

Four phases of  $[\text{Ni}(\text{H}_2\text{O})_6](\text{NO}_3)_2 \cdot (15\text{-crown-5}) \cdot 2\text{H}_2\text{O}$  have been found between 90 and 294 K: an ordered phase below 198 K (IV,  $P2_1/c$ ,  $Z' = 1$ ), an unusual commensurately modulated superstructure between 198 and 227 K (III,  $B2_1$ ,  $Z' = 7$ ), a partially disordered phase between 227 and 283 K (II,  $P2_1/m$ ,  $Z' = 1/2$ ) and a more disordered phase above 283 K (I,  $I2/m$ ,  $Z' = 1/4$ ). Phase III was found metastable at 90 K and the structures of all phases have been determined. The phase sequence was found *via* differential scanning calorimetry and all phases are related by reversible solid-solid phase transitions with no loss of crystallinity.



In all phases, the three dimensional  $\text{HO} \cdots \text{H}$  network is similar and best described as a 1-D chain and a 2-D plane of H-bonds. The 1-D chains are built by a set of H-bonds between 15-crown-5 and  $\text{Ni}(\text{H}_2\text{O})_6^{2+}$ ,

whereas lattice water molecules and nitrate anions enable the propagation of H-bonds in 2-D planes. Interactions along 1-D chains may change through the phase sequence: some interactions between 15-crown-5 and  $\text{Ni}(\text{H}_2\text{O})_6^{2+}$  may be more favorable in phase IV and less favorable in phase II. Phase III is best understood as a transitional phase that is similar to phase IV in some regions and similar to phase II in other regions.

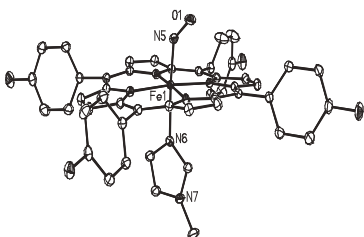
**10.01.03 Crystal Structure of  $\alpha$ -Nitro-*trans*-stilbene.** Carly S. Anderson<sup>1</sup>, Gary W. Breton<sup>1</sup>, Edwin D. Stevens<sup>2</sup>, and Kenneth L. Martin<sup>1</sup>, <sup>1</sup>Dept. of Chemistry, Berry College, Mt. Berry, GA, <sup>2</sup>Dept. of Chemistry, Univ. of New Orleans, New Orleans, LA.

The compound *cis*-3,4-diphenyldiazetene-1,2-dioxide thermally decomposes, a minor biproduct of which is  $\alpha$ -nitro-*trans*-stilbene. 5688  $\text{Mo-K}_\alpha$  reflections were measured at 150 K via Bruker SMART 1-K CCD single-crystal diffractometer. 4  $\text{C}_{14}\text{H}_{11}\text{NO}_2$  molecules are found in the unit cell with parameters:  $a = 16.262(3)$  Å,  $b = 6.305(1)$  Å,  $c = 12.710(3)$  Å,  $\alpha = 90^\circ$ ,  $\beta = 118.22(3)^\circ$ , and  $\gamma = 90^\circ$ . There is sufficient evidence for a C-centered lattice, but determining the precise space group is problematic due to the extensive disorder of the molecules throughout the lattice – the central C=C may be found in two different orientations between the phenyl rings. Of structural importance is that the phenyl substituents are *trans* on the central C=C. Using the Cc space group, the *R*-factor was found to be 0.0649 for the 1797 strongest reflections. Using the C2/c space group, the *R*-factor was a higher value of 0.0879 for the strongest 967 reflections. After modeling the structure using both Cc and C2/c space groups, geometric considerations and comparison of *R*-factors demonstrated the Cc space group to be a better model for the compound. The structure was solved and refined by full-matrix least-squares method via *SHELXTL V 5.1*.

**10.01.04 [Fe(TPP)(1-MeIm)(NO)], A Tale of 1 Crystal, 3 Cells and Too Many Data Collections. Multiple Temperature Studies to Resolve Disorder and Twinning.** Bruce C. Noll, Nathan J. Silvernail, W. Robert Scheidt, Univ. of Notre Dame, Notre Dame, IN.

In our ongoing study of the environment of axial ligands in six-coordinate Fe porphyrins we commonly pursue a series of experiments at various temperatures to map out the conformational landscape of these groups. During the course of such an experiment, it was observed that the crystal under study, an iron-nitrosyl porphyrin, indexed at 100 K to a triclinic cell of twice the volume of the cell of the 293 K study. A cell of 3× the room-temperature volume was found at 224 K. The crystal could be indexed as a non-merohedral twin with two components at all temperatures. Cell dimensions of the twin cells were equivalent to the small 293 K cell. The system was refined as a twin at all three temperatures. In addition, both the 2× and 3× cells were solved and refined. Multiple orientations of the NO oxygen were present in all but the 100 K data sets. Tripling the cell at 224 K did nothing to isolate these orientations. No differences could be observed in the conformations of the two porphyrins of the asymmetric unit of the doubled 100 K cell.

A second crystal showed no indications of either twinning or a phase change. Complete experiments at 100 K, 224 K, 293 K and 350 K, where the crystal decomposed, exhibited alternate orientations in all but the 100 K data set.



**10.01.05 Experiences with Scaling and Absorption Corrections.** George M. Sheldrick, Lehrstuhl für Strukturchemie, Univ. Göttingen, Germany.

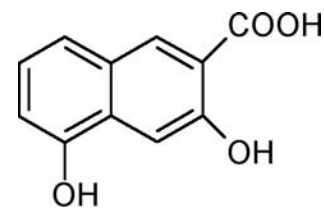
A brief review of techniques for scaling and absorption corrections of both small-molecule and macromolecular diffraction data collected with area detectors will be followed by some examples from the author's experience with the SADABS and TWINABS programs. The ability to perform a Gaussian absorption correction within the scaling program provides a good test of empirical absorption algorithms based on spherical harmonics, and also enables the linear absorption coefficient to be determined from the agreement of equivalent reflections. This makes it possible to apply face-indexed absorption corrections even when the contents of the unit-cell are not yet known, and may also be able to compensate for other systematic effects such as absorption by the crystal support. Even if the absorption is small, this calculation is required to find the mean path length through the crystal for use in extinction corrections for charge density studies. Problems that arise in the scaling and merging of data from non-merohedrally twinned crystals will also be discussed.

**01.01.06 Chemical Bonding in Pentaerythritol at Very Low Temperature or at High Pressure: An Experimental and Theoretical Study.** A.A. Pinkerton, E.A. Zhurova, V.G. Tsirelson, A.I. Stash, V.V. Zhurov, Dept. of Chem., Univ. of Toledo, Toledo, OH 43606; Mendeleev Univ. of Chem. Tech., Moscow, Russia; Karpov' Inst. of Phys. Chem., Moscow, Russia.

Chemical bonding in the pentaerythritol crystal based on the experimental electron density at 15(1)K, and theoretical calculations at the experimental molecular geometries obtained at room and low (15 K) temperatures has been analyzed and compared in terms of the topological analysis. Topological electron-density features corresponding to the high-pressure (1.15 GPa) geometry are also reported. In addition to the bond critical points (CPs) within the molecular layers, CPs between the atoms of different molecular layers have been located, and the bonding character of these relatively weak interactions discussed. Atomic charges and energies have been integrated over the atomic basins delimited by the zero-flux surfaces, and the intermolecular interaction energies have been calculated. The interaction between molecular layers in the crystal becomes stronger both at very low temperature and high pressure, as demonstrated by the more negative intermolecular interaction energies, higher electron density and energy density values at the CPs, and sharper electronic energy density profiles.

**01.01.07 Small Molecule Crystallography With Undergraduate Researchers.** Allison J. Dobson, Adam Donnelly, Bridgette Massey, Shae Vaughn, Kennon Deal, Lindsey Spedding, Georgia Southern Univ., Dept. of Chemistry.

The single-crystal structure of 3,5-dihydroxy-2-naphthoic acid and other small molecules will be discussed. All crystals were grown and mounted by undergraduate researchers from 2003-2006. In addition, data was collected by junior and senior undergraduates at Georgia Southern University during the same time period.



Title Compound

**10.01.08 Preparing Manuscripts for Acta Crystallographica C and E with Programs *publCIF* and *modiCIFer*.** Iliia A. Guzei, Chemistry Dept., Univ. of Wisconsin-Madison, Madison, WI, 53558.

The IUCr Editorial Office has released a new program *publCIF* that facilitates manuscript preparation for Acta Crystallographica C and E. *publCIF* allows editing of the content of Crystallographic Information Files (CIF) in a dual fashion – as a CIF with all the CIF field and data codes, and in a text editor similar to Wordpad. The latter shows the formatting of the title, author, abstract, comment, and reference sections as it will appear in print. The publication wizard feature helps create the abstract and comment as well as the author and reference databases. An important element of the program is its reference handling capability; it is now possible to conveniently sort the references in the alphabetical order and check for correspondence between the entries in the bibliography section and all citations in the body of the comment and crystallographic tables. These and other *publCIF* features will be shown in action.

As a user of the SHELXTL package I routinely modify CIF's produced by XL in order to insert the missing information and fields required for publication in Acta Cryst. C and E. To eliminate the repetitive nature of this task I wrote a PC program *modiCIFer* that takes a "raw" CIF file created by XL and inserts all the fields necessary to comply with the IUCr requirements. *ModiCIFer* makes use of a user/instrument specific initialization file and NAME.p4p, NAME.pcf, and NAME.res, to resolve missing items and to create a checkCIF compliant CIF that can be converted into a manuscript with *publCIF*.

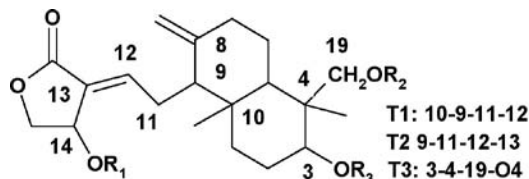
Both programs will be demonstrated with the emphasis on *publCIF*.

## 10.02 Natural Products and Drugs

**10.02.01 Effect of Blocking Groups on the Conformation and Intermolecular Interactions of Andrographolide.** C.H. Schwalbe<sup>1</sup>, C.J. Bache<sup>1</sup>, D.L. Rathbone<sup>1</sup>, S.R. Sagineedu<sup>2</sup>, S.R. Jada<sup>2</sup>, J. Stanslas<sup>2</sup>, M.F.G. Stevens<sup>3</sup>, <sup>1</sup>School of Life & Health Sciences, Aston Univ., Birmingham, UK, <sup>2</sup>Dept. of Biomedical Sciences, Univ. Putra Malaysia, Selangor, Malaysia, <sup>3</sup>The Pharmacy School, Univ. of Nottingham, Nottingham, UK.

The natural product andrographolide (**A**) has interesting biological effects, including anti-cancer, hypotensive, and anti-inflammatory, which it is desirable to elicit separately.

With R1 = R2 = R3 = H, **A** (CSD refcode ZZZLUK03) forms hydrogen-bonded chains at both ends of the molecule. We have blocked one or more of these sites: previously with R1 = acetyl in compound **I**, now with R2-R3 = the cyclic isopropylidene (**II**) and R1 = R2 = R3 = acetyl (**III**). In **I** and **II** the hydrogen-bonded chains persist where not blocked. With ranges for **A** – **III** of only 17° in torsion angle T1 and 10° in T2 the central chain is little affected by changes on the periphery, although computer models suggest other possible low-energy conformations. Products of addition to **III** at C8 such as the HCl adduct WUKXOP show a more kinked chain with smaller magnitudes of T1 and T2. T3 ranges from gauche to trans, the smallest magnitude found within the ring of **II** and the largest to accommodate the acetyl groups in **III**.



**10.02.02 Combined Vibrational Circular Dichroism and X-ray Powder Diffraction to Establish Absolute Stereochemistry and Structures of Small Molecules.** Gregory A. Stephenson, Krishna Chavali, Lilly Research Laboratories, Eli Lilly & Company, Indianapolis, IN 46285.

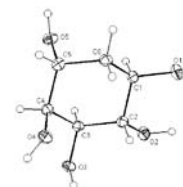
Computational chemistry has had a dramatic influence on the way that small-molecule organic research is being conducted. Application of density field theory to the determination of gas phase molecular conformations often serves as the starting point in understanding three dimensional organic structures. Molecular packing arrangements within the crystalline solids can be determined through use of simulated annealing or genetic algorithms for deriving atomic models used for comparison of calculated and observed powder diffraction patterns. Similarly, vibrational circular dichroism (VCD) uses computationally derived conformations to simulate spectra that are compared to experimental spectra and may be used to determine the absolute stereochemistry of molecules. While the role of single crystal diffraction for the determination of high resolution structure remains the undisputed favorite for organic chemists, the combination of powder diffraction and VCD techniques can be used as alternative methodologies for gaining much of the information that has traditionally been available only through single crystal diffraction. This talk will examine a number of examples of where these methods were employed to gain structural information in lieu of single crystal data and demonstrates the complimentary aspects of the combination of techniques.

**10.02.03 Electron Density Distribution in Crystals of Pharmacophores.** Tatiana V. Timofeeva, Andrey A. Yakovenko, Tiffany L. Kinnibrugh, Mikhail Yu. Antipin, Robert Long, Dept. of Natural Sciences, New Mexico Highlands Univ., Las Vegas, NM 87701, Eastern New Mexico Univ., Portales, NM 88130, [vtimofeeva@nmhu.edu](mailto:vtimofeeva@nmhu.edu)

Charge density distribution helps to investigate details of intramolecular chemical bonding and intermolecular interactions, that, in many cases, are the important reasons of such phenomena as polymorphism, formation of solvates and hydrates, solubility, and, as a result, of pharmacological activity. Piperazine is a pharmacophore that is widely used for combinatorial synthesis of potential drugs. Piperazine forms several hydrates that contains different amount of water. We investigated charge density distribution in the piperazine hydrates and compared their characteristics, related to electronic structure of these materials, to their physical properties and pharmacological activity.

**10.02.04 A New Biological Insight for the Organic Compounds C<sub>6</sub>H<sub>12</sub>O<sub>5</sub>** Hamilton Napolitano<sup>1</sup>, Ademir Camargo<sup>1</sup>, Jahyr Theodoro<sup>2</sup>, Marcelo Castilho<sup>2</sup> & Javier Ellena<sup>2</sup>, <sup>1</sup>Ciências Exatas e Tecnológicas, UEG & <sup>2</sup>Instituto de Física de São Carlos, USP.

Leishmaniasis is a tropical disease caused by a protozoal parasite of the order Kinetoplastid. Looking for new bioactive substances, potentially useful against leishmaniasis, we used both PRTase adenine phosphoribosyltransferase from *L. tarentolae* and parasite *L. major* as a model system to screen the inhibitory capacity of one quercitol compound from Brazilian plant. The data collection was performed using Enraf Nonius KappaCCD at room temperature. The structure was analyzed from 1425 reflections with  $I > 2\sigma(I)$  and refined to  $R_1$ -values of 0.033. The molecules are joined in crystal structure through five twice classical O–H...O hydrogen bonds linking the atoms O4–H4...O5<sup>i</sup> [ $i = -x+3, 0.5+y, -z+1$ ], O5–H5...O2<sup>ii</sup> [ $ii = x, y, 1+z$ ], O2–H2...O4<sup>iii</sup> [ $iii = x+2, y-0.5, -z$ ], O1–H1...O3<sup>iv</sup> [ $iv = x-1, y, z$ ] and O3–H3...O1<sup>v</sup> [ $v = -x+2, 0.5+y,$



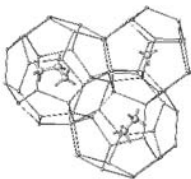
-z] with distances between donor and acceptor of 2.707(1), 2.808(1), 2.780(1), 2.736(1) and 2.843(2) Å, respectively. The nature of the hydrogen bonds O1–H1...O3<sup>iv</sup> and O3–H3...O1<sup>v</sup> observed in the crystal structure was theoretically investigated using the Kohn-Sham density functional theory (DFT).

Acknowledgment: CNPq, FAPESP and PrP (UEG).

**10.02.05 The Structure of Natural Gas Hydrates.** K.A. Udachin, H. Lu, J.A. Ripmeester, Steacie Inst. for Molecular Sciences, National Research Council, Ottawa, Ontario, Canada K1A 0R6

Natural gas hydrates are clathrate inclusion compounds of water and hydrocarbons plus small amounts of other gases such as CO<sub>2</sub>, H<sub>2</sub>S, etc, with the guest molecules trapped in cages in the hydrate crystal lattices. Their role in the geosphere is still very much under investigation, with potential impacts on the global energy supply, geohazards and global climate change.

The hydrates for which structures were reported were both recovered from the Cascadia Margin, offshore Vancouver Island. The first one crystal, found in an oil-stained sample taken from a hydrate outcrop on the sea floor, is cubic structure II (Figure), *Fd-3m*, *a* = 17.141(1) Å (composition: 2CH<sub>4</sub>·0.78C<sub>2</sub>H<sub>6</sub>·0.22C<sub>3</sub>H<sub>8</sub>·17H<sub>2</sub>O). The second, taken from 2.8m below the sea floor and associated with a cold vent field, is cubic structure I *Pm-3n*, *a* = 11.857(1) Å (composition: CH<sub>4</sub>·5.9 H<sub>2</sub>O). In all cases guest molecules are off the geometrical centers of the cages and are in van der-Waals contact with water molecules. The large cages of both cubic structures I and II were found to be 100% occupied with guest molecules.



**10.02.06 Hydrothermal Crystallization of Organic Molecular Solids: Applications to Pharmaceuticals, Co-crystal Engineering and Neutron Diffraction Studies.** Ian D. Williams, Fanny L-Y. Shek, Samuel M-F. Lo, Herman H-Y. Sung, Dept. of Chemistry, Hong Kong Univ. of Science and Technology, Clear Water Bay, Kowloon, Hong Kong, China.

The application of hydrothermal and related methodologies to the growth of organic crystals will be discussed. The advantages can include enhanced crystal size and quality, as well as high isolated yield. Hydrothermal crystallization can be applied to both natural product characterization and pharmaceutical formulation. We present several examples from this area; the anti-malaria drug artemisinin and its derivatives have been studied for polymorphism and hydrolytic breakdown products. The dopamine receptor antagonist dl-tetrahydropalmatine has been crystallized as a variety of salts and neutral co-crystals and its chiral resolution achieved. In the field of crystal engineering, hydrothermal methods can be used to form organic co-crystals between aromatic acids and bases with high phase purity and stoichiometric control. In certain systems the different molecular stoichiometries can have intriguing chemico-structural consequences, for example various bipyridines and phthalic acid form both a 1:1 neutral molecular adduct with N–HO hydrogen bonds, as well as a 1:2 organic salt with NH–O. In other crystals such as 2[4,4-bipyH<sub>0.5</sub>][C<sub>6</sub>H<sub>2</sub>1,2,4,5-(COO)<sub>4</sub>-H<sub>3</sub>] and dinicotinic acid short single well N-H–O hydrogen bonds are found. Crystals of 0.5cm dimension suitable for neutron diffraction, including deuterated forms, have been readily prepared by hydrothermal methods and the resulting studies allow new insight into this important class of hydrogen bond. Finally we have found facile formation of large crystals of cyclodextrin-adducts by this approach, which has implications for X-ray structural characterization of drug inclusion complexes.

We thank the Research Grants Council of Hong Kong for financial support of this work (6084/02P).

**10.02.07 Sesquiterpene Lactones Isolated from Plants of the Venezuelan Andes.** G. Díaz de Delgado,<sup>a</sup> J. Bruno C.,<sup>a</sup> V. Cote,<sup>a</sup> J.M. Amaro-Luis,<sup>b</sup> J.M. Delgado,<sup>a</sup> <sup>a</sup>Laboratorio de Cristalografía-LNDRX, <sup>b</sup>Laboratorio de Productos Naturales, Dept. de Química, Facultad de Ciencias, Univ. de Los Andes, Mérida, Venezuela, 5101.

The structures of several sesquiterpene lactones isolated from plants of the Venezuelan Andes will be discussed in this contribution. In particular, Dicorin diacetate, 4*S*,9*β*-diacetoxy-6*α*H,7*α*H,10*α*H-xanth-1,11(13)-dien-6,12-olide, C<sub>19</sub>H<sub>28</sub>O<sub>6</sub>, crystallizes in the orthorhombic system, space group *P2<sub>1</sub>2<sub>1</sub>2<sub>1</sub>* and unit cell parameters *a* = 7.3862(6), *b* = 14.7818(14), *c* = 17.6465(17) Å; *V* = 1926.7(3) Å<sup>3</sup>. Two C–H...O hydrogen bonds are observed for C3–H4...O6 [2.27Å°, 105°] and C13–H16...O4 [2.32Å°, 104°]. The C18, H25 and O4 atoms participate in an intermolecular hydrogen bond with H...Acceptor distance of 2.57 Å and a C18–H25...O4 angle of 146° to produce helical chains along the *b* axis. Burrodine, 2*β*-Hidroxi-4-Oxi-1*α*H,5*β*Me,7*α*H,8*α*H,10*α*H,10*α*H-11(13)-en-pseudoguaien-7(12)-olide, crystallizes in the monoclinic system, space group *P2<sub>1</sub>* and unit cell parameters *a* = 7.3393(16); *b* = 7.7573(16); *c* = 11.927(3) Å, *β* = 90.339(6)°; *V* = 679.03 Å<sup>3</sup>, *Z* = 4. The final discrepancy factors for the refinement were: *R*<sub>1</sub> = 0.0490, *wR*<sub>2</sub> = 0.1095, *S* = 1.005.

We thank R. Benson, Rigaku, USA, for support with data collection.

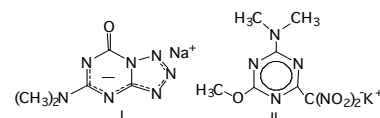
**10.02.08 Carbonyl...Ether Supramolecular Building Block in 25,26-Oxidofriedel-1,3-dione.** Kenneth J. Haller, Auphatham Phothikanith, School of Chemistry, Suranaree Univ. of Technology, Nakhon Ratchasima 30000 Thailand.

The crystal and molecular structure of 25,26-oxidofriedel-1,3-dione, isolated from *Salacia Chinensis* Linn is reported. The compound crystallizes in the monoclinic space group *P2<sub>1</sub>* with two molecules per unit cell. The crystal packing of the structure contains C–H...O hydrogen bonds and a rare supramolecular building block involving dipolar intermolecular contacts between the positive polarity carbon atom of a carbonyl group and the negative polarity oxygen atom of the ether linkage, C(δ<sup>+</sup>)...O(δ<sup>-</sup>). The new linkage is characterized from the structure and data in the Cambridge Crystal Structure Database.

Crystal Data: C<sub>30</sub>H<sub>46</sub>O<sub>3</sub>, *M<sub>r</sub>* = 454.67 D, monoclinic, *P2<sub>1</sub>*, *a* = 7.6688(1), *b* = 16.1829(2), *c* = 10.7132(2) Å, *Z* = 109.861(1) °, *V* = 1250.46(3) Å<sup>3</sup>, *Z* = 2, *D<sub>calc</sub>* = 1.208 Mg m<sup>-3</sup>, *T* = 150(2) K, *μ<sub>Mo</sub>* = 0.075 mm<sup>-1</sup>, Bruker Nonius KappaCCD, *R<sub>sym</sub>* = 0.055, 2903 refl, 2622 refl > 4σ(*F<sub>o</sub>*), *R<sub>i</sub>* = 0.036, *gof* = 1.048, *ρ<sub>max</sub>* = 0.27 e Å<sup>-3</sup>.

**10.02.09 The X-ray Structure of Novel Tetrazolo[1,5-a]-1,3,5-triazine and 1,3,5-triazine Derivatives.** E.V. Mironova<sup>1</sup>, D.B. Krivolapov<sup>1</sup>, I.A. Litvinov<sup>1</sup>, V.V. Baharev<sup>2</sup>, A.A. Gidasov<sup>2</sup>, A.E. Arbutov Institute of Organic and Physical Chemistry<sup>1</sup>, Russian Academy of Sciences, Kazan, 420088 Russia, Samara State Technical Univ.<sup>2</sup>, Samara, Russia.

Tetrazolo[1,5-a]-1,3,5-triazine derivatives are the 5,8-diazaanalogues of guanine, which is the one of



important building blocks of nucleic acid. The crystal and molecular structures of 5-aminotetrazolo[1,5-a]-1,3,5-triazin-7-one sodium salt (I) and 2-methoxy-4-dimethylamino-6-dinitromethyl-1,3,5-triazine potassium salt (II), which are used as precursors in the synthesis of the biologically active 1,3,5-triazine derivatives, are reported. In structure I two independent sodium cations have the special positions in the

center of symmetry. The sodium cations have practically undistorted octahedral configuration. The polymer chains containing of the four-membered non-planar  $\text{Na}_2\text{O}_2$  cycles are formed in crystal owing to the coordination of sodium cations with water molecules and with anions. The molecules I and II form the solvates with water. The anion of II is non-planar. The potassium cation is in general position and has nine coordination bonds. The potassium cations, anions and water molecules form the polymer chains similarly to I.

The work is supported by the Russian Foundation for Basic Research (grant N. 04-03-32156).

**10.02.10 Taxol - Single Crystal Structures and Solid State Behavior of Six Forms.** John DiMarco, Jack Gougoutas, Solid State Chemistry, Bristol-Myers Squibb Pharmaceutical Research Institute, Route 206 & Province Line Rd., Princeton, NJ 08543.

Taxol is a potent anti-cancer natural product discovered by the National Institutes of Health (NIH). Bristol-Myers Squibb Pharmaceutical Research Institute undertook the challenging research and development necessary to bring this drug to market. We have solved the structures and characterized the solid state behavior of five crystal forms, including the neat (solvent-free) crystal form A – the registered form of commerce. Our studies revealed a remarkably invariant hydrogen bonded “dimer” ( $Z'=2$ ) in all forms of Taxol. Most of the forms have been shown to be topotactic solid state precursors of form A and/or the tri-hydrate form B. The solid state molecule conformation in Tubulin.

## 10.03 Crystal Engineering: Supramolecular Chemistry: From Assembly to Structure and Function

**10.03.01 Can Co-crystals be Assembled Employing a Specific Hydrogen-Bonded Motif?** J. Bernstein, Dept. of Chemistry, Ben-Gurion Univ. of the Negev, Beer Sheva, Israel 84105.

In its ultimate manifestation crystal engineering [1] leads to a predicted desired *crystal structure*. In spite of some noteworthy successes in this effort, it is still not possible to design the crystal structure(s) of any particular substance given the structural formula. The recent piqued interest in co-crystals [2] has led to some impressive successes in preparing *crystals* of two or more components, but there still remains the considerable engineering challenge of designing and preparing *crystal structures* of systems with more than one molecular entity. We have been studying the hydrogen-bonding motif designated  $R_4^2(8)$  in the graph set notation, with the goal of utilizing the pattern in the generation of specific structural zero-, one-, two- and three dimensional structural features in co-crystals. Some successes and some ‘failures’ will be described, the latter nevertheless providing useful information for utilization and modification of the design strategy and crystal chemistry in general.

[1] G.R. Desiraju, *Crystal Engineering-The Design of Organic Solids*, Elsevier, Amsterdam, 1989

[2] Ö. Almarsson and M.J. Zaworotko, *Chem. Commun.*, 2004, 1989.

Supported by U.S.-Israel Binational Science Foundation Grant 2004118.

**10.03.02 The Influence of Disorder on Polymorphism.** A.G. Beasley, T.R. Welberry, D.J. Goossens, Research School of Chemistry, ANU, Australia.

Polymorphism is a matter of key importance in the pharmaceutical industry since the properties of polymorphs may vary, including the rate of uptake by the human body of pharmaceutical molecules. In this study we are using diffuse scattering methods to elucidate the disorder

in polymorphic systems, with a particular focus on disorder arising from the internal flexibility of molecules. The determination of crystal structures beyond the average structures which are available from Bragg data may provide additional information which may contribute to solving the problem of polymorph prediction and control.

The molecule p-methylbenzylidene-p-methylaniline (MeMe) has three polymorphs, all of which exhibit strong diffuse scattering indicating substantial disorder. Two of the polymorphs (MeMe1 and MeMe3) have orientational disorder in which the orientations are related by end-to-end and/or side-to-side “flips” of the molecule. Most remarkable is the MeMe2 form which is nominally perfectly ordered, and yet its diffraction pattern shows highly structured scattering indicating the presence of highly correlated displacive disorder. We have produced model crystals of the three polymorphs which reproduce the major features in their diffraction patterns. Exploration of such models provides information on intermolecular interactions.

**10.03.03 Space Group Frequencies of Hydrogen Bonded Networks.** Joseph W. Lauher, Dept. of Chemistry, State Univ. of New York, Stony Brook, NY 11794.

Crystal engineers and supramolecular chemists have achieved remarkable success in designing and preparing crystalline hydrogen bonded networks. These supramolecular constructs differ from normal molecules because they have one, two or three degrees of translational symmetry. Each network has its own symmetry group designation. A one-dimensional  $\alpha$ -network can be described by its rod group symmetry. A two dimensional  $\beta$ -network can be described by its layer group symmetry. A three dimensional  $\gamma$ -network can be described by its space group symmetry. In each case the symmetry group of the network must be a subgroup of the space group of the crystal. This requirement restricts the possible space group of any crystal that contains a given network. Software has been written to identify hydrogen bonded networks within the structures of the Cambridge Structural Database. The dimensionality of each network was determined and the appropriate rod, layer or space group was assigned. The results for each network were then correlated with the space group of the original crystals. Using this data new space group frequency tables have been constructed for crystals containing hydrogen bonded networks. Some significant differences are found when the numbers are compared to the standard frequency tables found for all organic molecules.

**10.03.04 Synergy of Intermolecular Forces in Self-Assembly of Propargylic Alcohols.** Michal Sabat, Marilise A. Hyacinth, Lin Pu, Dept. of Chemistry, Univ. of Virginia, Charlottesville, VA 22904.

We will discuss some of our recent findings indicating that the functional groups of propargylic alcohols not only make their self-assembly possible but also allow for a finely tuned cooperation (synergy) of interactions on a scale rarely observed in other supramolecular systems. For instance, diaryl-substituted chiral propargylic alcohols can form cyclic hexameric molecular assemblies as a result of the cooperation between three major intermolecular forces: the O-H...O hydrogen bonding, the C-H...F hydrogen bonding involving organic fluorine, and the  $\pi$  –  $\pi$  stacking interaction between the pentafluorophenyl and phenyl rings. We believe that this synergy of intermolecular forces could be utilized in a variety of applications, including chiral recognition and discrimination. Relevant structures and some theoretical aspects of the synergy will be discussed.

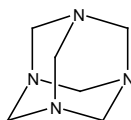
**10.03.05 Crystallographic Perspective of Pharmaceutical Co-crystals: Intermolecular H-Bonding between Heterocyclic Nitrogen Compounds and Carboxylic Acids.** Dedong Wu, James A. Osborn, Craig D. Collins, Jean M. Surian, AstraZeneca PLP, Wilmington, DE 19850.

Pharmaceutical co-crystals refer molecular complexes of active pharmaceutical ingredients (APIs) with other molecules. The technique of co-crystal formation is an important alternative method for pharmaceutical form selection. Intermolecular hydrogen bonding plays a key role in co-crystal formation in a pharmaceutical co-crystal. Thus, the study of molecular assembly to form co-crystals in the molecular level can be applied in understanding and designing new crystalline forms of pharmaceutical co-crystals. For the purpose of the study, we have employed heterocyclic aromatic compounds containing basic nitrogen and investigated their occurrence as co-crystals in the Cambridge Structural Database (CSD). Carboxylic acids have been selected as co-crystal agents. The presentation will demonstrate intermolecular bonding modes in crystal structures of co-crystals between heterocyclic nitrogen compounds and carboxylic acids. The tendency to form pharmaceutical co-crystals will also be discussed.

**10.03.06 Cocrystallization Tendencies of Hexamethylenetetramine.** K.A. Wheeler, P. Daka, Dept. of Chemistry, Eastern Illinois Univ., Charleston, IL 61920.

The controlled construction of multimolecular arrays has progressed over the last several years due in part to our improved understanding of non-bonded contacts. The extension of these efforts to cocrystalline systems is a current topic of interest that frequently follows the rational selection of fundamental components with complementary molecular features. Although studies in this area effectively produce predictable low dimensional molecular assemblies with discrete and 1D motifs, extending these patterns to yield 3D supramolecular frameworks has proven to be a challenging task.

In many ways hexamethylenetetraamine (HMTA) is a model candidate for use in cocrystallization studies. The hydrogen bond ability and tetrahedral arrangement of the four tertiary nitrogen atoms provides attractive features that could, in principal, form extended molecular architectures via cocrystallization with various donor molecules. Inspection of the Cambridge Structural Database (CSD) reveals a diverse collection of structure with HMTA/donor assemblies; even so, very few involve all HMTA nitrogen atoms in non-bonded contacts.



HMTA

This paper reports on the utility of HMTA as a functional building-block for controlled cocrystallization studies. The combination of both crystallographic studies of new HMTA/donor complexes and data retrieved from the CSD suggests important supramolecular tendencies.

**10.03.07 Design and Synthesis of Co-crystals using Molecular Sense and Supramolecular Sensibility.** Christer B. Aakeröy, Dept. of Chemistry, Kansas State Univ., Manhattan, KS, 66506, aakeroy@ksu.edu.

What is most likely going to happen when a homogeneous solution containing two different molecular solutes is allowed to evaporate to dryness? Unless a chemical reaction driven by the formation of covalent bonds takes place between the two solutes one would, as a rule, expect the appearance of two separate molecular solids. This is a manifestation of the inherent structural selfishness of molecules, something that is relied upon every time recrystallization is employed as a method of purification. Recrystallization processes are essential

in most covalent synthetic procedures and are performed on a regular basis in every synthetic laboratory. In the supramolecular laboratory, however, the very same process also provides an opportunity to move in the opposite direction – a co-crystallization is a deliberate attempt at bringing together different molecular species in one crystalline lattice without making or breaking covalent bonds. Since the odds are stacked firmly in favor of a homomeric product, how do we go about developing reliable and versatile synthetic methods for the directed assembly of co-crystals? This presentation will attempt to answer the question by outlining several modular hydrogen-bond driven strategies for the design and synthesis of binary and ternary supermolecules and co-crystals.

**10.03.08 A Way from Static to Dynamic Micropores in Crystalline Coordination Polymers.** S. Kitagawa, Dept. of Synthetic Chem. & Biological Chem., Kyoto Univ., Katsura, Kyoto, Japan.

The recent advent of porous coordination polymers (PCPs), as new functional microporous adsorbents, has attracted the attention of chemists due to scientific interest in the creation of unprecedented regular nano-sized spaces and in the finding of novel phenomena, as well as commercial interest in their application for storage, for separation and in heterogeneous catalysis.<sup>1-4</sup> One of the advantages of PCPs, as compared with other microporous inorganic materials such as zeolites, is flexibility accompanied with regularity, which provides unique sorption behaviors such as gated sorption for specific guests. We have succeeded in obtaining interesting array structures of adsorbed benzene,<sup>5</sup> acetylene,<sup>6</sup> O<sub>2</sub><sup>7</sup> molecules and so on. To this confinement phenomena, we have found flexible porous frameworks, which respond to specific guests, dissimilar to the conventional porous materials. [Cu(dhbc)<sub>2</sub>(4,4'-bpy)]<sub>n</sub> and [Cu(bdc)<sub>2</sub>(bpy)] are representatives.<sup>8</sup> Very recently, we found another flexible pores in {[Cu(pyrdc)(bpp)}(5H<sub>2</sub>O)]<sub>n</sub>.<sup>9</sup>

## References

*Reviews* 1) S. Kitagawa *et al.*, *Bull. Chem. Soc. Jpn.*, (Accounts), 1998, 71, 1739. 2) S. Kitagawa, *et al.*, *Angew. Chem. Int. Ed.*, 2004, 43, 2334. 3) S. Kitagawa *et al.*, *Chem. Soc. Rev.* 2005, 34, 109. 4) S. Kitagawa *et al.*, *Chem. Commun. Feature Article*, 2006, 701. *Original Papers* 5) R. Matsuda, *et al.*, *J. Am. Chem. Soc.* 2004, 43, 14063. 6) R. Matsuda, *et al.*, *Nature*, 2005, 436, 238. 7) R. Kitaura, *et al.*, *Science*, 2002, 298, 2358. 8) R. Kitaura, *et al.*, *Angew. Chem. Int. Ed.*, 2003, 43, 428. 9) K.T.Maji, *et al.*, *J. Am. Chem. Soc.* 2005, 127, 17152.

**10.03.09 Polyhedral Clusters and Networks with Host-type Ligands.** M.J. Hardie, C.J. Sumbly, School of Chemistry, Univ. of Leeds, Leeds, LS2 9JT, UK.

We have recently generated a series of host-type ligands based on the cyclotrivertatrylene framework. These ligands have rigid molecular cavities capable of binding other molecules. They can be incorporated into either discrete or polymeric metal-ligand systems, thus creating metallo-supramolecular assemblies or coordination polymers with specific molecular recognition sites. Complex [Ag<sub>3</sub>{tris(2-pyridylmethyl)cyclotrivertatrylene}]<sub>3</sub>.3PF<sub>6</sub><sup>-</sup>, for instance, has a 3-D [Ag<sub>3</sub>L<sub>2</sub>] coordination network with PF<sub>6</sub><sup>-</sup> anions in both lattice sites and within the molecular cavity of the ligand. The structure has cubic symmetry and is highly disordered. By making a single, simple assumption we are able to disentangle the disorder and make sense of the structure as a four-fold interpenetrating (10,3)-a network. An unusual "star-burst" tetrahedral assembly is formed in the complex



We can use host-guest chemistry to control the self-assembly outcome: the star-burst  $[Ag_4L_4]^{4+}$  tetrahedron is isolated in the presence of acetonitrile guest molecules, but in the presence of much bulkier glutaronitrile guest molecules a 2-D coordination polymer with 4.8<sup>2</sup> topology is formed instead.

**10.03.10 Design and Serendipity in the Construction of a Non-centrosymmetric Network Through  $\pi$ - $\pi$  Interactions.** J. Valdés-Martínez, J. M. Serrano-Becerra, S. Hernández-Ortega, David Morales-Morales, Inst. de Química, Univ. Nacional Autónoma de México, México DF, 04510, México.

The design and synthesis of non-centrosymmetric crystals is a difficult but important challenge in crystal engineering, due to their potential physical properties. We have used as strategy the design of non-centrosymmetric 2D networks organized through directional  $\pi$ - $\pi$  interactions. To achieve this directionality we have used an organic molecule with two phenyl rings one of them being pentafluorinated, 5Fph, and a step (imidazol) as a geometric restriction to favor non-centrosymmetry interactions between the ph and the 5Fph rings. The 2D layers organize into a non-centrosymmetric 3D structure due to ionic repulsions. The details of the above mentioned strategy as well as the crystal structure of the 1-benzyl-3-(2,3,4,5,6-pentafluorobenzyl)-1*H*-imidazolium bromide will be discussed.



**10.03.11 Synthetic Crystallography of Metal Complexes.** A. Guy Orpen, School of Chemistry, Univ. of Bristol, Bristol, UK.

The synthesis of designed crystal structures is part of a major strand of modern chemistry in which the focus has shifted from the analytical function of crystallography (the determination of crystal structures) to the synthetic. In synthetic crystallography, itself a branch of crystal engineering, a variety of means have been used in the attempt to plan and control the products and objectives of synthesis – the crystal structures.

Strategies that might be adopted to achieve this synthetic goal are considered. In particular, approaches based on supramolecular chemistry and molecular tectonics are examined. Progress is evaluated towards control of:

- The composition of the final synthetic product - the crystal structure.
- The supramolecular synthon formed.
- The periodic motif(s) formed.
- The entire crystal structure.

Applications and properties of such “engineered” solids is of importance. One property of particular interest to chemists is reactivity – this at the heart of the history of crystal engineering and has received sustained attention from a relatively small number of groups, primarily in solid state organic and organometallic chemistry. The prospects for the application of supramolecular crystals in synthesis and the opportunity to exploit the constraints imposed on molecular reactivity by the solid state are considered.

**10.03.12 Design, Synthesis And Application of N-Based Ligands for Coordination and Hydrogen Bonded Networks.** Eric Bosch, Chemistry Dept., Missouri State Univ., Springfield, MO 65804.

The design, synthesis and application of polytopic ligands to crystal engineering using metal coordination and hydrogen bonding will be presented. Ligands incorporating pyridine, pyrimidine, pyrazine and

triazine moieties were prepared. A variety of one-, two- and three-dimensional coordination networks were characterized following self-assembly of the ligands with inorganic salts primarily silver and copper salts. In contrast, hydrogen-bonded networks and capsules were formed following self-assembly of the ligands with polyphenols and carboxylic acids.

**10.03.13 Closed-Shell Interactions in Ag(I) Complexes: The Utility of the Metal-Ligand Mismatch.** Hilary A. Jenkins, Darren D.W. Mercer, Stephen A. Beaton, Dept. of Chemistry, Saint Mary’s Univ., Halifax, Nova Scotia, Canada, B3H 3C3.

Rational synthesis of metal-organic frameworks and polymers depends on many factors, not least of which is the preferred coordination geometry of the metal atom(s) involved. Silver(I) provides certain challenges in this area because of its somewhat unpredictable coordination geometry, and yet is often utilized specifically because it will bind to a wide variety of donors. Our recent work with simple tridentate N-donor ligands and normally four-coordinate Ag(I) has resulted in a series of compounds with closed-shell interactions between Ag(I) ions, and has given us an indication of what we can predict when synthesizing larger coordination polymers with bis(tridentate) ligands. Subtle changes in the ligand or counterions result in major changes in the overall structures, but certain patterns have emerged. In this presentation, we will discuss the effects of introducing aromatic and/or cationic spacers into tridentate ligands and the resultant formation of new polymeric and dimeric Ag(I) complexes. We will also examine the effects of varying the donor atoms in the ligands, progressing from an all-N system to mixed N,O-donors.

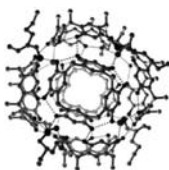
**10.03.14 Direct Crystallographic Observation of Chemical Transformations within a Self-Assembled Cages.** Makoto Fujita, Dept. of Applied Chemistry, School of Engineering, Univ. of Tokyo, and CREST, Japan Science and Technology Agency, 7-3-1 Hongo, Bunkyo-ku, Tokyo 113-8656, Japan.

Cavity-directed chemical transformations represent one of the most important features of three-dimensional hosts, but yet have been less explored in previous synthetic receptors. We are developing such functions with the large cavity of the self-assembled cages, particularly an  $M_6L_4$ -type cage complex. The photodimerization of olefins in this cage is featured, for example, by remarkable rate enhancement (>10<sup>2</sup> times), perfect regio- and stereo-selection, and high pairwise selection (when two different olefins are used) giving only a cross [2+2] adduct. In this paper, chemical reactions are carried out in a single crystalline state of the cage-substrate complex. Despite considerable change in the structures of the substrates, the cage framework is sufficiently robust enough to allow the direct crystallographic observation of the chemical reactions without losing the single crystallinity. The generation and trapping of an extremely labile unsaturated metal complex as well as solution-like behavior of an olefin in the [2+2] photoaddition in crystalline cage will be discussed.

**10.03.15 Designer Container-Molecule Materials.** K.T. Holman, S. T. Mough, O. Ugono, S.D. Drake, Dept. of Chemistry, Georgetown Univ., Washington, DC 20057.

So-called container molecules have received a great deal of attention in recent years related to their solution-phase binding properties and the unique behaviors of intimately associated “molecules within molecules.” Little is known, however, about the corresponding properties of materials derived from these remarkable molecules, though such materials might be expected to display recognition and storage prop-

erties commensurate with the molecular recognition properties of their building blocks. A design strategy toward functional soft materials derived from cup-like cavitands or container-like molecules will be outlined and some exemplary successes will be highlighted. The self-assembly of cup-like organic cavitands such as functionalized calix[4]resorcinarenes or cyclotrimeratrylenes into container-like and/or extended network solids will be described. Extended network structures derived from the self-assembly of cryptophane molecular containers will also be discussed.

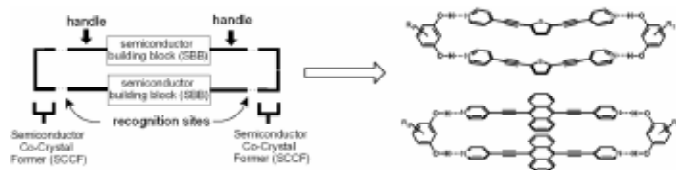


**10.03.16 From Covalent Synthesis to Supramolecular Assembly: The Investigation into Cavitand-Based Host-Guest Architectures.** N. Schultheiss, C.B. Aakeröy, J. Desper, Kansas State Univ., Manhattan, KS 66506.

Cavitands are excellent receptors for use in host-guest chemistry due to their bowl-shaped framework and a variety of covalent modifications can also be applied to both the upper and lower rims. Furthermore, the construction of cavitand-based capsules with tunable internal metrics allows for the encapsulation of specific sized guests. Accordingly, various pyridyl-functionalized cavitands were synthesized in good yields, by means of palladium catalyzed cross-coupling reactions. Through single-crystal X-ray analysis it has been shown that each of the derivatized cavitands exhibits an ability to accommodate guest molecules by way of multiple intermolecular interactions.

**10.03.17 Stacking of Semiconductor Molecules Enforced Through Hydrogen Bonding.** Anatoliy N. Sokolov, Leonard R. MacGillivray, Dept. of Chemistry, Univ. of Iowa, Iowa City IA, 52242.

In this presentation we describe a rational approach to direct the formation of face-to-face dimeric stacks of semiconductor building block (SBB) molecules (*J. Am. Chem. Soc.*, *in press*). The approach involves the functionalization of SBBs, namely 2,5-bis(4-pyridylethynyl)thiophene or 9,10-bis(4-pyridylethynyl)anthracene, with hydrogen bond acceptor sites. The subsequent co-crystallization of the SBB with a semiconductor co-crystal former (SCCF), in the form of a resorcinol derivative, results in the formation of hydrogen-bonded molecular assemblies in which the SBBs exhibit face-to-face  $\pi$ -stacked arrangements. The crystal structure of the pure compounds and related co-crystals will be reported and discussed in the context of engineering solids that exhibit efficient charge-transport properties.



**10.03.18 Challenges in the Drug Form Selection.** Z. Jane Li, Materials Science, Pfizer Global Research and Development, Pfizer Inc. Groton, CT 06340.

With increasing complexity of molecular structures of new drugs and variety of dosage forms, preparation and identification of the appropriate form and the Active Pharmaceutical Ingredient (API) with desired properties and functions become more challenging. Because the solid form of an API impacts stability, solubility, bioavailability and suitability for the dosage manufacture, understanding of the structures

and properties of the solid forms is critical in the drug development process. Case studies of the drug form selection will be presented. One involves the design and selection of a crystalline complex as an API, including the API form selection, crystal structural elucidation and crystallization scale-up issues. Another example is to address stability issues in the API form and drug product. These examples demonstrate that solid-state pharmaceuticals presents great opportunities for supramolecular synthesis and crystal engineering.

**10.03.19 Application of Crystallographic Information to Pharmaceutical Problems.** Matthew L. Peterson, TransForm Pharmaceuticals, Inc. 29 Hartwell Ave., Lexington, MA 02421, mpeterson@transformpharma.com

The topics presented will showcase the application of X-ray crystallography, highlighting its use as a powerful complement to more standard analytical techniques within the pharmaceutical preformulation and development arena. Utilization of crystal structure information to rationalize dramatic increases in stability of pharmaceutical compounds in the crystalline state versus the amorphous state will be addressed. Advances in crystal engineering, focusing predominantly on the design of novel materials with enhanced physicochemical properties, will also be discussed. Finally an analysis of polymorphism using the CSD, along with some simple molecular modeling techniques, will be shown.

## 11.01 Radiation Damage and Macromolecular Crystallography

**11.01.01 Thermal Imaging Applied to Cryocrystallography: Cryocooling and Beam Heating.** Edward Snell<sup>1</sup>, Henry Bellamy<sup>2</sup>, Gerd Rosenbaum<sup>3</sup>, Mark van der Woerd<sup>4</sup>, Michael Kazmierczak<sup>5</sup>, <sup>1</sup>Hauptman-Woodward Medical Research Inst., Buffalo NY, <sup>2</sup>CAMD, Louisiana State Univ., Baton Rouge, LA, <sup>3</sup>Dept. of Biochemistry, Univ. of Georgia, SER-CAT, APS, Argonne, IL, <sup>4</sup>BAE Systems, Huntsville, AL, <sup>5</sup>Dept. of Mechanical, Industrial & Nuclear Engineering, Univ. of Cincinnati, Cincinnati, OH.

Thermal imaging provides a non-invasive method to study both the cryocooling process and heating due the X-ray beam interaction with the sample. The method has been used successfully to image cryocooling in a number of experimental situations, i.e. cooling as a function of sample volume and as a function of cryostream orientation. There are experimental limitations to the method but it has proved a powerful technique to aid cryocrystallography development. Due to the rapid spatial temperature information provided about the sample it has also proved powerful in the testing of mathematical models.

Recently thermal imaging has been used to measure the temperature distribution on both model and typical crystal samples illuminated by an undulator produced X-ray beam. A brief overview of thermal imaging, and previous results will be presented. Following that a detailed description of the calibration then experimental and modeling aspects of the beam heating experiments will be described.

**11.01.02 Helium Temperature Mitigation of Radiation Damage.** B. Leif Hanson<sup>⊘</sup>, Unmesh Chinte<sup>⊘</sup>, Binal Shah<sup>\*</sup>, John Ruble<sup>#</sup>, Keith Brister<sup>^</sup> Connie Schall<sup>\*</sup>, B.-C. Wang<sup>#</sup>, Alan Pinkerton<sup>⊘</sup>. <sup>⊘</sup>Chemical Engineering and <sup>⊘</sup>Chemistry, Univ. of Toledo, OH; <sup>#</sup>Biochemistry and Microbiology, Univ. of Georgia, Athens, GA; and <sup>^</sup>formerly BioCARS, now LS-CAT, APS, ANL, Argonne, IL.

Previous work by our group has shown some abatement of radiation

damage in macromolecular crystals when using a Pinkerton Device open-flow helium cryostat delivering 15K data at the crystal position [Hanson et al. (2002) *J. Synchrotron Rad.* 9: 375-381]. Systematic studies at Bio-CARS of matched crystals at 15K and 100K have enabled us to quantify the improvement in lifetime in the highest resolution shell diffraction seen with the He temperature data. This can be as high as a 33% extension in diffractive lifetime in the highest resolutions shells. Improvements in lower resolution data measured at Cr wavelength has also been measured and will be detailed, as will anomalous diffraction studies with Se soaked crystals measured with 1.0Å X-rays. He cost with a Pinkerton device for a single crystal data set at APS is \$10-\$15. Since the use of cryogenic helium for data collection at a synchrotron source results in significant abatement of radiation damage, it should be considered for macromolecular data collection especially for proteins sensitive to radiation damage.

**11.01.03 Effects of Absorbed Dose on X-ray Radiation Damage in Protein Crystals at Cryogenic Temperatures.** J. Kmetko, N.S. Hussein, M. Naides, Y. Kalinin, R.E. Thorne, Physics Dept., Cornell Univ., Ithaca, NY 14853.

X-ray radiation damage to biological crystal is known to depend on parameters of the experimental setup (e.g. beam size, shape and energy, oscillation mode, etc.) as well as on the crystal itself (e.g. its size and shape, composition, etc.). We have measured how radiation damage at cryogenic temperatures depends on the crystal constituents and structure of four proteins: lysozyme, catalase, thaumatin, and apoferritin. We characterize radiation damage as degradation of relative B-factors per absorbed dose and define a coefficient of sensitivity to absorbed dose

$$S_{AD} = \frac{\Delta \langle u^2 \rangle}{\Delta D} = \frac{\Delta B_{rel}}{8\pi^2 \Delta D}$$

that serves as a robust measure of damage. Our results show that at cryogenic temperatures, the relative B factor per incident photon fluence increases linearly with the mass-energy absorption coefficient. The change in relative B-factor per dose, however, stays roughly independent of the mass-energy absorption coefficient (given by the crystal composition) and is about the same for all crystals, with  $S_{AD} \sim 0.014 \text{ \AA}^2/\text{MGy}$ . These results suggest that cryogenic radiation sensitivities per absorbed dose are unlikely to show significant protein-to-protein variations, and that radiation damage may in some cases be reduced by using salts with lower atomic number constituents.

We thank CHESS for access to beamline F3. This work was funded by the National Institute of Health (R01 GM65981).

**11.01.04 Radiation Damage of Protein Crystal in Various X-ray Energies.** N. Shimizu<sup>a</sup>, K. Hasegawa<sup>a</sup>, G. Ueno<sup>b</sup>, M. Yamamoto<sup>a,b</sup>, <sup>a</sup>Structural Biology Group, JASRI/SPring-8, <sup>b</sup>Div. of Synchrotron Radiation Instrumentation, RIKEN SPring-8 Center, 1-1-1 Kouto, Sayo, Sayo, Hyogo 679-5198 Japan.

The radiation damage of biological crystal sample always becomes a serious problem for the structural analysis. Most protein crystallographers expect that the use of high energy X-ray is one of

the methods to overcome it. However, no one might systematically verify the effect. In order to examine the effect of X-ray energy on radiation damage, we collected 12 ~ 15 data sets from one crystal at 9 different X-ray energies (6.5, 7.1, 8.3, 9.9, 12.4, 16.5, 20.0, 24.8 and 33.0 keV).

Lysozyme crystals with tetragonal form ( $P4_32_12$ ) were used as a sample for this comparison. The diffraction experiments were performed at BL41XU of SPring-8. One data set includes 180 images recorded with an oscillation step of  $1.0^\circ$ . The exposure time was set to 0.3 ~ 5 seconds according to the energy. Our data indicated that the increase of mosaicity started by the irradiation of photons larger than  $10^{13}$  for all X-ray energies. On the other hand, the amount of the change of mosaicity in high energy was shown smaller than that in low energy. In the presentation, we want to discuss the radiation damage of protein crystals by using all other data.

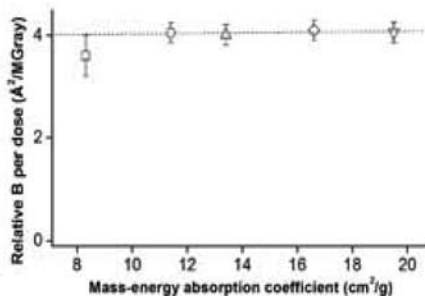
**11.01.05 Anomalous Diffraction at Ultra High Energy for Protein Crystallography.** Jean Jakoncic, Marco di Michiel, Zhong Zhong, Veijo Honkimaki, Peter David Siddons, Yves Jouanneau, Vivian Stojanoff, National Synchrotron Light Source, Brookhaven National Laboratory, Upton, NY.

Multiwavelength Anomalous Diffraction (MAD) and Singlewavelength Anomalous Diffraction (SAD) phasing at ultra high energy X-rays, 55 keV, are used to successfully determine a high quality and high resolution experimental electronic density map. The 2.5 % anomalous signal, at the Ho K edge, from three Ho atoms found in the model protein, Hen Egg-White Lysozyme, was sufficient to obtain a remarkable electron density and build the 3D molecular model in its integrity. Advantages and disadvantages on the use of ultra high energy X-rays are discussed in light of radiation damage problems and phasing power.

**11.01.06 Computational Removal of Radiation-induced Changes.** Zbyszek Otwinowski Dominika Borek Marcin Cymborski Wlodek Minor, Biochemistry, UT Southwestern Medical Center at Dallas, 5323 Harry Hines Blvd, Dallas, TX 75390-8816.

The dominant characteristics of radiation-induced changes, described either in real or reciprocal space, can vary between experiments. Real-space characteristics are important for the chemical interpretation of a crystal structure and could potentially also be used for phasing. On the other hand, the reciprocal-space characteristics consist of resolution-dependent decay combined with each reflection having an independent, continuous change of the structure factor with dose. Prior to an experiment, the magnitude and character of these changes cannot be accurately predicted. However, for the purpose of data analysis, a particular model of radiation damage must be assumed in order to avoid adding an unreasonable number of parameters. This procedure is additionally complicated by the fact that the magnitude of phasing signals and error estimators are unknown.

We present a number of examples showing which particular model of radiation damage in reciprocal space is most suitable for individual cases. Often, making the right choice has a dramatic impact on the structure solution process.



## 13.01 Crystalline Materials for Storage and Containment

**13.01.01 Investigation of the Microstructure of Ti-Doped Sodium Aluminum Hydride.** Martin Sulic, Craig Jensen, Lance Culnane, Bjorn Hauback, Hendrick Brinks, Mark Pitt, Ian Robertson, Chemistry, Univ. of Hawaii, 2545 McCarthy Mall, Honolulu, HI 06822.

It has been found that both doping and cycling of Ti-doped NaAlH<sub>4</sub> result in a decrease the crystal domain size and an increase anisotropic strain (Gomes, Renaudin, Hagemann, Yvon, Sulic, and Jensen, *J. Alloys and Compd.*, 390, 2005, 305). In order to further elucidate the relationship between the microstructure of the hydride and kinetics of its reversible dehydrogenation, we have conducted X-ray and neutron diffraction studies in tandem with tunneling electron microscopy. In previous studies of Ti-doped NaAlH<sub>4</sub>, we found that Ti-dopant undergo a progression of metamorphoses during the early cycles of dehydrogenation and re-hydrogenation. Therefore, unlike earlier structural investigations, the present study was focused on materials that had been subjected to multiple cycles. Our results have provided new insights the connection between the Ti-dopants and the microstructure of the hydride. The details of our studies will be presented and discussed in terms of their implications on the mechanism of hydrogen cycling in the doped hydride.

**13.01.02 Probing Structure and Bonding in Hydrogen-Storage Materials by Combined Neutron-Scattering Techniques and First-Principles Calculations.** T.J. Udovic, NIST Center for Neutron Research, NIST, 100 Bureau Dr., MS 8562, Gaithersburg, MD 20899.

The novel properties of the neutron such as its large scattering cross section for hydrogen can be routinely exploited by a variety of experimental neutron methods in order to probe the amount, location, bonding states, and motion of hydrogen in any promising hydrogen-storage material. For example, neutron powder diffraction (NPD) is critical for probing the structural details of hydrogen-storage materials and locating the positions of the absorbed hydrogen atoms and/or molecules. Neutron vibrational spectroscopy (NVS) complements NPD structural studies by revealing the local bonding potentials of the absorbed hydrogen. The results of both NPD and NVS measurements can be used to validate the fundamental physical description resulting from first-principles computational methods and thus deepen our overall understanding of the technologically important materials properties. This talk will provide recent examples of combined neutron and computational studies of new hydrogen-storage materials performed at the NIST Center for Neutron Research, including destabilized alkaline and alkaline-earth hydrides and metal-organic-framework structures.

**13.01.03 Diffraction Studies of Complex Al-based Hydrides for Hydrogen Storage.** Y. Nakamura<sup>1</sup>, M.H. Sørby<sup>1</sup>, A. Fossdal<sup>1</sup>, D. Blanchard<sup>1</sup>, H.W. Brinks<sup>1</sup>, C.M. Jensen<sup>2</sup>, B.C. Hauback<sup>1</sup>, <sup>1</sup>Dept. of Physics, Inst. for Energy Technology, P.O. Box 40, NO-2027 Kjeller, Norway, <sup>2</sup>Dept. of Chemistry, Univ. of Hawaii, Honolulu, HI 96822.

Complex Al-based hydrides, so-called 'alanates', have been investigated intensively as a candidate for hydrogen-storage materials with a high gravimetric capacity since reversible hydrogenation was reported for Ti-doped samples[1].

In this study, crystal structures of a series of alanates, *e.g.* LiAlD<sub>4</sub>, NaAlD<sub>4</sub>, KAlD<sub>4</sub>, Li<sub>3</sub>AlD<sub>6</sub> and Mg(AlH<sub>4</sub>)<sub>2</sub>, have been determined by powder neutron diffraction (PND) and synchrotron powder X-ray diffraction (SR-PXD). Mixed alanates Na<sub>2</sub>LiAlD<sub>6</sub> and K<sub>2</sub>NaAlH<sub>6</sub> have

been successfully synthesized and their structures have also been determined. Decomposition reaction has been investigated by *in situ* PND and SR-PXD. Effects of Ti additives for improving kinetics have been studied from viewpoints of unit cell dimensions and Al-Ti phase development.

The PND data were collected at the JEEP II reactor at IFE, Norway. The SR-PXD data were collected at the Swiss-Norwegian Beamline at ESRF, Grenoble, France.

Financial support from the European Commission and the Research Council of Norway is acknowledged. [1] B. Bogdanovic, M. Schwickardi, *J. Alloys Compd.*, 253-254 (1997) 1.

**13.01.04 Characterization of Phase Compositions and Structures for Metal Hydrides Used in Hydrogen Storage.** R.C. Bowman, Jr., J.G. Kulleck, JPL, Caltech, Pasadena, CA 91109, S.-J. Hwang, Caltech, Pasadena, CA 91125, M.R. Hartman, T.J. Udovic, J.J. Rush, NIST, Gaithersburg, MD 20899.

Knowledge of the phase diagrams and crystal structures of metal hydrides aids in development of these hydrogen storage materials for fuel cells and other energy technologies. The phase compositions and structures at the various stages of reaction with gaseous hydrogen have been examined in some promising systems by the combination of solid state nuclear magnetic resonance (NMR), powder x-ray diffraction (XRD), and neutron scattering methods. This approach will be illustrated with recent results obtained on two systems: (1) ZrNiD<sub>x</sub> over the composition range 0.8 < x < 3.0 where changes in structure and deuterium site occupancy are observed in two nonstoichiometric hydride phases and (2) The destabilized Li-Si-H systems where initial mixtures of LiH and Si convert into known Li-Si intermetallic phases as hydrogen is desorbed. A previously unknown ternary Li-Si-H phase has been found and characterized using NMR, neutron vibration spectroscopy, and neutron powder diffraction. While these reactions are reversible over portions of the Li-Si-H composition range, incomplete recovery of the original LiH + Si phases was also observed and will be related to formation of intermediate phases.

**13.01.05 Crystal Structure and Reaction Mechanism of Complex Metal Hydrides Studied by *in-situ* Synchrotron and Neutron Techniques.** Yan Gao, Job Rijssenbeek, GE Global Research, One Research Circle, Niskayuna, NY 12309.

Various light-weight complex metal hydrides, including sodium alanate and lithium magnesium imide, have been the focus of recent research in searching for ideal hydrogen storage materials for automotive application. Whereas these appear to be simple inorganic compounds, the challenges to the researchers who pursue a more fundamental understanding in these materials have been on the role of catalysts which make the hydrogenation process reversible under milder conditions, the reaction mechanism during hydrogen release and hydrogenation, and the crystal structures of intermediate and final reaction products in which the hydrogen positions become important. While *in-situ* diffraction is not new, our particular contributions as its application to hydrogen storage materials are to perform the *in-situ* diffraction (1) under hydrogen pressure of 2000 psi so that the reversible hydrogen release and uptake can be studied in real time and (2) under vacuum during hydrogen release so that the released gases can be analyzed by mass spectrometry in the same time as the diffraction data are taken. In addition, x-ray absorption fine structure (XAFS) analysis was applied to the study of Ti catalyst, and neutron diffraction and high-resolution powder diffraction were used to elucidate the crystal structures in more detail.

This talk is to demonstrate how the combined use of these crystallo-

graphic techniques can provide unprecedented insight to the mechanism of these reactions, which is of unquestionable importance to the design and discovery of new and more promising hydrogen storage materials that one day may be found under the hood of a car.

**13.01.06 Crystal Structures of and Charge Density Distributions in Perovskite-type Hydrides as a New Series of Hydrogen Storage Materials.** K. Ikeda, S. Kato, Y. Nakamori, S. Orimo, Inst. for Materials Research, Tohoku Univ., Sendai, Japan.

Some ternary hydrides have been reported to exhibit perovskite structures, typically expressed as ABH<sub>3</sub>, and their formation abilities were reasonably explained from the viewpoint of the geometric restrictions on ions, using Goldschmidt tolerance factors<sup>[1]</sup>. In addition, the reversible hydrogen storage abilities have been recently demonstrated for the first time on the hydride<sup>[2]</sup>. For improving the hydrogen storage abilities, it is necessary to clarify the atomistic bonding characters of the hydrides. In this study, the crystal structures and the charge density distributions precisely determined by synchrotron X-ray powder diffraction measurement and its MEM/Rietveld analysis will be presented on the perovskite-type hydrides such as NaMgH<sub>3</sub>, CaNiH<sub>3</sub>, and their related systems.

This study was partially supported by the Research Fellowships of the Japan Society for the Promotion of Science for Young Scientists.

[1] K. Ikeda, Y. Nakamori, and S. Orimo, *Acta Mater.*, **53** (2005) 3453.

[2] K. Ikeda, Y. Kogure, Y. Nakamori, and S. Orimo, *Scripta Mater.*, **53** (2005) 319.

## 13.02 Whole-Molecule Disorder

**13.02.01 About Whole-Molecule Disorder.** Håkon Hope, Dept. of Chemistry, Univ. of California, Davis, Davis, CA 95616.

Crystals grow by adding particles (molecules, atoms or ions) to an existing crystal. The approaching particle will only be added if its orientation is energetically favorable. If one particular orientation has an energetic advantage over all other orientations, the particle will settle in that orientation. If two or more orientations are close in energy, the particle may settle in one of these several orientations. Ideally, the orientations will follow a Boltzmann distribution. For example, if two orientations have the same energy, they will be represented by equal probabilities; the result will be a 50-50 disorder.

The crystal structure of azulene provides a well-studied example where the crystal is unable to discriminate between the two rings.

A false appearance of disorder can be the result of incorrect determination of unit cell size. Impurity molecules can compete for a place in the crystal. Alpha-D-galactose provides a tricky example. Ingenious studies of effects of impurity inclusion by Lahav, Leiserovitz and coworkers (e. g. in *Faraday Discuss.* 1993, 95, 307) have shown that reduction of local symmetry in regions of an intact crystal can occur, although the average symmetry of the whole crystal may be the same as for the pure material. The result could be the appearance of disorder.

**13.02.02 The Use of Advanced Refinement Techniques to Model Whole Molecule Disorder: Examples of Applications in Chemical Crystallography.** Charles Campana, Bruker AXS Inc., 5465 East Cheryl Pkwy., Madison, WI 53711.

There are numerous examples of chemically important crystal structures for which chemically and crystallographically acceptable results are not easily obtained, even though the crystalline specimens are of excellent quality and the experimental data are collected carefully

and correctly. These problems are usually tractable with the use advanced features of generally available programs, combined with some practical experience.

The diagnosis and treatment of problem crystal structures requires a logical, step-wise approach. We first look for symptoms which will reveal systematic errors in data, incorrect unit cells and/or space groups, twinning or incommensurate structures. Each of these problems has a treatment and a cure.

If none of the above conditions exist, and there is still a problem in solving and refining the structure, we may be able to analyze the structure and to refine it using disorder models and advanced refinement techniques.

We will present a series of chemically interesting structures to illustrate the method we have successfully used to analyze and refine complex disorders, including whole molecule disorders. All of the examples utilize advanced features available in the public-domain SHELXL program.

**13.02.03 Searching for WMD.** Peter Mueller, Chemistry, MIT, 77 Massachusetts Ave., Bldg. 2, Rm. 325, Cambridge, MA 02139.

Whole Molecule Disorder (or WMD) is a phenomenon that exists at least theoretically. Practically, however, this phenomenon has not been described very often and, besides the fullerenes, there are few examples in the literature. In this talk I will present a few examples where WMD appeared the right or at least a possible way to describe a structure.

**13.02.04 Penta-Tert-Butyl-Corannulene vs. Corannulene: Structure, Disorder, and Reactivity.** Y. Sevryugina<sup>1</sup>, E.A. Jackson<sup>2</sup>, L.T. Scott<sup>2</sup>, M.A. Petrukhina<sup>1\*</sup>, <sup>1</sup>Dept. of Chemistry, Univ. at Albany, SUNY, Albany, NY, 12222, <sup>2</sup>Dept. of Chemistry, Merkert Chemistry Center, Boston College, Chestnut Hill, MA, 02467-3860.

As part of a broad study on the reactivity of open geodesic polyaromatic hydrocarbons having curved unsaturated  $\pi$ -carbon surfaces that map onto the surface of C<sub>60</sub>-fullerene, we have accomplished the structural characterization of 1,3,5,7,9-penta-*tert*-butyl-corannulene (C<sub>40</sub>H<sub>50</sub>). Its molecular geometry and solid state packing have been compared with that of the parent bowl-shaped corannulene (C<sub>20</sub>H<sub>10</sub>). 1,3,5,7,9-Penta-*tert*-butyl-corannulene does not show  $\pi$ - $\pi$  stacking interactions and has a very loose packing in the solid state, compared to corannulene, due to peripheral crowding by the bulky *tert*-butyl groups. Difficulties in structure solution of the symmetrical C<sub>40</sub>H<sub>50</sub> bowl associated with the existence of various rotational orientations and with a statistical mixture of enantiomers will be discussed in detail. The effect of the ligand geometry and curvature on the outcome of gas phase complexation reactions of C<sub>20</sub>H<sub>10</sub> and C<sub>40</sub>H<sub>50</sub> with electrophilic volatile ruthenium(I) complexes will also be presented.

This work is supported by the American Chemical Society Petroleum Research Fund (PRF-42910-AC3) and the National Science Foundation Career Award (NSF-0546945).

**13.02.05 Disordered Structures: Identification and Interpretation.** Peter Y. Zavalij, Dept. of Chemistry and Biochemistry, Univ. of Maryland, MD 20742.

Crystal structures often exhibit different kinds of disorder from simple and frequent solvent disorder and rotational disorder of terminal groups to quite rare whole molecule disorder and to complex micro-twinning and OD structures. Usually significant disorder can be easily identified by high R-factor, strange ellipsoids, or senseless difference

peaks. However, sometimes disorder is not obvious and can be detected only by looking for some small, seemingly insignificant features, for example, difficulties in refinement of H atoms or presence of residual peaks even as small as hydrogen atom that are not near heavy atoms or in the middle of bonds, while the displacement ellipsoids are good and R-factor is just slightly higher than desired.

This presentation discusses identification and interpretation of the disordered structures covering several structures with whole molecule disorder, OD structure, an interesting stacking disorder in packing of 16! symmetrically independent molecules, and several structures of centrosymmetric host with non-centrosymmetric guest. The latter rises problem of choice between “classic” disordered structure and merohedral twinning: F vs. F<sup>2</sup>. It was noticed that in many cases structure disorder happens in the presence of “unrealized” local symmetry of the molecules or other building blocks.

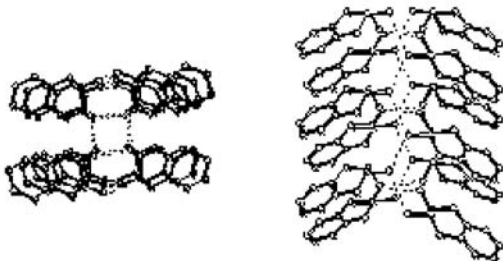
**13.02.06 Solid-State Compound Formation between Stereoisomers: 2,3-Tetralindiol.** Carolyn P. Brock, Sean Parkin, Brian Patrick, Dept. of Chemistry, Univ. of Kentucky, Lexington, KY 40506.

The existence of a 1:1 compound of *cis* and *trans*-2,3-tetralindiol, which represents a striking failure of fractional crystallization, was reported by Leroux in 1909, but the structure of this compound is unpublished. The compound dominates the ternary phase diagram (*cis* isomer and resolvable *trans* isomers; Lettré & Lerch, 1952), but its crystals grow as very small needles, which are both disordered and twinned. Data that refined satisfactorily were finally obtained using Cu radiation from a rotating-anode source.

Columns of H-bonded tetrameric units related by translation make up the structure; each unit contains two *cis* and two *trans* isomers. The overall packing and most of the H-bonding pattern can be maintained when *cis* and *trans* isomers are switched. While the isomers appear to be totally disordered, more detailed analysis indicates that a crystal containing only one of the *trans* enantiomers might be fully ordered.

Comparisons of this structure with the structures of the pure *cis* and enantiomerically pure *trans* isomers suggest reasons for the surprising stability of the *cis-trans* compound. The structure of the *trans* racemate remains unknown.

Leroux (1909). *Comptes Rendus* **148**, 931-933. Lettré, H. & Lerch, I. (1952). *Chem. Ber.* **85**, 394-397.



**13.02.07 Whole-Molecule Disorder in Adenine Salts and Substituted Adenine Derivatives.** John Desper, Christer Aakeroy, Michelle Smith, Goran Wennerberg, Chemistry, Kansas State Univ., 304 King Hall, Manhattan, KS 66506 USA.

A pair of co-crystals containing adenine or an adenine derivative and a carboxylic acid were analyzed by single-crystal X-ray diffraction. Although both structures contained both expected components, refinement as single ordered species proved unsatisfactory. In both cases, successful refinement was achieved by incorporating two structural models, disordered over a single site, for the adenine fragment. Disorder consists of exchanging the position of the 5-membered (imidazole) and 6-membered (pyrimidine) rings. The combination of both

fragments significantly improved refinement, as reflected both in statistical figures of merit and difference density maps.

**13.02.08 Examples of Crystal Structures with Whole Molecule Disorder.** G.D. Enright, J.A. Ripmeester, Steacie Inst. for Molecular Sciences, National Research Council, Ottawa (ONT.), Canada.

Small molecule crystal structures that exhibit whole-molecule disorder present considerable challenges in collection, solving, and refinement. Diffraction patterns from such crystals contain significant diffracted intensity outside of the Bragg reflections in the form of diffuse scattering or as satellite reflections. Examples of both types will be presented.

In the first example we present the single-crystal structure of the high temperature polymorph of caffeine. Our study confirms some features of a recent PXRD structure determination except the space group is R-3c and the molecule is disordered over *six* symmetry related positions. The molecules are  $\pi$ -stacked along the c axis. The diffraction pattern contains intense diffuse bands that occur at *d*-spacings that correspond to the distance (and subharmonics) between molecules.

In a second example we will present the structure of a five-membered heterocyclic carbene. The diffraction patterns indexed as F-centered orthorhombic with a weak set of satellite peaks. The primary cell was solved in space group Fdd2 with the molecules fully disordered about a two-fold axis.

For both examples it was necessary to greatly expand the number of trial sets to find an initial solution and a large number restraints were applied to stabilize the refinement.

**13.02.09 Disorder may be a Misnomer.** Brahma D. Sharma, PO Box 1626, Pismo Beach, CA 93448-1626.

The assignment of space group may be unambiguous, as centric or non-centric. The centric space group assignment in conjunction with number of units per asymmetric unit some times leads to the conclusion of “disorder” description of the structure.

An interesting example is a very old crystal structure presented by this author in collaboration with Late Jerry Donohue, namely, 2-phenylazulene<sup>[1]</sup>.

This ambiguity became an issue of contention in relation to the proof of the Watson-Crick base pairs by Fourier methods<sup>[2]</sup>.

We will present a proposal that the usual space disorder of whole molecules can be resolved by the well-known proposal of “mosaic” aspects of crystals, by Darwin.

However, the “time” averaging is another factor that must be given serious consideration as was done for N–H...N hydrogen bond by this author<sup>[3]</sup>.

#### References:

- [1] B. D. Sharma, and J. Donohue, (1961) *Nature*, 192, 863. J. Donohue, and B. D. Sharma, (1953) *Nature*, 198, 878
- [2] J. Donohue (1970) *Science*, 167, 1700, J. Donohue (1970) *Nature*, 227, 317
- [3] Brahma D. Sharma, American Crystallographic Association Abstracts of Papers, 5, (1967).

## 13.03 PDF Analysis of Industrially Relevant Materials

**13.03.01 Total Scattering: The Key to the Local and Medium Range Structure of Complex Materials.** Th. Proffen, Los Alamos National Laboratory, Lujan Neutron Scattering Center, Mailstop H805, Los Alamos, NM 87545.

The key to understanding the properties of complex materials is often an understanding of its local, medium- and long-range atomic structure. Structural characterization is usually based on the measurement of *Bragg intensities* and yields the *average* structure of the crystalline material. However, this approach ignores any defects or local structural deviations that manifest themselves as *diffuse scattering*. It also fails in case of disordered materials, badly crystalline such as many nano-materials, or not crystalline at all, such as glasses. In some cases crystalline and amorphous phases coexist making the traditional crystallographic structure refinement difficult or incomplete. The total scattering pattern, however, contains structural information over all length scales [1] and can be used to obtain a complete structural picture of complex materials. Here we present a number of examples of this technique to industrially relevant materials.

Th. Proffen, S.J.L. Billinge, T. Egami and D. Louca, *Z. Krist.* 218, 132-143 (2003).

**13.03.02 Structural Disorder in the Negative Thermal Expansion Material  $ZrW_2O_8$  and Quartz-based Piezoelectrics: An RMC Analysis of Total Scattering Data.** D.A. Keen<sup>1</sup>, M.G. Tucker<sup>1</sup>, M.T. Dove<sup>2</sup>, A.L. Goodwin<sup>2</sup>, S.A. Wells<sup>3</sup>, J.S.O. Evans<sup>4</sup>, J. Haines<sup>5</sup>, O. Cambon<sup>5</sup>, <sup>1</sup>ISIS Facility, Rutherford Appleton Laboratory, Oxon UK, <sup>2</sup>Earth Sciences Dept., Cambridge Univ., Cambridge, UK, <sup>3</sup>Biological Physics, Arizona State Univ., Tempe, AZ, <sup>4</sup>Chemistry Dept., Durham Univ., Durham, UK, <sup>5</sup>UMR CNRS 5617, Univ. Montpellier II, Montpellier 5, France.

Total scattering data from disordered crystals gives information on the long-range average structure via the Bragg intensities and local deviations from this average via the pair distribution function. The reverse Monte Carlo (RMC) method is an ideal way to analyse these data to provide self-consistent structural models. Disorder plays an important role in the NTE behaviour of  $ZrW_2O_8$  and the reduced piezoelectric performance in a-quartz  $SiO_2$  and a-berlinite  $GaPO_4$  resonators at high temperature. This talk will describe how results from RMC analysis of total scattering have been able to identify local structural features which are responsible for the observed macroscopic behaviour in these two materials. In particular, it is found that complex motion of “rigid” structural units provides the mechanism for thermally induced contraction of  $ZrW_2O_8$  and the dissipation of induced dipoles in  $SiO_2$  and  $GaPO_4$ .

**13.03.03 Diffraction Studies of Nanocrystalline Diamond and SiC in Real and Reciprocal Spaces.** Bogdan Palosz, Inst. of High Pressure Physics, Polish Academy of Sciences, Warsaw, Poland.

Nanocrystals have a non-uniform structure, where the arrangement of atoms in the grain interior (the core) is different than that at the surface (the surface shell). This difference may be very small and missed in a conventional diffraction experiment. We show that the key in a quantitative characterization of the atomic structure of nanocrystals is acquiring a diffraction data in a very large range of the reciprocal space ( $>Q = 20\text{-}30 \text{ \AA}^{-1}$ ), what requires high energy X-rays or hot neutrons. Only such data can provide the accuracy needed for a meaningful description of the atomic structure of nano-grains. It concerns the analysis in real (Bragg) as well as in reciprocal spaces (PDF). With ap-

plication of very large- $Q$  neutron diffraction at LANSCE (HIPPO and NPDF stations,  $Q$  up to  $50 \text{ \AA}^{-1}$ ) we were able to examine distribution of strains in nano-diamond and SiC as a function of the grain size, and trace their evolution in nano-ceramics sintered under high pressures. Also, using the Wilson method, different atomic thermal vibrations of the inner and surface atoms were evaluated.

We thank LANSCE for access to beamlines HIPPO and NPDF. This research is supported by the Polish Ministry of Education and Science, grant 3 T08A 020 29, and NSF grant DMR 0502136.

**13.03.04 Internal Strain Measurements using PDF Analysis.** B. Clausen<sup>1</sup>, Th. Proffen<sup>1</sup>, E. Üstündag<sup>2</sup>, <sup>1</sup>Lujan Center, Los Alamos National Laboratory, NM 87545, <sup>2</sup>Dept. of Mat. Sci. and Eng., Iowa State Univ., Ames, IA 50011.

Today, routine measurements of internal and residual strains in crystalline materials are performed using neutron and synchrotron X-ray based diffraction methods. The diffraction technique has proven invaluable for validating constitutive models for polycrystalline materials. Recently, the approach has been extended to bulk metallic glasses, and preliminary results show that changes in the position of the “*first sharp diffraction peak*” in  $S(Q)$  and nearest-neighbor peaks in  $G(r)$  correlate well with the macroscopic strain in uniaxial loading tests. However, it is clear that rigorous structure refinement is required for quantitative strain determination based upon pair distribution function analysis.

**13.03.05 Collective Properties from RMC Analysis of Total Scattering Data: Excitations, Modulations and Some Limitations.** A.L. Goodwin<sup>1</sup>, M.T. Dove<sup>1</sup>, E.R. Cope<sup>1</sup>, M.G. Tucker<sup>2</sup>, D.A. Keen<sup>2</sup>, <sup>1</sup>Dept of Earth Sciences, Cambridge Univ., Cambridge CB2 3EQ UK <sup>2</sup>ISIS Facility, Rutherford Appleton Laboratory, Oxon OX11 0QX UK.

The reverse Monte Carlo (RMC) structural refinement method provides a powerful means of generating atomistic configurations from total scattering data. These configurations represent at once both elastic and inelastic contributions to the scattering process: the former is reflected in the average periodic structure of the configuration, and the latter in local deviations from this average structure. Inelastic scattering from collective excitations such as phonons will then enter the RMC configurations in the form of correlated atomic displacements. This talk will describe how information regarding the phonon spectrum can be retrieved from analysis of large numbers of RMC configurations, enabling the calculation of phonon dispersion curves from powder diffraction data. The known limitations of the approach will be discussed. The extension of the RMCProfile implementation to allow refinement of magnetic structures will also be described, together with its role in the discovery of structural modulations in the benchmark antiferromagnet MnO. Finally, it will be shown that spin-wave dispersion curves can be recovered from these magnetic RMC configurations.

**13.03.06 Uncovering Structural Features Related to the Material Properties by the PDF Method.** Wojtek Dmowski<sup>1</sup>, Karen E. Swider-Lyons<sup>2</sup>, Takeshi Egami<sup>1,3</sup>, <sup>1</sup>Dept. of Materials Science and Engineering, Univ. of Tennessee, Knoxville, TN 37996, <sup>2</sup>Code 6170, Naval Research Laboratory, Washington, DC 20375, <sup>3</sup>Oak Ridge National Laboratory, Oak Ridge, TN 37831.

Atomic pair-density function (PDF) analysis is an ideal approach for examining the local- and medium-range atomic structures of materials. PDF has been widely used in the studies of glasses and liquids and has also been applied successfully to characterize the local and complex structures of crystalline solids. Using PDF analysis, we

demonstrate that important conclusions can be drawn about how the short- and long-range atomic structure of several materials, including catalysts, structural materials and ferroelectrics, relates to their physical and electrochemical properties. We demonstrate that PDF can be extended to study local atomic dynamics.

## 13.05 Difficult Organic/Organometallic Structures

**13.05.01 Synthetic Small-molecule Models of Peptides and Nucleic Acids – The Definitive Not-so-small Molecules.** Lee M. Daniels<sup>1</sup>, Ivan Huc<sup>2</sup>, Jean-Michel Leger<sup>2</sup>, <sup>1</sup>Rigaku Americas Corp., 9009 New Trails Dr., The Woodlands, TX, <sup>2</sup>Inst. Européen de Chimie et Biologie, 2, Rue Robert Escarpit, Pessac Cedex, France.

As small-molecule crystallography marches into the realm of the not-so-small, new challenges arise and new techniques become important. Modern molecular modeling tools and synthetic techniques allow the design and preparation of increasingly large and complex non-natural mimics of the folded conformations of peptides and nucleic acids. Determining 3-dimensional structures of these materials from diffraction data is difficult. There are crystal-growth challenges, frequent data collection and processing complications, and of course structure solution and refinement obstacles. Several examples of these systems will be discussed.



**13.05.02 A Nitrosyl Heme Thiolate Product from a Heterogeneous Reaction.** Douglas R. Powell, Nan Xu, Lin Cheng, and George B. Richter-Addo, Dept. of Chemistry and Biochemistry, Univ. of Oklahoma, 620 Parrington Oval, Norman, OK 73019.

Heme thiolate proteins display rich and diverse reactivities that include nitric oxide (NO) biosynthesis, NO reduction, hydroxylation, and detoxification of xenobiotics. Attempts to make model nitrosyl heme thiolate compounds by solution methods have, so far, been unsuccessful. However, such a model compound has been prepared from a heterogeneous reaction of crystals of  $[\text{Fe}^{\text{III}}(\text{oep})(\text{thiolate})]$  and NO gas.<sup>1</sup> The resulting crystal diffracted to only 1.0 Å resolution. The volume of the crystal lattice increased from 2266.3(6) Å<sup>3</sup> for the crystal without NO to 2360(2) Å<sup>3</sup> after NO addition. The NO ligand is bent with an angle of 159.6(8)°. The nitrosyl N is tilted 9.1° from the normal to the porphyrin plane. The Fe atom is displaced 0.05 Å toward the NO ligand from the porphyrin plane. This work was supported by the U.S. National Institutes of Health (GM64476).

<sup>1</sup>Nan Xu, Douglas R. Powell, Lin Cheng, and George B. Richter-Addo, *Chem. Comm.*, 2006, submitted.

**13.05.03 Crystal Structures and Solid Forms of 6-OH Buspirone.** <sup>1</sup>Qi Gao, <sup>1</sup>Dedong Wu, <sup>2</sup>Garry McGeorge, <sup>3</sup>Larry Parker, Bristol-Myers Squibb Pharmaceutical Research Inst., <sup>1</sup>Analytical Research & Development, Wallingford, CT, <sup>2</sup>Analytical Research & Development, New Brunswick, NJ, <sup>3</sup>Process Research & Development, New Brunswick, NJ.

6-OH Buspirone is a potent 5-HT<sub>1A</sub> partial agonist that exhibits anxiolytic activity in animal models. It is one of the major metabolites of the anxiolytic drug Buspar<sup>®</sup> and was found in a 3:1 isomer ratio of S:R in humans after chronic Buspar exposure. The development of this drug candidate for the treatment of anxiety was inspired by the prediction that it would provide a significantly larger amount of

the active drug with much reduced levels of other metabolites. This paper presents structural studies that were crucial to the understanding of the nature of solid materials and more importantly to the chemical development of 6-OH Buspirone. Discussions will focus on problems such as structure disorders, space group ambiguities, crystallization, phase transitions and racemic modifications.

**13.05.04 Enhanced Resolution PDF from Home Lab Based X-ray Scattering.** Alex Yokochi<sup>1</sup>, Larry Marple<sup>2</sup>, <sup>1</sup>Dept. of Chemical, Biological and Environmental Engineering, Oregon State Univ., Corvallis, OR 97331, <sup>2</sup>School of Electrical Engineering and Computer Science, Oregon State Univ., Corvallis, OR 97331.

Synthetic research in coordination chemistry often yields the famous “intractable insoluble material” that resists crystallization. A technique that may yield useful structural insights on the synthesized material is total scattering. In this technique, very high resolution scattering data is collected for the material in question ( $Q = 40 \text{ \AA}^{-1}$  is typical), from which a radial distribution curve is then reconstructed by Fourier transformation. However, for total scattering to be useful to guide daily activities in the laboratory, the data should be able to be produced in house with a conventional diffractometer. Unfortunately, using current methodology for spectrum reconstruction it is found that resolution limitations resulting from the limited range of data using home laboratory based instruments ( $Q_{\text{max}} = 24 \text{ \AA}^{-1}$  when using  $\text{AgK}\alpha$ ) drastically reduces the usefulness of information obtained with this technique.

A desire to be able to use total scattering techniques from home lab data has led us to investigate the possibility of applying modern signal processing and spectrum reconstruction techniques to enhance the information content of the derived radial distribution curve.

This presentation will report our experiences and insights whilst pursuing this work.

## 13.06 Structural Genomics Big and Small

**13.06.01 The Joint Center for Structural Genomics: A Multi-tiered Approach to Structural Genomics.** Ian A. Wilson, Joint Center for Structural Genomics (JCSG), La Jolla, CA 92037 USA.

The JCSG ([www.jcsg.org](http://www.jcsg.org)) has developed an integrated high throughput (HT) production pipeline for all steps from target selection, cloning, expression, crystallization to structure determination, and applied it to *Thermotoga maritima* (TM), as well as other bacterial and eukaryotic targets. We have determined over 150 structures of the predicted 1877 ORFs which, with other PDB TM structures, gives direct structural coverage of 32% of the expressed soluble proteins and ~12% of the proteome. After homology modeling and fold recognition, this represents one of the highest structural coverages (72%) of any organism. As a result of such HT studies, we have tested and validated strategies to improve yield and lower cost per structure through implementation of a three-tiered approach that includes a number of diverse salvage pathways. Many of these advances in technologies and methodologies can now be implemented on a smaller scale in individual structural biology labs. The JCSG is located at The Scripps Research Institute, Genomic Institute of the Novartis Research Foundation, U.C. San Diego, Burnham Institute, and the Stanford Synchrotron Radiation Laboratory/Stanford University. JCSG is supported through the NIH Protein Structure Initiative (U54 GM074898), ([www.nigms.nih.gov/funding/psi.html](http://www.nigms.nih.gov/funding/psi.html)).

**13.06.02 Expression, Purification and Crystallization Methods Developed at the MCSG Adoptable to a Structural Biology Laboratory.** M. Zhou, Y. Kim, P. Quartey, H. Li, C. Hatzos, Ry. Wu, L. Volkart, G. Joachimiak, M. Donnelly, A. Joachimiak, Midwest Center for Structural Genomics, Argonne National Laboratory, Argonne IL 60439.

The MCSG has developed an effective, low cost protein structure determination pipeline. New vectors and media allow protein expression using inexpensive laboratory incubators and vessels. Proteins are purified using semi-automated procedure and robot-assisted crystallization trials are inspected with the imager. One person can readily complete purification and crystallization of 16 different proteins over two week period. Typically 3-5 proteins will crystallize resulting in 1-2 new crystal structures. To increase the success rate we implemented savage pathways: 1) improve the protein expression by adding MBP fusion that can be removed *in vivo*, 2) increase crystallization success rate using semi-automated chemical modification, 3) screen for additives during crystallization. The pipeline is capable producing ~150 new structures/year. All the instruments are commercially available and procedures can be easily adapted to the medium-size crystallography laboratory.

This work was supported by the grants from the NIH (GM62414 and GM074942) and the U.S. Department of Energy, OBER under Contract W-31-109-ENG-38.

**13.06.03 High Throughput Optimization of Initial Crystallization Conditions.** J.R. Luft<sup>1,2</sup>, S.M. Gulde<sup>1</sup>, A.M. Lauricella<sup>1</sup>, M.I. Said<sup>1</sup>, J.L. Smith<sup>1</sup>, M. Thayer<sup>1</sup>, C.K. Veatch<sup>1</sup>, J.R. Wolfley<sup>1</sup>, M.G. Malkowski<sup>1,2</sup>, G.T. DeTitta<sup>1,2</sup>, <sup>1</sup>The Hauptman Woodward Medical Research Inst., <sup>2</sup>Dept. of Structural Biology, SUNY at Buffalo, 700 Ellicott St., Buffalo, NY 14203.

An established High Throughput infrastructure screens 200 biological macromolecules against 1536 chemical conditions each month to determine initial chemical crystallization conditions (1). The majority of these samples are provided by structural biologists with a subset of difficult to crystallize targets from *Saccharomyces cerevisiae* supplied by the CHTSB consortia. High Throughput optimization methods are under development to use information obtained from the screening experiments to produce crystals of sufficient size and quality for X-ray diffraction. First phase optimization trials use a simple volumetric approach to refine crystallization conditions in the experiment drop (2). This method was applied to 17 samples from the structural biology community set up in replicate 1536 well plates, incubated at four different temperatures. The outcomes of these experiments and other optimization methods that are under investigation will be described. This work is supported in part by NIH U54 GM074899-01.

1) *Journal of Structural Biology* **142**, 170-179 (2003)

2) *Structure* **10** (2) 147-151 (2002)

**13.06.04 Biological Crystallization Resource: Facilitating Knowledge-Based Biological Macromolecule Crystallization.** Chunmin Li, Kevin Kirkwood, Brayer Gary, Biochemistry and Molecular Biology, Univ. of British Columbia, 2350 Health Sciences Mall, Vancouver BC V6T 1Z3, CANADA.

The Biological Crystallization Resource (BCR) is a database that has been constructed to facilitate the discovery of the relationships between the properties of biological molecules and their optimal crystallization conditions. Through the use of advanced data mining and manipulation techniques the BCR is able to accept multiple parameter searches, where the resultant output allows an investigator to design customized crystallization screens for the biological macromolecules under investigation. The BCR URL is [www.growcrystal.com](http://www.growcrystal.com). A free

demonstration version of the database targeting the customized crystallization screen design of carboxylic ester hydrolases (E. C. 3. 1. 1. -) and a manual detailed the access and applications of the database can be found at the above web site.

**13.06.05 Structural Genomics Experimental Pipelines - Insights from the First Five Years.** O. Kirillova, M. Grabowski, H. Zheng, Z. Otwinowski, W. Minor, Dept. of Molecular Physiology and Biological Physics, Univ. of Virginia, Charlottesville, VA.

Worldwide structural genomics (SG) initiatives, aiming to rapidly elucidate the structures of a large number of strategically selected proteins, have produced more than 2000 structures out of a target list of around 96,000. About two thirds of SG structures were non-redundant (<30% sequence identity in the PDB at the time of deposition), which constituted close to a third of all non-redundant depositions. In 2005 the SG efforts contributed 45% of all non-redundant PDB depositions.

To estimate the potential of the second phase, we examined the dynamics of the SG experimental pipeline based on target data released by various centers, using the techniques of survival analysis.

The comparison of overall target progression rates at the stages of expression, purification, crystallization, and diffraction has shown that the pipeline efficiency varied significantly for different genomes and was influenced by protein characteristics and degree of similarity to proteins of known structure. For eukaryotic targets, most attrition was due to failure of expression and/or purification, while for prokaryotes it was due to failure of obtaining diffraction-quality crystals.

The high-throughput approach did not compromise structure quality. The quality of SG deposits has been steadily improving over time, despite the fact that the average time between data collection and completion of refinement was shortened from 242 days in 2003 to 175 in 2005.

**13.06.06 Probability-based Cryo Condition Optimization Procedure for High-throughput X-ray Crystallography.** M. Yu<sup>1</sup>, E.H. Bursey<sup>1</sup>, T. Radhakannan<sup>1</sup>, L-W. Hung<sup>1,2</sup>, <sup>1</sup>Physical Biosciences Div., Lawrence Berkeley National Lab, Berkeley, CA 94720, <sup>2</sup>Physics Div., Los Alamos National Laboratory, Los Alamos, NM 87545.

An empirical probability-based cryo condition selection procedure for high-throughput diffraction screening and data collection has been developed at the ISFI/TBSGC X-ray crystallography facility at the Lawrence Berkeley National Laboratory. This method is based on (1) diffraction experiments from about 3000 crystals of 62 unique TBSGC targets conducted in 2004-2005, and (2) empirical compatibilities between cryo-additives and crystallization reagents. The results have been cross-validated with over 700 independent data from the Cryoprotectant Database ([http://idb.exst.jaxa.jp/db\\_data/protein/200304E02478000.html](http://idb.exst.jaxa.jp/db_data/protein/200304E02478000.html)) with highly positive correlations. Our procedure selects 2-20 cryoprotectant candidates for initial diffraction screening according to the contents of the crystallization mother liquor. A 'score of merit' (SOM) combining the diffraction resolution, the mosaicity, and the presence of ice rings are used to track the successfulness of each cryo condition. Using this procedure, we have obtained high success rate to rapidly determine an optimal cryo condition for crystals from a board range of proteins.

**13.06.07 Robotic Crystal Harvesting: The Final Frontier in Automated High Throughput Crystallography.** Bernhard Rupp<sup>1</sup>, Peter Carmen<sup>2</sup>, Jace Walsh<sup>2</sup>, Echo Miller<sup>2</sup>, Robert Viola<sup>2</sup>. <sup>1</sup>q.e.d. life science discoveries, Livermore, CA, <sup>2</sup>Square One Systems Design, Jackson, WY.

High throughput crystallography has reached a level of automation, where complete computer-assisted robotic crystallization pipelines are capable of cocktail preparation, crystallization plate setup, and inspection and interpretation of results. Mounting of crystal pins, data collection and structure solution are also highly automated. The remaining challenge towards full automation is crystal harvesting and cryo-cooling. These critical operations occur late in the crystallization process and are a major source of loss of valuable crystals.

To address the final frontier in achieving fully automated high throughput crystallography, we have designed and tested an anthropomorphic, 6-axis Universal Micromanipulation Robot (UMR) capable of reliably harvesting and cryo-quenching protein crystals as small as 10µm from a variety of 96 well plates. The UMR arm is equipped with a versatile tool exchanger. Tape cutters, harvesting pins with MiTeGen MicroLoops, cryo-liquid exchange and custom tools provide additional operational flexibility. The current user interface is a simple game-style keyboard layout allowing intuitive manual control. Semi-automated process steps such as tool location, loop approach to crystals, as well as fully automated tape cutting and quenching have been implemented in the prototype. Integrated machine vision and object tracking are in development to achieve minimally supervised, automated crystal harvesting.

Work sponsored by NIH Grant No. R41 GM073278-01.

**13.06.08 The Role of Follow-Up Studies at the Center for Eukaryotic Structural Genomics.** J.G. McCoy, A. Arabshahi, E. Bitto, C.A. Bingman, F.J. Ruzicka, P.A. Frey, G.N. Phillips Jr., Dept. of Biochemistry, Univ. of Wisconsin-Madison, Madison, WI 53706.

A primary goal of the Center for Eukaryotic Structural Genomics (CESG) is to solve protein structures unrelated to those already in the PDB. A byproduct of this goal is an accumulation of structural data for proteins of unknown or misannotated function, or known function but an incomplete understanding of functional details. To help resolve these issues, CESG has begun to perform follow-up studies on a select group of enzymes. Two examples of these studies are given here. The first is the protein product of *Arabidopsis thaliana* gene At5g18200. We have identified it as an ADP-glucose phosphorylase and solved the structures of the adenylyl-enzyme intermediate (His<sup>186</sup>-AMP) to 1.83 Å resolution and the inactive H186G mutant complexed to ADP-glucose to 2.23 Å. In the second example, the structure of the protein product of *A. thaliana* gene At3g03250, a UDP-glucose pyrophosphorylase, complexed with UDP-glucose and glucose-1-phosphate has been solved to 1.64 Å. This revealed loop motions involved in substrate binding and significant interdomain motion within the crystal. This work was supported by the NIH grants, PSI U54 GM 074901, GM30480, and NLM training grant LM007359. The authors also thank the CESG team.

## 13.07 Remote Data Collection

**13.07.01 STaRBURSTT - CIC: CyberEnabled Instrumentation Access.** A.D. Hunter<sup>a</sup>, P.S. Szalay,<sup>i</sup> T.R. Wagner,<sup>a</sup> M. Zeller,<sup>a</sup> M. Bond,<sup>b</sup> R.J. Butcher,<sup>c</sup> G. Crundwell,<sup>d</sup> G.M. Ferrence,<sup>e</sup> K. Kantardjieff,<sup>f</sup> L. Ramirez,<sup>g</sup> T. Higgins<sup>h</sup>, <sup>a</sup>Youngstown State Univ., <sup>b</sup>South East Missouri State Univ., <sup>c</sup>Howard Univ., <sup>d</sup>Central Connecticut State Univ., <sup>e</sup>Illinois State Univ., <sup>f</sup>California State Univ. Fullerton, <sup>g</sup>East Los Angeles College, <sup>h</sup>Harold Washington College, <sup>i</sup>Muskingum College.

The STaRBURSTT-CIC (Science Teaching and Research Brings Undergraduate Research Strengths Through Technology - CyberInstrumentation Consortium) is a national consortia of made up primarily of Predominantly Undergraduate Institutions, Historically Black Colleges and Universities, and Hispanic Serving Institutions having strong interests in X-ray diffraction. Continuing advances in hardware and software are making it increasing easy to collect and process data from modern scientific instruments. Undergraduates and other novices are therefore increasingly able to successfully use these tools in their coursework and research. Unfortunately, no Predominantly Undergraduate Institution has the resources to purchase and maintain any but a selected sample of the instrumentation that they would like to have access to. Remote access over the WEB via instrumentation consortia offer a potentially effective solution. The advantages and disadvantages to such a remote access approach will be discussed.



**13.07.02 Remote Monitoring and Access to Instruments and Data. The CIMA Crystallography Portal.** John C. Huffman<sup>\*a</sup>, Donald F. McMullen<sup>b</sup>, Kianosh L. Huffman<sup>b</sup>, <sup>a</sup>Indiana Univ. Molecular Structure Center, <sup>b</sup>Pervasive Technology Laboratories, Indiana Univ., Bloomington, IN 47405.

The Common Instrument Middleware Architecture (CIMA) project, supported by the National Science Foundation Middleware Initiative, is aimed at “Grid enabling” instruments as real-time data sources to improve accessibility of instruments and to facilitate their integration into the Grid. CIMA middleware is based on current Grid implementation standards and accessible through platform independent standards such as the Open Grid Services Architecture (OGSA) and the Common Component Architecture (CCA). The CIMA Crystallography Portal is designed to allow remote monitoring of instruments and provide an environment that will allow authenticated collaborators to access and process data as it is collected using simple web services. The system has been designed so that long-term data integrity is assured using distributed university maintained resources. The data captured during the experiment will include the raw data frames and the raw data converted to the imgCIF format. It will also include extensive metadata that allow the user to easily review an experiment at a later date. The CIMA Crystallography Portal is currently in operation or being implemented for instruments in the IUMSC, the ChemMatCARS beamline at ANL, and three other university sites.



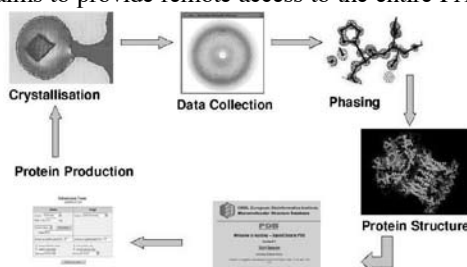
**13.07.03 Protein Crystallography in the 21st Century.** S. Michael Soltis and PX Group, Protein Crystallography Group, SSRL, Menlo Park, CA.

The macromolecular crystallography beam lines at SSRL have evolved into efficient and productive X-ray diffraction data acquisition and processing facilities for determining macromolecular structures. The traditionally heroic synchrotron experiment is now a technically robust and automated research tool for the biomedical research community. With the development of remote access tools, the facilities can be successfully utilized by scientists around the world. Enabling developments in instrument control, automation and remote access tools for streamlined experimental design and execution including the interface with the home laboratory will be presented.

**13.07.04 DNA & e-HTPX: High Throughput and Remote Access PX.** Graeme Winter<sup>a\*</sup>, DNA Developers<sup>abcdg</sup>, e-HTPX Developers<sup>adeh</sup>, <sup>a</sup>Daresbury Laboratory, UK, <sup>b</sup>ESRF, France, <sup>c</sup>MRC LMB, Cambridge, UK, <sup>d</sup>EMBL Grenoble, France, <sup>e</sup>EBSI, UK, <sup>f</sup>York Univ., UK, <sup>g</sup>EMBL Hamburg, Germany, <sup>h</sup>Wellcome Trust Centre for Human Genetics, Oxford, UK.

The DNA project<sup>[1]</sup> has developed reliable automation for data collection and processing of PX data. DNA consists of a number of separate modules: Beamline control; Data processing; Analysis and decision making. This has led to a highly portable system, which is currently operating at the ESRF, SRS, EMBL Hamburg and NSLS.

The e-HTPX project aims to provide remote access to the entire PX pipeline through a standard web interface. This has been achieved by contribution to existing efforts, including the DNA project and CCP4<sup>[2]</sup>. Web service interfaces to all of the key stages have been provided, as well as a single portal to unify the workflow into a "1-stop shop" for PX.



To provide this kind of services, there are three main areas of development work needed: A simple but powerful and intuitive interface; Instill "expertise" in the services; Development of the technologies; The challenges and solutions we have found will be described.

The development audience for e-HTPX has included academic and commercial groups.

e-HTPX is an e-Science Pilot Project funded by the BBSRC.

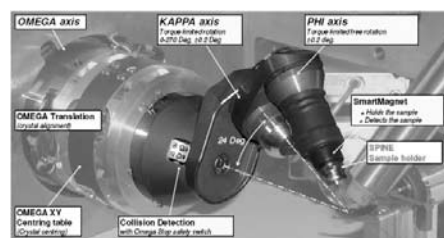
[1] <http://www.dna.ac.uk>

[2] <http://www.ccp4.ac.uk>

**13.07.05 Routine Crystal Reorientation.** S. Brockhauser<sup>1</sup>, F. Cipriani<sup>1</sup>, S. McSweeney<sup>2</sup>, R. Ravelli<sup>1</sup>, The DNA Collaboration ([www.dna.ac.uk](http://www.dna.ac.uk)) <sup>1</sup>EMBL-Grenoble, France, <sup>2</sup>ESRF, Grenoble, France.

Macromolecular crystallographers (MX) in general use simple single-axis goniometers for data collection, and most automation and remote data collection efforts exclude the use of multi-axis goniometers. However, the call for more degrees of freedom to re-orient the sample has never completely faded. The reimplementing of "old" methods of collecting truly redundant data is becoming more and more important with the increased use of very small anomalous signals for solving macromolecular structures.

The construction of a MiniKappa Goniometer Head has allowed us to reduce one of the major risks of traditional multi-axes goniometers: that of collisions. This small device offers routine crystal re-orientation and fast data collection sweeps without stability problems. A comprehensive software package that includes modules for calibration, 3D virtual beamline simulation, crystal re-orientation calculation, automated sample re-centring as well as smart multi-pass strategy calculation is being developed and integrated with the data collection system DNA (automated collection of data).



We will present the general use of DNA for service data collection with particular emphasis on exploitation of multi-axes goniometers.

Work funded in part by BIOXHIT.

**13.07.06 Methods, Hardware, and Software for High-Throughput and Remote Data Collection in Macromolecular Crystallography: The Brookhaven Experience.** D.K. Schneider, H. Robinson, A. Héroux, A. Soares, A. Saxena, J. Skinner, R. Buono, M. Cowan, H. Bosshard, R.M. Sweet, Biology Dept., Brookhaven National Laboratory, Upton, NY 11973.

The PXRR ([www.px.nsls.bnl.gov](http://www.px.nsls.bnl.gov)) operates six beam lines at the NSLS for macromolecular crystallography (PX). Two of these are high intensity insertion-device beam lines. We have defined a new paradigm for use of the synchrotron by structural biologists. Rapid Access is the norm for most beam line visits and daily open slots on our premier facilities are allocated over night to deserving projects or specimens. We implemented a mail-in service and promote a remote data collections capability with a resident PX-Operator staff that provides nearly 24h/7day facility support. To accomplish this we provide a pool of equipment, including ALS-style automounters, and software with very similar feel and layout across our facilities. An experiment-tracking database, PXdb, which carries information from beam time request to the final reduced data, is of critical importance in connecting dipole beam lines where users may screen specimens for quality, with ID lines where they may measure final data.

This work is supported by the NCRR of the National Institutes of Health, and the OBER of the US Department of Energy.

**13.07.07 Automatic Beamline Operation at Spring-8 RIKEN Structural Genomics Beamlines.** M. Yamamoto<sup>1&2</sup>, G. Ueno<sup>1</sup>, R. Hirose<sup>3</sup>, K. Hasegawa<sup>2</sup>, Okazaki<sup>2</sup>, T. Kumasaka<sup>1&4</sup>, <sup>1</sup>RIKEN Spring-8 Center, Sayo, Hyogo 679-5148 JAPAN, <sup>2</sup>JASRI/Spring-8, Sayo, Hyogo 679-5148 JAPAN, <sup>3</sup>PharmAcess Inc., Kamigori, Hyogo 678-1205 JAPAN, <sup>4</sup>Tokyo Tech, Midori-ku, Yokohama, 226-8505 JAPAN.

RIKEN Structural Genomics Beamlines (BL26B1&B2) at the Spring-8 have been constructed for high throughput protein crystallography. The beamline operation is automated cooperating with the sample changer robot SPACE [1]. Since October 2003, BL26B2 has been continuously operated with SPACE. In 2005 fiscal year, more than twenty crystals a day have been constantly delivered by sample tray to the beamline. The operation software BSS [2] and beamline management database D-Cha (Diffraction Check Assistance utilities) provide the intuitive GUI and unified control of beamline instruments. Combination of BSS, SPACE and D-cha enables Mail-in data collection that consists of day time crystal screening and night time full automatic data collection. Web interface of D-Cha allows user to deposit

measurement condition or to observe recorded images from home laboratory. The crystal screening at the beamline finished within day-time in the rate of 10 min/sample. Our mail-in system is now routinely operated at BL26B2.

[1] Ueno, G. et al. *J. Synchrotron Rad.* (2005). 12, 380-384

[2] Ueno, G. et al. *J. Appl. Cryst.* (2004). 37, 867-873

**13.07.08 The SER-CAT Remote User Participation Program.** J.P. Rose, J. Chrzas, Z. Jin, J. Fait, V. Babson, B.C. Wang, SER-CAT, APS, Argonne National Laboratory, Dept. of Biochemistry and Molecular Biology, Univ. of Georgia, Athens, GA 30602.

Striving to meet the growing demands for timely access to its beamlines, the Southeast Regional Collaborative Access Team (SER-CAT, Sector 22 APS) has developed an innovative program for secure remote user data collection on its bending magnet beamline. This is important to the SER-CAT membership since most users are located hundreds of miles from the beamlines.

The system consists of a locally modified ALS-style crystal mounter, the SERGUI user interface and a secure Access Grid based communication link between the remote user and the beamline. The automounter allows for uninterrupted screening or data collection on up to 96 samples. The SERGUI user interface provides tab notebook style access to all beamline control and data collection functions, and to data reduction and analysis software. Since all data remains on SER-CAT computers the communications overhead is dramatically reduced.

The remote access system has been under alpha testing by researchers at the University of Georgia for the past 10 months with a planned release to the SER-CAT membership in mid 2006. The automounter coupled with the ability to initiate and/or supervise data collection remotely via SERGUI and Access Grid will enable SER-CAT to begin exploring the possibility of restructuring its current 24 hr minimum beam time allocation into smaller but more frequent 4, 6, or 8 hr shifts. This would give SER-CAT members better access to the facility and allow them to plan their experiments and beamline use more efficiently.

**13.07.09 From Sample to Structure: Automation at SER-CAT.** James Fait<sup>1,2</sup>, John Chrzas<sup>1,2</sup>, John Goczy<sup>1,2</sup>, Andy Howard<sup>3</sup>, Zhongmin Jin<sup>1,2</sup>, John Rose<sup>2,1</sup>, B. C. Wang<sup>2,1</sup>, SER-CAT, APS, ANL, 9700 S. Cass. Ave., Argonne, IL, <sup>2</sup>Dept. of Biochemistry & Molecular Biology, Univ. of Georgia, Athens, GA, <sup>3</sup>Biological, Chemical, & Physical Sciences Dept., Illinois Inst. of Technology, Chicago, IL.

Automation has been extended to all aspects of the synchrotron experiment for biological macromolecular structure determination. At SER-CAT, beamline setup, sample handling, sample alignment, strategy, data collection, data reduction, structure solution and data archive have all been automated or are in the process of being automated. Use of robotics, image processing, and multiprocessor computing all contribute to the ease of completing the synchrotron experiment, with the user able to attempt the phasing of the sample on site, while it is still possible to augment the collected data, if necessary. Details of the implementation of various aspects of the automation process will be presented, along with several case studies.

## 13.08 Complementary Methods to Macromolecular Crystallography

**13.08.01 Atomic Force Microscopy in Structural Biology.** A. McPherson, Dept. of Molecular Biology and Biochemistry, The Univ. of California, Irvine, CA 92697.

Atomic force microscopy (AFM) is relatively new to structural biology, achieving some degree of popularity only in the past five years. It is one of several probe microscopy techniques that emerged from the field of physics. It has the unique virtues of being able to operate in fluid medium, is non perturbing and non destructive, scans on a time frame compatible with many active processes, and is able to visualize objects of the order of individual proteins, nucleic acids, and viruses. We subsequently explored the use of AFM for the investigation of living cells, then cells infected with viruses, and now individual virus particles. Even with current technology, AFM allows the resolution of surface features on macromolecular complexes of one to two nanometers, adequate to see the capsomeres on virus capsids of 30 to 200 nm diameter, clusters of proteins on retroviral surfaces, and the emergence of nucleic acid from the virions. In conjunction with controlled disruption of viruses by chemical or enzymatic means it allows the investigator to see internal structure as well. AFM allows one to take the results of X-ray crystallography, macromolecular structure, and extend it upwards to nanoscale complexes, and even organelles.

**13.08.02 Molecular Envelope Determination and *ab initio* Phasing.** Quan Hao, MacCHESS, Wilson Synchrotron Lab, Cornell Univ., Ithaca, NY 14853.

Small angle X-ray scattering (SAXS) or electron microscopy (EM) data have proven to be very useful in providing low resolution structural details of proteins and other macromolecules. To utilize the envelope information for crystallographic phasing, it is essential to develop a method for correctly positioning the known envelope in a crystallographic unit cell. The low resolution phases calculated from the correctly positioned molecular envelope can be used as a good starting point for phase extension. I will describe the development of the FSEARCH program for locating envelopes in the unit cell and plans to extend phases to crystallographic data resolution. This work is supported by the NIH grant RR01646.

**13.08.03 Time-resolved Crystallographic Studies of a Cooperative Dimeric Hemoglobin.** W.E. Royer<sup>1</sup>, J. E. Knapp<sup>1</sup>, R. Pahl<sup>2</sup>, V. Srajer<sup>2</sup>, <sup>1</sup>Dept. of Biochemistry & Mol. Pharm., Univ. of Massachusetts Med. School, Worcester, MA 01605, <sup>2</sup>Dept. of Biochemistry & Mol. Biol., CARS, Univ. of Chicago, Chicago, IL 60637.

Despite the availability of static structures of different states in a number of allosteric proteins, information about the kinetic pathway between such alternate states is limited. We have carried out nanosecond time-resolved diffraction experiments on single crystals of *Scapharca* dimeric hemoglobin, a protein whose alternate states show strong functional differences, despite relatively localized transitions that are compatible with the crystal lattice. Within 5ns of the photolytic release of ligands, an intermediate forms as R-state protein subunits respond to the presence of unliganded heme groups. Transition to this intermediate involves structural changes in the heme groups, neighboring residues and interface water molecules. The intermediate changes very little during the ns time-domain and lays a foundation for apparently concerted tertiary and quaternary structural changes that occur on a microsecond time scale and are associated with the transition to a low affinity T-state structure. Persistence of a T-state structure even after ligands rebind suggests a slow T to R transition that may result from the greater dimeric stability in the T-state.

**13.08.04 Diffraction Microscopy a New Tool for Structural Biologists.** Andrew A. Stewart<sup>1</sup>, Enju Lima<sup>1</sup>, Huijie Miao<sup>1</sup>, Xiaojing Haung<sup>1</sup>, David Shapiro<sup>3</sup>, Pierre Thibault<sup>2</sup>, Veit Elser<sup>2</sup>, Chris Jacobsen<sup>1</sup>, Janos Kitz<sup>3</sup>, David Sayre<sup>1</sup>, <sup>1</sup>Dept. of Physics & Astronomy, Stony Brook Univ., Stony Brook, NY 11794, <sup>2</sup>Dept. of Physics, Cornell Univ., Ithaca, NY, 14853, <sup>3</sup>Advanced Light Source, Lawrence Berkeley National Laboratory, Berkeley, CA 94720.

The Emerging technique of diffraction microscopy opens up the possibility of studying macromolecular assemblies within a cell and has the potential to become a powerful tool for structural biology. Unlike crystallography the technique does not require multiple copies of an object to be built into a crystal, only one copy of the object is needed, thus allowing structural biology to access information about objects which were until now the exclusive domain of electron microscopy. The advantage of this new technique is that it has the ability to study larger objects such as whole cells without sectioning. In principle, resolution in diffraction microscopy is only limited by radiation damage, to about 10nm resolution. The technique has many parallels with crystallography. The sample is inserted into a X-ray beam, the far field diffraction pattern is recorded, and the recorded diffraction intensities need to be phased to produce an image.

A 2-D image of a freeze dried yeast cell has already been reconstructed<sup>1</sup>. We will present the latest advances towards 2-D frozen hydrated specimens and 3-D reconstruction of cells. We will discuss the limitations and benefits of this new technique, and implications they for structural biology, with particular respect to complexes and macromolecular assemblies within cells, and cell structure.

<sup>1</sup>Shapiro, *et al.* Proceedings of the National Academies of Sciences, Vol 102 No. 43, 15343 - 15346.

**13.08.05 Determining the Phospholipid Packing within a Lipoprotein Particle Using Diffuse Scattering from Crystals and SAXS** C. Peters-Libeu, Y. Newhouse, K. Weisgraber J. David Gladstone Inst. of Neurological Disease, 1650 Owens St., San Francisco, CA 94158.

Human apolipoprotein E•DPPC dipalmitoylphosphatidylcholine (DPPC) particles mimic apoE-containing high density lipoprotein particles found in the brain and plasma. These high density lipoproteins play an active role in cholesterol transport through binding between apoE and members of the LDL-receptor family. Although the apoE•DPPC particles crystallize readily and diffract anisotropically to 7-12Å, the diffraction patterns are a composite of Bragg scattering from the ordered protein atoms and diffuse scattering from the partially ordered phospholipid. Analysis of the diffuse scattering reveals the shape of the apoE•DPPC particle, defines the orientation of the lipids with respect to the molecular envelope of the protein and defines average packing parameters for the phospholipid hydrocarbon tails. SAXS was used to confirm the shape of the apoE•DPPC particle in solution. Using this information, we have generated a model of apoE•DPPC particles in which the overall shape of the particle is spheroidal in contrast to the prevailing assumption that these particles would be discoidal. In addition, we modeled the conformational change which occurs in the LDL-receptor binding region of apoE when it binds to DPPC.

**13.08.06 Biophysical Characterization of  $\alpha$  to  $\beta$  Transition Observed in Collagen Binding Domain.** Philominathan Sagaya Theresa Leena, Osamu Matsushita, Joshua Sakon, Dept. of Chemistry and Biochemistry, Univ. of Arkansas.

*Clostridium histolyticum* ColG collagenase activated by Ca<sup>2+</sup> is responsible for extensive tissue destruction, and the CBD is a segment of the multi-domain enzyme. Binding of two Ca<sup>2+</sup> on CBD is

co-operative and is both enthalpically and entropically driven ( $K_{d1} = 2.13\mu\text{M}$ ;  $K_{d2} = 4.63\mu\text{M}$ ). Structures in the presence and absence of Ca<sup>2+</sup> have been solved at ultrahigh resolution (<1.2Å). N-terminus 14 residues of CBD adopt a  $\alpha$ -helical conformation however, addition of Ca<sup>2+</sup> unwinds the linker into a new  $\beta$ -strand. To rule out the crystal-packing artifact, NMR titration studies were done and it confirms the conformational structure change upon addition of Ca<sup>2+</sup>. The changes in Stokes and hydrodynamic radii as measured by size exclusion chromatography and dynamic light scattering experiments showed drastic transition upon Ca<sup>2+</sup> addition; however far UV-CD was not as sensitive. With Ca<sup>2+</sup> CBD becomes thermally stable (TM>90°C), protease insensitive and stable against chemical denaturants. Different metals trigger different degree of transition and as mutation of metal chelating amino acids. Not only this study provide insights into the drastic structure change thought to accompany upon secretion of the enzyme but also to provide insights into amyloidosis.

**13.08.07 Biophysical Analysis of Virus Particles and their Maturation: Insights into Elegantly Programmed Nanomachines** J.E. Johnson, Dept. of Molecular Biology, The Scripps Research Inst., La Jolla, CA, 92037.

Bacteriophages, herpesviruses and other large dsDNA viruses contain powerful molecular machines that pump DNA into preassembled procapsids triggering maturation. This event commences when DNA pressures within the capsid exceed 10-fold that of bottled champagne and are detected by a protein switch that transduces a signal outside of the particle. We investigated two bacteriophage systems to understand the structural basis for these events. The asymmetric structure of the mature P22 bacteriophage was determined to 17Å resolution by cryoEM and image processing, revealing the portal protein implicated in DNA packaging and pressure sensing as well as ordered dsDNA in the vicinity of the portal. Virus particle maturation was studied with the  $\lambda$ -like bacteriophage HK97. Intermediates in the maturation trajectory were characterized by cryoEM, solution x-ray scattering, crystallography and single particle fluorescence, allowing the creation of a movie<sup>[1]</sup> that depicts the particle dynamics.

[1] Wikoff, W., Conway, J., Tang, J., Lee, K., Gan, L., Cheng, N., Duda, R., Hendrix, R., Steven, A., and Johnson, J. 2006. Time-resolved molecular dynamics of HK97 virus maturation interpreted by electron cryo-microscopy and X-ray crystallography. *J Struct Biol* 153:300-306.

## 13.09 Time-Dependent Investigations

**13.09.01 The Spallation Neutron Source: On Time.** I. S. Anderson, Oak Ridge National Laboratory, Oak Ridge, TN 37831.

Neutron scattering methods allow the determination of dynamical processes in materials, at the atomic and molecular level, over a wide range of time scales. The next generation of spallation neutron sources will offer pulsed neutron fluxes significantly more intense than presently available and will enable time dependent processes to be followed using pulse probe methods operating at frequencies up to 60 Hz. Hence new sources, such as the Spallation Neutron Source, due to come into operation in June 2006, will enable real time studies to be carried out at characteristic time scales that have previously been difficult to investigate. New capabilities enabled by these techniques will be discussed.

**13.09.02 High Flux Neutron Diffractometers on Reactor Sources for Real-Time Crystallography.** Alan W. Hewat, Inst. Laue-Langevin, B.P. 156X Grenoble Cedex 9, FRANCE.

New high flux diffractometers on the US Spallation Neutron Source (SNS), such as VULCAN, POWGEN3 and TOPAZ will be world leading, and present a real challenge to machines on the European High Flux Reactor (ILL). In an attempt to compete, ILL will build on its strengths, which include high time-averaged flux on the sample obtained by focusing a wide band of wavelengths from the continuous source. We will emulate the best spallation source machines by using very large angle detectors. This combination of high flux and large detectors was shown at the US Shelter Island workshop to be the key to the most efficient use of existing neutron sources. For example, the quasi-Laue single crystal diffractometers LADI and VIVALDI use  $2\pi$  image-plate detectors on almost white beams, where the continuous intensity from a super-mirror guide can reach  $10^9$  n.cm<sup>-2</sup>.sec<sup>-1</sup>. Our new proposal CYCLOPS will use a 70%  $4\pi$  neutron CCD detector on a focussing super-mirror guide, which will allow real-time exploration of the whole of reciprocal space for the first time. Our new SALSA strain scanner also uses a wide band of wavelengths focussed for a small scattering range near 90°; it will nicely complement powerful TOF strain-scanning machines such as VULCAN. Finally, we are also investing in large 2D gas detectors of the kind constructed for Los Alamos by BNL, only twice as large. One of these 1+ steradian detectors has already been constructed for our single crystal protein diffractometer D19, and a second is planned for a new real-time powder Diffractometer for Rapid Acquisition (DRACULA).

**13.09.03 Time Resolved Neutron Diffraction Studies of the Hydrogen Storage Material Li<sub>3</sub>N.** Ashfia Huq<sup>1</sup> James W. Richardson<sup>1</sup> Evan R. Maxey<sup>1</sup> Dhanesh Chandra<sup>2</sup> Wen-Ming Chien<sup>2</sup>, <sup>1</sup>Intense Pulsed Neutron Source, Argonne National Laboratory, Argonne, IL 60439, <sup>2</sup>Metallurgical and Materials Engineering, Univ. of Nevada, Reno, Reno NV 89557.

The search for alternative fuel has spurred interest in complexes with high hydrogen absorption-desorption capacities. Among these compounds complex metal hydrides have received much attention. More recently it was proposed that simple metal nitrides such as Lithium Nitride (Li<sub>3</sub>N), with its 9 wt % recyclable hydrogen uptake, could be good candidates for reversible hydrogen storage. In this presentation we present the results of detailed structural study of Li<sub>3</sub>N through the temperature range 20K to 673K using Neutron Powder Diffraction. Commercially purchased compound showed a coexistence of alpha and beta phases of Li<sub>3</sub>N. We observed a steady decline of the beta phase above 473K and a very small fraction (~3 wt %) was frozen in at 673K. This transformation ( $\beta$  to  $\alpha$ ) was not reversible on cooling. We will also present the findings of in-situ neutron diffraction measurements of hydrogen absorption and desorption of the title material in the presence and absence of the  $\beta$  phase.

Work at ANL supported by the U.S. DOE, Basic Energy Sciences--Materials Sciences, under Contract W-31-109-ENG-38.

**13.09.04 Time-Resolved Studies at the Wide Angle Neutron Diffractometer\*** J. A. Fernandez-Baca<sup>1</sup>, Y. Ishii<sup>2</sup>, <sup>1</sup>Center for Neutron Scattering, Oak Ridge National Laboratory\*\*, Oak Ridge, TN 37831, <sup>2</sup>Japan Atomic Energy Agency, Tokai, Ibaraki 319-1195, Japan.

The Wide Angle Neutron Diffractometer (WAND) at the High Flux Isotope Reactor in Oak Ridge is a high-intensity, medium-resolution powder instrument, well suited to perform time-resolved experiments of structural transformations having short time-constants. Fast data collection is achieved with the combination of an intense neutron beam

( $10^7$  n/cm<sup>2</sup>.s) and a curved one-dimensional <sup>3</sup>He position sensitive detector covering 125° of scattering angle. The detector is a multi-anode type (624 anodes and a 0.2° pitch) <sup>3</sup>He gas counter specially designed and built for this instrument by ORDELA. Each of the anodes has an amplifier, a shaping amplifier, and a discriminator. In this talk we will present recent examples of time-resolved studies at the WAND, including the study of the kinetics of the nucleation and growth of Ice XI.<sup>§</sup>

\*The WAND was built at ORNL in collaboration with the Japan Atomic Energy Research Institute (now Japan Atomic Energy Agency) under the US-Japan Cooperative Program on Neutron Scattering Research. \*\*ORNL is managed by UT-Batelle, LLC under DOE BES Contract No. DE-AC05-00OR22725. §H. Fukazawa, unpublished.

**13.09.05 Center for Nanophase Materials Sciences.** Linda L. Horton, Center for Nanophase Materials Sciences, Oak Ridge National Laboratory, Oak Ridge, TN.

The Center for Nanophase Materials Sciences (CNMS) is the newest user facility at Oak Ridge National Laboratory. CNMS is co-located with the Spallation Neutron Source and has ties to the National Leadership Computing Facility, and the microscopy facilities in the Shared Research Equipment User Program and High Temperature Materials Laboratory. CNMS has a new 80,000-ft<sup>2</sup> building with a 10,000-ft<sup>2</sup> nanofabrication clean room facility. The CNMS houses both off-the-shelf instrumentation and state-of-the-art, unique (or nearly so) tools, including electron microscopes, scanning probes, synthesis instrumentation, and a wide range of characterization tools, such as x-ray diffraction and a tunable micro-Raman system.

The CNMS supports research on macromolecular materials, catalysts, functional nanomaterials, and nanomagnetism and quantum transport. Use of the CNMS facilities and collaborative support from CNMS staff are free-of-charge for users doing non-proprietary research with intent to publish. User research proposals are brief and focused, with a research description limited to 2 pages. Selection of proposals is based on their scientific and technical merit as evaluated by an external Proposal Review Committee. To learn more, visit <http://www.cnms.ornl.gov/>. The CNMS is sponsored by the Dept. of Energy's Office of Basic Energy Sciences.

**13.09.06 In-situ Synchrotron X-ray Studies of Creep Damage in CuZn-alloys.** A. Pyzalla<sup>1,2</sup>, A. Isaac<sup>1,2</sup>, B. Camin<sup>3</sup>, A. Kottar<sup>2</sup>, H. Kaminski<sup>2</sup>, T. Buslaps<sup>4</sup>, M. Di Michiel<sup>4</sup>, W. Reimers<sup>3</sup>, <sup>1</sup>TU Wien, Karlsplatz 13-308, Wien, Austria, <sup>2</sup>Max-Planck-Inst. for Iron Research, Max-Planck-Str.1, Düsseldorf, Germany, <sup>3</sup>TU Berlin, Ernst-Reuter-Platz 1, Berlin, Germany, <sup>4</sup>European Synchrotron Radiation Facility, ESRF, Grenoble, France.

The combination of tomography and diffraction experiments gives the unique opportunity to follow the development in the microstructure of materials and the subsequent changes in their texture and/or internal stress state due to external loading.

Combined tomography and diffraction carried out continuously *in-situ* and during only one experiment significantly increases the understanding of microstructure changes during creep, where it is important to characterise the dynamics in the early stages of the process. We performed combined diffraction/ tomography experiments, which aimed at determining *in-situ* the creep damage evolution and its correlation to texture development of CuZn-alloys.

The results of the experiments reveal the development of creep voids and damage in CuZn-alloys with increasing creep time. The experiments also show an influence of loading conditions (temperature, stress) on the void size and void growth mechanisms. We attempt to link creep damage, microstructure and microstrain development during the creep process.

**13.09.07 Simultaneous *in-situ* Neutron Diffraction Measurement of Rapid Transient Temperature and Stress Fields.** Z. Feng<sup>a</sup>, W. Woo<sup>b</sup>, X.-L. Wang<sup>a</sup>, D.W. Brown<sup>c</sup>, B. Clausen<sup>c</sup>, K. An<sup>a</sup>, C. Hubbard<sup>a</sup>, H. Choo<sup>b</sup>, S. A. David<sup>a</sup>, <sup>a</sup>Oak Ridge National Laboratory, Oak Ridge, TN, <sup>b</sup>Univ. of Tennessee, Knoxville, TN, <sup>c</sup>Los Alamos National Laboratory, Los Alamos, NM.

We present a novel experimental approach and results of direct, experimental measurement of the temperature and thermal stress *inside* the stir zone during friction-stir welding (FSW) of 6061-T6 aluminum plate using *in-situ* neutron diffraction measurements. This novel technique is based on the “quasi-steady state” phenomenon induced by moving, localized thermomechanical processing of the material of interest. The quasi-steady state circumvents the neutron flux limitation for studying the rapid transient material behavior. A specially designed portable thermomechanical processing system based on the friction stir welding process was designed and built for this test. Decomposition of the thermal and elastic strains from the lattice spacing changes measured using the neutron diffraction, for the first time, revealed the transient temperature and stress state under the tool shoulder during the FSW.

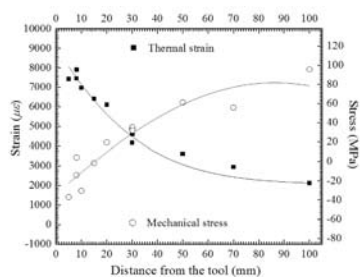


Figure 1. Thermal strain and longitudinal stress variation as function of distance from welding zone as determined from *in-situ* neutron diffraction experiment. This research is sponsored by the Laboratory Directed Research and Development program of Oak Ridge National Laboratory (ORNL), managed by UT-Battelle, LLC for the U. S. Department of Energy under Contract No. DE-AC05-00OR22725.

**13.09.08 *In-situ* Time-Resolved Study of Nanocrystallization in Zr-Based Bulk Metallic Glass.** X.-L. Wang<sup>1</sup>, L. Yang<sup>1,2</sup>, A.D. Stoica<sup>1</sup>, J. Almer<sup>3</sup>, <sup>1</sup>Spallation Neutron Source, Oak Ridge National Laboratory, Oak Ridge, TN 37831, <sup>2</sup>Dept. of Chemical and Materials Engineering, Univ. of Cincinnati, Cincinnati, OH 45221, <sup>3</sup>Advanced Photon Source, Argonne National Laboratory, Argonne, IL 60439.

Nanocrystallization in bulk metallic glass is a rather unique phenomenon in which partial crystallization leads to a homogenous microstructure with a high-density ( $10^{23}$ – $10^{24}$  m<sup>-3</sup>) of nanoscale crystalline particles embedded in an amorphous matrix. We report an *in-situ* high-energy synchrotron experiment on  $Zr_{32.5}Cu_{17.9}Ni_{14.6}Al_{10}Ti_5$  bulk metallic glass, revealing in detail the evolution of local atomic ordering and microstructure during nucleation. A nanoscale intermediate phase was identified, which develops and later dissolves as the final crystallization (to the tetragonal  $Zr_2Ni$  phase) takes place. By making simultaneous, time-resolved measurements of wide-angle diffraction and small-angle scattering, we demonstrate that the final crystallization is accompanied by concurrent redistribution of the chemical constituents, which indicates a close relationship between structural and chemical ordering within the system.

This research was supported by Division of Materials Sciences and Engineering, Office of Basic Energy Sciences, U.S. Department of Energy under Contract DE-AC05-00OR22725 with UT-Battelle, LLC. Use of the Advanced Photon Source was supported by the U. S. Department of Energy, Office of Science, Office of Basic Energy Sciences, under Contract No. W-31-109-Eng-38.

## 13.10 Canadian Light Source Symposium

**13.10.01 The Canadian Macromolecular Crystallography Facility 08ID-1 Beamline at the Canadian Light Source.** L.T.J. Delbaere<sup>1</sup>, P. Grochulski<sup>1,2</sup>, I. Blomqvist<sup>2</sup>, L. Prasad<sup>1</sup>, J. Puttick<sup>1</sup>, J. Côtélesage<sup>1</sup> <sup>1</sup>Biochemistry, Univ. of Saskatchewan <sup>2</sup>Canadian Light Source, Saskatoon, S7N 5E5 Canada.

The 08ID-1 beamline is the initial phase of the Canadian Macromolecular Crystallography Facility (CMCF). The CLS is a 2.9 GeV ring that produced its first light in the diagnostic beamline in December of 2003. At 08ID-1 the first light was detected at the front end in September 2005, the first monochromatic light after the double crystal monochromator in November 2005 and the first monochromatic light in the experimental enclosure in December 2005. We have been commissioning a beamline which is illuminated by a small-gap in-vacuum hybrid undulator (SGU), located in the upstream half of the straight section and chicaned inboard by 0.75 mrad. The downstream half of this section is reserved for the future SGU for the 08ID-2 beamline. The scientific goal of the 08ID-1 beamline is to operate a protein crystallography beamline suitable for studying small crystals and crystals with large unit cells.

Structural studies at other synchrotrons have been carried out on PEP carboxykinase, which is a key enzyme in gluconeogenesis. The overall structure represents a new protein fold. In addition there is a unique mononucleotide fold.

Funded by CFI, NSERC and CIHR in Canada.

**13.10.02 Beamline and Infrastructure for High-Throughput Protein Crystallography at the Canadian Light Source.** Ernst M. Bergmann, Alberta Synchrotron Inst., Edmonton, ALB, Natalie S. Strynadka, Dept. of Biochemistry, Univ. of British Columbia, Vancouver, BC, Louis Delbaere, Dept. of Biochemistry, Univ. of Saskatchewan, Saskatoon, SK, Canada, Pawel Grochulski, Russ Berg, Michel Fodje, Emil Hallin, Canadian Light Source, Saskatoon, SK, Canada.

The Canadian Light Source (CLS) in collaboration with the Canadian community of macromolecular crystallographers is designing, building and commissioning a beamline dedicated to high-throughput structure determination of biological macromolecules by X-ray crystallography. This facility will combine a third-generation synchrotron beamline with advanced robotics, automation and IT infrastructure. The beamline will be developed to automate every aspect of crystal screening and data collection. It will be capable of screening a large number of crystals without user intervention. The software will be developed to accept input parameters for data collection via user interface, scripted commands or an intelligent database of parameters. The infrastructure will be connected with a 1Gbps fibre optic link via CA4net, Canada's high speed research network, to all major research centres in Canada. This will allow remote observation and control of the experiment. The beamline will be integrated with the currently commissioned first macromolecular crystallography beamline at the CLS. Our goal is an infrastructure that will allow screening and analysis of all protein crystals from Canadian researchers within at most a few weeks.

This project is funded by the Canada Foundation for Innovation, the British Columbia Knowledge Development Fund, Western Economic Diversification Canada and Boehringer Ingelheim, Laval PQ.

**13.10.03 Structure of MRSA Resistance Determinant PBP2a in Complex With an Efficient  $\beta$ -lactam.** Andrew L. Lovering<sup>1</sup>, Franck Danel<sup>2</sup>, Malcolm G.P. Page<sup>2</sup>, Natalie C.J. Strynadka<sup>1</sup>, <sup>1</sup>Dept, Biochemistry and Molecular Biology, Univ. of British Columbia, Vancouver, Canada, <sup>2</sup>Basilea Pharmaceutica AG, Basel, Switzerland.

The emergence of MRSA as an important clinical pathogen has necessitated the search for an effective antibiotic, one that succeeds where traditional  $\beta$ -lactams cannot. Conventional  $\beta$ -lactams have a well-documented mode of action, that of the covalent modification and subsequent inactivation of a group of enzymes known as penicillin-binding proteins (PBPs). These enzymes are responsible for the peptidoglycan cross-linking stage of bacterial cell wall synthesis, and once this activity has been inhibited, lysis of the cells occurs shortly afterward. Upon being challenged with  $\beta$ -lactams, MRSA strains will express PBP2a, which has a lower affinity for these compounds and can remain catalytically active.

We have expressed PBP2a in a truncated form (lacking the membrane spanning region) and have crystallized it in complex with an effective  $\beta$ -lactam inhibitor. The enzyme adduct is probably present in several conformations, consistent with findings from UV-circular dichroism studies. The information gained from this crystal structure explains the efficacy of this particular inhibitor, and will hopefully be of use in the design of even more potent compounds.

**13.10.04 Toward the Design of Aminoglycoside Kinase Inhibitors.** D. Fong<sup>1</sup>, B. Xiong<sup>2</sup>, J. Hwang<sup>1</sup>, A. Berghuis<sup>1,2</sup>, Depts. of <sup>1</sup>Biochemistry and <sup>2</sup>Microbiology & Immunology, McGill Univ., Montreal, QC, Canada.

Aminoglycosides are a group of antibiotics that target the 30S bacterial ribosome. Resistance to aminoglycosides is most commonly caused by enzyme-catalyzed modification and detoxification of the drug. Two examples of aminoglycoside kinase are APH(3')-IIIa and APH(9)-Ia. APH(3')-IIIa is produced by pathogenic Gram-positive bacteria such as *Enterococci* and *Staphylococci*. It is capable of conferring resistance to at least ten aminoglycoside antibiotics that contain a 2-deoxystreptamine ring. In contrast, APH(9)-Ia is found in the Gram-negative bacteria *Legionella pneumophila* and operates exclusively on spectinomycin which has an actinamine moiety.

The overall structure of APH(3')-IIIa and APH(9)-Ia are very similar to that of eukaryotic protein kinases. It has also been shown that several isoquinolinesulfonamide type protein kinase inhibitors are good inhibitors of these two aminoglycoside kinases. These inhibitors target the nucleotide-binding pocket of the enzyme, thus detailed structural information is crucial to the design of ligands that selectively inhibit the bacterial enzymes. The crystal structures of APH(3')-IIIa and APH(9)-Ia bound with one such inhibitor, CKI-7, and comparison to isoquinolinesulfonamide-bound structures of eukaryotic protein kinases will be presented.

**13.10.05 Structural Studies of BTB Domains from Transcription Factors and their Complexes with Corepressors.** A.F. Ghetu, G.G. Privé, Ontario Cancer Institute, Toronto, ON, Canada.

The human oncogene BCL6 is a BTB-zinc finger transcriptional repressor involved in the pathogenesis of B-cell lymphomas. The N-terminal BTB domain of BCL6 forms an obligate homodimer that associates with BTB binding domains (BBDs) of various corepressors, including SMRT and BCoR. Our previous crystallographic work revealed that the 17 residue SMRT BBD binds into the BCL6 BTB lateral groove. We have now determined the 2.4 Å crystal structure of BCL6 BTB in complex with the BCoR BBD. The space group

is P6(1)22, the unit cell dimensions are (a,b) = 150 Å, c = 312 Å, and each asymmetric unit contains 8 BTB chains and 8 BCoR BBD peptides. The structure was solved with PHASER using a BCL6 BTB dimer as a search model. The BBDs of SMRT and BCoR share no sequence similarity, yet the peptides follow very similar surfaces along the BCL6 BTB lateral groove. The majority of BTB-BBD interactions involve conserved mainchain interactions, however alanine scanning mutagenesis showed that each BBD has a unique set of side-chain that are essential for BTB binding. We also find that histidine 116 of BCL6 acts as a toggle switch that is flipped in or out upon SMRT and BCoR binding, respectively. In conclusion, our results illustrate a mechanism by which one binding site can recognize multiple non-conserved sequences.

**13.10.07 SAXS of Biological Macromolecules and the Canadian Light Source.** Brian H. Shilton, Dept. of Biochemistry, The Univ. of Western Ontario, London, ONT., Canada.

Small Angle X-ray Scattering (SAXS) is used to determine the size and shape of macromolecules in solution. The data from SAXS experiments are complementary to structural information obtained from high resolution X-ray crystallography or NMR spectroscopy. For example, in the case of multi-domain proteins, individual domain structures determined at high resolution can be used with SAXS data to model the structure of the complete protein in solution. SAXS is useful for detecting conformational changes attendant upon ligand binding, and it can detect crystal packing effects in high resolution structures. The basic principles of a SAXS experiment will be outlined along with examples of SAXS experiments that have been used for structural studies of biological macromolecules. The possibilities for incorporation of a biological SAXS beamline at the CLS will be discussed. Because the user community is relatively small, such a beamline would likely have to be multifunctional.

**13.10.08 Materials under Extreme Conditions: Their Crystalline Structures by X-Ray Diffraction with the use of Synchrotron Radiation.** Serge Desgreniers, Laboratoire de physique des solides denses, Ottawa-Carleton Inst. of Physics, Univ. of Ottawa, Ottawa, Ontario, Canada. K1N 6N5.

The advent of third-generation synchrotron radiation sources has contributed significantly to the essor of physics of materials under extreme conditions. In this presentation, I will review recent developments in techniques for the generation of very high pressures and temperatures on materials and the use of high brilliance synchrotron light to probe the crystalline state of condensed matter by X-ray diffraction. Following a general introduction on the physics of materials subjected to extreme pressures and temperatures, I will concentrate on recent studies of the crystalline structures of high-density phases of materials carried out by X-ray diffraction techniques using synchrotron radiation. Results are discussed for dense phases of "guest-host" systems like gas hydrates and alkali metal-Group IV element clathrates, as well as simple molecular systems like solid oxygen. I will then conclude with a discussion of prospects for a structured program of science at extreme conditions at the Canadian Light Source.

**13.10.09 The Brockhouse X-Ray Diffraction and Scattering Sector for Materials Science.** Stefan Kycia, Dept. of Physics, Univ. of Guelph, Guelph, ON, N1G 2W1 Canada.

An overview of the layout and science driving the proposed Brockhouse Sector will be presented. The facility will enable structural characterization of many forms of materials systems. Some potential

applications include structural studies of polymers, drugs, emulsions, biomaterials, novel batteries, petroleum products and quantum materials. The instrumentation will provide excellent performance over the 3–60keV x-ray energy range. To achieve this, two complimentary insertion device (ID) beamlines will be incorporated into the Canadian Light Source. An undulator beamline will cover energies from 3–20keV and a superconducting wiggler beamline will cover energies from 15–60keV. Sharing a single straight section, the two ID's will operate simultaneously. The first of three hutches will support micro and anomalous single crystal crystallography, high-resolution powder diffraction, *ab-initio* structure solution, Rietveld refinement, and combinatorial materials research. A second hutch will aim at high-resolution PDF measurements at extreme environments. Diamond anvils, furnaces, and cryostats will create these environments. The third hutch will support SAXS/WAXS and have a diffractometer for inelastic scattering and reciprocal space mapping.

## 13.11 Combined Techniques in Materials Science

**13.11.01 Combined Scattering Techniques for the Characterization of Polymer Crystallization.** Bart Goderis, Catholic Univ. of Leuven, Chemistry Dept., Div. of Molecular and Nanomaterials, Celestijnenlaan 200F, 3001 Heverlee, Belgium.

Due to their long chain architecture, crystallizable polymers rarely reach a fully crystalline state. In most cases they adopt a semicrystalline morphology consisting of alternating crystalline and amorphous layers. Stacks of such nano-layers are further arranged in micrometer sized, spherulitic aggregates. The one dimensional stack morphology is most conveniently characterized by small angle X-ray scattering (SAXS), yielding the thickness of the layers, thickness distributions and crystalline fractions. Using synchrotron radiation, the transformation of a polymer melt into semicrystalline layers stacks can be followed. Methods to characterize this space filling process, based on a combination of SAXS and small angle light scattering, are introduced. Finally, because of rapid cooling procedures, applied in day-to-day practice, polymer crystals may display considerable branching. It is illustrated how a thorough image analysis of AFM images helps developing structural models for a better interpretation of the SAXS data.

**13.11.02 Probing Nanoscale Structure and Dynamics in Polymer Nanocomposites by SAXS and XPCS.** R. Aravinda Narayanan<sup>1,3</sup>, S. Lewis<sup>4</sup>, A. Bansal<sup>5</sup>, L.S. Schadler<sup>4</sup>, L.B. Lurio<sup>6</sup>, S. Narayanan<sup>2</sup>, P. Thiyagarajan<sup>1</sup>, <sup>1</sup>IPNS, <sup>2</sup>APS, Argonne National Lab, Argonne, IL, <sup>3</sup>Oak Ridge National Lab, Oak Ridge, TN, <sup>4</sup>Rensselaer Polytechnic Inst., Troy, NY, <sup>5</sup>GE Global Research, Niskayuna, NY, <sup>6</sup>Northern Illinois Univ., DeKalb, IL.

Polymer nanocomposites exhibit radically different thermo-mechanical properties which are, generally, attributed to the larger interfacial area of the nanoparticle which increases the polymer-filler interactions; and the nanoscale confinement of the polymer by nanoparticles leading to changes in the polymer dynamics. Our SAXS studies reveal the presence of hierarchical particle structures that varies with the particle surface chemical treatment, which is performed to tune the polymer-particle interactions. Using XPCS we show for the first time that the internal stress at the interface due to the presence of nanoparticles could be measured. It is found that the internal stress, which arises due to the entropic penalty that the polymer faces in the presence of the nanoparticles, engenders heterogeneous dynamics: The faster relaxation modes are significantly affected by the interface and

are uniquely related to the bulk properties. Using SAXS and XPCS we attempt to provide a general framework for understanding the relationship between the nature of the interfaces and thermo-mechanical properties.

This work benefited by the use of APS and IPNS funded by DOE-BES under contract #W-31-109-ENG-38.

**13.11.03 Combined XRD and Raman Combinatorial Screening System.** Bob He, Chris Frampton, Juergen Sawatzki, Bruker AXS, 5465 East Cheryl Parkway, Madison, WI 53711.

Combinatorial investigations require rapid screening techniques to test and evaluate variations of composition, structure and property within a material library. X-ray diffraction provides abundant information on the atomic arrangement of the sample revealed through the diffraction pattern. Raman spectroscopy measures the characteristic vibration frequencies determined by the chemical composition and chemical bond. Both X-ray diffraction and Raman spectroscopy are non destructive methods that require virtually no sample preparation, thus, allowing samples to be analyzed simply and quickly in their natural form. Combinatorial screening based on spectroscopic and diffraction techniques is of high importance *e. g.* for drug substances and formulations since the polymorphism of active ingredients has to be controlled to achieve a reliable product quality which will satisfy the regulatory authorities.

This presentation covers the development of an innovative instrument consisting of XRD and Raman spectroscopy for combinatorial screening. The X-ray source, X-ray optics, X-ray detector, laser source, Raman probe and an auto-zoomed video microscope are all integrated into a single platform so that the X-ray diffraction pattern, Raman spectrum and optical image from the same sample or sample area can be measured in a single load. The software associated with the system can treat data from the various techniques and analyze the results in correlation.

**13.11.04 Factors Affecting the Self Assembly of Amyloid Peptides.** S.V. Pingali<sup>1</sup>, Y. Liang<sup>3</sup>, P. Liu<sup>3</sup>, S.W. Childers<sup>3</sup>, K. Lu<sup>3</sup>, L. Guo<sup>2</sup>, D.G. Lynn<sup>3</sup>, P. Thiyagarajan<sup>1</sup>, <sup>1</sup>IPNS, <sup>2</sup>BioCAT, APS Beamline, Argonne National Lab, IL, <sup>3</sup>Emory Univ., Atlanta, GA.

Amyloid peptide's unique amphiphilic character allows the peptide to self-assemble in aqueous media into well-organized fibrillar structures. In order to study the self-assembly process of the smaller variant A $\beta_{16-22}$  (KLVFFAE), fluorescent labels such as Rhodamine 110 (Rh) and Rhodamine B (Rb) are used. Our studies show that fluorescent labels strongly influence the morphology of the self assembled nanotubes. A 9:1 mixture of A $\beta_{16-22}$  and Rhodamine 110 attached A $\beta_{17-22}$  (Rh-LVFFAE) as well as a 9:1 mixture of A $\beta_{16-22}$  and Rhodamine 110 attached A $\beta_{16-22}$  (Rh-KLVFFAE) results in the formation of narrower tubes. Interestingly, when a glycine is used to link Rhodamine 110 to A $\beta_{16-22}$  (Rh-G-KLVFFAE) or when Rhodamine B is attached to Lysine (Rb-KLVFFAE), the mixture self assembles into nanobubes with similar outer radius as A $\beta_{16-22}$ . We believe that the difference in the morphology of the nanotubes is due to the alteration of the packing parameter of the hydrophobic moieties and the effective charge of the peptides leading to variation in the interfacial curvature.

Work benefited from the use of IPNS and APS funded by the DOE, BES under contract W-31-109-ENG-38 to the U. Chicago and funding from DOE ER15377 to DGL.

**13.11.05 Characterization of Epoxy-Silane Films by Combined Scattering Techniques.** Peng Wang, Dale W. Schaefer, Dept. of Chemical and Materials Engineering, Univ. of Cincinnati, Cincinnati, OH 45221.

Bis-silanes with the general formula of  $(\text{RO})_3\text{Si}(\text{CH}_2)_3\text{-R}'$ - $(\text{CH}_2)_3\text{Si}(\text{OR})_3$ , where OR represents an alkoxy group and R is an organic functionality, show excellent performance as coupling agents in anti-corrosion films; Epoxy resin also has superior chemical and corrosion resistance as well as outstanding mechanical toughness. A combination of silane and epoxy is an excellent coating system with high hardness based on the mixture of epoxy (EPI-REZ™ 5003-W-55) and bis-sulfur silane ( $\text{R}' = \text{S}_2$ ). This one step coating provides excellent anti-corrosion protection of metals substrates. The goal of this study is to fully understand this two component system. Morphology, thickness, chemical composition, water barrier properties, response to organic solvents as well as hydrothermal degradation were investigated using x-ray and neutron reflectivity; Phase separation was studied by small angle scattering of neutron and X-ray scattering. Minority phase distribution profile was elucidated by using GISAXS.

Acknowledgment: This research is supported by SERDP.

**13.11.06 Fluctuation X-ray Microscopy – a Novel Approach for Characterization of Medium-Range Order in Noncrystalline Systems.** L. Fan<sup>1</sup>, D.J. Paterson<sup>2</sup>, I. McNulty<sup>1</sup>, M.M.J. Treacy<sup>3</sup>, D. Kumar<sup>3</sup>, P. Du<sup>4</sup>, U. Wiesner<sup>4</sup>, J.M. Gibson<sup>1</sup>, <sup>1</sup>Advanced Photon Source, Argonne National Laboratory, Argonne, IL 60439, <sup>2</sup>Australian Synchrotron, Clayton, Victoria 3068, Australia, <sup>3</sup>Dept. of Physics and Astronomy, Arizona State Univ., Tempe, AZ 85287, <sup>4</sup>Materials Science & Engineering, Cornell Univ., Ithaca, NY 14853.

The characterization of medium-range order (MRO) is a challenging problem. At present no x-ray technique effectively probes MRO. We have developed fluctuation X-ray microscopy (FXM) which offers quantitative insight into MRO in materials at nanometre- and larger-length scales. FXM examines spatially resolved fluctuations of X-ray speckle patterns. Systematically measuring the speckle variance as a function of the scattering vector and the X-ray spot-size produces information about the degree of MRO and the correlation length. To demonstrate this new technique we have studied a model system comprised of polystyrene spheres. Using nanofocusing optics, we have further developed fluctuation X-ray microscopy for the study of nanomaterials. The MROs in polymer-inorganic hybrids are quantitatively determined by FXM.

Use of the Advanced Photon Source was supported by the U.S. Department of Energy, Office of Science, Office of Basic Energy Sciences, under Contract No. W-31-109-ENG-38.

**13.11.07 Combination of Three-Beam Diffraction and Resonant Scattering for Study of Orbital Ordering in Microcrystal of  $\text{LaMnO}_3$ .** Qun Shen<sup>1</sup>, K.D. Finkelstein<sup>2</sup>, R. Colella<sup>3</sup>, <sup>1</sup>Advanced Photon Source, Argonne National Laboratory, <sup>2</sup>Cornell High Energy Synchrotron Source, Cornell Univ., <sup>3</sup>Dept. of Physics, Purdue Univ.

The (300) reflection in  $\text{LaMnO}_3$  has been observed at Mn K-edge and interpreted as the effect of orbital ordering by virtue of on-site 4p-3d Coulomb repulsion. An alternative interpretation is the effect of cooperative Jahn-Teller distortion of the oxygen octahedron surrounding Mn. Ordinarily these two effects are not distinguishable in resonant x-ray scattering experiments. However, they cause a phase difference of  $180^\circ$  in the resonantly scattered beam, which can be measured by phase-sensitive three-beam diffraction. We have performed such a three-beam experiment on  $\text{LaMnO}_3$ . The recorded three-beam interference profiles show that the mechanism of resonant scattering is the cooperative Jahn-Teller distortion rather than 4p-3d Coulomb repulsion. It demonstrates that the resonant technique supplemented

by three-beam diffraction is a very powerful tool capable of providing unique information to distinguish different electronic models responsible for the resonant scattering.

This work was supported by NSF Grant DMR 0225180 and NIH Grant EB002057 through CHESS. The Advanced Photon Source is supported by DOE Contract W-31-109-ENG-38.

**13.11.08 X-ray Imaging of Electro-deposited Microparticles by Near-Field Coherent Diffraction.** Martin de Jonge, Xianghui Xiao, Yong Chu, Qun Shen, Advanced Photon Source (APS), Argonne National Laboratory, Argonne, IL.

Coherent x-ray diffraction imaging is a potentially powerful technique for studying noncrystalline microstructures with resolution down to few-nm scales.

We report recent such studies of lead microparticles by electro-deposition onto a silicon-nitride membrane. The measurements were made using a highly-coherent x-ray beam of 8-keV at 32-ID of the APS. A pinhole was used to define an illumination region on the specimen, and further pinholes were used to remove high-order Airy rings and parasitic scattering from the illuminating beam. Coherent diffraction Images were recorded in the intermediate regime with a Fresnel number around unity. These not-so-far field diffraction patterns help to resolve the twin-image problem that exists in the far-field regime. Preliminary analysis suggests that reconstruction of these particles to  $\sim 100$  nm resolution may be possible, based on images collected with a lens-coupled CCD, and to significantly higher resolutions when using a direct-detection CCD. The goal of this work is to obtain reconstructed structures at few-nm scales and to find the optimum geometry for coherent diffraction imaging experiments.

This work was supported by the U.S. Department of Energy under contract No. W-31-109-ENG-38

## 13.12 Metal-Organic Hybrids-Crystal Engineering

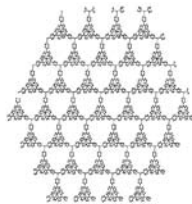
**13.12.01 Hybrid Materials from the F Elements.** Christopher L. Cahill, Lauren A. Borkowski, Daniel T. De Lill, Dept. of Chemistry, The George Washington Univ., Washington, DC 20052.

Our group has been focusing on the synthesis and structural systematics of lanthanide and actinide containing metal-organic framework materials (MOFs) and coordination polymers. Each of these systems displays a unique set of structural features which in turn gives rise to unprecedented topologies as well as tunable electronic properties. For example, Ln-carboxylates exhibit edge sharing of Ln-O polyhedra so that at least one dimension of these structures contains robust Ln-oxide bonding. Further, we are able to manipulate the topologies of these compounds through ‘templating’ in which non-coordinated, aromatic guest molecules can be utilized to influence both the crystal structure as well as Ln luminescence.

Hybrid materials containing the uranyl cation ( $\text{UO}_2^{2+}$ ) also display a wide range of structure types. Rather than templating, this system employs the use of multiple linker molecules (that is, carboxylate/pyridyl combinations) to promote assembly of extended structures. Interestingly, U-pyridine linkages are quite rare in extended structures, despite their ubiquity in uranyl-containing molecular compounds and transition metal MOFs. We have tailored appropriate pyridyl/carboxylate pairings to crystallize structures in which the aromatic serves as either a linker, or a charge balancing/space filling guest. In all cases, the aromatic component serves to sensitize  $\text{UO}_2^{2+}$  luminescence. Further, polymerization of uranyl centers to form oligomeric secondary building units is seen as a function of linker geometry.

**13.12.02 Heterometallic Metal-Organic Frameworks: Metal-ligands vs. Organic Ligands.** Seth M. Cohen, Sara R. Halper, Drew L. Murphy, Dept. of Chemistry and Biochemistry, Univ. of California, San Diego, La Jolla, CA 92093.

Inspired by the extensive work into metal-organic frameworks (MOF) based on simple organic ligands as 'linkers' and metal ions or metal ion clusters as 'nodes', we have investigated approaches to enhance these architectures by the incorporation of highly chromophoric metal centers. By designing 'metalloligand' precursors we have attempted to reproduce known MOF structures that possess augmented spectroscopic features based on the introduction of the second metal center. Several findings along this line of investigation will be discussed, which include a wide variety of new MOF structures (see figure), pronounced anion templating effects on structure, as well as the ability of these MOFs to readily undergo anion exchange.



**13.12.03 The Use of Pi-Bonded Organometallic Quinonoid Complexes in the Construction of Self-Assembled Metal-Organic Hybrid Materials.** D.A. Sweigart, S.U. Son, J.A. Reingold, S.B. Kim, G.B. Carpenter, Dept. of Chemistry, Brown Univ., Providence, RI 02912.

The coordination of organometallic fragments such as  $[\text{Mn}(\text{CO})_3]^+$  or  $[\text{Rh}(\text{P}(\text{OPh})_3)_2]^+$ , to the carbocyclic ring in hydroquinone, 1,4- $\text{C}_6\text{H}_4(\text{OH})_2$ , results in activation of the  $-\text{OH}$  groups to deprotonation. The resulting pi-bonded quinone complexes function as ligand spacers by connecting through the oxygen atoms to metallic nodes. The 1-, 2-, or 3-D metal-organometallic coordination networks formed in this manner span an interesting range of architectural motifs that depend in a predictable manner on the nature of the node and the experimental conditions.

Crystal engineering of the salt  $[(1,4\text{-hydroquinone})\text{Rh}(\text{P}(\text{OPh})_3)_2]^+\text{X}^-$  is possible because of *charge-assisted* hydrogen-bonding to the anion  $\text{X}^-$ . The structure of the solid network depends on the nature of the anion

( $\text{SbF}_6^-$ ,  $\text{OTf}^-$ ,  $\text{OTs}^-$ ,  $\text{PF}_6^-$ ,  $\text{PF}_2\text{O}_2^-$ ,  $\text{BF}_4^-$ ,  $\text{ClO}_4^-$ ), and can be monomeric, dimeric, 1-

D polymeric,  $\text{C}_2$  helical or  $\text{C}_3$  helical. These materials exhibit three types of noncovalent interactions – hydrogen-bonding, charge pairing, and pi-pi stacking of the aromatic hydroquinone rings. The hydrogen-bonding from the  $-\text{OH}$  groups to the anion, illustrated for  $\text{X}^- = \text{BF}_4^-$ , results in a supramolecular assembly featuring hydrophobic channels of aromatic phenyl rings from the triphenyl phosphite ligands. The nature of the channels may make this material a useful model for certain guest-host studies.

We gratefully acknowledge support from the National Science Foundation and the Petroleum Research Fund, administered by the American Chemical Society.

**13.12.04 Hybrid Materials Based on Chalcogenide Tetrahedral Clusters and Functional Organic Molecules.** Pingyun Feng, Dept. of Chemistry, Univ. of California, Riverside, CA 92521.

Hybrid materials based on chalcogenide tetrahedral clusters and organic functional molecules represent an interesting class of materials that integrate the unique features from both materials. The materials can consist of single-sized tetrahedral clusters and organic ligands that act as molecular building blocks in the formation of well-ordered su-

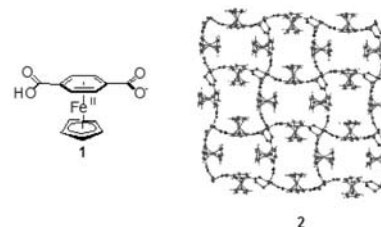
perlattices from zero to three dimensions. Alternatively the tetrahedral clusters can be joined directly to produce inorganic frameworks and organic molecules serves as templating agents to direct the formation of these materials. Some of these inorganic frameworks may contain organic ligands as surface capping groups. Both main-group and transition metals have been incorporated into clusters to allow the modification of structural and physical properties. Different types of organic molecules have been incorporated into the superlattice through either covalent bond, electrostatic interaction or other weaker interactions. The structural analysis based on single crystals reveals detailed information that could help the structural elucidation of larger colloidal nanostructures. The synthesis, structures, and various properties of these materials will be discussed.

**13.12.05 Tunable Inorganic-Organic Hybrid Nanostructures by Crystal Engineering.** Xiaoying Huang, Wooseok Ki, Jing Li, Dept. of Chemistry and Chemical Biology, Rutgers Univ., Piscataway, NJ 08854.

Research in inorganic-organic hybrid materials is a rapidly developing area of materials science. Hybrid materials can combine the superior electronic, magnetic, and optical properties and thermal stability of inorganic frameworks with the structural diversity, flexibility, high processability, and light-weight of organic molecules. These materials can enhance and strengthen the functionality and performance and, thus, have both fundamental and technological importance. We have recently developed a unique class of crystalline inorganic-organic hybrid nanostructured materials with systematically tunable structures and properties. The structures of these materials are comprised of II-VI semiconductor nanometer sized motifs (inorganic component) and suitable organic spacers (organic component). They possess numerous improved properties over conventional II-VI semiconductor bulk materials, including broad band-gap tunability, high absorption coefficients and exciton binding energies, all very desirable for optoelectronic applications such as photovoltaics, solid state lighting and UV emitting devices. More significantly, they exhibit extremely strong quantum size effect and their nano-properties are independent on particle sizes, and can be systematically tuned by changing the structure and dimensionality of the inorganic motifs.

**13.12.06 Metal-Organometallic Frameworks Derived from Facially Metalated Arylcarboxylates.** S.A. Kumalah, K.T. Holman, Dept. of Chemistry, Georgetown Univ., Washington, DC, 20057.

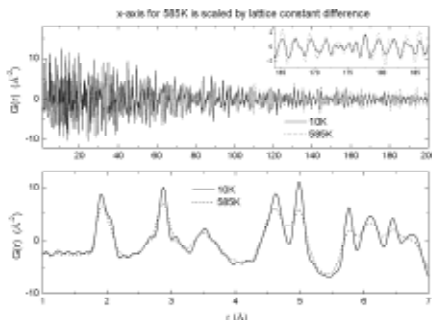
In recent years, remarkable progress has been made in the use of coordination chemistry to design materials, commonly known as metal organic frameworks or coordination polymers, via the use of various transition metals and organic bridging ligands. In this context, the use of *organometallic* bridging ligands, which have the obvious potential to introduce unique functionality, have been relatively unexplored. The synthesis and characterization of a series of metal-organometallic framework (MOMF) materials, derived from simple  $[\text{CpFe}(\eta^6\text{-arene-carboxylate})]$  bridging ligands, will be presented. For example, the reaction of  $\text{Co}(\text{NO}_3)_2 \cdot 6\text{H}_2\text{O}$  with  $[\text{CpFe}]^+$ -metalated 1,4-benzenedicarboxylic acid results in  $[\text{Co}_3(1\text{-H})_4(\text{H}_2\text{O})_2(\mu\text{-H}_2\text{O})_2][\text{NO}_3]_2$  (2), a 3D framework material constructed of square grid cobalt-carboxylate networks that are interconnected in the third dimension through additional cobalt ions.



## 13.13 Exploring Structures from the Near Neighbor to the Nanometer Scale Using Pair Distribution Function Analysis and Small Angle Scattering

**13.13.01 Nanometer Range Local Atomic Structure Probed by the PDF Method.** T. Egami, Univ. of Tennessee, Knoxville, TN 37996, Oak Ridge National Laboratory, Oak Ridge, TN 37831.

The method of atomic pair-density function (PDF) analysis has traditionally been applied mainly to study the short range structure within 0.5 nm or so. This is because the PDF analysis has been primarily used for liquid and glasses, which do not have much structure beyond nm. However, the PDF can be determined over larger distances, particularly when the measurement is made with higher Q-resolution. Using the NPDF of Los Alamos NL that has the Q resolution  $\Delta Q/Q = 1.5 \times 10^{-3}$ , the PDF can



now be determined up to 30 nm. With this capability it is now possible to determine the hierarchical structure in different lengthscales. We discuss examples of such study, in 1) relaxor ferroelectrics in which the local atomic polarizations are non-collinear, and are different from the average polarization in nano-domains, 2) nickelate compounds in which the local environment of Ni ion is Jahn-Teller distorted, but shows no macroscopic distortion due to formation of sublattices and nano-domains. The figure shows the PDF of  $\text{LiNiO}_2$  determined at 10 and 585 K.

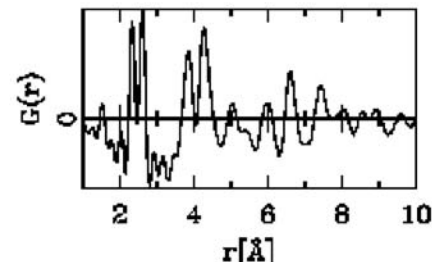
Work supported by the NSF DMR04-04781.

**13.13.02 The Probability Distribution Function in Small-angle Scattering.** R.P. Hjelm, Los Alamos Neutron Science Center, Los Alamos National Laboratory, Los Alamos, NM 87545.

A typical small-angle scattering (SAS) measurement on particles in solution on length scales from 1 to 100 nm. Ideally, the particles will not be correlated in position and orientation, in which case the SAS measurement gives information on the spherically-averaged particle structure. Because of the disorder that is inherent in these types of systems, the probability distribution function,  $p(r)$ , is a natural way of representing the information that is available from the SAS measurement, including particle size, shape and internal structure. The probability distribution function is related to the measured intensity by the sine-transform,  $p(r)/r = \frac{2}{\pi} \int_0^\infty Q I(Q) \sin Qr dQ$ , and is thus related to the Debye-Bueche correlation function,  $\gamma(r)$ , as  $p(r) = 4\pi r^2 \gamma(r)$ . Features of  $p(r)$  have led to the development of algorithms, notably those of Glatter and of Moore), for the calculation of  $p(r)$ , which account for instrument resolution functions, and which allow for detailed comparison with model calculations. We will discuss some examples of results from systems where such comparisons have led to detailed information on the particle structure.

**13.13.03 Structure of CdSe/ZnS Core/Shell Nanoparticles.** R.B. Neder, Institut fuer Mineralogie, Univ. Wuerzburg, Am Hubland, 97074 Wuerzburg, Germany.

The structure of CdSe/ZnS core/shell nanoparticles was determined from pair distribution function (PDF), small angle X-ray scattering, standard and anomalous powder diffraction, and EXFAS data. The particles were prepared as described by [1]. The powder pattern reveal broad maxima that indicate a zincblende structure and particles with approximately 3 to 4 nm in diameter. Both, EXAFS and PDF data reveal that the first neighbour distances Cd-Se (2.61) and Zn-S (2.33) correspond to their respective bulk values. The PDF data furthermore show that also the next few neighbour distances are identical to the respective bulk values as well. The width of the first neighbour distributions is not wider than that of standard reference samples. This proves that the CdSe core and the ZnS shell are free of substantial strain. The thin ZnS shell is thus not epitaxially grown with pseudomorphic lattice constants but has already relaxed to the bulk structure. The complementary combination of the experimental data enabled to determine and refine a full structural model.



[1] Dabbousi, B. O., Rodriguez-Viejo, J., Mikulec, F. V., Heine, J.R., Mattoussi, H., Ober, R., Jensen, K. F. & Bawendi, M. G. J. Phys. Chem. B, 101, 9463 (1997).

**13.13.04 Investigating the Structure of Proteins in Solution by Small-angle Scattering.** Lise Arleth, The Royal Veterinary and Agricultural, Univ., Dept. of Natural Sciences, Thorvaldsensvej 40, DK-1871 Copenhagen, Denmark.

Small-angle scattering (SAS) of x-rays or neutrons is a well-established technique for investigating structures on the length scale of 1-100 nm. The technique is gaining increased importance in the determination of the structure of proteins and more general biomacromolecules in solution and is a strong complement to protein crystallography. In a SAS experiment, the Fourier transform of the 3-dimensional structure of the sample (in terms of the scattering length density fluctuations) is measured. After a simple data analysis, the radius of gyration, the maximum diameter and the molecular weight of the biomacromolecule or biomacromolecular complex is obtained. A more advanced analysis allows for determining the full 3-D structure of the biomacromolecule with a resolution down to 0.5-1.0 nm. One of the main advantages of SAS is that no special sample preparation is needed prior to analysis: The biomacromolecules can be studied in their native state in a physiologically relevant concentration and environment.

**13.13.05 Pair Distribution Function Analysis: The Dependence of Entropic PDF's upon Non-Uniform Priors.** R.J. Papoular, Laboratoire Léon Brillouin CEA/CNRS UMR12, Gif sur Yvette 91191, France.

Since their original introduction to study the local structure of crystals in the 1980's by Egami's group ( e.g., [1] and references therein ), PDF analyses have undergone tremendous developments. Evolving alongside with the latter are the quest for the accuracy of PDF's [1], efficient programs such as PDFFIT [2] to compute them and the proper assessment of the standard uncertainties associated with them [3]. The present work focuses on yet another aspect linked to the reliability of PDF's: how many of them can be computed from a single dataset S(Q)? Whilst conventional PDF analyses involve a straightforward

Sine Fourier transform, we use Maximum Entropy (MEM) to obtain  $g(r)$  from  $S(Q)$ , as initially pioneered by Daniell's group in the 1980's to study liquids and amorphous materials<sup>[4]</sup>. We show that the retrieved PDF's are much dependent upon a MEM related device: the non-uniform PDF prior (NUP), which may range from totally disordered (liquid) to fully ordered (perfect crystal). The related PDF deviations are compared with the standard uncertainties.

[1] Toby *et al.*, *Acta Cryst.* **A48**, 336(1992).

[2] Proffen *et al.*, *J. Appl. Cryst.* **32**, 572(1999).

[3] Toby *et al.*, *Acta Cryst.* **A60**, 315(2004).

[4] Daniell *et al.*, *Maximum Entropy & Bayesian Methods, Skilling* (ed.), Kluwer(1989).

### 13.13.06 Pair Distribution Function Analysis of Nanosystems.

Katharine Page, Ram Seshadri, Anthony K. Cheetham, Materials Research Lab & Materials Dept., Univ. of California, Santa Barbara, CA.

The limited translational periodicity in nanomaterials renders reciprocal space methods of limited utility for structural studies, but real-space methods are showing a great deal of promise. Our early work with 5nm gold nanoparticles demonstrated the power that pair distribution function refinement can bring to structural descriptions on the nano-scale.<sup>1</sup> These results will be presented, along with our more recent study of gold nanoparticles under pressure. We shall also describe the use of total neutron scattering powder diffraction patterns and the pair distribution function to attain quantitative structural information for other nanoparticle systems, including core-shell hard-soft magnetic metal oxides and novel intermetallics. We will demonstrate the problems arising from incoherent hydrogen scattering that are inherent to organically capped nanoparticles, and present complementary synchrotron x-ray data for some of our systems. The potential applications, power and current limitations of real-space methods for analysis of structure in the nano-regime will be discussed.

<sup>1</sup>K. Page, Th. Proffen, H. Terrones, M. Terrones, L. Lee, Y. Yang, S. Stemmer, R. Seshadri, A. K. Cheetham, Direct observation of the structure of gold nanoparticles by total scattering powder neutron diffraction, *Chem. Phys. Lett.* **393** (2004) 285-288.

### 13.13.07 The Whole Particle Structural Analysis on TiO<sub>2</sub> and Ge<sub>2</sub>Sb<sub>2</sub>Te<sub>5</sub> Nanoparticles.

S. Shamoto<sup>1</sup>, K. Kodama<sup>1</sup>, S. Iikubo<sup>1</sup>, T. Taguchi<sup>1</sup>, Th. Proffen<sup>2</sup>, N. Yamada<sup>3</sup>, <sup>1</sup>Quantum Science Directorate, Japan Atomic Energy Agency, Tokai, Ibaraki, Japan, <sup>2</sup>Los Alamos National Laboratory, Los Alamos, NM, <sup>3</sup>Matsushita Electric Industrial Co., Ltd., Moriguchi, Osaka, Japan.

A nanoparticle has large surface area in the ratio, which would have different crystal structure from the inside. As for a catalyst, the surface plays an important role in the functionality. Structural analysis of the whole particle is an important step toward understanding the property. Recent high intensity quantum beams, such as pulsed neutron and synchrotron x-ray provide us a possibility for the analysis, which needs high Q-resolution and high intensity simultaneously. TiO<sub>2</sub> and Ge<sub>2</sub>Sb<sub>2</sub>Te<sub>5</sub> nanoparticles are photocatalyst and optical recording materials, respectively. The former particles are isolated individually, while the latter particles are embedded in an amorphous matrix. These two typical nanoparticles have been studied by the atomic pair distribution function (PDF) analysis with the spherical particle form factor [1] using neutron powder diffraction data obtained at NPDF in LANSCE as shown in Fig. 1.

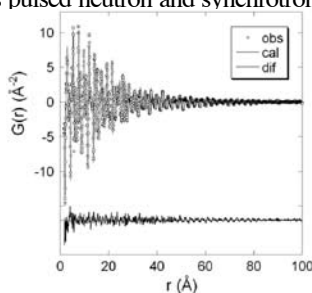


Figure 1. Observed, calculated and difference PDFs with the spherical particle form factor for TiO<sub>2</sub> nanoparticle.

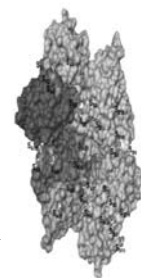
[1] K. Kodama, S. Iikubo, S. Shamoto, cond-mat/0511246.

## 13.14 Cool Structures

### 13.14.01 The High-Resolution Structure of a Processive Exopolyphosphatase with a Novel Regulatory GTPase Fold.

D.A. Sanders, J. Alvarado A. Ghosh, M.S. Hasson\*, Markey Center for Structural Biology, Dept. of Biological Sciences, Purdue Univ., West Lafayette, IN 47906, \*Deceased.

The *E. coli* Ppx exopolyphosphatase degrades long-chain polyphosphates in a highly processive reaction & hydrolyzes the terminal 5' phosphate of guanosine 5' triphosphate 3' diphosphate (pppGpp). The structure of Ppx has been determined to 1.9Å resolution by X-ray crystallography. Remarkably, 29 sulfate ions are found bound to the Ppx dimer, & they occupy sites where the polyP chain is likely to bind. An aqueduct that passes through the enzyme provides a physical basis for the enzyme's high processivity. The amino-terminal region containing the polyPase active site is a member of the ASKHA (Acetate and Sugar Kinases, Hsp70, Actin) phosphotransferases. A Domain III six-helix claw homologous to the catalytic core of eukaryotic cyclic nucleotide phosphodiesterases is probably the pppGppase. PolyPase activity regulation by pppGpp hydrolysis is reminiscent of the regulation of biochemical reactions by G proteins & other GTPases. Recent enzymological studies of mutant Ppx proteins provide additional insight into the regulation of the bacterial stringent response to nutrient deprivation. A new genus of 3-dimensional protein animation, which illustrates the path of the polyP chain, will be presented.



### 13.14.02 Conformational Microheterogeneity Shapes the Photochemical Response of the Bacterial Photoreceptor PYP.

P.-D. Coureux, Z. P. Fan, U.K. Genick, Biochemistry Dept., Brandeis Univ., Waltham, MA 02454.

Protein molecules do not adopt a single, fixed structure. Instead, their structures fluctuate to populate an ensemble of many hierarchically nested conformational substates. Since, "structure determines function", each structural substate should also correspond to a functional substate. One of the untested assumptions of structural biology has been that subtle changes in structure lead to equally subtle changes in function. Is this assumption correct? Here we report experiments on the bacterial photoreceptor PYP where we probed a cryogenically trapped ensemble of conformational substates for their ability to facilitate the light-driven isomerization of PYP's *para*-coumaric acid chromophore. Spectroscopic experiments coupled with ultra-high resolution X-ray crystallography revealed that structural states with minimal conformational differences display dramatically different functional properties. Notably, the dominant structural state proved to be inert to light activation, while the biologically-relevant chromophore-isomerization activity can be attributed to a minor conformational substate.

### 13.14.03 What Does George Lucas Know About Crystallography?

Patrick J. Carroll, Dept. of Chemistry, Univ. of Pennsylvania, Philadelphia, PA.

A collection of interesting structures from the past couple years done in the X-ray Facility in the Department of Chemistry at the University of Pennsylvania is presented. Included are large structures, twinned structures, structures with  $Z' \gg 1$ , structures with disorder, structures with large numbers of solvent molecules, several still "unsolved" structures, and a few structures that are difficult to classify.

**13.14.04 Low-Melting Organic Salts: Phase Transitions, Twinning, and Disorder.** Victor G. Young, Jr.,<sup>1</sup> Wesley A. Henderson,<sup>2</sup> Stefano Passerini,<sup>3</sup> Paul C. Trulove,<sup>2</sup> Hugh C. DeLong<sup>2</sup>; <sup>1</sup>X-Ray Crystallographic Lab, Chemistry Dept., Univ. of Minnesota, Minneapolis, MN, <sup>2</sup>U.S. Naval Academy, Dept. of Chemistry, Annapolis, MD, <sup>3</sup>ENEA, Casaccia Research Center, Rome, Italy.

Low-melting organic salts often exhibit complex temperature-dependent properties. Below melting temperatures these are best described as crystalline materials with liquid-like properties where some or all of the cations and/or anions are disordered. At yet lower temperatures, as monitored by DSC, these undergo stepwise phase transitions to ordered systems where some are twinned by non-merohedry and have high  $Z'$  structures. Many of these have intermediate phases with both ordered and/or disordered species. For example,<sup>1</sup> the salt  $\text{PYR}_{12}\text{TFSI}$  undergoes four known solid-solid phase transitions before melting at 91°C. At -120°C, the crystal structure consists of ordered ions (Phase IV). This crystal structure is found in space group  $P\bar{1}$  with  $Z'=8$  as a non-merohedral twin. Above the phase transition at -85°C all of the  $\text{PYR}_{12}^+$  and TFSI<sup>-</sup> ions become disordered forming a plastic crystalline phase (Phase III). This crystal structure is found in space group  $P2_1/n$  with  $Z'=2$  as a non-twinned, single crystal. The crystal structures of both Phase II and Phase I have not been determined due to their inherent liquid-like properties. The structures and phase behavior of several new low-melting organic salts will be presented in this paper.

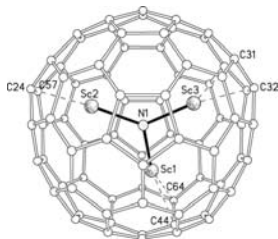
<sup>1</sup>Wesley A. Henderson, Victor G. Young, Jr., Stefano Passerini, Paul C. Trulove, and Hugh C. DeLong, Chem. Mater. (2006) 18, 934.

**13.14.05 Chemical Reaction in a Single Crystal: Monitoring Structural Changes in a Multi-Step Oxidation Process by Single Crystal X-Ray Crystallography.** Xiaoping Wang<sup>1,2</sup>, Qinliang Zhao<sup>2</sup>, Rongmin Yu<sup>2</sup>, Carlos A. Murillo<sup>2</sup>, F. Albert Cotton<sup>2</sup>, Dept. of Chemistry, Univ. of North Texas, Denton, TX 76203; <sup>2</sup>Laboratory for Molecular Structure and Bonding, Texas A&M Univ., College Station, TX 77842.

An unusual case of multi-step single-crystal to single-crystal (SCSC) conversions via chemical oxidation has been observed for the dimolybdenum molecular pair  $\text{Mo}_2(\text{DAniF})_3(\mu\text{-OD})_2\text{Mo}_2(\text{DAniF})_3$ , where DAniF is the anion of *N,N'*-di-*p*-anisylformamidinate. It reacts readily with atmospheric oxygen and undergoes two successive SCSC oxidative conversions in about three weeks. First to form a mixed-valence compound,  $\text{Mo}_2(\text{DAniF})_3(\mu\text{-O})(\mu\text{-OD})\text{Mo}_2(\text{DAniF})_3$ , which is inaccessible by a solution reaction, and then to a doubly oxidized product,  $\text{Mo}_2(\text{DAniF})_3(\mu\text{-O})_2\text{Mo}_2(\text{DAniF})_3$ . "Snapshots" of the structural changes were obtained from single-crystal structures solved during the oxidation process.

**13.14.06 Surprising New Results Concerning the Endohedral Fullerene Structures of  $\text{C}_{80}$ ,  $\text{C}_{82}$ ,  $\text{C}_{84}$ ,  $\text{C}_{86}$ , and  $\text{C}_{88}$ .** Marilyn M. Olmstead, Christine M. Beavers, Alan L. Balch, Univ. of California, Davis, Harry C. Dorn, Virginia Polytechnic Inst. and State Univ.

Endohedral fullerenes—large, even numbered carbon cages with positively charged species inside—differ in many respects from their empty cage congeners. All known empty cage fullerenes obey the isolated pentagon rule (IPR) in which pentagons are only fused to hexagons. We have already reported the first single crystal structure determination of a non-IPR endohedral fullerene,  $\text{Sc}_3\text{N@C}_{68}$ , where three pentagon-pentagon fusions occur in a  $D_3$  symmetric arrangement. Moreover, among the seven possible



IPR isomers of  $\text{C}_{80}$ , the  $I_h$  isomer is predicted to be the least stable, but in the set of endohedral molecules  $\text{M}_3\text{N@C}_{80}$  ( $\text{M}=\text{Sc}, \text{Y}, \text{Lu}$ , or lanthanide), the  $I_h$  isomer is the most stable. We now report a number of structures which feature some of the following surprises: a second isomer of  $\text{M}_3\text{N@C}_{80}$  with  $D_{5h}$  symmetry; a second non-IPR endohedral fullerene,  $\text{Tb}_3\text{N@C}_{84}$ ; an egg-shaped fullerene of  $\text{Tb}_2(\text{C}_2)\text{@C}_{88}$  as well as a new isomers of  $\text{M}_3\text{N}$  clusters within  $\text{C}_{86}$  and  $\text{C}_{88}$ . Examination of these structures reveals clues about the formation of fullerenes, information about the distribution of charge within the fullerene cages and the strength of  $\pi\text{-}\pi$  intermolecular interactions between the fullerene and cocrystallized porphyrin molecules.

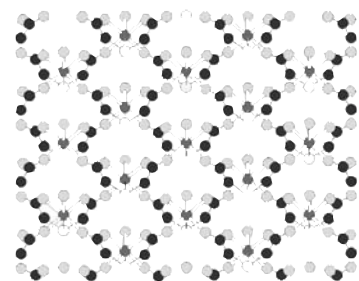
## 13.15 Science at X-Ray and Neutron Facilities Around the Pacific Rim

**13.15.01 The High Resolution X-Ray Structure of Taka-Amylase; The Crystal Grown in Microgravity Environment.** Akifumi Higashiura<sup>1</sup>, Hiroaki Tanaka<sup>2</sup>, Koji Inaka<sup>4</sup>, Masaru Sato<sup>3</sup>, Shigeru Sugiyama<sup>4</sup>, Sachiko Takahashi<sup>2</sup>, Mari Yamanaka<sup>2</sup>, Moritoshi Motohara<sup>3</sup>, Satoshi Sano<sup>3</sup>, Tomoyuki Kobayashi<sup>3</sup>, Mamoru Suzuki<sup>1</sup>, Tet-suo Tanaka<sup>3</sup>, Atsushi Nakagawa<sup>1</sup>, <sup>1</sup>Inst. for Protein Research, Osaka Univ., <sup>2</sup>Japan Space Forum, <sup>3</sup>Japan Aerospace Exploration Agency, <sup>4</sup>Maruwa Food Ind., Inc.

Recently, high brilliance and highly focused synchrotron beam lines, X-ray data collection at low temperature and technical advances in crystallographic analysis have significantly improved the resolution of X-ray crystallography. A crystallization in microgravity environment is one of the technique for the determination of high resolution structure. In this study Taka-amylase, a glycoprotein derived from *Aspergillus oryzae*, was used as a model protein for high resolution X-ray crystal structure analysis. The space crystals were produced in the JAXA-GCF (Japan Aerospace Exploration Agency –Granada Crystallization Facility) project. Taka-amylase structure was refined against X-ray data recorded on beamline BL44XU of SPring-8 to resolution of 1.0Å. This high resolution structure was providing us with a more reliable picture of the geometric and conformational properties of proteins and implied the necessity to improve bond length and angle restraints.

**13.15.02 Synthesis and Thermodecomposition Study of  $\text{Zn}(\text{tda})\text{H}_2\text{O}$  (tda = thiodiacetate).** Ming-Chen Wu<sup>1</sup>, Hwo Shuenn Sheu<sup>2</sup>, Chi-Shen Lee<sup>1</sup>, <sup>1</sup>Dept. of Applied Chemistry and Inst. of Molecular Science, National Chiao Tung Univ., 1001 Ta-Hsueh Rd., Hsinchu 30010, Taiwan, <sup>2</sup>National Synchrotron Radiation Research Center, Taiwan.

A novel two dimensional coordination polymer  $\text{Zn}(\text{tda})\text{H}_2\text{O}$  (tda =  $\text{O}(\text{CH}_2\text{COO})_2^{2-}$ ) was synthesized under hydrothermal condition. The compound crystallized in the monoclinic space group  $P2_1$  with  $a = 16.437 \text{ \AA}$ ,  $b = 5.2098 \text{ \AA}$ ,  $c = 16.437 \text{ \AA}$ ,  $\beta = 114.201^\circ$ ,  $V = 1060.2(6) \text{ \AA}^3$ , and  $Z = 4$ . The structure features two dimensional, noncentrosymmetric networks with a pseudo hexagonal network of Zn(II) coordinated by tda and water molecules. The  $\text{Zn}(\text{tda})\text{H}_2\text{O}$  decomposed at  $T > 550 \text{ C}$  to form ZnO sponge with the surface area  $\sim 30 \text{ m}^2/\text{g}$ , which make it an attractive precursor for one step synthesis of nanoporous ZnO.



The two dimensional structure of  $\text{Zn}(\text{tda})\text{H}_2\text{O}$  projected along [010].

We thank NSRRC for access to beamline. The temperature dependent Powder X-ray diffraction data were collected using synchrotron radiations at NSRRC BL01C2 beam line. This research was supported by National Science Council (NSC94-2113-M-009-012) and Institute of Nuclear Energy Research, Atomic Energy Council, Taiwan (NL940251).

**13.15.03 Small-Angle Scattering with a Focus on Bio-molecular Structure in Australia.** Jill Trehwella, Univ. of Sydney and Bragg Institute, ANSTO.

There has been a recent surge of interest in small-angle scattering for studying bio-molecules in recent years. As the molecular structural problems become more challenging, researchers are turning to small-angle scattering data as a potential source of complementary information that can aid in importing the accuracy of NMR derived structures (Grishaev *et al.* 2005, *JACS* **127**, 16621) or in order to be able to build models of complexes for which there are crystal or NMR structures of components but the components may have flexible linkers that inhibit crystallization (Vigil *et al.* 2005, *JBC* **280**, 35521). At this opportune time, Australia is investing in instrumentation for small-angle scattering using laboratory based X-ray sources, high brilliance X-rays from the new Australian Synchrotron under construction in Melbourne, and neutron beams from the new Open Pool Australian Light Reactor (OPAL) that is in commissioning at Lucas Heights, near Sydney. This talk will briefly describe the existing and planned facilities, and the science that is being and will be enabled.

**13.15.04 A New Macromolecular Crystallography Beam Line at the Stanford Synchrotron Radiation Laboratory Designed for the Analysis of Very Small Crystals.** Daniel Harrington, Andy Ringwall, Jean-Charles Castagna, Armin Busse, James Safranek, Aina Cohen, Thomas Rabedeau, Stanford Synchrotron Radiation Laboratory, Stanford Univ., Menlo Park, CA 94025.

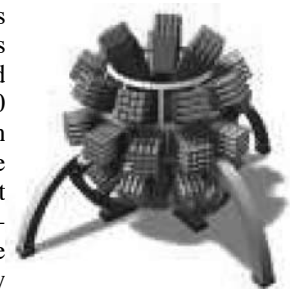
The Stanford Synchrotron Radiation Laboratory, through a generous contribution from the California Institute of Technology, is building a new macromolecular crystallography beam line that will take full advantage of the new SPEAR3 source.

Particular attention is being given to producing a beam line capable of analyzing extremely small crystals, both by maximizing the radiation brilliance and developing tools necessary to easily align and collect data on these samples. The source of the X-rays will be a mini-gap, in-vacuum undulator in the east pit region of the SPEAR3 ring arranged in a chicane with a second, future beam line source. The source phase space will be coupled to the focal position phase space via 3 rhodium-coated mirrors, two of which will independently focus the beam in the horizontal and vertical directions. A liquid nitrogen-cooled pair of Si(111) crystals will provide monochromatic radiation between 6 and 18keV (2.07 - 0.69Ångstroms). This design has been analyzed using ray tracing, FEA of thermally sensitive components, and various flux calculations. New devices are being developed or acquired which will permit the visualization of crystals on the 5µm scale and the automated screening of crystals. When completed, 60% of the beam time for this resource will be available for the general user community.

**13.15.05 IBARAKI Biological Crystal Diffractometer in J-PARC (BIX-P1) – General View.** I. Tanaka<sup>1</sup>, N. Niimura<sup>1</sup>, T. Ozeki<sup>2</sup>, T. Ohhara<sup>3</sup>, K. Kurihara<sup>3</sup>, K. Kusaka<sup>3</sup>, K. Aizawa<sup>3</sup>, Y. Morii<sup>3</sup>, M. Arai<sup>3</sup>, K. Ebata<sup>4</sup>, Y. Takano<sup>4</sup>, <sup>1</sup>Ibaraki Univ., Hitachi, Ibaraki 316-8511, Japan, <sup>2</sup>Tokyo Inst. of Tech., Meguro, Tokyo, Japan, <sup>3</sup>JAEA, Tokai, Ibaraki, Japan, <sup>4</sup>Ibaraki Pref. Gov., Mito, Ibaraki, Japan.

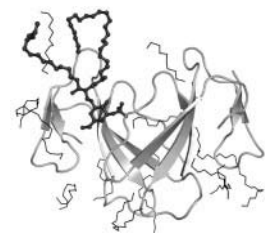
Ibaraki Prefectural Government in Japan has started to construct a neutron diffractometer for biological macromolecules for industrial

use at J-PARC. The diffractometer is designed to cover the sample crystals which have their cell edges up to around 150 Å. It is expected to measure 100 samples per year if they have 2mm<sup>3</sup> in crystal volume. The efficiency is more than 50 times larger than the present high performance diffractometers, BIX-4 in JRR-3 reactor in JAEA. To realize this performance, two important and key items should be developed; a detector and a software in data reduction. The current status of these developments will be reported with the latest parameters of this diffractometer, including detector, optics and shielding information.



**13.15.06 Glycosphingolipid-Facilitated Membrane Insertion and Internalization of Cobra Cardiotoxin: Crystal Structure of The Cardiotoxin/Sulfatide Complex.** Jung-Hung Liu<sup>1,3</sup>, Chia-Hui Wang<sup>2,3</sup>, Shao-Chen Lee<sup>2</sup>, Wen-guey Wu<sup>2</sup>, Chwan-Deng Hsiao<sup>1</sup>, <sup>1</sup>Inst. of Molecular Biology, Academia Sinica, Taipei, Taiwan, <sup>2</sup>Dept. of Life Sciences and Inst. of Bioinformatics and Structural Biology, National Tsinghua Univ., Hsinchu, Taiwan, Republic of China. <sup>3</sup>These authors contributed equally to this work.

Cobra cardiotoxins, a family of basic polypeptides having lipid- and heparin-binding capacities, induce severe tissue necrosis and systolic heart arrest in snakebite victims. Recent studies showed that CTX A3, the major cardiotoxin from Taiwan cobra venom, binds sulfatide in the outer leaflet of the plasma membrane, and consequently sulfatide mediates CTX A3-induced membrane leakage and CTX A3 internalization into mitochondria. Sulfatide is a glycosphingolipid with 3'-sulfated galactose headgroup. Here we describe the crystal structure of a CTX A3/sulfatide complex in a membrane-like environment at 2.3 Å resolution. CTX A3 recognizes both the headgroup and the ceramide interfacial region of sulfatide and induces a lipid conformational change that may play a key role in CTX A3 oligomerization and cellular internalization.



We thank NSRRC, Taiwan for access to beamline 17B2. This research was supported by NSC and Academia Sinica, Taiwan.

**13.15.07 Cephalosporin Acylase: A Protein with Two Chemistries.** Jin kwang Kim, In Seok Yang, Hye Jung Shin, Ki Joon Cho, Eui Kyung Ryu, Sun Hwa Kim, Sung Soo Park, Kyung Hyun Kim, Dept. of Life Sciences & Biotechnology, School of Life Sciences & Biotechnology, Anam-dong, Sung-buk ku, Seoul SOUTH KOREA.

Cephalosporin acylase (CA), a member of the N-terminal nucleophile (Ntn) hydrolase family, is activated through sequential primary and secondary autoproteolytic reactions with the release of a pro-segment. We have determined crystal structures of four CA mutants. Two mutants are trapped after the primary cleavage, and the other two undergo secondary cleavage slowly. These structures provide a first look at the pro-segment conformation during activation in Ntn hydrolases. The highly-strained helical conformation of the precursor pro-segment is transformed into a relaxed loop conformation in the intermediates, suggesting that the relaxation of structural constraints drives the primary cleavage reaction. The secondary autoproteolytic step has been proposed to be intermolecular. However, our analysis provides evidence that CA is processed in two sequential steps of intramolecular autoproteolysis involving two distinct proteolytic mechanisms, the first mediated by a serine residue and the second by a glutamate.

## AW.01 Buerger Award Structural Biology from all Angles

**AW.01.01 A Personal Journey through Structure Space.** Helen M. Berman, Rutgers, The State Univ. of New Jersey, Dept. of Chemistry and Chemical Biology, Piscataway, NJ 08854.

Integrative, systematic studies of molecules require large and well-organized data sets. My longstanding research interests in the structures and interactions of biological macromolecules have helped to motivate and inform the development of the Nucleic Acid Database and the Protein Data Bank. This talk will focus on the interplay of the systematic studies of DNA, collagen, and CAP-DNA and the growth and vision of the NDB and PDB.

The NDB is supported by funds from the NSF. The RCSB PDB is supported by funds from NSF, NIGMS, Office of Science, DOE, NLM, NCI, NCRR, NIBIB, and NINDS. CAP-DNA studies are supported by NIGMS.

**AW.01.02 An Anthropological Review of the Development of mmCIF.** Paula M. D. Fitzgerald<sup>1</sup>, J. Westbrook<sup>2</sup>, <sup>1</sup>Merck Research Laboratories, Rahway, NJ, <sup>2</sup>Rutgers, State Univ. of New Jersey, Dept. of Chemistry and Chemical Biology, Piscataway, NJ.

The creation of the mmCIF dictionary was a community-based project, with input from many individuals within the crystallographic and related communities. As with any such project, particularly one that generated such a large and complicated data structure, there were many changes of direction along the way, and keeping the project moving forward was at times a major challenge.

The core team that guided the development of the dictionary consisted of Paula Fitzgerald, John Westbrook, Brian McMahon, Phil Bourne, Keith Watenpaugh, and our Buerger award winning Helen Berman. This presentation will focus on the human aspects of the project, in which Helen played a key role – particularly the fall weekends spent at Rutgers hammering out the original data model, followed over the next few years by workshops at York, Brussels, Tarrytown, and Rutgers elaborating the model and changing it to meet the desires of the community.

The mmCIF data model has now been fully vetted and published in the recent volume International Table of Crystallography Volume G: Definition and exchange of crystallographic data. The data model has been widely adopted, and this presentation will also survey the many ways in which the data model has facilitated the development of software that allows crystallographic commuting, structural bioinformatics, and data archiving to evolve while working in the context of a well-defined data structure.

**AW.01.03 Drug-Nucleic Acid Structures: Thirty Years On.** Stephen Neidle, CRUK Biomolecular Structure Group, The School of Pharmacy, Univ. of London, London WC1N 1AX, UK.

The recognition of nucleic acids by small molecules is of importance in the action of an extraordinarily wide range of drugs active against bacterial and fungal infections, viruses, human cancers and a number of parasitic diseases. These molecules have been mostly targeted against double-helical DNA, and their discrimination for particular sequences is based in large part on hydrogen-bonding to base-pair edges; the more subtle and detailed sequence-dependent differences in backbone geometry and base morphology are probably of lesser importance. All this has been revealed by single-crystal studies of drug-nucleic acid complexes and some of this information has been useful in drug design studies. More recently, it has become apparent

that some DNA sequences, notably those within guanine-rich tracts, can form a wide diversity of higher-order quadruplex structures. These present altogether much more selective drug targets.

This lecture will review the progress of drug-DNA crystallography during this period, taking as exemplars a number of complexes with acridine-based drugs.

**AW.01.04 Collagen Crystallography: From Early Fiber Diffraction to High-resolution Structures.** Jordi Bella, Wellcome Trust Centre for Cell-Matrix Research, Faculty of Life Sciences, Univ. of Manchester, Manchester M13 9PT, UK.

Fifty years ago the collagen triple helix was derived from fiber diffraction analysis. The resulting low-resolution models remained controversial for decades on the precise conformational parameters of the helices and the nature and patterns of hydrogen bonding. Crystallographic studies on synthetic peptides with collagen-like sequences have confirmed the essential features of the collagen triple helix and have clarified many of these long-standing controversies. High-resolution crystal structures have established that: (1) the collagen triple helix contains structural waters; (2) the degree of triple-helical twist is dependent on collagen sequence and environment; (3) the lateral packing of triple helices in the crystal lattices shows the intermolecular spacing and quasi-hexagonal arrangement seen in collagen fibrils; (4) peptides with an extremely simple charge distribution are capable of generating staggered arrangements; and (5) weak C $\alpha$ -H $\cdots$ O=C hydrogen bonding interactions occur systematically in the collagen triple helix and cooperate with conventional hydrogen bonds. This talk will review the main findings of the high-resolution crystallographic studies to date and will include new data from two recent crystal structure determinations.

**AW.01.05 Electron Cryomicroscopy of Macromolecular Assembly at Subnanometer Resolution.** W. Chiu, National Center for Macromolecular Imaging, Baylor College of Medicine, Houston, TX

Electron cryomicroscopy has been advanced to resolve structures of large macromolecular assemblies at resolution range of 5–10 Å without using crystals. At this resolution, we are able to resolve long alpha helices and large beta sheets of protein components or subunit domains of the assembly. Using model building, the folds of components and domains may be derived. Alternatively, if the crystal structures of components and domains are known, they can be docked into the cryomicroscopy density map by rigid body or flexible fitting. A valuable application of electron cryomicroscopy is to study the structural changes of assembly during different physiological states. Currently, all these structural informatics are not easily accessible to the public. An extension of the already successful infrastructure of PDB to archive the electron cryomicroscopy density map is certainly timely and critical. Such a publicly accessible structural informatics will provide biological end-users to mine structures and other biological information to understand structure and function relationship of assemblies which are the building blocks of physiological processes.

Acknowledgment: This research is supported by NIH grant P41RR02250.

**AW.01.06 Fragment Based Drug Discovery for Oncology Targets.** Stephen K. Burley, Chief Scientific Officer and Senior Vice-President Research, SGX Pharmaceuticals, Inc., San Diego, CA.

SGX Pharmaceuticals, Inc. (SGX) has developed a fragment based drug discovery platform that utilizes high-throughput X-ray crystallography for lead identification/optimization. The proprietary FAST<sup>TM</sup> (Fragments of Active Structures) process exploits crystallographic screening to detect, visualize, and identify small ligands (MW 150-

200) that are bound to the target protein. Each member of the *FAST*<sup>TM</sup> fragment/scaffold library was selected to be amenable to rapid chemical elaboration at two or three points of chemical diversity using parallel organic synthesis. Initial lead optimization involves using our knowledge of the co-crystal structure of the target-fragment complex and advanced computational chemistry tools to guide synthesis of small focused linear (one-dimensional) libraries. These linearly elaborated fragments/scaffolds are then evaluated with *in vitro* biochemical and cellular assays and co-crystal structure determinations. Thereafter, optimal variations at each point of chemical diversity are combined to synthesize focused combinatorial (two- or three-dimensional) libraries that are again examined with assays and crystallography. (The potential chemical diversity of the fully elaborated *FAST*<sup>TM</sup> fragment/scaffold library far exceeds 160 million compounds.) Active compound series are prioritized for further medicinal chemistry and compound development efforts using the results of *in vitro* and *in vivo* ADME and *in vitro* toxicology studies. Successful applications of the *FAST*<sup>TM</sup> fragment-based lead discovery/optimization process will be presented for a portfolio of well validated oncology targets, including wild-type and Gleevec-resistant BCR-ABL.

## AW.02 Warren Award The Development of Neutron Reflectometry and its Applications to Magnetism, Soft Matter, and Biology

**AW.02.01 Investigating the Structures of Thin Films and Multilayered Materials by Neutron Reflectometry.** C.F. Majkrzak, NIST Center for Neutron Research, Gaithersburg, MD 20899.

With both isotopic and magnetic sensitivity, neutron reflectometry has become an established technique for studying the nanometer scale structure of thin films and multilayered matter. From measurements of the intensity of specularly reflected neutrons, the depth profile of the scattering length density (SLD), and ultimately information about the chemical composition, along the surface normal can be deduced whereas nonspecular reflection reveals in-plane density variations. Specular neutron reflection with polarized beams yields the *vector* magnetization depth profile. Polarized neutron reflectometry studies of synthetically grown sandwiches and superlattices of magnetic layers interspersed with materials possessing other physical properties, such as superconductivity, have proven to be particularly powerful. Furthermore, with the development of exact methods for phase determination employing adjacent references, dynamical specular neutron reflection data can be directly inverted to obtain, in principle, and largely in practice, a unique SLD profile. An introduction to the basic theory and experimental methods of neutron reflectometry, together with a sampling of typical current applications in several different fields, is presented. In conclusion, the bright outlook for future advances in neutron reflectometry is considered.

**AW.02.02 Ordering and Orienting Block Copolymer Nanostructures: The Influence of Ions.** Thomas P. Russell, Polymer Science and Engineering Dept., Univ. of Massachusetts, Amherst, MA 01003.

The directed self-assembly of block copolymers is emerging as a simple tool for the fabrication of nanostructured materials. Trace ionic impurities or added salts are shown to have profound influence on the ease of orienting arrays copolymer microdomains and on inducing

ordering transitions that can reduce the size scale of the domains to the nanometer level using an applied electric field. Complexation of one of the blocks with salt is shown to markedly increase the segmental interactions, as evidenced by the narrowing of the interfacial width determined from neutron reflectivity measurements. In addition, the complexation, coupled with controlled solvent evaporation, is shown to provide a simple route to induce highly oriented arrays of the copolymer microdomains having long-range lateral order. By controlling the level of ions in the copolymer, the time scale over which the domain are ordered and oriented is markedly increased. Consequently, an avenue is opened in enhancing the processing of these versatile materials and opening potential routes to addressable nanostructured materials.

**AW.02.03 Neutron Reflectometry Investigation of Interfacial Structure in Tethered Polymer Systems.** M.D. Foster, Dept. of Polymer Science, The Univ. of Akron, Akron, OH 44325.

When a polymer chain is tethered to a surface or various portions of a polymer chain are tethered to one another, as in a long-branched polymer chain, the behavior of the polymeric material interface can be altered. Neutron scattering measurements have been key in elucidating both the bulk thermodynamics of binary polymer blends containing a linear component and a branched component and the interfacial behavior of these blends. Reflectometry is also useful for clarifying the internal structure of diblock copolymer brushes in which the tethering of each diblock chain to a surface results in interesting properties. This system represents a special case in which each chain exhibits both internal tethering of the one block to the other and tethering to a surface external to the molecule.

**AW.02.04 Ph-Dependent Conformational Changes and Insertion of Diphtheria Toxin Adsorbed to Lipid Membranes by Neutron and X-Ray Reflection.** M.S. Kent, H. Yim, S. Satija, I. Kuzmenko, Sandia National Laboratories, Albuquerque, NM.

Several important bacterial toxins, such as diphtheria, tetanus, and botulinum, invade cells through a process of high affinity binding, internalization via endosome formation, and subsequent membrane penetration of the catalytic domain activated by a pH drop in the endosome. These toxins are composed of three domains: a binding domain, a translocation domain, and an enzyme. In each case, the translocation process is not well understood with regard to the detailed conformational changes that occur at each step or how the relatively large catalytic domains can pass through the membrane. Several groups have recently advanced the hypothesis that the catalytic domains unfold and the translocation domains chaperone their refolding into translocation competent conformations. To begin to address this, we performed neutron reflectivity measurements for diphtheria toxin bound to lipid membranes as a function of pH. Work to date has focused on the early stages. In particular, we show that no adsorption occurs at pH = 7.6, but strong adsorption occurs over a pH range from 6.5 to 6.0. Upon binding at pH 6.5, the toxin can be modeled as a single layer. However, upon further acidification at least two domains can be resolved and these undergo distinctly different conformational changes with pH. At least two stages of conformational change occur, as the thickness of the outer layer increases from pH 6.3 to 5.3 and then decreases from pH 5.3 to 4.5. In addition, the extent of segment insertion into the membrane was determined at various pH values by X-ray reflection and grazing incidence X-ray diffraction.

**AW.02.05 Neutron Reflectometry from Biological Thin Films at the NIST Center for Neutron Research: Past, Present and Future.**

S. Krueger, NIST Center for Neutron Research, Gaithersburg, MD.

During the past decade, neutron reflectometry has increasingly become an important technique for the characterization of supported planar biological and biomimetic thin films. Advancements in instrumentation, sample environment and measurement protocols now make it possible to obtain Angstrom-level information about the composition of these materials along the axis perpendicular to the plane of the membrane. A newly developed phase-sensitive neutron reflectometry technique now allows direct inversion of the reflectivity data to obtain unique compositional depth profiles of the films. The development of these neutron reflectometry methods at the NIST Center for Neutron Research will be reviewed and some examples pertaining to the study of peptide and protein interactions with planar bilayer model membranes will be illustrated. The use of neutron reflectometry for the study of systems of importance for biomedical and bioengineering applications will also be examined. Examples of the characterization of such systems using the phase-sensitive neutron reflectometry technique will be presented. Finally, future experiments will be discussed in light of advances in both experiment and computational techniques.

**AW.02.06 Bio-Membranes: X-ray and Neutron Scattering Studies.** J. Majewski, C. Miller, T. Kuhl\*, Los Alamos National Laboratory, Los Alamos, NM, \*Univ. of California, Davis, CA.

Cells are highly organized with many functional units defined by lipid membranes. The lipid membrane, composed of lipid and proteins molecules, forms a barrier to keep various gradients between the inside and outside of the cell and perform functions from selective transport and recognition to sequestration.

Several scattering techniques have been developed for probing the surface structure of the 2-D arrays of lipids at different interfaces. These include neutron and x-ray reflectometry and x-ray grazing incidence diffraction. As will be shown in this presentation, these techniques can be successfully implemented for studying structures of lipid membranes and their interactions with bio-polymers (for example, toxins) with sub-nanometer resolution.

The properties of bio-membranes are of general interest to a wide scientific audience working in the fields of chemistry and biology since they are relevant to such areas as biosensors, advanced drug delivery, and polymer-membrane interactions. Understanding how membranes assemble on the *nm*-scale would be profound for the understanding of how bacteria, toxins, and viruses penetrate cell walls and are transmitted.

Work supported by DOE contract W7405-ENG-36 and the DOE Office of Basic Energy Sciences.

**AW.02.07 Polarized Neutron Reflectivity for the Analysis of Nanomagnetic Systems.** H. Zabel, K. Theis-Broehl, B.P. Toperverg, Dept. of Physics, Ruhr-Univ. Bochum, D 44780 Bochum, Germany.

In recent years polarized neutron reflectivity has played an essential role for the exploration of magneto- and spintronic nanostructures. Well known systems extensively studied include exchange coupled magnetic superlattices, exchange spring valves between soft and hard magnetic films, exchange bias systems between ferromagnetic and antiferromagnetic films, and more recently magnetic semiconductors and ferromagnetic Heusler alloy films and superlattices. In addition to studies of layered systems, neutron scattering has now also expanded in the direction of laterally structured magnetic media such as stripes and islands on the sub-micrometer scale. Although the competition with x-ray resonant magnetic scattering (XRMS) has increased in recent years, there are some advantages PNR offers that are hard to challenge.

Those are the analysis of the data with the Born approximation or with the distorted wave Born approximation (DWBA), the well known cross sections, and the magnetic spin flip scattering, which has no counterpart in XRMS. The latter one allows evaluation of magnetization fluctuations transverse to the neutron polarization axis and gives access to magnetic roughness and magnetic domain states. In this contribution specular and off-specular PNR work of most recent examples from Heusler alloy multilayers and lateral exchange biased stripes will be presented.

**AW.02.08 Origin of Positive and Negative Exchange Bias in Co/FeF<sub>2</sub>.** M.R. Fitzsimmons, B. Kirby, Los Alamos National Laboratory, Los Alamos, NM 87545, S. Roy, Zhi-Pan Li, Igor V. Roshchin, S.K. Sinha, Ivan K. Schuller Dept. of Physics, Univ. of California - San Diego, La Jolla, CA 92093.

Exchange coupling across an antiferromagnetic-ferromagnetic interface can produce a shift of the ferromagnetic hysteresis loop about the zero of applied field; hence the phenomenon is called exchange bias. The shift can be very large; thus, in small fields, typical of applications in magnetic recording or magnetic random access memory, the magnetization of the ferromagnet is effectively pinned, providing a magnetic reference state required in these applications. Despite the technological importance of exchange bias, a detailed understanding of its origin has been elusive. A critical piece that has long been missing is quantitative information about the spatial distribution of pinned and unpinned magnetization in exchange bias systems. We have used polarized neutron beams with polarization analysis to obtain the magnetization depth profile across an exchange bias bilayer comprised of Co (the ferromagnet) and FeF<sub>2</sub> (the antiferromagnet). Our Co/FeF<sub>2</sub> system is unusual in that depending upon the magnitude of the field in which the sample was cooled (through the Néel temperature of FeF<sub>2</sub>), the exchange bias can be either positive or negative. By comparing the magnetization depth profiles of the same sample for the two biases, we were able to identify how the distribution of pinned magnetization changes with the sign of bias, providing a unique insight into the origin of positive and negative exchange bias.

Work funded in part by the U.S. DOE, BES-DMS.

**AW.02.09 Magnetic Behavior of Rare Earth Thin Films and Superlattices.** Ph. Mangin\*, K. Dumesnil+, C. Dufour+, \*Laboratoire Léon Brillouin CEA/CNRS UMR12, Gif sur Yvette 91191 France, +Laboratoire de Physique des Matériaux, Univ. Henri Poincaré/CNRS UMR 7556, BP 239, 54506 Vandoeuvre les Nancy France.

Since the pioneering works of C.F. Majkrzak et al [1] et Salamon et al [2] on Gd/Y and Dy/Y superlattices, a lot works have been devoted to the magnetic behavior of epitaxial films and superlattices of rare earths. We first summarize the results obtained on a lot of systems exhibiting a large variety of behaviors. Then we present recent results from bcc-europium. Eu thin films exhibit a helical magnetic ordering along the cubic axes [100], [010] (out of the plane of the sample) and [001] (in the plane of the sample), which gives rise to three kinds of magnetic domains D1, D2 and D3 respectively. As the temperature is lowered, two phenomena are observed: i) The wave vectors of the D1 and D2 domains leave the cubic directions and rotate through an angle  $\beta(T)$ . ii) The D3 domains vanish and are only restored if a critical field  $H_c(T)$  is applied along [001].  $\beta(T)$  and  $H_c(T)$  are shown to be correlated to the epitaxial strains and we will discuss several mechanisms including magnetoelastic contributions and exchange anisotropy induced by the deformations [3].

[1] C.F. Majkrzak et al. Phys. Rev. Lett. 56,2700(1986), [2] M.B. Salamon et al. Phys. Rev. Lett. 56,259(1986), [3] S. Soriano et al. Phys. Rev. B71, 092409(2005)

**AW.02.10 Elements of Neutron Specular Reflection Phase-Inversion.** N.F. Berk, NIST Center For Neutron Research, 100 Bureau Dr., Gaithersburg, MD 20899.

Neutron specular reflection probes the laterally averaged scattering length density (SLD) depth profile of thin films. The power of the technique stems in part from its underlying mathematical coherence. Because specular reflection can be cast formally as a one-dimensional wave mechanics problem, it admits to exact solutions of both the “direct” problem of calculating the reflection amplitude spectrum from any SLD profile, and of the “inverse” problem of retrieving the SLD profile from the amplitude spectrum. The formalities establish a one-to-one correspondence between the amplitude spectrum and the profile (for a broad and useful class of SLD profiles), thus enabling reliable interpretations of neutron measurements. What is needed to complete the direct-to-inverse cycle are the means of determining the complex reflection amplitude from measurements of its square modulus, the reflectivity. Reference-layer methods have been developed to solve this “phase” problem exactly for neutrons, thus making “phase-inversion” a realistic measurement technique. In this talk we summarize the basic formal and practical elements of phase-inversion.

**AW.02.11 Echoes from Nanostructured Films.** Roger Pynn, Physics Dept., Indiana Univ., Bloomington, IN 47405.

In spite of the success of neutron reflectometry in providing many key insights into the layering of natural and man-made thin films, the technique has provided little information about the lateral structure of such films. Partly this is a result of the fact of their weak scattering. This is exacerbated by fact that structural motifs are often large compared to the neutron’s wavelength so neutron beams have to be well collimated to obtain information about lateral structure by conventional diffraction techniques. In an attempt to overcome these limitations, a number of groups are pursuing a technique that uses Neutron Spin Echo to measure scattering angles for uncollimated beams. I will discuss the use of birefringent prisms to implement this method. The essence of the idea is to separate the two quantum spin states of a neutron in space using suitable magnetic prisms. The two quantum states interact with the scattering sample at different points in space and are then recombined by further prisms. The interference between the two quantum states is used to determine the correlation between the scattering potentials at the two scattering points. Conceptually, understanding the apparatus used for these studies is almost identical to understanding why a ray of light passes through a glass slab with a lateral displacement of its trajectory.

**AW.02.12 Off-Specular Grazing Incidence Scattering from Surfaces: Theory and Applications.** Sunil K. Sinha Physics Dept., Univ. of California San Diego, La Jolla, CA 92093, LANSCE, Los Alamos National Laboratory, NM 875411.

Grazing incidence scattering studies of surfaces, in the form of off-specular diffuse scattering, grazing incidence small angle scattering and grazing incidence diffraction have become active areas of research and are a useful complement to specular reflectivity studies. Such studies are now being carried out at most major facilities with X-rays and neutrons to study the morphology of both magnetic and non-magnetic interfaces. We shall briefly review how these types of scattering can be analyzed to yield information about quantities such as structural and magnetic roughness, domains and patterning in thin films, dot arrays and thermal interface fluctuations. We shall illustrate this with examples from recent experiments. The use of coherent X-ray beams in such studies will also be discussed.

The work reported here was carried out at the Advanced Photon Source, Argonne, the

Advanced Light Source Berkeley and the Manuel Lujan Neutron Scattering Facility, Los Alamos. This work has been supported by Grant DE-FG02-03ER46084 from Basic Energy Sciences, D.O.E.

## AW.03 Etter Early Career Award

**AW.03.01 X-rays, Action, Camera! The Joys and Heartaches of Making Movies of Redox Enzymes in Motion.** Carrie M. Wilmut, Dept. of Biochemistry, Molecular Biology & Biophysics, Univ. of Minnesota, Minneapolis, MN 55455.

Except in rare cases, X-ray crystal structures of enzymes are at the resolution of medium sized atoms, not the individual electrons/protons that reveal the details of catalysis. In contrast, various spectroscopic techniques are very good at defining the positions of electrons/protons. By combining crystallography and spectroscopy a level of structural insight can be achieved that has never before been possible. Many enzymes are catalytically active in the crystal, and due to the restraints imposed by the crystal lattice the rates of individual reaction steps are often slower than in solution. This means that transient reaction intermediates that have been difficult to characterize in solution, build up to accessible levels in crystals. By running kinetics in crystals, the extraordinary potential to “see” these intermediates, and then solve their structures to near atomic resolution, is enormous. Flash freezing is used to press the “pause” button on the enzymatic reaction in the crystal, while spectroscopy ensures the correct assignment of the catalytic state of the crystalline enzyme, and allows the resulting X-ray crystal structure “snapshot” to be precisely placed along the reaction co-ordinate to build up a “movie” of catalysis at the molecular level.

**AW.03.02 Effect of Hydrophobic Mutations on Proton Transfer and Active Site Structure in Human Carbonic Anhydrase II.** S.Z. Fisher<sup>§</sup>, D. Bhatt<sup>¶</sup>, C.K. Tu<sup>¶</sup>, M. Agbandje-McKenna<sup>§</sup>, D.N. Silverman<sup>¶</sup>, R. McKenna<sup>§</sup> <sup>§</sup>Dept. of Biochemistry and Molecular Biology, <sup>¶</sup>Dept. of Pharmacology and Therapeutics, College of Medicine, Univ. of Florida, Gainesville, FL, 32610.

The mammalian  $\alpha$ -carbonic anhydrases ( $\alpha$ -CAs) are ubiquitous zinc metalloenzymes that catalyze the reversible hydration carbon dioxide to form bicarbonate. The rate-limiting step in catalysis by human CA II is the transfer of a proton from the Zn-H<sub>2</sub>O to bulk solvent via the proton-shuttling residue, H64. The intra-molecular proton transfer proceeds through a well-ordered chain of H-bonded solvent molecules. The solvent molecules are coordinated through H-bonds by several active site residues and other solvent molecules. We have constructed, three single site CA II mutants, replacing 3 polar residues that assist in the solvent coordination with hydrophobic residues (Y7F, N62L, and N67L). We report the crystal structures of all 3 mutants (1.6 – 1.8 Å resolution) at different pHs (6.0- 10.0), and discuss the observed conformational changes in the active site architecture, solvent order, and subsequent measured increases and decreases in proton transfer efficiencies, as compared to wild type CA II.

**AW.03.03 Structural Studies in Rieske Dioxygenase Electron Transport.** E.N. Brown, D. Ferraro, C.-L. Yu, D.T. Gibson, S. Ramaswamy, Dept. of Biochemistry, Univ. of Iowa, Iowa City, IA 52242.

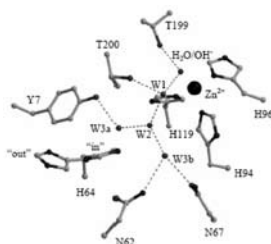
Rieske dioxygenase systems are multi-protein systems of interest for their potential use in “green” chemistry, drug precursor synthesis, and environmental cleanup. Commercial use of dioxygenase systems requires an understanding of substrate specificity, product stereospecificity, and electron transport efficiency. New structures of the Rieske ferredoxin component of two dioxygenase systems are presented:

*Pseudomonas putida* Naphthalene Dioxygenase Ferredoxin and *Sphingomonas yanoikuyae* B1 Biphenyl Dioxygenase Ferredoxin. Continuum electrostatics methods accurately predict ferredoxin reduction potential based solely on the structures of 13 Rieske ferredoxin proteins ( $R^2 = 0.94$ ). Potential binding interactions between Rieske ferredoxin proteins and dioxygenase enzymes are determined with computational docking and refined using molecular dynamics simulations. Resulting Rieske [2Fe-2S] cluster distances of 11 – 14 Å are compatible with intra-protein electron transfer.

We thank ESRF for access to beamline ID14-1 and IMCA-CAT for access to beamline 17-ID. This research is supported by a graduate student fellowship from the University of Iowa Center for Biocatalysis and Bioprocessing and USPHS Grant #GM62904.

**AW.03.04 Structures of Wild Type *E. coli* Adenylosuccinate Lyase and a Mutant-substrate Complex Provide New Insights Into the Enzymatic Mechanism.** M. Tsai<sup>1,2</sup>, P. Yip<sup>1</sup>, J. Koo<sup>1,2</sup>, M.L. Segall<sup>3</sup>, R.F. Colman<sup>3</sup>, P.L. Howell<sup>1,2</sup>, <sup>1</sup>Hospital for Sick Children, <sup>2</sup>Univ. of Toronto, Toronto, Ont., Canada; <sup>3</sup>Univ. of Delaware, Newark, DE.

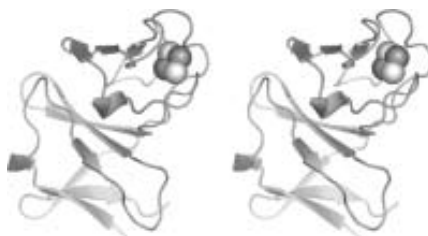
Adenylosuccinate lyase (ADL) participates in the *de novo* purine biosynthetic pathway where it catalyzes the breakdown of adenylosuccinate (ADS) to AMP and fumarate. ADL is a member of the class II fumarase superfamily, which includes argininosuccinate lyase (ASL)/ $\delta 2$ -crystallin, fumarase C, L-aspartase, and 3-carboxy-*cis-cis*-muconate lactonizing enzyme. To gain further insight into the ADL enzymatic mechanism, and those of the other superfamily members, we have determined the crystal structures of wild type *E. coli* ADL and an H171A mutant with bound substrate to 2.0 and 1.85 Å resolution, respectively. The H171A-ADS complex has enabled us to precisely identify for the first time the residues involved in substrate binding, as well as the putative catalytic residues for this enzyme. Furthermore, structural comparisons suggest conformational changes occur in ADL upon substrate binding and catalysis, similar to those observed previously in ASL/ $\delta 2$ -crystallin. Details regarding the catalytic mechanism of ADL and those of other superfamily members have been re-examined in light of the current results.



**AW.03.05 X-ray Structural, Thermodynamic and Laser T-jump Kinetic Studies of Villin.** Thang K. Chiu, Jan Kubelka, James Hofrichter, William A. Eaton, David R. Davies. Lab of Molecular Biology, NIDDK, NIH, 9000 Rockville Pike, Bethesda, MD 20892.

Understanding the fundamental processes which govern protein folding is medically important because protein misfolding are associated with numerous diseases.

We have used x-ray crystallography, CD spectroscopy and laser T-jump kinetic measurements to study the folding of a 35 amino acid fragment of the villin headpiece domain. This is the smallest naturally occurring protein which folds without the need for ion or ligand, and has been the subject of numerous molecular dynamics simulations to study its folding behavior. Our atomic resolution x-ray structures reveal important details of packing of the hydrophobic core and some new features, such as inter-helical hydrogen bonds which bridge adjacent alpha helices. In addition, the structure and folding parameters of several mutants were determined to high-

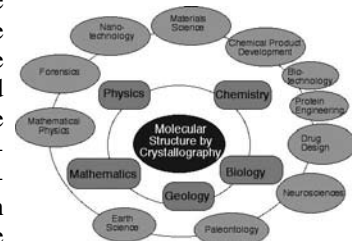


light the contribution of each residue to the overall folding of this small protein. We observed that removal of two buried charges reflected in the norleucine for lysine substitutions dramatically stabilizes the protein and increases its folding rate. Thus, relief of electrostatic repulsion among charged residues may play a key role in protein folding. This double mutant is the fastest-folding protein observed to date: ~700 ns. To better understand the contribution of the hydrophobic core to overall folding, we also determined the x-ray structure of a much smaller peptide fragment. This structure may shed some light on the folding pathway of its larger 35 amino acid counterpart.

## SP.01 Undergraduate Research Showcase

**SP.01.01 Sustaining Crystallography in the 21<sup>st</sup> Century: Crystallography Education Policies for the Physical and Life Sciences.** K.A. Kantardjieff, Keck Center for Molecular Structure, CSU Fullerton, U.S. National Committee for Crystallography and American Crystallographic Assn.

The USNC/Cr conducted two surveys to determine the content and extent of coverage of crystallography in university curricula, as well as the views of the greater crystallographic community on the status of crystallography education and training in the US, in both physical and life sciences. Recognizing the opportunity to communicate to the broader scientific community the research opportunities afforded by crystallography, as well as the value of crystallographic information, the ACA and USNC/Cr organized an education summit, which took place at the conclusion of the ACA national meeting in Orlando.



The outcome is a consensus policy statement on crystallography education and training that makes recommendations for a comprehensive re-evaluation of crystallography education and suggests ways to develop in the broader scientific community an appreciation for the value of crystallographic information. The ACA and USNC/Cr intend that this white paper on crystallography education and training provides guidelines to professional societies and academic departments for crafting future crystallography curricula.

The education summit was funded by the USNC/Cr, ACA, CSUPERB and the NSF.

**SP.01.02 The STaRBURSTT - CIC - Teaching Initiative.** A.D. Hunter<sup>a</sup>, P.S. Szalay,<sup>i</sup> M. Zeller,<sup>a</sup> M. Bond,<sup>b</sup> R.J. Butcher,<sup>c</sup> G. Crundwell,<sup>d</sup> G.M. Ferrence,<sup>e</sup> K. Kantardjieff,<sup>f</sup> L. Ramirez,<sup>g</sup> T. Higgins<sup>h</sup>, <sup>a</sup>Youngstown State Univ., <sup>b</sup>South East Missouri State Univ., <sup>c</sup>Howard Univ., <sup>d</sup>Central Connecticut State Univ., <sup>e</sup>Illinois State Univ., <sup>f</sup>California State Univ. Fullerton, <sup>g</sup>East Los Angeles College, <sup>h</sup>Harold Washington College, <sup>i</sup>Muskingum College.

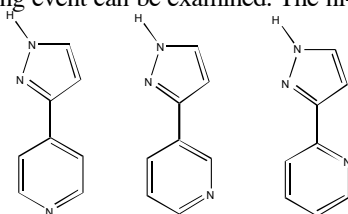
The STaRBURSTT-CIC (Science Teaching and Research Brings Undergraduate Research Strengths Through Technology - CyberInstrumentation Consortium) is a national consortia of made up primarily of Predominantly Undergraduate Institutions, Historically Black Colleges and Universities, and Hispanic Serving Institutions having strong interests in X-ray diffraction. This presentation will emphasize new curriculum materials developed and tested by this



group, including: computer labs on structure determination, local and remote access labs for unknown structure determination, and mini- and full scale student research projects; safety procedures; crystal growth; the selection, mounting, and evaluation of crystals; data collection strategies, structure solution using SHELX, powder diffraction for bulk phase confirmation, using crystallographic data bases, and writing and evaluating crystallographic papers. The remote collection of crystallographic data via the internet will be emphasized.

**SP.01.03 The Good, the Bad, and the Ugly: Balancing Interactions that Drive the Formation of Co-Crystals.** Meg E. Fasulo, Christer B. Aakeroy, John Desper, Dept. of Chemistry, Kansas State Univ., Manhattan, KS.

Pyrazole and pyridine both have the ability to form co-crystals when combined with carboxylic acids. When these two moieties are united in the same molecule, an interesting event can be examined. The nitrogen atom of the pyridine ring is considerably more basic than the nitrogen atom of the pyrazole ring, meaning that it is a much better hydrogen-bond acceptor. However, the N-H of the pyrazole is much more acidic than the C-H of the pyridine ring, meaning it is a much better hydrogen-bond donor. Will the combination of a bad acceptor and good donor (pyrazole) outweigh the combination of a good acceptor and bad donor (pyridine) when interacting with carboxylic acids? This talk will focus on synthesis and characterization of 3-(pyridyl)pyrazole ligands, and examine the site at which interactions with carboxylic acids occur.



**SP.01.04 A Systematic Approach to the Selection of Automated Docking Programs for Screening and Structure-Based Inhibitor Design.** Katagiri, Kazuo, Xia, Jiarong, Stieglitz, Kimberly, Dept. of Chemistry, Univ. of Massachusetts, Boston, MA.

A structural-based approach to drug design and screening has become increasingly important as the number of protein-ligand complexes available in the Protein Data Bank continues to increase rapidly. A large number of molecular docking programs have recently been developed with the goal of extracting all available structural and chemical information that can be derived from proteins, ligands and protein-ligand complexes.

The quality of the results from virtual screening is directly related to the ability of a particular software program to position the ligands into a targeted binding site (called a targeted receptor molecule) with accuracy and precision. Because of the different algorithms used by various docking programs combined with the inherent differences in shape of a binding pocket for ligand-bound proteins, a particular program may be appropriate for one targeted binding site, while another docking program may not. In order to better understand and reconcile these differences, three docking programs are evaluated for accuracy and precision in this comparative study: AutoDock3, DOCK5, Surflex, and GOLD. Differences between the algorithms of these programs are presented. A novel method utilizing geometric shapes to characterize specific binding pockets is presented to select the best match of docking program and protein-ligand structure. Two allosterically regulated proteins are utilized in the evaluation of the docking programs: Aspartate Transcarbamoylase and Fructose 1-6 biphosphatase (FBPase). Each program “claims” to be superior to the other. Testing the programs against the target receptor site with known inhibitors already evaluated through “actual” not “virtual” screening provides the most

effective method to select the appropriate program for each individual binding site. An automated approach to evaluating docking programs for use with available structures in the protein data bank is presented.

## TR.01 The Future of Neutron Crystallography: Smaller Crystals, Larger (Macro) Molecules

**TR.01.01 Capabilities of Single-crystal Neutron Diffraction: A Summary and a Discussion of Future Potential.** Robert Bau, Chemistry Dept., Univ. of Southern California, Los Angeles CA 90089.

The various capabilities of single crystal neutron diffraction are presented in this introductory talk. In brief, the technique is currently being used for (1) accurately locating the positions of light atoms (in most cases hydrogen) in molecules when they are surrounded by much heavier atoms (for example, H atoms in metal cluster complexes); (2) distinguishing between certain isotopes (most notably H from D), and (3) studies of magnetic structure. In some cases, examples from the author’s own work will be presented to illustrate the usefulness of the technique. Advantages as well as disadvantages of single-crystal neutron diffraction will be discussed, and future directions will be prominently featured: in particular, new facilities will be described which are intended to markedly reduce (a) crystal size and/or (b) data collection times. Finally, we will mention very briefly exciting new developments in the applications of this technique to macromolecular structure, which will be elaborated in more detail by subsequent speakers in this Transactions Symposium.

**TR.01.02 Single Crystal Diffraction at Pulsed Neutron Sources: Present and Future Capabilities.** A.J. Schultz, IPNS, Argonne National Laboratory, Argonne, IL 60493.

The single crystal neutron time-of-flight Laue technique for small molecule crystallography has been very successful at pulsed sources such as the IPNS and at the ISIS (UK) facility. Some examples of recent accomplishments will be presented. For larger macromolecules, the Protein Crystallography Station [1] has been in operation since 2002 at the Los Alamos LANSCE spallation neutron source. Two new sources with much higher flux that will begin producing neutrons either this year or in the near future are the JSNS in Japan and the SNS at the Oak Ridge National Laboratory, USA. At the SNS, the small molecule diffractometer, Topaz, is under construction and will be available for users in 2009. It will allow data collection on “x-ray size” crystals, which is predicted to have a major impact on neutron chemical crystallography. During the past three years we have also developed and optimized the design for a macromolecular neutron diffractometer (MaNDi) which will be capable of collecting complete data sets for macromolecular crystals in as little as one day [2]. DOE has now approved its construction at the SNS and a beam line position has been secured.

Work at Argonne was supported by the U.S. DOE, BES-MS.

[1] P. Langan *et al.*, *J. Appl. Cryst.* **2004**, *37*, 24.

[2] A. J. Schultz *et al.*, *J. Appl. Cryst.* **2005**, *38*, 964.

**TR.01.03 Beyond the Folding Structure of Biomolecules. Structural Chemistry and Molecular Recognition in Biomolecules Evolved at J-PARC.** Nobuo Niimura, Inst. of Applied Beam Science, Ibaraki Univ., Hitachi 316 8511, Japan.

The J-PARC project in Japan for a 1 MW spallation neutron source is now under construction. There, the construction of dedicated neutron diffractometer for protein crystallography named BIX-P1 is also un-

der construction. At the new instrument, the neutron intensity at the sample position will become about 100 times higher than at the current BIX-type diffractometer installed at JRR-4 in JAEA.

Neutron bio-macromolecular crystallography provides the accurate information of hydrogen & hydration in proteins and nucleic acids. This will open the new field beyond the folding structure of bio-macromolecules such as:

- 1) Recognition of proteins and nucleic acids through the network structure of water molecules surrounding bio-macromolecules, and
- 2) The nature of chemical bond in proteins and nucleic acids elucidated by the accumulation of accurate structural information of hydrogen atoms.

**TR.01.04 LMX: Large Molecule Neutron Diffractometer for Supramolecular Chemistry and Biological Structure.** Lee Brammer, Dept. of Chemistry, Univ. of Sheffield, Brook Hill, Sheffield S3 7HF, UK, lee.brammer@sheffield.ac.uk

In the past neutron diffraction has required the use of very large crystals due to flux limitations and has been confined to the study of systems with relatively small numbers of independent atoms. A major change is taking place with the development of new diffractometers and new (spallation) sources that promises to deliver opportunities to study crystals of a size that was in common usage for X-ray diffraction only 20-30 years ago. Much larger unit cells will also be accessible.

This talk will focus on the potential new areas of chemistry, materials and structural biology that will become accessible to structural investigation by neutrons in the coming years. In the UK, our efforts are focussed on development of the LMX diffractometer on the new cold neutron target station (TS2) at the ISIS spallation neutron source. The areas of application we envisage for this new instrument include supramolecular chemistry, organometallic chemistry, molecular magnets and single molecule magnets, zeolites and inorganic framework materials, organometallic chemistry, partially ordered fibers of synthetic and biological polymers and protein crystallography.

**TR.01.05 Protein Crystallography with Spallation Neutrons.** Leighton Coates, Paul Langan, Benno Schoenborn, Bioscience Div., MS M888, Los Alamos National Lab, Los Alamos, NM, 87545.

The PCS (Protein Crystallography Station) at Los Alamos Neutron Science Center, is a high performance neutron protein crystallography beam line funded by the office of Biological and Environmental Research of the U.S. Department of Energy. Beam-time is free to expert and non-expert users and is allocated twice a year through a call for proposals and a peer review process.

Although most protein structures are determined using X-rays the position of hydrogen atoms and the coordination, sometimes even the position of water molecules cannot be directly determined at resolutions typical for most protein crystals. Hydrogen atoms are the primary motive force in most enzymatic processes. Neutron diffraction is a powerful technique for locating hydrogen atoms even at resolutions of 2-2.5 Å and can therefore provide unique information about enzyme mechanism and hydrogen bonding.

**TR.01.06 Neutron Diffraction from Cyclodextrin Hydrates to Photosystem II.** W. Saenger, Inst. of Chemistry & Biochemistry /Crystallography, Free Univ. Berlin, Takustr. 6, 14195 Berlin, Germany.

Cyclodextrins or cycloamyloses consist of 6 to 10  $\alpha$ -1,4 linked D-glucoses with 3 O-H groups in each glucose. The neutron structures

of their hydrates show extended networks of  $\cdots\text{O}\cdots\text{H}\cdots\text{O}\cdots\text{H}\cdots\text{O}\cdots\text{H}\cdots$  hydrogen bonds that are mostly homodromic (in the same direction) and cooperative. These motifs will be illustrated with cyclodeca-amylose  $\bullet 27 \text{H}_2\text{O}$ . In cycloheptaamylose  $\bullet 12 \text{H}_2\text{O}$ , many of the  $\text{H}_2\text{O}$  and O-H groups are disordered, giving rise to flip-flop hydrogen bond disorder that is due to rotation of O-H groups and is dynamic,  $\text{O}\cdots\text{H}\cdots\text{O} \leftrightarrow \text{H}\cdots\text{O}\cdots\text{H}$  [1]. The flip-rate was determined by quasi-elastic neutron scattering [2].

Photosystem II is embedded in the thylakoid membrane of plants. The cyanobacterial variety consists of 20 protein subunits and 77 cofactors, the most interesting being a cluster consisting of 4 Mn(III) and Mn(IV) cations and one Ca(II), in short  $\text{Mn}_4\text{Ca}$ , where water is oxidized to atmospheric oxygen [3]. Since X-rays rapidly reduce  $\text{Mn}_4\text{Ca}$  to inactive Mn(II) associated with destruction of the  $\text{Mn}_4\text{Ca}$  architecture, neutron diffraction is the radiation of choice to derive the true architecture of  $\text{Mn}_4\text{Ca}$ .

W. Saenger et al., Chem Rev. 98, 1787-1802 (1998).

T. Steiner et al., Mol. Phys. 72, 1211-1232 (1991).

B. Loll et al., Nature 438, 1040-1044 (2005).

**TR.01.07 Complementary 2.2Å Neutron and 0.8Å X-Ray Diffraction Studies Reveal a Catalytic Proton Pathway in Fully Deuterated Human Aldose Reductase.** A. Podjarny<sup>1</sup>, A. Mitschler<sup>1</sup>, M. Blakeley<sup>2</sup>, F. Ruiz<sup>1</sup>, S. Ginell<sup>3</sup>, M. Haertlein<sup>4</sup>, I. Hazemann<sup>1</sup>, F. Meilleur<sup>4</sup>, A. Joachimiak<sup>3</sup>, D. Myles<sup>2</sup>, <sup>1</sup>IGBMC, CNRS, ULP, INSERM, Illkirch, France, <sup>2</sup>EMBL Grenoble Outstation, ILL, Grenoble, France, <sup>3</sup>SBC, ANL, Argonne, IL 60439, <sup>4</sup>ILL, Grenoble, France.

The enzymatic mechanism of human aldose reductase (h-AR) includes a hydride donation from the coenzyme NADPH and a proton donation from the enzyme. Neutron Laue diffraction data from the fully deuterated protein (h-AR(D), ILL, Grenoble) complexed with the inhibitor IDD594 and  $\text{NADP}^+$ , were collected to a resolution of 2.2 Å at room temperature with a small crystal (0.15 mm<sup>3</sup>). The neutron density maps increased the overall observation rate of H(D) atoms from 54 % (0.66 Å X-ray data) to 61 % (neutron data). This increase is most evident for the mobile H(D) atoms ( $B > 5 \text{Å}^2$  at 100K). Furthermore, the identity between the complexes of h-AR(D) and of h-AR(H) was demonstrated by a helium-cooled X-ray structure of h-AR(D) ( $C\alpha$  rms difference = 0.1Å; 15K; SBC-191D, resolution 0.8Å, mosaicity 0.2°, R-merge 2.3 %, R-Factor 11.5%). The h-AR(D) X-ray structure suggested a catalytic proton pathway W-Asp43-Lys77-Tyr48, which could be clearly confirmed by the neutron structure.

**TR.01.08 Location of Active-site Hydrogen Atoms in D-Xylose Isomerase.** Gerard J. Bunick<sup>§</sup>, Amy Katz<sup>\*§</sup>, Xinmin Li<sup>§</sup>, Jenny P. Glusker<sup>\*</sup>, H.L. Carrell<sup>\*</sup>, B.L. Hanson<sup>^</sup>, Paul Langan<sup>#</sup>, Leighton Coates<sup>#</sup>, Benno Schoenborn<sup>#</sup>, <sup>§</sup>Univ. of Tennessee, Knoxville, TN, <sup>\*</sup>Fox Chase Cancer Center, Phila., PA, <sup>^</sup>Univ. of Toledo, Toledo, OH, <sup>#</sup>Biosciences Div., LANL, Los Alamos, NM.

Time-of-flight neutron diffraction has been used to locate hydrogen atoms that define the ionization states of amino acids in D-xylose isomerase (XI) from *Streptomyces rubiginosus*. XI is one of the largest enzymes studied to date at high resolution (1.8 Å) by this method. We have determined the position and orientation of a metal ion-bound water molecule located in the active site. This water is thought to be involved in the isomerization step in which D-xylose is converted to D-xylulose or D-glucose to D-fructose. Under the conditions of measurement (pH 8.0) it is found to be a water molecule rather than a hydroxyl group. One lysine appears to have an  $-\text{NH}_2$  terminal group (rather than  $\text{NH}_3^+$ ). The ionization state of each histidine residue has also been determined. High-resolution X-ray studies (0.94 Å) indicate disorder in some side chains when a truncated substrate is bound. This suggests

how they might move during catalysis. This combination of techniques can contribute greatly to the elucidation of enzyme mechanisms.

Research supported by NIH GM-29818, CA-10925, CA-06927, NASA NAG8-1826, and the USDOE Office of Science, OBER.

**TR.01.09 Neutron Diffraction Structure of *E. coli* Dihydrofolate Reductase in Complex with the Chemotherapeutic Methotrexate at 2.2Å Resolution.** Brad Bennett\*, Paul Langan†, Leighton Coates†, Marat Mustyakimov†, Benno Schoenborn†, Elizabeth Howell\*, Chris Dealwis\*\*, \*Dept. of Biochemistry, Cellular and Molecular Biology, Univ. of Tennessee, Knoxville, TN, †Los Alamos National Lab, Biosciences Div., Los Alamos, NM.

The role hydrogen atoms play in biochemical processes cannot be overstated, yet they are difficult to visualize by X-ray crystallography. Neutron crystallography has a proven track record in locating hydrogen, but limited neutron fluxes and accessibility to reactor sources have made it impractical. Spallation neutron sources provide a new arena for protein crystallography, as higher fluxes and time-of-flight measurements enhance data collection efficiency. Here we report a 2.2Å resolution neutron structure and a 1.0Å ultrahigh resolution X-ray (UHRX) structure of *E. coli* Dihydrofolate Reductase (DHFR) in complex with methotrexate (MTX), a chemotherapeutic agent. Neutron data were collected on a 0.25mm<sup>3</sup> D<sub>2</sub>O-soaked crystal at the Protein Crystallography Station (PCS) at the spallation source operated by Los Alamos Neutron Scattering Center (LANSCE). This study provides an example of using spallation neutrons to identify protonation states *directly* in macromolecules from nuclear density maps. In particular, the neutron structure reveals the N1 atom of MTX is protonated, and thus charged, when MTX is bound to DHFR. In contrast, the UHRX structure does not directly identify the protonation state of either MTX or the active site Asp27 residue. However, results from full matrix refinement of this structure show that the Asp27 carboxylate bond lengths are equivalent, indicating the Asp27 is charged when MTX is bound. Taken together, these results clarify a long-standing controversy, revealing that the Asp27•MTX interaction is ionic in nature. Additionally, the neutron maps show that nearly 2/3 of amide backbone hydrogens in DHFR have been exchanged for deuterium.

**TR.01.10 Smaller Crystals, Larger Proteins: Deuterium Labeling for Neutron Crystallography.** Dean Myles<sup>1</sup>, Kevin Weiss<sup>1</sup>, Dale Pelletier<sup>2</sup>, <sup>1</sup>Center for Structural Molecular Biology, <sup>2</sup>Life Sciences Div., ORNL, PO Box 2008 Oak Ridge, TN 37831, weisskl@ornl.gov, mylesda@ornl.gov.

Neutron scattering provides a unique, non-destructive probe of delicate biological materials and higher order assemblies and the design and production of H/D labeled material permits selected parts of macromolecular structures to be highlighted and analyzed *in situ*. In neutron protein crystallography, deuteration improves the signal to noise ratio of the data by an order of magnitude, allowing higher quality data to be collected from smaller crystals of larger macromolecular systems. In order to exploit this potential, we have established a Deuteration Laboratory for the *in vivo* production of H/D labeled protein, nucleic acids and other bio-macromolecules to support the user research programs at the HFIR and the SNS neutron scattering facilities at ORNL. The Deuteration Laboratory will provide the support, expertise, training and facilities required to produce specific, selective and randomly H/D labeled proteins and other macromolecules for neutron protein crystallography, small angle scattering, reflectivity and spectroscopic analysis. We will describe the development and application of deuterium labeling for neutron analysis of the structure, function and dynamics of proteins and macromolecular assemblies.

**TR.01.11 New Possibilities for the Determination of Macromolecular Structures from Selected H/D Derivative Crystals Utilizing Neutron Data Alone.** Herbert A. Hauptman, David A. Langs, Hongliang Xu, Hauptman-Woodward Medical Research Inst., 700 Ellicott Street, Buffalo, NY.

The impending development of higher flux neutron spallation facilities has generated a renewed interest in the possibilities for structure determination using neutron beams. Much of the interest in biological circles stems from being able to use the differences in scattering between H and D to answer important questions concerning macromolecules. For the most part these investigations rely on the structural results from previous X-ray studies to seed their investigations. In this presentation we would like to call attention to some interesting possibilities that neutron diffraction offers toward the actual structure determination of macromolecules by exploiting perdeuterated proteins that have been selectively hydrogenated for specific amino acid residues. It is our contention that such structures can be solved *ab initio* by direct methods procedures if suitable H/D derivatives can be synthesized.

Research support from NIH grant GM-46733 is gratefully acknowledged.

## WK.02 The Management of Synchrotron Image Data: The imgCIF File System and Beyond

**WK.02.01 imgCIF: The Management of Synchrotron Image Data.** Robert M. Sweet<sup>1</sup>, Herbert J. Bernstein<sup>2</sup>, <sup>1</sup>Biology Dept., Brookhaven National Laboratory, Upton, NY 11973, <sup>2</sup>Dept. of Mathematics and Computer Science, Dowling College, Oakdale, NY 11769.

This workshop is being organized with the encouragement and cooperation of the Data, Standards, and Computing Committee of the American Crystallographic Association (ACA). The principal objective of this workshop is to encourage adoption of the existing IUCr standard for image data, imgCIF/CBF. This standard will be discussed in some detail, and the participants will leave with a clear roadmap to the adoption of an agreed approach to achieving data portability.

A secondary goal will be to discuss ways that this standard might be extended in the future through new, emerging standards to achieve maximal data portability. If the first workshop is successful two additional workshops will be held over the next year. These will be to consider what data need to be managed, what metadata need to be packaged with the data, what formats need to be discussed (imgCIF, CBF, HDF, XML), and what other improvements might be made.

### WK.03 An Introduction to Grazing Incidence Small Angle Scattering with X-rays and Neutrons

**WK.03.01 Grazing Incidence Small Angle Neutron Scattering Techniques and Applications to Bilayer Membranes.** David Worcester, Biology Div., Univ. of Missouri-Columbia, Cold Neutrons in Biology & Technology Project, NCNR, NIST, Gaithersburg, MD.

Biological and artificial bilayer membrane structures include aspects that can be studied by grazing incidence small angle neutron scattering. These are primarily in-plane or near-in-plane features. Of special current interest is the demixing or partial demixing of lipid mixtures resulting in putative raft formation, which can be studied by using certain of the lipid components in deuterated form to provide in-plane contrast. Techniques for such measurements are developing and will be discussed. Other areas of interest include 2D crystals of membrane components, which for grazing incidence produce Bragg rods of diffraction whose intensity perpendicular to the in-plane axis provides structural characterization in 3D. Applications to membrane proteins are of particular interest.

**WK.03.02 Practical Aspects of GISAXS.** Byeongdu Lee,<sup>1</sup> X-Ray Science Div., Advanced Photon Source, Argonne National Laboratory, 9700 S. Cass Ave., Argonne, IL 60439.

The grazing-incidence small-angle X-ray scattering (GISAXS) technique is attracting much attention in the study of nanostructures such as a thin film on a substrate as well as particles on a substrate. In addition to the information derived from conventional transmission SAXS, GISAXS can deliver three-dimensional information about the thin film. In many cases, a substrate induces orientation of the particles. Compared to the powder pattern, the oriented GISAXS pattern enables an easier structure solution with better confidence in the results. However, evaluation of GISAXS data is still challenging. In this presentation, characteristic features and new measuring methods for GISAXS will be presented for several sample systems such as block copolymers, metallic catalyst clusters and bio-particles.

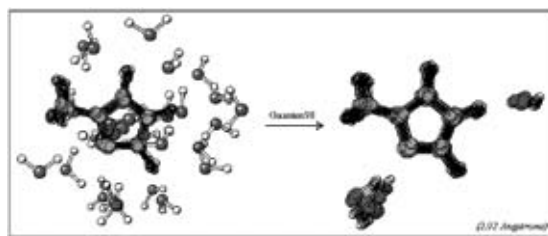
This work was benefited by the use of APS funded by DOE-BES under contract # W-31-109-ENG-38.

**S-P001 Crystal Structure of RecF Exhibits Structural Conservation With Rad50: Implications for DNA Recognition and Formation of Presynaptic Complexes.** O. Koroleva, N. Makharashvili, S. Korolev, Biochemistry and Molecular Biology, Saint Louis Univ. School of Medicine, St. Louis, MO.

DNA damage encountered during replication is a primary cause of mutations, genomic rearrangements, and lethality in all cells. Prokaryotic RecF, together with RecO and RecR, belong to a ubiquitous group of recombination mediators (RMs) that include such eukaryotic proteins as Rad52 and BRCA2. RMs are thought to help maintain genome stability in the presence of DNA damage by loading RecA-like recombinases and displacing ssDNA binding proteins at single-stranded DNA regions. We present the crystal structure of RecF from the extremely radiation resistant bacteria *Deinacoccus radiodurans*. The protein contains conserved sequence motifs characteristic of ATP-binding cassette (ABC) ATPases, and found in DNA repair and structural maintenance of chromosome (SMC) proteins. RecF lacks long coiled-coil region, but exhibits a high degree of structural similarity to the head domain of Rad50. This structural homology extends beyond the ATPase subdomain and encompasses the so-called "lobe 2" subdomain of Rad50. The high degree of structural conservation of bacterial RecF to the evolutionarily diverged eukaryotic Rad50 implies a common function of similar structural elements likely in DNA binding and, particularly, in double-stranded DNA boundaries recognition. RecF structure also sheds light on the mechanism by which RecF, along with RecR and RecO, may promote the presynaptic complex formation to initiate the processing at sites of DNA damage.

**S-P003 Distribution of Water Around Amino Acid Side Chains: Statistical and Computational Analysis.** R.H. Lai, K.A. Kantardjieff, Dept. of Chemistry and Biochemistry and W.M. Keck Foundation Center of Molecular Structure, California State Univ., Fullerton, CA.

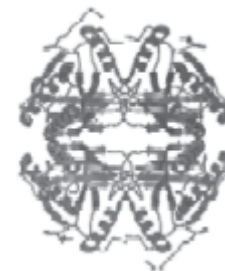
The structure of water around proteins is of interest to explain protein folding and stability, as well as function. In crystallography, knowledge of water structure is important for refining protein structures determined by X-ray. The calculated model for a protein, based on electron density derived from X-ray diffraction data, usually refines with a significantly higher residual factor (R value) than that for small molecules. Knowledge of structural propensities for water in protein



crystals can provide additional parameters in refinement, which ultimately improve the accuracy of the calculated model (reflected in a lower R value). A better understanding of the role(s) and function(s) of water molecules requires a general 'map' of localized hydrogen bonding interactions between the side chains and water. Here, we present the results from theoretical calculations and statistical analyses, which show strong agreement for the distances, locations, as well as orientations of water molecules around the 20 amino acid side chains. These distribution data indicate that water structures around amino acid side chains exhibit propensities that can be used to parameterize and improve X-ray crystallographic refinement.

**S-P005 Crystal Structures of Chicken Muscle Lactate Dehydrogenase.** L. Grant, E.R. Greiner, J.M. Warfel, N. Polder, G. Watanabe, C. Smith, B. Rupp, X. Ouyang, S.R. Herron, C.R. Meyer, C. Srinivasan, K.A. Kantardjieff, *et al.*, Dept. of Chemistry and Biochemistry and W.M. Keck Foundation Center of Molecular Structure, California State Univ., Fullerton, CA.

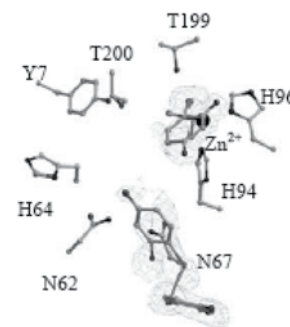
Lactate dehydrogenase (LDH) is a tetrameric, 331 residue oxidoreductase essential to ATP synthesis under anaerobic conditions which catalyzes the reversible reduction of pyruvate to lactate. Evolutionary alterations in the flexibility of the molecule and patterns of sequence conservation suggest the active site of LDH-A should be viewed as an extended unit involving most of the enzyme's structure for which substrate binding induces the loop region to fold over the active site. LDH-A was purified from chicken breast muscle and crystals obtained using Hampton screens via vapor diffusion. The native enzyme crystallized in space group P2<sub>1</sub>2<sub>1</sub>2, with cell dimensions, in Å, of a = 84.04 Å b = 126.78 Å and c = 252.74 Å. A putative pyruvate complex has been crystallized in space group C2 with dimensions of a = 75.16 Å b = 152.40 Å c = 142.79 Å and β = 93.5°.



Crystals were flash cooled and shipped to the Stanford Synchrotron Radiation Laboratory where 1.92 Å native data were collected. The native structure has been solved by molecular replacement using porcine LDH-A as the probe. Data refinement and structure determination of complexed crystals has begun.

**S-P007 Structural Comparison of the Binding Mode of a Thioxolone Ester Product to Classic Sulfonamide Inhibitors in Carbonic Anhydrase II.** C. Genis<sup>1</sup> S.Z. Fisher<sup>1</sup>, L. Govindasamy<sup>1</sup>, M. Agbandje-McKenna<sup>1</sup>, J. N.Orwenyo<sup>2</sup>, J. Kiddle<sup>2</sup>, R. McKenna<sup>1</sup>,<sup>1</sup>Dept. of Biochemistry and Mol. Biol., Coll. of Med., Univ. of Florida, Gainesville, FL, <sup>2</sup>Dept. of Chemistry, Western Michigan Univ., Kalamazoo, MI.

Carbonic anhydrases (CAs) are zinc metalloenzymes that catalyze the reversible hydration of carbon dioxide. The role of this reaction in physiology has made it a target of many therapeutic approaches, as enzyme inhibition is related to the treatment of glaucoma, hypertension, epilepsy, and altitude sickness. Most CA inhibitors currently known are sulfonamide-based. Thioxolone (6-hydroxy-1, 3-benzoxathiol-2-one), is a novel non-sulfonamide that has been found to have CA inhibitory activity.



The structure determined, from CA II crystals soaked with thioxolone at 1.6 Å resolution, revealed the ester product 4-mercaptobenzene-1, 3- diol bound in the active site. This work has shown the hydrolytic catalysis of CA II on thioxolone and gives a structural basis for the understanding the inhibitory nature of the resultant ester product. This result also provides information on which amino acids are important for the ester product binding and possible CA isoform specificity. This binding mode will also be compared to currently used sulfonamide-based CA inhibitors.

**S-P009 Determination of Sialic Acid Binding Region of Adeno-associated Virus 5.** M DiMattia<sup>1</sup>, L Govindasamy<sup>1</sup>, B Whitaker<sup>1</sup>, R McKenna<sup>1</sup>, S Zolotukhin<sup>2</sup>, N Muzyczka<sup>3</sup>, M Agbandje-McKenna<sup>1</sup>, <sup>1</sup>Dept. of Biochem. & Mol. Bio., <sup>2</sup>Dept. of Pediatrics, <sup>3</sup>Dept. of Mol. Genetics and Microbiology, COM UF Gainesville, FL 32610.

Adeno-associated virus 5 (AAV5) is under development for gene-therapy applications for treatment of cystic fibrosis. Belonging to the *Dependovirus* genus of the ssDNA *Parvoviridae*, this non-lytic virus is highly applicable for packaging and delivery of recombinant therapeutic DNA into target tissues due to its non-pathogenic nature and ability to establish long-term expression. Different AAV serotypes have distinct cell surface tropisms mediated through differential recognition of cell surface carbohydrates. AAV5, known to bind sialic acid (SA), is significantly more effective at transducing the apical surface of airway epithelia than AAV2. Crystals of AAV5 soaked with SA have been used to determine the structure of the AAV5-SA complex to 3.5 Å resolution. F<sub>o</sub>-F<sub>c</sub> density observed at the icosahedral 3-fold axis is consistent with ordered SA. The structure determination of the complex and the analysis of receptor-capsid interactions will be presented. Mapping of this receptor attachment site represents another step toward our understanding of the AAV5 structure and will lead to engineering of novel vectors, expanding the repertoire of tissues that can be targeted by AAV5 vectors.

**S-P011 Structure of Adeno-associated Virus 1 to 8.6 Å Resolution by Cryo-electron Microscopy.** E.B. Miller<sup>1</sup>, B. Guda-Whitaker<sup>1</sup>, L. Govindasamy<sup>1</sup>, X. Yan<sup>2</sup>, R. McKenna<sup>1</sup>, S. Zolotukhin<sup>3</sup>, N. Muzyczka<sup>4</sup>, T.S. Baker<sup>2</sup>, M. Agbandje-McKenna<sup>1</sup>, <sup>1</sup>Dept. of Biochem. & Mol. Biol., <sup>3</sup>Dept. of Pediatrics, <sup>4</sup>Dept. of Mol. Genetics and Microbiology, COM, UF, FL, <sup>2</sup>Dept. of Chem./Biochem. & Mol. Biol., UCSD, CA.

Adeno-associated viruses (AAV) are non-pathogenic ssDNA parvoviruses. Members of this genus require co-infection with a helper virus for successful replication. Recombinant AAV (rAAV) show great potential as vectors for therapeutic gene delivery. *In vitro* and *in vivo*, rAAV1 vectors show superior transduction of muscle cells compared to rAAV2, despite being ~83% identical to the latter virus at the amino acid sequence level. Thus the need for rational selection of an appropriate AAV serotype for tissue specific gene therapy applications has generated interest in the structural features of the capsids responsible for capsid-tissue interactions. Towards mapping the AAV1 capsid features responsible for its enhanced muscle transduction, we have determined its structure to 8.6 Å resolution by cryo-electron microscopy and image reconstruction. A pseudo-atomic model of the AAV1 capsid VP has been built into the reconstructed density based on the crystal structure of AAV2. Comparison of the surface topology of the AAV1 capsid with those available for AAV2, AAV4, AAV5, and AAV8 will be presented.

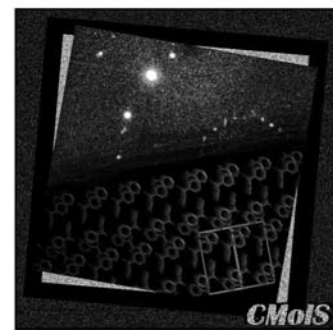
**S-P013 Differential Recognition of the Type-I and Type-II H-Antigen Acceptors by the Human ABO(H) Blood Group A and B Glycosyltransferases.** J.A. Letts<sup>‡</sup>, N.L. Rose<sup>§</sup>, Y.R. Fang<sup>§</sup>, S.N. Borisova<sup>‡</sup>, N.O.L. Seto<sup>‡</sup>, M.M. Palcic<sup>§</sup>, S.V. Evans<sup>‡</sup>, <sup>‡</sup>Dept. of Biochemistry & Microbiology, Univ. of Victoria, Victoria, BC, Canada, <sup>§</sup>Dept. of Chemistry, Univ. of Alberta, Edmonton, AB, Canada.

The human ABO(H) blood group A and B antigens are generated by the homologous glycosyltransferases GTA and GTB, which respectively add the monosaccharides N-acetylgalactosamine and galactose to the H antigens. In the first comprehensive structural study of the

recognition by a glycosyltransferase toward a panel of substrates corresponding to acceptor fragments, 14 high-resolution crystal structures of GTA and GTB have been determined in the presence of oligosaccharides corresponding to different segments of the H type I and type II antigens. GTA and GTB differ in only four critical amino acid residues. As these enzymes both utilize the H antigen acceptors, the four residues had been thought to be involved strictly in donor recognition; however, we now report that acceptor binding and subsequent transfer is significantly influenced by two of these residues. Further, these structures show that acceptor recognition is dominated by the central galactose residue and they give direct insight into the design of model inhibitors for GTA and GTB.

**S-P015 The W.M. Keck Foundation Center for Molecular Structure: A Core Facility of CSUPERB and Core Node of the STaRBURSTT-CyberDiffraction Consortium.** X. Ouyang, K. Kantardjiev, Dept. of Chemistry and Biochemistry and W.M. Keck Foundation Center of Molecular Structure, California State Univ., Fullerton, CA 92834.

The W.M. Keck Foundation Center for Molecular Structure (CMoIS), a core facility of CSUPERB, is the first comprehensive X-ray crystallographic and computational facility located at a predominantly undergraduate institution. CMoIS is also the west coast “core node” of the “Science Teaching and Research Brings Undergraduate Research Strengths Through Technology Cyber Diffraction Consortium” (STaRBURSTT-CDC). As a “collaboratory” and a “virtual laboratory”, CMoIS provides faculty and student investigators throughout the 23-campus California State University, regional colleges and universities, and the United States with local and remote access to instrumentation, software and databases for research and training involving both small and macromolecular structure. Furthermore, CMoIS offers experiments and tutorials for the undergraduate curriculum, as well as annual professional development workshops for undergraduate faculty, covering small molecule crystallography, macromolecular crystallography, molecular modeling and simulation, and structure-guided drug design. These national workshops are among a variety of courses offered by the Center for Workshops in the Chemical Sciences, a consortium of 12 universities funded by the National Science Foundation. Through its networks and partnerships, CMoIS has enhanced the research and educational infrastructure of the CSU, and students have benefited from the collaborative aspects of molecular science.



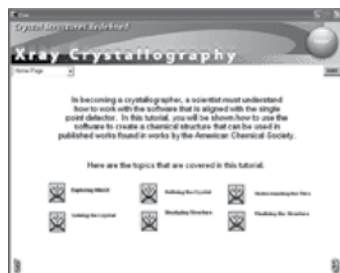
**S-P017 Novel Iron-Sulfur Cluster in *Pseudomonas aeruginosa* Adenosine Phosphosulfate Reductase.** J. Chartron<sup>1</sup>, K. S. Carroll<sup>2</sup>, H. Gao<sup>2,3</sup>, H. Chen<sup>2</sup>, J.A. Leary<sup>3</sup>, C.R. Bertozzi<sup>2</sup>, C.D. Stout<sup>1</sup>, <sup>1</sup>Dept. of Molecular Biology, The Scripps Research Inst., La Jolla, CA, <sup>2</sup>Depts. of Chemistry and Molecular and Cell Biology, Univ. of California, Berkeley, <sup>3</sup>Dept. of Chemistry and Molecular Cell Biology, Genome Center, Univ. of California, Davis.

APS reductase (APSR) catalyzes the first committed step in sulfur assimilation in pathogenic bacteria, including *Mycobacterium tuberculosis*, and is a promising target for drug development, as the enzyme does not occur in mammals. The thiosulfonate intermediate of APSr

derived from adenosine 5'-phosphosulfate (APS) with sulfite attached to Cys256 has been crystallized anaerobically in the presence of excess APS. The structure was solved by Fe K-edge MAD and refined at 2.7 Å resolution. The asymmetric unit contains two tetramers; APS is bound in a deep active site cleft, but the C-terminal, thiosulfonated peptide is disordered. The [4Fe-4S] cluster is ligated by the unique Cys139-Cys140 motif within a helix, and by Cys228 and Cys231. The structure, and biochemical and spectroscopic experiments, support a two-step mechanism in which the thiosulfonate is reduced by thioredoxin at a site on the enzyme distal from the cluster. Features of the structure suggest a role for the cluster in conformational changes.

**S-P019 Cyber-tutorials for Undergraduate Crystallographic Education.** Gregory M. Ferrence, Elizabeth Tabler, CB 4160, Dept. of Chemistry, Illinois State Univ., Normal, IL.

A decade of rapid desktop computer and crystallographic software advances has led to the emergence of many non-specialists engaging in crystallographic activities far beyond the relatively simplistic utilization of reports generated by professional crystallographers. With increasing numbers of non-expert crystallographic practitioners, a critical need to improve widespread basic crystallographic education exists. Non-specialists need to better appreciate disciplinary limitations and pitfalls as well as the importance of the professional crystallographer. Technology has made it possible to teach practical, "hands-on" crystallography to undergraduates. Materials, particularly worked examples and tutorials, to teach crystallography remain scarce. We are designing and building computer based tutorials for aid in crystallography education, including as components of a distance learning chemical crystallography course designed for non-specialists. Tutorials are geared to help students learn: 1) the process of translating a diffraction data set into a set of atomic coordinates representing the 3-D solid state molecular structure, 2) validation of crystallographic results, and 3) contextual analysis of results through literature and Cambridge Structural Database comparison.



**S-P021 Quokka: The Small-angle Neutron Scattering Instrument at OPAL.** E.P. Gilbert, Bragg Inst., ANSTO, PMB 1, Menai, NSW 2234, Australia, e-mail: epg@ansto.gov.au.

A small-angle neutron scattering (SANS) instrument is being designed as part of the initial instrument suite for the 20-MW Australian Reactor, OPAL. The new instrument, receiving neutrons from a large liquid-D<sub>2</sub> cold source, will be in the spirit of the world's best facilities and will greatly build upon the Australian Nuclear Science and Technology Organisation's existing expertise and facilities. Scheduled for operation in January 2007, it will provide Australian and international researchers with opportunities to access state-of-the-art SANS instrumentation. The details of the new SANS will be presented.

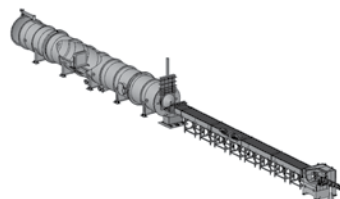


Figure 1 - Quokka - the SANS instrument at OPAL.

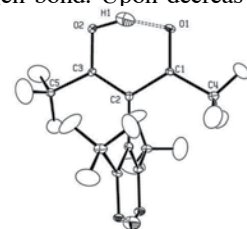
[1] E.P. Gilbert, J.C. Schulz and Terry J. Noakes, *Physica B*, (2006) in press.

**S-P025 Vector Resolution of a Focusing SANS Instrument.** Kenneth C. Littrell, IPNS Argonne National Laboratory, Argonne, IL.

Small angle neutron scattering (SANS) is one of the most popular and oversubscribed techniques at every user facility for neutron scattering studies of condensed matter that offers it. The limiting features in SANS experiment design and the applicability of a given instrument to a particular problem of scientific interest are the length of time required to make a measurement and the minimum momentum transfer  $Q$  that can be measured. In the traditional pinhole-camera geometry, these two constraints are inextricably linked, forcing tradeoffs. However, instruments based on lenses have been developed demonstrating how this linkage can be broken, allowing higher throughput while retaining high resolution and a low minimum  $Q$ . Previous experiments have shown that this is true for the vector resolution as well as the scalar, or orientationally averaged resolution. Here, we extend the previous results describing the theoretical resolution function of a focused SANS instrument to include the vector resolution, enabling the calculation of resolution broadening effects in oriented systems measured on a lens-based instrument.

**S-P027 Neutron Diffraction and X-ray Charge Density Studies of Tetraacetylene.** P. Piccoli<sup>a</sup>, E. Zhurova<sup>b</sup>, J. Eckert<sup>c</sup>, A. Pinkerton<sup>b</sup>, T. Koetzle<sup>a</sup>, A. Schultz<sup>a</sup>, D. Hadzi<sup>d</sup>, <sup>a</sup>IPNS, ANL, Argonne, IL, <sup>b</sup>Dept. of Chemistry, Univ. of Toledo, Toledo, OH, <sup>c</sup>Materials Research Laboratory, Univ. of California, Santa Barbara, CA, <sup>d</sup>National Inst. of Chemistry, Ljubljana, Slovenia.

Single crystal neutron diffraction data have been collected on a sample of tetraacetylene (TAE) at five temperatures between 20 and 298 K in order to characterize the temperature-dependent behavior of the short, strong, intramolecular hydrogen bond. Upon decreasing the temperature from 298 K to 20 K, the O2-H1 distance decreases from 1.17(1) to 1.081(2) Å while the O1...H1 distance increases from 1.33(1) to 1.386(6) Å. The convergence of the C-O bond lengths to identical values (1.285(4) Å) at 298 K, from inequivalent distances at low temperature, illustrates the dynamic equilibrium between the keto- and enol tautomers of this compound and is consistent with a resonance-assisted hydrogen bond. The O...O distance (2.432 ± 0.006 Å) varies little with temperature. Sub van der Waals intermolecular C-H...O contacts may be responsible for this ordering at low temperature. Preliminary experimental charge density results from low temperature X-ray diffraction will also be presented.



Work at ANL supported by the U.S. DOE, Basic Energy Sciences--Materials Sciences, under Contract W-31-109-ENG-38.

**S-P029 Variable Low-temperature Data Collection and Hierarchical Refinement to Study an Order-Disorder Phase Transition.** Weenawan Somphon<sup>1</sup>, Kenneth J. Haller<sup>1</sup>, A. David Rae<sup>2</sup>, <sup>1</sup>School of Chemistry, Inst. of Science, Suranaree Univ. of Technology, Nakhon Ratchasima 30000 Thailand, <sup>2</sup>Research School of Chemistry, The Australian National Univ., Canberra, ACT 0200 Australia.

The polymorphic structure of Ag(bipy)NO<sub>3</sub>, which undergoes a reversible order-disorder transformation at ~150 K, was studied by variable temperature (100-296 K). Synthetic precession photographs show *Fddd* symmetry and diffuse scattering above 150 K, but a loss of systematic absences below 150 K, indicating *F12/d1* (*i.e.* *C2/c*) symmetry, and essential disappearance of the diffuse scattering. The

100 K structure is an ordered structure with twin components related by a rotation around  $c^*$ . Features of the program RAELS (including refinable local coordinates relative to refinable orthonormal axial systems, refinable  $TL$  and  $TLX$  thermal models to describe rigid body motions, and constraints and restraints that can be used to impose more rational models and control refinement pathways by decreasing the effective number of refinable variables) were used to define and control the hierarchical refinements. Bruker-Nonius KappaCCD data collection; Oxford Cryosystems low temperature device; unit cells from  $\phi/\chi$  scan data; EvalCCD data reduction; SORTAV absorption corrections and data merging.

**S-P031 High-energy X-ray Diffraction PDF Study of a Novel Class of Supermicroporous Alumina/Silica/Manganese Materials.** Lev N. Zakharov<sup>1</sup>, Boris G. Shpeizer<sup>1</sup>, Abraham Clearfield<sup>1</sup>, Asel Sartbaeva,<sup>2</sup> Simon Billinge<sup>3</sup>, <sup>1</sup>Dept. of Chemistry, Texas A&M Univ., P.O. Box 30012, College Station, TX 77842, <sup>2</sup>Dept. of Physics and Astronomy, Arizona State Univ., P.O. Box 871504, Tempe, AZ 85287-1504, <sup>3</sup>Dept. of Physics and Astronomy, Michigan State Univ., East Lansing, MI 48824-2320.

The structure of amorphous supermicroporous Al/silica/Mn materials with different concentrations of Al and Mn were studied by the high-energy X-ray diffraction atomic pair distribution function (PDF) method. Experiments were carried out with the BESSRC/XOR 11-ID-C and 6ID-D MUCAT beamlines at the Advanced Photon Source (APS), Argonne National Laboratory. The PDF data indicate that at low Al concentrations, Al atoms substitute for Si in the framework, and at high Al concentrations, a longer-range ordered Al/Mn-oxide structure is formed. Comparison of our PDF data with the PDF profiles for pure silica and, from single crystal structures of Mn,Si,O-complexes, indicates the existence of the Si-O-Mn and Al-O-Mn fragments in the material structure, suggesting that the Mn is incorporated into the bulk structure.

**S-P033 Identification of a Novel *Escherichia coli* O157:H7 Heme Oxygenase ChuS and its Structural Similarity to ChuX.** M.D.L. Suits, G.P. Pal, Z. Jia, Dept. of Biochemistry, Queen's Univ., Kingston, Ontario, K7L 3N6 Canada.

Heme oxygenases (HOs) catalyze the oxidation of heme to biliverdin, carbon monoxide (CO), and free iron. For pathogenic microorganisms, heme uptake and degradation is one of the critical mechanisms for iron acquisition that enables multiplication and survival within hosts they invade. Here we report the functional identification of a novel heme oxygenase ChuS from the *Escherichia coli* O157:H7, along with its apo and heme complex structures. ChuS is structurally unique compared to other HOs with respect to overall architecture and heme coordination. Spectral analysis and CO detection by gas chromatography confirm that ChuS is capable of using either ascorbic acid or cytochrome P450 reductase-NADPH as sources of electrons for heme oxygenation. As such, ChuS is the first HO to be identified in any strain of *E. coli*. Sequence analysis suggests that homologues of ChuS are present in many other pathogenic bacteria. Furthermore, we present the structure of another member of the heme utilization operon, ChuX, which superimposes with the structural repeats of ChuS. This structural conservation suggests a similar method of heme coordination. The functional implication of this new structural information is discussed in the context of enteric iron acquisition.



**S-P035 Achieving Successful Discovery Through Effective Lab Management.** M. Rabiyaathul Thanuja, J. Jabarullahan, Madurai Kamaraj Univ., Madurai - 625 021, India.

A scientist's creative and intuitive potential leads to the success of any research project, and his or her management abilities, which play a major role at the background, like a shadow business partner. Due to the lack of administrative training during their careers, most scientists seek assistance from lab managers to administer the non-science responsibilities. A manager's responsibilities often include procurement of lab supplies and instruments and sometimes recruitment. The manager helps lower expenditures and improves time management, making the research process more efficient.

Early 2005, we initiated a study to accumulate information regarding various aspects of lab management including cost and time to create a hypothetical model for variable cost analysis. This study will enable managers to find efficient procedures and consistent results. We have limited our studies to the selected biological labs. Materials and method sections from recent publications were collected to identify the reagents, costs, etc., and tabulated the data. The data was used to design non-redundant hypothetical experimental model and variable cost analysis. We will be discussing our protocol and the results will encourage managers and young scientists to operate cost effective labs in both university and industry settings

**S-P037 Synthesis, Structural Characterization and Study Kinetic of Ruthenium Complex with Phosphinics and Bipyridinics Derivatives Ligands (X-BIPY) (X = CL-, MeO, AND Me-).** Lincoln Lucilio Romualdo, Fabio Bastista do Nascimento, Javier Ellena, Eduardo Castellano, Alzir Azevedo Batista, <sup>1</sup>Dept. de Química, Univ. Federal de São Carlos, São Carlos, SP, Brazil, <sup>2</sup>Inst. de Química de São Carlos, Univ. de São Paulo, São Carlos, SP, Brazil.

Three new ruthenium complex with phosphinics and bipyridinics derivatives ligands was synthesized, characterized structurally and a study of the kinetic properties was accomplished with the purpose of evaluating the speed of leaves of a strong donor sigma ligand and it changes for the of a ligand pi donor. The pKa different of the bipyridinics ligands which present different groups donors and withdrawing electrons, generate different react speedy of the compounds, turning an excellent kinetic study in inorganic chemistry.

**S-P039 Cyclization of N(4)-R Thiosemicarbazones Derived from 2-formyl and 2-acetylpyridine (R = alkyl or aryl).** Fábio B. do Nascimento<sup>1</sup>, Cláudia Rodrigues<sup>1</sup>, Letícia R. Teixeira<sup>1</sup>, Alzir A. Batista<sup>1</sup>, Heloisa Beraldo<sup>2</sup>, Javier Ellena<sup>3</sup>, <sup>1</sup>Dept. de Química, Univ. Federal de São Carlos, São Carlos, SP, Brazil, <sup>2</sup>Dept. de Química, Univ. Federal de Minas Gerais, Belo Horizonte, MG, Brasil, <sup>3</sup>Inst. de Física de São Carlos, Univ. de São Paulo, São Carlos, SP, Brasil.

Thiosemicarbazones and their metal complexes are of considerable interest due to their beneficial biological applications<sup>1</sup>. The 2-heterocyclic thiosemicarbazones have been subject of numerous studies<sup>2</sup>. The presence of alkyl or aryl groups at the terminal N(4) position can considerably increase the biological activity of these compounds<sup>3</sup>. In the present work reactions of  $VO(SO_4)_2$  with 2-formyl and 2-acetylpyridine N(4)-R thiosemicarbazones (H2Fo4R, H2Ac4R, R = alkyl or aryl) were explored in ethanol. With H2Fo4Ph the corresponding vanadium(IV) complex  $[VO(H2Fo4Ph)H_2O]SO_4$  was isolated and its mother liquors afforded a crystal that was refined by X-ray diffraction and gave the correspondig thiosemicarbazone cyclized.

<sup>1</sup>H. Beraldo, D. Gambino, *Mini-Reviews on Medicinal Chemistry* 4 (2004) 159.  
<sup>2</sup>D.X. West, S.B. Padhye, P.S. Sonawane, *Struct. Bond.* 76 (1991) 1 and refs therein.  
<sup>3</sup>A.E. Liberta, D.X. West, *Biometals* 5 (1992) 121.

**S-P043 Crystallization Studies of the MgO-ZrO<sub>2</sub>-WO<sub>3</sub> System.** Amy Gindhart, Cora Lind, Dept. of Chemistry, Univ. of Toledo, Toledo, OH.

There has been interest in negative thermal expansion (NTE) materials because of the effects seen when they are incorporated into composites. The incorporation of such materials could reduce the overall thermal expansion of their respective composites. Previous work done in the A<sub>2</sub>(WO<sub>4</sub>)<sub>3</sub> system has shown that the thermal expansion is dependent on the identity of the A<sup>3+</sup> cation. Suzuki and associates have substituted the A site by a mixture of Hf<sup>4+</sup> and Mg<sup>2+</sup>. There have not been any other reports of different M<sup>II</sup>M<sup>IV</sup> cation mixtures on the A site in the A<sub>2</sub>(WO<sub>4</sub>)<sub>3</sub> system.

The cations of interest in this paper are Mg<sup>2+</sup> and Zr<sup>4+</sup>, which can combine to form a previously unknown NTE compound in this family. There are several possible pathways that can be explored for the preparation of this material. These include solid state routes, dissolution and evaporation of water soluble precursors, hydrothermal treatment, heating of preformed binary and ternary compounds, and a non-hydrolytic sol-gel process. The formation of unreactive MgWO<sub>4</sub> was observed in several approaches, which is why some traditional solid-state methods cannot be used. Crystallization studies were performed on samples prepared by different methods to establish what phases are preferentially formed, and to investigate suitable methods for the facile preparation of MgZr(WO<sub>4</sub>)<sub>3</sub>.

**S-P045 Crystal Structures of [M(H<sub>2</sub>O)<sub>6</sub>](BF<sub>4</sub>)<sub>2</sub>, M = Mg, Mn, Fe, Co, Ni, and Zn.** James A. Kaduk, Innovene USALLC, P.O. Box 3011 MC F-9, Naperville IL 60566.

Although hexagonal lattice parameters have been reported for these compounds [1], their crystal structures have never been reported. The structure of a plausible analog, Mg(ClO<sub>4</sub>)<sub>2</sub>(H<sub>2</sub>O)<sub>6</sub>, has been reported in *Pmn2<sub>1</sub>* [2]. Isolation of the Fe species in a plant deposit prompted laboratory synthesis of the other compounds. The crystal structures of these hygroscopic compounds (which melt near room temperature) were refined using the Rietveld method.

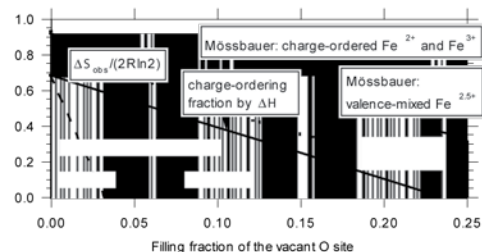
The Fe compound was identified by indexing the powder pattern and using lattice matching techniques. The orthorhombic [Mg(H<sub>2</sub>O)<sub>6</sub>](ClO<sub>4</sub>)<sub>2</sub> model yielded a successful refinement, but the displacement coefficients of one of the two independent tetrafluoroborate anions were larger than seemed reasonable, given the strong O-H...F hydrogen bonds. This feature persisted in the refinements of the Mg, and Co structures, while the Mn and Zn structures seemed more chemically-reasonable. In the Ni structure, a second Ni site seemed to be populated. Grinding generated profile broadening characteristic of stacking faults in this compound. In an attempt to decide whether the true symmetry was orthorhombic or hexagonal, single crystals of the Mg and Ni compounds were grown. The Mg compound is orthorhombic, but the Ni compounds seems to be truly hexagonal. Quantum chemical calculations have been used to derive accurate hydrogen positions and to quantify the strengths of the hydrogen bonds.

[1] K. C. Moss, D. R. Russell, and D. W. A. Sharp, *Acta Cryst.*, 14, 330-330 (1961).

[2] C. D. West, *Zeit. Krist.*, 88, 480-493 (1935).

**S-P049 Verwey Transition in Ideal Settings and Under Valence Frustration.** Pavel Karen, Dept. of Chemistry, Univ. of Oslo, POB 1033 Blindern, 0315 Oslo, Norway.

Owing to controversy about charge order in the complex low-temperature phase, Verwey transition in magnetite (Fe<sub>3</sub>O<sub>4</sub>) remains a puzzle. The A-site ordered perovskite RBaFe<sub>2</sub>O<sub>5</sub> (R is a rare-earth atom) stabilizes mixed-valence iron in an orthogonal network of coordination square pyramids with oxygen vacancies confined to the R layer. Consequently, RBaFe<sub>2</sub>O<sub>5</sub> exhibits all symptoms of the Verwey transition: change in volume, entropy, electrical conductivity, and magnetization. <sup>57</sup>Fe Mössbauer spectroscopy detects about 90% of iron states as Fe<sup>2.5+</sup> above the Verwey transition and as locally ordered Fe<sup>2+</sup>/Fe<sup>3+</sup> below that. For long-range ordering into di- and trivalent iron at low temperatures, neutron and synchrotron X-ray powder diffraction each suggest about 70%. A corresponding fraction of the ideal transition entropy 2Rln2 per formula unit is detected by scanning calorimetry. Filling oxygen vacancies decreases transition entropies and charge-freezing temperatures like an ideal solution of RBaFe<sub>2</sub>O<sub>6</sub> in the RBaFe<sub>2</sub>O<sub>5</sub> solvent. Accounting by <sup>57</sup>Fe Mössbauer spectroscopy for all iron coordination-, spin- and valence states suggests that the valence-mixed and valence-ordered states of iron do not have the same stability against oxygen nonstoichiometry, except at zero nonstoichiometry when they both have a maximum concentration. Structurally, Verwey transition is a klassengleich first-order transition between two cooperative systems: a valence-mixed halfmetal and a valence-ordered semiconductor with one and only one singly or doubly occupied *d* orbital of *t<sub>2g</sub>* symmetry ordered.



charge-freezing temperatures like an ideal solution of RBaFe<sub>2</sub>O<sub>6</sub> in the RBaFe<sub>2</sub>O<sub>5</sub> solvent. Accounting by <sup>57</sup>Fe Mössbauer spectroscopy for all iron coordination-, spin- and valence states suggests that the valence-mixed and valence-ordered states of iron do not have the same stability against oxygen nonstoichiometry, except at zero nonstoichiometry when they both have a maximum concentration. Structurally, Verwey transition is a klassengleich first-order transition between two cooperative systems: a valence-mixed halfmetal and a valence-ordered semiconductor with one and only one singly or doubly occupied *d* orbital of *t<sub>2g</sub>* symmetry ordered.

**S-P051 Phasing and Modeling of Large Structures with Se-SAD - Crystal Structure of Deblocking Aminopeptidase.** A. Joachimiak<sup>1</sup>, C. Chang<sup>1</sup>, R. Wu<sup>1</sup>, J. Abdullah<sup>1</sup>, M. Cymborowski<sup>2</sup>, W. Minor<sup>2</sup>, <sup>1</sup>Midwest Center for Structural Genomics and Structural Biology Center, Biosciences, Argonne National Laboratory, Argonne, IL 60439, <sup>2</sup>Univ. of Virginia, VA 22908.

Structure of deblocking aminopeptidase (DAP) from *B. cereus* was solved as part of Midwest Center for Structural Genomics project. DAP from *B. cereus* is a 349 amino acids protein that assembles into large multi-subunit structure. The Se-Met labeled crystals were obtained that belong to R3 rhombohedral space group (*a*=240.9 Å, *b*=240.9 Å, *c*=294.8 Å). An asymmetric unit contained sixteen molecules corresponding to 5,584 residues (632 kDa) with 112 potential Se sites. The SAD (0.9794 Å) data set to 2.65 Å was collected at 19-ID beamline and phased with HKL2000-PH. Auto-chain tracing failed using conventional programs. The initial model was built manually and refined to R=19.4 % (R<sub>free</sub>=26.4 %). Final structure has one dodecamer and 1/3 of another dodecamer/A.U. The biological unit resembles tetrahedral aminopeptidase. This is the largest protein structure/A.U. solved by Se-SAD among PDB-deposited coordinates. Details assembly and function will be presented.

This work was supported by the grants from the NIH (GM62414 and GM074942) and the U.S. Department of Energy, OBER under Contract W-31-109-ENG-38.

**S-P053 Controlled-temperature Diffraction Measurements on Samples in Glass Capillaries.** Brian Litteer, Martijn Fransen and Richard Glazer\*\*, PANalytical Inc., Natick MA, USA, \*PANalytical B.V., Lelyweg 1, 7602 EA Almelo, The Netherlands, \*\*Oxford Cryosystems, 3 Blenheim Office Park, Lower Road, Long Hanborough, Oxford, OX29 8LN, UK.

The measurement of samples in glass capillaries has advantages for certain types of materials, for instance samples with anisotropic crystallite shapes or crystallites in liquids. With the introduction of multi-purpose X-ray powder diffractometers, the capillary technique has become a standard addition to the conventional Bragg-Brentano reflection geometry. For controlled temperature experiments, however, the reflection geometry is still mostly used, especially in the case of low-temperature measurements.

In order to obtain a controlled-temperature device for capillary powder diffraction, a Cryostream (an established product in the single crystal community) has been modified, in close collaboration between Oxford Cryosystems and PANalytical. Key question in this integration is of course the accuracy of the sample temperature along the capillary length. In this study, we determined the temperature accuracy of the Oxford Cryostream for this powder diffraction application and show an example of what can be done with this capillary heater-cooler.

**S-P055 Vacancy Ordering in LSM Materials for SOFC Cathodes - A Combined Neutron and X-ray Diffraction Study.**

L. Suescun, J. Mais, B. Dabrowski, J.D. Jorgensen, E.R. Mackay, J.D. Richardson Jr., Y. Ren, Materials Science Division, Bldg 223, Argonne National Lab, Argonne, IL

Fast oxygen conductivity combined with electronic conductivity have been observed in  $\text{La}_{0.8}\text{Sr}_{0.2}\text{MnO}_{3-d}$  (LSM) materials. This has made  $\text{La}_{0.8}\text{Sr}_{0.2}\text{MnO}_{3-d}$  the most used cathode material in Solid Oxide Fuel Cell devices. These properties have been attributed to the oxygen vacancy disorder present in the materials with a small amount of oxygen deficiency. On the other hand, similar compounds showing ordered vacancies and orbital ordering of Mn cations have shown to be poor ionic and electronic conductors. Electrochemical and chemical stability studies performed on LSM's with  $0.7 < y < 0.9$  have shown that  $\text{La}_{0.2}\text{Sr}_{0.8}\text{MnO}_y$  ( $x = 0.8$ ) could be a better cathode material for SOFC than the currently used  $\text{La}_{0.8}\text{Sr}_{0.2}\text{MnO}_{3-d}$  ( $x = 0.2$ ). *In-situ* neutron TOF diffraction (at Argonne's IPNS-GPPD) and synchrotron X-ray diffraction experiments (at APS-11ID-C station) have been performed to characterize the vacancy ordering process in highly oxygen deficient LSM's ( $x = 0.8$  and 1) and the stability of these phases at different temperatures and oxygen partial pressures. New vacancy ordered phases displaying charge and oxygen/vacancy ordering have been characterized by Rietveld refinement of NPD and Synchrotron XPD patterns and will be presented.

This work has been supported by the Department of Transportation.

**S-P057 Structural Basis for  $\text{O}_2$  Activation in Extradiol Ring Cleaving Dioxygenases.** E. G. Kovaleva, and J. D. Lipscomb, Dept. of Biochemistry, Molecular Biology, and Biophysics, Univ. of Minnesota, Minneapolis, MN 55455.

Homoprotocatechuate (HPCA) 2,3-dioxygenase (2,3-HPCD) catalyzes proximal extradiol ring-cleavage of catecholic substrates. Substrate binding to the active site Fe(II) promotes binding and activation of  $\text{O}_2$  as well as the subsequent insertion of both oxygen atoms to yield the product. Here, we use structural approaches to explore the mechanistic consequences of: (1) replacing an electron supplying substrate ring substituent with an electron withdrawing group, and (2) making

subtle changes in a 2<sup>nd</sup> sphere amino acid residue. High-resolution crystal structures and optical spectra in combination with kinetic studies show that 4- $\text{NO}_2$ -catechol (4NC) binds in the same site as HPCA and undergoes either ring oxidation to the quinone or ring cleavage depending on the active site amino acid composition. A residue capable of acid-base chemistry is required near the  $\text{O}_2$  binding site in order to observe the ring-cleaved 4-NC product. When HPCA is bound instead of 4-NC, or when the normal acid-base residue is present, ring cleavage is always observed, suggesting that both the substrate and the active site acid-base contribute to reaction fidelity. The techniques developed here are being used to structurally characterize reaction cycle intermediates for the first time.

**S-P059 Crystal Structure of the Catalytic Core Domain of a Novel Histone Demethylase.**

Xia Hong, Zhongzhou Chen, Jangye Zang, Johnathan Whetstone, Yang Shi, and Gongyi Zhang#, Dept. of Immunology, National Jewish Medical and Research Center, Denver, CO 80206, #Correspondence should be addressed to: Gongyi Zhang, Tel: 303-398-1715, Zhangg@njc.org.

Posttranslational modifications of histones regulate chromatin structure and gene expression. Histone demethylases, members of a newly emerging transcription factor family, remove methyl groups from the lysine residues of the tails of histone proteins, and thereby regulate the transcriptional activity of target genes. JmjC domain-containing proteins have been predicted to be demethylases. For example, the JmjC-containing protein JHDM2 has been characterized as a H3-K9me3- and H3-K36me3-specific demethylase. Structures of the catalytic core domain of JHDM2 with and without  $\alpha$ -ketoglutarate in the presence of Fe(II) have been determined by X-ray crystallography. Analysis of the core domain revealed novel structures of the JmjN domain, the JmjC domain, the C-terminal domain, and a zinc finger motif. These unique structural features create a potential substrate binding pocket. Structure-based sequence alignment of the JHDM2 family members further suggests a potential mechanism for the substrate specificity of individual family members.

**S-P061 Protein Crystallization Optimization Techniques and Cryoprotectant Selection at Ontario Center for Structural Proteomics.**

X. Xu, T. Skarina, E. Evdokimova, M. Kudritska, J. Gu, H. Zheng, O. Kagan, O. Onoprienko, O. Egorova, A.M. Edwards, A. Savchenko, University Health Network, Univ. of Toronto, Ontario, Canada.

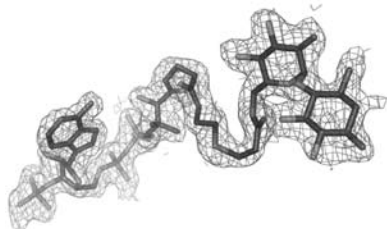
The Ontario Centre for Structural Proteomics is a Canadian Institute that is affiliated with both the Northeast Structure Genomics Consortium and the Midwest Centre for Structural Genomics. Since 1998, we have contributed more than 200 diffracted crystals of structural genomics targets.

The quality of the crystal is the key for the structure determination. Production of well-diffracting crystals is still a bottleneck in this process. We will present a refined complex approach to optimize protein crystals for diffraction including microcrystal seeding, temperature variation and small molecule co-crystallization.

Cryocrystallography has become an essential and routine tool in structural biology over the last decade as a result of observation of great reduction in radiation damage to protein crystals during X-ray diffraction experiments at cryotemperatures. The most critical step in this process is selection of suitable cryoprotectant, which is usually done empirically. We will present our method for cryoprotectant selection based on extensive experience gained during Structural Genomics program.

**S-P063 Probing Protein Mechanisms of Antibiotic Resistance Factors Using Potential Transition State Mimics in Structural Studies.** O.M. Baettig<sup>1</sup>, A. Sharma<sup>2</sup>, A.M. Berghuis<sup>1&2</sup>, <sup>1</sup>Dept. of Biochemistry, <sup>2</sup>Microbiology & Immunology, McGill Univ., Montreal, Canada.

The rise in antibiotic resistance has emphasized the need for studying the mechanisms that confer resistance. Resistance to aminoglycoside antibiotics is primarily due to enzymatic modification of the aminoglycoside. The enzyme of study, Aminoglycoside 6'-N-acetyltransferase-Ii (AAC(6')-Ii), acetylates a broad spectrum of aminoglycosides at the 6' amino group. Crystal structures of AAC(6')-Ii in complex with its co-enzyme acetyl-CoA have previously been reported<sup>[1]</sup>. However, all attempts to co-crystallize AAC(6')-Ii with its aminoglycoside substrates have failed. To circumvent the difficulty of co-crystallizing AAC(6')-Ii with aminoglycosides, we proposed to use potential transition state mimics in which co-enzyme A is covalently linked to an acetylated aminoglycoside (see picture)<sup>[2]</sup>. Here, we report the crystal structures of AAC(6')-Ii in complex with several of these transition state mimics. Preliminary analysis reveals binding interactions between the enzyme and antibiotic moieties.



[1] Wybenga-Groot L.E. *et al*, *Structure* 1999;7(5):497-507.  
[2] Gao F. *et al*; *Angew Chem Int Ed Engl* 2005;44(42):6859-62.

**S-P065 Structures of Human Deoxycytidine Kinase in Complex with L-Nucleoside Analogs Give Insight into the Enzyme's Non-Enantioselective Catalytic Activity.** E. Sabini, S. Hazra, A. Lavie, Dept. of Biochemistry and Molecular Genetics, UIC, 900 S. Ashland Ave, Chicago 60607, IL.

L-nucleosides analogs such as L- $\beta$ -2',3'-dideoxy-3'-thiacytidine (3TC) and its 5-fluoro-3'-thia-derivative (FTC) show potent anti-HIV and anti-HBV activity. The antiviral activity of 3TC and FTC is due to the fact that the triphosphate forms of the two drugs are good substrates for the HIV-1 reverse transcriptase and the HBV DNA polymerase, yet show lower affinity towards the human DNA polymerases compared to the corresponding D-enantiomers, leading to decreased toxicity. On the other hand, the dioxolane analogue of 3TC, L-OddC (L- $\beta$ -2'-deoxy-3'-oxacytidine) is the first L-nucleoside showing antitumor activity due to the ability of its triphosphate to inhibit human DNA polymerases. The rate-limiting step in the activation pathway of 3TC, FTC and L-OddC is catalyzed by human deoxycytidine kinase (dCK). In addition to phosphorylating its physiological substrates dC, dA and dG, dCK is responsible for the phosphorylation of several nucleoside analogs, and lacks selectivity between D- and L-enantiomers. Here we present the high resolution structures of dCK in complex with 3TC/ADP, FTC/ADP and L-OddC/ADP. The structures reveal how this non-enantioselective enzyme can accommodate both D- and L-configurations.

**S-P067 CMP-Induced Structural Changes in a Multifunctional Sialyltransferase from *Pasteurella multocida*.** Lisheng Ni,<sup>1</sup> Mingchi Sun,<sup>1</sup> Harshal Chokhawala,<sup>1</sup> Xi Chen,<sup>1</sup> Andrew J. Fisher<sup>1,2</sup>, <sup>1</sup>Dept. of Chemistry, <sup>2</sup>Section of Molecular and Cellular Biology, Univ. of California, Davis, CA.

Sialyltransferases catalyze the transfer a sialic acid from CMP-sialic acid to an acceptor (galactose, N-acetylgalactosamine, or sialic

acid). They are key enzymes in the synthesis of sialic acid-containing oligosaccharides, polysaccharides, and glycoconjugates and play pivotal roles in many physiological processes including cell recognition, bacterial infection, and tumor metastasis. The structures of truncated multifunctional *Pasteurella multocida* sialyltransferase, with and without CMP, have been determined at 2.0 and 1.65 Å resolution, respectively. The structure represents the first sialyltransferase structure that belongs to glycosyltransferase-B structural group. The CMP binding site is located in a cleft between the two Rossmann domains. Yet, the CMP only interacts with residues in the C-terminal domain. The binding of CMP to the protein causes a large closure movement of the N-terminal Rossmann domain towards the C-terminal nucleotide-binding domain. Additionally, a short helix near the active site seen in the apo structure becomes disordered upon binding to CMP. This helix may swing down upon binding to donor CMP-sialic acid to form the binding pocket for an acceptor.

**S-P069 Thioesterase Domain of Human Fatty Acid Synthase: Structural Insights into Chain-length Selectivity.** C.W. Pemble<sup>1</sup>, S.J. Kridel<sup>2</sup>, W.T. Lowther<sup>1</sup>, <sup>1</sup>Dept. of Biochemistry, <sup>2</sup>Dept. of Cancer Biology, School of Med., Wake Forest Univ., Winston-Salem, NC.

Human fatty acid synthase (hFAS) is responsible for the *de novo* biosynthesis of long-chain fatty acids. hFAS has been shown to play a pivotal role in the supply of fatty acids important for growth and survival of many human carcinomas, underscoring its importance in tumor biology. The large multifunctional hFAS complex consists of three major domains acting in concert to ensure nascent fatty-acyl maturation. Interestingly, the terminating activity provided by the resident C-terminal thioesterase domain (hFAS-TE) is responsible for catalyzing the highly selective liberation of thioester-linked palmitoyl-acyl (C<sub>16</sub>) substrates. The remarkable degree of chain-length specificity attributed to hFAS-TE historically has been a topic not completely understood. We have solved to 1.7 Å and 2.3 Å resolution the structures of hFAS-TE in complex with palmitate and a novel, potent inhibitor, respectively. The structures revealed a pronounced hydrophobic binding channel that contacts the C<sub>16</sub> fatty-acyl moieties of both palmitate and the core fragment of the inhibitor. These ligand interactions offer the first evidence for substrate selectivity and the intermediary steps of catalysis.

**S-P071 Crystal Structure of Human Urokinase Complexed with a Cyclic Peptidyl Inhibitor, Upain-1.** Mingdong Huang, Gengxiang Zhao, Cai Yuan, Chuanbing Bian, Troels Wind, Peter Andreasen, Xiaoming Ye, Zixian Huang, State Key Lab on Structural Chemistry, Fujian Inst. of Research on the Structure of Matter, 155 Yang Qiao Xi Lu, Fuzhou Fujian, China.

The urokinase-type plasminogen activator (uPA) is implicated in tumor cell migration, invasion and metastasis. The inhibition of uPA activity represents a promising mechanism for anti-tumor therapy. The structure analysis of protease-inhibitor complexes helps understanding the mechanism of inhibitor action and the design of inhibitors. A cyclic peptidyl inhibitor (CSWRGLENHRMC, upain-1) was identified (Hansen *et al*. *J Biol Chem* **280**, 38424-37) as an effective and highly specific uPA inhibitor with a *K<sub>i</sub>* of 500 nM. We determined the crystal structure of uPA in complex with upain-1 at 2.14Å resolution. The structure reveals that the upain-1 binds with the S<sub>1</sub> and S<sub>2</sub> pockets of uPA, and with the 60-loop of uPA that renders it specific for uPA. The oxyanion hole of uPA was occupied by the Glu7 of upain-1, forcing upain-1 to behave as an inhibitor rather

than a substrate of uPA. This study provides mechanistic information about the enzyme-inhibitor interaction, and a new pharmacophore for the design of specific uPA inhibitor.

**S-P073 Crystallographic Studies of HTLV-1 Protease.** Mi Li<sup>1,2</sup>, Alla Gustchina<sup>1</sup>, Gary Laco<sup>3</sup>, Jan Rozycki<sup>3</sup>, Jerry Alexandratos<sup>1</sup>, Mariusz Jaskolski<sup>4</sup>, and Alexander Wlodawer<sup>1</sup>, <sup>1</sup>MCL, NCI at Frederick, Frederick, MD, <sup>2</sup>Basic Research Program, SAIC-Frederick, Frederick, MD, <sup>3</sup>National Cancer Inst., Bethesda, MD, <sup>4</sup>Dept. of Crystallography, A. Mickiewicz University, Poznan, Poland.

The success of structure-assisted drug design targeting HIV-1 protease (PR) has changed the clinical outcome of AIDS and validated the approach of targeting retroviral enzymes for the purpose of designing and improving therapeutic agents. HTLV-1 is a retrovirus clinically associated with diseases such as adult T-cell leukemia. HTLV-1 encodes a 125-amino acid long protease that shares 24% identity with HIV-1 PR, and thus provides an appealing new drug target. We have solved the structure of a truncated version of HTLV-1 PR consisting of residues 1-116 in complex with a statine-based inhibitor extending from subsites P5 to P5'. Significant structural differences are found in several loop areas, which include the functionally important flaps, previously considered to be structurally highly conserved. Potential key residues responsible for the resistance of HTLV-1 PR to anti-HIV drugs are identified. The extensive interactions between the inhibitor and the enzyme provide sufficient data to describe the substrate binding sites and elucidate the specificity of HTLV-1 PR.

**S-P075 Towards Crystals of Proteorhodopsin.** P. Gourdon, R. Berntsson, N. Bonander, A. Snijder, R. Neutze, Dept. of Chemistry and Biotechnology, Chalmers Univ. of Technology, 413 90 Gothenburg, Sweden.

Membrane proteins are associated with many important biological functions. There is only a limited knowledge of the 3D structures and the reaction cycles of membrane proteins. We are presently seeking conditions that yield crystals of the membrane protein proteorhodopsin. This rhodopsin, related to G protein coupled receptors, was discovered in seawater in year 2000. It is thought to participate in creating the proton motive force, which is involved in energy metabolism. Thus, proteorhodopsin may play an important role in the energy balance of the earth's biosphere. Although the structure of at least three archeal rhodopsins have been obtained by X-ray crystallography, no homologue from the kingdom of bacteria has ever been structurally characterised. Here we present results from a successful expression, isolation, solubilisation, and a three-step purification procedure. We also show preliminary crystallisation results. The ultimate goal of this research includes the elucidation of structure-function relationships of these enzymes by determining reaction intermediates.

**S-P077 Dioxygen Activation in *Hansenula polymorpha* Amine Oxidase.** B.J. Johnson<sup>a</sup>, A. Pearson<sup>a</sup>, J. Klinman<sup>b</sup>, C. Wilmore<sup>a</sup>, <sup>a</sup>Dept. of Biochem., Mol. Biol. and Biophys., Univ. of Minnesota, Minneapolis, MN 55455, <sup>b</sup>Depts. of Chem. and Mol. and Cell Biol., Univ. of California, Berkeley, CA 94720.

Copper amine oxidases (CAO) are homodimeric enzymes that convert primary amines to aldehydes and O<sub>2</sub> to H<sub>2</sub>O<sub>2</sub>. Each monomer contains a Cu(II) ion and a 2,4,5-trihydroxyphenylalanine quinone (TPQ) cofactor. O<sub>2</sub> is essential in the oxidative-half reaction of CAO, returning the substrate reduced aminoquinol TPQ back to the oxidized quinone state. However, the exact location and timepoint of O<sub>2</sub> binding and activation in the oxidative half-reaction remains unclear.

The crystal structure of oxidized *H. polymorpha* amine oxidase (HPAO) was solved previously [1]. In this study, gas binding is observed in freeze-trapped HPAO. Xe can be used to map hydrophobic sites in proteins where molecular O<sub>2</sub> may bind. CO and NO are oxygen mimics used extensively in solution studies to probe dioxygen activation. These gases are complexed to oxidized HPAO as well as anaerobically methylamine reduced HPAO in the crystal. The resulting structures give insight into O<sub>2</sub> binding and activation.

[1] Li R., Klinman J.P., Mathews F.S., *Structure*. 1998, 6(3), 293.

**S-P079 Complete Reaction Cycle of a Cocaine Catalytic Antibody at Atomic Resolution.** Xueyong Zhu<sup>1</sup>, Tobin J. Dickerson<sup>2,3</sup>, Claude J. Rogers<sup>2,3</sup>, Gunnar F. Kaufmann<sup>2,3</sup>, Jenny M. Mee<sup>2,3</sup>, Kathleen M. McKenzie<sup>2,3</sup>, Kim D. Janda<sup>2,3,4,\*</sup>, Ian A. Wilson<sup>1,4</sup>, Depts. of <sup>1</sup>Molecular Biology, <sup>2</sup>Chemistry, <sup>3</sup>Immunology, The Skaggs Inst. for Chemical Biology<sup>4</sup>, The Scripps Research Inst., La Jolla, CA.

Abuse of cocaine is a major public health problem, and has been a significant social problem since the late 70's and early 80's when crack-cocaine was first introduced. Unfortunately, FDA-approved treatments do not exist for cocaine abuse, addiction, and overdose. Immunopharmacotherapy has been proposed as a promising means to treat cocaine abuse. The murine cocaine catalytic antibody 7A1 hydrolyzes of the benzoate ester of cocaine to produce the nonpsychoactive metabolites ecgonine methyl ester and benzoic acid. 7A1 Fab' fragment and six complexes with substrate cocaine, transition state analog, both products (ecgonine methyl ester and benzoate), one product ecgonine methyl ester, and finally the other product benzoate, as well as heptaethylene glycol were determined at 1.5-2.3 Å resolution. Here, we present the snapshots of the complete cycle of the cocaine antibody catalytic reaction at atomic resolution. Significant conformational changes occur along the 7A1-catalyzed cocaine hydrolysis pathway, but are generally limited to the active site, including some key residues and ligands themselves. Antibody CDR loop movements (up to 2.3 Å) and substantial side-chain rearrangements (up to 9 Å) alter the shape and size (~320 - 500 Å<sup>3</sup>) of the antibody active site from "open" to "closed" to "open" for the substrate, transition state and product states, respectively. From this comprehensive series of crystal structures, the catalytic mechanism is discussed, and the possible mutations have been proposed to explore how to improve catalytic proficiency.

**S-P081 Substrate Recognition and Catalysis in Thimet Oligopeptidase.** Nicholas Noinaj, David Rodgers, Univ. of Kentucky Dept. of Molecular and Cellular Biochemistry and Center for Structural Biology, Lexington, KY.

GPCR signaling is crucial for the regulation of neuronal communication. Here, neuropeptides serve as signaling molecules which transduce a signal from one neuron to the next and are then terminated through several mechanisms, one of which involves neuropeptide degradation via a class of enzymes known as neuropeptidases. Thimet oligopeptidase (TOP) is a neuropeptidase that hydrolyzes many diverse substrates with cleavage sites that have no apparent consensus. The TOP crystal structure has previously been reported and despite significant efforts, specificity remains a mystery. Recently though, we have determined crystal structures of TOP bound with fragments from seven different peptides. Our results indicate



that TOP is able to recognize diverse substrates via a novel multipurpose binding surface that is relatively flat and composed mainly of aromatic and hydrophobic residues that interact primarily with C-terminal backbone atoms. This surface is located on a wall opposite the active site, providing further indication that a hinge-like conformational change is required for catalysis. Our work has also shown that a previously reported potent inhibitor of TOP, dynorphin A<sub>1-13</sub>, is in fact hydrolyzed and that a product fragment acts as the true inhibitor. *NIH/NIDA/NINDS/ACS-PRF*.

**S-P083 Extended CIF Validation Software.** Georgi Todorov, Kostadin Z. Mitev, Herbert J. Bernstein, Dept. of Mathematics and Computer Science, Dowling College, Oakdale, NY 11769.

Recent revisions to the CIF standard, the growing number of dictionaries and the critical role played by CIF in the IUCr publication process led the IUCr to fund a two year project to upgrade portions of the existing CIF software base to support longer lines and more rigorous validation of CIFs against multiple layered dictionaries. The work on handling of long lines was reported earlier. We present a database-based approach to validation to ensure compliance with data range and enumeration specifications, to ensure compliance with parent-child relationships, and to detect missing and duplicated tags. This approach to validation is being extended to support the handling of binary synchrotron imgCIF data.

Work funded in part by the IUCr.

**S-P085 Structure of Ras-like GTPase Cdc42 Bound to a GTP Analogue GMPPCP.** M. Phillips, G. Calero, R. Cerione, Cornell Univ., Ithaca NY 14853.

Rho GTPases are important molecular “switches” that are involved in the regulation of numerous cellular processes such as cell trafficking, cytoskeletal rearrangement, nuclear signaling, and apoptosis. Activation of these proteins occurs by binding of GTP to the active site while deactivation is achieved by hydrolysis of GTP to GDP and P<sub>i</sub>. Structures of Ras as well as other small GTPases have revealed two regions that move upon GTP binding which have been named Switch 1 and Switch 2. Here we present the 2.4 Å resolution structure of GMPPCP-bound Cdc42. This structure is interesting in that there are no major conformational changes between the GDP (inactivated) and the GMPPCP (activated) structures, unlike many other Ras-like GTPases. This indicates a new model for the activation of Cdc42 whereby target binding induces a conformational change in Switch 1 that can only be stabilized in the GTP bound form, due to coordination of key residues in Switch 1 to the γ-phosphate of GTP.

**S-P087 Evaluation of Target Residues for Crystallization by Surface Entropy Reduction.** David R. Cooper<sup>1</sup>, Tomasz Boczek<sup>1,3</sup>, Katarzyna Grelewska<sup>1,3</sup>, Malgorzata Pinkowska<sup>1,3</sup>, Michal Zawadzki<sup>1,3</sup>, Lukasz Goldschmidt<sup>2,3</sup>, David Eisenberg<sup>2,3</sup>, Zygmunt Derewenda<sup>1,3</sup>, <sup>1</sup>Dept. of Molecular Physiology and Biological Physics, Univ. of Virginia, Charlottesville, VA, <sup>2</sup>Dept. of Chemistry and Biochemistry, Univ. of California, Los Angeles, Los Angeles, CA, <sup>3</sup>PSI Center for Structure and Function Innovation.

The fact that crystallization remains a bottleneck for the structure determination of even well-behaved, soluble proteins is leading more laboratories to use mutagenesis to facilitate crystallization. The Surface Entropy Reduction (SER) approach that our lab has focused on has shown to be quite successful. Although intuitively alanine is a good target amino acid and has proven to aid crystallization, preliminary successes with other residues have led us to

perform a more extensive examination of the role of the target residue. Nine sets of mutations were chosen for a model protein, and five target residues (A, S, T, H, & Y) were systematically examined for their ability to facilitate crystallization. We also evaluated the use of alternate reservoirs for crystallization. Although no one target residue stands out as the magic bullet, this study suggests a crystallization strategy that can dramatically increase the chances of obtaining crystals of difficult proteins.

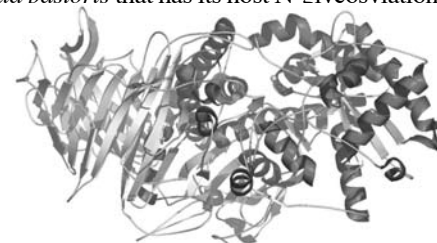
**S-P089 Cytochrome *ba3* Oxidase in Nanoscale Lipid Bilayers: A Roadmap to Crystallization.** V. Mitch Luna, James A. Fee, C. David Stout, Dept. of Molecular Biology, The Scripps Research Institute, La Jolla, CA, 92037.

Cytochrome *ba3* oxidase is a respiratory enzyme that catalyzes the reduction of molecular oxygen to water in aerobic organisms. Here we present a novel assembly procedure of *Thermus thermophilus* cytochrome *ba3* oxidase in nanoscale lipid bilayers (nanodiscs) as a model for integral membrane protein incorporation in nanodiscs. This procedure increases homogeneity for the purpose of high-resolution structure determination through crystallization and avoids the use of detergents. Utilizing the His-tag engineered at the N-terminus of subunit I, we are able to bind cytochrome *ba3* oxidase to Nickel resin and conduct the nanodisc assembly on the resin, which allows us to separate empty nanodiscs, and nanodiscs that incorporated the cytochrome *ba3* oxidase. Through this procedure, we are able to obtain cytochrome *ba3* oxidase in a native, detergent free, lipid bilayer environment. Here the enzyme is fully active as a cytochrome *c* oxidase and retains its unique spectroscopic properties. Cytochrome *ba3* oxidase in nanodiscs offers a unique avenue for structure determination and presents a membrane protein in a more native-like lipid environment.

**S-P091 Investigating the Catalytic Mechanism of Golgi alpha-mannosidase II: A Possible Target for Cancer Chemotherapy.** N. Shah, D.A. Kuntz, D.R. Rose, Dept. of Medical Biophysics, Univ. of Toronto, Ontario Cancer Inst., University Health Network, Toronto, ON, Canada.

A feature typical of many cancerous cells is their altered cell surface glycosylation. Golgi alpha-mannosidase II (GMII, 125 kDa) catalyzes the committed step of complex N-glycan formation in the N-glycosylation pathway. Inhibition of GMII by small molecule inhibitors is known to reduce metastasis in cancer patients and generally improve clinical outcome. GMII catalyzes the hydrolysis of two different mannose-mannose bonds converting GnMan<sub>5</sub>Gn<sub>2</sub> to GnMan<sub>3</sub>Gn<sub>2</sub>. Its catalytic action is highly specific and unique.

Our laboratory has previously solved the crystal structure of GMII from *Drosophila melanogaster* and has studied many potential inhibitors against this enzyme. Through current work, we aim to gain insight into the catalytic mechanism of GMII. The objective of my work is to study the enzyme interacting with its natural substrate. Isolation of this complex, branched polysaccharide has been a challenging task. We are attempting to purify the GMII natural substrate by exploiting a strain of *Pichia pastoris* that has its host N-glycosylation system knocked out, followed by introduction of certain elements of the human N-glycosylation system. Our progress to this end will be presented.



**S-P093 Towards a Better Understanding of Exopolysaccharide Export in Gram-Negative Bacteria.** C-L. Keiski<sup>1,2</sup>, P. Yip<sup>1</sup>, L.L. Burrows<sup>1,3</sup>, P.L. Howell<sup>1,2</sup>, <sup>1</sup>Hospital for Sick Children, <sup>2</sup>Univ. of Toronto, Toronto, ON, Canada, <sup>3</sup>McMaster Univ., Hamilton, ON, Canada.

Bacterial exopolysaccharides are a primary component of the biofilm matrix and despite their key role in determining its architecture, little is known about the proteins responsible for their production. One of the most extensively studied exopolysaccharide biosynthetic pathways in bacteria is the production of alginate by the opportunistic pathogen *Pseudomonas aeruginosa* in the cystic fibrosis lung. The biosynthesis of the alginate precursor sugar, GDP-mannuronic acid is well understood, however the subsequent steps of polymerization and export are less well characterized. AlgK is a periplasmic protein of unknown function believed to be involved in alginate export. We are focusing on the structural and functional characterization of this protein. AlgK has been overexpressed and purified to >95% homogeneity. Crystals that diffract to 8Å have been obtained and are currently being optimized. Antibodies targeting purified AlgK have been produced and will be used in subsequent functional studies.

**S-P095 Structural Studies of the Prion Replicative Interface.** C.R. Kimberlin<sup>1</sup>, A. Bellon<sup>1</sup>, G. Abalos<sup>1</sup>, J. Cruite<sup>1</sup>, R.A. Williamson<sup>1</sup>, E.O. Saphire<sup>1</sup>, <sup>1</sup>Dept. of Immunology, The Scripps Research Institute, La Jolla, CA 92037.

Neurodegenerative prion diseases such as Creutzfeldt-Jakob disease and bovine spongiform encephalopathy have been closely linked to the conversion of normal cellular prion protein (PrP<sup>C</sup>) to an alternate, misfolded conformation (PrP<sup>SC</sup>). Previous studies have shown that antibodies directed against PrP regions containing residues 96-104 and 133-158 can inhibit the conversion of normal PrP<sup>C</sup> to PrP<sup>SC</sup> suggesting that these regions play a critical role in the replicative interface between PrP<sup>C</sup> and PrP<sup>SC</sup>. A high-resolution structure of PrP<sup>SC</sup> would provide valuable insight into the mechanism by which the conversion process occurs. However, the natural tendency for PrP<sup>SC</sup> to self-assemble into aggregates hinders crystallization efforts. Thus, to further investigate regions of PrP involved in structural conversion, PrP residues 89-112 and 136-158 were each grafted into the heavy-chain complementarity-determining region 3 (HCDR3) of the recombinant human IgG b12 antibody. These PrP motif-grafted antibodies were found to bind specifically to PrP<sup>SC</sup> with nanomolar affinity. Fab portions of the b12 antibodies with PrP residues 89-112 or 136-158 grafted into the HCDR3 have been expressed and purified. Microfluidic free-interface-diffusion screens yielded crystals that diffract to 2.5Å belonging to space group P2<sub>1</sub> which show evidence of pseudomorphological twinning. Refinement is currently in progress.

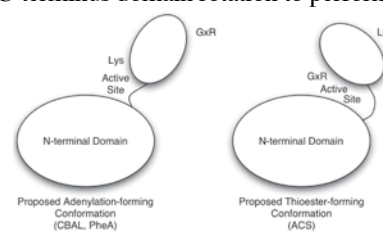
**S-P097 Mechanism of Hexamerization of gpU, the Tail Terminator Protein from Bacteriophage Lambda.** L. Pell<sup>1,2</sup>, A. Liu<sup>1</sup>, L. Edmonds<sup>3</sup>, L. Donaldson<sup>3</sup>, P.L. Howell<sup>1,2</sup>, A.R. Davidson<sup>1</sup>, <sup>1</sup>Univ. of Toronto <sup>2</sup>Hospital for Sick Children <sup>3</sup>York Univ., Canada.

The lambda tail terminator protein, gpU, binds to the major tail protein (gpV), halting gpV polymerization at precisely the correct tail length. Recombinant gpU is monomeric in solution; however, addition of Mg<sup>2+</sup> induces oligomerization, yielding hexameric rings. *In vivo* gpU functions as a hexamer, likely to complement the stoichiometry of hexameric gpV. Several gpU mutants have been identified that are unable to form hexamers *in vitro* upon Mg<sup>2+</sup> addition. The monomeric solution structure of gpU reveals an  $\alpha/\beta$  topology and a ferredoxin-like fold. To gain insight into the mechanism of hexamerization, crystallization studies were pursued. Se-Met derivative crystals of gpU-D74A

have been grown and MAD data to 2.6Å resolution collected. The Se atoms were found using SHELX and interestingly, the initial experimental electron density map clearly shows 12 molecules arranged in two stacked rings. Crystallization screening of wild type gpU both in the presence and absence of Mg<sup>2+</sup> is currently in progress. The structure of gpU-D74A as well as its implications in the oligomerization mechanism of gpU will be presented.

**S-P099 Structure and Function of Adenylate Forming Enzymes: A ~140° C-terminus Domain Rotation.** Albert S. Reger, Jill M. Carney, Andrew M. Gulick, SUNY, Dept. of Structural Biology, Hauptman-Woodward Medical Inst., Buffalo, NY.

The adenylate-forming enzymes, including Acyl-CoA Synthetases and the adenylation domains of Non-Ribosomal Peptide Synthetases, perform two half-reactions in a ping-pong mechanism. We have proposed that upon completion of the initial adenylation reaction, these enzymes use a 140° C-terminus domain rotation to perform the second thioester forming half reaction. Structural and kinetic data of mutant enzymes support this hypothesis. Mutations were made to Acetyl-CoA Synthetase that specifically affect the individual half-reactions. Substitution of K609A results in an enzyme unable to catalyze the adenylation reaction, while G524L is unable to catalyze the thioester-forming half reaction. Kinetic data including hinge mutants D517P and D517G and structures of the mutants R194A, R584A, R584E, and K609A will be presented in support of the stated hypothesis.



**S-P101 Enolase and Its Role in Accumulation of Cholesteryl Esters.** Ramin Radfar, Jason Holliday, Wofford College, Chemistry Dept., Spartanburg, SC 29303.

Atherosclerosis, the most common form of arteriosclerosis, is characterized by the presence of arterial thickening deposits (plaque) of almost pure cholesteryl esters in the inner lining of an artery. Plaques can grow large enough to significantly reduce the blood's flow through an artery. Enolase may have a role in accumulation of these deposits by inhibiting activity of cholesterol ester hydrolase and formation of a complex with cholesteryl ester.

We thank Dr. Lukasz Lebioda for beamline access. This research is supported by Cottrell College Science Award No CC6029.

**S-P103 An Innovative Method to Produce Recombinant Human Telomerase Reverse Transcriptase (hTERT).** Edward Wu, Stephen Hughes, HIV-Drug Resistance Program, National Cancer Institute, Frederick, MD 21702.

Telomerase is a ribonucleoprotein complex that adds telomeric DNA repeats to the end of chromosomes, which are iteratively shortened as cells divide. Activation of the complex is critical to the immortalization of normal cells. Telomerase has become an important molecular marker for the diagnosis, prognosis, and treatment of cancer. The lack of purified hTERT, the catalytic subunit of complex, is a major problem. The primary difficulty in generating active recombinant hTERT appears to be the protein folding. We used a GFP-hTERT fusion to monitor folding in insect cells. Folding was not improved by the co-expression of the human heat shock proteins hsp70 and hsp90. We used the intrinsic cellular chaperones

that reside in specific cytoplasmic compartments to assist the folding process. We directed the transport of the GFP-hTERT fusion to mitochondria and the endoplasmic reticulum (ER). The GFP fluorescence was enhanced when the GFP-hTERT fusion was directed to the ER, and the folding and solubility of the ER-transported protein was improved. This improvement makes it possible to purify and assay the recombinant hTERT protein.

**S-P105 Crystal Structure of Nudix Family Proteins BT0354 and EF2700.** C. Chang, E. Duggan, J. Abdullah, A. Joachimiak, Midwest Center for Structural Genomics and Structural Biology Center, Biosciences, Argonne National Laboratory, 9700 South Cass Ave., Bldg 202, Argonne, IL 60439.

The Nudix family is widespread among eukaryotes, bacteria, archaea and viruses and consists mainly of pyrophosphohydrolases that act upon substrates of general structure Nucleoside Diphosphate linked to another moiety, X (NDPX) to yield NMP and P-X. This family is defined by conserved 23 amino acid Nudix sequence motif: GxxxxxExxxxx[UA]xRExxEExGU, where U is an aliphatic, hydrophobic residue. Sequence data analysis suggests that BT0354 from *B. thetaiotaomicron* and EF2700 *E. faecalis* belong to Nudix family. The crystal structures of both proteins have been determined by SAD method. The structure of BT0354 (225 residues) was refined to 2.4 Å resolution ( $R=19.8\%$ ,  $R_{\text{free}}=25.1\%$ ) with two dimers in the asymmetric unit. The structure of EF2700 (273 residues) was refined to 2.26 Å resolution ( $R=20.1\%$ ,  $R_{\text{free}}=24.3\%$ ) as dimer. Although these proteins belong to Nudix family, they show some striking differences. The structural comparisons with other Nudix proteins would be presented.

This work was supported by the grants from the National Institute of Health (GM62414 and GM074942) and the U.S. Department of Energy, Office of Biological and Environmental Research under Contract W-31-109-ENG-38.

**S-P107 New Approaches to High-throughput Crystallization Based on Contact Line Pinning.** Robert E. Thorne<sup>1,2</sup>, Yevgeniy Kalinin<sup>1</sup>, Viatcheslav Berejnov<sup>1</sup>, <sup>1</sup>Physics Dept., Cornell Univ., Ithaca NY, <sup>2</sup>Mitegen, LLC, Ithaca, NY.

Macromolecular crystal growth via vapor diffusion relies on solvent evaporation from drops of mother liquor. Drop shape affects the evaporation rate and can have especially large effects on nucleation rates, but is poorly controlled in existing crystallization methods. We have microfabricated micrometer-size patterns that strongly pin drop contact lines, allowing precise control of drop shapes and positions. Uncertainties in evaporation rate are greatly reduced, providing better-defined crystallization conditions and improved reproducibility of results. Drops of protein, surfactant and salt solutions pinned in this manner are highly stable against vibrations and tilts, allowing the substrate to be flipped for hanging drop crystallization. Based on these results, we have designed a new class of crystallization trays that allow *in-situ* X-ray examination and easy crystal retrieval.

This work was funded by the National Institutes of Health (R01 GM65981) and by NASA (NAG8-1831).

**S-P109 New Methods to Prepare Iodine Derivatives by Vaporizing Iodine Labeling (VIL) and Hydrogen Peroxide VIL (HYPER-VIL).** Hideyuki Miyatake, Tomokazu Hasegawa, Akihito Yamano, RIKEN Harima Inst./SPring-8, Sayo-cho, Japan.

We developed new techniques, vaporizing iodine labeling (VIL) and hydrogen peroxide VIL (HYPER-VIL), for the preparation of iodine derivatives. In the VIL, a small amount of KI/I<sub>2</sub> solution is

enclosed in a crystallization well, with the result that the gaseous I<sub>2</sub> molecules diffuse into the crystallization droplets without exerting substantial changes of ionic strength in the target crystals. Once they have diffused into the droplet, the I<sub>2</sub> molecules often iodinate accessible tyrosines at *ortho*-positions. When the iodination is insufficient or does not occur, we can further apply the HYPER-VIL technique to increase the iodination ratio by addition of a small droplet of hydrogen peroxide (H<sub>2</sub>O<sub>2</sub>) to the crystallization well; the gaseous H<sub>2</sub>O<sub>2</sub> also diffuses into the crystallization droplet to catalyze the iodination. These techniques are suitable for phase determination when coupled with softer X-rays, such as those from CuK $\alpha$ /CrK $\alpha$  radiations. In addition, synchrotron radiation of longer wavelengths are also effective for phasing with the iodine derivatives. We assessed the effectiveness of these techniques using five different crystals. Consequently, four of the crystals were successfully iodinated providing sufficient phasing power.

**S-P111 Towards the Structural Basis for Bacterial Two-partner Secretion.** Hye-Jeong Yeo<sup>1</sup>, Katarzyna Walkiewicz<sup>1</sup>, Michal Szymanski<sup>1</sup>, Takeshi Yokoyama<sup>1</sup>, Joseph St. Geme<sup>2</sup>, <sup>1</sup>Dept. of Biology and Biochemistry, Univ. of Houston, Houston, TX, <sup>2</sup>Dept. of Pediatrics, Duke Univ. Medical Center, Durham, NC.

*Haemophilus influenzae* is an important human pathogen and especially common as a cause of localized respiratory tract diseases. The *H. influenzae* HMW1 protein is a High-Molecular Weight non-pilus adhesin that mediates attachment to human epithelial cells, an essential step in the pathogenesis of *H. influenzae* infections. The HMW1 adhesin belongs to a protein family secreted via the Two-Partner Secretion (TPS) pathway, which is utilized to translocate large protein virulence factors across the outer membrane in many pathogenic bacteria. The TPS systems are composed of two major component proteins, with TpsA being the secreted protein and TpsB its specific transporter. HMW1 is an example of TpsA proteins, and is translocated to the cell surface by virtue of the HMW1B outer membrane translocator (a TpsB protein). The HMW1 adhesin is synthesized as a 160 kDa precursor protein that consists of three domains: a signal sequence, an N-terminal secretion domain, and a C-terminal mature adhesin domain. The HMW1B translocator, a bacterial Omp85-like protein, is a large protein (~60 kDa) forming a tetrameric pore (~240 kDa) in the outer membrane. To understand the structural basis for Two-Partner Secretion, we aim to determine the crystal structures of the component proteins in the *H. influenzae* TPS pathway. We have obtained crystals of the HMW1B outer membrane protein and of the HMW1 secretion domain. Crystals of the HMW1 secretion domain diffract to a resolution of 2.4 Å. Our progress on the project will be presented and discussed.

This work was supported by Robert A. Welch Foundation grant # E-1616 to H.J.Y.

**S-P113 Structure-based Fragment Screening Using High Throughput Crystallography.** R.J. Rosenfeld, J. Badger, P. Collins, D. Bensen, L. Tari, R. Athay, D.E. McRee, ActiveSight, 4045 Sorrento Valley Blvd., San Diego CA 92121.

Fragment-based screening is a method for developing novel lead compounds. The goal of fragment screening is to identify small fragments that bind efficiently in an active site and can be linked together to create new high affinity scaffolds for drug design. We present a complete home laboratory system for rapid structure based fragment screening. In our pilot project, we created a library of 450 small molecular weight fragments (mw. 100-300 Da). We soaked apo protein crystals in solutions containing four fragments and performed follow-up experiments with single soaks to verify fragment

hits. We used the ACTOR automated robot crystal-mounting system and automated data collection on a high intensity FR-E home x-ray source with CCD detector. Integrated automated processing, refinement and fitting software developed by Molecular Images was used to quickly generate refined structures with electron density maps that were viewed in MiFit. Our pilot project resulted in a 4% hit rate for fragments in our library binding to a protein kinase. This validates our library and demonstrates that structure based fragment library screening can be achieved rapidly and successfully in a home laboratory.

**S-P115 Crystal Structure of *Arabidopsis* Dehydroquinase-Shikimate Dehydrogenase.** S. Singh, D. Christendal, Univ. of Toronto, ON, Canada.

The shikimate pathway (SP) is involved in the biosynthesis of the aromatic amino acids and a variety of other aromatic compounds in bacteria, apicomplexa, fungi and plants, but is absent in animals. The SP consists of seven enzymatic steps which end with the formation of chorismate, the precursor to metabolic pathways involved in the synthesis of amino acids, lignins, and ubiquinones, to name just a few. Each of the seven enzymes is encoded by a single gene in most prokaryotes whereas enzymes two to six comprise a multidomain, fusion product in fungi, collectively known as the AROM complex. Plants, however, contain a bifunctional fusion product of enzymes three and four, dehydroquinase and shikimate dehydrogenase (DHQ-SDH), but all other enzymes are encoded by separate genes. To date, all seven SP enzyme protein structures have been determined; however there are no representatives from the plant kingdom.

This study is the first to present a structure of a plant SP enzyme, DHQ-SDH, the only bifunctional SP enzyme known to date. DHQ-SDH was co-crystallized with a tartrate molecule in the DHQ active-site, and with a shikimate molecule in the SDH active-site. Despite the number of SDH structures available, this is the first to present a SDH-substrate complex which has guided site-directed mutagenesis studies of some of the key residues interacting with shikimate. We also present the kinetic data of these active-site mutants.

**S-P117 Fingerprint and Structural Analyses in a Putative Short Chain Oxidoreductase Enzyme.** Robert Huether<sup>1</sup>, Bi-Cheng Wang<sup>4</sup>, James Zhi-Jie Liv<sup>4</sup>, Vladimir Pletnev<sup>3</sup>, Timothy Umland<sup>12</sup>, Qilong Mao<sup>2</sup>, Leah Gambino<sup>2</sup>, and William Duax<sup>1</sup>, <sup>1</sup>SUNY at Buffalo, Dept of Structural Biology, NY, <sup>2</sup>Hauptman-Woodward MRI NY, <sup>3</sup>Inst. Bioorg. Chem., RAS, Moscow, Russia <sup>4</sup>Univ. of Georgia, GA.

We have identified a highly conserved fingerprint of 40 residues in the TGxxxGIG subfamily of the Short chain oxidoreductase (SCOR) enzymes. The subfamily is made up of over 7900 members with an amino acid length of ~250. The 40 fingerprint residues are critical to catalysis, cofactor binding, protein folding and oligomerization. They give us insight into evolution of the folding and function of SCORs enzymes. We have identified a putative SCOR enzyme from *C. thermocellum* (Cth1068) that contains 30 of the 40 fingerprint residues. Of the 10 variants from the fingerprint, one is a Gly substitution of a highly conserved Asn residue that plays significant structural and catalytic roles; no previously reported TGxxxGIG SCOR crystal structure contains this N→G mutation. We are undertaking crystal structure analysis to determine the impact of this variation on the hydride transfer network, the conformation of helix 5 and oligomer formation. We have a 1.8Å resolution dataset on a tetragonal crystal form (I4<sub>1</sub>22).

Supported by NIH Grant No. DK26546 (WLD)

**S-P119 A Ribonucleotide Reductase Small Subunit from *M. Tuberculosis* with a More Protected Tyrosyl Radical.** J.S. Davis, H. Rubin, Dept. of Biochemistry & Molecular Biophysics, Univ. of Pennsylvania, Philadelphia, PA 19104.

Ribonucleotide reductases (RNRs) are enzymes that provide deoxyribonucleotides for DNA synthesis and repair in all organisms. These enzymes are classified into three classes based on cofactor requirement and the type of protein radical formed. Class I RNRs consist of  $\alpha_2\beta_2$  proteins, both the large subunit (NrdE) and small subunit (NrdF) are needed for catalysis. While many organisms contain more than one class of RNRs, it is unclear why *Mycobacterium tuberculosis* contains three small subunit class Ib proteins; NrdF1, NrdF2 and NrdB. The function of NrdB is unclear, NrdF2 is functional under normal growth conditions, and NrdF1 appears to be important in response to DNA damaging conditions.

NrdF1 can bind to NrdE in the absence of NrdF2, and is catalytically active. The tyrosyl radical appears to be better protected from hydroxyurea, which suggests a more buried active site, and hence an overall difference in active site structure.

Based on the current structure of NrdF2, we suggested that the major differences would be in the C-termini of these proteins. However, recent data suggests that the active sites of these proteins may be different. The native enzyme with 322 residues diffracted to 3 Å in-house and crystallizes in space group P4<sub>2</sub>2<sub>1</sub>2.

**S-P123 Structure of A Novel Acetylcitrulline Deacetylase from *Xanthomonas campestris*.** D. Shi, X. Yu, L. Roth, M. Tuchman and N.M. Allewell, Children's National Medical Center, Washington, DC 20010, USA, College of Chemical and Life Sciences, Univ. of Maryland, College Park, MD 20742.

The structures of a novel *N*-acetylcitrulline deacetylase from a plant pathogen *Xanthomonas campestris* have been solved using a three-wavelength dataset collected from a single crystal of SeMet protein. Six selenium sites were found using SOLVE and 82% of the polypeptide chain was automatically traced using RESOLVE. Refinement was carried out using CNS with 1.75 Å datasets to a crystallographic R factor of 19.8% and a free R factor of 22.4%. The structure of the monomer consists of two domains. The catalytic domain provides ligands for the metal ions in the active site. The other domain forms the dimer interface through hydrophobic interactions between helices and hydrogen bonding between two  $\beta$  strands forming a continuous  $\beta$  sheet across the dimer. The polypeptide fold of the monomer is similar to the fold of *Pseudomonas* sp. carboxypeptidase G2 and *Neisseria meningitidis* succinyl diaminopimelate desuccinylase. The availability of three-dimensional structures of this protein allows us to identify the residues that are important to the substrate binding and catalytic reaction.

**S-P125 Structural and Biophysical Characterization of Two hEphB4 Complexes: Insights into Modulating Protein-protein Interactions.** Jill E. Chrencik, Alexei Brooun, Michael I. Recht, Michelle L. Kraus, Anand R. Kolatkar, Peter Kuhn, Dept. of Cellular Biology, The Scripps Research Inst., La Jolla, CA 92037.

The Eph family of receptor tyrosine kinases and their ligands, the ephrins, regulate numerous biological processes in developing and adult tissues, and have more recently been implicated in cancer progression and in pathological forms of angiogenesis. Recent biochemical studies suggest that agonizing EphB4 signaling, or antagonizing ephrin-B2 signaling, results in the inhibition of cellular proliferation in vitro. Here we present the 1.65 Å crystal structure of the ligand

binding domain of EphB4 in complex with an antagonistic peptide that inhibits ephrin-B2 binding and exhibits anti-tumorigenic properties in vivo. Further, we present the 1.9 Å crystal structure of the EphB4-ephrin-B2 complex. A thorough comparative analysis of the two structures reveals how subtle differences in the amino acid composition of the receptor G-H and J-K loops results in the recruitment of a unique set of ligands to the cell surface. ITC and FP studies further reveal the molecular determinants for the directed specificity unique to the EphB4 receptor, allowing the first insights into modulating pathways resulting in tumorigenesis and angiogenesis that rely on EphB4-ephrinB2 signaling.

**S-P127 Complexed Crystal Structure of Primosomal Protein PriB Reveals a Novel Single-stranded DNA Binding Mode.**

C.Y. Huang, C.H. Hsu, Y.J. Sun, H.N. Wu, C.D. Hsiao, Inst. of Molecular Biology, Academia Sinica, Taipei, Taiwan.

PriB is a primosomal protein required for replication restart in *Escherichia coli*. PriB stimulates PriA helicase activity via interaction with single-stranded DNA (ssDNA), but the molecular details of this interaction remain unclear. Here, we report the crystal structure of PriB in a complex with a 15-mer oligodeoxythymidylate (dT15) at 2.7 Å resolution. Although PriB shares structural similarity with the *E. coli* single-stranded DNA-binding protein (*EcoSSB*), the structure of the PriB-dT15 complex reveals that PriB and *EcoSSB* differ in the way they bind ssDNA. Filter-binding assays showed that the PriB-ssDNA interaction is salt-sensitive and cooperative. Mutational analysis confirmed that the loop L<sub>45</sub> plays an important role in ssDNA binding. We propose a cooperative binding mechanism of PriB to ssDNA and a model for the assembly of the PriA-PriB-ssDNA complex. This is the first structure showing a replication restart primosomal protein in a complex with ssDNA, and it provides a novel model to elucidate how a dimeric oligonucleotide-binding-fold protein binds ssDNA.

**S-P129 Crystal Structure of Human Apolipoprotein A-I: Insights into its Protective Effect Against Cardiovascular Diseases.**

A. Abdul Ajees\*, G.M. Anantharamaiah†, Vinod K. Mishra‡, M. Mahmood Hussain§, H.M. Krishna Murthy\*, \*Center for Biophysical Sciences and Engineering, †The Atherosclerosis Research Unit, Depts. of Medicine, Biochemistry and Molecular Genetics, Univ. of Alabama at Birmingham, Birmingham, AL, §Depts. of Anatomy, Cell Biology and Pediatrics, SUNY Downstate Medical Center, Brooklyn, NY.

Despite three decades of extensive studies on human apolipoprotein A-I (apoA-I), the major protein component in high density lipoproteins, the molecular basis for its antiatherogenic function is elusive, in part due to lack of a structure of the full-length protein. We describe here the crystal structure of lipid-free apoA-I at 2.4 Å. The structure shows that apoA-I is comprised of an amino-terminal four-helix bundle and two carboxy-terminal helices. The N-terminal domain plays a prominent role in maintaining its lipid-free conformation, indicating that mutants with truncations in this region form inadequate models for explaining functional properties of apoA-I. This structure provides for the first time a much-needed structural template for exploration of molecular mechanisms by which human apoA-I ameliorates atherosclerosis and inflammatory diseases.

**S-P131 Crystal Structures of Free Textilinin-1 and its Complex with the Catalytic Domain of Human Plasmin.** Emma-Karin I. Millers<sup>1</sup>, Geoff Birrell<sup>2</sup>, Paul P. Masci<sup>3</sup>, Martin F. Lavin<sup>2</sup>, John de Jersey<sup>1</sup>, Luke W. Guddat<sup>1</sup>, <sup>1</sup>School of Molecular and Microbial Sciences, Univ. of Queensland, Brisbane, <sup>2</sup>The Queensland Cancer Fund Research Unit, The Queensland Inst. of Medical Research, Herston, Brisbane, <sup>3</sup>Dept. of Medicine, Univ. of Queensland, Princess Alexandra Hospital, Woolloongabba, Brisbane 4102, QLD, Australia.

Textilinin-1 (Txln-1) is a small multiply disulfide bonded protein isolated from the venom of the Australian common brown snake, *Pseudonaja textilis textilis*. It is a Kunitz type serine protease inhibitor that works as an anti-fibrinolytic agent by blocking the activity of plasmin and/or other proteases involved in fibrinolysis. The crystal structures of free recombinant Txln-1 and its complex with human recombinant microplasmin, the catalytic domain of plasmin; residues 542-791, have been determined to 1.63 Å and 2.8 Å resolution respectively. The primary binding loop of Txln-1 to microplasmin adopts multiple conformations in the free structure. However, when bound in the complex this loop is ordered, forming a stable Michaelis complex with microplasmin. Arginine 17 from Txln-1 (ArgT17) protrudes into the specificity pocket (P1 site) of microplasmin making ionic contact with aspartate 735 (AspP735). The carbonyl carbon of ArgT17 makes a shorter than van der Waals contact with the hydroxyl of SerP741, a residue in the catalytic triad. The side chain of HisP603, which is also part of the catalytic triad, has an orientation not observed in any other plasmin structure. The structure of the complex between Txln-1 and microplasmin will assist in the development of antifibrinolytic therapeutic agents.

We acknowledge the Australian Research Council and QRxPharma for financial support.

**S-P133 Crystal Structure of HP0242, a Hypothetical Protein from *Helicobacter pylori* with a Novel Fold.** Jia-Yin Tsai, Bo-Tsang Chen, Hui-Chun Cheng, Hsin-Yi Chen, Nai-Wan Hsiao, Ping-Chiang Lyu, and Yuh-Ju Sun, Inst. of Bioinformatics and Structural Biology, National Tsing Hua Univ., Hsinchu 300, Taiwan, Republic of China.

HP0242 is a hypothetical protein from a human gastric pathogen, *Helicobacter pylori*. Here, we report the first crystal structure of HP0242 determined at 2.27 Å resolution by multiwavelength anomalous dispersion (MAD) phasing. The overall structure of HP0242 folds like a musical instrument-triangle with four helices. Two monomers tightly interlock each other by Helix2 to form a dimer with extremely strong interactions. Helix2 is essential in the formation of HP0242 dimer. We suggest that dimer might represent the functional state for HP0242. A structure-based homology analysis with the DALI algorithm indicates that HP0242 has a novel fold. To date, none of the HP0242 and its homologues has been assigned a cellular function. Our results may shed a light on further functional studies based on the unique protein folding.

**S-P135 Kinetic and Structural Properties of Triosephosphate Isomerase from *Helicobacter pylori*.** Chen-Hsi, Chu, Yi-Ju, Lai and Yuh-Ju Sun, Inst. of Bioinformatics and Structural Biology, National Tsing Hua Univ., Hsinchu 300, Taiwan, Republic of China.

The glycolysis enzyme triosephosphate isomerase (TIM) has been cloned from *Helicobacter pylori*. Biochemical characterizations of the recombinant expressed protein (HpTIM) revealed a high degree of similarity to other species TIMs and its enzymatic activity towards the substrate D-glyceraldehyde-3-phosphate was determined ( $K_m = 2.92 \pm 0.19$  mM,  $k_{cat} = 5.4 \times 10^4$  min<sup>-1</sup>, and  $V_{max} = 9.70 \pm 0.89$

$\mu\text{M min}^{-1}$ ). The HpTIM crystal structure was determined by molecular replacement method at 2.3Å resolution. The overall structure is  $(\beta/\alpha)_6(\beta/\alpha)_6$ , resemble to the common TIM barrel folding with  $(\beta/\alpha)_6$ . From the conformation of loop 6, connecting  $\beta\text{F}$  and  $\alpha\text{8}$ , and binding of phosphate ion, the HpTIM was recognized as the “closed” state. The conserved salt bridge between Arg and Asp among other TIMs was absence in HpTIM, the corresponding residues were Lys183 and Ser211. However, HpTIM has a unique salt bridge between Lys183 and Asp213. For clarification of the significance of this salt bridge to TIM, the enzymatic activity of salt bridge mutants of HpTIM was determined. The results suggested that the conserved salt bridge might not be necessary for TIM enzymatic activity but contribute to its conformational stability.

**S-P137 Crystal Structures of  $\Delta^1$ -pyrroline-2-carboxylate Reductase from *Pseudomonas*.** Masaru Goto, Hisashi Muramatsu, Hisaaki Mihara, Tatsuo Kurihara, Nobuyoshi Esaki, Rie Omi, Ikuko Miyahara, Ken Hirotsu, Dept. of Biochemistry, Osaka Medical College, Takatuki City, Osaka, Japan.

$\Delta^1$ -Piperidine-2-carboxylate/ $\Delta^1$ -pyrroline-2-carboxylate reductase from *Pseudomonas syringae* pv. tomato belongs to a novel subclass in a large family of NAD(P)H-dependent oxidoreductases distinct from the conventional MDH/LDH superfamily characterized by the Rossmann fold. We have determined the structures of the following three forms of the enzyme: the unliganded form, the complex with NADPH, and the complex with NADPH and pyrrole-2-carboxylate at 1.55, 1.8, and 1.7 Å resolutions, respectively. The enzyme exists as a dimer, and the subunit consists of three domains, domain I, domain II (NADPH binding domain), and domain III. The core of the NADPH binding domain consists of a SEven-Stranded predominantly Antiparallel  $\beta$ -Sheet, which is called “SESAS”, fold characteristic of the new oxidoreductase family. The enzyme’s preference for NADPH over NADH is explained by the cofactor binding site architecture. A comparison of the overall structures revealed that the mobile domains I and III change their conformations to produce the catalytic form. This conformational change plays important roles in substrate recognition and the catalytic process.

**S-P139 Structural Basis for the Dehalogenation of Fluoroacetate by Fluoroacetate Dehalogenase.** Rie Omi, Keiji Jitsumori, Tatsuo Kurihara, Nobuyoshi Esaki, Ikuko Miyahara, Ken Hirotsu, Inst. for Chemical Research, Kyoto Univ., Kyoto, Japan.

Fluoroacetate dehalogenase (FAC-DEX) isolated from *Burkholderia* sp. FA1 catalyzes the hydrolytic cleavage of the stable carbon-fluorine bond of fluoroacetate to produce glycolate. FAC-DEX is the only enzyme which shows the high activity toward fluoroacetate and the low activity toward chloroacetate and bromoacetate. In order to elucidate the structure-function relationship of FAC-DEX, we have determined the three-dimensional structures of the native FAC-DEX, the D104N FAC-DEX complexed with fluoroacetate, and the ester intermediate. FAC-DEX consists of two domains (a core domain and a cap domain) and includes Asp104 and His271 as the catalytic nucleophile and base, respectively, in the core domain. One of the striking features of FAC-DEX is the conformational change of the loop region which exists in the vicinity of active-site entrance, depending on the binding of the substrate. This conformational change is related to the substrate recognition and plays an important role in the catalytic action of the enzyme. The fluoroacetate molecule was observed in the active site of the D104N-fluoroacetate and the fluorine atom of the fluoroacetate makes a contact with the guanidino group  $\text{NH}_2$  of Arg108.

**S-P141 Structural Analysis of ROM Mutants Using Crystallographic and NMR Techniques.** Evi B. Struble<sup>1</sup>, Danielle M. Barbazon<sup>2</sup>, Jane E. Ladner<sup>1</sup>, John P. Marino<sup>1</sup>, <sup>1</sup>Center for Advanced Research in Biotechnology of the Univ. of Maryland Biotechnology Inst., and the National Inst. of Standards and Technology, Rockville, MD, <sup>2</sup>Loyola College in Maryland, Baltimore, MD.

Solution studies of the ROM protein from ColE1 plasmid have determined that single point mutations at position 14 have deleterious effect on the binding of this protein to kissing loop RNA dimers. We solved the x-ray structures for three of these mutants F14Y, F14W, and F14H. All the three dimensional structures are essentially the same as the native ROM protein, with evidence of increased conformational variability of the amino acid side chain at the mutation site. Surprisingly, solution NMR data, in particular <sup>1</sup>H, <sup>15</sup>N relaxation and residual dipolar coupling (RDC) measurements show significant differences between native and mutant ROM structures. These differences are not limited at the mutation site and suggest that Phe 14 may be important in fine-tuning the presentation of the helical surface of the Rom dimer to the RNA kissing complex. A side-by-side comparison between RDC values predicted from the crystal structures and the ones measured using NMR will be presented and the significance of such comparisons will be discussed.

**S-P143 Crystal Structure of Shikimate Dehydrogenase from *Aquifex Aeolicus*.** J.H. Gan<sup>1</sup>, P. Prabakaran<sup>1</sup>, Y. Li<sup>2</sup>, Y. Gu<sup>1</sup>, M. Andrykovitch<sup>1</sup>, H. Yan<sup>2</sup>, X. Ji<sup>1</sup>, <sup>1</sup>Macromolecular Crystallography Laboratory, National Cancer Inst., National Institutes of Health, Frederick, MD, USA; <sup>2</sup>Dept. of Biochemistry and Molecular Biology, Michigan State Univ., East Lansing, MI.

Shikimate dehydrogenase (SD) catalyzes the fourth reaction in the shikimate pathway, the NADP-dependent reduction of 3-dehydroshikimate (3-DS) to shikimate acid (SA). The shikimate pathway, a seven-step metabolism leading from phosphoenolpyruvate and erythrose 4-phosphate to chorismate, is essential for aromatic biosynthesis in bacterial, fungi, plants, and apicomplexan parasites, but is absent from mammals, which makes it an ideal target for development of antimicrobials, herbicides, and antiparasite agents. Three classes of SD enzymes (YdiB, AroE, and SD-like) were identified and characterized, and a few three-dimensional structures were reported. However, none of the structures has either 3-DS or SA bound in the active site. Here, we present three crystal structures of SD from *Aquifex Aeolicus* (AaSD), including apo-AaSD, AaSD•Hg<sup>2+</sup>, and AaSD•NADP•SA (a ternary complex with both the cofactor and the product bound in the active center). These structures provide insight into the catalytic mechanism of SD, and assist structure-based design of novel antimicrobials, herbicides, and antiparasite agents.

**S-P145 Structures of 5-methylthioribose Kinase Phased by ADP-2Ho: Catalytic Mechanism and Drug Design.** S-Y. Ku<sup>a,b</sup>, P. Yip,<sup>b</sup> K.A. Cornell,<sup>c</sup> M.K. Riscoe,<sup>d</sup> P.L. Howell<sup>a,b</sup>, <sup>a</sup>Univ. of Toronto and <sup>b</sup>Hospital for Sick Children, Toronto, ON, Canada, <sup>c</sup>Boise State Univ., ID, <sup>d</sup>Portland State Univ., OR.

Methionine plays critical roles in many cellular functions but is energetically costly to synthesize; thus pathways to salvage methionine have evolved in all organisms. 5-methylthioribose (MTR) kinase is a key enzyme in this pathway in microorganisms and certain plants, and the absence of a mammalian homolog makes the enzyme a good target for the design of selective antibiotics and herbicides. Recombinant *B. subtilis* MTR kinase has been crystallized with the detergent CHAPS, and structures of the apo enzyme, ADP, AMPPCP and AMPPCP-MTR complexes determined to 2.1Å,

2.2Å, 2.0Å, and 2.3Å resolution, respectively. MTR kinase has an eukaryotic protein kinase fold, and is structurally similar to 3',5'-aminoglycoside phosphotransferase and choline kinase. No global conformation movement is observed upon substrates binding and a dissociate mechanism for phosphate transfer is proposed. The structure was phased using the anomalous signal of holmium. Two holmium ions replace the magnesium ions in the ADP-2Ho protein complex, suggesting that holmium could serve as a convenient and powerful phasing tool to aid the structure determination of other nucleotide binding proteins.

**S-P147 Crystal Structure of Penicillin Binding Protein 4 (dacB) from *Escherichia coli*, Both in the Native Form and Covalently Linked to Various Antibiotics.** Hiroyuki Kishida, Satoru Unzai, Jeremy R.H. Tame and Sam-Yong Park, Protein Design Laboratory, Yokohama City Univ., Tsurumi-ku, Yokohama, Japan.

The crystal structure is presented of penicillin binding protein 4 (PBP4) from *Escherichia coli*, a bifunctional enzyme with both DD-endopeptidase and DD-carboxypeptidase activity. PBP4 is one of 12 penicillin binding proteins in *E.coli* involved in the synthesis and maintenance of the cell wall. The model contains a penicillin binding domain similar to known structures, but includes a large insertion which folds into domains with unique folds. The structures of the protein covalently attached to five different antibiotics presented here show the active site residues are unmoved compared to the apo protein, but nearby surface loops and helices are displaced in some cases. Movement of conserved residues suggests a possible cause for the slow deacylation rate of PBP4.

**S-P149 Crystal Structure of Methionyl-tRNA Formyltransferase from *Clostridium thermocellum*.** H. Yang, I. Kataeva, H. Xu, M. Zhao, J. Chang, Z. Liu, L. Chen, W. Tempel, D. Lee, D. Lin, J.P. Rose, B.C. Wang, Dept. of Biochemistry and Molecular Biology, Univ. of Georgia, Athens, GA 30602.

Methionyl-tRNA formyltransferase (FMT) is the enzyme responsible for the formylation of the amino terminus of the acyl moiety of tRNA<sup>Met</sup>, a key step in the targeting of initiator tRNA towards the translation start machinery in bacteria. The structure of *Clostridium thermocellum* FMT has been determined to 2.05 Å resolution. Crystals of selenomethionine protein were grown by the microbatch method using 2.5M ammonium sulfate, 0.1M sodium citrate, pH 5.6 as the precipitant. The crystals belong to space group P4<sub>2</sub>,2<sub>1</sub> with a = 85.4Å and c = 104.27Å. Protein phases and the initial electron density map were generated from single wavelength anomalous scattering data ( $\lambda = 0.9794\text{Å}$ ), collected at SER-CAT, using the SCA2Structure pipeline. The resulting model was refined against a native 2.05Å resolution data set and converged to an R-value of 20.9% (R-free = 23.7%). The coordinates have been deposited in the Protein Data Bank, entry 1ZGH. The protein has a Formyl\_trans\_N domain structure at N-terminal domain resembles a Rossman fold.

Work supported by NIGMS (GM062407), the Georgia Research Alliance, and The UGA Research Foundation.

**S-P151 The Reaction of PMM/PGM: Structural Insights Into a Simple Processive Enzyme.** Andrew M. Schramm, Catherine Regni, Lesa J. Beamer, Dept. of Biochemistry, Univ. of Missouri-Columbia, MO.

The enzyme phosphomannomutase/phosphoglucosmutase (PMM/PGM) belongs to the  $\alpha$ -D-phosphohexomutase enzyme superfam-

ily and catalyzes the reversible conversion of 1-phospho to 6-phosphosugars. The reaction entails two phosphoryl transfers, with an intervening 180° reorientation of the reaction intermediate (e.g., glucose 1,6-bisphosphate) during catalysis. Reorientation of the intermediate occurs without dissociation from the active site of the enzyme, and is thus a simple example of processivity, as defined by multiple rounds of catalysis without release of substrate.

Structural characterization of two PMM/PGM intermediate complexes with glucose 1,6-bisphosphate provides new insights into the reaction catalyzed by the enzyme, including the reorientation of the intermediate. Kinetic analyses of site-directed mutants reveal active site residues critical for maintaining association with glucose 1,6-bisphosphate during its dynamic reorientation in the active site of PMM/PGM.

**S-P153 Structural and Biochemical Studies of Carnitine Acyltransferases.** Yu-Shan Hsiao, Gerwald Jogl and Liang Tong, Dept. of Biological Sciences, Columbia Univ., New York, NY.

Carnitine acyltransferases catalyze the exchange of acyl groups between carnitine and coenzyme A (CoA). The enzymes of this family are classified based on their substrate preferences, including carnitine acetyltransferase (CrAT), carnitine octanoyltransferase (CrOT), and carnitine palmitoyltransferases (CPTs). CPT I and CPT II are crucial for the  $\beta$ -oxidation of long-chain fatty acids in the mitochondria by enabling their transport across the mitochondrial membrane. The unique sensitivity of CPT I to malonyl-CoA is a crucial regulatory mechanism for fatty acid oxidation. Mutation and dysregulation of CPTs are strongly linked to many human diseases, and they are promising targets for developing therapeutic agents against obesity and type 2 diabetes. We have determined the crystal structures of mouse CrAT and CrOT, alone and in binary and ternary complexes with various substrates and products. Our structural, mutagenesis and biochemical studies have elucidated the molecular basis for the substrate selectivity of these enzymes between short- and medium-chain fatty acids.

**S-P155 Structure of the Type IV Pilus Scaffold Protein PilF from *P. aeruginosa*.** J. Koo<sup>1,2</sup>, S.-Y. Ku<sup>1,2</sup>, L. Sampaleanu<sup>1</sup>, L.L. Burrows<sup>1,3</sup>, P.L. Howell<sup>1,2</sup>, <sup>1</sup>Hospital for Sick Children, <sup>2</sup>Univ. of Toronto, Toronto, ON, Canada, <sup>3</sup>McMaster Univ., Hamilton, ON, Canada.

Type IV pili (T4P) are long, thin, flexible filaments that are required for the initiation of infection by many human, animal and plant pathogens including *P. aeruginosa*. While T4P are composed of 1000's of copies of a single protein, PilA, mutational data have implicated over 50 genes in the regulation, biosynthesis, assembly and function of T4P in *P. aeruginosa*. Of interest to us are the *pilF* gene and the *pilMNOPQ* gene cluster. The protein products of these genes are hypothesized to form a multi-protein complex that spans the intricate, 3-layered Gram-negative bacterial cell wall to provide a conduit for passage of the pilus. PilF, a predicted periplasmic lipoprotein, is believed to stabilize oligomerization of the secretin PilQ, an outer membrane protein that forms a dodecameric pore through which the pilus is extended and retracted. To investigate how PilF affects PilQ function, we have determined the structure of PilF at 2.0 Å resolution using SeMet incorporation and the SAD technique. The protein contains 6 tetratricopeptide repeat (TPR) domains, a common protein-protein interaction motif, arranged in a superhelix. The structure and its implications for PilF function will be presented.

**S-P157 Crystal Structure of Quinolinate Synthase, an Enzyme Involved in the *de novo* NAD Biosynthesis.** Erika Soriano, Ethan C. Settembre, Tadhg P. Begley, Steven E. Ealick, Dept. of Chemistry and Chemical Biology, Cornell Univ., Ithaca, NY.

Nicotinamide adenine dinucleotide (NAD) is an essential cofactor in several metabolic pathways and has recently been shown to play a role in several signaling pathways. Consequently, there is great interest in the biosynthesis of NAD. Quinolinate is the universal precursor in the *de novo* biosynthesis of NAD and can be synthesized starting from either tryptophan in the case of eukaryotes or from aspartate in most prokaryotes. The aspartate pathway begins with L-aspartate oxidase, which converts aspartate to iminoaspartate. Quinolinate synthase (QS) catalyzes the condensation of iminoaspartate and dihydroxyacetone phosphate to form quinolinic acid. This enzyme has been difficult to characterize due to either instability or inactivity when it is overexpressed and purified. QS is the final enzyme in this pathway to be structurally characterized (1WZU; Sakuraba, *et al.*, *J. Biol. Chem.* **280**:26645-8 (2005)). We have determined the crystal structure of QS from *Pyrococcus furiosus* at 2.8 Å resolution. The crystal structure and sequence alignments provide insights into the details of the active site and the enzyme's evolution.

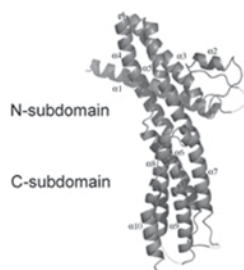
**S-P159 Crystal Structures of the Nitric Oxide Complexes of Horse Heart Myoglobin.** Daniel M. Copeland<sup>1</sup>, Alexei S. Soares<sup>2</sup>, Ann H. West<sup>1</sup>, George B. Richter-Addo<sup>1</sup>, <sup>1</sup>Dept. of Chemistry and Biochemistry, Univ. of Oklahoma, Norman, OK, <sup>2</sup>Macromolecular Crystallography Research Resource, National Synchrotron Light Source, Brookhaven National Laboratory, Upton, NY.

The interactions of nitric oxide (NO) and nitrite with heme proteins are physiologically relevant. Nitrite binds to ferric and ferrous synthetic porphyrins through its N atom. The crystal structures of the nitrite adducts of some heme proteins also show the N-binding of nitrite to the iron center. We have determined the high resolution crystal structure of the nitrite adduct of ferric horse heart myoglobin (hh Mb) to 1.20 Å resolution. The nitrite moiety is bound directly to the iron atom of the heme group, and is stabilized by hydrogen bonding to the distal His64 residue. We have also determined the crystal structures of nitrosyl horse heart myoglobin. We find that the FeNO conformation is dependent on the method of preparation of the nitrosyl myoglobin.

This work was supported by the U.S National Institutes of Health (GM 64476; GBR-A).

**S-P161 Sec15 Interacts with Rab11 via a Novel Domain and Affects Rab11 Localization *in vivo*.** Shuya Wu,<sup>1</sup> Sunil Q. Mehta,<sup>2</sup> Franck Pichaud,<sup>5</sup> Hugo J. Bellen,<sup>2,3,4</sup> Florante A. Quijcho<sup>1,4</sup>, <sup>1</sup>Dept of Biochemistry and Molecular Biology, <sup>2</sup>Program in Developmental Biology, <sup>3</sup>Depts of Molecular Human Genetics and of Neuroscience, <sup>4</sup>Howard Hughes Medical Inst., Baylor College of Medicine, Houston, TX, <sup>5</sup>LMCB, Univ. College London, London, UK.

Sec15, a component of the exocyst, recognizes vesicle associated Rab GTPases, helps target transport vesicles to the budding site, and is thought to recruit other exocyst proteins. Here, we report the characterization of a 35 kDa fragment which comprises most of the C-terminal half of *Drosophila* Sec15. This C-terminal domain was shown to bind a subset of Rab GTPases, especially Rab11, in a GTP-dependent manner. We also provide evidence that in the fly photoreceptors Sec15 co-



calizes with Rab11 and loss of Sec15 affects rhabdomere morphology. Determination of the 2.5 Å crystal structure of the C-terminal domain revealed an elongated structure with a novel fold consisting of 10 α helices equally distributed in two subdomains (N- and C-subdomains). We show that the C-subdomain, via mainly a single helix, is sufficient for Rab binding. Since the C-subdomain shares no sequence and structure homology to any known Rab effectors, the structure highlights a new Rab-binding domain.

**S-P163 Discovery of the HCV NS3/4A Protease Inhibitor SCH503034. Key Steps in Structure-Based Optimization.** Andrew J. Prongay, Zhuyan Guo, John Pichardo, Nanhua Yao, Thierry Fischmann, Joseph Myers, Jr., Patricia C. Weber, Bruce Malcolm, Brian M. Beyer, Richard Ingram, Rumin Zhang, Ashok Arasappan, Frank Bennett, Stephane L. Bogen, Kevin Chen, Edwin Jao, Raymond G. Lovey, Srikanth Venkatraman, F. George Njoroge, Vincent Madison, Schering-Plough Research Inst., Kenilworth, NJ.

The structures of both native and S139A apo-HCV NS3/4A protease domain were solved to high resolution. Subsequently, structures were determined for a series of ketoamide inhibitors in complex with the protease. The changes in the inhibitor potency were correlated with changes in the buried surface area upon binding the inhibitor to the active site. The largest contributions to the binding energy arises from the hydrophobic interactions of the P1 and P2 groups as they bind to the S1 and S2 pockets. This correlation of the changes in potency with increased buried surface area contributed directly to the design of a potent tripeptide inhibitor of the HCV NS3/4a protease that is currently in clinical trials.

**S-P165 Structural Studies and Comparison of the Crystal Structures of Human Apo- and Holo-Cellular Retinoic Acid Binding Protein (CRABP) II.** Soheila Vaezeslami, Erika Mathes, Chrysoula Vasileiou, Babak Borhan, James H. Geiger, Dept. of Chemistry, Michigan State Univ., East Lansing, MI.

CRABP II is a small, cytosolic protein that solubilizes and transfers retinoic acid (RA) to the nucleus while also enhancing its transcriptional activity. We have determined the first high-resolution structure of apo-wild type (WT) CRABP II at 1.35 Å. Using three different data sets collected on apo-WT CRABP II we have shown that apo- and holo-CRABP II share very similar structures. Binding of RA appears to increase the overall rigidity of the structure, although the induced structural changes are not as pronounced as previously thought. The enhanced structural rigidity may be an important determinant for the enhanced nuclear localization of the RA-bound protein. Comparison of our apo-WT with the apo-R111M structure shows that mutation of Arg111, a conserved residue of CRABP II and a key residue in RA binding, causes major structural changes in the molecule. We further investigated the structural importance of Arg111 by determining the structures of four other CRABP II mutants. Our structures also demonstrate structural changes induced by crystal packing and show that a crystal can harbor demonstrative structural differences in the asymmetric unit.

**S-P167 Crystal Structure of D-Ribulose 5-Phosphate 3-Epimerase in Complex with D-Xylitol 5-Phosphate.** Alexander A. Fedorov, Elena V. Fedorov, Julie Akana\*, John A. Gerlt\*, Steve C. Almo, Dept. of Biochemistry, Albert Einstein College of Medicine, Bronx, NY 10461 \*Dept. of Biochemistry, Univ. of Illinois, at Urbana-Champaign, Urbana, IL 61801.

D-Ribulose 5-Phosphate 3-Epimerase belongs to the "ribulose phos-

phate binding" superfamily defined by the Structural Classification of proteins (SCOP). The crystal structure of D-Ribulose 5-Phosphate 3-Epimerase from *Streptococcus pyogenes* complexed with D-Xylitol 5-Phosphate and Zn was solved by molecular replacement with EPMR using model derived from the *Synechocystis* RPE hexamer (PDB file 1TQJ). The refinement was carried out using CNS at 1.8 Å resolution to a  $R_{\text{cryst}}=0.224$  and  $R_{\text{free}}=0.256$ . The final structure contains 19748 protein atoms, 12 inhibitor molecules, 12 Zn atoms and 991 water molecules for two hexamers of the complex in the asymmetric unit. Every Zn atom in the structure is coordinated by two oxygens from the inhibitor and by His 34, Asp 36, His 67 and Asp 176 from the enzyme. The functional and structural correlations for D-Ribulose 5-Phosphate 3-Epimerase will be presented.

**S-P169 Substrate-assisted in Oxygen Activation by Cytochrome P450 158A2: A New Mechanism of Proton Transfer.** Bin Zhao, F. Peter Guengerich, Markus Voehler, Michael R. Waterman, Dept. of Biochemistry, Vanderbilt Univ. School of Medicine, Nashville, TN.

CYP158A2 as well as other related P450s regarding CYP101A1 (Schlichting *et al* (2000) *Science* 287, 1615-1622, and Nagano *et al* (2005) *J. Biol. Chem.* 280, 31659-31663) and CYP107A1 (Nagano *et al* (2005) *J. Biol. Chem.* 280, 22101-22107) have solved the X-ray crystal structure of the ferrous-dioxygen bound P450s at high resolution, revealing the structural basis for proton transfer and dioxygen activation in P450s. The ferric substrate analogue complex and the unique short-lived intermediate ferrous-dioxygen complex structures identify the role of active site water molecules that are critical for proton transfer during catalytic cycle, which are supported by biochemical studies. This has important implications not only for understanding the structural basis of a proton transfer pathway for oxygen activation via water molecules in CYP158A2 but also classifying two classes of P450s based on the pathway of proton transfer, one self-assisted enzyme involving the highly conserved threonine in the I-helix (CYP101A1) and the substrate-assisted enzyme requiring the substrate molecules either to directly transfer protons (CYP107A1) or to stabilize a water pathway for proton transfer (CYP158A2).

**S-P171 Binding of the Substrate Analog Azide to the Active Site of Human Manganese Superoxide Dismutase.** J.F. Domsic<sup>§</sup>, P.S. Quint<sup>¶</sup>, L. Govindasamy<sup>§</sup>, C.K. Tu<sup>¶</sup>, D.N. Silverman<sup>¶</sup>, R. McKenna<sup>§</sup>, <sup>§</sup>Dept. of Biochemistry and Molecular Biology, <sup>¶</sup>Dept. of Pharmacology and Therapeutics, College of Medicine, Univ. of Florida, Gainesville, FL, 32610.

Human Manganese superoxide dismutase (MnSOD) is a mitochondrial enzyme that scavenges superoxide radicals from its environment. MnSOD catalyzes the disproportionation of superoxide, leading to the formation of oxygen and hydrogen peroxide. However, during the oxidation of the manganese ligand, a product inhibited form occurs, consisting of a side-on or end-on peroxo complex. In order to better understand how this inhibition occurs, we used crystallographic and spectrophotometric analyses to observe the binding of the substrate analog azide in the active site pocket. The crystal structure of MnSOD bound with azide was solved to 2.3 Å resolution with an  $R_{\text{cryst}}$  of 0.201. Azide is positioned such that one end interacts with the hydroxyl group on the side chain of Tyr34 while the other coordinates with the Mn ligand. This orientation corroborates well with the previously solved structure of azide bound to MnSOD from *Thermus thermophilus*. It is also further supported by UV/Vis spectrophotometry, which revealed that azide binding was greatly inhibited by the presence of 3-fluorotyrosine substituted at position 34.

**S-P173 Structure and Catalytic Mechanism of S-adenosylmethionine Synthetase.** Fusao Takusagawa, Junichi Komoto, Taro Yamada, George Markham, Molecular Biosciences, Univ. of Kansas, Lawrence, KS 66045.

S-Adenosylmethionine synthetase (MAT) catalyzes formation of S-adenosylmethionine (SAM) from ATP and L-methionine (Met) and hydrolysis of triphosphosphate to  $\text{PP}_i$  and  $\text{P}_i$ . *E. coli* MAT (eMAT) has been crystallized with the ATP analogue AMPPNP and Met, and the crystal structure has been determined at 2.5 Å resolution. eMAT is a dimer of dimers and has a 222 symmetry. Each active site contains the products (SAM and PPNP). A modeling study indicates that the substrates (AMPPNP and Met) can bind at the same sites of the products and only a small conformation change of the ribose ring is needed in conversion of the substrates to the products. On the basis of the ternary complex structure and a modeling study, a novel catalytic mechanism of the SAM formation is proposed. In the mechanism, neutral His14 acts as an acid to cleave the C5'-O5' bond of ATP while simultaneously a change in the ribose ring conformation from C4'-*exo* to C3'-*endo* occurs, and the S of Met makes a nucleophilic attack on the C5' to form SAM. All essential amino acid residues for substrate binding found in eMAT are conserved in the rat liver enzyme, indicating that the bacterial and mammalian enzymes have the same catalytic mechanism. However, a catalytic mechanism proposed recently by González *et al.* based on the structures of three ternary complexes of rat liver MAT (*J. Mol. Biol.* **331**, 407 (2003)) is substantially different from our mechanism.

**S-P175 Structural Basis of Why a Thermophilic Acylphosphatase is a Poor Enzyme at Lower Temperatures.** Kam-Bo Wong, Sonia Y. Lam, Rachel C.Y. Yeung, Dept. of Biochemistry, Centre for Protein Science and Crystallography, The Chinese Univ. of Hong Kong, Shatin, Hong Kong, China.

Acylphosphatase is a small enzyme (~90-100 residues) that catalyzes the hydrolysis of carboxyl-phosphate bond in acylphosphates. We have determined the crystal structures of a thermophilic acylphosphatase from *Pyrococcus horikoshii* (PhAcP) to 1.5 Å; and a mesophilic homolog, human common-type acylphosphatase to 1.45 Å. PhAcP is an extremely stable protein with a melting temperature of ~110°C. Enzyme kinetics reveals that PhAcP is less catalytically efficient than its mesophilic homolog at 25°C. Structural comparison has revealed that the active site residue, Arg-20, forms an extra salt-bridge to the carboxyl group of the C-terminal Gly-91. To investigate if this salt-bridge contributes to the reduced catalytic efficiency of PhAcP, we disrupt the salt-bridge by replacing the Gly-91 with an alanine, as the formation of the salt-bridge requires the glycine residue to adopt a phi angle of ~180 deg. Crystal structure of the G91A variant shows that the salt-bridge is disrupted without affecting the active site structure. The significant increase of catalytic efficiency of G91A variant suggests that the salt-bridge between Arg-20 and Gly-91 does play a role in reducing the activity of PhAcP.

**S-P177 Effect of Solution Stirring on Protein Crystallization.** Ryota Murai, Shinya Nakata, Masafumi Kashii, Hiroaki Adachi, Kazufumi Takano, Hiroyoshi Matsumura, Satoshi Murakami, Tsuyoshi Inoue, Yusuke Mori, Takatomo Sasaki, Osaka Univ., SOSHO Inc., Suita, Osaka, Japan.

In order to produce high-quality protein crystals, we have developed solution stirring technique. Stirring a protein solution during the crystallization decrease the number of crystals produced, and an increase in the size and quality of the crystals<sup>[1]</sup>.

This time, we investigate the supersaturation condition which stirring technique works effectively. Supersaturation was controlled by

temperature, because it can control the supersaturation easily and precisely from outside. This experiment was conducted with a new temperature control tool TAON which we had developed<sup>[2]</sup>. TAON can produce multi-temperature conditions on a micro-plate by generating a temperature gradient. Using TAON, we can stir various temperature protein solutions at one time.

Stirring technique worked well in the high supersaturation conditions. However, when the supersaturation became too high, the effect of stirring was not seen. From this results, we found suitable conditions to produce high quality protein crystals with stirring technique.

[1] M. Yaoi, H. Adachi, K. Takano, H. Matsumura, T. Inoue, Y. Mori and T. Sasaki: *Jpn. J. Appl. Phys.* **43** (2004) 686.

[2] H. Adachi, A. Niino, K. Takano, H. Matsumura, S. Murakami, T. Inoue, Y. Mori and T. Sasaki: *Jpn. J. Appl. Phys.* **44** (2005) 4080.

**S-P179 Protein Crystal Processing Using Ultraviolet Laser Irradiation.** Kazufumi Takano, Hiroshi Kitano, Hiroaki Adachi, Masafumi Kashii, Hiroyoshi Matsumura, Satoshi Murakami, Tsuyoshi Inoue, Yusuke Mori, Masaaki Doi, Takatomo Sasaki, Osaka Univ., SOSHO Inc., Nikon Corp., Suita Osaka, Japan.

We have developed a protein crystal processing technique, pulsed UV laser soft ablation (PULSA). The complicated and precise processing of protein crystals, which is not possible at present using conventional mechanical tools, has been achieved using PULSA without causing significant damage. The processing was effective for various protein crystals. In the case of a partially cracked protein crystal, the diffraction pattern was considerably improved by eliminating the damaged section with the PULSA processing. Furthermore, a laser-processed protein crystal was seeded and grown larger than its original size. PULSA also successfully processed not only cryo-cooled crystals but also nylon loops and cryoprotectants at a cryogenic temperature. This new approach will enable us to reliably process biological macromolecular crystals, and to expand the limits of crystal species that can currently be used for XRD measurement.

**S-P181 Structural Studies on a NADP<sup>+</sup>/H Dependent Oxidoreductase Contributes to Investigate Coenzyme Specificity.** M. Medina, M. Martínez-Júlvez, J.R. Peregrina and J. Hermoso. Dept. de Bioquímica y Biología Molecular y Celular, Facultad de Ciencias y BIFI, Univ. de Zaragoza, España, Grupo de Cristalografía Macromolecular y Biología Estructural, Inst. Química-Física Rocasolano. C.S.I.C. Madrid, España.

In this work we propose the model for the structure of a mutated species of ferredoxin-NADP<sup>+</sup>/H reductase (FNR). This enzyme catalyses the reduction of NADP<sup>+</sup> to NADPH during photosynthesis, being this reaction highly specific for NADP<sup>+</sup>/H versus NAD<sup>+</sup>/H. The mechanism of recognition of either NADP<sup>+</sup>/H or NAD<sup>+</sup>/H coenzyme by NAD(P)<sup>+</sup>/H-dependent reductases is not yet completely understood. The aim of the current project is to study this coenzyme specificity in FNR based on the structure of T155G/A160T/L263P/R264P/G265P FNR. Those residues have been substituted by other residues conserved in NAD<sup>+</sup>/H dependent reductases in similar positions. The presented structural analysis of the FNR mutant shows a local similar conformation to that present in NAD<sup>+</sup>/H-dependent reductase, which may explain the observed increase of mutant affinity for NAD<sup>+</sup>/H by biochemical characterisation experiments. Also, we are working on the resolution of complexes formed by mutated species of FNR and NAD<sup>+</sup> with the aim to elucidate the possible role of some residues in coenzyme specificity.

**S-P183 Structures of AlkA:DNA Complexes in Search Mode.** D.A. Lehtinen, T. Hollis, The Center for Structural Biology, Dept. of Biochemistry, Wake Forest Univ. Health Sciences, Winston-Salem, NC 27157.

The *Escherichia coli* 3-methyladenine glycosylase, AlkA, is a base excision repair (BER) enzyme that repairs alkylated damaged DNA using a base-flipping mechanism that exposes the damaged nucleotide allowing hydrolysis of the glycosylic bond. AlkA contains a versatile active site that successfully removes a wide range of alkylated bases, cyclic adducts and deaminated bases. In order to address how AlkA selectively recognizes and excises such chemically diverse damaged DNA from the vast excess of normal DNA, crystal structures were determined of AlkA bound to DNA containing a T:T mismatch and DNA containing 1, N<sup>6</sup>-ethenoadenine. The double-stranded DNAs were designed to represent weak substrates in attempts to capture the DNA bound at different stages of the catalytic reaction. These AlkA-DNA structures revealed non-specific DNA binding that is dramatically different from the previously solved AlkA-DNA structure where the DNA was bound at the active site. The new AlkA:DNA structures, together with the previously identified structure, support two different modes of AlkA-DNA binding, one in catalytic mode and one in search mode. We propose that in search mode the DNA is bound non-specifically, thus allowing the AlkA enzyme to scan along the DNA searching for damaged bases.

**S-P185 The Refined Structure of Hypothetical Protein Pf0725 from *P. furiosus* Confirms its function as a CoA Binding Protein.** M. Zhao, J. Chang, J. Habel, H. Xu, L. Chen, D. Lee, D. Nguyen, S.H. Chang, P. Horanyi, Q. Florence, W. Tempel, W. Zhou, D. Lin, H. Zhang, J. Praissman, F.E. Jenney Jr., M.W.W. Adams, Z.J. Liu, J.P. Rose, B.C. Wang, Dept. of Biochemistry and Molecular Biology, Univ. of Georgia, Athens, GA.

As part of an ongoing structural genomics study we have determined the structure of hypothetical protein Pf0725 by Se-SAS to 1.70 Å resolution.

The selenomet protein was crystallized from a solution containing 0.3M sodium thiocyanate and 35% PEG 3350 by the microbatch method at 291K. The crystals belong to space group P6, with a = 79 Å and c = 36 Å. The structure was determined on-site at SER-CAT from a single SAS dataset collected at the selenium edge on 22ID using the SCA2Structure pipeline. Total time for data collection and structure determination was under 12 hours. The refined structure (R = 22.3%, R free = 24.5%) has been deposited in the Protein Data Bank, entry 1Y81. Analysis of the electron density maps revealed the presence of bound Coenzyme A (CoA). The presence of CoA together the structure's similarity to the *T. thermophilus* CoA binding protein TT1466 suggests that Pf0725 is a CoA-binding protein.

Work supported by NIGMS (GM062407), the Georgia Research Alliance, and The UGA Research Foundation.

**S-P187 Crystal Structure of the Ternary Complex of Allantoate-Amidohydrolase with its Substrate and A Ligand: A Crucial Enzyme of Purine Catabolism from *E. coli* K12.** Rakhi Agarwal, Subramanyam Swaminathan, Biology Dept., Brookhaven National Laboratory, Upton, NY, 11973

Allantoate-amidohydrolase, one of the enzymes involved in purine degradation pathway, is responsible for the breakdown of allantoate to CO<sub>2</sub>, NH<sub>3</sub> and ureidoglycine and is conserved among species. We determined the crystal structure of allantoate-amidohydrolase from *E. coli* K12 by Se-MAD at 2.25Å resolution. The protein is a homodi-

meric subunit, consisting of one large catalytic domain with a dizinc center and a small domain mainly involved in dimerization. Each domain has an interesting mixed  $\alpha/\beta$  topology similar to the family of dizinc-dependant exopeptidases suggesting a common origin. The substrate allantoate binds to the deep cleft of the active site and the ligand binds close to the active site. Allantoate-amidohydrolase with the bound substrate and ligand provides insight into its mechanism of carbamoyl exopeptidase nature of action. The ligand sulfate anion presumably acts as an allosteric effector.

Acknowledgement: Research supported by a National Institutes of Health grant (GM62529) to the NYSGXRC under DOE Prime Contract No. DEAC02-98CH10886 to Brookhaven National Laboratory.

**S-P189 Structural Analysis of *E. coli*  $\beta$ -sliding Clamp 148-152 Ala Mutant and its Role in DNA Polymerase V-dependent Translesion DNA Synthesis.** Vivian Cody, Jim Pace, Edward Snell, Hauptman-Woodward Medical Research Inst. Buffalo, NY 14203, Mark D. Sutton, Laurie Sanders, Sarah Ponticelli, Jill Duzen, Robert Maul, Univ. at Buffalo, Buffalo, NY 14214.

Damaged bases in the DNA that are not repaired prior to replication can act as potent blocks to polymerization, leading to replication fork arrest. We previously described a mutant form of the *E. coli*  $\beta$  sliding clamp protein bearing alanine substitutions in place of residues 148-152 ( $\beta$ -148-152) that was severely impaired for pol IV-dependent translesion synthesis *in vivo*. We have solved the crystal structure of the mutant  $\beta$ -148-152 clamp protein. Data were measured to 1.75 Å resolution for the homodimeric *E. coli*  $\beta$ -148-152 mutant that crystallizes in a triclinic lattice. The current model reveals that the loop encompassing the mutations adopts an alternative conformation from the wild type protein. In addition, BIAcore and gel filtration chromatography data for the interactions of wild type and  $\beta$ -148-152 clamp proteins with various *E. coli* pols indicate that residues 148-152 define a surface of the clamp that is critically important for the proper functioning of some, but not all, *E. coli* pols. These data suggest that these residues play a vital role in DNA polymerase switching. Supported in part by GM66094 (MDS).

**S-P191 The Structural Biology Center User Program at the Advanced Photon Source, Argonne National Laboratory.** S.L. Ginell, R.W. Alkire, C. Chang, M.E. Cuff, N.E.C. Duke, Y.-C. Kim, K. Lazarski, J. Osipiuk, G. Rosenbaum, F.J. Rotella, R-g. Zhang, A. Joachimiak, Structural Biology Center, Biosciences, Argonne National Laboratory, Argonne, IL.

The Argonne's Structural Biology Center (SBC) operates a national user facility for macromolecular crystallography at sector 19 of the Advanced Photon Source. Both the 19ID and 19BM beamlines are equipped with high-resolution optics, Kappa goniostat, a low noise, large area CCD detectors, advanced software for data analysis, processing and structure determination, and other equipment to enable the collection of best diffraction data on the most challenging projects. Highlights for this past year include the deposit of the 1000<sup>th</sup> structure in the PDB from data collected at the SBC, the commissioning of the SBC crystal mounting robot at 19BM, the availability of cooling crystals to 15-20K using a helium cryostat, and the implementation of a version of HKL2000 that allows data processing through structure solution and model building in near real time. Information on the user program and the sector 19 beamlines will be provided and can also be obtained from the SBC web site (<http://www.sbc.aps.gov>).

This work is supported by the U.S. Department of Energy, Office of Biological and Environmental Research, under Contract W-31-109-ENG-38.

**S-P193 Antibody Complex of a Cockroach Allergen Bla g 2.** Alla Gustchina<sup>1</sup>, Mi Li<sup>1,2</sup>, Sabina Wünschmann<sup>3</sup>, Martin D. Chapman<sup>3</sup>, Anna Pomés<sup>3</sup>, Alexander Wlodawer<sup>1</sup>, <sup>1</sup>MCL, NCI at Frederick, <sup>2</sup>Basic Research Program, SAIC-Frederick, Frederick, MD, <sup>3</sup>INDOOR Biotechnologies, Inc., Charlottesville, VA.

Cockroaches excrete a potent allergen, Bla g 2, which elicits IgE responses at exposure levels that are 10-100 fold lower than other common indoor allergens. Exposure and sensitization to cockroach allergens such as Bla g 2 is a major risk factor for asthma mortality and morbidity. IgE-binding inhibition experiments showed that the monoclonal antibody mAb 7C11 inhibits IgE antibody binding up to 25-40%, despite of binding to only a small part of the total Bla g 2 surface. F(ab')<sub>2</sub> fragments of mAb 7C11 were generated by pepsin cleavage and crystal structure of the Bla g 2-Fab complex was solved by molecular replacement. Bla g 2 is present in the complex in a dimeric state, unusual for the aspartic protease family. Two Fab molecules interact with a dimer in such a way that the vast majority of the interactions are formed between one Fab and one of the two Bla g 2 molecules. Interactions with the antibody are dominated by a number of charged residues of the allergen. Determination of the molecular structure of Bla g 2-Fab complexes facilitates epitope mapping and enables a rational approach to the engineering of allergen molecules with reduced IgE antibody binding.

**S-P195 Crystal Structure of PurO from *Methanobacterium thermoautotrophicum*.** You-Na Kang<sup>a</sup>, Robert H. White<sup>b</sup>, Steven E. Ealick<sup>a\*</sup>, <sup>a</sup>Dept. of Chemistry and Chemical Biology, Cornell Univ., Ithaca, NY, 14853, <sup>b</sup>Dept. of Biochemistry, Virginia Tech, Blacksburg, VA 24061.

Inosine 5'-monophosphate cyclohydrolase (IMPCH) catalyzes the cyclization of 5-formaminoimidazole-4-carboxamide ribonucleotide (FAICAR) to IMP in the final step of *de novo* purine biosynthesis. Two major types of this enzyme have been discovered to date; PurH in Bacteria and Eukarya, and PurO in Archaea. The structure of MTH1020 from *Methanobacterium thermoautotrophicum* was previously solved without functional annotation (PDB 1KUU) but shows high sequence similarity to the archaeal IMPCH (PurO). We determined the crystal structures of MTH1020 in complex with either IMP or AICAR. Based on the sequence analysis, structures, and biochemical data, MTH1020 is confirmed as an archaeal IMPCH, thus designated as MthPurO. MthPurO has  $\alpha$ - $\beta$ - $\beta$ - $\alpha$  core structure showing an N-terminal nucleophile (NTN) hydrolase fold. The active site is located at the deep pocket on the surface and contains residues strictly conserved within PurOs. Biochemical studies show that R30 and E104 act as critical residues for catalysis. Comparisons of the two types of IMPCH, PurO and PurH, revealed that there are no similarities in sequence, structure, or the active site architecture, suggesting they are evolutionarily not related with each other.

**S-P197 MD Reveals the Binding Conformation of HIV Protease With the MAC4A Binding Domain of GAG.** Philip D. Martin, Ladislau Kovari, Wayne State Univ., Biochemistry and Molecular Biology, Detroit, MI 48201.

There are three basic crystallographic conformations for HIV protease. A "closed" form (1MUI with Lopinavir, 1KJ4 with an octapeptide), an "open" form (wild type HIV protease, 3PHV), and a "wide open" form (multidrug resistant mutant MDR-769, 1TW7).

The N-terminus of AVC4A contains the wild type HIV binding peptide (SQNYPIV). If one tries to dock this natural substrate, the AVC4A substructure of the GAG protein, into the HIV protease ac-

tive site, numerous disastrous collisions occur. None of the HIV protease crystal structures can bind this “native” format without major conformational changes.



These crystal structures were subjected to 5-ns of molecular dynamics (MD) with GROMACS. We found that all the structures opened up even further (the “fully open” form). We could then dock the AVC4A polypeptide into the active site of HIV protease with only minor VDW contacts. The RMS delta CA for the middle four substrate residues (NYPI) start out at only 0.4 Å relative to that found in the 1KJ4 structure. We will present the results of the MD simulations on the various HIV protease crystal structures and of the complex.

Supported by NIH grants GM62990 and A1065294 and a Michigan Life Sciences Corridor grant to the Structural Biology Facility at Wayne State University.

**S-P199 Phasing in the Home Laboratory.** Joseph D. Ferrara, Cheng Yang, Robert Bolotovskiy, James W. Pflugrath, Rigaku Americas Corp., The Woodlands, TX, 77381.

Many examples of S-SAD and Se-SAD phasing have been reported with diffraction data collected using copper radiation (1.54 Å) or radiation at the selenium K absorption edge (0.98 Å). With recent advances in X-ray technology, chromium radiation (2.29 Å) is now available for in-house data collection and appears to be ideally suited for measuring anomalous signals from weak anomalous scatterers such as sulfur, selenium, calcium and other atoms commonly found in protein crystals. The results of a number of successful SAD experiments using Cr radiation have been published by several groups including our own.

With the addition of Cr radiation to the crystallographer’s toolkit, in-house X-ray sources can provide at least two routinely useful wavelength options for macromolecular crystallography. This report also discusses the results of phasing by combining diffraction data collected using both Cu and Cr radiation sources.

Finally, we report the results of data collection with a new imaging plate detector (R-AXIS HR) designed specifically for use with Cr radiation. This new detector allows the collection of data suitable for both phasing and refinement with Cr radiation from a single crystal in a single, simple diffraction experiment.

**S-P201 Searching for Silver Bullets: An Alternative Strategy for Crystallizing Macromolecules.** Bob Cudney<sup>1</sup>, Alexander McPherson<sup>2</sup>, <sup>1</sup>Hampton Research, 34 Journey, Aliso Viejo, CA 92656, <sup>2</sup>Univ. of California, Dept. of Molecular Biology & Biochemistry Irvine, CA 92697.

Based on a hypothesis that various small molecules might establish stabilizing, intermolecular, non covalent cross links in protein crystals and thereby promote lattice formation, we carried out three separate experiments. We assessed the impact of more than 200 chemicals on the propensity of 81 different proteins and viruses to crystallize. The compounds were formulated as 115 overlapping reagent mixes, each containing 1 to 20 individual components. The experiments were comprised of 18,240 vapor diffusion trials. A salient feature of the experiments was that, aside from the inclusion of the reagent mixes, only two fundamental crystallization conditions were used, 30% PEG 3350, and 50% Tacsimate™ at pH 7. Overall, 65 proteins (85%) were crystallized. Most significant was that 35 of the 65 (54%) crystallized only in the presence of one or more reagent mixes, but not in control samples lacking any additives. Based on these experiments, we propose that an alternate approach

to crystallizing proteins might be developed, which employs a limited set of fundamental crystallization conditions combined with a broad screen of potentially useful small molecule additives.

**S-P203 Is the Protein Folding Problem Solvable? The Structure of Tetrameric Impase from *T. Maritima* Shows Unusual Protein Plasticity.** Boguslaw Stec<sup>1</sup>, Kimberly A. Stieglitz<sup>2</sup>, Mary F. Roberts, <sup>1</sup>The Burnham Inst. for Medical Research, La Jolla CA 92307, <sup>2</sup>Dept. of Chemistry, Merkert Chemistry Center, Boston College, Chestnut Hill MA 02467.

The thermodynamic hypothesis of protein folding has become an important paradigm of modern biology. Substantial progress was made towards understanding the main factors influencing folding. However, recent developments question the general validity of this hypothesis. We will review the experimental and theoretical work aimed at defining the relation of the protein sequence to the protein structure. We also present an interesting example that questions the uniqueness of solution of this problem. In this work we present a structure of the first tetrameric inositol monophosphatase (IMPase) from *Thermotoga maritima*. The structure provides insights into evolutionary specialization of function and emergence of allosteric regulation by transition from dimeric IMPase fold to tetrameric FBPase fold. The tetrameric structure of this unregulated enzyme is similar in its quaternary assembly to the allosterically regulated tetramer of fructose 1,6 bisphosphatases (FBPase), while individual dimers are similar to human IMPase. It also offers a more detailed view into the protein folding problem by focusing on a fragment of the protein found in two seemingly opposing secondary structure arrangements. In the first crystal form the tetramer is symmetric, while in the second form it is asymmetric. In the asymmetric form the active site loop, adopts the β-structure in the upper dimer, while it takes on an α-helical conformation in the lower dimer.

**S-P205 Playing LEGO with BRCT-repeats, FHA-domains and C/EBP Transcription Factors.** Maria Miller, Macromolecular Crystallography Laboratory, CCR, NCI at Frederick, Frederick, MD 21702.

CCAAT/enhancer-binding proteins (C/EBPs) are important transcriptional regulators implicated in cell growth, differentiation, survival and tumorigenesis. Sequence analysis revealed several motifs containing serine and threonine residues, which upon phosphorylation conform to known recognition sites for the BRCT-repeats and FHA-domain containing proteins, e.g., PTIP, BRCA1, and MDC1. These molecules act as scaffolds facilitating protein-protein interactions and formation of functional multiprotein complexes involved in DNA repair and cell cycle control. Structural basis for phosphopeptide recognition has been defined by numerous crystal structures. We are currently using a wealth of available information to link C/EBPs to their partners in cellular machinery. Conclusions concerning specificity of interactions will be presented for the following complexes: (1) Phosphopeptides from the transactivation domains of C/EBP delta (residue range: 57-68) and C/EBP beta (residue range: 84-95) with tandems of BRCT domains from the PTIP and BRCA1 proteins respectively: based on coordinates 1T29, 1Y98, and 1KZY. (2) Phosphopeptide derived from C/EBP alpha basic region (residue range: 277-288) with MDC1, based on the crystal structure of the MDC1 bound to histone tail of gamma-H2AX; pdb code: 2AZM.

**S-P207 Microfluidic Chips for Parallelized Analytical Crystallization.** Andrew May, David Cohen, Suzanne Weaver, Yong Yi, Kevin Farrell, R&D, Fluidigm Corp., S. San Francisco, CA.

Macromolecular crystallization has traditionally relied upon the selection of a limited set of reagent formulations from within the vast potential reagent space that could result in the growth of diffraction-quality crystals. The number of experiments and resulting reagent space is typically limited by the amount of sample available and the number of reagent formulations that can be prepared for the experiment. Structural biologists increasingly explore variations in the sample (alternative constructs, ligands, substrates, etc.) as a method for increasing the success rates for crystallization of any particular target. Decisions on which of these samples to pursue often rely on the correlation between orthogonal biophysical techniques and the propensity of a sample to crystallize.

The TOPAZ® family of microfluidic screening chips have been designed for multiple samples to be run in parallel against the same 96-solution reagent set using a total of 1.4 ul per sample. The limited sample volume requirements allow TOPAZ chips to be used to generate analytical crystallization data for each of the samples prepared in parallel. Crystallization data from TOPAZ® chips provides a direct readout of the propensity of any given sample or construct to crystallize. When employed early on in the purification process, this information can be used to decide which sample variant to pursue. It also facilitates parallel processing of samples for crystallization early in the structure determination pipeline.

Data will also be presented from studies demonstrating the use of microfluidic liquid diffusion-based crystallization in a more traditional crystallization pipeline. Follow-on translation strategies from initial screening hits will also be described. Data will be presented from projects which have led to the successful determination of structures from TOPAZ® screening hits.

**S-P209 Optimization of Crystallization Condition in Gel-Tube Method.** H. Tanaka<sup>a\*</sup>, M. Yamanaka<sup>a</sup>, K. Inaka<sup>b</sup>, M. Sato<sup>c</sup>, S. Takahashi<sup>a</sup>, S. Sugiyama<sup>b</sup>, S. Sano<sup>c</sup>, M. Motohara<sup>c</sup>, T. Kobayashi<sup>c</sup>, and T. Tanaka<sup>c</sup>, <sup>a</sup>Japan Space Forum, Tokyo, Japan, <sup>b</sup>Maruwa Food Industries, Inc., Nara, Japan, <sup>c</sup>Japan Aerospace Exploration Agency, Ibaraki, Japan.

'Gel-Tube' is a method for a protein crystallization using a simplified counter-diffusion technique<sup>[1]</sup>, based on gel-acupuncture method<sup>[2]</sup>. A gel in a silicon tube, through which protein and precipitant solution diffuse each other from different direction, can be easily attached to the end of a capillary. Using 1-dimensional (1-D) simulation, it is possible to estimate the diffusion process inside the capillary and to design crystallization conditions, such as protein and precipitant concentration, gel-tube and sample solution lengths, pre-mixing precipitant concentration in protein solution and pre-saturating precipitant concentration in gel-tube, and time to obtain the first crystal. We will introduce some tips for optimization of crystallization condition and also a method for controlling diffusion in a capillary.

We thank Professor Garcia-Ruiz and the members of his laboratory in CSIC-University of Granada for their helpful discussion.

[1] Tanaka, H. *et al.*, *J. Synchrotron Rad.*, 2004, 11, 45-48.

[2] Garcia-Ruiz, JM., Moreno, A., *Acta Cryst.*, 1994, D54, 484-490.

**S-P211 Structural and Biochemical Analysis of Nucleotide Binding in *B. subtilis* SecA.** D. Kim., J.F. Hunt, Dept. of Biological Sciences, Columbia Univ., New York, NY 10027 USA.

Protein translocation through the cytoplasmic membrane in bacteria

is achieved through the Sec system. SecA is a peripheral membrane protein that acts as an ATPase and uses the energy derived from binding and/or hydrolysis of ATP to push the preprotein successively through the SecYEG channel; however, the exact nature of these steps is unclear. *ecA* in an ATP-bound conformation would provide insight into the fundamental role of nucleotide binding and hydrolysis in the conformational cycle of this mechanoenzyme. Non-hydrolysable ATP analogs do not bind SecA with high affinity and therefore are not useful for this study. Instead, a mutagenesis strategy was employed to engineer proteins that could bind but not hydrolyze nucleotide. Structural and biochemical studies of these mutants are underway.

We thank the NSLS at Brookhaven National Laboratory for access to Beamline X12B. This research is supported by the Biophysics Training Grant GM08281-17.

**S-P213 The Refined Crystal Structures of Flock House Virus and Virus-like-particles Reveal Structural Features Important to the Virus Maturation and Assembly.** Zhongguo Chen, Vijay Reddy, John E. Johnson, Dept. of Molecular Biology, The Scripps Research Institute, La Jolla, CA 92037.

Flock house virus (FHV) is a member of Nodaviridae, a group of icosahedral insect viruses with a bipartite, single stranded RNA genome. Each virus particle is assembled from 180 copies of capsid protein containing 407 amino acid residues in a  $T=3$  quasi symmetry and encapsidates the bipartite genome. During maturation, the capsid protein is auto-cleaved into two polypeptides with the cleavage of the scissile bond between Asn363-Ala364.

We refined 4 crystal structures of FHV, one authentic virus and 3 virus-like particles (VLP), to near atomic resolution. All 4 structures share similar features, except that a Ca ion and a sulfate ion can be found in the VLP structures at the quasi three-fold axes, but not in the authentic FHV. The fold of the capsid protein is a canonical virus  $\beta$  sandwich with residues 92-320 forming the core of the  $\beta$  domain. An internal helical domain is formed by three  $\alpha$  helices from the N and C-termini in the interior of capsid. A portion of the duplex RNA genome can be imaged in the crystal structure, however, the B factors are high, indicating disorder or non-strict conformation to the icosahedral symmetry. Segment 72-82 is flexible with higher B factors. We postulate that the flexibility of this segment helps in catalyzing the cleavage of the scissile bond, and plays an essential role in the capsid maturation, as well as the formation of subunit contacts during the assembly.

**S-P215 New Tools for Protein Crystal Retrieval and Handling.** R.E. Thorne, G. Chew, M. Sochor, Cornell Univ., Ithaca, NY 14853.

Conventional metal microtools (developed for electron microscopy sample preparation) are ill-suited to the small size and extreme fragility of protein crystals. We have developed a set of microfabricated tools for common crystal manipulation tasks including (1) dislodging crystals adhered to slides or crystallization trays, (2) separating crystals or crystal fragments, (3) transferring crystals between soaking solutions, (4) cutting protein skins, gels and lipid phases to extract crystals, (5) measuring dimensions of crystals as small as 20 microns, and (6) actively grabbing crystals so that they are immobilized without damage. Made of 10 micron thick polyimide, these transparent tools are rigid, yet they can easily be deformed to press flat against well bottoms, and their spring-like action minimizes the chance of crystal damage. These properties make them well-suited to both manual and automated crystal manipulation.

**S-P217 The CombiClover 384™ Plate: A Novel High-Density Plate for Protein Crystallization.** Hidong Kim, Craig Sterling, Lance Stewart, deCODE biostructures, Inc., and Emerald BioSystems, Inc., Bainbridge Island, WA 98110.

A novel plate has been developed for protein crystallization. The CombiClover 384 plate is an SBS-format protein crystallization plate containing 96 Clover crystallization chambers. The patented Clover chamber (US patent # 6,039,804) allows simultaneous crystallization screening of up to four different target samples against a single crystallization condition. The 96 Clover chambers of the CombiClover 384 plate comprise 384 crystallization drop chambers, and permit the simultaneous crystallization screening of four different protein samples against typical 96-condition crystallization screens in a single plate. The spacings between either neighboring drop chambers or reservoirs within rows and columns are the same, facilitating programming for crystallization robots. The CombiClover 384 plates are molded in cyclic olefin copolymer (COC). COC is an excellent material for protein crystallization applications due to its high transparency, low water permeability, and broad-range chemical resistance. The CombiClover 384 plate is a crystallization plate designed for the high-throughput demands of modern protein crystallography.

**S-P219 Global Protein Surface Survey: A Comprehensive Survey of Protein Surface Features.** T.A. Binkowski, A. Joachimiak, Structural Biology Center & Midwest Center for Structural Genomics, Argonne National Laboratory, Argonne, IL.

As structural genomics efforts continue to populate the protein fold space at rapid pace, an exponential growth in protein surface information follows suit. These surfaces contain a wealth of information about protein function. The Global Protein Surface Survey (GPSS) is the first effort to identify and organize surfaces from structures deposited in the Protein Data Bank. Surface libraries have been compiled that represent all geometrically defined solvent accessible cavities and interior voids as well as ligand, metal, DNA and peptide binding surfaces. Publicly available annotation is mapped onto surfaces. The role of surface analysis in understanding the biological roles of proteins is becoming an increasingly important part of the effort at the Midwest Center for Structural Genomics. Utilizing a novel search algorithm, hypothetical protein surfaces are queried against the GPSS libraries for function prediction. We present results utilizing surface comparisons from several newly solved structures. The GPSS is available at <http://gpss.mcsg.anl.gov>.

This work was supported by the grants from the NIH (GM62414 and GM074942) and the U.S. Department of Energy, Office of Biological and Environmental Research under Contract W-31-109-ENG-38.

**S-P221 What Makes MAP2Ks Dual Specificity Kinases?** J.M. Humphreys, S.-J. Lee, P. Madhavapeddi, T. Zhou, E.J. Goldsmith, UTSouthwestern Medical Center, 5323 Harry Hines Blvd., Dallas, TX, 75235

MAP2Ks belong to a small group of “dual specificity” kinases which phosphorylate target proteins at both S/T and Y, and activated MAP2Ks are themselves doubly phosphorylated. We have expressed active MAP2Ks with mutations that mimic native mono and di-phosphorylated MEK6, and we have developed an HPLC-based technique to quantify mono and di-phosphorylated MAPK products.

Preliminary results indicate that MEK6DD phosphorylates p38 $\alpha$  primarily through a Y\* intermediate, as does activated wild-type

MEK6. Both MEK6AD and MEK6DA monophosphorylated mimics show varying bias toward initial tyrosine phosphorylation, however the MEK6DA mutant first phosphorylates tyrosine almost exclusively. p38 $\alpha$  phosphorylation by MEK6DA approaches what is observed for MEK6DD, suggesting the increase of Y\* intermediate is at the expense of T\*. MEK6AD has a much lower turnover but a higher T\*/Y\* intermediate ratio than MEK6DA. This data suggests that the type of reaction (S/T or Y phosphorylation) catalysed by MEK6 is effected by its phosphorylation state.

Crystallographic studies of the mechanism(s) behind this phenomenon are being conducted using truncated MEK6 proteins co-crystallized with peptide-ATP analogue bisubstrates.

This research is supported by a grant from the National Institutes of Health (ND46993).

**S-P223 Helium-cooled X-ray Diffraction Studies Enhance the Visibility of a Proton Pathway in Human-Aldose Reductase.** A. Mitschler<sup>1</sup>, S. Ginell<sup>2</sup>, A. Cousido<sup>1</sup>, T. Petrova<sup>1,2</sup>, V. Lunin<sup>3</sup>, I. Hazemann<sup>1</sup>, M. Van Zandt<sup>4</sup>, A. Joachimak<sup>2</sup>, A. Podjarny<sup>1</sup>, <sup>1</sup>IGBMC-CNRS-INSERM-ULP, Strasbourg-Illkirch, France, <sup>2</sup>ANL-SBC, Argonne, IL, <sup>3</sup>IMPB, Puschino, Russia, <sup>4</sup>IDD,CT

Human aldose reductase (h-AR) is involved in severe diabetic complications, and is a clinical target for drug design. Its enzymatic mechanism is based on the transfer of a hydride from coenzyme NADPH and of a proton from the h-AR. The crystal structure (0.66Å/100K) of the ternary complex (h-AR-NADP<sup>+</sup>-inhibitor IDD594) indicated that the visibility of H atoms in difference density maps is correlated to the B values of the corresponding bonded atoms (in the active site, 77% of H are seen when B<5 Å<sup>2</sup>). X-ray diffraction data sets were collected at resolutions <0.9 Å, at APS-SBC ID19, from He-cooled (15K) crystals of h-AR complexed with different inhibitors. A comparison with the 100 K structures indicates an overall decrease (1.7 Å<sup>2</sup>) of B values in the ordered parts of the protein. Difference density maps show clearer densities, *e.g.*, for a double conformation of the carboxylate of inhibitor IDD676 and for the double conformations of D-atoms in a proton pathway along water-Asp43-Lys77-Tyr48 for the complex h-AR(D)-NADP<sup>+</sup>-IDD594.

This work is supported by the U.S. Department of Energy, OBER, under Contract W-31-109-ENG-38.

**M-P002 IBARAKI Biological Crystal Diffractometer in J-PARC (BIX-P1), Optimization of Design Parameters.** K. Kusaka<sup>1</sup>, T. Ohhara<sup>1</sup>, I. Tanaka<sup>2</sup>, N. Niimura<sup>2</sup>, T. Ozeki<sup>3</sup>, K. Kurihara<sup>1</sup>, K. Aizawa<sup>1</sup>, Y. Morii<sup>1</sup>, M. Arai<sup>1</sup>, K. Ebata<sup>4</sup>, Y. Takano<sup>4</sup>, <sup>1</sup>JAEA, Tokai, Ibaraki, Japan, <sup>2</sup>Ibaraki Univ., Hitachi, Ibaraki, Japan, <sup>3</sup>Tokyo Inst. of Tech., Meguro, Tokyo, Japan, <sup>4</sup>Ibaraki Pref. Gov., Mito, Ibaraki, Japan.

The TOF neutron biological diffractometer in J-PARC proposed by Ibaraki prefectural government is designed to cover the samples have their cell edges up to 135Å, and to realize the efficiency is more than 50 times larger than the present high performance diffractometer, BIX-4 (JRR-3, JAEA). To achieve this performance, the diffractometer will be installed on a coupled moderator has more intense peak and integrated intensity but wider pulse shape than a decoupled one. The overlapping of Bragg spots along the time-axis expected should be considered for the determination of optic parameters and it is necessary to de-convolute the overlapped spots with higher accuracy. The original simulation programs of TOF diffraction data with designed parameters were developed to obtain information of spot-overlapping, completeness of Bragg spots and spot profiles along time-axis. In this paper, the consideration of important designed parameters focused on biological macromolecular and the strategy of de-convoluting overlapped spots will be reported based on the simulation results.

**M-P004 Crystallization Phase Diagram of Several Proteins.** Y. Ohnishi<sup>1,2</sup>, Y. Kobayashi<sup>2</sup>, M. Yamashita<sup>2</sup>, K. Ebata<sup>2</sup>, Y. Sawa<sup>2</sup>, I. Tanaka<sup>2</sup>, N. Niimura<sup>2</sup>, <sup>1</sup>Kaken Co. Ltd., <sup>2</sup>Ibaraki Univ., Hitachi-shi, Japan.

Neutron diffraction provides an experimental method of directly locating hydrogen atoms in proteins and hydration structure of proteins. The bottle neck of neutron macromolecular crystallography is that large crystals are needed: currently, the volume of crystals should be larger than 1 mm<sup>3</sup>. We have found that one rational way to find the proper conditions to grow large single crystals using established crystallization phase diagram. A large single crystal can be grown under supersaturated conditions close to the solubility boundary. Indeed, large single crystals from proper condition on the phase diagram of proteins were suitable for use in neutron protein data collection.

We have made crystallization phase diagram of some basic proteins such as insulin (2Zn) and Ribonuclease A, and succeeded in growing large crystals which are applicable to neutron diffraction experiment. The large crystal growth of the other basic proteins is also under way by using the phase diagram strategy.

**M-P006 Crystallization of a Large Single Crystal of  $\beta$ -lactoglobulin for Neutron Protein Crystallography.** D. Yagi<sup>1</sup>, Y. Ohnishi<sup>2</sup>, I. Tanaka<sup>1</sup>, N. Niimura<sup>1</sup>, <sup>1</sup>Ibaraki Univ., <sup>2</sup>Kaken, Hitachi City, Japan.

$\beta$ -lactoglobulin is a typical model globular protein for studies of protein folding. The  $\beta$  sheets structure is formed through  $\alpha$ -helix structure in folding process. ( $\alpha$ - $\beta$  transition) The  $\alpha$ - $\beta$  transition includes the rearrangement of H-bonds from intra- $\alpha$ -helix to inter- $\beta$  strands. In order to elucidate the  $\alpha$ - $\beta$  transition from the atomic view point of H-bonds, the neutron diffraction experiment of  $\beta$ -lactoglobulin has been scheduled.

Neutron diffraction needs a large single crystal of protein. The large single crystal of  $\beta$ -lactoglobulin (1mm  $\times$  0.4mm  $\times$  0.5mm in size) has been grown in the meta-stable zone on the basis of the crystallization phase diagram, which has been determined by a dialysis

method. The quality of the crystal was assessed by the developed Wilson plot method. The preliminary neutron diffraction from the crystal has been carried out.

**M-P008 Neutron Diffraction from Cubic Insulin at pD6 and 7.** T. Ishikawa<sup>1</sup>, Y. Oonishi<sup>2</sup>, I. Tanaka<sup>1</sup>, T. Chatake<sup>3</sup>, K. Kurihara<sup>4</sup>, T. Tamada<sup>4</sup>, R. Kuroki<sup>4</sup>, N. Niimura<sup>1</sup>, <sup>1</sup>Ibaraki Univ., <sup>2</sup>Kaken, <sup>3</sup>Chiba Scie. Univ., <sup>4</sup>JAEA, Hitachi City Ibaraki 316-8511, Japan.

X-ray diffraction experiment of porcine cubic insulin has shown the conformational change of the 10<sup>th</sup> histidine and the absence of the change of the 5<sup>th</sup> histidine and these conformational changes is pH-dependent. Maeda et al have carried out the neutron diffraction experiment of porcine cubic insulin at pD=9, and the experiment has revealed that the protonation and deprotonation of histidine residues are the cause of the pH-dependent structural changes.

We have carried out the neutron diffraction experiment of porcine cubic insulin at pD=6 and 7. Cubic insulin was grown to a size of 1mm<sup>3</sup> in volume by a dialysis method on the basis of the crystallization phase diagram. The crystal was soaked at pD6 and 7. Neutron diffraction experiment was carried out with BIX-4 installed at the JRR-3 of the Japan Atomic Energy Agency (JAEA).

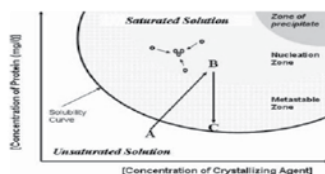
**M-P010 Flash-cooling and Preliminary Low Temperature Neutron Diffraction Studies of the Crenarchaeal *Aeropyrum pernix* Flap Endonuclease-1 (FEN-1).** S.J. Tomanicek<sup>1</sup>, B. Shah<sup>2</sup>, C.A. Schall<sup>2</sup>, T.C. Mueser<sup>1</sup>, B.L. Hanson<sup>1</sup>, <sup>1</sup>Chemistry and <sup>2</sup>Chemical Engineering, The Univ. of Toledo, Toledo, OH.

The flap endonuclease-1 (FEN-1) enzymes are structure-specific 5' to 3' DNA endonucleases that are members of the RAD2/RAD27 family of eukaryotic nucleases. FEN-1 enzymes are involved in the recognition and cleavage of flap DNA that is generated during the processing of Okazaki fragment primers during lagging-strand DNA synthesis and in processing strands displaced during DNA synthesis associated with repair. We have previously solved the X-ray structure of the native metal free *Aeropyrum pernix* (Ape) FEN-1 enzyme at 1.4 Å resolution. Low temperature neutron diffraction studies of Ape FEN-1 are aimed at examining the role of solvent in substrate recognition and the role of divalent metal ions in the catalytic mechanism of the FEN-1 enzymes. We have recently developed a method to reliably flash-cool large Ape FEN-1 crystals (0.3 mm<sup>3</sup>) with a mosaicity of approximately 0.2°. Following deuterium exchange of Ape FEN-1, crystals are grown using vapor diffusion experiments in the presence of a deuterated cryoprotectant. The crystals are then cryogenically preserved using a helium cryostat at 40K. Using one of our smallest crystals of Ape FEN-1 (0.064 mm<sup>3</sup>) we were able to attain diffraction at PCS.

**M-P012 CyBi®-HTPC Work Station for Protein Crystallization. Automation of Protein Crystallization in Sitting Drop.** Harris Grevelis<sup>1</sup>, I. Broutin<sup>2</sup>, F. Bonhure<sup>2</sup>, <sup>1</sup>CyBio Inc., Woburn, MA, I. Crystallography Lab. et RMN Biologiques, CNRS, Univ. of Pharmaceutical, Paris.

Recent developments in genomics and proteomics have led to an increase in the number of macromolecules requiring structural elucidation. Moreover, the increased size of complex proteins often requires the use of crystallography as a structural method. The protein structure of a gene product can then be determined by this technique, but first the crystal must be obtained. This process is inconsistent however, since it is not possible to determine the crystallization conditions in advance using information regarding sequence and physicochemical

features of a protein. Instead, the protein is tested against a matrix of varying standard conditions to determine those optimum for crystallization. The throughput and reliability of this process can be improved considerably using automation.



The behavior of a molecule dependant on variations in its environment can be described via a phase chart. The balance between the solution phase and the solid phase is called the solubility curve. Above this curve is the meta-stable zone where over saturation results in conditions that are too weak for crystal growth without any external supply of energy.

For a macromolecule to crystallize, it must go over this area without reaching the precipitation zone. The molecule will then be in an over-saturation stage which allows crystallization to commence.

Due to the numerous conditions that must be tested, it is vital to conduct all experiments with an increased focus on accuracy and reproducibility.

**M-P014 A Data Processing Software for Neutron (Quasi-) Laue Diffraction.** Z. Ren, Renz Research, Inc., P. O. Box 605, Westmont, IL 60559.

A highly-automated data processing software Precognition™ is developed for neutron (quasi-)Laue diffraction. The software starts from analysis of diffraction images recorded on normal or arbitrarily-included flat detector or cylindrical detector, and results in fully-reduced structure factor amplitude in three steps. Step 1 establishes an accurate geometric model of each diffraction pattern in a dataset, including auto-indexing, refinement of various parameters of crystal and experimental apparatus, and corrections for detector distortion. Step 2 integrates and isolates the intensity of each predicted spot, some easily observable by eye, some not, and some sharing the same detector pixels with each other, known as spatial overlap. Step 3 compares all integrated intensities together in order to reveal therefore to reduce systematic errors, and to identify therefore to reject random noise. The most significant systematic correction is normalization of incident beam intensity at all wavelengths, which process requires no prior measurement of the spectrum of the neutron beam. Crystallographic and structural results from dihydrofolate reductase complex with a drug methotrexate (Bennett *et al.*, *Acta Cryst.* D61, 574-579, 2005) and other testing cases will be presented. This software is being extended to process time-of-flight images.

**M-P016 New Possibilities Offered by Current Progress in Neutron Macromolecule Crystallography.** Flora Meilleur, Inst. Laue Langevin, BP156, 38042 Grenoble, France, meilleur@ill.fr.

Neutron macromolecule crystallographic studies are providing unique and complementary insights on hydrogen and hydration in protein crystal structures that are not available from X-ray structures alone. Recent progress in neutron protein crystallography instrumentation have dramatically improved the speed and precision with which neutron protein structures can now be determined. Ongoing developments will further extend the size and complexity of systems that can be studied. Parallel improvements in modern molecular biology now allow fully (per)deuterated protein samples to be produced for neutron scattering that essentially eradicate the large hydrogen incoherent scattering background that has hampered such studies in the past. High quality neutron data can now be collected to near atomic resolution (~2.0Å) for proteins of up to ~50 kDa molecular weight

using crystals of volume ~0.1 mm<sup>3</sup>. The ability to flash-cool and collect high resolution neutron data from protein crystals at cryogenic temperature (15 K) now opens the way for kinetic crystallography on freeze trapped systems.

**M-P018 Increasing Crystallization Trials Productivity through Imaging Automation.** Pierre Le Magueres<sup>1</sup>, Eric Hnath<sup>1</sup>, Jian Xu<sup>2</sup>, <sup>1</sup>Rigaku Americas, 9009 New Trails Dr., The Woodlands, TX 77381, Rigaku Automation Group, 5999 Avenida Encinas, Suite 150, Carlsbad, CA 92008.

The Minstrel I crystal imaging platform from Rigaku, consisting of a Minstrel I imager, a plate hotel and the database CrystalTrak, is designed to automate the process of recording, tracking and optimizing a vast number of protein crystallization trials.

The Minstrel I captures high quality images of crystallization drops from most commercial crystallization plates due to a flexible and upgradeable plate type library. The possibility to manually select different light patterns and polarized light filters further aids the identification of such critical features as crystalline precipitate, phase separation and crystals down to a size of a few microns.

Linked to a plate hotel with up to 160 SBS-type plates, and combined with the CrystalTrak database, the Minstrel I imaging system allows crystallographers to frequently image crystallization trials and electronically record relevant of data. Thanks to the option in CrystalTrak to automatically optimize crystallization conditions, the platform (Minstrel I + plate hotel + CrystalTrak) represents a solution for increasing crystallization trial productivity, and thus reduce the amount of time in obtaining crystals suitable for X-ray diffraction.

**M-P020 Automated Ligand Refinement with a Combined Force Field and Shape Potential.** S. Wlodek, A.G. Skillman, A. Nicholls, OpenEye Scientific Software, 3600 Cerrillos Rd., Santa Fe, NM 87507.

An automated computational procedure for fitting a ligand into its electron density with the use of the MMFF94 force field and a Gaussian shape description has been developed. It employs a series of adiabatic optimizations of gradually increasing shape potential. Starting from a set of energy-relaxed ligand conformations, the final results are structures realistically strained to fit the crystallographic data.

**M-P022 Description of Software for the Planning, Execution, and Refinement of Crystallography Experiments.** Paige N. Vinson, Thermo Electron Corporation, Brentwood, TN, USA 37027, E-mail: paige.vinson@thermo.com.

A modular and highly integrated software package will be described which takes the crystallographer from the planning stage through to the refinement of the experimental process. Some key features include reagent/protein management, screen design, database query tools, and graphical image control. Each application is specialized for a specific function but provides input to other applications. For example, while viewing experimental images, a user may choose an image deemed “interesting” and have the conditions for that site sent to the Screen Designer application for the starting conditions of a fine screen.

Data generated from experiments can be mined using a novel, graphical query tool. Query results may be sent to the image viewing and analysis application for further study, as well as to the screen design application for use in designing additional rounds of refined experiments.

These and other features of the software will be presented in a format describing typical scenarios and methods of use.

**M-P024 Software for Efficient Co-crystal Structure Determination.** J. Badger, P. Collins, R. Rosenfeld, B. Smith, R. Atha, D.E. McRee, Molecular Images and ActiveSight, 4045 Sorrento Valley Blvd., San Diego CA 92121.

Iterative drug design projects that include protein crystallographic data typically require that structure results are returned to synthetic chemists within weekly cycles. Similarly, the viability of crystallographic fragment-based lead discovery projects depends on being able to analyze 100's of data sets within a few weeks. ACTOR/FR-E systems provide the hardware for unattended repetitive data collection but automated software is required for structure determination.

To manage the raw data processing needs of high volume co-crystallography projects, we have developed *PyDInt* (Python Distributed Integration system). This client-server software system uses D\*TREK as its processing engine and only requires a target list of image directories to automatically process multiple data sets in the expected space group. We have also developed a Python application (*BNG*) for automating structure solution from multiple data sets. *BNG* takes the integrated data and runs molecular replacement and refinement programs (CCP4) to solve each structure. *BNG* outputs include logs of the structure solution history and session files for the MIFit model-building program. These session files enable immediate viewing of each structure in the context of its electron density map.

**M-P026 Structure of Human MAPKinase Kinase 1 (MEK1) Reveals a Novel Mode of Non-Competitive Kinase Inhibition: A Case Study in Industrial Crystallography.** J.F. Olsen, H. Chen, A. Pavlovsky, C. Whitehead, E. Zhang, C. Wang, S.M. Cornell, J. Sebolt-Leopold, H. Teclé, C.A. Hasnain, Pfizer Global Research and Development, Michigan Laboratories, Ann Arbor, MI 48105.

MEK1 is dual-specificity, tyrosine/serine protein kinase found in the Ras/Raf/MEK/ERK mitogen-activated protein kinase (MAPK) signalling pathway. Approximately 30% of all human cancers have a constitutively activated MAPK pathway, making MEK1 an excellent target for therapeutic intervention in the treatment of cancer. In order to improve our understanding of the function and regulation of human MEK1 we determined its crystal structure as a ternary complex with MgATP and an inhibitor related to the clinical candidate CI-1040. The MEK1 crystal structure reveals a unique inhibitor-binding pocket adjacent to the MgATP-binding site. The presence of the potent inhibitor in this pocket induces several conformational changes in the unphosphorylated MEK1 enzyme that locks it into a closed but catalytically inactive species. Thus, the structure reveals a novel, non-competitive mechanism for protein kinase inhibition. In addition, the structure determination of MEK1 will be discussed as a case study for performing macromolecular crystallography in an industrial setting.

**M-P028 Structural Flexibility of *E. coli* Peptide Deformylase Deduced from Multiple Independent Crystal Lattices.** Nandini Sharma, P.M.D. Fitzgerald, Merck Research Laboratories, Rahway, NJ.

Deformylation of newly synthesized proteins is an essential step in bacterial protein production. As this pathway is present in bacteria but absent in higher organisms, peptide deformylase (PDF), the enzyme that catalyzes the reaction, has been studied as a potential target for a novel antibiotic. In the course of a program aimed at identifying such an antibiotic, the crystal structure of *E. coli* peptide deformylase was determined.

PDF was found to be an exceptionally easy protein to crystallize. Using standard commercial screens, crystals useful for data collec-

tion were obtained in more than 25% of the crystallization wells. Each of the crystals obtained in these screens was characterized crystallographically, and five unique crystal forms were identified. Subsequently a sixth crystal lattice was identified, one that grew under the same conditions as one of the original five lattices, and later a seventh lattice was obtained in complex with an inhibitor.

Crystallization conditions were optimized for each of the seven lattices to produce the best possible diffraction quality crystals. Eventually a monoclinic lattice was used to determine phases for the structure using the heavy atom isomorphous replacement method. Using a refined model for the structure obtained in the monoclinic system, the structures of the protein in the other six lattices were determined by the molecular replacement method.

This rich source of independent structural data has allowed us to compare the structure of PDF in a number of truly independent crystalline environments. To this set of structures, the structure of a C-terminally truncated short form of the enzyme was later added. The greatest structural flexibility is found in the C-terminal alpha helix; small but significant structural plasticity is found in other regions of the protein.

**M-P030 Crystal Structure of Proline-rich Tyrosine Kinase 2.** Kam Y.J. Zhang, Abhinav Kumar, Yoshihisa Suzuki, Ben Powell, Brandi P. Grondona, Heike Krupka, James Tsai, Chao Zhang, Gideon Bollag, Plexxikon Inc., 91 Bolivar Dr., Berkeley, CA 94710.

Integrin-linked signaling is important for regulating cell adhesion and motility. Proline-rich tyrosine kinase 2 (PYK2) is one of the key mediators of integrin-dependent signals. PYK2 mediate cytoskeletal rearrangements as a consequence of integrin ligation. PYK2 is localized to the sites of cell-cell contacts, and becomes activated in response to calcium mobilization. PYK2 activation leads to apoptosis in fibroblasts. PYK2 plays a key role in tumor invasion and metastasis. In order to facilitate the structure-based design of potent and selective PYK2 inhibitors as anti-cancer drugs, we have determined the crystal structure of PYK2 both apo and complexed with AMPPNP at 1.45 Å and 1.8 Å resolution respectively. These structures have revealed a unique conformation of the activation loop. The binding of AMPPNP has provided insights to the design of small molecule inhibitors.

**M-P032 Novel Binding Site for Protein Kinase Inhibitors.** Radha Akella, Xiaoshan Min, Elizabeth Goldsmith, UT Southwestern Medical Center at Dallas, 5323 Harry Hines Blvd Dallas TX 75390.

MAP kinases and their upstream activators MEKs are drug targets for rheumatoid arthritis, cancer, inflammatory bowel disease, psoriasis and others. PD98059 binds specifically to the inactive form of MEK1, preventing its activation by c-Raf and other upstream activators (Alessi et. al 1995) It has been shown to be non-competitive with respect to ATP (Dudley, et.al 1995). Crystallographic studies were undertaken using p38 as a model system to identify the sites of binding of PD98059. We found that PD98059 bound to a novel site which is outside the catalytic site p38 alpha; at the hinge point between the two kinase domains flanked by the  $\beta$ -sheets 3 and 7. This site is distinctly different from the site previously reported for other non-ATP competitive inhibitors of MEK1 by Ohren *et. al* (2004). Crystal structures of MEK6 and MEK1 bound to these inhibitors will also be discussed.

Alessi, D.R., *et al.* 1995. *J Biol Chem*, **270**, 27489-94.

Dudley, D.T., *et al.* 1995. *Proc Natl Acad Sci USA*, **92**, 7686-9.

Ohren, J.F. *et al.* 2004 *Nature structural and Molecular biology* **11**:1192-1197

**M-P034 Crystal Structure of the Human Rhinovirus RNA Polymerase.** T.C. Appleby<sup>1</sup>, H. Luecke<sup>2</sup>, J.H. Shim<sup>1</sup>, J.Z. Wu<sup>1</sup>, I.W. Cheney<sup>1</sup>, L. Vogeley<sup>2</sup>, Z. Hong<sup>1</sup>, N. Yao<sup>1</sup>, <sup>1</sup>Valeant Pharmaceuticals International, Costa Mesa, CA, <sup>2</sup>Dept. of Molecular Biology and Biochemistry, Univ. of California at Irvine, Irvine, CA.

Human rhinoviruses are members of the *Picornaviridae* family and are the primary infectious agents responsible for symptoms associated with the common cold. Picornaviruses utilize virus-encoded RNA-dependent RNA polymerases and uridylylated protein primers to initiate replication of the complete single-strand RNA genome. The molecular details of this mechanism are not well understood due to the lack of structural information. We report the crystal structure of human rhinovirus serotype 16 3D RNA-dependent RNA polymerase (HRV16 3D<sup>pol</sup>) at 2.4Å resolution. HRV16 3D<sup>pol</sup> shares the canonical features of other known polymerases and contains an N-terminal region that tethers the *fingers* and *thumb* subdomains, forming a completely encircled active site cavity which is accessible through a small tunnel on the backside of the molecule. The small *thumb* subdomain contributes to the formation of a large cleft on the front face of the polymerase which also leads to the active site. The cleft is large enough to accommodate a template:primer duplex during RNA elongation and most likely serves as the site for peptide uridylylation and subsequent protein-primed initiation.

**M-P036 Advances in Crystallographic Hardware and Software for Structural Biology.** Cary B. Bauer, Matthew M. Benning, David M. Khazins, Vladislav Sedov, Sergei Medved, Bruker AXS Inc., 5465 E. Cheryl Parkway, Madison, WI 53711.

In recent years the number of protein structures solved by X-ray crystallography has grown tremendously. As a result, the demands placed on X-ray hardware and software have also increased greatly. This presentation will highlight recent advances in hardware and software from Bruker AXS, specifically involving products designed for protein crystallography. One such product is the AXIOM 200. This is a new, large format photon counting area detector based on microgap technology. This type of detector offers many advantages over traditional detectors including maximum sensitivity, ultra-low noise and high dynamic range. In addition, the extremely fast readout eliminates the need for an experimental shutter. Developments in X-ray sources and optics will also be discussed as well as crystallographic results obtained using these new instruments.

**M-P038 Design, Synthesis and X-ray Structure of Protein-Ligand Complexes: Important Insight into Selectivity of Beta-secretase Inhibitors.** Lin Hong, Arun K. Ghosh, Azhar K. Husain, Lui Lei, Chun-Feng Liu, Thippeswamy Devasamudram, Vajira Weerasena, Robert Turner, Gerald Koelsch, Vajira Weerasena, Robert Turner, Geoffrey Bilcer, Jordan Tang, Zapaq Inc., Oklahoma City, OK, Depts. of Chemistry and Medicinal Chemistry, Purdue Univ., West Lafayette, IN, Protein Studies Program, Oklahoma Medical Research Foundation and Dept. of Biochemistry and Molecular Biology, Univ. of Oklahoma Health Science Center, Oklahoma City, OK.

The proteolytic enzyme beta-secretase (memapsin 2, BACE-1) has emerged as a leading target for therapeutic intervention of Alzheimer's disease (AD). It is one of the two proteases that cleave the beta-amyloid precursor protein to generate the 40/42 residue amyloid-beta peptide. The excess level of A-beta leads to formation of amyloid plaques and neurofibrillary tangles in the brain, which are believed to be the pathological causes of AD. Our structure-based design led to the discovery of very potent and highly selective beta-secretase inhibitors and our X-ray structural analysis of protein-inhibitor com-

plexes has uncovered potentially important molecular interactions useful in the design of selectivity for beta-secretase inhibitors.

**M-P040 Structural Basis of Apramycin Recognition of the Ribosomal Decoding Site.** Qing Han, Qiang Zhao, Sarah Fish, Klaus B. Simonsen, Dionisios Vourloumis, Jamie Froelich, Dan Wall, Thomas Hermann\*, Anadys Pharmaceuticals, Inc., 3115 Merryfield Row, San Diego, CA 92121, \*Dept. of Chemistry and Biochemistry, UCSD, La Jolla, CA 92093.

Aminoglycoside antibiotics bind to 16S rRNA near the mRNA decoding site and induce miscoding during translation. Apramycin is unique among aminoglycosides in achieving antibacterial specificity by substitution of the 2-DOS ring at the 4-position only. In contrast to other aminoglycosides, the main effect of apramycin is inhibition of elongation by blocking translocation. To decipher the molecular recognition of the rRNA target by apramycin, we determined the crystal structure of apramycin bound to an oligonucleotide containing the bacterial decoding site.

The crystal structure reveals a unique mode of apramycin interaction with the decoding-site RNA. Apramycin binds to the decoding-site internal loop in the major groove and extending into the minor groove. A pseudo-base pair interaction of the apramycin bicyclic sugar with A1408 and alignment of the terminal sugar with C1409-G1491 in a pseudo-base triple are key interactions. Docking of the complex structure to the 30S subunit indicates that apramycin binding might involve ribosomal protein S12, which is a key trigger element for ribosome translocation.

**M-P042 The Crystal Structure of the Chimeric Bt Cry1A.105 Insecticidal Protein at 3.0 Å Resolution.** T.J. Rydel, E.J. Sturman, T.C. Lee<sup>#</sup>, N.N. Bogdanova<sup>#</sup>, T.M. Malvar\*, Monsanto Company, Chesterfield, MO, <sup>#</sup>Creve Coeur, MO, \*Mystic, CT.

Genetically modified (GM) crops are engineered for herbicide tolerance, insect resistance (IR), or virus resistance. Corn and cotton GM IR crops contain one or more specific genes from the soil bacterium *Bacillus thuringiensis* (Bt), which produce insecticidal crystalline (Cry) proteins during sporulation. Cry1's control Lepidoptera (moths and butterflies) larvae, Cry3's control Coleoptera (beetles) larvae, and Cry2's control Lepidoptera and Diptera (mosquitoes) larvae. Crystal structures are publicly available for Cry1Aa, Cry2Aa, Cry3Aa, and Cry3Bb Bt proteins, and they all display a common 3-domain topology.

We have solved the crystal structure of Cry1A.105 to 3.0 Å resolution. Cry1A.105 is a chimeric protein containing domains I and II of Cry1Ab and domain III of Cry1F. The Cry1A.105 crystal structure was solved by molecular replacement methods using synchrotron data and either the Cry1Aa crystal structure or a Cry1A.105 protein structure model for phasing. This poster will review the experimental work, and how the Cry1A.105 crystal structure compares to the crystal structures of Cry1Aa, other 3-domain Cry crystal structures and to the modeled Cry1A.105 protein structure.

**M-P044 Electrostatic Potential of Aminoacyl-tRNA Synthetase Navigates tRNA on its Pathway to the Binding Site.** M. Safro, D. Tworowski, A. Feldman, Dept. of Structural Biology, Weizmann Inst. of Science, Rehovot 76100, Israel.

The aaRSs catalyzing the same overall aminoacylation reaction vary greatly in subunit organization, structural domain composition and amino acid sequence. The diffusion-controlled associa-

tion of aaRS and tRNA was found to be governed by long-range electrostatic interactions when homogenous negative potential of tRNA fits to the patches of positive potential produced by aaRS: one patch for each tRNA substrate molecule. Considering aaRS as a molecule with anisotropic reactivity and based on the continuum electrostatics and Smoluchowski's theory, the reaction conditions for tRNA-aaRS diffusional encounters were formulated. The domains, categorized as enzymatically relevant, appeared to be non-essential for field sculpturing at long distances. On the other hand, set of complementary domains exerts primary control on the aaRS's isopotential surface formation. Subdividing the aaRS's charged residues into native, conservative and non-conservative subsets we evaluated the contribution of each group to long-range electrostatic potential (EP). Surprisingly, the EP landscapes generated by native and non-conservative subsets are fairly similar, thus suggesting the non-conservative subset being specifically developed for efficient tRNA attraction.

**M-P046 Crystal Structure of Mouse Cleavage Stimulation Factor 77 (CstF-77).** Yun Bai, Thierry Auperin, James L. Manley, Liang Tong, Dept. of Biological Sciences, Columbia Univ., New York, NY 10027.

The 3'-end processing of eukaryotic mRNA precursors has two steps, endonucleolytic cleavage and polyadenylation. A series of RNA-binding proteins and RNA-processing enzymes are involved in this process. Among them is cleavage stimulation factor (CstF), a multisubunit protein of special importance. Mammalian CstF is a heterotrimer containing three subunits, CstF-50, CstF-64 and CstF-77. CstF-77 is involved in protein-protein interactions with CstF-50, CstF-64 and the cleavage and polyadenylation specificity factor (CPSF) subunit, CPST-160. It is important for the assembly and function of the complex. CstF-77 contains 12 HAT (Half A Tetratricopeptide) motifs at the N-terminus and a Pro-rich domain at the C-terminus. We have determined the crystal structure of a fragment of mouse CstF-77, which contains 7 of the HAT repeats and forms a dimer in the crystal. There is a large groove in the center of the dimer, which might be involved in binding other proteins of the CstF or CPST complexes.

**M-P048 Processing Conformation of MAP Kinases.** E.J. Goldsmith, T. Zhou, J. Humphreys, R. Akella, Dept. of Biochemistry, Univ. of Texas Southwestern Medical Center at Dallas, 5323 Harry Hines Boulevard, Dallas, TX.

MAP kinases interact with docking motifs in activating kinases, phosphatases, and substrates that bind to sites outside the kinase active site. Here we report a 1.9 Å crystallographic analysis of inactive ERK2 bound to a "D-domain" docking motif peptide (pepHePTP) derived from hematopoietic tyrosine phosphatase, a negative regulator of ERK2. In this complex, the complete D-domain docking motif interaction defined by mutagenic analysis is observed for the first time, including extensive electrostatic interactions with the "CD site" of the kinase. Large conformational changes occur affecting the activation loop conformation: the phosphorylation sites, which are buried in the inactive form of ERK2, become exposed to solvent, which may promote processing. Similar conformational changes occur in a complex between ERK2 and a MEK2 (MAP/ERK kinase 2)-derived peptide. The peptide binding interaction and conformational changes are similar yet unique among the MAP kinases ERK2, p38 $\alpha$  and JNK1, offering insights into the mechanisms of specificity determination.

**M-P050 Small Angle X-ray Scattering with the NanoSTAR on Biological Macromolecules.** Kurt Erlacher, Bruker AXS, 5465 E. Cheryl Parkway, Madison, WI 53711.

Biological macromolecules can be analyzed using the SAXS technique to reveal their size, shape, and low resolution structure. The laboratory small-angle X-ray scattering camera NanoSTAR is specially equipped for studying these systems. For analyzing biological samples in solution they are filled into a capillary, which seals the specimen from the surrounding vacuum, which is necessary for optimal SAXS conditions. For most samples it is essential to control the sample temperature during data acquisition. This can be achieved with the instrument in a temperature range from -30°C to 300°C.

The nanostructure analysis becomes possible by use of a strong collimated point beam and a high speed area detector. Several examples of the system configuration as well as applications on various biological macromolecules like the protein b-lactoglobulin, Lysozyme and the sweet tasting protein Thaumatin are discussed.

**M-P052 The 40 Residues that Control Folding, Cofactor Binding, Catalysis, Oligomerization and Function of 13000 Short Chain Oxidoreductase Enzymes.** W.L. Duax<sup>1</sup>, R. Huether<sup>1</sup>, V. Pletnev<sup>2</sup>, C.M. Weeks<sup>1</sup>, T. Umland<sup>1</sup>, Q. Mao<sup>1</sup>, L. Gambino<sup>1</sup>, <sup>1</sup>Hauptman-Woodward Inst., Buffalo, NY, <sup>2</sup>Inst. Bioorg. Chem., RAS, Moscow.

The short-chain oxidoreductase (SCOR) family of enzymes has over 13,000 putative members in bacteria, plants, insects, and mammals that catalyze oxidation, reduction and epimerization. Over 70% (~7,900) of the putative family members belong to a single subfamily that contains the signature sequence TGxxxGIG in the  $\beta 2\alpha 3$  turn of the Rossmann fold. The crystal structures of 50 of these have been reported. Although there is not one residue fully conserved, there are 40 fingerprint residues that are conserved at 70% identity or greater. We are determining the roles of each of the fingerprint residues in controlling protein folding, cofactor binding, catalysis, and function. Cofactor selectivity is controlled by two adjacent residues in the  $\beta 2\alpha 3$  turn of the Rossmann fold. Seven residues may be critical to catalysis. C-H $\cdots$ O hydrogen bonds may play a significant role in catalysis and a  $3_{10}$  kink at the center of helix 5 and patterns of aromatic amino acid substitution on helix 5 may control dimer formation. The  $\phi, \psi$  values of seven of the 12 Gly residues in the fingerprint fall in a region of the Ramachandran plot where the other 19 amino acids are rarely observed. Gly residues in these positions are nearly indispensable for the maintenance of the Rossmann fold.

This work is supported by NIH Grant No. DK26546.

**M-P054 A Structural Genomics Analysis of Histidine Kinase Sensor Domains.** J. Cheung, W. A. Hendrickson, Dept. of Biochemistry and Molecular Biophysics, Howard Hughes Medical Inst., Columbia Univ., New York, NY, 10032.

Two-component protein signaling systems in prokaryotes and lower eukaryotes relay external environmental signals to internal adaptive cellular responses. Signal transduction occurs via phosphotransfer between a histidine kinase sensor protein and a response regulator which interact in tandem. The sensor is usually a transmembrane protein that contains a conserved cytoplasmic histidine kinase transmitter domain and a modular periplasmic sensor domain. The response regulator is cytoplasmic protein that contains a receiver domain that interacts with the histidine kinase, and an output domain that interacts with regulators of transcription or chemotaxis. Our work focuses on the X-ray structure determination of a variety

of bacterial histidine kinase sensor domains, guided by a structural genomics analysis of the entire sensor domain family. Structures of five sensor domains have been solved to atomic resolution, some in both ligand-bound and ligand-free states, revealing several distinct structural folds. An analysis of the structures reveals a possible mechanism of transmembrane signaling, and a comprehensive pan-genomic bio-informatics analysis of all sensor domain sequences allows fold prediction for over 350 sensor domains.

**M-P056 *In situ* Extension as a Protocol for Identifying Novel Alpha-Amylase Inhibitors.** G.D. Brayer, C. Li, A. Begum, S.G. Withers, Dept. of Biochemistry, Molecular Biology, and Chemistry, Univ. of British Columbia, Vancouver, BC, Canada.

Human pancreatic alpha-amylase (HPA) is responsible for cleaving large malto-oligosaccharides, such as starch, to maltose and cross-linked junction points. Post-prandial blood glucose levels are correlated to this digestive process and therefore alpha-amylase inhibitors have the potential to be therapeutic agents in the treatment of diabetes and obesity. Despite considerable interest, it has proven difficult to develop inhibitors for HPA that are both specific and of high affinity. Recently we have designed and refined a new high-throughput approach for the discovery and subsequent structural elucidation of oligosaccharide-based inhibitors for HPA, based upon auto-glucosylation. This approach has demonstrated the ability to transform poor HPA inhibitors into significantly improved inhibitors with enhanced specificity and binding affinity profiles. Application of our multi-step high-throughput screening approach has identified a number of new classes of potential HPA inhibitors. Supported by the Canadian Institutes of Health Research.

**M-P058 An Automated Image Collection System For Crystallization Experiments Using SBS Standard Microplates.** Erik Brostromer<sup>a</sup>, Jie Nan<sup>a</sup>, Xiao-Dong Su<sup>a</sup>; <sup>a</sup>National Laboratory of Protein Engineering and Plant Genetic Engineering, Peking Univ., Beijing, China.

As part of a university laboratory structural genomics platform, a low-cost, in-house developed, automated imaging system for SBS microplate experiments has been designed and constructed. The imaging system can scan a microplate in around one to six minutes depending on the plate layout and scanning options. A web-based crystallization database system has been developed, enabling users to follow their crystallization experiments from a web browser.

The system is mechanically simple and leaves room for further developments and additions, but the basic idea is for the system to be non-complicated, robust and low-cost. The software is developed in-house and consists of a robot controlling software and an Image Management system. The software is stand-alone, but we have chosen to partly integrate the image management system into our in-house developed lab information management (LIMS), thus making it an integrated part of our lab environment.

**M-P060 A Laboratory Information Management System For High Throughput Laboratory Environment.** Jie Nan<sup>a</sup>, Xiao-Dong Su<sup>a</sup>; <sup>a</sup>National Laboratory of Protein Engineering and Plant Genetic Engineering, Peking Univ., Beijing 100871, China.

In the post-genomic era, high throughput (HTP) methods for Structural Genomics (SG) have become indispensable. In the environment of high-performance machines and parallelization techniques, a management system for handling data is crucial to meet the increased amount of information. Thus, we have developed an in-house Laboratory In-

formation Management System (LIMS). Using the Browser/Server mode, the system was built by Linux+Apache+MySQL+Php (LAMP) with a Web-interface. The main part of LIMS is Data Management, which assists data collection and storage in all stages of protein-structure projects. Authentication is added to make sure that all the users could access most information, but only the user who works on a project could change its information. There is a set of in-house developed tools LIMS, such as for primer design and the generation of structural-based multi-alignment graphics.

To avoid user-error and to reduce manual input, we are currently in the process of connecting LIMS to the computer connected equipment in the lab, and right now the LIMS was already integrated with our in-house developed Imaging Robot system. Additional functions like the management of seminars, notes and publications are also included to simplify the lab management.

**M-P062 The Joint Center for Structural Genomics: A Multi-tiered Approach to Structural Genomics.** Marc Elsiger, A. Deacon, A. Godzik, S.A. Lesley, K.O. Hodgson, J. Wooley, K. Wuthrich, I.A. Wilson, The Joint Center for Structural Genomics, The Scripps Research Institute, La Jolla, CA.

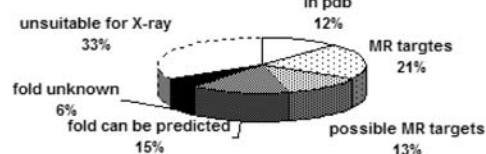
The Joint Center for Structural Genomics ([www.jcsg.org](http://www.jcsg.org)) pipeline is constructed around a flexible, 3-tiered approach to structural genomics, which is used to efficiently characterize, optimize and solve each target. This hierarchical strategy makes full use of parallel processing methods; however, it does not rely on a single processing protocol. Instead, it seeks to minimize the effort and resources to obtain a structure for every target of interest, regardless of whether they prove to be difficult or straight forward. Tier 1 is focused primarily on gathering experimental data on the proposed targets and is reliant on complete automation and the processing of a large number of targets through initial crystallization trials. Targets are then either advanced towards structure determination or enter appropriate Tier 3 salvage pathways, which focus on identifying and creating parallel routes to retrieve more challenging targets. These pathways include alternative routes of expression, construct optimization, and alternative crystallization strategies. This behavior-driven approach is an efficient way to address large numbers of diverse targets and has been successfully tested for both prokaryote and eukaryote proteomes during PSI-1. Our current production center (JCSG-2) will continue to develop and optimize HT approaches to advance the frontiers of structural genomics through the determination of a large number of high-value targets that populate protein fold and family space.

**M-P064 Improved Success Rate of Molecular Replacement.** Lukasz Jaroszewski, Robert Schwarzenbacher, Adam Godzik, Joint Center for Structural Genomics, TBI, La Jolla, CA.

The most important goals of the Structural Genomics Initiative are: determining new protein folds and extending "structural coverage" of large protein families with known structures. It is possible to significantly reduce the costs of the second goal by using molecular replacement (MR) phasing method.

We have recently shown (Schwarzenbacher, *et. al.*, 2004) that the success rate of MR can be improved by using advanced modeling methods and parallel processing of multiple MR searches.

Here we present a full analysis of



over 70 successful and 15 unsuccessful MR trials performed at the Joint Center for Structural Genomics. We show that in the most difficult cases several variants of alignments and search models had to be used. We present the method of predicting probability of successful MR phasing based on the features of the alignment between the protein and its modeling template. We predict the number of MR targets in the proteome of *t. maritima* and show that about 30% of structures from typical bacterial proteome can be solved with MR: Structural coverage of the proteome of *t.maritima*.

Schwarzenbacher, R., Godzik, A., Grzechnik, S.K., Jaroszewski, L. (2004). The importance of alignment accuracy for molecular replacement. *Acta Cryst. D60*, 1229-1236.

**M-P066 Generation of Expression Clones Using High-Throughput Technologies for Protein Structure Determination and Drug Discovery.** S. Moy, Y-c. Kim, C-s. Chang, J. Osipiuk, R-g. Zhang, H. Li, R-y. Wu, F. Collart, A. Joachimiak, Midwest Center for Structural Genomics and Structural Biology Center, Biosciences, Argonne National Laboratory, Argonne, IL.

With the development of high-throughput (HTP) technologies, elucidation of protein structures is at fast-pace and lower cost. At MCSG, adaptation of HTP cloning in 96-well plate format utilizing the Beckman-Coulter system accelerated the generation of expression clones for protein purification and determination of new structures. This technology can also aid in drug discovery. The structure of a penicillin-binding protein from *B. steraothermophilus* may offer opportunities in the optimization of the penicillin-like antibiotics. Structures of transcriptional regulators might aid discovery of new drugs – TetR from *B. cereus*, TetR and MarR from *E. faecalis*, MarR from *P. gingivalis*, and ROK from *V. cholerae*. These transcriptional factors are up- or down-regulated by small co-regulators. Identification of these ligands combined with structure determination of complexes can aid drug design.

This work was supported by the grants from the National Institute of Health (GM62414 and GM074942) and the U.S. Department of Energy, Office of Biological and Environmental Research under Contract W-31-109-ENG-38.

**M-P068 Structure of *B. subtilis* NrdI - An Auxiliary Protein of Class Ib Ribonucleotide Reductase has Flavodoxin Fold and Binds FMN.** R-y. Wu, R-g. Zhang, M. Shu, A. Joachimiak, The Midwest Center for Structural Genomics and Structural Biology Center, Biosciences, Argonne National Laboratory, Argonne, IL.

Ribonucleotide reductases (RNRs) catalyze the reduction of ribonucleotide di- or tri-phosphates to the corresponding deoxyribonucleotides for DNA replication and repair. This reaction requires a source of electrons. In *B. subtilis*, only one locus is dedicated to deoxyribonucleotide biosynthesis and is composed of *nrdI*, *nrdE* and *nrdF* genes. The *nrdI* is strictly conserved in the locus of Ib RNRs. To reveal NrdI's function we have determined the first crystal structure of the NrdI protein at 1.9 Å. The protein has flavodoxin fold with five parallel β-strands flanked on both sides by four α-helices. A FMN co-factor is bound at the carboxy-terminal end of the β-sheet. The structure suggests that the NrdI/FMN complex serves as an electron donor in the ribonucleotide reduction reaction.

This work was supported by the grants from the National Institute of Health (GM62414 and GM074942) and the U.S. Department of Energy, Office of Biological and Environmental Research under Contract W-31-109-ENG-38.

**M-P070 Structure of Toprim Domain-containing Protein from *Bacillus stearothermophilus*.** P. Rezacova<sup>1</sup>, D. Borek<sup>1</sup>, S. Moy<sup>2</sup>, A. Joachimiak<sup>2</sup>, Z. Otwinowski<sup>1</sup>, <sup>1</sup>Dept. of Biochemistry, UT Southwestern Medical Center, Dallas, TX, <sup>2</sup>Biosciences Div. and Structural Biology Center, Argonne National Laboratory, Argonne, IL.

The crystal structure of Midwest Center for Structural Genomics target APC35832, a 14.7-kDa protein from *Bacillus stearothermophilus*, has been determined at 1.6 Å by SAD from mercury soaked crystals.

APC35832 structure has a conserved Toprim fold with a 4-stranded β-sheet surrounded by 4 α-helices. Toprim domain is a part of the catalytic core in number of enzymes catalyzing formation or cleavage of phosphodiester bond. The closest structural homolog of APC35832 is domain in T7 primase, in which the conserved acetic residues coordinate Mg<sup>2+</sup> ion and conserved glutamate was found to be critical for formation of phosphodiester bond.



In order to determine if the metal-binding function is preserved in APC35832, the protein was co-crystallized with MgCl<sub>2</sub> and the structure was determined at 1.6 Å. One Mg<sup>2+</sup> ion is coordinated by side chains of conserved residues D58, D60 and E88.

The metal binding and the presence of conserved glutamate E14 suggest that Toprim domain of APC35832 can participate in a catalytic activity. Nevertheless, protein APC35832 lacks the additional domains necessary for catalytic activity of proteins belonging to Toprim superfamily. Protein consisting of Toprim domain alone thus might represent modules for construction of novel class of multimeric nucleotidyl transferases or nucleases. Potential interaction partners and biological function of the APC35832 protein are yet to be identified.

**M-P072 CrystalMation: Capacity, Reproducibility and Efficiency of a Fully Integrated Automatic High-Throughput Crystallization Platform.** Jian Xu, David Robbins, Rollan Mosko, Matt Lundy, Tom Vorndran, Mandel Mickley, Michael Willis, Rigaku Automation, Carlsbad, CA 92008.

CrystalMation is the first fully and seamlessly integrated robotic system commercially available on the market for automating the crystallization process from protein to crystal. It consists of crystallization screen creation, plate setup, reservoir & protein dispense, plate storage & handling, image inspection & scoring, one-click optimization and software applications for experiment management and decision making. We report here a system successfully built and optimized for JCSG and IAVI, which has been shown to meet the high-throughput criteria. Large scale, systematic and functional tests have been performed on the system, including various volumes, proteins, screens, and plate types. The results indicate the system sets up 96 well SBS format plates at a rate of 4.5 minutes per plate or less. Liquid dispensing was consistent and reproducible, even at low volumes. Inspections of all plates were completed within individually specified schedules and stored in the database. The statistics from this large dataset also suggested that all crystallization conditions that give rise to crystals were repeatable.

We thank Joint Center for Structural Genomics for collaboration.

**M-P074 Structural Investigations of the Hydrophobic Core of the Flavin-Dependent Thymidylate Synthase.** Irimpan I. Mathews<sup>1</sup>, Heath Klock<sup>2,3</sup>, Eileen Ambing<sup>2,3</sup>, Scott A. Lesley, Ashley M. Deacon<sup>1,2</sup>, <sup>1</sup>Stanford Synchrotron Radiation Laboratory, <sup>2</sup>The Joint Center for Structural Genomics, Stanford Univ., 2575 Sand Hill Rd, SSRL MS 69, Menlo Park CA 94025, <sup>3</sup>The Genomics Inst. of Novartis Research Foundation, 10675 John Jay Hopkins Dr., San Diego, CA 92121.

The functional role of two of the highly conserved residues from the hydrophobic core of flavin-dependent thymidylate synthase (thyX/Thymidylate Synthase Complementing Protein) has been analyzed by stability measurements and structural studies. We have solved five structures of the double mutants of the highly conserved residues from the hydrophobic core of FDTS. These results emphasize the importance of the rigidity of the hydrophobic core and its plasticity to accommodate small changes in the size of the contributing side chains. Interestingly, while the drastic changes in the sizes of the side chains affected the cofactor and substrate binding properties, enzyme was able to maintain its overall fold. In conclusion, the current study shows that small changes in the sizes of the hydrophobic residues do not affect the overall fold and supports the earlier suggestion of a common overall fold for the FDTS/TSCP family of enzymes.

**M-P076 Structural and Biochemical Studies of the Tryptophan 2,3-Dioxygenase Reveal the Molecular Detail of Tryptophan Oxidation.** Farhad Forouhar,<sup>1</sup> Ross Anderson,<sup>2</sup> Chris Mowat,<sup>2</sup> Sergey M. Vorobiev,<sup>1</sup> Mariam Abashidze,<sup>1</sup> Arif Hussain,<sup>1</sup> Seetharaman Jayaraman,<sup>1</sup> Chiara Bruckmann,<sup>2</sup> Sarah Thackray,<sup>2</sup> Todd Tucker,<sup>1</sup> Haleema Janjua,<sup>3</sup> Rong Xiao,<sup>3</sup> Thomas B. Acton,<sup>3</sup> Gaetano T. Montelione,<sup>3</sup> Steve Chapman,<sup>2</sup> Liang Tong<sup>1\*</sup>, <sup>1</sup>Dept. of Biological Sciences, Northeast Structural Genomics Consortium, Columbia Univ., New York, NY, <sup>2</sup>School of Chemistry, Univ. of Edinburgh, Edinburgh, <sup>3</sup>Center for Advanced Biotechnology and Medicine, Northeast Structural Genomics Consortium, Rutgers Univ., Piscataway, NJ.

The essential but least abundant amino acid L-tryptophan is a precursor for serotonin, NAD/NADP, and polyADP-ribose. Tryptophan 2,3-dioxygenase (TDO) is a hemoprotein that catalyzes the first and rate-limiting reaction of tryptophan degradation via the kynurenine (KYN) pathway, by incorporating a dioxygen into the indole moiety of tryptophan. In mammals, more than 90% of the total tryptophan is degraded by TDO in the liver through the KYN pathway. The related enzyme, indoleamine dioxygenase, is a target for the treatment of cancer and autoimmune diseases. Here we present extensive structural and biochemical studies of the *Xanthomonas campestris* TDO and a related enzyme from *Shewanella oneidensis*. These studies provide molecular insight into the mechanism of tryptophan oxidation.

**M-P078 Optimization of Protein Crystallization Screens at the Ontario Centre for Structural Proteomics.** T. Skarina\*, E. Evdokimova\*, X. Xu, A. Ignatchenko, A.M. Edwards, A. Savchenko, Ontario Centre for Structural Proteomics, Univ. of Toronto, University Health Network, Toronto, ON, Canada, tsarina@uhnres.utoronto.ca, evdokimo@uhnres.utoronto.ca, \*Corresponding authors.

Obtaining diffracting protein crystals is a key step in protein structure determination using X-ray crystallography. It is particularly critical in Structural Genomics projects, which require structural characterization of hundreds of poorly characterized protein families. Thus defining efficient and cost effective strategies for protein crystallisation is crucial for such large scale projects as well for the structural studies of individual proteins.

Since 1998 the Ontario Centre for Structural Proteomics (Canadian and NIH-funded Centre affiliated with the Midwest Center for Structural Genomics in the US) have been focused on the optimization of protein crystallization process by developing more effective crystallization screens. Our database currently contains the results on crystallization trials for over 1300 unique proteins from all three kingdoms of life (Bacteria, Archaea and Eukarya). Initial crystallization conditions were obtained for 500 of these proteins. More than 160 of them had been optimized to lead to the protein structure determination using X-ray crystallography.

Statistical analysis of this data allowed us to come up with optimized the screen that includes 90% of non-redundant crystallization conditions. We have also developed specific crystallization screens for DNA-binding and membrane proteins.

**M-P080 Identification of Small Molecule Ligands for Structural Genomics Targets and their Application in Crystallization Trials.** E. Evdokimova\*, T. Skarina\*, M. Kudritska, X. Xu, O. Egorova, M. Pennycook-Brown, A. Ezersky, A.M. Edwards, A. Yakunin, A. Savchenko, Ontario Centre for Structural Proteomics, Univ. of Toronto, Univ. Health Network, Toronto, ON, Canada, evdokimo@uhnres.utoronto.ca, tsarina@uhnres.utoronto.ca, \*Presenting authors.

A large number of protein functions depend on the interactions with small molecules. The molecular mechanisms of these interactions are usually revealed through structural studies of protein-small molecule complexes. Structural Genomics targets poorly characterized protein families for large-scale three-dimensional structure determination. Identification of small molecule ligands for these proteins not only provides an insight into their function but also facilitates structural studies of these proteins.

At Ontario Centre for Structural Proteomics (Canadian and NIH-funded Centre affiliated with the Midwest Center for Structural Genomics in the US) we are using two main methods for identification of small molecule ligands of structural genomics targets: 1) generic enzymatic assays; 2) miniaturized high-throughput protein stability assays.

Using these approaches, we have identified several potential ligands and enzymatic substrates for previously uncharacterized proteins. Interactions of these proteins with small molecules were confirmed by determination of their complex structures.

**M-P082 The Undiscovered Bourne: The Helsinki Low-Volume Medium-Throughput Crystallisation Facility.** A. Goldman, P. Heikinheimo, S. Mäki, V.-P. Jaakola, L. Lehtiö, H. Repo, Inst. of Biotechnology, Univ. of Helsinki, FIN-00640 Helsinki, Finland.

We recently installed an automated protein crystallisation system, including a Hamilton Microlab STAR liquid handling robot for preparing screens, a Cartesian Microsys for protein drops and a Thermo Rhombix Imager for imaging. Thermo Rhombix software integrates all the components, so we can run individual steps, store experiment design and history and query the results. A full-time technician runs the service.

Our goal was to provide a crystallisation centre in Finland: *i.e.* to crystallise proteins at 50-200 nl volumes, to provide premixed screens for those wishing to screen at home and to provide imaging services. We currently crystallise protein from seven different groups. Crystallisations are performed twice a week and after the experiment is set up, end-users are notified by email when their experiments are imaged. Plates are imaged on the day of setup, weekly till a month old and once a month until four months old.

The scientist can analyse the drop images from their own computer either through the web or *via* the Oracle database. We will present results from our first year of operation.

We thank the Academy of Finland, Sigrid Juselius Foundation, the Institute of Biotechnology and Biocentrum Helsinki for support.

**M-P084 A Nearly-Automated High-Throughput Method for Identifying Well-Expressed Soluble Protein Variants.** E.H. Bursey\*, T.C. Terwilliger† L-W. Hung\*†, \*Lawrence Berkeley National Laboratory, Berkeley, CA 94720, Los Alamos National Laboratory, Los Alamos, NM 87545.

Low protein expression levels and poor solubility are commonly encountered in a large percentage of recombinant proteins. These problems are especially challenging for laboratories in the field of Structural Genomics, whose objective is to produce structural information about a diverse set of proteins in a high-throughput manner. We have developed a rapid, high-throughput method for increasing the expression and solubility of recombinant proteins through the generation of protein variants by site-specific truncation of the DNA coding region. These truncation variants are expressed using a commercially available *in vitro* protein expression system and are quantified by dotblot. This method has been streamlined by the development of a computer program which designs truncation variants and the associated PCR primers and by the development of a platform to automate the wet-lab work based on a Tecan liquid-handling robot. The method described here can be used to screen the expression and solubility of up to 94 truncation variants in just 13 hours.

This research was supported by Mycobacterium Tuberculosis Structural Genomics Consortium.

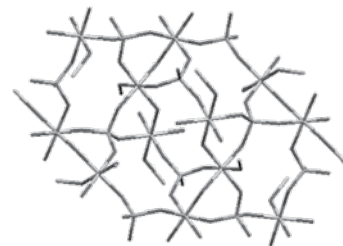
**M-P088 Biosynthesized Magnetic (Zn<sub>1-x</sub>Fe<sub>x</sub>)Fe<sub>2</sub>O<sub>4</sub> Nanoparticles.** C.J. Rawn<sup>1</sup>, L.W. Yeary<sup>2</sup>, J.-W. Moon<sup>3</sup>, B.C. Chakoumakos<sup>1</sup>, M.E. Madden<sup>3</sup>, T.J. Phelps<sup>3</sup>, L.J. Love<sup>2</sup>, <sup>1</sup>Materials Science and Technology Div., <sup>2</sup>Engineering Science and Technology Div., <sup>3</sup>Environmental Sciences Div., Oak Ridge National Lab., Oak Ridge, TN.

Magnetic nanoparticles are needed for rapidly expanding applications in the biomedical and engineering fields. The biomineralization process used for this study is of interest due to the synthesis at relatively low temperatures that produces nanoparticles without milling. These factors reduce processing costs and the method is promising for its scale up ability to produce large quantities of material. Nanoparticle magnetite with Zn substituting for some of the Fe has been synthesized at 60°C by a biologically induced mineralization method using thermophilic bacteria. Pure magnetite and magnetite with increasing amounts of Zn have been studied using time-of-flight powder neutron diffraction, X-ray powder diffraction, TEM, and magnetic susceptibility. The addition of Zn increases the lattice parameter, the background, and the peak width. The latter two results suggest an increase in disorder, a decrease in crystallinity, and/or a decrease in crystallite size. Rietveld refinements show that the Zn prefers the tetrahedral site in the structure and the refined site occupancies for the samples with Zn are  $x = 0.629(7)$  and  $x = 0.804(7)$  atom per formula unit with corresponding lattice parameters of  $a = 8.4040(1)$  and  $a = 8.4253(1)$  Å compared to the sample without Zn that has a lattice parameter of  $a = 8.36965(6)$ .

This work was supported by the Defense Advanced Research Projects Agency (DARPA) Biomagnetics Program under Contract 1868-HH43-X1. Oak Ridge National Laboratory is managed by UT-Battelle, LLC, for the U.S. Department of Energy under Contract DE-AC05-00OR22725.

**M-P090 Synthesis and Structure of an Aluminophosphate Built from 3-rings.** Hemant P. Yennawar<sup>#</sup>, David E. W. Vaughan<sup>+</sup> and Anthony J. Perrotta<sup>+</sup>, <sup>#</sup>Dept. Biochemistry and Molecular Biology, Althouse Lab., <sup>+</sup>Materials Research Lab., Materials Research Inst., The Pennsylvania State Univ., University Park, PA, 16802.

Reacting a pre-made aluminophosphate (ALPO, P/Al=0.9) gel with an aqueous-triethylamine solution of KOH and TMAOH we have synthesised a new porous 3D crystalline structure (PSU-2) under high pH conditions. Single crystal structure analysis shows that the orthorhombic crystal is built from two different pairs of 3-rings of P-tetrahedra and Al-octahedra. This is the first known ALPO built only from 3-ring secondary building units. Associated phases include ALPO analogs of the zeolites sodalite, analcime and natrolite, the last not hitherto reported in an ALPO composition.



**M-P094 Some New Results by Using the Transmission Electron Microscopes to Study the Alloy Nd-Fe-Co-Al.** V. Vong, L.T. Hung, N.H. Dan, M. Hietschold, Laboratory of Electron Microscopy-Vietnamese Academy of Science and Technology, 18 Hoangquocviet Rd., Cauaiay-Hanoi Vietnam.

The Nd-Fe-Al bulk amorphous hard magnetic alloy discovered by Inoue *et al.*[1996] with  $R_c \sim 102$  K.s-1,  $H_c \sim 300$  kA/m. This kind of materials have attracted many researchers by virtue of both the application potential and the natural of the hard magnetic mechanism. The Co, B improve GFA,  $H_c$ , (BH)max and TC of these alloys (N. X. Phuc *et al.*). The high  $H_c$ , Tc and (BH)max in these alloys were supposed that is due to single domain-like structures formed by nanosized clusters of nanocrystallites.  $Nd_{55-x}Co_xFe_{30}Al_{10}B_5$  ( $x = 0,5,10,15$  and 20) and  $Nd_{40-x}Co_xFe_{30}Al_{10}B_{x+5}$  ( $x=0,5$  and 10) rods with dimensions of  $1 \times 10 \times 30$  mm fabricated by copper mold suction-casting method in an arc-melting furnace.  $Nd_{35-x}Fe_{30+x}Co_{20}Al_{10}B_5$  ( $x = 0,10,20$  and 30) and  $Nd_{25}Co_{30}Fe_{30}Al_{10}B_5$  were prepared by melt-spinning method with quenching rate of  $v=30$ m/s and  $v=10, 15, 20$  and 25m/s, respectively. We achieved the Nd-Fe-Al based alloys and then the materials were studied by transmission electron microscopes (TEM,HREM). The results show that the prepared materials have nano-structure and nano-size. The characterizations as well as high Tc,  $H_c$  and (BH)max ... of the prepared materials were investigated. Many authors supposed that the nanosized clusters of this material can be improved the materials, especially magnetic property. In the work we proved this one. With the method for preparation of the sample can create the changing of the material structure.

**M-P096 On Diamond Nucleation Sites and Relativistic Rehybridization in Pyramidalizing Reactions.** Boris Udovic, Sezanska 11, 6210 Sezana, Slovenia, boris.udovic@email.si.

The experienced low tendency toward carburization reactions and carbon solubility make rather outstanding the chemical behaviour of non-transition elements as metal Sn and Pb atoms among the potential combinations of some most celebrated  $3d \rightarrow 6d$  carbide formers in diamond phase synthesis. In the lower valence state a stable but sterically active  $6s^2$  electron pair is projected out one side of the Pb atom, generating an asymmetric structure upon filling one of the hybrid orbitals originated from their  $6s$  and  $6p$  atomic components. The relativistic contraction of the  $6s$  orbital and the expansion of the full filled  $5d$  kernel envelope promote the reshape of the nearest bonding

orbitals. In a possible alloy of more noble metals and non-transition elements as Pb, which are combined with a carbide-former of the iron group (Fe, Th, etc.), the last elements react as carbon attractors while the non-transition element Pb behaves as a repeller-expeller of dissolved carbon atoms. The antagonistic expelling action is expected to involve at least one single bond between surface Pb and carbon adatoms. The interacting field turns into the change of the symmetry of the potential energy of surface Pb atoms, which is further desymmetrized and its wavefunction is changed to rehybridize forming the sterically active  $6s^2$  lone pair in pyramidal electronic redistribution. The repelling Pauli fields torque the vicinal  $p_z$  carbon orbital and gain to release more paraffinic than olefinic bonds in comparison to stronger attractive interactions with carbide and graphite-former elements.

**M-P098 Anomalous Scattering of HgSe Nanoclusters in Zeolites using Synchrotron X-ray Radiation.** M. Castro-Colin, A.M. Milinda, S.C. Moss, W. Donner, A.J. Jacobson, E. Anokhina, Physics Dept., Chemistry Dept., U. of Houston, Houston, TX 77204.

HgSe, has been grown inside LTL and Nd-Y zeolites (tubular and spherical nanosized pores, respectively). A first sharp diffraction peak is observed in an X-ray diffraction profile associated to the clustering of HgSe, whose size is bound by the zeolite pore diameter. The combined effect of guest materials properties as well as the charge imbalance inside the pore, affect the cluster-cluster correlation (clusters in separate pores), via occupational and/or orientational order. These correlations are expressed through a broad diffuse modulation, absent in the pure host, upon which the more obvious, Bragg peaks are imposed. This effect is suggested through preliminary pair-distribution function (PDF) data. Anomalous scattering experiments carried out both below the Se K-edge and the Hg L-edge, as well as off-edge for each zeolite, aided in calculating average crystallographic parameters of HgSe. These results and further PDF analyses promise to reveal an understanding of the structural configuration and cluster allocation mechanisms. A potential technological application of this system could arise, due to the transparency of these zeolites and ease of interaction of visible light with species contained within the pores.\* M.C.C. now at U.T. El Paso.

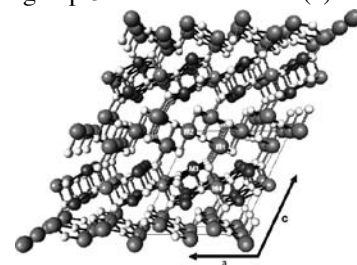
Research is supported by DOE/BES DE-FG02-04ER46160.

**M-P100 Structural Phase Transitions Coupled with Magnetic Order in the Geometrically Frustrated Triangular Lattice Antiferromagnet  $\text{CuFeO}_2$ .** Q. Huang,<sup>1</sup> F. Ye,<sup>2</sup> Y. Ren,<sup>3</sup> J.A. Fernandez-Baca,<sup>2,4</sup> Pengcheng Dai,<sup>4,2</sup> J.W. Lynn,<sup>1</sup> T. Kimura<sup>5</sup>. <sup>1</sup>NIST Center for Neutron Research, NIST, Gaithersburg, MD, <sup>2</sup>Center for Neutron Scattering, ORNL, Oak Ridge, TN, <sup>3</sup>X-ray Science Div., ANL, Argonne, IL, <sup>4</sup>Dept. of Physics and Astronomy, The Univ. of Tennessee, Knoxville, TN, <sup>5</sup>Los Alamos National Laboratory, Los Alamos, NM.

Neutron and synchrotron X-ray diffraction were used to study the geometrically frustrated triangular lattice antiferromagnet  $\text{CuFeO}_2$ . The compound exhibits an incommensurate and a commensurate magnetic order at  $T_{N1} \sim 13$  K and  $T_{N2} \sim 11$  K, respectively, accompanied by a second- and a first-order structural phase transitions from hexagonal to monoclinic structure. Application of magnetic field from 0 T to 7 T lowers the transition temperatures by 1 K, to  $T_{N1} \sim 12$  K and  $T_{N2} \sim 10$  K, respectively, and induces an additional structural modulation in the temperature region where the field-driven ferroelectricity occurs. This suggests a strong magneto-elastic coupling that is intimately related to the multiferroic effect.

**M-P102 Synthesis and Characterization of Quaternary Chalcogenide  $\text{In}_1\text{Sn}_4\text{Bi}_3\text{Se}_8$ .** Ming-Fang Wang, Chi-Shen Lee<sup>1\*</sup>, Chia-Jyi Liub<sup>2</sup>, <sup>1</sup>Dept. of Applied Chemistry and Inst. of Molecular Science, National Chiao Tung Univ., 1001 Ta-Hsueh Rd., Hsinchu 30010, Taiwan, <sup>2</sup>Dept. of Physic, National Changhua Univ. of Education, 1 Jin-De Road, Changhua, Taiwan 500, Republic of China.

A new quaternary compound  $\text{In}_2\text{Sn}_4\text{Bi}_6\text{Se}_{16}$  was synthesized by direct combinations of the In:Sn:Bi:Se = 1:2:3:8 at 1023 K. The compound crystallized in the monoclinic space group  $C2/m$  with  $a = 13.557(3)$  Å,  $b = 4.1299(8)$  Å,  $c = 15.252(3)$  Å,  $\beta = 115.73(3)^\circ$ ,  $V = 769.3(3)$  Å<sup>3</sup>,  $Z = 1$ , and  $R/wR_g/\text{GOF} = 0.0213/0.052/1.089$ . The structure of  $\text{In}_1\text{Sn}_2\text{Bi}_3\text{Se}_8$  features three-dimensional framework consisting of rectangular NaCl-type infinite rod unit running parallel to the  $a$ -axis, which are stitched together by Bi-Se. Electronic structure calculation based



Perspective view of the structures of  $\text{InSn}_2\text{Bi}_3\text{Se}_8$  along the  $b$ -axis.

on the model  $\text{In}_2\text{Sn}_4\text{Bi}_6\text{Se}_{16}$  suggests that the material is a narrow band gap semiconductor. Thermopower of  $\text{In}_1\text{Sn}_2\text{Bi}_3\text{Se}_8$  is  $-270$  (20)  $\mu\text{V/K}$  over temperature range between 300 and 700 K. Electrical conductivity and thermal conductivity of  $\text{In}_1\text{Sn}_2\text{Bi}_3\text{Se}_8$  at room temperature are  $1645(7)$   $\text{Sm}^{-1}$  and  $0.36$   $\text{W/mK}$ , respectively, which indicating the Figure of Merit ( $ZT$ ) at room temperature close to 0.1.

This project was supported by National Science Council (NSC94-2113-M-009-012).

**M-P104 Chemical Disorder in As-Te Glasses Studied by Pulsed Neutron and High-Energy X-ray Diffraction.** Eugene Bychkov, Mariana Milochova, LPCA UMR CNRS 8101, Univ. of Littoral, 59240 Dunkerque, France.

The As-Te glassy system differs from other binary chalcogenide glasses. First, a significant chemical disorder was found for both stoichiometric,  $\text{As}_2\text{Te}_3$ , As- and Te-rich non-stoichiometric glasses using anomalous X-ray scattering<sup>[1]</sup>. Second, we found that the position of the First Sharp Diffraction Peak (FSDP) is different if studied using neutrons or X-rays. This difference seems also be related to the chemical disorder and different coherent scattering lengths,  $b_{\text{Te}}/b_{\text{As}} = 0.88$  but  $Z_{\text{Te}}/Z_{\text{As}} = 1.58$ , i.e., nearly a factor of 2. We carried out a detailed analysis of our high-resolution neutron and X-ray data in the As-Te glassy system and confirmed the hypothesis of chemical disorder. A possible explanation of the observed phenomenon is a relatively low temperature for the semiconductor – metal transition in As-Te melts<sup>[2]</sup>.

[1] Q. Ma, D. Raoux, S. Benazeth, *Phys. Rev. B* **48** (1993) 16332.

[2] N.F. Mott and E.A. Davis, *Electron processes in non-crystalline materials* (Clarendon Press, Oxford, 1979).

**M-P106 Exploring Local Distortion Modes Via Single-Crystal Diffuse Scattering.** Branton J. Campbell, Harold T. Stokes, Dept. of Physics & Astronomy, Brigham Young Univ., Provo, UT 84602.

Diffraction studies of long-range order often permit one to unambiguously determine the structure of a low-temperature distorted phase in considerable detail. In contrast, short and intermediate-range distortions lead to weak diffuse peaks that can be difficult to detect, even at advanced neutron and synchrotron x-ray facilities. When there are not enough well-defined peaks to reliably develop a distortion model, the ability to quickly enumerate and test potential candidate structures against limited experimental data is essential. Here, we present the straight-forward use of the ISODISPLACE software package to characterize local atomic displacements in important material systems.

**M-P108 Molecular Motion and Macroscopic Actuation in Liquid Crystal Elastomers.** J.R. Deschamps<sup>1\*</sup>, J. Konnert<sup>1</sup>, C. Spillmann<sup>2</sup>, J. Naciri<sup>2</sup>, B. Ratna<sup>2</sup>, <sup>1</sup>Code 6030, Naval Research Laboratory, Washington, DC, deschamps@nrl.navy.mil; <sup>2</sup>Code 6930, Naval Research Laboratory, Washington, DC.

The use of liquid crystals is well known in electrooptics, yet their potential use in other areas of technology is ever increasing. For example, liquid crystals in the nematic phase have been incorporated into cross-linked polymer networks to form materials capable of reversible, uniaxial contraction for use as mechanical actuators<sup>1,2</sup>. It has been shown that when an electric field is applied to chiral smectic A liquid crystals in the layer plane, the transverse dipole of the molecules couple to the electric field and tilt the molecules in a plane perpendicular to the electric field direction<sup>3</sup>. Therefore, it is possible to produce reversible, macroscopic dimension changes in a smectic elastomer by applying an electric field to cause molecular tilting of the liquid crystal molecules. In this study, we observe the molecular response, via x-ray scattering, of a smectic A elastomer while subjected to electric field. We examine the diffraction patterns in order to develop an understanding of the relation between changes at the molecular level and the accompanying macroscopic changes in the LC elastomer.

[1] Gleim, W. & Finkelmann, H. Thermoelastic and Photoelastic Properties of Cross-Linked Liquid-Crystalline Side-Chain Polymers. *Makromolekulare Chemie-Macromolecular Chemistry and Physics* 188, 1489-1500 (1987).

[2] Thomsen, D. L., Keller, P., Naciri, J., Pink, R., Jeon, H., Shenoy, D. & Ratna, B. R. Liquid crystal elastomers with mechanical properties of a muscle. *Macromolecules* 34, 5868-5875 (2001).

[3] Garoff, S. & Meyer, R. B. Electroclinic Effect at the Ac Phase-Change in a Chiral Smectic Liquid-Crystal. *Physical Review A* 19, 338-347 (1979).

**M-P110 Teaching Crystallography in a Materials Science Program.** Maureen M. Julian, Dept. of Materials Science and Engineering, Virginia Tech, Suite 302 Collegiate Square, Blacksburg, VA 24060.

I propose to discuss several ideas I use in my textbook, 'Foundations of Crystallography, from lattices to electron density maps', a work in progress. I use case studies drawn from Materials Science and Engineering examples in polymers, metals and ceramics. The emphasis is on understanding the basics by working in two-dimensions. For example the 2-D point group trees and space group trees can be completely constructed. Advanced computer exercises are used, in our case the program is MATLAB. The 3-D structures are drawn in MATLAB and can be viewed in perspective as well as the projections. I use symmetry illustrations from prehistoric ornamental art as well as molecular drawings. Sample student reports will be available as well as my own text.

**M-P112 High-Pressure Diffraction Study of the  $A_2M_3O_{12}$  Family.** Stacy Gates, Cora Lind, Univ. of Toledo, Chemistry Dept., Toledo, OH.

Recently, interest in negative thermal expansion (NTE) materials has increased because of their effects when incorporated into composites. Incorporation of NTE materials into composites can favorably reduce thermal expansion in applications with metals, ceramics, and polymers. However, there is concern about their stability under pressure. Earlier attempts to prepare composites with NTE materials have failed due to irreversible transformations of the NTE material to a high-pressure phase that no longer displays NTE. Some of the NTE materials in the  $A_2M_3O_{12}$  family are known to undergo phase transitions as a function of temperature, while others show phase transitions that are induced by pressure.

In this paper results on the synthesis and characterization of  $Y_2Mo_3O_{12}$ , and  $Ga_2Mo_3O_{12}$  are presented. Characterization includes thermal analysis (TG-DTA), scanning electron microscopy (SEM), and powder X-ray diffraction (PXRD). Variable temperature X-ray diffraction was used to investigate the phase transition behavior. To address the materials' behavior under pressure, an *in situ* diffraction study was carried out in a diamond anvil cell (DAC) using synchrotron radiation. We found that both  $Ga_2Mo_3O_{12}$ , and  $Y_2Mo_3O_{12}$  undergo pressure-induced phase transitions, followed by pressure-induced amorphization.

**M-P114 Crystal Structure of Solid  $SiH_4$  at High Pressure.** O. Degtyareva\*, X. Chen, V.V. Struzhkin, H-k. Mao, R.J. Hemley, Geophysical Laboratory, Carnegie Inst. of Washington, 5251 Broad Branch Rd. N.W., Washington D.C. 20015. \*now at School of Physics, Univ. of Edinburgh, Mayfield Road, Edinburgh EH9 3JZ, UK.

Despite considerable experimental effort, the metallic state of solid hydrogen has not been achieved so far at as high pressures as 3 Mbar<sup>[1-3]</sup>. Hydrogen-rich compounds of C, Si and Ge recently received a lot of attention by theoreticians as likely candidates for high-temperature superconductors in their dense metallic form<sup>[4,5]</sup>. Hydrogen can be viewed in these systems as being "chemically pre-compressed", which lowers the metallization pressure, as it was shown for  $SiH_4$ <sup>[5]</sup>. The crystal structure of solid  $SiH_4$  is however unknown.

Here we investigate experimentally the crystal structure of high-pressure phase III of solid  $SiH_4$ , stable from 7 GPa up to at least 40 GPa. Powder X-ray diffraction data were collected at beam line 16-ID-B (HPCAT) at the Advanced Photon Source. Crystal structure of  $SiH_4$  phase III is monoclinic, space group  $P2_1/c$ , and contains four tetrahedrally bonded molecules ( $SnBr_4$  structure type).

[1] C. Narayana et al, *Nature* 393, 46, 1998 [2] A.F. Goncharov et al, *PNAS* 98, 14234, 2001 [3] P. Loubeyre et al, *Nature* 414, 613, 2002 [4] N.W. Ashcroft, *Phys. Rev. Lett.* 92, 187002, 2004 [5] J. Feng et al, *Phys. Rev. Lett.* 96, 017006, 2006

**M-P116 Pressure Dependence of Tolerance Factor of  $Sr_{0.7}Ca_{0.3}MnO_3$ .** R. Kiyonagi, O. Chmaissem, B. Dabrowski, J.D. Jorgensen, J.W. Richardson, J. Fieramosca, IPNS ANL, Argonne, IL 60439, Dept. of Physics, Northern Illinois Univ., Dekalb, IL 60115, MSD ANL, Argonne, IL 60439.

$Sr_{1-x}Ca_xMnO_3$  is one of the  $ABO_3$  type perovskite compound which has been investigated intensively. A previous work on this material demonstrated that a magnetic phase transition at low temperature and structural changes due to the size of the A-site ion are describable by a tolerance factor which is a function of Sr/Ca-O and Mn-O bond lengths. Thus this factor is considered an important parameter to predict a stable structure when synthesizing a new perovskite compound. In order to study a pressure dependence of the tolerance factor of  $Sr_{0.7}Ca_{0.3}MnO_3$ , neutron powder diffractions were carried out under high pressure. We found that the tolerance factor is pressure independent within the applied pressure (up to 5.5 Kbar). However the pressure dependencies of Sr/Ca-O and Mn-O bond lengths differ relative to each other. According to Sr/Ca-O bond the change in length corresponds to a temperature change by 50 K while change in Mn-O bond length corresponds to a change by 120 K. In a low temperature antiferromagnetic phase it was revealed that the spin moment lies in the *a-b* plane instead of along the *c*-axis.

Work at ANL supported by the U.S. DOE, BES--Materials Sciences, under Contract W 31-109-ENG-38.

**M-P118 Pressure-induced FE to AFE Phase Transition of PZT95/5-2Nb: A Neutron Diffraction and Dielectric Study.** Bruno Morosin, Maxim Avdeev, James Jorgensen, Simine Short, Eugene Venturini, Pin Yang, George Samara, Sandia National Laboratories, Albuquerque, NM and Argonne National Laboratory, Argonne, IL.

Zr-rich, Nb-doped lead zirconate titanate powder and ceramic samples with composition near  $\text{Pb}_{0.99}(\text{Zr}_{0.95}\text{Ti}_{0.05})_{0.98}\text{Nb}_{0.02}\text{O}_3$  (known as PZT95/5-2Nb) have been studied in the range of hydrostatic pressure 0 - 6.2 kbar and temperature 10 - 295K by time-of-flight neutron diffraction and dielectric measurements. At 295K the diffraction study shows that the sample undergoes a sharp phase transition from the rhombohedral ferroelectric R3c phase ( $F_{\text{R(LT)}}$ ) to the antiferroelectric orthorhombic Pbam phase ( $A_0$ ) at 2.1 kbar; at 200K this transition occurs at 1.1 kbar. The transformation is incomplete: after the initial sharp drop of the  $F_{\text{R(LT)}}$  content, 20% of the sample remains in this low pressure phase. Above the transition, the fraction of the  $F_{\text{R(LT)}}$  phase, which exists as a minority phase in the high pressure  $A_0$  phase, continues to decrease, but even at our highest pressure of 6.2 kbar, ~8% of the sample remains in the  $F_{\text{R(LT)}}$  phase. The 10% volume contraction at the  $F_{\text{R(LT)}}$ -to- $A_0$  transition unexpectedly results in the retained minority  $F_{\text{R(LT)}}$  being anisotropically “clamped”, with its *a* axis slightly expanded and *c* axis contracted at the phase transition. On pressure release, 26% of the  $F_{\text{R(LT)}}$  phase remains at ambient pressure in the “clamped” state because of the majority  $A_0$  phase. The most pronounced structural changes of the  $F_{\text{R(LT)}}$  result from temperature changes rather than pressure and these involve the B metal site oxygen octahedra distortions.

The work at the Argonne National Laboratory was supported by the U.S. Department of Energy, Office of Science, Contract No. W-31-109-ENG-38. The work at Sandia National Laboratories was supported by the U.S. Department of Energy's National Nuclear Security Administration. Sandia is operated by Sandia Corporation, a Lockheed Martin Company, for the Department of Energy under Contract DE-AC04-94AL85000.

**M-P120 Solid State Structure of 1,2,3-selenadiazole Derivatives.** Nigam P. Rath<sup>a</sup>, A. Marx<sup>b</sup>, V. Manivannan<sup>b</sup>, S. Saravanan<sup>c</sup>, S. Muthusubramanian<sup>c</sup>, <sup>a</sup>Dept. of Chemistry and Biochemistry, Univ. of Missouri- St. Louis, <sup>b</sup>Dept. of Physics, Presidency College, Chennai-600005, India, <sup>c</sup>Dept. of Organic Chemistry, Madurai Kamaraj Univ., Madurai-625021, India.

Heterocyclic compounds containing selenium are of interest due to their biological and synthetic applications. 1,2,3-selenadiazoles have attracted much attention as versatile intermediates in organic synthesis and for their biological properties. For example, some of the 1,2,3-selenadiazole derivatives exhibit antifungal, antibacterial, antimicrobial and insecticidal activities. As naturally occurring nitro compounds exhibit broad antibiotic activity and certain alkyl nitro compounds exhibit antitumor activity we decided to synthesize and structurally characterize a set of 1,2,3-selenadiazoles with nitro group in the side chain. Geometrically, the conformation around the CH-CH in the side chain and the possible hydrogen bonding of nitro group with other substituents in the ring in the solid state and in solution may be of interest in these compounds. In order to better understand the structural properties of these compounds we have determined the solid state structure of several 1,2,3-selenadiazoles using single crystal x-ray diffraction studies. The results of these studies will be presented in this poster.

**M-P122 Crystal Structure of Carbonic Anhydrase Complexed with Bicarbonate from *Pyrococcus horikoshii* OT3.** J. Jeyakanthan, C. Kuroishi, S. Kuramitsu, S. Yokoyama, Y. Shiro, RIKEN SPring-8 Centre, 1-1-1, Kouto, Sayo-Cho, Sayo-Gun, Hyogo, 679-5148 Japan.

Carbonic anhydrases are widely distributed in nature and participate in different functions. It is a zinc-containing metalloenzyme that catalyzes the reversible conversion of  $\text{CO}_2$  and  $\text{HCO}_3^-$ . On the basis of specific amino acid sequence similarities, three major classes of carbonic anhydrases have been described:  $\alpha$ ,  $\beta$ , and  $\gamma$ . Here, we report on the novel x-ray structures of free and bicarbonate-bound forms from the *Pyrococcus horikoshii* OT3, at 1.5 and 2.3 Å resolution, using molecular replacement phasing. The polypeptide chain fold is a left-handed  $\beta$ -helix, and the most important feature of the active site cavity is a zinc ion, complexed with three histidyl residues, and a zinc-ion-bound water molecule in a tetrahedral arrangement. The bicarbonate anion binds to the zinc ion as an essential ligand at the tetrahedral site, replacing the activity linked  $\text{H}_2\text{O}/\text{OH}^-$  ion group in the native enzyme. The bicarbonate is stabilized by the coordination of oxygen directly with the active-site zinc ion. Interestingly, we also observed a calcium ion bound with this enzyme. The current structure shows that the overall fold and catalytically-active site is similar to that observed  $\gamma$ -class of carbonic anhydrases from *Methanosarcina thermophila*.

**M-P124 Crystal Structure of  $\beta$ -Hemolysin: Mechanism of Sphingomyelin Cleavage.** Medora Huseby, Ke Shi, Cathleen Earhart, Douglas Ohlendorf, Dept. of Biochemistry, Molecular Biology and Biophysics, Univ. of Minnesota.

$\beta$ -hemolysin is a virulence factor of *Staphylococcus aureus* that catalyzes the cleavage of sphingomyelin in biological membranes to ceramide and phosphorylcholine causing lysis of erythrocytes.  $\beta$ -hemolysin belongs to the neutral sphingomyelinase C family, and shares homology to mammalian neutral sphingomyelinase C enzymes which are important in sphingolipid signaling and metabolism. Crystals were found to be fully merohedrally twinned. Diffraction data were collected at the Molecular Biology Consortium facilities on beam line 4.2.2 at the Advanced Light Source. The structure was solved via molecular replacement using SmcL (sphingomyelinase C from *Listeria ivanovi*) as the search model and refined to 2.4 Å resolution.  $\beta$ -hemolysin belongs to  $\alpha/\beta$  protein family and is arranged in a 4-layer sandwich, adopting a similar structure to that of SmcL. The structural features provide insight into the mechanism of neutral sphingomyelinase C along with the protein interaction with a sphingomyelin substrate. A C-terminal  $\beta$ -hairpin is thought to penetrate the lipid bilayer and aid in substrate binding and positioning. This mechanism is also assisted by a hydrophobic loop which is nearby the active site. Inactive mutants are being used to study the structure of the substrate complex.

[1] [www.cdc.gov/](http://www.cdc.gov/) [2] Openshaw et al. *JBC*, 2005.

**M-P126 Aerolysin Binding to a GPI Anchor Core Glycan: High-Resolution Structure of Proaerolysin in Complex with the Receptor Component Mannose-6-phosphate.** C.L. Brooks, S.N. Borisova, J.T. Buckley, S.V. Evans, Dept. of Biochemistry and Microbiology, Univ. of Victoria, Victoria, B.C., V8P 3W6 Canada.

Aerolysin is a bacterial channel-forming toxin produced by *Aeromonas* species. The toxin and its inactive precursor proaerolysin are both known to bind with high affinity to the conserved glycan core of glycosylphosphatidylinositol (GPI) anchored proteins, although the specific nature of these interactions was unknown. Here we report to 2.49 Å resolution the first structure of proaerolysin in complex with a component of its putative GPI glycan receptor, mannose-6-phosphate. The structure unequivocally identifies the binding site on the protein as well as some of the GPI glycan residues involved in binding. The mannose-6-phosphate residue fills part of a large groove on the surface of the protein, with the sugar ring recognized via hydrophobic stacking interactions and the phosphate moiety via

specific charged-residue interactions. This structure gives unique insight into the observed different receptor specificities of related toxins that also bind to GPI anchored proteins.

**M-P128 Crystal Structure of Staphylococcal Enterotoxin I in Complex with a Human MHC II Molecule.** R. Guan<sup>1,2</sup>, M.M. Fernández<sup>1</sup>, E.L. Malchiodi<sup>1</sup>, R.A. Mariuzza<sup>1</sup>, <sup>1</sup>Center for Advanced Research in Biotechnology, Univ. of Maryland Biotechnology Inst., Rockville, MD 20850, <sup>2</sup>Laboratory of Molecular Biology, National Inst. of Diabetes and Digestive and Kidney Diseases, National Institutes of Health, Bethesda, MD 20892.

Superantigens (SAGs) are immunostimulatory and disease-causing proteins of bacterial or viral origin that can be presented by MHC II molecules to T cell receptors. Staphylococcal enterotoxin I (SEI), a SAG belonging to the Zn<sup>2+</sup> SAG family, binds MHC II molecules through a Zn<sup>2+</sup> containing high affinity site. We determined the crystal structure of SEI in complex with HLA-DR1, an MHC II molecule, loaded with an influenza hemagglutinin (HA) peptide. SEI and DR1/HA bury a much smaller surface area but have a higher shape correlation compared with other SAG-MHC/peptide complexes. Most of the interactions between SEI and DR1/HA are with the  $\beta$  chain of DR1 and there is no interaction with the  $\alpha$  chain. Zn<sup>2+</sup>, which plays important role in stabilizing the SEI and DR1 complex, is coordinated by residues H169, H207 and D209 from SEI and H81 from DR1  $\beta$  chain. SEI makes less contacts with HA than that in other SAG-MHC/peptide complexes, by forming only one side chain H-bond with Kp-1 at the N-terminal of HA, which indicates that SEI binds DR1 irrespective of peptide sequence.

**M-P130 Solution of Protein Crystallographic Structures by High Pressure Cryocooling and Noble Gas Phasing.** Chae Un Kim, Quan Hao, Sol M. Gruner, CHESS, Cornell Univ., Ithaca, NY.

Room pressure flash cryocooling of protein crystals is the standard way to reduce radiation damage during data collection. However, it is necessary to find cryoprotection conditions by trial and error, a process that can be time consuming and is not always successful. Recently a new method, high pressure cryocooling, was developed that does not require penetrative cryoprotectants and typically yields very high quality diffraction (Kim *et al.*, 2005, *Acta Cryst. D61*, 881-890). This method was successfully extended to diffraction phasing by incorporating heavy noble gas, krypton. Here, the modified high pressure cryocooling procedure is described. Porcine pancreas elastase (PPE, 240 residues, 26 kDa) prepared by the method was selected as a test case. Excellent diffraction was achieved without any penetrating cryoprotectants and a single 31 % occupied krypton (Bijvoet amplitude ratio ( $\langle |\Delta F| \rangle / \langle F \rangle$ ) of 0.53 % on PPE) was successfully used for SAD phasing at 1.3 Å resolution. The anomalous difference map showed a 100  $\sigma$  peak in the krypton site and 6 additional peaks at 3.6  $\sigma$ , which were assigned to naturally present sulfur atoms that had the anomalous strength of only 0.18 electrons. The modified high pressure cryocooling method has potential to greatly simplify obtaining protein structures.

**M-P132 A Prediction System for Protein Crystallization Conditions.** Koji Inaka<sup>1</sup>, Shigeru Sugiyama<sup>1</sup>, Fujiko Shibata<sup>1</sup>, Yoshiko Kobayashi<sup>1</sup>, Kaoru Sugimori<sup>2</sup>, Michiyo Takeuchi<sup>2</sup>, Jose Martin Ciloy<sup>2</sup>, Masato Kitajima<sup>2</sup> <sup>1</sup>MARUWA Food Industries, Inc. Yamatokoriyama, Japan, <sup>2</sup>Fujitsu Kyushu System Engineering Ltd. Fukuoka, Japan.

A prediction system for crystallization conditions has been developed.

This system will help guide the user to a rational and highly confident crystallization method. This system consists of a database that contains not only detailed information on crystallization conditions extracted from published crystallization and structural analysis reports, but also biological information for each macromolecule that is essential for protein crystallization experiments. Each crystallization condition related to a specific target protein can be easily searched and extracted by providing only the amino acid sequence information and a few keywords. Moreover, crystallization data stored by each user can be linked conveniently to the system. Since comparison and data mining of the search results readily reveal trends in the crystallization parameters, each crystallization parameter can be narrowed down and estimated before any screening experiment is started. This prediction system is an efficient approach to crystallization since it helps reduce unnecessary screenings in the process.

**M-P134 Gene Composer: A Tool for Designing and Optimizing Protein Constructs for X-ray Crystallography.** Mark Mixon, John Walchli, Kai Post, Peter Nollert, Lance Stewart, Alex Burgin, deCODE biostructures and Emerald BioSystems, 7869 NE Day Rd W., Bainbridge Island, WA 98110.

The diligent crystallographer will often consult many different software packages in order to make decisions about how to design a protein construct and to maximize the likelihood of success for crystallizing a protein. Since information that impacts the design process comes from disparate sources, it is often a laborious task to assemble a unified view of sequence and structural information. We have developed software and a database, called Gene Composer that neatly bundles the process into one package. The Protein Design Module contains alignment as well as web access tools that allow users to rapidly place sequence information in the context of homologous structural models. Information about solvent accessible regions, crystal contacts, B-factors, as well as ligand, and water contacts are displayed so that important structural and functional regions of homologous sequences can be rapidly identified. The Protein-to-DNA Design Module allows users to design a novel nucleic acid coding sequence with optimized open reading frame features for different heterologous expression systems (preferred codon usage, minimized mRNA secondary structure, eliminated or introduced restriction sites, regulatory elements, etc.). Various features of the software will be discussed together with examples of how Gene Composer can aid researchers in designing protein constructs and nucleic acid coding sequences for improved protein expression and crystallization.

**M-P136 Biophysical Characterization of Collagenase S1 Domain.** C.R. Sides, S.T. Leena, Philominathan, O. Matsushita, J.J. Sakon, Univ. of Arkansas, Fayetteville, AR 72701.

Previous ColH collagenase studies from *Clostridium histolyticum* propose that the catalytic domain of the protein is the S1 domain. Studying the active site architecture for this novel class of zinc proteases is important for understanding the mechanism of collagenase and as a target for drug development for gas gangrene or wound healing. No homologous structure to collagenase S1 domain is known; therefore, biophysical characterization experiments are beneficial to learning the basic physical properties, such as folding and binding, which provide insight to S1 crystallization. Properties of S1 domains from five different *Clostridium* species have been analyzed both in the presence and absence of calcium because calcium is thought to activate collagenase. Circular dichroism and dynamic light scattering showed that although calcium is important in the dynamics of the enzyme, no secondary structural change accompanies calcium addition.

Furthermore, isothermal calorimetry binding curves showed little indication for calcium binding to the S1 domain, thus suggesting that although calcium is useful in crystallization, calcium only plays a significant role in collagenase S3 domains and not in the S1 domain.

**M-P138 X-ray Structures of Methylamine Dehydrogenase Reaction Intermediates.** Teresa De la Mora-Rey, Arwen R. Pearson, Kevin T. Watts, Ed Hoeffner, Carrie Wilmot, Univ. of Minnesota, Dept. of Biochemistry, Molecular Biology & Biophysics, Minneapolis, MN 55455, dela0174@umn.edu.

Methylamine dehydrogenase (MADH) catalyzes the oxidation of methylamine to formaldehyde and ammonia. It is upregulated by the presence of substrate and enables bacterial growth on methylamine as the sole carbon, nitrogen and energy source. The redox center is tryptophan tryptophylquinone (TTQ) which is composed of two Trp residues posttranslationally modified by the addition of a covalent cross-link and two oxygens to form an O-quinone. Amicyanin (a type I blue Cu protein) is the redox partner of MADH and it is also induced in the presence of methylamine. The reaction during turnover gives distinct spectral features in the visible region, which define specific electronic states of the cofactor.

The use of single crystal kinetics, microspectrophotometry and X-ray crystallography of the holo- (with Cu) and apo- (without Cu) complexes of MADH with amicyanin allows the trapping of different catalytic intermediates in the crystal and the determination of their x-ray structures. In this presentation the structural features of O-quinone, N-quinol and N-semiquinone catalytic intermediates will be discussed in terms of the current model for catalysis and electron transfer.

**M-P140 Crystal Structure of AAV8 and Structural Implications of Acidification.** H Nam<sup>1</sup>, M Lane<sup>1</sup>, B Gurda-Whitaker<sup>1</sup>, R McKenna<sup>1</sup>, S Zolotukhin<sup>2</sup>, N Muzyczka<sup>3</sup>, M Agbandje-McKenna<sup>1</sup>, <sup>1</sup>Dept. Biochemistry and Molecular Biology, <sup>2</sup>Dept. Pediatrics, <sup>3</sup>Dept. Molecular Genetics and Microbiology, College of Medicine Univ. of Florida Gainesville, FL 32610.

Transduction of Parvoviruses into host cells depends on endosomal processing, and its mechanisms, including the effect of low pH on viral capsids, are poorly understood. Adeno-associated viruses (AAVs), members of the *Parvoviridae*, are being actively investigated as gene therapy vectors. AAV serotype 8, in particular, is a promising candidate for liver targeted gene therapy. We have determined the crystal structure of the AAV8 viral capsid at four different pHs, 7.5, 6.0, 5.5, and 4.0, that represent pHs of endosomal compartments. The general fold of the AAV8 is similar to those of previously determined AAVs. The most pronounced differences in AAV8 compared to other AAVs reside in regions near the three-fold axis that are important for receptor binding and host cell tropism. Structural variations at different pHs are also observed at the interior and exterior surfaces of the three-fold capsid region. Our studies are identifying specific capsid regions responsible for AAV8's preferential tropism for liver cells, and the structures at various pHs aid our understanding of the effects of endosomal processing on AAV viral capsids.

**M-P142 X-ray Structure of AAV5, A Gene Therapy Vector for Cystic Fibrosis.** L. Govindasamy<sup>1</sup>, M. DiMattia<sup>1</sup>, H. Levy<sup>1</sup>, B. Gurda-Whitaker<sup>1</sup>, J.A. Chiorini<sup>2</sup>, R. McKenna<sup>1</sup>, N. Muzyczka<sup>3</sup>, S. Zolotukhin<sup>4</sup>, M. Agbandje-McKenna<sup>1</sup>, <sup>1</sup>Dept of Biochem. and Mol. Biol., <sup>2</sup>Dept. of Mol. Genetics and Microbiology, <sup>3</sup>Dept. of Pediatrics, COM, UF, Gainesville, FL, <sup>4</sup>GTTB, NIDCR, NIH, Bethesda, MD.

Adeno-associated virus serotype 5 (AAV5), is a small, nonpathogenic,

non-enveloped icosahedral capsid of ~260Å in diameter. This virus, belonging to the *Dependovirus* genus of the *Parvoviridae* is under development for gene therapy applications to treat cystic fibrosis. To identify the structural features of AAV5 that contribute to its enhanced transduction of the apical surface of airway epithelia compared with other AAV serotypes, we have determined its capsid structure by X-ray crystallography. AAV5 crystals belong to the orthorhombic space group  $P2_12_12_1$ , with unit-cell parameters  $a = 264.7$ ,  $b = 447.9$ ,  $c = 629.7$  Å. There is one complete  $T = 1$  viral capsid per asymmetric unit. The structure of the capsid was determined to 3.2 Å resolution by molecular replacement. Structural comparison of AAV5 with those already available for AAV2, AAV4, and AAV8 clearly shows structural re-arrangements in surface loop regions of the capsids that co-localize with regions identified as being important for AAV2 receptor attachment, transduction efficiency, and antigenic reactivity.

**M-P144 Biophysical and Structural Characterization of Adaptor-related Protein Complex 4.** Lauren Parker, Helen Kent, Phil Evans, MRC Laboratory of Molecular Biology, Cambridge, UK.

Adaptor-related complex 4 (AP-4) is a member of a family of homologous heterotetrameric protein complexes that play a role in various intracellular trafficking pathways. While other members of the family have been well characterized both structurally and functionally, very little is known about the role of AP-4 within the cell. The C-terminal domain of the  $\mu 4$  subunit is known to interact with Yxx $\Phi$  binding motifs found in cargo molecules. Isothermal titration calorimetry has been used to verify potential motifs and to characterize their binding affinities with  $\mu 4$ . Some of the main sequence differences between AP-4 and its homologues lie in the appendage "ear" domains of the two largest subunits,  $\epsilon$  and  $\beta 4$ . These domains interact with regulatory and accessory proteins, and hence, much of the functional diversity is assumed to be in these regions. Crystals of the  $\mu 4$  C-terminal domain and of both appendage "ear" domains have been obtained; all are being optimized for data collection. Additionally, portions of the four subunits that together constitute the AP-4 core have been cloned and co-expressed in *E. coli*. Structural studies of this core are currently underway.

**M-P146 A New Crystal Form of the 70S Ribosome Functional Complex.** A. Korostelev, S. Trakhanov, M. Laurberg, A. Baucom, L. Lancaster, H. Asahara, W. Scott, H. Noller, Center for Molecular Biology of RNA and Dept. of MCD Biology, UCSC, Santa Cruz, CA.

Ribosomes are large (2.5 MDa) ribonucleoprotein complexes responsible for synthesis of proteins based on messenger RNA (mRNA) sequences in all living cells. Previously, we reported the 5.5 Å structure of functional complexes of the *Thermus thermophilus* 70S ribosome containing a model mRNA and two or three tRNAs, which allowed fitting of backbone models for the RNA and protein components of the complex.

Here, we report a 4.5-Å structure of a natural functional complex of the *T. thermophilus* ribosome containing mRNA and 2 tRNAs. We utilized a new crystal form of the 70S ribosome, in which the c axis of the tetragonal unit cell is shortened by 110 Å, owing to disruption of one of the coaxially stacked RNA-RNA crystal contacts. The structure was solved by the molecular replacement method followed by rounds of increasingly finer rigid-body refinement and energy minimization. Changes in the overall conformation of the ribosome identify flexible features of the structure that are potentially involved in functional dynamics. Composite omit electron density maps resolve interactions of the ribosome with mRNA and tRNAs and provide new insights into how the ribosome optimally positions its substrates.

**M-P148 Structure of an Electron Transfer Complex Between Plant Ferredoxin and Sulfite Reductase.** G. Kurisu<sup>1</sup>, M. Nakayama<sup>2</sup>, M. Kusunoki<sup>2</sup>, T. Hase<sup>2</sup> <sup>1</sup>Dept. of Life Sci., Univ. of Tokyo, Komaba, Tokyo 153-8902, Japan, <sup>2</sup>Inst. for Protein Res., Osaka Univ., Suita, Osaka 565-0871 Japan.

Plant sulfite reductase (SiR) catalyzes the six-electron reductions of sulfite using reduced ferredoxins (Fds), and is a key enzyme to sulfur assimilation. The physiological functional unit is a 65 kDa monomer with a siroheme and a [4Fe-4S] cluster as redox centers. The bacterial SiR, whose 3D structure has already been reported, is obviously different from the plant SiR, since the bacterial one is independent of Fd and physiologically functions as an oligomeric form. We have been studying the electron transfer interaction between plant Fd and SiR using the recombinant maize proteins. It was confirmed that Fd and SiR form a stable protein-protein complex electrostatically. We crystallized the Fd:SiR e-transfer complex in three different space groups,  $P4_12_12$ ,  $P6_1$  and  $P2_12_12$ . The initial structure was solved by a Fe-MAD method using the data from a tetragonal crystal. The best model was refined to  $R_{\text{cryst}} = 0.22$  and  $R_{\text{free}} = 0.28$  for the 2.0 Å data from an orthorhombic crystal. In the crystals of three space groups, Fd and SiR molecules faced each other in the same manner. The redox centers were found to be in a close proximity and several charged residues seemed to be involved in the molecular interaction.

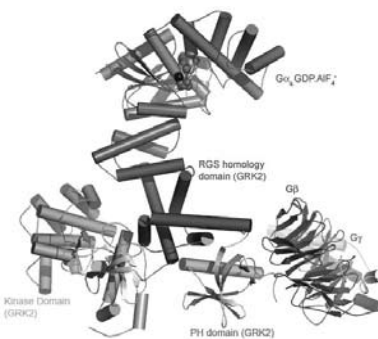
**M-P150 Structural Basis of Phosphorylation-Independent Desensitization of Gq-Coupled Receptors.** Aruna Shankararayanan<sup>‡</sup>, Valerie M. Tesmer<sup>‡</sup>, Takeharu Kawano<sup>§§</sup>, Tohru Kozasa<sup>§</sup> and John J.G. Tesmer<sup>‡</sup>, <sup>‡</sup>Inst. for Cell and Molecular Biology, Dept. of Chemistry and Biochemistry, Univ. of Texas, Austin, TX, Dept. of Pharmacology, Life Sciences Inst., Univ. of Michigan, Ann Arbor, MI, <sup>§</sup>Dept. of Pharmacology, <sup>§§</sup>Dept. of Anatomy and Cell Biology, Univ. of Illinois & College of Medicine, Chicago, IL.

G-protein coupled receptor kinase 2 (GRK2) desensitizes G-protein coupled receptor by phosphorylating activated receptors and sequestering activated G $\alpha$  and G $\beta\gamma$  subunits. Herein, we present the crystal structure of G $\alpha_q$ -GRK2-G $\beta\gamma$  complex that serves as a model for phosphorylation independent desensitization of GPCRs. In the structure, activated G $\alpha$  and G $\beta\gamma$  subunits are completely dissociated from one another and they are in an unusual orientation with respect to each other and with respect to the predicted cell membrane when compared to that of inactive G $\alpha\beta\gamma$  heterotrimer. The structure reveals that G $\alpha_q$  makes novel effector-like interactions with the RGS homology domain of GRK2 that also permits the binding of classic RGS proteins providing evidence for the assembly of higher order complex of GPCRs, GRK2, activated G $\alpha$  and G $\beta\gamma$  and RGS proteins at the cell membrane.

Reference: Snapshot of Activated G Proteins at the Membrane: The G $\alpha_q$ -GRK2-G $\beta\gamma$  Complex. *Science* 9 Dec 2005; 310: 1686-1690

Supported by: National Institute of Health, American Heart Association and American Cancer Society

We thank ALS for access to beam line 8.3.1.



**M-P152 The  $\beta$ -lactam Sensor of *Staphylococcus aureus* and its Role in Triggering Antibiotic Resistance.** Mark S. Wilke<sup>1</sup>, Tanya L. Hills<sup>1</sup>, Hong-Zhong Zhang<sup>2</sup>, Henry F. Chambers<sup>2</sup>, Natalie C. J. Strynadka<sup>1</sup>, <sup>1</sup>Dept. Biochemistry and Molecular Biology, Univ. of British Columbia, Vancouver, Canada, <sup>2</sup>Dept. Medicine, Univ. of California, San Francisco, CA, USA,

Superbug strains of *Staphylococcus aureus* evolved resistance to  $\beta$ -lactam antibiotics (BLAs) by the acquisition of two mechanisms: (i) secretion of hydrolytic  $\beta$ -lactamase enzymes, and (ii) production of  $\beta$ -lactam-insensitive cell wall transpeptidases (PBP2a). Despite their distinct modes of resistance, expression of these proteins is controlled by homologous regulation systems, including a repressor (BlaI/MecI) and a multidomain transmembrane receptor (BlaR1/MecR1). The extracellular domain of BlaR1/MecR1 acts as a 'sensor' for BLAs and structurally resembles the  $\beta$ -lactamases and BLA-binding domain of the cell wall transpeptidases. Through X-ray crystallography, we've observed that the BlaR1 sensor domain is acylated by BLAs, but conformationally unchanged by the acylation. In order to study the transduction of the BLA-binding signal across the membrane, we are presently using nuclear magnetic resonance and X-ray crystallographic methods to investigate the theory that an adjacent extracellular loop of BlaR1 interacts with the sensor domain in its BLA-free form and that acylation by BLAs alters or destroys that interaction.

**M-P154 Novel Cu<sup>2+</sup> binding site in C<sub>2</sub>A Domain of Synaptotagmin I.** F. Guo, D. Rajalingam, T.K.S. Kumar, J. Sakon, Univ. of Arkansas, Fayetteville, AR 72701.

Synaptotagmins are synaptic vesicle membrane proteins which consist of calcium binding C<sub>2</sub>A and C<sub>2</sub>B domains. They are involved in membrane traffic and signal transduction as neurotransmitter release through its calcium dependent interactions with syntaxin and phospholipids. C<sub>2</sub>A is an ~18kD all-beta-sheet protein. Structure of C<sub>2</sub>A with calcium is well characterized by both NMR and X-rays. Recent studies show that C<sub>2</sub>A domain has a high binding affinity for copper and triggers multiprotein complex release like human acidic fibroblast growth factor (hFGF-1). The 1.4 Å resolution structure of C<sub>2</sub>A with Cu<sup>2+</sup> shows only single histidine ligating the metal. Compared to our 1.2 Å resolution structure of C<sub>2</sub>A, a conformational change takes place upon Cu<sup>2+</sup> binding. <sup>15</sup>N-<sup>1</sup>H HSQC titration confirmed the Cu<sup>2+</sup> bound in the vicinity of His254 which is located in the loop between beta-strands 7 and 8. Results from isothermal calorimetry (ITC) show that C<sub>2</sub>A has extraordinary binding affinity with copper (in the nanomolar range). The elucidation of copper binding site in C<sub>2</sub>A indicates that the synaptotagmin I may switch function though binding different metal ions and it is an effective strategy to inhibit the FGF-1-induced pathogenesis by prevention of the formation of the copper-bound state of C<sub>2</sub>A.

**M-P156 NeXus With Binary XML - Efficient Support of Binary Data in the XML Implementation of the NeXus File Format.** Georgi Darakev, Vassil Litchev, Kostadin Z. Mitev, Herbert J. Bernstein, Dept. of Mathematics and Computer Science, Dowling College, Oakdale, NY 11769.

There are two formats for the management of synchrotron image data under serious consideration to facilitate moving raw image data among beam lines and user home institutions: imgCIF and NeXuS. imgCIF provides a very efficient representation of large binary image data in its native binary form. NeXuS is equally efficient in internal storage and in transfer as an image of its internal HDF4/5 format, but to date it lacks an agreed efficient external representation. Use of SOAP serialization of the internal objects has been proposed, but that imposes a serious performance penalty in working with XML, since XML does

not directly support a binary representation. For the smaller volumes of data seen in collecting neutron data, this has not been a serious problem. For high-data-rate synchrotron data collection, efficiency is more important. We propose a new, reasonably efficient format with only a 1 part in 15 overhead for encoding as printable characters, and have augmented the NeXuS and CBFlib APIs to support this format. These augmented APIs support encoding and decoding of binary data thereby producing valid UTF-16 XML documents, or if desired, mixed UTF-8/UTF-16 XML documents by use of non-character codepoints as control flags (extending the UTF-16 BOM convention). The availability of these APIs should contribute to achieve seamless transitions among imgCIF, NeXuS, imgML (an XML presentation of imgCIF) and SOAP serializations of NeXuS data and internal NeXuS file formats.

**M-P158 MX at Diamond.** J. Brandao-Neto, L. Johnson, E. Duke, G. Evans, K. McAuley, R. Flaig, T. Sorensen, A. Wagner, A. Grant<sup>++</sup>, G. Preece, R. Wooliscroft, A. Ashton, M. Harding, D. Butler, A. Taylor, Diamond Light Source, Chilton, UK, <sup>++</sup>Synchrotron Radiation Source, Daresbury, Warrington, UK.

Diamond is the largest scientific investment in the UK for 30 years and is funded by the UK Government and the Wellcome Trust. Phase I of Diamond includes the construction of the machine and seven beamlines and will be complete in 2007. A further 15 beamlines will be built in Phase II. Three of the Phase I and two of the Phase II beamlines are dedicated to macromolecular crystallography (MX).

The Phase I MX beamlines will receive radiation from in-vacuum undulators and will be tunable between 0.5 Å–2.5 Å with operation optimised at 1 Å. A flux of  $10^{12}$  photons/s in a  $100\mu\text{m} \times 100\mu\text{m}$  spot at the sample is expected. All beamlines will be equipped with robotic sample changers, CCD detectors and other essential equipment associated with MX beamline operation. In addition one of the beamlines is being designed to permit data collection on samples from Category 3 pathogens.

The first Phase 2 MX beamline is being designed as a microfocus beamline with a beam focus down to  $5\mu\text{m}$ , whereas the second one will be a fixed wavelength station operating at 0.93 Å. Additionally there are plans for a beamline optimised for longer wavelengths (2 Å+).

**M-P160 The SSRL Macromolecular Crystallography Facility.** A. Cohen, P. Dunten, A. Gonzalez, D. Harrington, I. Mathews, M. Soltis, representing the SMB group, Menlo Park, CA.

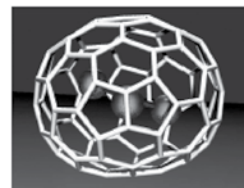
The SSRL Structural Molecular Biology group operates 5 crystallography beam lines, BL1-5, BL9-1, BL9-2, BL11-1, and BL11-3. BL7-1, which has been upgraded to fully utilize the SPEAR3 source including a new wiggler and x-ray optics, will be commissioned later this year. Users of these beam lines have the option to conduct experiments while remaining at their home institution and in 2006 nearly half of experiments were conducted remotely. Using the Stanford Auto-Mounting system and the Blu-Ice control system, remote users have the ability to mount, center, and screen samples, and collect diffraction datasets. Data collected during sample screening are automatically analyzed and the results, which include the number of spots, Bravais lattice, unit cell, estimated mosaicity, and resolution, are visible through Web-Ice and Blu-Ice. To address the needs of remote experimenters, new automated capabilities have been released including sample washing, sample annealing, and an improved sample illumination system. Additionally, work is in progress to expand the scientific capabilities of the beam lines. Users will be able to conduct single crystal UV-visible microspectrophotometry experiments during diffraction data collection. BL12-2, a new undulator station optimized for data collection with small crystals, will be completed in 2007.

**M-P162 Synthesis and Characterization of Novel 2D Organic-Inorganic Hybrid Cobalt and Nickel Vanadates.** Kittipong Chainok<sup>1</sup>, Kenneth J. Haller<sup>1</sup>, Herman S.-Y. Sung<sup>2</sup>, Ian D. Williams<sup>2</sup>, <sup>1</sup>School of Chemistry, Inst. of Science, Suranaree Univ. of Technology, 30000, Thailand, <sup>2</sup>Dept. of Chemistry, Hong Kong Univ. of Science and Technology, Clear Water Bay, Kowloon, Hong Kong, China.

Two new isomorphous 2D organic-inorganic hybrid metal vanadates with general formula  $[\text{M}_2(\text{Im})_8\text{V}_4\text{O}_{12}]$ , (M = Ni, Co, and Im = imidazole) have been hydrothermally synthesized. The crystal structure of both compounds consists of  $\{\text{V}_4\text{O}_{12}\}^{4+}$  clusters covalently attached to four  $\{\text{M}(\text{Im})_4\}^{2+}$  moieties via bridging oxo groups. Each M(II) displays distorted octahedral geometry, defined by one nitrogen atom from each of four equatorially coordinated imidazole ligands, and one oxygen atom from each of two  $\{\text{V}_4\text{O}_{12}\}^{4+}$  subunits in the axial positions. Alternatively, the structure consists of distorted  $\text{MN}_4\text{O}_2$  octahedra and distorted  $\text{VO}_4$  tetrahedra. Two cyclic constructs define the oxide layer, four  $\text{VO}_4$  tetrahedra edge connect to form small rings, and four  $\text{MN}_4\text{O}_2$  octahedra and eight  $\text{VO}_4$  tetrahedra connect to form large  $\{\text{M}_4\text{V}_8\text{O}_{12}\}$  rings which fuse to produce the two-dimensional connectivity. The supramolecular hydrogen bonding (N–H $\cdots$  $\pi$ , C–H $\cdots$ O, and N–H $\cdots$ O) plays a significant role in the formation and stability of the structure, binding adjacent oxide layers together to generate the three-dimensional structure. Further characterization of the compounds by EDX, FTIR, TGA, elemental analyses, and magnetic susceptibility is also reported.

**M-P164 Tb<sub>3</sub>N@C<sub>84</sub> – A Non-IPR isomer of C<sub>84</sub>.** Christine M. Beavers, Marilyn M. Olmstead, Alan L. Balch, Univ. of California, Davis & Harry C. Dorn, Virginia Polytechnic Inst. and State Univ.

A new isomer of C<sub>84</sub> was recently determined from the structure of an endohedral metal nitride fullerene co-crystallized with nickel octaethylporphyrin (NiOEP). Tb<sub>3</sub>N@C<sub>84</sub> was isolated and characterized by mass spectrometry to have the stated formula, but the isomer was unknown.



The surprising result was that the fullerene cage violated the Isolated Pentagon Rule (IPR), making it part of an exclusive group of known Non-IPR fullerene structures. Non-IPR fullerenes have fused five-membered rings. This 5,5 bond is relatively electron rich; the greater electron density is demonstrated by the totally ordered terbium atom  $\pi$ -bonded to the 5,5 junction. The other two terbium atoms in the nitride were disordered, with the major conformation appearing at approximately fifty percent occupancy. The fullerene cage itself has interesting structural aspects. It has two distinct ends: a pointed beak where the fused pentagons reside, and a rounded end that resembles half of a C<sub>80</sub>. These ends are joined by a contiguous band of ten hexagons. The beak end has mm symmetry, but the round end has fivefold rotational symmetry. Overall, the fullerene has m symmetry. This new isomer will be compared to more symmetric IPR endohedral fullerenes with respect to nitride orientation, and co-crystallization  $\pi$ -stacking.

**M-P166 Crystallographic Studies of Pyruvate-formate lyase Activase.** J Vey<sup>\*1</sup>, M Li<sup>2</sup>, J Yang<sup>2</sup>, J Broderick<sup>2</sup>, C Drennan<sup>1</sup>, <sup>1</sup>Dept. of Chemistry, MIT, Cambridge, MA, 02142, <sup>2</sup>Dept. of Chemistry & Biochemistry, Montana State Univ., Bozeman, MT.

One newly discovered and exciting role for iron-sulfur clusters in biology is in the initiation of protein-mediated radical chemistry. The SAM Radical protein superfamily uses an iron-sulfur cluster and S-adenosylmethionine (SAM) to generate substrate- or protein-bound radicals via a 5'-deoxyadenosyl radical. As the reactions that follow

this initial step are highly diverse, this family is thought to be a metabolically and evolutionarily important group of proteins.

PflAE catalyzes the SAM-dependent activation of pyruvate-formate lyase (PFL) by formation of a catalytic glycy radical on G734 of PFL. We are continuing our studies<sup>1</sup> of the SAM Radical superfamily with PflAE with the hope of adding to our understanding of formation and control of the 5'-deoxyadenosyl radical by these enzymes for reaction with highly diverse substrates.

The structure of PflAE was solved in space groups  $P3_1$  and  $P3_121$ . Difficulties encountered during the refinement led to the investigation of possible problems such as twinning and alternate space groups. Current progress towards refinement of the x-ray crystal structure will be presented.

[1] Berkovitch et al. *Science* (2004) **303** (5654): 76-9.

[2] Nicolet Y and Drennan CL. *Nuc Acid Res* (2004) **32** (13): 4015-25.

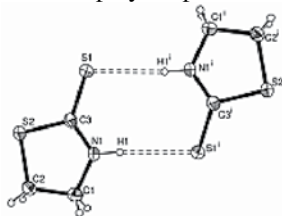
**M-P168 Structural Biology of the Type II Secretion System from *Vibrio cholerae*.** J. Abendroth, P. Murphy, A. Kreger, M. Sandkvist, WG. Hol, Howard Hughes Medical Inst. and Univ. of Washington, Seattle, WA 98195.

The human pathogen *Vibrio cholerae* employs the Type II Secretion System (T2SS) for the export of its major pathogenic agent, cholera toxin, from the periplasm of *V. cholerae* through the outer membrane into the intestine of its host. The T2SS, a large protein machinery that consists of 12-15 proteins, is a highly regulated system that spans the cell envelope from the cytoplasm to the outer cell membrane. X-Ray structures of several soluble cytoplasmic and periplasmic protein domains and complexes have been solved using Se-Met anomalous diffraction techniques. Pathways how experimental problems such as disorder of anomalous scatterers, low phasing power at high and medium resolution and the selection of the crystallizable fragments were overcome will be presented along with the current set of structures, and ongoing efforts to express, purify and crystallize complexes of integral membrane proteins of the T2SS.

**M-P170 Quantum Mechanics Studies on 2-Mercaptothiazoline Polymorphs.** Salloum R., Ellena J., Inst. de Física de São Carlos, Univ. de São Paulo, 13560-970 São Carlos, SP, Brasil.

2-Mercaptothiazoline is an important organic compound used as a corrosion inhibitor in many industrial processes. A novel polymorph of this compound, showing a planar conformation, has recently been studied for the first time<sup>[1]</sup>. The new triclinic polymorph<sup>[1]</sup> was compared in terms of its molecular conformation and intermolecular interactions with the previously known monoclinic polymorph<sup>[2]</sup>.

Quantum mechanics calculations in monomers and dimers have been carried out using Gaussian03 package of programs in order to investigate differences found in solid state. DFT/6-311++g(2d,p) calculations showed that the planar conformation has an additional energy of 15.6878 kcal mol<sup>-1</sup> with respect to the conformation found by Flakus *et al.*<sup>[2]</sup>. Such a difference in energy seems to be balanced by hydrogen bonds intermolecular interactions that give rise to the formation of dimers such as shown in above.



[1] R.S. Corrêa, S.A. Santana, R. Salloum, R.M. Silva & A.C. Doriguetto, A triclinic polymorph of 1,3-thiazolidine-2-thione (2-mercaptothiazoline), *Acta Cryst. C* **62**, o115-o117 (2006).

[2] H.T. Flakus, A. Miros & P.G. Jones, Polarization IR spectra of model crystals containing cyclic N...S bonded dimers: 2-mercaptothiazoline and 2-mercapto-1-methylimidazole, *Spectrochimica Acta Part A* **58** (2002).

**M-P172 Degree-of-freedom-based Methods for Phasing Centrosymmetric Structures from X-ray Diffraction Data.** A. B. Smith, N.V. Sahinidis, Dept. of Chemical and Biological Engineering, Univ. of Illinois at Urbana-Champaign, Urbana, IL 61801.

The phase problem has recently been approached via combinatorial optimization techniques that are guaranteed to find a global optimum of a certain minimal principle formulation for centrosymmetric structures<sup>[1,2]</sup>. However, this formulation falls short from accounting for translational symmetry and atomicity constraints.

In this paper, a new integer minimal principle for centrosymmetric structures is presented; one which fully accounts for reciprocal space phase shifts resulting from translational symmetry relations. Additionally, to enforce atomicity constraints, characterization of false minima is done in terms of even and odd triplets. Based on this characterization, an n-best triplet method is proposed: Gaussian elimination using only a subset of reliable triplets. Phase solution sets are generated by enumerating the degrees of freedom present. A reciprocal space solution filter is introduced to further decrease the number of candidate phase solutions. Computational results are presented for a few challenging structures.

[1] A. Vaia and N.V. Sahinidis. An integer programming approach to the phase problem for centrosymmetric structures. *Acta Crystallographica A*, **59**:452-458, 2003.

[2] A. Vaia and N.V. Sahinidis. Polynomial-time algorithms for the integer minimal principle for centrosymmetric structures. *Acta Crystallographica A*, **61**:445-4528, 2005.

**M-P174 Evaluation of the Different Choice Method of Absorption Correction Used in the Structural Determination in Complex with Heavy Metals.** Sauli Santos-Jr<sup>a</sup>, Javier Ellena<sup>b</sup>, <sup>a</sup>Núcleo de Física, Curso de Engenharia de Alimentos, Univ. Federal do Tocantins - UFT, <sup>b</sup>Inst. de Física de São Carlos, Univ. de São Paulo - USP, Brazil.

The determination of three-dimensional structures with heavy metals is a very important tool in the study of complexes that can be able to act as antidotes in the poisoning by ingestion of these kinds of substances. A detailed knowledge of these complexes is important to help in the modeling of new molecular structures and in the determination of more effective procedures in the neutralization of the processes, developed for individuals with chronic heavy metals poisoning. It is known some techniques of X-ray absorption correction for diffraction data from monocrystals. During the data reduction many corrections take place, such as: Lorentz, polarization, absorption and eventually correction for deterioration of the sample. The absorption correction is strongly recommended for crystals with strong absorbers in its structural form. The effect of the absorption of X-ray in crystalline samples had been studied and a comparison of the results using different methods was made. This work that showed different forms of absorption correction, we observed significant differences in the figures of merit, peaks and valleys of residual charge density and parameters of anisotropic displacements. Peaks and valleys of residual charge density that they located close to heavy metals had drastically diminished the height or depth after the appropriate absorption correction, respectively. Bond distances and angles, on the other hand, did not change significantly.

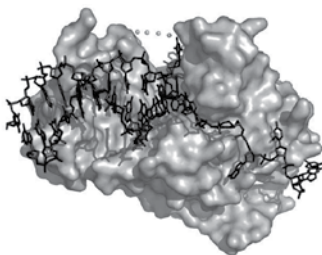
**M-P176 X-ray Crystallography at the University of the West Indies (UWI), Jamaica: Structures of Novel Metal Complexes and the H-Bonding Interactions Featured in Them.** Marvadeen A. Singh-Wilmot, Univ. of the West Indies, Mona, Kingston Jamaica.

The structures of complexes of the transition metal and lanthanide ions are critical to their applications in medicine, catalysis and materials science. As part of two different programs to relate structures of

complexes containing organic ligands tethered to i) transition metal ions and ii) lanthanide ions, we have solved the structures of a variety of novel 3d and 4f complexes including some metal clusters. The compounds were crystallized using slow evaporation and vapor diffusion techniques. Data were collected at room temperature on a Bruker P-4 Single Crystal Diffractometer and the structures were solved by Direct and Patterson Methods.

**M-P178 Co-crystal of Bacteriophage T4 RNase H with a Fork DNA Substrate: Insight into Lagging Strand RNA Primer Removal from Okazaki Fragments.** J.M. Devos<sup>1</sup>, C.E. Jones<sup>2</sup>, N.G. Nossal<sup>2</sup>, T.C. Mueser<sup>1</sup>, <sup>1</sup>Dept. of Chemistry, The Univ. of Toledo, Toledo, OH. <sup>2</sup>National Institutes of Health, Bethesda, MD.

Bacteriophage T4 RNase H is a 5' exonuclease responsible for removal of RNA primers from lagging strand fragments during DNA replication. T4 RNase H, a member of the flap endonuclease (Fen-1) family of enzymes, acts as a 5' exonuclease on duplex substrates and as a flap endonuclease on branched substrates. We have previously reported the structure of native T4 RNase H (pdb 1TFR). Here we present the crystal structure of the D132N active site mutant of T4 RNase H with a fork DNA substrate. The complex reveals the molecular interactions for substrate recognition and provides structural insight into the catalytic mechanism. The duplex interacts with an extended loop of the HhH motif. The 5' overhang crosses over the active site through the central cleft of the protein. The 3' overhang reaches close to binding sites for the T4 32 protein and the T4 45 clamp, at the C- and N- termini respectively. The preferred cut site for T4 RNase H on this fork DNA is between the first two duplex nucleotides next to the 5' overhang.



This work was supported by National Science Foundation (MCB – 034696) and the Intramural Research Program of NIDDK, National Institutes of Health.

**M-P180 Manganese Protoporphyrin-IX Reconstituted Myoglobin and its Complexes with Various Ligands.** Zaki N. Zahran, Lilian Chooback, Daniel M. Copeland, Ann H. West, George B. Richter-Addo, Dept. of Chemistry and Biochemistry, Univ. of Oklahoma, 620 Parrington Oval, Norman, OK 73019.

Manganese protoporphyrin-IX (Mn-PPIX) has been used as a synthetic heme cofactor in some studies of heme proteins. Such Mn-PPIX-reconstituted proteins have previously been characterized by spectroscopy. To the best of our knowledge, no high-resolution X-ray crystal structures of Mn-PPIX proteins have been reported. We now report the 1.6 Å resolution crystal structures of Mn-PPIX-reconstituted myoglobin (MnMb) in its oxidized (Mn<sup>III</sup>Mb) and reduced form (Mn<sup>II</sup>Mb). In addition, we report the crystal structures of the MnMb complexes with azide, methanol, nitrite and nitric oxide to 1.6-1.9 Å resolution. The structures of the Mn-PPIX-reconstituted myoglobin compounds provide interesting comparisons with the native Mb derivatives.

This work was supported by the U.S. National Institutes of Health (GM 64476; GBR-A).

**M-P182 Structure of the Bi-functional ATP Sulfurylase/APS Kinase from *Aquifex aeolicus*, a Chemolithotrophic Thermophile.** Z. Yu, I. MacRae, E. Lansdon, I. Segel, A. Fisher, Univ. of California, Davis, CA 95616.

The chemolithotroph *Aquifex aeolicus* derives its energy from re-

duced sulfur in the environment. ATP sulfurylase catalyzes the last step in the sulfur oxidation pathway to produce ATP and sulfate. Our lab recently demonstrated that this enzyme also possesses APS kinase activity making it a bifunctional enzyme. APS kinase phosphorylates APS to produce PAPS, the universal sulfate donor. The arrangement of domains in *Aquifex* is reminiscent of fungal ATP sulfurylase where the APS kinase-like domain allosterically regulates the ATP sulfurylase but has no kinase activity. The fungal ATP sulfurylase catalyzes the sulfur assimilatory reaction to produce APS and PP<sub>i</sub>, which is the opposite direction to the *Aquifex* enzyme. To better understand the structural and functional differences between the different physiological roles of this enzyme in diverse organisms, we determined the structures of these enzymes from a number of sources. This poster presents the 2.3Å resolution structure of ATP sulfurylase/APS kinase from *Aquifex*. The enzyme forms a homodimer through the APS kinase domain. ADP molecules bound in both ATP sulfurylase and APS kinase active sites. In the APS kinase active site, the P-loop substitution S381P and a non-conserved disulfide bond explains the low kinase activity.

**M-P184 Crystal Structure of the Ligand-bound Saccharopine Reductase from *Saccharomyces cerevisiae*.** Babak Andi, Paul F. Cook, Ann H. West, Dept. of Chemistry and Biochemistry, The Univ. of Oklahoma, 620 Parrington Oval, Norman, OK 73019.

Saccharopine reductase (SR) is the penultimate enzyme of the unique  $\alpha$ -aminoadipate pathway for the biosynthesis of lysine in fungi important for developing new specific antimycotic agents. The enzyme catalyzes the NADPH-dependent condensation reaction of the  $\alpha$ -aminoadipate delta-semialdehyde with glutamate to make saccharopine. The crystal structure of the apo-SR has been previously solved in space group  $P3_121$  with unit cell dimensions of  $a = b = 85.28 \text{ \AA}$ ,  $c = 141.98 \text{ \AA}$  from crystals grown in ammonium sulfate. Recent studies show that the apo-SR crystals can also be obtained using PEG-MME 2000 as a precipitant, which was used to obtain a structure of ligand-bound SR. In this study, the crystal structures of the ligand-bound SR obtained from the crystals grown in ammonium sulfate and PEG-MME 2000 are compared.

This work is supported by the NIH grant (GM 071417).

**M-P186 Crystal Structure of Conserved Hypothetical Protein Rv0390 from *Mycobacterium tuberculosis*.** T. Radhakanan<sup>\*</sup>, E.H. Bursey<sup>\*</sup>, M. Yu<sup>\*</sup>, B.W. Segelke<sup>§</sup>, T. Lakin<sup>§</sup>, D. Toppani, C.-Y. Kim<sup>†</sup>, S.T.A. Kaviratne<sup>†</sup>, T. Woodruff<sup>†</sup>, T.C. Terwilliger<sup>†</sup>, L.-W. Hung<sup>\*,†</sup>, <sup>\*</sup>Lawrence Berkeley National Laboratory, Berkeley, CA 94720, <sup>§</sup>Lawrence Livermore National Laboratory, Livermore CA 94550, <sup>†</sup>Los Alamos National Laboratory, Los Alamos NM 87545.

We report the crystal structure of a conserved hypothetical protein, Rv0390, from *Mycobacterium tuberculosis*. The initial phase information was obtained by SAD method using Br derivative and the resulting model was refined to a final R factor of 17.5% and free-R factor of 21.8% at 1.8Å resolution. The overall structure of Rv0390 consists of one central parallel five-stranded  $\beta$ -sheet surrounded by  $\alpha$ -helices on both sides. The sequence of Rv0390 is homologous to the uncharacterized rhodanese homology domain (RHOD\_1) super family. Its 3-dimensional structure is similar to that of sulfurtransferase, which is also a member of the rhodanese family. A detailed structure description and a hypothetical function of Rv0390 will be presented.

**M-P188 Structural Differences Between *E. coli* and *A. thaliana* MTA Nucleosidase Explain Divergence in Substrate Specificity.** K.K.W. Siu<sup>1</sup>, J.E Lee<sup>1,\*</sup>, J. Sufirin<sup>2</sup>, B. Moffatt<sup>3</sup>, P.L. Howell<sup>1</sup>. <sup>1</sup>The Hospital for Sick Children and Univ. of Toronto, ON, Canada, <sup>2</sup>Roswell Park Cancer Inst., Buffalo, NY, <sup>3</sup>Univ. of Waterloo, ON, Canada. \*Present Address: The Scripps Research Inst., CA.

*E. coli* 5'-methylthioadenosine (MTA)/S-adenosylhomocysteine (SAH) nucleosidase (MTAN) is a dual substrate specific enzyme that plays a key role in methionine recycling and polyamine biosynthesis, and transmethylation reactions and quorum sensing, respectively. The enzyme has been identified as a target for antibiotic development because it is essential for viability in multiple pathogenic bacterial species, but is absent in mammals. MTAN is also present in plants, but the plant enzyme lacks specificity towards SAH and metabolizes only MTA. To gain insight into this loss of substrate specificity, we have determined the structures of wild-type *A. thaliana* MTAN in its apo-form and complexed with the inhibitors, formycin A and methylthiotubercidin to 2.0Å, 1.9Å and 1.8Å, respectively. The tertiary structure of *A. thaliana* MTAN is highly similar to the bacterial enzyme; however a detailed comparison of the active sites reveals significantly fewer conformational changes in the plant enzyme upon ligand binding as well as steric hindrances in the 5'alkylthio-binding site that would prevent SAH binding.

**M-P190 X-ray Crystallographic Study of CBL3-interacting Protein, C38 from *Arabidopsis thaliana*.** Eun young Park<sup>1</sup>, Seung-Ick Oh<sup>1</sup>, Jeong Sheop Shin<sup>1</sup>, Kyung-Nam Kim<sup>2</sup>, Hyun Kyu Song<sup>1</sup>. <sup>1</sup>School of Life Sciences and Biotechnology, Korea Univ., Korea, <sup>2</sup>Dept. of Biology, Sejong Univ., Korea.

In the cytoplasm of plant cells, the alteration of Ca<sup>2+</sup> concentration induces signal transduction. This alteration is caused by many extra-cellular stresses including light, biotic, and abiotic stress factors. CBLs (Calcinuerin B-Like protein family) are small proteins in *Arabidopsis thaliana* that interact with CIPKs (CBL-Interacting Protein Kinases) under the influence of this alteration. CBL3 is one of these CBL family proteins, known to SOS3 like calcium-binding protein 6. Recently we have identified a new target of the CBL3 protein, which is designated to C38 using a yeast-two hybrid screening system. C38 interacts with CBL3 in a calcium dependent manner. We have determined the crystal structure of C38 at 1.5 Å resolution in the product complex state. Based on our structural studies, characterization of the enzymatic function of C38 is in progress. In addition, some of our biochemical data confirm the *in vitro* complex formation between CBL3 and C38.

**M-P192 Structural and Kinetic Analysis of Mutants of an Active Site Base in a Non-Heme Extradiol Dioxygenase.** Rebecca D. Hoelt, Stephanie L. Groce, John D. Lipscomb, Douglas H. Ohlendorf, Dept. of Biochemistry, Molecular Biology and Biophysics, Univ. of Minnesota.

The key step in aerobic microbial degradation of aromatic compounds is often performed by a dioxygenase enzyme, which catalyzes aromatic ring cleavage. The iron containing dioxygenase enzymes consist of two families, extradiol (Fe<sup>2+</sup>) and intradiol (Fe<sup>3+</sup>). These enzymes have shown very high substrate and cleavage specificity. Homoprotocatechuate 2,3-dioxygenase (HPCD) from the Gram-positive soil bacterium *Brevibacterium fuscum* is an extradiol dioxygenase that catalyzes the ring cleavage of 3,4-dihydroxyphenylacetate to  $\alpha$ -OH- $\delta$ -carboxymethyl cis,cis-muconic semialdehyde. One residue thought to be important in ring cleavage

specificity in this enzyme is the highly conserved H200. A series of mutations at this site have been created and, to date, three of these mutants H200N, H200Y and H200F have been crystallized. H200Y is red in color; H200N kinetic data reveals an oxygenated intermediate not seen in wild type enzyme; and H200F has been shown to switch from extradiol cleavage to intradiol cleavage of an alternate substrate. Data from these mutants and their complexes are currently being collected and analyzed. Insights into the molecular mechanism resulting from this analysis will be presented.

**M-P194 Crystal Structure of NH<sub>3</sub>-dependent NAD<sup>+</sup> Synthetase from *Bacillus anthracis*.** H. McDonald<sup>1</sup>, C. Deivanayagam<sup>1,2</sup>, L. DeLucas<sup>1,2</sup>, I. Protassevitch<sup>1</sup>, P. Pruet<sup>1</sup>, W. Brouillette<sup>1,3</sup>, C. Brouillette<sup>1,2</sup>, Univ. of Alabama at Birmingham, Center for Biophysical Sciences and Engineering<sup>1</sup>, Dept. of Vision Sciences<sup>2</sup>, Dept. of Chemistry<sup>3</sup>.

The threat of anthrax being used as a weapon became a reality for Americans in 2001 when the postal system was used to spread anthrax. NAD<sup>+</sup> synthetase (NADS) is a ubiquitous enzyme that catalyzes the last step of nicotinamide adenine dinucleotide biosynthesis, and is considered to be a potential target for the development of novel antibacterial agents. Therefore, the crystal structure of NADS from *Bacillus anthracis* has been elucidated and refined to 1.9 Å resolution with a current R-factor = 23.2 % and R<sub>free</sub> = 25.3 %. X-ray diffraction data were collected at the SER-CAT ID beamline at APS. The crystal belongs to space group P2<sub>1</sub>2<sub>1</sub>2<sub>1</sub>, with unit cell parameters of a=84.4, b=85.6, and c=245.4 Å. The structure was solved using molecular replacement with *B. subtilis* NADS (1EE1.pdb) as the model. Although *B. anthracis* NADS shares 78% sequence identity with *B. subtilis*, there are notable differences observed between the two crystal structures. We will present these observations and discuss the design of specific inhibitors that could result in a new class of antibacterial agents.

**M-P196 Crystal Structures of Multi-Drug Resistant HIV-1 Protease Mutants Define a New Target For Protease Inhibitor Design.** R.S. Yedidi, G. Proteasa, J.L. Martinez, J.F. Vickrey, P. Martin, L.C. Kovari, Dept. of Biochemistry and Molecular Biology, School of Medicine, Wayne State Univ., Detroit, MI.

Life cycle of HIV-1 reveals that the protease is critical for viral maturation and a very important target for designing inhibitors as a part of the highly active antiretroviral therapy (HAART). Accumulation of mutations causes the clinical failure of most protease inhibitors. The high resolution (1.3 Å) "wide open" structure of MDR769HIV-1 protease, recently solved by our group, has a set of mutations (L10I, M36V, M46L, I54V, I62V, L63P, A71V, V82A, I84V, L90M). Structural analysis indicated an expanded active site cavity and wide open flaps. We examined the impact of the drug resistance mutations at codon 82 and we report the MDR crystal structures of A82S, A82T and A82F at 1.85-2.25 Å resolution. All of these structures support the active site expansion hypothesis regarding the development of drug resistance. We are employing solvent mapping techniques to identify cavities for the design of small molecule inhibitors against the MDR HIV-1 protease.

This work is supported by NIH grant AI 065294 to LCK.

**M-P198 Crystal Structure of a Putative pduO-type ATP:cobalamin Adenosyltransferase from *Mycobacterium tuberculosis*.**

Jin Ho Moon<sup>1</sup>, Anthony Kaviratne<sup>1</sup>, Minmin Yu<sup>2</sup>, Evan H. Bursey<sup>2</sup>, Li-Wei Hung<sup>3</sup>, Timothy P. Lakin<sup>4</sup>, Brent W. Segelke<sup>4</sup>, Thomas C. Terwilliger<sup>1</sup>, Chang-Yub Kim<sup>1</sup>, <sup>1</sup>Bioscience Div., Los Alamos National Laboratory, Los Alamos, NM 87545 <sup>2</sup> Physical Biosciences Div., Lawrence Berkeley National Berkeley, Berkeley, CA 94720 <sup>3</sup> Biological and Quantum Physics Group, Physics Div., Los Alamos National Laboratory, Los Alamos, NM 87545 <sup>4</sup> Biosciences Div., Lawrence Livermore National Laboratory, Livermore CA 94551.

ATP:cobalamin adenosyltransferase catalyze the final step in the conversion of Vitamin B<sub>12</sub> into coenzyme B<sub>12</sub> (adenosylcobalamin). Three classes of this enzyme have been identified cobA, pduO and eutT based on primary sequences. The gene coding Rv1314c from *Mycobacterium tuberculosis* classified to pduO type. The pduO members are associated with genes encoding adenosylcobalamin-dependent diol or glycerol dehydratase or methylmalony-CoA mutase. We have determined the crystal structure of a putative pduO-type ATP:cobalamin adenosyltransferase from *Mycobacterium tuberculosis* at 2.0 Å resolution by multiple wavelength anomalous dispersion experiments using bromide ion as anomalous scatterers. The monomer consists of a five-helix bundle and two short beta strands. And the oligomeric structure has shown to be trimer which is formed by the interactions between the helix.

**M-P200 Structural Basis of Serpin Inhibitory Mechanism.**

Soon-Hee Sul, and Elizabeth Goldsmith, Dept. of Biochemistry, UT Southwestern Medical Center at Dallas, 5323 Harry Hines Blvd., Dallas, TX 75390.

The serpins belong to a superfamily of proteins that employs a unique suicide substrate-like inhibitory mechanism. Recent X-ray structure of a serpin-protease complex confirmed that the serpins undergo dramatic conformational changes when cleaved by the protease they inhibit and the protease is translocated 70Å from one pole to the other of serpin. However, the factors causing the conformation change of the serpin are not fully understood. A crystallographic approach was used to understand how the inhibitory mechanism of serpin works. First, the complex structures of the mutant *M.sexta* serpin 1B(A353K, S354A) with trypsin S195A and the mutant serpin 1B (A353K, I350A) with trypsin have been determined. These structures elucidate the role of specific sequences within the reactive center loop for serpin inhibitory mechanism. Second, the structure with aldehyde peptide having serpin reactive center loop with wild type trypsin is being investigated. The major significance of this work is to understand how the hydrolysis reaction is arrested at the covalent intermediate acyl enzyme stage.

**M-P202 Crystal Structure of IMP Dehydrogenase from *Bacillus anthracis*.**

R-g. Zhang<sup>1</sup>, R-y. Wu<sup>1</sup>, L.E. Volkart<sup>1</sup>, G. Joachimiak<sup>1</sup>, P. Gornicki<sup>2</sup>, A. Joachimiak<sup>1</sup>, <sup>1</sup>Structural Biology Center, Biosciences, Argonne National Laboratory, 9700 South Cass Ave., Bldg 202, Argonne, IL 60439, <sup>2</sup>Dep. of Mol. Gen. and Cell Biol., Univ. of Chicago, 920 E. 58th St., Chicago, IL 60637.

IMP dehydrogenase (IMPDH) is an essential enzyme that catalyzes the conversion of IMP to XMP, a unique step in GTP synthesis. IMPDH inhibitors have broad clinical utility in the treatment of malignancy, viral diseases and as immunosuppressive agents. To provide a basis for the evaluation of IMPDH inhibitors as antimicrobial agents, we have determined the crystal structures IMPDH from *B. anthracis* at 2.2 Å with substrate and product bound in the active site. The IMPDH is a tetramer with its four subunits related

by a crystallographic fourfold axis. The enzyme is composed of two domains: a TIM barrel domain that embodies the catalytic site and a CBS dimer domain. The structure of *B. anthracis* IMPDH is similar to *S. pyogenes* IMPDH which we reported earlier. Structural comparisons of IMPDH from bacterial and eukaryotic sources will contribute to understanding of their distinct properties and the design of specific bacterial IMPDH inhibitors.

This work was supported by the grant from the NIH (AI057153) and the U.S. Department of Energy, OBER under Contract W-31-109-ENG-38.

**M-P204 Modulation of Axial Methionine Coordination in Type-1 Copper Sites.** Iain MacPherson, Michael E. P. Murphy, Biochemistry and Molecular Biology, Univ. of British Columbia, Vancouver, BC.

Type-1 copper sites are characterized by their strong absorbance at 600 nm and sometimes 460 nm, giving rise to an intense blue-to-green color. A typical type-1 copper site contains three strong ligands, two histidines and one cysteine, and one weaker axial methionine. Whether the four-coordinate copper site lies in the blue or green end of the spectrum (ratio of  $A_{600}/A_{460}$ ) depends largely on the geometry of the axial methionine with respect to the other three ligands and the copper, affecting the ratio of  $A_{600}/A_{460}$ . The type-1 copper protein, nitrite reductase from the soil bacteria *Alcaligenes faecalis* (AfNiR), is characterized by its intense absorbance at 589 and 460 nm, giving rise to a strong green color. Random mutagenesis and screening resulted in two variants of nitrite reductase, H60Y and H60R. Their electronic spectra differ significantly from the native enzyme with  $A_{600}/A_{460}$  ratios of 0.85 and 1.18, respectively, compared to 0.81 from native AfNiR, leading to a marked blue shift in color. X-ray structural analysis of the H60Y and H60R variants show a change in the  $\beta$ -strand containing non-coordinating residues Met62 and Phe64, whose side chains flank the axial Met150. The changes observed in the structures of H60Y and H60R are discussed and related to the close homologue, nitrite reductase from *Alcaligenes xylosoxidans*, which differs from AfNiR with its axial methionine coordination and intense blue color.

**M-P206 Structural Constraints on Protein Autoprocessings through an N-O or N-S Acyl Shift.** Y. Sun, Y. Wang, H.-C. Guo, Dept. of Physiology and Biophysics, Boston Univ. School of Medicine, Boston, MA 02118.

Proteolysis is involved in activating many biological functions. A unique type of proteolysis, protein autoprocessing, has emerged as novel mechanism of posttranslational modification. It is initiated by a nucleophilic attack of a threonine, serine, or cysteine residue at the scissile peptide bond, leading to an N-O or N-S acyl shift. From that intermediate, a diverse group of proteins undergo various types of peptide-bond rearrangements. Intramolecular autoproteolysis is one such novel mechanism found to activate human nucleoporin hNup98 and glycosylasparaginase (GA). We have determined precursor structures of the *Flavobacterium* GA and hNup98 autoproteolytic domain, both at 1.9 Å resolution. Interestingly, structural constraints are found near the scissile peptide bonds of both precursors. Structural comparisons of these two precursor structures are underway to study mechanistic similarities and differences between them.

**M-P208 Crystal Structure of Thermophilic Cytochrome P450 from *Picrophilus torridus*.** Winny W. Ho, Huiying Li, Clinton Nishida, Paul Ortiz de Montellano, Thomas Poulos, Dept. of Molecular Biology and Biochemistry, Univ. of California, Irvine, CA 92697, Dept. of Pharmaceutical Chemistry, School of Pharmacy, Univ. of California, San Francisco, CA 94143, winny@uci.edu.

Cytochrome P450s are found in all organisms including bacteria, fungi, plants, insects, and vertebrates and provide one of the primary roles by which the body removes toxic substances. Another type of cytochrome P450 enzyme is thermophilic cytochrome P450s, which can survive at extreme conditions, such as high temperature of 60° C and highly acidic pH 0.7 environments. Also, these enzymes function in extremely low intracellular pH conditions. Two new thermophilic P450s in *Picrophilus torridus* (PTO1399 and PTO0085) were found while conducting a BLAST analysis of current available genomes of thermophilic organisms. [1] The function of both enzymes is still unknown. So far, we have been successful in crystallizing PTO 1399 and data collected have a resolution of 2.5 Å. We are now in the process of refining this structure. By understanding the structural basis for the stability of proteins from thermophilic organisms, we can further apply this information for drug synthesis.

[1] O. Fütterer, A. Angelov, H. Liesegang, G. Gottschalk, C. Schepers, B. Schepers, C. Dock, G. Antranikian, W. Liebl., *PNAS*, 2004, 101, 9091-9096.

**M-P210 Crystal Structure of the Aerobic FMN-Dependent Azoreductase (AzoA) from *Enterococcus faecalis*.** Z.-J. Liu<sup>1,2</sup>, H. Chen<sup>3</sup>, L. Chen<sup>1</sup>, S.L. Hopper<sup>3</sup>, C.E. Cerniglia<sup>3</sup>, Neil Shah<sup>2</sup>, J. P. Rose<sup>1</sup>, B.-C. Wang<sup>1</sup>, <sup>1</sup>Dept. of Biochemistry and Molecular Biology, Univ. of Georgia, Athens, GA 30605, USA, <sup>2</sup>National Laboratory of Biomacromolecules, Inst. of Biophysics, Chinese Academy of Sciences, Beijing 100101, China, <sup>3</sup>National Center for Toxicological Research/FDA, Jefferson, AR 72079, USA.

Azo dyes are a class of colorants used in tattooing, cosmetics, foods, and consumer products. In bacteria, azo dyes are mainly metabolized by azoreductases to colorless aromatic amines, some of which are carcinogenic. The crystal structure of AzoA from *E. faecalis* has been determined to 2.0 Å. AzoA has a broad spectrum of substrate specificity and is capable of degrading a wide variety of azo dyes. The structure was determined by single wavelength anomalous scattering from Se-Met labeled protein using the UGA Sca2Structure pipeline. The AzoA structure is a dimer with an FMN molecule bound to each monomer. The AzoA monomer shows the typical NAD(P)-binding Rossmann fold with the FMN cofactor lying on top of the C-terminal end of the central  $\beta$ -sheet, inside a positively charged pocket. The FMN phosphoribityl moiety is buried deeply within the protein while the FMN isoalloxazine ring remains partially accessible to the solvent.

**M-P212 Crystal Structure of MC159 Reveals Molecular Mechanism of DISC Assembly and FLIP Inhibition.** Jin Kuk Yang, Liwei Wang, Lixin Zheng, Fengyi Wan, Misonara Ahmed, Michael J. Lenardo, Hao Wu, Dept. of Biochemistry, Weill Medical College of Cornell Univ., New York, NY 10021.

The death-inducing signaling complex (DISC) comprising Fas, Fas-associated death domain (FADD), and caspase-8/10 is assembled via homotypic associations between death domains (DDs) of Fas and FADD and between death effector domains (DEDs) of FADD and caspase-8/10. Caspase-8/10 and FLICE/caspase-8 inhibitory proteins (FLIPs) that inhibit caspase activation at the DISC level contain tandem DEDs. Here, we report the crystal structure of a viral FLIP, MC159, at 1.2 Å resolution. It reveals a noncanonical fold of DED1, a dumbbell-shaped structure with rigidly associated DEDs and a differ-

ent mode of interaction in the DD superfamily. Whereas the conserved hydrophobic patch of DED1 interacts with DED2, the corresponding region of DED2 mediates caspase-8 recruitment and contributes to DISC assembly. In contrast, MC159 cooperatively assembles with Fas and FADD via an extensive surface that encompasses the conserved charge triad. This interaction apparently competes with FADD self-association and disrupts higher-order oligomerization required for caspase activation in the DISC.

**M-P214 Crystal Structure of the BTB Domains from LRF and Kaiso: Implications for the Protein-protein Interaction Properties of BTB Transcription Factors.** P.J. Stogios<sup>1</sup>, L. Chen<sup>2</sup>, G.G. Prive<sup>1,2</sup>, <sup>1</sup>Dept. of Medical Biophysics, Univ. of Toronto, Toronto, Canada, <sup>2</sup>Ontario Cancer Inst., Toronto, Canada.

The BTB domain is a eukaryotic protein-protein interaction domain found in a variety of biological functions and contexts. There are many transcription factors (TF's) that contain the BTB domain and C2H2 zinc finger motifs, such as BCL6, PLZF, LRF, Kaiso and Miz1, each of which has been implicated in regulation of genes involved in cancer biology. In TF's that contain BTB domains, this domain's role is to mediate dimerization and in some cases, recruit enzyme complexes involved in chromatin remodeling and transcription regulation. Here we present recently solved structures of the BTB domains from the TF's LRF and Kaiso and progress towards the crystallization of the BTB domain from Miz1. In LRF-BTB, a protein-protein interaction groove that is utilized by some BTB domains to recruit transcription corepressors is lined with amino acids that are not compatible with corepressor binding. The BTB domain of Kaiso forms a double chain of oligomers in the crystal. This may reflect the tendency for BTB TF's to oligomerize on their DNA recognition sequences. Miz1-BTB crystals are currently being refined and improved to obtain well-diffracting crystals. These structures aid in our understanding of the mechanism of transcription regulation by BTB-zinc finger TF's and will be useful for future protein-protein interaction interference studies.

**M-P216 Asymmetric Hexameric Assembly of the Archaeal Secretion ATPase.** A. Yamagata, J.A. Tainer, Dept. of Molecular Biology, The Scripps Research Institute, La Jolla, CA, 92037.

Members of the large family of bacterial and archaeal secretion ATPases play key roles in macromolecular transport, pilin and flagellar assembly systems. The central function of these proteins in facilitating bacterial toxin export and cellular adherence to human cells necessitates further analysis of the poorly understood chemomechanical structural mechanisms of secretion ATPases and their role in virulence.

Here, we describe the crystal structure of *Archaeoglobus fulgidus* GspE2, a putative archaeal secretion ATPase, in complex with AMP-PNP. Two subunits in the asymmetric unit exhibit distinct open-closed conformations characterized by rigid-body movement of two defined N- and C- terminal domains. They further form the asymmetric hexameric ring structure along a 3-fold crystallographic axis. AMP-PNP in the open form is bound within C-terminal domain. However, in the closed form, two arginine residues (arginine fingers) from N-terminal domain interact with gamma-phosphate of AMPPNP, suggesting that these interactions are required to maintain the closed conformation. A magnesium ion that is essential for ATP hydrolysis is only observed in closed form, suggesting that the closed form is the catalytically active subunit. Based on these results, we propose the working model how ATP hydrolysis is coupled with the basic mechanism of secretion ATPases.

**M-P218 WRN Exonuclease Structure and Molecular Mechanism Imply an Editing Role in DNA End Processing.** J.J. P. Perry<sup>1</sup>, S. M. Yannone<sup>2</sup>, L.G. Holden<sup>1</sup>, C. Hitomi<sup>1</sup>, A. Asaithamby<sup>4</sup>, S. Han<sup>2,3</sup>, P.K. Cooper<sup>2</sup>, D.J. Chen<sup>4</sup>, J.A. Tainer<sup>1,2</sup>, <sup>1</sup>Molecular Biology, The Scripps Research Inst., CA, 92037, <sup>2</sup>Lawrence Berkeley National Labs, CA, 94720, <sup>3</sup>Pfizer Global Research & Development, CT, 06340, <sup>4</sup>UT Southwestern Medical Center, TX, 75390.

WRN is unique among five human RecQ DNA helicases by having a functional exonuclease domain (WRN-exo) and being defective in the premature aging and cancer-related disorder Werner syndrome. Here, we characterize WRN-exo crystal structures, biochemical activity and participation in DNA end-joining. Metal ion complex structures, active site mutations and activity assays reveal a two-metal-ion mediated nuclease mechanism. The DNA end-binding Ku70/80 complex specifically stimulates WRN-exo activity, and structure-based mutational inactivation of WRN-exo alters DNA end-joining in human cells. We furthermore establish structural and biochemical similarities of WRN-exo to DnaQ family replicative proofreading exonucleases, with WRN-specific adaptations consistent with dsDNA specificity and functionally important conformational changes. These results indicate WRN-exo is a human DnaQ family member and support analogous proof-reading activities that are stimulated by Ku70/80, with implications for WRN functions in age related pathologies and genomic integrity.

**M-P220 Structure of a Highly Active Insect  $\epsilon$ -class Glutathione S-transferase from a DDT-resistant Strain of the Malaria Vector *Anopheles gambiae*.** Yujun Wang<sup>1</sup>, Jing Zhou<sup>1</sup>, Janet Hemingway<sup>2</sup>, Hilary Ranson<sup>2</sup>, Edward J. Meehan<sup>1</sup>, Liqing Chen<sup>1</sup>, <sup>1</sup>Laboratory for Structural Biology, Dept. of Chemistry, Graduate Program of Biotechnology, Univ. of Alabama in Huntsville, Huntsville, AL 35899, <sup>2</sup>Vector Research Group, Liverpool School of Tropical Medicine, Liverpool L3 5QA, UK.

Insecticide resistance is consistently abating the global effort of controlling insect vectors of malaria, yellow fever, dengue and dangué haemorrhagic fever *etc.* Glutathione S-transferases (GSTs), a major family of detoxification enzymes, play a pivot role in the detoxification of insecticides in insects. In the mosquito, *Anopheles gambiae*, elevated expression of a highly active  $\epsilon$ -class GST, agGSTe2, confers resistance to the organochlorine insecticide DDT by converting it from reactive lipophilic molecules into water-soluble non-reactive conjugates. To elucidate its mechanism, the crystal structure of agGSTe2 in complex with glutathione (GSH) has been determined and refined at 1.4 Å. A structural comparison and analysis will provide further information about its unusual high activity.

Supported by NSF-EPSCoR.

**M-P222 Crystal Structure of Trehalose-6-phosphate Phosphatase Related Protein.** Krishnamurthy N. Rao, Subramanyam Swaminathan, Biology Dept., Brookhaven National Laboratory, Upton, NY 11973.

Trehalose-6-phosphate phosphatases catalyze de-phosphorylation of trehalose-6-phosphate (T6P) to trehalose and orthophosphate. Synthesis of trehalose, a common disaccharide crucial for organism survival under stress conditions, is dependent on trehalose phosphatase. Here, we report crystal structure of trehalose-6-phosphate phosphatase related protein (T6PP) from *Thermoplasma acidophilum*, determined by dual-wavelength anomalous diffraction (DAD) method. It represents the first structure of the trehalose 6-phosphate phosphatase family. T6PP possesses a core domain of known  $\alpha/\beta$  hydrolase fold, and a cap domain. An active site magnesium ion and a glycerol mol-

ecule bound at the interface between the two domains provide insight into the mode of substrate binding by T6PP. A trehalose-6-phosphate molecule modeled into a cage formed by the two domains makes favorable interactions with the protein molecule. We have confirmed that T6PP is a trehalose phosphatase from amino acid sequence, three dimensional structure, and biochemical assays.

Acknowledgements: Research was supported by a National Institutes of Health grant (GM62529) to the NYSGXRC under the auspices of the Protein Structure Initiative (DOE Prime Contract No. DEAC02-98CH10886 to Brookhaven National Laboratory).

**M-P224 Nerve Agent Processing by Human Carboxylesterase I.** Christopher D. Fleming<sup>1</sup>, Carol C. Edwards<sup>3</sup>, Douglas M. Cerasoli<sup>2</sup>, Philip M. Potter<sup>3</sup>, Matthew R. Redinbo<sup>1</sup>, <sup>1</sup>Univ. of North Carolina at Chapel Hill, Chapel Hill, NC, <sup>2</sup>U.S. Army Medical Research Inst., Bethesda, MD, <sup>3</sup>St. Jude Research Hospital, Memphis, TN.

Organophosphate nerve agents (OPs) are a class of neurotoxins that are deadly to a milligram level of exposure. OPs covalently modify the acetylcholinesterase (AChE) enzyme, causing rapid muscle paralysis. Given the limited treatment options that currently exist, the development of an effective OP hydrolase may provide a prophylactic option for military and civilian first responders. Human carboxylesterase I (hCE1), a promiscuous drug metabolism enzyme, is a candidate for development into an efficient nerve agent hydrolase. Here we present the crystal structures of hCE1 in covalent, protaged acyl-enzyme intermediate complexes with the nerve agents Tabun, Soman, and Cyclosarin to 2.7 Å, 2.7 Å, and 2.3 Å resolution, respectively. These results reveal that hCE1 is resistant to permanent covalent “aging” observed with other serine hydrolases, including AChE. These structures provide a framework to identify mutations that may increase the nerve agent hydrolase activity of hCE1.

**M-P226 Crystal Structure of Molybdopterin-Guanine Biosynthesis Protein B (Mob B).** Lakshminarasimhan Damodharan, Subramaniam Eswaramoorthy, Desigan Kumaran, Subramanyam Swaminathan, Biology Dept., Brookhaven National Laboratory, Upton, New York, NY 11973.

Mob B from *Archaeoglobus fulgidus* DSM 4304 is involved in the biosynthesis of molybdopterin guanine dinucleotide. We report the crystal structure of Mob B determined at 2.1 Å resolution by the single wavelength anomalous dispersion method (SAD) using selenomethionine protein. The protein crystallizes in the monoclinic space group  $P2_1$  with the asymmetric unit containing a homodimer. The molecule has an  $\alpha/\beta$  - fold with a major and a minor domain. The minor domain is involved in domain swapping between the protomers resulting in 16-stranded extended  $\beta$ -sheet. The protein contains two nucleotide binding motifs (Walker A) on the surface which might participate in GDP binding. During refinement, we identified a strong residual density that was modeled as praseodymium decahydrate which was used as an additive in crystallization. Praseodymium decahydrate solvent molecule is involved in molecular association.

Acknowledgement: Research was supported by the National Institutes of Health (GM074945) grant to NYSGXRC under Prime Contract No. DEAC02-98CH10886 with the Brookhaven National Laboratory.

**M-P228 Structural Basis for PYK2 Adhesion Targeting in Osteoclast Activation.** Wang Yimin, S. Ranganathan, Z. Qu, Xu Feng, W.-C. Xiong, R. Li, Southern Research Inst., Birmingham, AL, Dept. of Pathology, Univ. of Alabama, Birmingham, AL.

Proline-rich tyrosine kinase 2 (PYK2) is a major kinase in the integrin-mediated cell adhesion and is related to focal adhesion kinase (FAK). While FAK is widely expressed in various tissues, PYK2 is primarily expressed in the central nervous system and in cells derived from hematopoietic lineages, such as osteoclasts. PYK2 localizes to adhesion structures through interactions between its C-terminal region and cytoskeletal proteins and plays an important role in cell adhesion and migration. The PYK2 C-terminal region is highly homologous to the focal adhesion targeting (FAT) domain of FAK. However, PYK2, not FAK interacts with gelsolin, an actin-binding protein found in osteoclastic adhesion structures. This specific interaction regulates the osteoclastic actin ring formation and osteoclast activation and is a potential target for bone resorption and metastasis of common cancers. The PYK2 FAT domain containing 138 residues crystallizes in space group P21 with cell dimensions of  $a = 49.8 \text{ \AA}$ ,  $b = 130.8 \text{ \AA}$  and  $c = 49.9 \text{ \AA}$ . The crystal structure of the PYK2 FAT domain has been determined at  $2.5 \text{ \AA}$  resolution by molecular replacement. The current model contains four molecules in the asymmetric unit and has been refined to  $R_{\text{cryst}} = 0.20$  and  $R_{\text{free}} = 0.26$ . The crystal structure reveals a four-helix bundle with surface features required for binding to the LD motifs of paxillin and gelsolin. Comparison between PYK2 and FAK reveals the structural basis for specific interactions of PYK2 with gelsolin and a target site for specific inhibitor design to the integrin-mediated osteoclast activation.

We thank NE-CAT at APS for access to beamline 8-BM. This research is supported by NCI/NIH grant CA102998.

**T-P001 Simplified Models for Hierarchical Structures Based on Disks, Rods and Tubes.** Ryan S. Justice,<sup>a,b</sup> Jan Ilavsky,<sup>c</sup> Dale W. Schaefer,<sup>b</sup> <sup>a</sup>Air Force Research Laboratory, WPAFB, OH USA, <sup>b</sup>Univ. of Cincinnati, Dept. of Chemical and Materials Engineering, Cincinnati, OH, <sup>c</sup>Argonne National Laboratory, Argonne, IL.

With rising interest in utilization of polymer nanocomposites for structural applications, quantifying filler dispersion has emerged as a major challenge. To characterize nanocomposite systems with nanosilicates and carbon nanotubes, we have developed models for fractal disks, fractal rigid-rods, and simplified tubes to analyze scattering data. The fractal disk model, for example, incorporates the idea of semi-flexible disk-like entities, allowing the persistence length of the crumpled sheets to be quantified. Simplified rod and tube models capture the essential features of exact models but allow for easy incorporation of large-scale flexibility (worm-like rods and tubes). The mathematical simplicity of the models permits rapid extraction of size distributions when analyzing polydisperse systems.

The models are used to analyze ultra small-angle X-ray data on both water suspensions and composites formed with carbon and silicate colloids. Conclusions from small-angle scattering often conflict with those from electron imaging. Possible reasons why hierarchical morphologies have escaped detection by imaging methods will be discussed.

**T-P002 Robotic Crystallization and Precipitation Point Proximity.** Shahzad Majeed, Tongqing Zhou, Peter D. Kwong, Vaccine Research Center NIAID/NIH, 40 Convent Dr., Bethesda MD 20892.

Proteins tend to crystallize more frequently close to their precipitation points. In this experiment, we used three commercial screens, the Hampton Crystal Screen, the Wizard I screen and the Precipitant Synergy screen, in combination with robotic systems to test how precipitation point proximity affects crystallization. Variations of the three commercial screens were made with different degrees of precipitant optimization. These different screens were tested with five different proteins, three that crystallized readily (bovine pancreatic trypsin inhibitor, concanavalin A, and hen egg white lysozyme) and two that crystallized infrequently (bovine serum albumin and ovalbumin). We found that for readily crystallized proteins, a sparse grid of three to four precipitant concentrations was sufficient to maximize the number of unique conditions that gave crystals, and further optimization was of minimal benefit. For difficult to crystallize proteins, additional precipitant optimization doubled the number of unique conditions producing crystals. Thus the appropriate degree of precipitation point optimization was found to be dependent on the overall frequency with which each particular protein crystallized.

**T-P003 Bilayer Membrane and the Formation of Unilamellar Vesicles.** Thomas M. Weiss, SSRL/SLAC, Stanford Univ., Menlo Park, CA.

Self-assembled lipid and surfactant bilayers have received considerable attention in a wide variety of scientific areas ranging from fundamental research to applied biotechnology. Much of this research has been focused on understanding the dependence of the membrane properties based on its composition and chemical nature.

In this work we investigated the changes in the dynamics of unilamellar vesicle formation and the structural properties of the resulting vesicles using static and time resolved small angle x-ray scattering. We show how small changes in the chemical composition of the membrane, influences the propensity of the system to form unilamellar vesicles and relate this to the elastic properties of the bilayer.

**T-P004 Functional Diversity from a Simple Protein Fold.** M.L. Hackert, J.J. Almrud, W.H. Johnson<sup>†</sup>, C.P. Whitman<sup>‡</sup>, Dept. of Chemistry and Biochemistry, and <sup>†</sup>College of Pharmacy, The Univ. of Texas at Austin, Austin, TX 78712.

The tautomerase superfamily is represented by 4-Oxalocrotonate tautomerase (4-OT), 5-(carboxymethyl)-2-hydroxyruconate isomerase (CHMI), and macrophage migration inhibitory factor (MIF). 4-OT and many other proteins in this family are hexameric, while other members are trimeric or dimeric. However, all members of this enzyme superfamily share a simple folding unit represented by the 4-OT monomer that is remarkable for its small size (62 a.a.) and simple ( $\beta$ - $\alpha$ - $\beta$ ) fold. Some subunits, like those of CHMI and MIF, are nearly twice as large as the 4-OT subunit and probably arose by gene duplication. Members of this superfamily also share a key mechanistic feature - an active site amino-terminal proline, which sometimes has an unusually low  $pK_a$ , as the general base in keto-enol tautomerization.

Several new members of the 4-OT family have been identified and representative structures determined, although the function of many of these proteins remains unknown. Within the superfamily, dehalogenase and decarboxylase activities are now known in addition to the tautomerase, isomerase and MIF activities noted previously. The functional diversity in the 4-OT superfamily suggests that nature used these short sequences as building blocks to create new structures and activities. A summary of these results will be presented.

**T-P005 Low Temperature Mixed Lipid Phase: Understanding Bicelle Formation.** P.D. Butler<sup>1</sup>, D. Singh<sup>1,2</sup>, L. Porcar<sup>1,3</sup>, U. Perez-Salas<sup>4</sup>, W.A. Hamilton<sup>5</sup>, G. Lynn<sup>5</sup>, <sup>1</sup>National Institute of Standards and Technology, Gaithersburg, MD, <sup>2</sup>Johns Hopkins Univ., Baltimore, MD, <sup>3</sup>Univ. of Maryland, College Park, MD, <sup>4</sup>UC Irvine, Irvine CA, <sup>5</sup>Oak Ridge National Laboratory, Oak Ridge, TN.

Systems consisting of mixtures of a long and a short-tail lipid have recently shown promise in membrane protein crystallization and have been used for some time as an alignable media for use in NMR protein structure determination. However, the phase diagram of these lipid mixtures remains poorly understood. In particular, much of the literature posits the existence of bicelles, or discotic micelles, as the agents of the useful properties. Recent work however suggests that such structure only exist below the melting transition temperature of the long tail lipid, with a transition to a lamellar phase at higher temperature. A detailed understanding of the phase behavior is crucial to adapting these systems for more general applications. In this work, we report on a systematic study at the lowest temperature isotropic fluid like phase. Using a series of small angle neutron scattering (SANS) experiments with hydrogentaed and deuterated lipids, we show direct evidence of the discoidal morphology with the two lipids being segregated in different parts of the disk and show that a model which properly accounts for the geometric packing as well as the thermodynamic nature of the system, hitherto ignored, quantitatively predicts the sizes of the disks. At higher temperature, but still well below the chain melting temperature, the system clearly becomes much more complicated and we see evidence of mixing of the two lipids.

**T-P006 JAXA-GCF Project: High-performance Protein Crystallization in Space.** M. Sato<sup>a\*</sup>, H. Tanaka<sup>b</sup>, K. Inaka<sup>c</sup>, S. Shinozaki<sup>b</sup>, A. Yamanaka<sup>b</sup>, S. Takahashi<sup>b</sup>, M. Yamanaka<sup>b</sup>, E. Hirota<sup>b</sup>, S. Sugiyama<sup>c</sup>, M. Kato<sup>a</sup>, C. Saito<sup>a</sup>, S. Sano<sup>a</sup>, M. Motohara<sup>a</sup>, T. Nakamura<sup>a</sup>, T. Kobayashi<sup>a</sup>, T. Tanaka<sup>a</sup>, <sup>a</sup>Japan Aerospace Exploration Agency, Ibaraki, 305-8505 JAPAN, <sup>b</sup>Japan Space Forum, Tokyo, 100-0004 Japan, <sup>c</sup>Maruwa Food Industries, Inc., Nara, 639-1123 Japan.

Japan Aerospace Exploration Agency (JAXA) has conducted the proj-

ect (JAXA-GCF) for obtaining high-quality protein crystals twice a year since 2003. In this project, we have provided user-friendly experimental frame work, from optimization of crystallization condition to X-ray diffraction data collection. In technical point of view, we contrived gel-tube method for experimental device <sup>[1]</sup> based on the counter-diffusion crystallization technique <sup>[2]</sup>, and provided techniques for harvesting and cryoprotecting crystals before X-ray diffraction experiment for users. As a result, the success rate of the crystallization, mostly resulting in an improvement of the maximum resolution, has become increased, including some atomic-resolution crystals. In the near future, space experiment could be essential especially for obtaining atomic resolution crystals which will become significant for the drug design.

[1] Tanaka, H. *et al.*, *J. Synchrotron Rad.*, 2004, **11**, 45-48.

[2] Garcia-Ruiz, JM., Moreno, A., *Acta Cryst.*, 1994, **D50**, 484-490.

**T-P007 Model-independent Imaging of Interfacial Structures at the Mineral-Water Interface.** P. Fenter, C. Park, Z. Zhang, J. Catalano, M.J. Bedzyk, K.L. Nagy, N.C. Sturchio, D.J. Wesolowski, Argonne National Laboratory, 9700 South Cass Ave, CHM-200, Argonne, IL, Dept. of Materials Science and Engineering, Northwestern Univ., Evanston IL, Dept. of Earth and Environmental Sciences, Univ. of Illinois at Chicago, 845 West Taylor St, Chicago IL, Chemical Sciences Div., Oak Ridge National Laboratory, Oak Ridge, TN.

A grand challenge in interfacial science is the direct observation of interfacial structures, with both molecular-scale resolution and in the environment of interest. Recent work will be presented demonstrating the capability to image the mineral-water interface both perpendicular and parallel to the interface using advanced interfacial X-ray scattering techniques. These *in-situ* measurements directly reveal the interfacial hydration layer adjacent to the mineral surface (analogous to the hydration shell surrounding cations in aqueous solutions), as well as the distribution of cations attracted to the mineral surface charge.

This work was supported by the Geoscience Research Program, Office of Basic Energy Sciences, Office of Science, Department of Energy, both directly and through its support for the Advanced Photon Source at Argonne National Laboratory under contract W-31-109-ENG-38.

**T-P008 Function-biased Choice of Additives for Optimization of Protein Crystallization.** M. Chruszcz<sup>1</sup>, M.D. Zimmerman<sup>1</sup>, K. Koclega<sup>1</sup>, J. Raynor<sup>1</sup>, J.J. Petkowski<sup>1</sup>, M. Cymborowski<sup>1</sup>, X. Xu<sup>2</sup>, T. Skarina<sup>2</sup>, E. Evdokimova<sup>2</sup>, A. Savchenko<sup>2</sup>, A. Edwards<sup>2</sup>, Z. Otwinowski<sup>3</sup>, W. Minor<sup>1</sup>, <sup>1</sup>Univ. of Virginia, Charlottesville, VA 22908, <sup>2</sup>Univ. of Toronto, Toronto, ON M5G 1L6, Canada, <sup>3</sup>UT Southwestern Medical Center at Dallas, Dallas, TX 75390.

Well-diffracting single crystals of macromolecules are one of the most valuable pieces of matter. Production of crystals suitable for structure solution is still a bottleneck of the structure determination process. We present an approach to optimization of protein crystallization that is based on the LabDB knowledge database. LabDB keeps information on all experiments that were performed in order to obtain crystals. Crystallization optimization is based on application of different so-called 'additives' that may lead to better quality crystals in the same or a different crystal form. The choice of chemicals is based on the analysis of protein function and information stored in LabDB. The presented approach substantially increased the diffraction resolution limit for several crystals and in some cases its application gave different crystal form(s). The approach was also successfully used to prevent or reduce twinning. In one of the most successful applications of the optimization protocol (thioesterase from *Pseudomonas aeruginosa*; PDB code: 2AV9) three new crystals forms were obtained by a small variation of the original crystallization conditions. The resolution limit was extended from 2.4Å to 1.9Å.

**T-P009 *Ab initio* Structure Determination from Pair Distribution Function.** Pavol Juhas, Phillip M. Duxbury, Simon J.L. Billinge, Michigan State Univ., East Lansing, MI.

A vast majority of all known structures has been obtained by reciprocal space methods that require periodic long-range order in the material. However, many important systems, such as nanomaterials or non-crystallized molecules, have no periodic order at all and their structures cannot be solved using crystallographic methods. The analysis of the atomic Pair Distribution Function (PDF) is not limited by periodic order and it has yielded important atomic scale information on nanomaterials. However, PDF analysis is not simple and it typically consists of time consuming trial-and-error tests of different structure models. Our recent work [1] presents another way of extracting structure from PDF data and it demonstrates a complete *ab-initio* structure solution of a single-component molecule from PDF data alone. We will describe the extension of *ab-initio* PDF method to general, multi-component molecules and to periodic systems with large supercells. The application of chemical information, such as bond angle restraints or known structure fragments will also be discussed.

[1] P. Juhas, D. M. Cherba, P. M. Duxbury, W. F. Punch, S. J. L. Billinge, *Ab initio* determination of solid-state nanostructure, *Nature* (to be published in 2006).

**T-P010 The Inactivation of HAV 3C Protease by Peptide-based Ketone Inhibitors via an Unusual Episulfide Ring.** Jiang Yin<sup>1</sup>, Maia M. Cherney<sup>1</sup>, Ernst M. Bergmann<sup>1</sup>, Jianmin Zhang<sup>2</sup>, Hanna Pettersson<sup>2</sup>, John C. Vederas<sup>2</sup>, Michael N.G. James<sup>1</sup>, <sup>1</sup>Dept. of Biochemistry, Univ. of Alberta, Edmonton, AB, Canada, <sup>2</sup>Dept. of Chemistry, Univ. of Alberta, Edmonton, AB, Canada.

Most previously solved crystal structures of Hepatitis A viral 3C proteinase are of inactivated variants containing either an active site residue substitution (C172A) or an oxidized C172 in the active site. A recently described form of crystals, obtained by incubating HAV 3C with an N-cbz-L-serine- $\beta$ -lactone inhibitor, diffract to high resolution (beyond 1.4Å) at synchrotron X-ray sources. The  $\beta$ -lactone inhibitor binds to a surface histidine residue (H102), leaving the catalytic residue (C172) unmodified. In this study, three tetrapeptidyl inhibitors were soaked into pre-grown HAV 3C- $\beta$ -lactone crystals. The residues in the  $\beta$ -hairpin substructure (aa 138-158) are critical for enzyme-inhibitor interactions. The S<sup>γ</sup> of C172 forms two covalent bonds with each inhibitor, leading to an unusual episulfide cation (thiuranium ring). Our results offer high-resolution visualization of the substrate binding sites (S1 to S4) in HAV 3C and sheds light on the mechanisms underlying both the inactivation of HAV 3C by these inhibitors and on the proteolyses of natural substrates by this viral cysteine protease.

**T-P011 Neutron Structure of [Zn<sub>2</sub>[L-Sala)<sub>2</sub>(H<sub>2</sub>O)<sub>2</sub>].2H<sub>2</sub>O.** W.T. Klooster<sup>1</sup>, G.J. McIntyre<sup>2</sup>, J.J. Vittal<sup>3</sup>, <sup>1</sup>Australian Nuclear Science and Technology Organisation, Lucas Heights, Australia, <sup>2</sup>Inst. Laue-Langevin, France, <sup>3</sup> Dept. of Chemistry National Univ. of Singapore.

A brief overview of neutron diffraction and its (dis)advantages will be given. As example the data collection and results of the structure of [Zn<sub>2</sub>[L-Sala)<sub>2</sub>(H<sub>2</sub>O)<sub>2</sub>].2H<sub>2</sub>O, which has interesting hydrogen-bonding, will be discussed.

Data were collected on VIVALDI, the neutron single-crystal Laue diffractometer at the Institut Laue-Langevin, Grenoble, France. The new OPAL research reactor at ANSTO will have a similar instrument operational in 2006. The main features are data collection times of hours, using crystals with average size of ~0.1 mm<sup>3</sup>, a considerable improvement with current facilities.

**T-P012 Dual-wavelength X-ray Generation from one Machine to Facilitate Protein Structure Determination.** Kurt L. Krause, John Cutfield, Sue Cutfield, Peter Mace, Sigurd Wilbanks, Calum Smits, Catherine Day, Dept. of Biochemistry, Univ. of Otago, New Zealand.

We present our initial experience at using chromium and copper X-rays from the same generator to facilitate in-house determination of protein crystal structures. The availability of focussed high-flux chromium X-rays has greatly facilitated the in-house determination of protein crystal structures. At the same time in-house high-flux copper sources allow for improved native data collection at higher resolutions. Most commonly these two sources of X-rays are found on separate diffractometers at the same facility. Generating both wavelengths of X-rays from the same machine is cost effective, but can greatly increase the complications of the experimental set-up. Newer multi-layer optics that allow for more rapid switching between wavelengths have been developed that preserve the same Bragg angle for Copper and Chromium sources. The details of switching between these two-wavelengths will be described and illustrated in case studies.

**T-P013 Mail-in Crystallography Program at Brookhaven National Laboratory's NSLS: Update on our Operation.** A. Héroux, A.S. Soares, R.M. Sweet, H. Robinson, Biology Dept., Brookhaven National Laboratory, Upton, NY 11973.

For the last six years, the Macromolecular Crystallography Research Resource (PXRR) has been providing mail-in access to several beamlines at the National Synchrotron Light Source (NSLS) for x-ray diffraction. This program is available at no charge for academic users not only from the US but also from all around the world (<http://px.nsls.bnl.gov>). The use and success of this program has been on a steady rise since its creation. The needs of the "remote" synchrotron users (MAD, SAD, native data collections) are conveyed to our local scientific staff, which becomes their local experimenter. The Mail-in experimenter takes an active role in the design of the experiments in order for them to mature and be fruitful in an accelerated fashion. An update on the achievements of the Mail-in program will bring to light its productivity and how it is accelerating the innovation of new productivity tools, new ways of scheduling and a constant quality control of the beamlines, which benefit users who come to NSLS beamlines as well as those who use the Mail-in Program.

Sponsored by BER, DOE and the National Center for Research Resources of the US Nat.l Institutes of Health.

**T-P014 Microcrystallography at MacCHESS.** R.E. Gililan, M.J. Cook, S. Cornaby, T.A. Szebenyi, D.H. Bilderback, Cornell High-Energy Synchrotron Source, Ithaca NY 14853.

Small crystals seem to be a frequent occurrence in protein crystallography. Refinement of crystallization conditions to produce larger, better quality crystals is a time-consuming activity that is not always successful. Protein crystals, that are 30  $\mu$ m or smaller in their largest dimension, present special challenges in both handling and data collection. Typical 100 micron diameter beams produce unnecessary scattering from solvent surrounding the crystal and the result is degraded signal-to-noise ratios. While apertures and slits can reduce beam size, the number of photons reaching the sample remains the same. To meet the needs of an increasing number of researchers with smaller crystals, beamline F1 at CHESS now offers microbeam capabilities based on single-bounce high-gain capillary optics. Beams, 18 microns in diameter with a flux of  $1.4 \times 10^{10}$  photons/second, are now routinely available to regular users. In this poster we will discuss the details of our implementation, limitations due to source character-

istics, and our latest results using new 5 micron capillary optics. This poster will also demonstrate the improvement that can be achieved using a helium atmosphere to further reduce unwanted scattering and absorption. We have integrated a helium-enclosed microbeam environment with ALS-style sample automounting for convenient screening of microcrystals. We will also discuss our use of fluorescence microscopy to center crystals smaller than the resolving power of our visible light optics. The poster will conclude with a discussion of how Cornell's proposed Energy Recovery Linac, with its diffraction-limited, high spectral brightness source, is ideally suited to advance microcrystallography.

Many thanks to the staff of MacCHESS and CHESS who are supported through NIH NCCR grant RR-01646 and NSF award DMR 0225180

**T-P015 Crystallography in Fiction: The Sequel.** Frank R. Fronczek, Dept. of Chemistry, Louisiana State Univ., Baton Rouge, Louisiana, 70803.

Poster P152 at the Orlando ACA meeting presented examples of crystallography or crystallographers in novels and short stories, highlighting works by Kurt Vonnegut, Jr., Michael Crichton, C. P. Snow, and others. It contained an appeal for further examples known to the crystallographic community, and produced considerable feedback, the results of which will be presented here. More examples of novels and short stories will be given. For example, Nevil Shute's 1948 novel, *No Highway* deals with metal fatigue threatening to doom a commercial aircraft, and contains references to crystallography. Examples from poetry and movies will also be given, including John Updike's poem *Ode to Crystallization*, the 1971 Universal Pictures film *The Andromeda Strain*, based on Crichton's novel, and the 1951 20th Century Fox film *No Highway in the Sky*, based on Shute's novel. As before, I will be happy to hear of other examples.

**T-P016 Practical Application of Absorption Anisotropy Correction at Long Wavelengths.** K. Rajashankar, I. Kourinov, NE-CAT, Cornell Univ., Advanced Photon Source, Bldg. 436E, Argonne National Labs, Argonne, IL 60439.

Structure determination using weak anomalous scatterers like Sulfur usually requires data collected at longer wavelengths, typically higher than 1.5Å. Such experiments provide rather weak anomalous signal, hence very accurate data is essential to derive phase information. However, at longer wavelengths the anisotropic absorption effects introduce errors in the measurements. Correction for absorption anisotropy may be applied through empirical approach as proposed by Robert Blessing (Acta Cryst. A51, 1995, 33-38) and implemented in several data scaling software packages. However, there are no studies indicating the practical use of these procedures. We have carried out an extensive study on the use of absorption correction at longer wavelengths. It can be concluded that significant improvement in data quality can be achieved via application of empirical absorption corrections. In cases with high anisotropy in absorption, structure solution could be achieved only after application of the absorption corrections. In this presentation we will provide details of this study.

**T-P017 Metal Induced Alpha to Beta Transitions in Collagen Binding Domain.** Philominathan Sagaya Theresa Leena, Osamu Matsushita, Joshua Sakon, Dept. of Chemistry and Biochemistry, Univ. of Arkansas.

*Clostridium histolyticum* ColG collagenase activated by Ca<sup>2+</sup> is responsible for extensive tissue destruction, and the CBD is a seg-

ment of the multi-domain enzyme. Binding of two Ca<sup>2+</sup> on CBD is co-operative and is both enthalpically and entropically driven ( $K_{d1} = 2.13\mu\text{M}$ ;  $K_{d2} = 4.63\mu\text{M}$ ). Structures in the presence and absence of Ca<sup>2+</sup> have been solved at ultrahigh resolution (<1.2Å). N-terminus 14 residues of CBD adopt a  $\alpha$ -helical conformation however, addition of Ca<sup>2+</sup> unwinds the linker into a new  $\beta$ -strand. To rule out the crystal-packing artifact, NMR titration studies were done and it confirms the conformational structure change upon addition of Ca<sup>2+</sup>. The changes in Stokes and hydrodynamic radii as measured by size exclusion chromatography and dynamic light scattering experiments showed drastic transition upon Ca<sup>2+</sup> addition; however far UV-CD was not as sensitive. With Ca<sup>2+</sup> CBD becomes thermally stable ( $T_m > 90^\circ\text{C}$ ), less susceptible to proteolysis and stable against chemical denaturants. Different metals trigger different degree of transition and as mutation of metal chelating amino acids. Not only this study provide insights into the drastic structure change thought to accompany upon secretion of the enzyme but also to provide insights into amyloidosis.

**T-P018 Preliminary Protein Crystallization Using the Honeybee Crystallization Robot.** Milya Davlieva, Hamid Khoja, Anne Stone, Joseph Longtin, Ulrich Strych, Sanka Tennakoon, Kurt Krause, Biology and Biochemistry, Univ. of Houston, 4800 Calhoun, Houston, TX 77204.

Modern crystallization robots aim at widening the bottleneck of determining preliminary crystallization conditions in macromolecular structure determination. These machines claim to automate and accelerate the proven sparse-matrix approach employed in many laboratories. Here we present our experiences with the Honeybee crystallization robot (Genomic Solutions), enabling the rapid evaluation of proteins in sitting drop plates. We screened a total of 16 diverse proteins for crystallization with the robot:

Hen lysozyme, equine myoglobin, bovine ribonuclease A (RNAseA), hemoglobin and catalase, *Serratia marcescens* nuclease, two bacterial alanine racemases, five, yet uncharacterized streptococcal proteins, and three *Trichomonas vaginalis* ferredoxins. Ten of these proteins crystallized in at least one of the 96 conditions of the Hampton Research HR2-130 screen. Two proteins crystallized only when set up conventionally by hand, and four proteins (hemoglobin, myoglobin, one ferredoxin, one streptococcal protein) did not crystallize at all. Shape and size of the crystals obtained with the Honeybee robot were comparable to what was obtained through conventionally prepared sitting drop crystals.

**T-P019 Citrate-dependent and Heparan Sulfate-mediated Cell Surface Retention of Cobra Cardiotoxin.** C.-J. Chen<sup>a,c</sup>, H.-H. Guan<sup>a,b</sup>, S.-C. Lee<sup>b</sup>, W.-g. Wu<sup>b</sup>, <sup>a</sup>Life Science Group, National Synchrotron Radiation Research Center, <sup>b</sup>Inst. of Bioinformatics and Structural Biology, <sup>c</sup>Dept. of Physics, National TsingHua Univ., Hsinchu 300, Taiwan.

Cell surface retention of biologically active ligands through heparin or heparan sulfate (HS) binding plays an important role in certain disease states and cell development. Anionic citrate is a major component of venom but its role in toxicity remains puzzling. By immobilizing Chinese hamster ovary cells in microcapillary tubes and heparin on sensor chips, we showed that HS-mediated cell retention of the major cardiotoxin (CTX) from cobra, CTX A3, near membrane surfaces is citrate dependent. The CTX A3-heparin hexasaccharide complex structure with a bound citrate at 2.4 Å-resolution revealed a molecular model for toxin retention in which heparin induced conformational changes of CTX A3 lead to citrate-mediated dimerization. The results suggest a novel role for venom citrate in biological activity and reveal

a mechanism that explains cell retention of CTX A3 through HS-CTX interaction. The combined usage of the Surface Plasmon Resonance (SPR) method and the retention experiment in microcapillary provides the novel approach to address the dynamic features of the biological activities of protein-HS interaction that can not be acquired by crystallography alone.

Lee, S.-C. *et al. J. Biol. Chem.* **280**, 9567-9577, 2005

**T-P020 Effects of Mutations on a Pre-decarboxylation Reaction Intermediate Analogue-Pyruvate Dehydrogenase E1 Component Complex.** P. Arjunan<sup>1,2</sup>, K. Chandrasekhar<sup>1,2</sup>, N. Nemeria<sup>3</sup>, F. Jordan<sup>3</sup>, W. Furey<sup>1,2</sup>, <sup>1</sup>Biocrystallography Laboratory, VA Pittsburgh Healthcare System, University Dr. C, Pittsburgh, PA 15240, <sup>2</sup>Dept. of Pharmacology, Univ. of Pittsburgh, School of Medicine, Pittsburgh, PA 15261, <sup>3</sup>Dept. of Chemistry, Rutgers Univ., Newark, NJ 07102.

The thiamin diphosphate (ThDP) dependent E1 component of the pyruvate dehydrogenase multienzyme complex (PDHc) catalyzes the rate-limiting step of the overall PDHc reaction and subsequent acetyl transfer to a lipoyl-lysine residue from the E2 component. It therefore provides an ideal target for mechanistic structural investigation. In an effort to obtain structural information on the first ThDP-bound intermediate in the presence of the enzyme, we had previously reported the crystal structure of the reaction intermediate analogue  $\alpha$ -phosphonolactylthiamin diphosphate (PLThDP) in complex with the native E1. We have now studied the same complex with the active site variants H407A and E571A. While there are general similarities between the native and these two structures, there are significant differences in the active site. Regarding the PDHc specific reaction, the presence of PLThDP induces large-scale conformational changes in the enzyme. Comparison of these structures with catalytic activity will be presented.

**T-P021 The Implication of the Sequence of Disulfides Breaking in the Reductive Unfolding Pathways of Ribonuclease A.** Jun Wang, Igor Kourinov, Steve Ealick, NE-CAT, Cornell Univ., Ithaca, NY.

Time-resolved disulfides breaking of bovine pancreatic ribonuclease A (protein was from Dr. Scheraga group at Cornell) were observed by Fitscale, a novel data analysis method through a conventional single wavelength data collection. The study of the sequence of the disulfide bonds breaking from the native state and its mutants reveals that the disulfide bonds breaking due to X-ray irradiation is related to the disulfide bond unfolding pathways. The order of the disulfides breaking in native RNase A is consistent with the reductive unfolding pattern that the (40-95) and (65-72) disulfide bonds takes parallel reduction resulting from these two disulfide bonds have very similar accessibility to the solvent and more accessibility than the other two (58-110) and (26-84) disulfide bonds. By in silico mutation of the residue tyrosine (Y) 92 to glycine (G) and leucine (L), which tyrosine 92 is considered as a burial of the (40-95) disulfide bond to the solvent, the observation of the change of the sequence of the disulfide bonds breaking indicates the (40-95) disulfide is affected by the intramolecular interactions which demonstrated by its reduction unfolding pathway.

**T-P022 How a New Chemical Compatibility Test Facilitates Protein's Crystallization.** Jean-Pascal Viola\*, S. Tetreault, C. Houde, QIAGEN Canada Inc., Montreal, QC, Canada, Jean-Pascal.Viola@QIAGEN.com

In early stages of a macromolecule's crystallization, when little information is known about protein solubility versus various chemi-

cal, the selected strategy is to setup usual initial screens at protein concentration selected from past experience. Factors such as availability of protein or intrinsic protein physical properties can be used as guidelines, but again, they provide little help in selection of initial screens conditions.

During development of new optimization procedures and initial screens, we needed to find a new strategy which would address this question, and enable us to orient crystallization appropriately. Presented here is a new method to test a macromolecule's solubility against many chemicals which can be applied straightforwardly at experimental setup. Using this method, not only did we obtain a reasonable and necessary high level of precipitation in any selected initial screens, but results from this test can also be applied directly to optimization strategies like "Pro-Active" or "The Optimizer Series" presented earlier.

This strategy was applied to a series of 10 proteins where solubility was tested against a series of salts, polymers, organics and buffers. From results obtained, initial screens and optimization methods were selected. This preliminary solubility evaluation, performed prior to crystallization setup, benefited not only initial screening results but also accelerated optimization process, using less protein compare to the classical optimization method.

**T-P023 Accurate Single Crystal X-ray Charge Density Quality Data Collected at ChemMatCARS, Advanced Photon Source (APS).** Yu-Sheng Chen<sup>1</sup>, T. Graber<sup>1</sup>, P.J. Viccaro<sup>1</sup>, Rasmus Poulsen<sup>2</sup>, Henrik Clausen<sup>2</sup> and Bo Iversen<sup>2</sup>, <sup>1</sup>Center for Advanced Radiation Source (CARS), Univ. of Chicago, Argonne, IL 60439, <sup>2</sup>Dept. of Chemistry & Interdisciplinary Nanoscience Center (iNANO) Univ. of Aarhus, DK-8000 Århus C, Denmark.

Accurate X-ray charge density studies have been collected for single crystal metal-organic framework (MOF, M= Zn and Co) samples with dimensions less than 50  $\mu\text{m}$  crystals at low temperature (below 20K) using single crystal X-ray diffraction experiment at ChemMatCARS at the Advanced Photon Source (APS). The high accuracy charge density data were collected using a Bruker 6000 CCD detector, mounted on a HUBER 5020 diffractometer with Pinkerton's type open flow Helium Cyro-system. 30 keV were used for photon energy (wavelength  $\lambda = 0.41325\text{\AA}$ ). The detector settings were  $2\theta = 30^\circ$  and 1 second exposure time using  $0.3^\circ$  phi scans per frame. 2200 and 3200 total frames were collected for each crystal; M=Zn and Co respectively. One data collection was finished within 8 hours. The frames were integrated using SAINT, the oblique correction has been corrected by Oblique software and the data were sorted, averaged, merged and corrected for absorption using the SORTAV program. The  $R_{\text{int}} = 0.0583$  and 0.0562 for M = Zn and Co respectively. The statistical tables from the SORTAV will be presented and the selected deformation and Laplacian maps as well.

**T-P024 Novel Cell-free Expression System for Synthesis of Proteins Used in Structural Analyses.** Jean-Pascal Viola, Uritza von Groll\*, Annette Zacharias\*, Steve Tetreault†, Christian Houde†, Frank Schäfer\*, QIAGEN Research & Development, †QIAGEN Canada Inc., Montreal, QC, Canada, \*QIAGEN GmbH, Hilden, Germany.

A structural genomics project is a multidisciplinary process including several working steps. On of the most time-consuming steps is expression of labeled protein in amounts sufficient for structural analysis by either X-ray crystallography or NMR.

The dramatic reduction in the time required to obtain proteins of interest makes cell-free expression systems an attractive alternative

to conventional methods. Moreover, they do not require specialized equipment, use simple procedures, and offer the ability to express proteins that may be poorly expressed in in vivo systems. By employing large-scale reactions and adding an affinity tag to the expression construct, sufficient Se-Met or SI-labeled protein for a thorough structural determination can be synthesized and purified to homogeneity in a single working day.

We present a new technology, which following a small-scale construct evaluation step, can be used for expression of milligram amounts of functional proteins in a 2 hour procedure, and demonstrate its application to X-ray crystallography and NMR structural analysis of several prokaryotic and human proteins.

**T-P025 Upgrade of NSLS X25 Macromolecular Crystallography Beamline.** L.E. Berman<sup>1</sup>, J. Skaritka<sup>1</sup>, T. Tanabe<sup>1</sup>, G. Rakowsky<sup>1</sup>, D. Harder<sup>1</sup>, S. Ramamoorthy<sup>1</sup>, E. Zitvogel<sup>1</sup>, I. Pinayev<sup>1</sup>, T. Shaftan<sup>1</sup>, P. Montanez<sup>1</sup>, A. Lenhard<sup>1</sup>, S. LaMarra<sup>1</sup>, S. Hulbert<sup>1</sup>, D. Lynch<sup>1</sup>, M. Becker<sup>2</sup>, W. Nolan<sup>2</sup>, A. Saxena<sup>2</sup>, D. Schneider<sup>2</sup>, R. Sweet<sup>2</sup>, G. Rosenbaum<sup>3</sup>, <sup>1</sup>NSLS, <sup>2</sup>Biology Dept, BNL, Upton, NY 11973, <sup>3</sup>ANL, Argonne, IL 60439.

The radiation source, optics, and experimental station of the NSLS X25 beam line are being improved to optimize for macromolecular crystallography. We established a plan that would increase the intensity and quality of the X-ray beam delivered to the specimen, and improve the experimental sensitivity, especially for small crystals (~10 μm size). This is being done through the replacement of the original wiggler source by an in-vacuum small-gap undulator. This new source is 15 times brighter than the original one at 6.3 keV, and 6 times brighter at 10.5 keV. Upgrades to the beamline optics are also being pursued that will exploit the new source's properties. For the monochromator, we will implement cryogenic cooling of the first crystal and sagittal bending of the second crystal to permit horizontal focusing. A new bendable mirror, to permit vertical focusing, will be installed just after. Finally, the diffractometer in the station is being upgraded, in part to accommodate the use of a microfocusing optical element in the beam path just before the sample.

Sponsors: DOE, OBER and OBES; and NIH, NCR

**T-P026 Structure of a Ubiquitin Specific Protease 8 (USP8) - E3 Ligase Nrdp1 Complex.** J. R. Walker, G. Avvakumov, S. Xue, F. Mackenzie, E. M. Newman, S. Dhe-Paganon, Structural Genomics Consortium and Dept. of Physiology, Univ. of Toronto, 100 College St., Toronto, ON M5G 1L5, Canada.

The RING finger E3 ligase Nrdp1 catalyses the ubiquitination and degradation of members of the family of epidermal growth factor receptors, the antiapoptotic protein BRUCE, and the E3 ligase parkin. Nrdp1 auto-ubiquitination contributes to its own degradation by the proteasomal system, but this activity is countered by the association of Nrdp1 with the deubiquitylase ubiquitin specific protease 8 (USP8). USP8 contains multiple domains, including a catalytic domain, two coiled-coil domains, and a rhodanese domain. We report the high resolution crystal structure of the USP8 rhodanese domain in complex with the Nrdp1 C-terminal domain, which we have named the USP8 interaction domain. The Nrdp1 USP8 interaction domain forms a novel protein fold, and interacts with a conserved peptide loop of the rhodanese domain. The consensus sequence of this peptide loop is found in other Nrdp1 targets such as BRUCE and ErbB4, suggesting a common method of interaction. We have also determined the crystal structure of a coiled-coil domain of USP8, which contributes to USP8 dimerization and may play a role in the ability of Nrdp1 to interact with dimerized receptor molecules.

**T-P027 Cryogenic Automounters at the NSLS Facilitate Efficient Use of Undulator Beam Lines for Macromolecular Crystallography.** A.M. Saxena, D.K. Schneider, A. Soares, H. Robinson, M. Carlucci-Dayton, J. Skinner, R. Buono, G. Shea-McCarthy, W. Nolan, R. M Sweet, Biology Dept., Brookhaven National Laboratory, Upton, NY 11973.

Cryogenic automounters, in combination with semi-automated data collection software, greatly enhance the efficiency of screening the crystals of macromolecular assemblies to identify the best specimens for final data collection. This time consuming search is carried out at bending magnet beam lines of the Macromolecular Crystallography Research Resource at the NSLS (PXRR) where the automounter can collect data for a few frames and index them to determine their characteristics in a few minutes. The screening procedure then supplies the crystals for final data collection on a high intensity insertion device beamline, such as X29, where a window of a few hours is provided each day to collect high resolution data on such crystals that show promise of yielding the structure. This report summarizes key elements of the PXRR automounter program, including design features of our ALS type robots, its attendant software components, integrated scheduling methods, staff support commitments, and development plans.

This work is supported by the NCR of the National Institutes of Health, and the Office of Biological and Environmental Research of the US Department of Energy.

**T-P028 Structure of a General Anesthetic Binding Site on PKC.** S. Shanmugasundararaj, J. Das, K.W. Miller, Dept. of Anesthesia, MGH, Boston, MA, 02114.

Anesthetics are relatively nonspecific drugs that interact with many transmembrane ion channels and soluble proteins, often causing unwanted side effects. Gaining a detailed understanding of the structural motifs governing anesthetic-protein interactions is a critical step in elucidating the molecular mechanisms underlying general anesthesia. General anesthetics modulate phorbol ester binding and are therefore hypothesized to interact with the cysteine-rich diacylglycerol/phorbol ester-binding domain, C1 of protein kinase C, a tandem repeat of C1A and C1B subdomains. We have solved the crystal structure of the high affinity phorbol-binding subdomain, C1B of mouse PKC in the absence and presence of anesthetics and studied its interaction with general anesthetic alcohols. The cell parameters are a=43.715; b=32.597; c=49.719Å and β=94.2°. There is an anesthetic-binding pocket that is bounded by (Tyr-236, Asn-237, Tyr-238, Met-239 and Ser-240). This pocket is separated from the phorbol-binding pocket by a single strand of residues that include Met-239 and Ser-240. Mutations in this pocket designed to ablate or enhance general anesthetic binding would provide a powerful method for testing the hypothesis proposed above in cells and animals.

Supported by GM 69726 and the Department of Anesthesia and Critical Care.

**T-P029 Potential of an Energy Recovery Linac (ERL) X-ray Source for Structural Studies.** D. Szebenyi\*, CHESS, Cornell Univ., Ithaca, NY 14853 (\*for the LEPP/CHESS/MacCHESS development team.).

A new type of X-ray source using ERL technology is under development at Cornell (<http://erl.chess.cornell.edu>). A bright electron beam is produced using a DC photo cathode injector, accelerated to 5 GeV in a superconducting (SC) linac, passed once through a series of undulators to produce X-rays, and then dumped - with recovery of nearly all of the energy stored in the beam. A repetition rate of up to 1.3 GHz is possible. The resulting X-ray beams are small, round, very brilliant

and highly coherent. All standard crystallography experiments can be done at the ERL source, as well as frontier X-ray experiments which are difficult or impossible at current synchrotron sources. These include phase contrast imaging on the nanometer scale, time-resolved studies using 100 femtosecond pulses, and 3D structures of non-periodic specimens at near atomic resolution. A prototype electron injector, first SC accelerating cavity, and beam dump are under construction with an \$18M award from the National Science Foundation, and planning for the 5 GeV machine is well underway. Input from potential users is being sought; much has already been obtained through a June 2006 series of workshops on the scientific potential of the ERL.

**T-P030 Structural Insights into the Evolution of Drug Resistance in HIV-1 Protease.** H. Heaslet\*, V. Kutilek, G. Morris\*, Y.-C. Lin\*, J.H. Elder\*, B.E. Torbett, C.D. Stout\*, \*Dept. of Mol. Biol., Dept. of Mol. & Exp. Med., The Scripps Research Inst., La Jolla, CA.

The development of resistance to anti-retroviral drugs targeted against HIV is an increasing clinical problem in the treatment of HIV-1-infected individuals. Many patients develop drug resistant strains of the virus after treatment with inhibitor cocktails (HAART therapy), which include multiple protease inhibitors. Therefore, it is imperative that we understand the mechanisms by which the viral proteins, in particular HIV-1 protease, develop resistance. We have determined the three-dimensional structure of HIV-1 protease NL4-3 in complex with the potent protease inhibitor TL-3 at 2.0Å resolution. We have also obtained the crystal structures of three mutant forms of NL4-3 protease containing one (V82A), three (V82A, M46I, F53L) and six (V82A, M46I, F53L, V77I, L24I, L63P) point mutations in complex with TL-3. The three protease mutants arose sequentially under *ex vivo* selective pressure in the presence of TL-3, and exhibit 4-, 11-, and 30-fold resistance to TL-3 respectively. This series of protease crystal structures offers insights into the biochemical and structural mechanisms by which the enzyme can overcome inhibition by TL-3 while recovering some of its native catalytic activity.

Heaslet, H., Kutilek, V., Morris, G., Lin, Y.-C., Elder, J.H., Torbett, B.E. & Stout, C.D., Structural Insights into the Mechanisms of Drug Resistance in HIV-1 Protease NL4-3 (2006) *J. of Mol. Biol.*, In press.

**T-P031 Development of a Real Time Timing-shutter Performance Monitor for Protein Crystallography.** R.W. Alkire<sup>a</sup>, Michael Molitsky<sup>a</sup>, F.J. Rotella<sup>a</sup>, N.E.C. Duke<sup>a</sup>, John Lee<sup>b</sup>, Tim Madden<sup>b</sup>, Patrick De Lurgio<sup>c</sup>, <sup>a</sup>Structural Biology Center, Biosciences Div., <sup>b</sup>Advanced Photon Source, <sup>c</sup>High Energy Physics Division, Argonne National Laboratory, Argonne, IL 60439.

One of the many instrument challenges facing protein crystallography synchrotron beamlines is the synchronization of fast sample rotation with shutter timing. In order to monitor shutter timing events and long-range shutter performance accurately, a timing shutter monitor has been developed. This monitor uses a photodiode to capture x-ray-induced fluorescence from the shutter blade. When synchronized with goniometer and shutter timing signals, opening and closing shutter delay times can be measured, along with the total x-ray exposure time for each data frame. Data are measured using a National Instruments counter/timer card and output is displayed on a Windows-based computer via a Visual Basic interface. Each shutter cycle is time stamped and output is written to a log file. Performance data using this device on bending magnet beamline 19BM at the Advanced Photon Source will be presented, along with details outlining future improvements.

This work was supported by the U. S. Department of Energy, Office of Biological and Environmental Research and Office of Basic Energy Sciences, under Contract W-31-109-ENG-38.

**T-P032 Structures of Human  $\alpha$ -Phosphomannomutase 1 Reveal the Basis of Glycoprotein Syndrome Type 1a.** Nicholas R. Silvaggi<sup>1</sup>, Debra Dunaway-Mariano<sup>2</sup>, Karen N. Allen<sup>1</sup>, <sup>1</sup>Boston Univ. School of Medicine, Boston MA 02118; <sup>2</sup>Univ. of New Mexico, Albuquerque, NM 87131.

Carbohydrate-deficient glycoprotein syndrome type 1a, a congenital disease characterized by severe nervous system defects, is caused by mutations in  $\alpha$ -phosphomannomutase ( $\alpha$ PMM).  $\alpha$ PMM (there are two isozymes,  $\alpha$ PMM1 and 2) catalyzes the conversion of D-mannose 6-phosphate to  $\alpha$ -D-mannose 1-phosphate (M1P), a critical substrate in glycoprotein synthesis. The structure of human  $\alpha$ PMM1 (29.7kDa) was determined alone and bound to M1P.  $\alpha$ PMM1 crystallized in space group  $P4_32_12$  with unit-cell dimensions  $a=51.7\text{\AA}$  and  $c=216.0\text{\AA}$ . Surprisingly, molecular replacement using the structure of  $\alpha$ PMM2 failed, despite 65% identity between the isozymes. Ultimately, the structure was determined to 2.1Å resolution ( $R_{\text{cryst}}=0.191$ ,  $R_{\text{free}}=0.206$ ) using a three-wavelength SeMet MAD data set collected at NSLS beamline X12C. This structure was used to phase the 1.8Å structure of the  $\alpha$ -PMM1:M1P complex ( $R_{\text{cryst}}=0.205$ ,  $R_{\text{free}}=0.241$ ). The  $\alpha$ -PMM1:M1P structure represents a collision complex, the first encounter of enzyme and substrate, and not the Michaelis complex. The substrate binds first to a cap domain and then is swept into the active site upon cap closure. Mapping the mutations onto the structure allows them to be classified as affecting substrate binding and catalysis, dimerization, or protein stability, with the most severe mutations falling into the first class.

**T-P033 BioCARS: A Facility for Macromolecular Crystallography at the Advanced Photon Source.** R.W. Henning, V. Srajer, R. Pahl, T. Graber, S. Anderson, S. Ruan, G. Macha, J. VonOsinski, M. Bolbat, H. Brewer, N. Lei, H. Tong, K. Moffat, Consortium for Advanced Radiation Sources, The Univ. of Chicago, Chicago, IL.

The BioCARS facility is a part of the multi-disciplinary and multi-institutional Consortium for Advanced Radiation Sources (CARS) managed by the University of Chicago. CARS has designed, constructed and operates the experimental facilities at the Advanced Photon Source (APS) as National Synchrotron Resources available to the scientific community. BioCARS consists of two beamlines: an insertion device beamline 14-ID with an undulator and one experimental station (14-ID-B), and a bending magnet beamline 14-BM with two stations that are used simultaneously (14-BM-C and 14-BM-D). BioCARS provides state-of-the-art facilities and scientific and technical support for: studies of macromolecular assemblies that form crystals with large unit cells, MAD phasing, high resolution crystallography, Laue crystallography and time-resolved crystallography. BioCARS is also the only facility at the APS that has been approved for safe work on Biosafety Level 3 samples such as pathogenic human viruses.

Beamtime is allocated through peer review of proposals. To apply for beamtime or for more information about the BioCARS facility, visit: <http://biocars.org>.

**T-P034 Crystal Structure of the Platelet Integrin GPIIb/IIIa: A Target for Allo-, Auto-, and Drug-dependent Antibodies Associated with Immune Thrombocytopenia.** Tsan Xiao<sup>1</sup>, Bing-Hao Luo<sup>2</sup>, Timothy A. Springer<sup>2</sup>, <sup>1</sup>Laboratory of Immunology, National Institute of Allergy and Infectious Diseases, National Institutes of Health, 4 Center Dr., Bldg.4, Bethesda, MD 20892, <sup>2</sup>The CBR Inst. for Biomedical Research, Dept. of Pathology, Harvard Medical School, 200 Longwood Ave., Boston, MA 02115.

The complete ectodomain of the platelet integrin GPIIb/IIIa or  $\alpha$ IIb $\beta$ 3

is crystallized under physiological dication conditions and the structure is determined at 2.8 Å resolution. There are two  $\alpha$ IIb $\beta$ 3 molecules per asymmetric unit, and the overall structure of  $\alpha$ IIb $\beta$ 3 is in the bent conformation. The overall shape of the crystal structure resembles the EM images, suggesting that the conformation is representative of its structure in the aqueous solution. Three metal ions are present in the ligand binding  $\beta$  I domain, with a magnesium at the Metal-Ion Dependent Adhesion Site (MIDAS), and two calcium ions at the Adjacent to MIDAS (ADMIDAS) and Ligand-Induced Metal Binding Site (LIMBS), respectively. All of the domains in the  $\beta$ 3 leg region are resolved in the crystal structure, with an acute bent angle between domains I-EGF1 and I-EGF2, suggesting that the single connecting residue Glu472 serves an important role in integrin activation and extension.

**T-P035 Time-resolved Crystallography and Optical Studies of Single Crystals at BioCARS: Present Capabilities and Future Directions.** R. Pahl, V. Srajer, K. Moffat, Consortium for Advanced Radiation Sources, The Univ. of Chicago, Chicago.

Time-resolved crystallography is a unique technique for determining the structures of intermediates and excited states in biomolecular and chemical reactions. Using the Laue X-ray diffraction technique at the high-brilliance third-generation X-ray sources (ESRF, APS, SPring-8, etc.) snapshots are taken of molecules in action with a time resolution of about 100ps, the typical duration of a single X-ray pulse at synchrotron sources. We present the status of the user facility for time-resolved studies at BioCARS, an NIH/NCRR funded Synchrotron Structural Biology Resource at the Advanced Photon Source. During the past years a continuously growing time-resolved user community has developed; projects under investigation include light and chemically triggered reaction mechanism. Results from most recent studies of photo-sensitive proteins will be discussed. An overview will also be given on the current efforts in enhancing the technical capabilities for time-resolved diffraction experiments and spectrophotometry at BioCARS. The technical upgrades will improve resources for complementary optical monitoring of reactions in crystals, update the laser systems, and most importantly improve the X-ray optics to enable single xXray pulse experiments.

**T-P036 Crystal Structure of the C-terminal RNase III Domain of Human Dicer.** D. Takeshita<sup>1</sup>, S. Zenno<sup>2</sup>, W. C. Lee<sup>1</sup>, K. Nagata<sup>1</sup>, K. Saigo<sup>2</sup>, M. Tanokura<sup>1</sup>, <sup>1</sup>Dept. of Applied Biological Chemistry, Graduate School of Agricultural and Life Sciences, The Univ. of Tokyo, Tokyo, Japan, <sup>2</sup>Dept. of Biophysics and Biochemistry, Graduate School of Science, The Univ. of Tokyo, Tokyo, Japan.

In many eukaryotes, small RNAs trigger gene silencing in a sequence-specific manner. The Dicer protein is responsible for the production of small RNAs including short interfering RNAs (siRNAs) and microRNAs (miRNAs). The C-terminal RNase III domain (RNase IIIb) of human Dicer has been expressed, purified and crystallized. X-ray diffraction data have been collected to 2.0 Å resolution. The structure of the RNase IIIb domain was solved by molecular replacement using the program MOLREP, and refined to  $R$ -factor of 0.211 ( $R_{free}$  of 0.234). The asymmetric unit contained three molecules (molecules A, B, and C) of the RNase IIIb domain. The three molecules formed homodimers. One homodimer was formed between molecules A and C, and another homodimer was formed between molecules B and B'. These homodimers contained four magnesium ions in the active sites.

**T-P037 Automated Data Collection at the IMCA-CAT Advanced Photon Source User Facility.** A. Mulichak, K.P. Bataille, J.L. Muir, L.J. Keefe, Sector 17, Advanced Photon Source, Argonne National Laboratory, Argonne, IL 60439.

The Industrial Macromolecular Crystallography Association Collaborative Access Team (IMCA-CAT) operates a data collection facility for protein crystallography at Sector 17 of the Advanced Photon Source. Equipped with a Rigaku ACTOR robot, the IMCA-CAT insertion device beamline has offered automated sample mounting for routine use since 2004. Automated mounting, centering, and retrieval of protein samples enable high-throughput sample screening and unattended data acquisition, significantly reducing the time necessary for crystal screening and the need for direct operator interaction. The ACTOR system has also greatly facilitated the use of a mail-in data collection option for IMCA members. Recent upgrades of hardware and software, including a second system with higher storage capacity now installed at the bending magnet beamline, continue to expand the role of robotics at IMCA-CAT.

While targeting the needs of drug discovery research, the automation capabilities at IMCA-CAT are also ideally suited for structural genomics and other research efforts requiring high-throughput experiments. IMCA-CAT facilities are available to interested researchers through the APS General User Program.

**T-P038 Crystallographic Studies of Phosphoenolpyruvate Carboxykinase.** Julien J.H. Cotelesage<sup>a</sup>, Louis T.J. Delbaere<sup>a</sup>, Hughes Goldie<sup>a</sup>, J. Gregory Zeikus<sup>b</sup>, <sup>a</sup>Dept. of Biochemistry, Univ. of Saskatchewan, <sup>b</sup>Dept. of Biochemistry and Molecular Biology, Michigan State Univ.

The K213S mutant of the enzyme phosphoenolpyruvate carboxykinase (PCK) from the bacterium *Escherichia coli* has been found to have the unusual kinetic property of being inhibited by divalent manganese. Normally ionic manganese enhances the activity of PCK. A 2.0 Å crystal structure of K213S complexed with ATP, Mg<sup>2+</sup>, Mn<sup>2+</sup> and substrate-analogue pyruvate might explain the inhibitory effect of Mn<sup>2+</sup>. The structure reveals that with the side chain of lysine at position 213 missing, pyruvate is able to take an alternate orientation when coordinating the manganese ion. If the substrate oxaloacetate is able to coordinate Mn<sup>2+</sup> differently as well, it may not be able to react, thus explaining the inhibitory effect of Mn<sup>2+</sup>.

A novel technique to put carbon dioxide in the active site of crystallized PCK has been designed. It is based on the techniques used to make heavy atom derivatives of crystals with xenon gas. PCK from *E. coli* and *Anaerobiospirillum succiniciproducens* have been crystallized under a pressurized atmosphere of carbon dioxide. The results of this experiment will be discussed.

**T-P039 GM/CA: An NIH-Funded Dual Canted Undulator Sector for Protein Crystallography at the APS.** W.W. Smith<sup>a</sup>, R.F. Fischetti<sup>a</sup>, J.L. Smith<sup>b</sup>, D. Yoder<sup>a</sup>, R. Benn<sup>a</sup>, S. Stepanov<sup>a</sup>, S. Xu<sup>a</sup>, A. Urakhchin<sup>a</sup>, O. Makarov<sup>a</sup>, S. Devarapalli<sup>a</sup>, S. Corcoran<sup>a</sup>, M. Becker<sup>a</sup>, R. Sanishvili<sup>a</sup>, <sup>a</sup>Biosciences Div., Argonne National Laboratory, Argonne, IL, <sup>b</sup>Life Sciences Inst., Univ. of Michigan, Ann Arbor, MI.

The National Institute of General Medical Sciences and National Cancer Institute have established the GM/CA-CAT at the Argonne National Laboratory to build and operate a national user facility for crystallographic structure determination of biological macromolecules at the APS. The scientific and technical goals of the CAT address problems at the cutting edge of structural biology research, as well as targeted programs of the sponsoring institutes in structural genomics

and structure-based drug design, with an emphasis on streamlined, efficient throughput for a variety of sample types, sizes and qualities.

We are completing construction of a facility at Sector 23 consisting of three beamlines; two on independently-tunable canted-undulator sources and one on a tunable bending magnet. The undulator lines are equipped with focusing mirrors and are capable of producing a focused beam 25 microns in the vertical by 60 microns in the horizontal at the sample or at the detector surface. The energy range of one undulator line spans 3.5 KeV to 35 KeV. Beamline controls have been developed based on EPICS, and Blu-Ice provides the user interface to the experiment. User experiments are now being carried out on the first undulator line. Commissioning of the second undulator beam line is in progress. Development of an automounter for all 3 beamlines is well under way. The results of our experiences with the first undulator line will be described.

GM/CA-CAT has been funded in whole or in part with Federal funds from the National Cancer Institute (Y1-CO-1020) and the National Institute of General Medical Science (Y1-GM-1104).

**T-P040 Structure of CHIP, a Novel Chaperone-associated Ubiquitin Ligase.** Z. Xu, K.I. Devlin, S. Misra, The Cleveland Clinic Foundation, Cleveland, OH 44195.

The ubiquitin ligase CHIP (C-terminal of Hsp70 Interacting Protein) was identified as a co-chaperone that links the heat shock protein Hsc/Hsp70 and Hsp90 to the ubiquitin-proteasome protein degradation system. To understand the mechanisms of CHIP function as a co-chaperone and an ubiquitin ligase, we crystallized and solved the structure of the helical linker domain and U-box domain of zebrafish CHIP (*DrCHIP-HU*). The structure of *DrCHIP-HU* shows a symmetric homodimer. The conformation of the helical linker domains and the relative positions of the helical and U-box domains differ substantially in *DrCHIP-HU* from those in a recently published structure of an asymmetric dimer of Mouse CHIP. In addition, we used an *in vitro* ubiquitylation assay and two-dimensional NMR spectroscopy to probe the interaction between CHIP and its cognate ubiquitin conjugating enzyme UbcH5b. We identified the interactions between two long loops of the CHIP U-box domain and an UbcH5b interface composed of helix 1 and the L7 loop that provide specificity of CHIP for this particular ubiquitin conjugating enzyme. Our results provide new insights both into conformational variability in the domain arrangement of CHIP, and into U-box-mediated recruitment of particular ubiquitin conjugating enzymes for the ubiquitylation of specific targets.

**T-P041 Testing the Compact Light Source: A Miniature Synchrotron Light Source for the Homelab.** Ronald D. Ruth, Jeffrey Rifkin, Rod Loewen, Lyncean Technologies, Inc.

Past research at Stanford Linear Accelerator Center has led to a new x-ray source concept, a miniature synchrotron light source.\* This research spawned a new corporation, Lyncean Technologies, which has recently completed development of the Compact Light Source (CLS). The CLS is a tunable, homelab x-ray source with up to three beamlines that can be used like the X-ray beamlines at the synchrotrons—but it is about 200 times smaller than a synchrotron light source. The compact size is achieved using a laser undulator and a miniature electron-beam storage ring. The photon flux on a sample will be comparable to the flux of highly productive synchrotron beamlines. In this presentation, we will first introduce the Compact Light Source and show how it can bring the quality, tunability and flux of a synchrotron beam line into an X-ray scientist's local laboratory. At Lyncean Technologies, Inc. we have recently completed the construction of a production prototype source with funding from the NIGMS Protein Structure Initiative. We

will finish the presentation showing details of our initial testing of the prototype CLS, X-ray optics and endstation.

\*Z.Huang and R.D.Ruth, "Laser-Electron Storage Ring", *Phys. Rev. Lett.*, **80**:976-979, 1998.

Supported by the National Institute of General Medical Sciences, the National Institutes of Health, R44 GM665011.

**T-P042 Some Strategies to Get the Best MAD/SAD Data from Synchrotron Beamlines.** Xiaoping Dai, Ian Wilson, The Scripps Research Inst., La Jolla, CA.

From the early days of MAD development, strategies to collect the best, most accurate and complete data have always been an important issue for in-house X-ray sources<sup>[1]</sup>, to first generation synchrotron beamlines<sup>[2]</sup>, and today for second and third generation synchrotron beamlines. I will present recent trials from our lab on how to achieve high quality data from MAD/SAD experiments. Radiation damage is the most serious problem, especially for the brighter beamlines. The damage to the crystal is non-uniform and also time and orientation dependent. So it is very hard to adequately correct the X-ray data. Other key factors to consider are absorption near the absorption edge, energy resolution/stability, as well as exposure time to obtain suitable counting statistics. It is important to note that the best strategy is only best for the individual crystal conditions, such as the size, unit cell and space group of the crystal, its sensitivity to radiation, and diffraction strength and resolution.

[1] Dai, X. (1995), Ph. D. Thesis, UCSD; Ryu, S.-E et al (1990), *Nature*, **348**, 419.

[2] Hendrickson, W.A. (1991), *Science*, **254**, 51.

**T-P043 High Throughput Protein Crystallography at the NIGMS East Coast Structural Biology Facility.** Anubhav Jain<sup>2</sup>, Jean Jakoncic<sup>1</sup>, Marc Allaire<sup>1</sup>, Alec Berntson<sup>2</sup>, Kun Qian<sup>1</sup>, Fabiano Yokaichiya<sup>1</sup>, Vivian Stojanoff<sup>1</sup>, <sup>1</sup>Brookhaven National Laboratory, Upton, NY, USA, <sup>2</sup>Cornell Univ., Ithaca, NY.

High-throughput protein crystallography using industrial automation techniques have reduced the time needed to conduct protein structure experiments at many facilities around the world. The X6A beamline at the National Synchrotron Light Source (NSLS) has been dedicated to studies concerned to bio-molecular crystallography and the developments of automation techniques to help the biological-, biochemical- and biophysics- communities to explore all aspects of structural biology. The facility serves experts and non-experts crystallographers from protein purification to structural determination coordinates. For high sample throughput an automated sample changer has been commissioned allowing quick sample screening and high throughput data collection. Key to the operation is a new package for precise protein crystal centering based on expert system codes. Sample screening is performed according to protocols and a sample database automatically uploaded at the time users schedule their beam time on a electronic calendar available to the User at the Facility website (<http://protein.nsls.bnl.gov>).

**T-P044 Structural Studies of MosA, a Dihydrodipicolinate Synthase from *Sinorhizobium meliloti*.** K.H. Nienaber<sup>1</sup>, C.P. Phenix<sup>2</sup>, D.R.J. Palmer<sup>2</sup>, L.T.J. Delbaere<sup>1</sup>, <sup>1</sup>Dept. of Biochemistry, <sup>2</sup>Dept. of Chemistry, Univ. of Saskatchewan, 107 Wiggins Rd., Saskatoon, SK, Canada, S7N 5E5.

*Sinorhizobium meliloti* L530 is a bacterium found in soil that forms a symbiotic relationship with legumes. MosA has been isolated from *S. meliloti* L530 and was initially identified as an O-methyltransferase. Investigation by Dr. David Palmer and his lab has revealed that

MosA was mischaracterized and actually acts as a dihydrodipicolinate synthase (DHDPS). MosA is of particular interest as it is a part of the lysine biosynthesis pathway in most plants and bacteria, and thus is a potential drug target. Previous crystallographic structures revealed the presence of pyruvate covalently bound to a lysine residue in a Schiff base form in the active site. New data are being collected on crystals of complexes of MosA with (S)-aspartate- $\beta$ -semialdehyde, 2-oxobutyrate, lysine and pyruvate, and 2,6-pyridinedicarboxylic acid bound, representing a substrate, substrate analog, inhibitor, and product analog respectively. It is expected these structures will add weight to the argument that MosA is a DHDPS, as well as providing a possible drug target for other more harmful bacterium.

**T-P045 NorthEastern Collaborative Access Team (NE-CAT) Beam Lines at the Advanced Photon Source.** Craig M. Ogata, Steven E. Ealick, Malcolm Capel, Igor Kourinov, Ed Lynch, K. Rajashankar, Narayanasami Sukumar, John P. Unik, Jun Wang, James Withrow, X. Yang, NE-CAT, Argonne, IL, Dept. of Chem. & Chemical Biology, Cornell Univ., Ithaca, NY.

The Northeastern Collaborative Access Team (NE-CAT) facility at the Advanced Photon Source will consist of four beamlines. Three of the beamlines will come off of a novel canted undulator source. The novel source consists of two undulators in a single straight section. A bend magnet beamline completes the set of four beamlines. At the present time, there are two operational beamlines, one of the undulator beamlines (24ID Phase I) and the bend magnet beamline 8BM. A third beamline using the second undulator is scheduled for commissioning this summer. This beamline will have the ability to cover the selenium edge and a single high energy remote position. The bend magnet beamline (8BM) has been open for general users since Oct of 2004, it routinely covers the energy range from 7 – 13.5 keV. The operational undulator beamline (24ID Phase I) will open to general users later this year, it covers a range from 5 – 25 keV.

NE-CAT is a consortium of scientists organized to develop a structural biology sector at the Advanced Photon Source (APS). This facility will be used to focus on NE-CAT research on structural studies involving technically challenging crystallographic projects. In order to meet these needs, an ALS robot for screening a large number of sample crystals is now being commissioned and a microfocussing diffractometer is scheduled for installation on the insertion device beamline in the near future.

Funding for NE-CAT is provided through grant P41 RR015301 from the National Center for Research Resources of the NIH and from the NE-CAT member institutions.

**T-P046 Structural Analysis of an *E. coli* Phosphoenolpyruvate Carboxykinase (PCK) Complex with Carbon Dioxide.** J. Puttick<sup>1</sup>, H. Goldie<sup>2</sup>, and L.T.J Delbaere<sup>1</sup>, Depts. of Biochemistry<sup>1</sup> and of Microbiology and Immunology<sup>2</sup>, Univ. of Saskatchewan, 107 Wiggins Rd., Saskatoon, SK, Canada, S7N 5E5.

Phosphoenolpyruvate carboxykinase (PCK) is a key enzyme involved in gluconeogenesis. During the reversible decarboxylation and phosphorylation reaction, a carbon dioxide molecule is released or bound. Until now, only two other crystallographic structures containing CO<sub>2</sub> have been published. In the active site of this PCK structure, one of the oxygen atoms is hydrogen bonded to a water molecule and the side chain of an arginine residue, while the other oxygen atom is hydrogen bonded to the hydroxyl group of a tyrosine residue and another water molecule. The common feature of the three CO<sub>2</sub>-bound protein structures is the interaction of one oxygen atom of CO<sub>2</sub> with a basic amino acid side chain of the protein.

**T-P047 A New Method for Flash Cooling Protein Crystals.** M. Warkentin, V. Berejnov, R.E. Thorne, Physics Dept., Cornell Univ., Ithaca NY.

Despite the enormous success of cryocrystallographic techniques, there has been surprisingly little understanding of the fundamental mechanisms relevant to their successful application. We show that conventional flash cooling methods provide relatively slow cooling, and that cooling rate is largely unaffected when sample volumes are reduced below 0.1 mm<sup>3</sup>. We then describe a new flash cooling method that yields much larger cooling rates, especially for the very small crystals that can be mounted without excess liquid using microfabricated holders<sup>[1]</sup>. Cryoprotectant concentrations required to prevent formation of crystalline ice are dramatically reduced, simplifying cryoprotectant screening protocols and reducing the chances of crystal damage. Crystal mosaicities are reduced, increasing the quality of the structural information that is obtained.

This work was funded by the National Institute of Health (R01 GM65981).

[1] R. E. Thorne et al., *J. Appl. Cryst.* **36** (2003) 1455-1460.

**T-P048 The Crystal Structure of Cytochrome P460 from *N. europaea* Reveals a Novel Cytochrome Fold and Cross-linked Heme.** A.R. Pearson<sup>1</sup>, B.O. Elmore<sup>1</sup>, C. Yang<sup>2</sup>, A.B. Hooper<sup>1</sup>, C.M. Wilmot<sup>1</sup>, <sup>1</sup>Univ. of Minnesota, Minneapolis, MN, <sup>2</sup>RigakuMSC Inc., The Woodlands, TX.

Heme P460 is unusual among *c*-type hemes in that it contains three covalent links to a protein scaffold. Two are to thioethers from cysteines in the CXXCH motif, common to all *c*-type hemes; the third is between a protein sidechain and a *meso* carbon of the porphyrin ring.

Heme P460 has so far been identified and biochemically characterized in two proteins from *N. europaea*. In hydroxylamine oxidoreductase (HAO), a homo-trimer containing 21 *c*-hemes and 3 catalytic hemes P460, the additional crosslink involving a tyrosine sidechain has been confirmed by X-ray crystallography (Igarashi *et al.* [1997] *NSB* **4** 276-284).

We report the crystal structure of the second protein, cytochrome P460 (cytP460), a small 19 kDa mono-heme cytochrome, containing only a heme P460. The structure to 1.7 Å was determined by sulfur SAD using Cr K $\alpha$  X-radiation, revealing a novel *c*-type cytochrome fold which is predominantly  $\beta$ -sheet. The structure confirms biochemical analyses which indicated the third crosslink involves a conserved lysine residue, K70 (Arciero & Hooper [1997] *FEBS Lett.* **410** 457-460). In contrast to HAO, the crosslink is to the opposite *meso*-carbon of the porphyrin ring.

**T-P049 A State-of-the-Art Undulator Beamline for Time-Resolved Laue and Monochromatic Crystallography at BioCARS.** T. Graber\*, F. Westferro, M. Meron, P. J. Viccaro, R. W. Henning, V. Srajer, R. Pahl, S. Anderson, P. Anfinrud<sup>1</sup>, K. Moffat, Consortium for Advanced Radiation Sources, The Univ. of Chicago, Chicago, IL and <sup>1</sup>National Institutes of Health, Bethesda, MD, \*Corresponding author

BioCARS, a national facility for macromolecular and time-resolved x-ray crystallography located at the Advanced Photon Source, is in the process of upgrading their undulator beamline. Both monochromatic as well as highly focused pink-beam capabilities are being developed. A cryogenic Si (111) (Kohzu) monochromator with a variable offset of 15-25 mm and an energy range of 6-20 keV is presently being commissioned. Pink and monochromatic beam will be focused using a KB mirror pair (Oxford/SESO) with a vertical demagnification ratio of 5:1 and a horizontal demagnification of 8:1. Additionally, a dual in-line undulator configuration will be installed

with periods of 23 and 27 mm. These undulators are designed to give continuous first-harmonic coverage with a 6.8-20 keV energy range. The expected monochromatic flux is  $\sim 5 \times 10^{13}$  photons/sec into a 46 (V) by 75(H)  $\mu\text{m}^2$  focal spot. For time-resolved Laue experiments, the critical specification is the number of photons delivered to the sample from a single storage-ring electron pulse or bunch; this number is expected to be  $\sim 10^{10}$  photons.

To apply for beamtime or for more information about the Bio-CARS facility, visit: <http://biocars.org>.

**T-P050 Structural Basis for Inhibition of Translation by the Tumor Suppressor, Pdc4.** Nicole LaRonde-LeBlanc<sup>1</sup>, Arti Santhanam<sup>2</sup>, Nancy H. Colburn<sup>2</sup>, Alexander Wlodawer<sup>1</sup>, <sup>1</sup>Macromolecular Crystallography Laboratory and <sup>2</sup>Laboratory of Cancer Prevention, Center for Cancer Research, NCI, Frederick, MD 21702.

The tumor suppressor Programmed Cell Death 4 (*Pdc4*) inhibits the translation of mRNA with complex 5' untranslated regions through interactions with components of the translation initiation complex, eIF4F, in particular the RNA helicase eIF4A. These interactions occur through two MA3 domains in the Pdc4 molecule. We have determined the structure of the C-terminal MA3 domain of Pdc4 (cMA3) at 2.0 Å resolution. The crystals, which belong to space group P3<sub>1</sub>21 with 2 molecules per asymmetric unit, exhibit an unusual form of disorder. The final 2F<sub>o</sub>-F<sub>c</sub> electron density was excellent for molecule A, but considerably poorer for molecule B. Several scenarios were explored to explain this anomaly, but so far none was able to do so. Using the unquestionably correct structure of molecule A, we demonstrate that the cMA3 domain of Pdc4 shows remarkable structural similarity to an MA3 domain located near the C-terminus of eIF4G (eIF4Gc). We show that the cMA3 domain of Pdc4 competes with eIF4Gc for binding to eIF4A and that this MA3 domain alone is sufficient for inhibition of translation. This work provides a clear structural explanation for inhibition of eIF4A-mediated translation by Pdc4.

**T-P051 Next-Generation Automation for Biological Crystallography X-ray Data Collection.** Thomas Earnest, Carl Cork, Jim O'Neill, Physical Biosciences Div., Lawrence Berkeley National Laboratory, Berkeley CA 94720.

Automation of the structure determination process significantly benefits the structural biology community by increasing the overall speed and accuracy of data collection, and by providing the capability for the rapid screening of crystals to select those which will provide the best quality data. An automated crystal mounting and alignment system has been developed at Lawrence Berkeley National Laboratory and installed on three of the protein crystallography beamlines at the Advanced Light Source (ALS), and is currently being implemented at synchrotron crystallography beamlines at CHESS, NSLS, and the APS through a multi-institutional collaboration. There are several benefits to using an automounter system – i) optimization of the use of synchrotron beamtime, ii) facilitation of advanced data collection techniques, iii) collection of higher-quality data, iv) reduction of the risk to crystals during mounting, unmounting, and remounting, v) exploration of systematic studies of experimental protocols. Development of the next-generation automounter featuring a Cartesian geometry with three Adept motorized linear encoded stages, and smart cameras to enable a simple automated alignment procedure and state checking, is underway with improvements in robustness, simplicity of operation, and sample tracking.

Supported by National Institutes of Health / National Institute of General Medical Sciences R01 GM62648.

**T-P052 Mms2/Ubc13 with Covalently Bound Ubiquitin: Structural Basis of Linkage-specific Ubiquitin Chain Formation.** M.J. Eddins<sup>1</sup>, C.M. Carlile<sup>1</sup>, K.M. Gomez<sup>1</sup>, C.M. Pickart<sup>3</sup>, C. Wolberger<sup>1,2</sup>, <sup>1</sup>Dept. of Biophysics, Johns Hopkins School of Medicine, Baltimore, MD, <sup>2</sup>Howard Hughes Medical Inst., <sup>3</sup>Dept. of Biochemistry, Johns Hopkins Bloomberg School of Public Health, Baltimore, MD, <sup>4</sup>Claffin Univ., Orangeburg, SC.

The E2 ubiquitin conjugating enzyme Ubc13 in complex with the UEV protein Mms2 is involved in forming K63-linked polyubiquitin chains which are implicated in nonproteolytic signaling pathways. The Mms2/Ubc13 complex plays vital roles in DNA repair and the NF- $\kappa$ B pathway. We have determined the structure of the Mms2/Ubc13/ubiquitin complex by trapping the covalently linked donor ubiquitin to the active site residue of Ubc13. The complex shows the details of the active site of Ubc13 including the covalent link and specific interactions of the donor ubiquitin with the UEV/E2 complex. Crystal packing places an ubiquitin from one complex in the acceptor site of an adjacent complex placing K63 of the acceptor ubiquitin into the active site. Mutations that disrupt this acceptor site and confer UV sensitivity provide evidence that the ubiquitin in the crystal is in the acceptor site. Along with K63 of this acceptor ubiquitin making specific interactions with residues in the active site, this suggests a model for ubiquitin chain formation and substrate specificity.

**T-P054 Structure of GTP Dependent Phosphoenolpyruvate Carboxykinase (PCK) from *Corynebacterium glutamicum*.** Lata Prasad, Sanjukta Aich, Fumie Imabayashi, Louis Delbaere, Biochemistry, Univ. of Saskatchewan, 107 Wiggins Road, Saskatoon SK S7H 5J7, Canada.

Substrate free structure of GTP-dependent phosphoenolpyruvate carboxykinase (PCK) from gram positive bacterium *Corynebacterium glutamicum* has been solved from 2.1 Å resolution data. Initial phasing of the diffracted data has been obtained by PHASER program using 1KHF (human cytosolic PCK structure) as a starting model. It shows a P2 (1) symmetry with a=72.336, b=118.055, c=152.931,  $\beta$ = 96.443 and have 4 molecules in each asymmetric unit. PCK is one of the key enzymes in the gluconeogenesis process which controls the blood sugar level during fasting in mammals. All the eukaryotic mammalian PCKs are GTP-specific though eukaryotic archae species show mostly ATP specificities. Bacterial PCKs can be ATP-or GTP-specific but all plant PCKs are ATP-specific. Alignment of PCK enzymes shows that the ATP- and GTP- specific binding sites are somewhat conserved based on the nucleotide binding specificities with few exceptions which do not have any clear ATP- or GTP-specific binding sites. Phylogenetic studies have been performed to understand the evolutionary relationship of various PCKs from different sources. This research was funded by a CIHR grant to L.T.J.D.

**T-P055 The SIBYLS beamline (ALS 12.3.1) at the Advanced Light Source: A Valuable Resource for Both SAXS and Protein Crystallography.** Scott Classen, Greg Hura, Ken Frankel, Susan Tsutakawa, John Tainer, Lawrence Berkeley National Laboratory, Berkeley, CA.

Structural characterizations of large, conformationally-variable, multi-component, and radiation sensitive macromolecules are essential to understand many important cellular processes. However, such structural studies require flexible experimental systems to overcome problem-specific challenges. To meet these demands, the Structurally Integrated Biology for Life Sciences (SIBYLS) beamline at the Advanced Light Source (ALS) has been developed. This beamline

has been optimized to accommodate both the individual and the combined effectiveness of protein crystallography (PX) and small angle X-ray scattering (SAXS). The SIBYLS beamline has incorporated many useful features for maximizing the future adaptability of the beamline and individual endstations to the users experimental systems. SIBYLS has a unique dual double monochromator design with both Si(111) crystal and multilayer mirrors. A large, walk in, hut was chosen to accommodate developing technologies such as sample delivery systems required for high throughput SAXS and robotic crystal mounting technologies. The individual endstations have incorporated detectors optimized to their particular application, a MarCCD 165 detector for the SAXS endstation and an ADSC Quantum315 for the PX endstation.

**T-P056 Crystal Structure of a LDLR/RAP Complex: Insights into Ligand Binding and Intracellular Trafficking of the LDLR Family Proteins.** Natalia Beglova, Carl Fisher, Stephen C. Blacklow, Dept. of Pathology, Brigham and Women's Hospital, Harvard Medical School, Boston, MA 02115.

Proteins of the LDLR family bind a diverse range of ligands, yet the basis for ligand recognition is poorly understood. We solved the 1.3 Å X-ray structure of a complex between a two-module region of the ligand-binding domain of the LDLR and the third domain of RAP, an escort protein for LDLR family members. Each LA module combines four residues to create a virtually identical binding pocket for a lysine side-chain protruding from the second helix of RAP. All four LA residues that form the binding pocket participate in calcium coordination and, as a consequence, the relative positions of their side chains are constrained. This calcium-dependent mode of electrostatic recognition, together with avidity effects resulting from the use of multiple sites, represents a general binding strategy likely to apply in the binding of other basic ligands to LDLR family proteins. Complexes dissociate, when the pH drops below 6.5. Titration of histidine residues oriented toward the interior of the helical hairpin of RAP-D3 results in unfolding of the helix bundle and release of the receptor.

Data were collected at beamline X29A of the NSLS. This work was supported by the NIH RO1 to SCB and AHA SDG to NB.

**T-P057 Structural Basis of Human Hookworm - Host Interactions and Vaccine Development.** Oluwatoyin Asojo, Pathology and Microbiology Dept., Univ. of Nebraska Medical Ctr, Omaha, NE.

Human hookworm infection is a major cause of anemia and malnutrition of adults and children in the developing world. As part of ongoing efforts to control hookworm infection, The Human Hookworm Vaccine Initiative has identified candidate vaccine antigens from the infective L3 larval stages and adult stages of the parasite. The L3 larval stages including a family of pathogenesis related-1 (PR-1) proteins known as the ancylostoma secreted proteins (ASPs). A novel crystal structure of *Na*-ASP-2, a PR-1 protein secreted by L3 infective larvae of the human hookworm, *Necator americanus*, has been solved to resolution limits of 1.68 Å and to R factor 17% using the recombinant protein expressed in and secreted by *Pichia pastoris*. The overall fold of *Na*-ASP-2 is a 3 layer alpha-beta-alpha sandwich flanked by an N-terminal loop and a short cysteine rich C-terminus.

Adult stage antigens include the cytosolic glutathione-S-transferases (GSTs). Nematode GSTs facilitate the inactivation and degradation of a variety of electrophilic substrates (drugs) via the nucleophilic addition of reduced glutathione. Parasite GSTs also play significant roles in multi-drug resistance and the modulation of host-immune defense mechanisms. In an effort to clarify the structural basis of the failure of hookworm chemotherapy, we have recently solved the

structures of two major GSTs, *Na*GST-1 and *Na*GST-2 from *Necator americanus*, to the resolution limits of 2.2 Å and 1.8 Å (respectively) using recombinant protein expressed in and secreted by *Pichia pastoris*. The structures are complexes with glutathione usurped during the fermentation process. *Na*-GST-1 has typical GST fold and dimer. The *Na*-GST-1 structure reveals a novel binding cavity for glutathione. This mode of binding is unique and different from all previously observed structures as typified by *Na*-GST-2.

**T-P058 Crystal Structure of Mouse Nicotinamide Phosphoribosyltransferase.** Tao Wang, Xiangbin Zhang, Cynthia Wolberger, Dept. of Biophysics and Biophysical Chemistry, Howard Hughes Medical Inst. and Johns Hopkins Univ. School of Medicine, 725 N Wolfe St, Baltimore, MD 21205.

Mammalian nicotinamide phosphoribosyltransferase (Namp) catalyzes the reaction of nicotinamide + PRPP → NMN + PPi. Recent studies have showed this reaction is the rate-limiting reaction in NAD biosynthesis pathway in the mammalian systems. We report the crystal structure of a mouse Namp apoenzyme at 1.94 Å resolution and the crystal structure of Namp complexed with NMN at 2.1 Å resolution. The overall folding of Namp structures reveals that Namp belongs to TYPE II phosphoribosyltransferases. The folding of Namp structures resembles the folding of nicotinic acid phosphoribosyltransferase (NaPRTase) from thermoplasma acidophilum rather than the folding of NaPRTase from yeast. Namp forms a dimer in the crystals. NMN is located at the intensive dimeric interface. While the nicotinamide ring of NMN faces the inside of the active site pocket, the phosphate moiety of NMN is located at the entrance of the active site pocket. An aspartic acid, absent in the active site pockets in the structures of nicotinic acid phosphoribosyltransferases, H-bonds to nicotinamide moiety of NMN and thus recognizes nicotinamide but not nicotinic acid specifically.

**T-P059 Unusual Features of a Rare V $\lambda_x$  Antibody Fab Fragment that Neutralizes the Ebola Virus.** Jeffrey E. Lee<sup>1</sup>, Mary Kate Hart<sup>2</sup>, Erica Ollmann Saphire<sup>1</sup>, <sup>1</sup>The Scripps Research Inst., La Jolla, CA; <sup>2</sup>USAMRIID, Fort Detrick, Frederick, MD.

13F6-1-2 is a murine monoclonal antibody that recognizes the heavily glycosylated mucin-like domain of the virion-attached glycoprotein (GP) and protects animals against lethal viral challenge [Wilson, *et al* (2000) *Science* 287 1664-6.]. 13F6-1-2 was sequenced and its Fab fragment crystallized in complex with its Ebola virus GP peptide epitope and structure determined to 2.0 Å resolution. 13F6-1-2 utilizes a rare V $\lambda_x$  light chain. Surprisingly, the 3 CDR light chain loops do not adopt any of the canonical conformations and represent a new class of structures. The peptide binds in an extended conformation, anchored primarily by interactions to the heavy chain. The light chain makes 4 H-bonds to the peptide, but interestingly, all contacts are mediated through germline-encoded residues. Two GP residues, Gln406 and Arg409, make extensive side chain H-bond and electrostatic interactions to the antibody and are likely critical for recognition and affinity. The 13F6-1-2 V $\lambda_x$  light chain shares strong sequence identity to human V $\lambda$  subgroup VIII, thus providing a framework for humanization. This first structure of a V $\lambda_x$  light chain and Ebola virus neutralizing antibody is an exciting step towards the development of a therapeutic antibody.

**T-P060 Crystal Structures of ColE7 in Complex DNA/ $Zn^{2+}$  and Im7/ $Ni^{2+}$  Show How a Transition Metal Ion Bound ColE7 Binds and Cleaves DNA.** L.G. Doudeva<sup>1</sup>, H. Huang, Z. Shi<sup>1</sup>, C.-L. Li<sup>1</sup>, W.-C. Chu<sup>2</sup>, H.S. Yuan<sup>1</sup>, <sup>1</sup>Inst. of Molecular Biology, Academia Sinica, Taipei, Taiwan, ROC, <sup>2</sup>Inst. of Biomedical Engineering, National Yang Ming Univ., Taiwan, ROC.

The nuclease domain of ColE7 (N-ColE7) contains an H-N-H motif which folds in a metal finger topology. Here we report the crystal structures of a  $Zn^{2+}$ -bound N-ColE7 (H545E mutant) in complex with a 12-bp duplex DNA (5'-CGGGATATCCCG-3') and a  $Ni^{2+}$ -bound N-ColE7 in complex with the inhibitor Im7 at a resolution of 2.5 Å and 2.0 Å, respectively. Metal-dependent cleavage assays and site-directed mutagenesis showed that N-ColE7 cleaves double-stranded DNA with a single metal ion cofactor,  $Ni^{2+}$ ,  $Mg^{2+}$ ,  $Mn^{2+}$  and  $Zn^{2+}$ . In the crystal structure of N-ColE7-DNA complex, the zinc ion is directly coordinated to three histidines and the DNA scissile phosphate in a tetrahedral geometry. In contrast,  $Ni^{2+}$  is bound in N-ColE7 in two different modes, to four ligands (three histidines and one phosphate ion), or to five ligands with an additional water molecule. These data suggest that the divalent metal ion in the His-metal finger motif can be coordinated to six ligands, such as  $Mg^{2+}$  in I-PpoI, *Serratia* nuclease and Vvn, five ligands or four ligands, such as  $Ni^{2+}$  or  $Zn^{2+}$  in ColE7. Universally, the metal ion in the His-metal finger motif is bound to the DNA scissile phosphate and serves three roles during hydrolysis: polarization of the P-O bond for nucleophilic attack, stabilization of the phosphoanion transition state and stabilization of the cleaved product.

**T-P061 Alternative Intermolecular Contacts of the VP5\* Antigen Domain Underlie the Two- to Three-fold Reorganization of the Rotavirus Spike Protein.** Joshua D. Yoder, Philip R. Dormitzer, Program in Virology, Harvard Medical School, and the Laboratory of Molecular Medicine, Children's Hospital, 320 Longwood Ave., Boston, MA 02115.

The rotavirus spike protein VP4 adopts at least 3 conformations during cell entry. VP4 is flexible prior to priming. After trypsin primes the virion by cleaving VP4 into VP5\* and VP8\*, portions of the spike protruding from the virion acquire a rigid conformation with approximate two-fold symmetry. The molecular envelope of the primed spike is known from cryo-EM image reconstructions of virions. Following an unknown triggering event, the protruding parts fold back and undergo a two- to three-fold rearrangement to a putative post membrane-interaction conformation. The VP5\* antigen domain, which contains key heterotypic neutralizing epitopes, is a potential vaccine candidate, and corresponds to the spike body. We have expressed this domain and determined its structure in two forms: a 1.6 Å dimer that fits the molecular envelope of the spike body and a 2.0 Å trimer. The structures reveal identical elements in alternative conformations allowing formation of dimers or trimers. The ability to associate as dimers and trimers underlies the VP5\* two- to three-fold organization.

**T-P062 Kinetic and Structural Properties of Inorganic Pyrophosphatase from *Helicobacter pylori*.** Y.-J. Sun, T.-C. Chao, J.-Y. Tsai, C.-Y. Huang, H. Huang, Inst. of Bioinformatics and Structural Biology National Tsing Hua Univ., Hsinchu 300, Taiwan, ROC.

Inorganic pyrophosphatase (PPase) catalyzes the hydrolysis of pyrophosphate (PPi) to orthophosphate (Pi) and controls the level of PPi in cells. PPase plays an essential role in energy conservation and provides the energy for many biosynthetic pathways. The *Helicobacter pylori* pyrophosphatase (HpPPase) gene was cloned, expressed, purified. The  $K_m$  and  $V_{max}$  of HpPPase were determined. The effects of

the inhibitors NaF, ATP, iminodiphosphate, and N-ethylmaleimide on HpPPase activity were evaluated. NaF showed the highest inhibition of the enzyme. Crystal structures of HpPPase and the PPI-HpPPase complex were determined. HpPPase comprises three  $\alpha$ -helices and nine  $\beta$ -strands and folds as a barrel structure. HpPPase forms a hexamer in both the solution and crystal states, and each monomer has its own PPI-binding site.

**T-P063 Structure Determination of Two Extracellular Ig-like Domains of Human Myeloid Cell Inhibitory Receptor Siglec-5.** M.A. Zhuravleva, P.D. Sun, National Inst. of Allergy and Infectious Diseases, NIH, Rockville, MD 20852.

Siglecs (sialic-acid Ig-like binding lectins) are a family of immunoglobulin lectins implicated in adhesive and signaling functions through recognition of glycans containing sialic acid. Siglec-5 is expressed on the cells of the innate immunity and exhibits biochemical features of inhibitory receptor. To understand the molecular basis for the sialic acid-dependent adhesion implemented by Siglecs and to get an insight into receptor specificity, structural studies have been carried out using two Ig-like N-terminal domains of Siglec-5. The crystal structure (Sp.Gr. R32,  $a=94.044\text{\AA}$ ,  $c=209.888\text{\AA}$ ) of such two-domain Siglec has been determined for the first time and is presented here. Structure solution using MR with phased translation function uncovered unparalleled features not seen in other one-domain structures of related Siglecs, including a unique interdomain disulfide bond between the V- and C2-set domains and an unusual conformation of variable loop C-C' of the ligand-binding domain. The latter is believed to be important in determining the binding specificities of Siglecs. The role of the interdomain disulfide in ligand recognition is investigated. The attempts to obtain a receptor-ligand complex using various sialylated oligosaccharides are underway.

**T-P064 Structural Basis for Sequence-dependent DNA Cleavage by the Non-Specific Endonuclease.** W. Yang, Y. Wang, L.G. Doudeva, C.-L. Li, H. S. Yuan, Inst. of Molecular Biology, Academia Sinica, Taipei, Taiwan, ROC.

Non-specific endonucleases hydrolyze DNA without sequence specificity but with sequence preference that they cleave at some sites more efficiently than others. However, the structural basis for sequence-dependent cleavage by the non-specific endonucleases remained elusive. Here we use the non-specific endonucleases ColE7 to dissect this problem. DNA foot printing assays showed that the nuclease domain of ColE7 (N-ColE7) cleaves DNA with a preference for making nicks after (at 3'O-side) thymine bases. The crystal structure of N-ColE7 (H545Q mutant) in complex with an 18-bp DNA was determined at a resolution of 2.8 Å. In the N-ColE7-DNA structure, a preferred thymine residue is located right before the scissile phosphate and the structure of this "preferred" complex was compared with the previously determined "non-preferred" complexes in which a guanine is located before the scissile phosphate. The structural comparison shows that the phosphate backbone in the "preferred" complex is distorted the most, leading to a shorter distance between the zinc ion and the scissile phosphate. This result suggests a general structural basis for the sequence-dependent DNA cleavage that the enzyme-induced DNA backbone conformational change is the local determinant for non-specific endonucleases to decide whether to cleave or not to cleave a DNA.

**T-P065 Structural Basis for Recognition of a Mutated Human Melanoma Antigen by an Anti-tumor T Cell Receptor.** Lu Deng<sup>a</sup>, Ries Langley<sup>a</sup>, Suzanne L. Topalian<sup>b</sup>, Roy Mariuzza<sup>a</sup>, <sup>a</sup>Center for Advanced Research in Biotechnology, Univ. of Maryland, Rockville, MD, <sup>b</sup>Surgery Branch, NCI, NIH, Bethesda, MD.

CD4<sup>+</sup> T cells play an important role in generating and maintaining immune responses against cancer. T cell receptor (TCR) E8, isolated from tumor-infiltrating CD4<sup>+</sup> T cells, recognizes a melanoma antigen restricted by the MHC class II molecule HLA-DR1. The mutated antigen is a peptide derived from the glycolytic enzyme triosephosphate isomerase (TPI<sub>23-37</sub>) with a single amino acid substitution (Thr28Ile). Here we present the crystal structures of TCR E8 in free form, and of the trimolecular complexes E8/wild type TPI<sub>23-37</sub>/HLA-DR1 and E8/mutant TPI<sub>23-37</sub>/HLA-DR1. The structures show substantial conformational changes for CDR3 $\alpha$  of E8 upon binding to peptide/MHC. E8 primarily recognizes the central to N-terminal portion of TPI<sub>23-37</sub> in contrast with both anti-microbial and alloreactive TCRs which focus on the peptide center, and autoimmune TCRs, which recognize the N-terminal peptide segment. This study provides the structural basis of the dramatically altered T cell stimulation capacities of the wild type and mutant TPI peptide, and offers insights into CD4<sup>+</sup> T cell responses to MHC class II-restricted tumor antigens in general.

This research is supported by NIH grant AI36900 to RAM.

**T-P066 Crystal Structures of the Biotin Protein Ligase and Biotin Carboxyl Carrier Protein from *Pyrococcus horikoshii* OT3: Stages of Biotin Activation and Biotinylation.** Bagautdin Bagautdinov, Naoki Kunishima, Advanced Protein Crystallography Research Group, RIKEN SPring-8 Center, Harima Inst., Kouto, Hyogo, Japan.

Biotin protein ligase (BPL) catalyses synthesis of an activated form of biotin, biotinyl-5'-AMP, from substrates biotin and ATP, and followed biotinylation of the biotin carboxyl carrier protein (BCCP) subunit of acetyl-CoA carboxylase. Here we present the crystal structures of BPL and BCCP from *Pyrococcus horikoshii* OT3. BPL structures liganded with biotin, ATP, ADP, ADP:biotin, biotinyl-5'-AMP, biotinyl-5'-AMP:Mg<sup>2+</sup>(Mn<sup>2+</sup>) as well as of the mutated K111G (K111A) BPL protein in apo- and in complexes with biotinyl-5'-AMP have been analyzed. The structures reveal the tight dimer through N-termini as the functional unit (Bagautdinov *et al. J. Mol. Biol.* **353**, 322). The catalytic requirement of the BPL active site is positioning of reactants and neutralization of their negative charges by K111, R48, R51, R233. At mutation of K111 to G(A) BPL produces biotinyl-5'-AMP, possibly due to the neutralization of the reactant ends by three positively charged arginines. Presence of the divalent metals Mg<sup>2+</sup>(Mn<sup>2+</sup>) at reaction causes trapping of leaving  $\beta$ -,  $\gamma$ -phosphates in the active site cavity. The biotinyl domain BCCP structure characterized by higher mobility of the local residues -M111-K112-M113-, where K112 is candidate for biotinylation by BPL. The details of the BPL-BCCP interactions involved at biotinylation will be discussed.

**T-P067 Architecture and Affinity Maturation of Shark New Antigen Receptors.** R.L. Stanfield, H. Dooley, M.F. Flajnik, I.A. Wilson, The Scripps Research Inst., 10550 N. Torrey Pines Road, La Jolla, CA 92037.

Cartilaginous fish, such as sharks, skates and rays, are the oldest living organisms known to possess an adaptive immune system. In addition to conventional light-heavy chain antibody isotypes called IgW and IgM, sharks have a very unusual heavy chain isotype termed 'new antigen receptor' (IgNAR), which consists of one variable and five constant domains. Electron microscopy reveals that two heavy chains dimerize via their constant region to form an elongated structure, with

two free variable domains at the tip. While mammalian antibodies achieve their enormous diversity from the large number of V, D, and J genes that can be recombined to form the germline antibody, IgNAR genes are arranged in a 'cluster' configuration with 1 V, 3D, and 1 J gene segment, and recombination takes place only within that cluster. This type of gene rearrangement focuses germline diversity to the CDR3 region, with antigen-driven somatic mutation then used to further increase antigen affinity. Here we report crystal structures of germline and somatically mutated IgNAR variable domains, with and without bound antigen. Unique features of this unusual shark antibody and its affinity maturation process will be described.

**T-P068 Crystal Structure of SO1698 Protein from *Shewanella oneidensis*, a Putative Aspartic Endopeptidase.** J. Osipiuk, R. Mulligan, M. Bargassa, F. Collart, A. Joachimiak, The Midwest Center for Structural Genomics and Structural Biology Center, Biosciences, Argonne National Laboratory, Argonne, IL 60439.

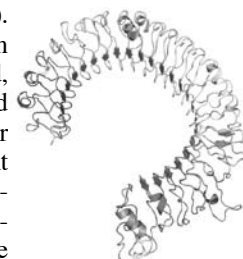
The crystal structure of SO1698 protein from *S. oneidensis* was determined by a single wavelength anomalous diffraction method and refined to 1.6 Å. The 125 residues protein crystallizes in space group H32 with cell dimensions of  $a=b=100.0$  Å and  $c=100.9$  Å. The protein structure is a  $\beta$ -barrel and unexpectedly includes two polypeptides, N-terminal 1-116 and C-terminal 117-125 residues respectively. Excellent electron density revealed a break in the polypeptide chain, which is likely caused by auto-catalytic cleavage. In addition, electron density revealed the Lys97 side chain covalently linked to Asp116. The protein is a dimer in the crystal and shows some structural features typical of aspartic endopeptidases, but doesn't show a nonspecific protease activity. The putative active site residues involved in auto-cleavage were identified and point mutants were produced. Biochemical and structural analysis and possible mechanism of auto-cleavage will be presented.

This work was supported by the grants from the National Institute of Health (GM62414 and GM074942) and the U.S. Department of Energy, Office of Biological and Environmental Research under Contract W-31-109-ENG-38.

**T-P069 The dsRNA binding site of human Toll-like Receptor 3.** Jessica K. Bell<sup>1</sup>, Janine Askins<sup>2</sup>, Pamela R. Hall<sup>1</sup>, David R. Davies<sup>1</sup>, David M. Segal<sup>2</sup>, <sup>1</sup>Laboratory of Molecular Biology, National Institutes of Diabetes & Digestive & Kidney Diseases, Experimental Immunology Branch, National Cancer Institute, National Institutes of Health, Bethesda, MD.

Pathogen recognition by Toll-like receptors (TLRs) initiates an innate response that is essential for inhibiting pathogen dissemination, and for the development of acquired immunity. The TLRs recognize pathogens with their N-terminal ectodomains (ECD) but the molecular basis for this recognition is not known. Recently, we reported the X-ray structure for unliganded TLR3-ECD. The molecule resembles a 23 loop solenoid bent into the shape of a horseshoe, with each loop consisting of one leucine-rich repeat (LRR). Although it has proven difficult to obtain a crystal structure of TLR3 with its ligand, dsRNA, we have now located the ligand binding site by mutational analysis. Of over 50 single residue mutations, only two point mutations resulted in the loss of TLR3 activation and ligand binding functions. These mutations locate the dsRNA binding site on the glycan-free lateral surface of TLR3 and suggest how dsRNA could bind and activate TLR3.

This work was supported by NIH Intramural Research and an NIAID Biodefense Award.



**T-P070 Crystal Structure of the Human TRPV2 Channel Ankyrin Repeat Domain.** Clare J. McCleverty, Eric Koesema, Ardem Patapoutian, Scott A. Lesley, Andreas Kreusch, Protein Sciences, Genomics Inst. of the Novartis Research Foundation, San Diego, CA, 92121.

Transient receptor potential vanilloid (TRPV) channels are polymodal integrators of noxious stimuli mediating thermosensation and nociception. The structure of a TRPV channel has not yet been elucidated and the molecular mechanisms by which external stimuli translate into channel gating are unknown. Here, we report the first structure from the TRPV channel subfamily, a 1.7 Å resolution crystal structure of the ankyrin repeat domain (ARD) from human TRPV2. The ARD, which is a common protein-protein recognition domain motif, is conserved in the N-terminal intracellular domain of all TRPV channels. Our crystal structure reveals a six ankyrin repeat stack with multiple insertions in each repeat generating a surface distinct from other known ARD structures. A prominent kink resulting from a large rotational shift of the last two repeats may function to create two distinct binding sites in the ankyrin groove, the surface typically used for ligand recognition. The TRPV2 ARD provides the first structural insight into a domain which coordinates nociceptive sensory transduction and is likely to be a prototype for other TRPV channel ARDs.

**T-P071 Structural Work on Potential Drug Targets from Tropical Parasites.** T Arakaki<sup>1,2</sup>, M Holmes<sup>1,2</sup>, I Le Trong<sup>1,2</sup>, J Caruthers<sup>2,3</sup>, E Boni<sup>1,2</sup>, E Phizicky<sup>2,4</sup>, E Quarterly<sup>2,4</sup>, G DeTitta<sup>2,5</sup>, J Luft<sup>2,5</sup>, A Lauricella<sup>2,5</sup>, O Kalyuzhnyi<sup>1,2</sup>, J Ross<sup>1,2</sup>, F Buckner<sup>2,6</sup>, W Van Voorhis<sup>2,6</sup>, C L M J Verlinde<sup>1,2</sup>, W G J Hol<sup>2,7</sup>, E A Merritt<sup>1,2</sup>, Depts of <sup>1</sup>Biochemistry and <sup>6</sup>Medicine, Univ. of Washington, Seattle, <sup>2</sup>Structural Genomics of Pathogenic Protozoa Consortium, <sup>3</sup>Stanford Univ., <sup>4</sup>Univ. of Rochester School of Medicine, <sup>5</sup>Hauptman Woodward Inst., <sup>7</sup>Howard Hughes Medical Inst., UW.

Diseases caused by eukaryotic pathogens such as *Plasmodium spp.*, *Leishmania spp.*, and *Trypanosoma* afflict billions of people in the poorest developing countries. The Structural Genomics of Pathogenic Protozoa Consortium is studying selected proteins from these protozoans, seeking potential targets for drugs to mitigate these diseases. Target proteins include phosphatases, lipid binding proteins, and enzymes from the pentose phosphate and pyrimidine biosynthesis pathways. Several structures will be presented, including that of a tyrosine phosphatase from *L. major*, a phosphatidylethanolamine-binding protein from *P. vivax*, and the *T. brucei* dihydroorotate dehydrogenase (DHODH), from the pyrimidine biosynthetic pathway. DHODH oxidizes dihydroorotate to orotate and comparison with other DHODH structures offers insights for the development of a broad, general inhibitor of trypanosomatid DHODHs.



**T-P072 Ternary Substrate Complex Structures of DNA Polymerase  $\beta$  with Mutagenic DNA Intermediates: Active Site Constraints for Mismatch Extension.** Batra, V.K., Beard, W.A., Pedersen, L.C., Wilson, S.H., Laboratory of Structural Biology, National Inst. of Environmental Health Sciences, Research Triangle Park, NC.

DNA polymerases, including DNA polymerase  $\beta$  (Pol  $\beta$ ), occasionally insert the wrong (incorrect) nucleoside triphosphate (dNTP). For this base substitution error to become a mutation, the mismatch must be extended. Earlier, we compared the extension efficiency of all 12 possible mispaired primer termini (Beard et al., 2004). Although the extension of terminal mispairs is kinetically challenging, transition in-

termediates were generally extended more easily than transversions. Mismatches at the primer terminus diminished correct nucleotide insertion efficiency without affecting DNA binding affinity. Here, we present ternary complex structures of Pol  $\beta$  with most of the mismatched primer termini and an incoming non-hydrolyzable dNTP analogue (dUMPNPP). These structures reveal that extension efficiency correlates well with the observed distance ( $d$ ) between the primer 3'-OH and  $\alpha$ -phosphate of the incoming nucleotide. This distance ranges from 3.4 Å (correctly paired primer terminus) to  $> 9$  Å. Mismatches with distances between 4 – 6 Å were extended, albeit poorly. When the observed distance increases further ( $d > 6$  Å), extension was nearly completely impeded.

Beard, W.A., Shock, D.D., and Wilson, S.H. (2004) Influence of DNA structure on DNA Polymerase  $\beta$  active site function: Extension of mutagenic DNA intermediates. *J. Biol. Chem.*, 279, 31921-31929.

**T-P073 Recognition of Human Epithelial Cells by *Moraxella* Pathogens.** Rebecca Connors<sup>a</sup>, Darryl Hill<sup>b</sup>, Richard Sessions<sup>a</sup>, Tony Clarke<sup>a</sup>, Tim Joseph-Horne<sup>a</sup>, Mumtaz Virji<sup>b</sup>, R. Leo Brady<sup>a</sup>, <sup>a</sup>Dept. of Biochemistry and <sup>b</sup>Dept. of Cellular and Molecular Medicine, Univ. of Bristol, UK.

*Moraxella catarrhalis* is a human specific pathogen responsible for localized ear, throat and lung infections. It also causes widespread blood and brain infections in immuno-compromised individuals. The bacteria adhere to specific receptor molecules on human epithelial cells before subsequent invasion and resulting disease. We have created a recombinant fragment of the *Moraxella catarrhalis* adhesion molecule which has retained its ability to bind to the human receptor. The fragment has been crystallized and diffraction data collected to 1.9Å resolution. Partial solutions have been obtained by molecular replacement using Phaser and support a trimeric alpha-helical coiled coil structure. We aim to use the structural information, in association with molecular modeling studies and site-directed mutagenesis to investigate the interactions formed between adhesion molecule and receptor protein.

**T-P074 Structural Determination of Yeast CPSF-100 and Direct Biochemical Evidence for Endoribonuclease Activity of CPSF-73.** Corey Mandel, Hailong Zhang, Syuzo Kaneko, Damara Gebauer, Vasupradha Vethantham, James L. Manley, Liang Tong, Dept. of Biological Sciences, Columbia Univ., New York, NY.

Most eukaryotic messenger RNA precursors (pre-mRNAs) must undergo extensive maturational processing, especially 3'-end cleavage and polyadenylation. Several proteins have been characterized that are required for cleavage; however, the specific protein that catalyzes the hydrolysis is unknown. Indirect evidence suggests that the 73 kD subunit of the cleavage and polyadenylation specificity factor complex (CPSF-73) may be the endonuclease for this reaction but there is no direct evidence of this activity. To help elucidate the endonuclease, we solved the crystal structure of yeast CPSF-100, which shares recognizable sequence homology with CPSF-73, as well as a model for the active site of CPSF-73. Both proteins contain two domains, a metallo- $\beta$ -lactamase domain and a new domain called the CASP domain. The modeled active site of CPSF-73 is located between the two domains and should possess hydrolytic activity. Our biochemical studies suggest recombinant CPSF-73 has endoribonuclease activity, while mutations of the active site reduce this activity. Our results provide the first direct evidence that CPSF-73 is the endonuclease involved in 3' pre-mRNA processing.

**T-P075 The Secret of Broadly Neutralizing Anti-HIV-1 Antibody b12.** Tongqing Zhou<sup>1</sup>, Ling Xu<sup>1</sup>, Barna Dey<sup>1</sup>, Shi-Hua Xiang<sup>2</sup>, Dennis R. Burton<sup>3</sup>, Joseph G. Sodroski<sup>2</sup>, Richard T. Wyatt<sup>1</sup>, Gary J. Nabel<sup>1</sup>, Peter D. Kwong<sup>1</sup>, <sup>1</sup>Vaccine Research Center, National Inst. of Allergy and Infectious Diseases, National Institutes of Health, Bethesda, MD 20892, <sup>2</sup>Dept. of Cancer Immunology and AIDS, Dana-Farber Cancer Inst., Div. of AIDS, Harvard Medical School, Boston, MA 02115, <sup>3</sup>The Scripps Research Inst., Dept. of Immunology, 10550 North Torrey Pines Rd., La Jolla, CA 92037.

We use atomic-level design coupled to feedbacks from crystallographic, thermodynamic, and surface-plasmon resonance data to stabilize the gp120 envelope glycoprotein into the conformation induced by the primary HIV-1 receptor, CD4. A gp120 core partially stabilized by interdomain disulfides and cavity-filling mutations kept CD4 binding, but lost binding to all CD4-binding-site-directed antibodies tested, except for the broadly neutralizing antibody, b12. Structural analysis at 2.3Å resolution of the antigen-binding fragment of b12 in complex with this gp120 core revealed that b12 bound primarily to the functionally critical CD4-binding loop of gp120 and in a manner that avoided gp120-conformational fixation. Our results provide atomic-level details for how the immune system can exploit functional constraints of CD4 binding to produce antibodies that broadly and potently neutralize HIV-1.

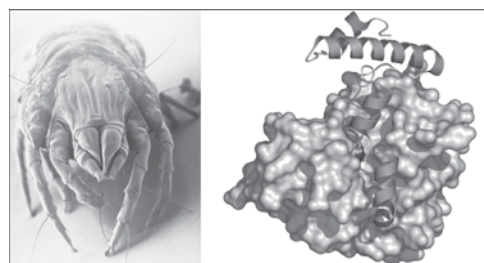
**T-P076 Crystal Structure of a *S. aureus* Pathogenicity Island Protein, EAR.** Ramachandraiah Gosu, C. Kent Brown, Zu-Yi Gu, Patrick Schlievert<sup>§</sup>, Cathleen Earhart, Douglas Ohlendorf, Biochem., Molecular Biol. & Biophysics, <sup>§</sup>Microbiology, Univ. of Minnesota, Minneapolis, MN 55455.

Pathogenicity islands are defined as elements of DNA that are heterologously present in bacteria, carry virulence factors, and are not identified as bacteriophages, transposons or plasmids. One such island found in *S. aureus* Gram-positive bacteria is named SaPI3. EAR, Enterotoxin-associated Ampicillin Resistance protein, corresponds to ORF4 in SaPI3. Seleno-Methionine labeled double-mutant (L64M/I108M) EAR protein, Mw 20kDa crystallizes in space group P4<sub>3</sub>2<sub>1</sub>2 with cell constants a=b= 48.86 Å, c=154.03 Å having ~62% solvent content with one molecule in the asymmetric unit. Crystal structure was solved using both SAD (Single-wavelength Anomalous Dispersion) and MAD (Multi-wavelength Anomalous Dispersion) phasing (2 Se) and refined to a final R factor 21.4 % (R<sub>free</sub> 24.5%) for 1.95Å data. Structure looks having a pattern similar to one domain of β-lactamase comprising a sheet made up of 6 anti-parallel β strands and two helices running across the sheet. The conserved motif SXXK observed in all serine dependent hydrolases (Class A, C or D β-lactamases) forms part of the active site situated at the beginning of a helix, spatially located at the interface of two domains, surprisingly seen in the crystal structure of EAR protein in a different secondary structure i.e. at the beginning of a strand but in closer proximity to the observed active site of β-lactamase upon overlay. Existence of ampicillin resistance of EAR protein when cloned in *E.coli*, structural similarity at the domain level with respect to β-lactamase and the presence of conserved motif SXXK suggest that it might be in consonance with another protein or ORF might be involved in carrying out β-lactamase type of activity.

**T-P077 Analysis of the Crystal Structure of the Major House Dust Mite Allergen Der p 1.** K. Meno<sup>1</sup>, P.B. Thorsted<sup>1</sup>, H. Ipsen<sup>1</sup>, O. Kristensen<sup>2</sup>, J.N. Larsen<sup>1</sup>, M.D. Spangfort<sup>1</sup>, M. Gajhede<sup>2</sup>, K. Lund<sup>1</sup>, <sup>1</sup>ALK-Abelló A/S, Denmark, <sup>2</sup>The Danish Univ. of Pharmaceutical Sciences, Denmark.

Inhalation allergy to house dust mite is among the most prevalent aller-

gic diseases worldwide and proteins belonging to group 1 mite allergens are major elicitors of this. Group 1 contains cysteine proteases located in the alimentary canal of



the mite. Recombinant Der p 1 (rDer p 1) from *Dermatophagoides pteronyssinus* as a tool for allergy diagnosis or immunotherapy is an attractive prospect. However, the proteolytic activity or presence of the pro-peptide on the immature protein is of concern. An enzymatically inactive rproDer p 1 variant was produced that yielded crystals diffracting to a resolution of 1.61 Å thus resulting in the first structure of Der p 1. The mature region adopts a conformation similar to the mature form of other cysteine proteases suggesting that no major structural changes are induced by maturation. The pro region adopts a unique fold, which interacts with the active site cleft and a substantial adjacent area on the mature region. The antibody binding properties of pro and mature rDer p 1 were assessed by immunological techniques. Mature rDer p 1 showed antibody-binding properties indistinguishable from the natural protein but several epitopes are covered by the pro-peptide.

**T-P078 Structural Studies on Two Dioxygenases in the Prokaryotic Tryptophan-based Quinolate Biosynthetic Pathway.** Y. Zhang, K.L. Colabroy, S.A. Kang, S. Bale, T. Mukherjee, B.R. Crane, T.P. Begley, S.E. Ealick, Dept. of Chemistry and Chemical Biology, Cornell Univ., Ithaca, NY 14853.

It has been generally believed that the biosynthesis of quinolate from tryptophan is unique to eukaryotes, while in prokaryotes quinolate is derived from aspartate and dihydroxyacetone phosphate. However, the tryptophan-based quinolate biosynthetic pathway has been recently identified in bacteria including *Ralstonia metallidurans*. In the tryptophan-based quinolate biosynthetic pathway, tryptophan dioxygenase (TDO) catalyzes the first step to form N-formyl kynurenine; 3-hydroxyanthranilate-3,4-dioxygenase (HAD) catalyzes the last enzymatic step, which is the oxidative ring opening of 3-hydroxyanthranilate. The crystal structures of TDO and HAD from *R. metallidurans* were determined at 2.5 Å and 1.9 Å resolution, respectively. TDO is a tetramer with cofactor heme bound at the active site. Biochemical studies are underway. HAD is a dimer of cupin fold with a catalytic iron buried inside the cupin barrel in a distorted octahedral geometry. In addition, a FeS<sub>4</sub> center is found close to the solvent surface but its biochemical function is unknown. Based on the HAD crystal structures, mutagenesis studies were carried out and an enzymatic mechanism is proposed.

**T-P079 Crystal Structure of the Trimeric Complex of Interleukin-13, IL-13 Receptor α1 and the Binding Domain of the Inhibitory Antibody Fab13.2.** Kevin Parris, John Dumas, Marion Kasaian, Amy Tam, Tim Cook, Lioudmila Tchistiakov, Xiang-Yang Tan, Kimberly Marquette, James Wilhelm, Laura Lin, Lidia Mosyak, Wyeth Research, Cambridge, MA 02140.

Interleukin 13 is a pleiotropic cytokine generated early in immune responses driven by T helper 2 cells and plays a critical role in mediating T helper 2-type immunosuppressive activities. Administration of recombinant IL-13 has been shown to induce the pathophysiological features of asthma, whereas neutralization of IL-13 ameliorated/attenuated the asthma phenotype. IL-13 has also been shown to play a prominent role in parasitic infections, atopic dermatitis and cancer. To gain insight into the mechanism of IL-13 regulation, we utilized

the Fab fragment of an IL-13 inhibitory antibody (mAb13.2) as a tool to facilitate crystallization of IL-13 singly (1.8Å) and in complex with IL-13 $\alpha$ 1 receptor (2.2Å). We find that IL-13R $\alpha$ 1 grasps IL-13 in a pincer-like fashion where the Ig3 domain interacts with C-terminal end of the D-helix and the Ig1 domain interacts with loops near the N-terminal end of the D-helix. This interaction with Ig1 induces beta-strand structure onto two loops of the IL-13 molecule forming an extended beta sheet across the two molecules. The Fab fragment binds to the C-helix, where the IL-4 receptor would normally bind.

**T-P080 Crystallization of Partially Trypsinized *E. coli* PEP Carboxykinase.** K.C. Klemmer<sup>1</sup>, H. Goldie<sup>2</sup>, L. Prasad<sup>1</sup>, L.T.J. Delbaere<sup>1</sup>, Depts. of Biochemistry<sup>1</sup> and Microbiology & Immunology<sup>2</sup>, Univ. of Saskatchewan, S7N 5E5, Canada.

Phosphoenolpyruvate carboxykinase [ATP dependent] (PCK) from *Escherichia coli* is activated by Ca<sup>2+</sup> or by Mn<sup>2+</sup> in the presence of saturating concentrations of MgATP. Partial digestion of PCK with trypsin abolishes activation by Ca<sup>2+</sup> but not via Mn<sup>2+</sup>. A 120-minute trypsin digest of PCK produced PCKD, which crystallized in space group P2<sub>1</sub>, a novel space group for PCK. The crystal structure revealed no electron density for amino acid residues 390-400 but the remainder of the C-terminal polypeptide was present. Amino acid residues from 442-455 were demonstrated to have a unique orientation. These latter residues form the P-loop, which is important for binding and stabilizing the phosphate backbone of ATP. SDS-PAGE verified the trypsin cleavage at Arg396, through the separation of PCK into two distinct fragments, 45 and 15 kDa in size. Strikingly, kinetic assays of PCKD demonstrated Ca<sup>2+</sup> activation is partially regained. Ca<sup>2+</sup> activation is restored through gel filtration and/or a freeze thaw cycle. A possible mechanism thought to result in the restoring of Ca<sup>2+</sup> activation, is by a conformational change.

**T-P081 Crystal Structure of Imidazolonepropionase from *Agrobacterium tumefaciens* at 1.87 Å Resolution.** Rajiv Tyagi, Desigan Kumaran, Subramanyam Swaminathan, Biology Dept., Brookhaven National Laboratory, Upton, NY 11973.

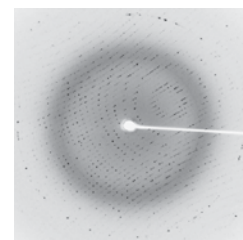
Imidazolonepropionase (imidazolone-5-propionate hydrolase; EC 3.5.2.7) a 45.6 kDa protein is member of amidohydrolase superfamily and catalyses the conversion of imidazolone-5-propanoate to N-forminio-L-glutamate in the histidine degradation pathway. We have determined the first three dimensional structure of this enzyme from *Agrobacterium tumefaciens* at 1.87 Å resolution using Mercury-MAD. The asymmetric unit contains two monomers, where each monomer is composed of a small N-terminal domain and a large C-terminal domain having classic TIM barrel fold. The active site is contained within each monomer and its organization displays the landmark feature of amidohydrolase superfamily showing a metal ligand (iron), four histidines and one aspartic acid.

Acknowledgements: Research was supported by the National Institutes of Health (GM074945) under Prime Contract No. DEAC02-98CH10886 with Brookhaven National Laboratory.

**T-P082 Crystallization and Preliminary X-ray Analysis of the Laccase from *Coriopsis gallica*.** E. De la Mora, A. Resines, B. Valderama, E. Horjales, E. Rudiño-Piñera, IBT-UNAM, Cuernavaca, Mexico.

Laccases belong to the blue oxidases family. These are multi-copper enzymes catalyzing the four-electron reduction of molecular oxygen to water with concomitant one-electron oxidation of the substrate. We have crystallized laccase from *C. gallica* at different pHs; at its opti-

mum for activity (pH 4 and 4.5) and around its inactivation point (pH 6.5 to 8). Crystals at low pHs grown using the hanging drop method with a mother liquor containing 5% PEG 1K, 5% PEG 8K, Mes 50mM at 277 K. While crystals at pH 7 grown with 13% PEG 1K, 13% PEG 8K and HEPES 50mM also at 277 K. Two data-sets have been collected. In the first one a diffraction pattern at 1.8 Å was obtained but with a mosaicity of 2° (see figure). From the second crystal we got a pattern at 3.0 Å resolution, with completeness of 60% and R<sub>merge</sub> of 24%. Crystals belong to space group P2<sub>1</sub>2<sub>1</sub>2<sub>1</sub> with cell dimensions of a=56.4, b=85.9, c=152.1. High mosaicity and low resolution appear to be consequences of the sensibility of the crystals to changes in temperature. Although the completeness, clear positive peaks are visible for the four coppers in the catalytic center of the enzyme. Currently, we are carefully dehydrating crystals. While crystals seem to be stable, it is still necessary to corroborate any change over the diffraction quality.



**T-P083 Crystal Structure of Hypothetical Protein TM1727 of *Thermotoga maritima*.** Mahendra Madegowda, Subramaniam Eswaremoorthy, Jayaraman Seetharaman, Subramanyam Swaminathan, Biology Dept., Brookhaven National Laboratory, Upton, NY 11973.

The hypothetical protein TM1727 of *Thermotoga maritima* (T1650 of NYSGRC) belongs to a large family of proteins, with homologues in bacteria, archaea, and eukaryotes. The amino acid sequence of T1650 does not share any recognizable homology with proteins of known functions or structures. To correlate the biological function, we have determined its crystal structure at 2.6 Å using Se-MAD phasing. The structure reveals the presence of two domains, one larger and one smaller and the dimer interface occur through the smaller domain which is made of helical bundles. A residual density near the GTGTLT sequence motif at the N-terminal  $\alpha\beta$  domain may be explained as due to the co-factor. The detailed structure-function and characterization are underway and will be presented.

Acknowledgement: Research was supported by the National Institute of Health (GM074945) grant to NYSGXRC under Prime Contract No. DEAC02-98CH10886 with the Brookhaven National Laboratory.

**T-P084 Crystal Structure of Metastasis-associated Protein S100A4 in the Calcium-Bound Form.** Puja Pathuri, Hartmut Luecke, Dept. of Molecular Biology & Biochemistry, Univ. of California, Irvine, CA 92697.

S100A4 is a member of the S100 family of calcium binding proteins that is directly involved in tumorigenesis. Currently the only structural information available is the apo or calcium-free form of the protein, which was determined by NMR (nuclear magnetic resonance). Here we report the crystal structure of human S100A4 in the calcium-bound state at 2.7Å resolution. Upon calcium binding a large conformational change in the three-dimensional structure of the dimeric S100A4 protein occurs. This calcium dependent conformational change opens up a hydrophobic binding pocket that is capable of binding to intracellular targets such as Annexin A2, p53 tumor suppressor protein and myosin IIA. The structure of the calcium-bound form of S100A4 will give us a better insight on its interactions with protein targets and possibly a better understanding on its in metastasis.

**T-P085 Towards Data Management for PX Structure Determination Within CCP4.** Peter Briggs, Wanjuan Yang. CCP4, CCLRC-Daresbury Laboratory, Warrington, UK, Contact: p.j.briggs@dl.ac.uk.

BIOXHIT is an Integrated Project within the 6<sup>th</sup> Framework Programme of the European Commission, which is coordinating scientists at all European synchrotrons alongside leading software developers in a timely and unprecedented joint effort to develop, assemble and provide a highly effective technology platform for Structural Genomics.

A key part of the integrated technology platform being delivered by the BIOXHIT project is the development of automated structure determination software pipelines covering the latter stages of structure solution by protein X-ray crystallography (PX). Within such pipelines it is essential to accurately record, organise and track the data, something that becomes increasingly important as the throughput of structures solved using these procedures rises.

Therefore as part of BIOXHIT, CCP4 (the Collaborative Computational Project No. 4, a UK-based software project that provides a suite of programs for the determination of macromolecular structures via X-ray crystallography) is developing a system for performing data management in order to address this need. The system will integrate with existing software such as CCP4i (the CCP4 graphical interface) as well as with new automated pipelines such as that being developed by the CCP4 Automation Project. This poster reports on recent progress towards realising this system.

**T-P086 The Crystal Structure of a Birnavirus RNA Polymerase Reveals a Distinct Active Site Topology and a Novel Protein-Priming Domain.** Junhua Pan<sup>1</sup>, Vikram N. Vakharia<sup>2</sup>, Yizhi Jane Tao<sup>1</sup>, <sup>1</sup>Dept. of Biochemistry & Cell Biology, Rice Univ., Houston, TX 77005, <sup>2</sup>Center for Biosystem Research, Univ. of Maryland, College Park, MD 20742.

RNA-dependent RNA polymerases (RdRps) are often excellent targets for antiviral drug design because of their virus-specific functionalities. Birnavirus VP1 is a multifunctional protein that serves as both RdRp and protein-primer for initiation of RNA synthesis. Here we report the 2.5Å structure of a birnavirus VP1 determined by multiple isomorphous replacement and anomalous scattering (MIR-AS). Close inspection of this structure reveals that VP1 adopts a novel active site topology that has never been observed in other polymerase structures. Additionally, VP1 contains only two aspartate residues in the active site, another highly unusual feature for RNA-dependent polymerases. The putative guanylation site residue, which functions in initiating protein-primed RNA synthesis, resides in VP1 but is found 23Å away from the polymerase active site. Our results indicate that the novel topology in the active site may represent a dead-end product in evolution, and birnavirus VP1 is likely to be a descendant of polymerases from tetraviruses in the alphavirus superfamily, revealing the evolutionary relationship between dsRNA and +ssRNA viruses.

**T-P087 Complete Automation of Molecular Replacement.** F. Long, A.A. Vagin, G.N. Murshudov, Chemistry Dept., Univ. of York, York, YO10 5YW, UK.

Analysis of the PDB shows that this year around 67% of all the deposited structures are solved by molecular replacement. With better algorithms and organisation of data bank it can be expected that this number will be substantially higher. This talk will describe a complete automation of molecular replacement. There are three main components of this work: (1) Reorganisation of database of proteins. All entries in the PDB have been analysed

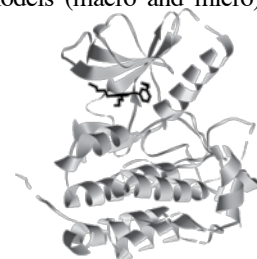
and only non-redundant sets of protein structure, domains and tertiary information were stored. Hierarchical database according to sequence identities was organised. It means that search for similar structure is very fast (less than 10 seconds). (2) Automatic molecular replacement system was designed using python. The system requires only experimental data – sequence the reflection data. The system begins searching the database and extracting candidate structures. It also analyses the experimental data and makes such decisions as resolution limit, existence of pseudo-translation. Then the system starts molecular replacement and refinement on the candidate structures using several protocols (3) Programs such as MOLREP, REFMAC. We have already tested more than 1000 cases and success rate is more than 75%. It is expected that more than 80% of structures will be solved completely automatically.

**T-P088 Crystal Structure of the Hypothetical Protein Xcc0516 from *Xanthomonas campestris*: A Novel Quaternary Structure Assembled by Five Four-Helix Bundles.** Li-Ying Lin, Chung-Lun Ching, Ko-Hsin Chin, Shan-Ho Chou, and Nei-Li Chan, L.-Y. Lin and C.-L. Ching contributed equally to this work, Inst. of Biochemistry, College of Life Sciences, National Chung Hsing Univ., Taichung, Taiwan.

The crystal structure of Xcc0516 (SwissProt accession number: Q8PD29), a 14.6-kDa conserved hypothetical cytosolic protein from plant pathogen *Xanthomonas campestris*, has been determined at 2.5 Å resolution by the multiwavelength anomalous diffraction method. Xcc0516 was selected as a target for structural determination because it exhibits no apparent sequence homology to any structure in the Protein Data Bank. While it turns out that the Xcc0516 monomer adopts a common four-helix bundle fold with a typical up-down-up-down arrangement of helices, interestingly, five monomers associate to form a pentameric ring structure with C5 symmetry. To our knowledge, this is the first example of a pentameric toroid formed by non-transmembrane four-helix bundle domain. Self-association of four-helix bundles into a toroid-like oligomer is predominantly achieved by aligning the principle (pseudo-4-fold) axis of individual subunit approximately along the main oligomer axis. In contrast, the Xcc0516 monomer tilts by ~50 degree about the C5 axis. A BLAST search revealed that Xcc0516 can be aligned over its entire length with the bacterial 23S rRNA proteins of the Ribosomal\_S23p protein family (Pfam domain PF05635), with E values around e-36. Since residues involved in Xcc0516 pentamer formation are highly conserved among Ribosomal\_S23p family members, they are likely to adopt a similar quaternary architecture.

**T-P089 Computational Studies at the Micromolecule/Macromolecule Interface.** William B. Gleason<sup>1,3,4</sup>, Eric R.A. Johnson<sup>3</sup>, Derek Straka<sup>1,2</sup>, Jane Shvelidze<sup>3</sup>, Caroline Nibbe<sup>1</sup>, David MacDonald<sup>2</sup>, Jack Anderson<sup>1</sup>, Depts. of <sup>1</sup>Chemistry, <sup>2</sup>Biochemistry, <sup>3</sup>Biomedical Engineering, <sup>4</sup>Laboratory Medicine & Pathology, Univ. of Minnesota, Minneapolis, MN 55406.

Docking remains a popular technique in drug design business, because it is believed that it may help to constrain the enormous cost of drug development. Docking requires either models (macro and micro) derived from experimental data or, preferably, real structures of ligand/macromolecular complexes. Various authors, e.g. Gerard Kleywegt, have reviewed the situation from the small molecule perspective. We will present from our own work (“tips and tricks”) that may be useful. Examples of the binding of sulfated model compounds



to heparin-binding proteins will be given. Using AUTODOCK3 we have found that the implementation of rotational constraints leads to much better results for ligands with many degrees of rotational freedom. We will also present examples of docking involving HIV protease inhibitors as well as work with docking inhibitors of the EGFR receptor kinase. A brief discussion of how these inhibitors relate to the very useful empirical rules of Lipinsky will be given.

We thank the Minnesota Supercomputer Institute for computer time, technical support, and summer support for ERAJ, DS, and JS.

**T-P090 Purification, Crystallization and Structure Solution of the Complex between p38 $\alpha$  and its Substrate MK2.** Giovanna Scapin<sup>1</sup>, Sangita B. Patel<sup>1</sup>, James Thompson<sup>2</sup>, Joseph W. Becker<sup>1</sup>, Julie DeMartino<sup>2</sup>, Dennis Zaller<sup>2</sup>, Stephen O'Keefe<sup>2</sup>, Depts. of <sup>1</sup>Medicinal Chemistry and <sup>2</sup>Immunology & Rheumatology, Merck Research Laboratories, PO BOX 2000, Rahway, NJ, 07065.

The p38 mitogen-activated protein kinase pathway is required for the production of proinflammatory cytokines (TNF $\alpha$  and IL-1) that mediate the chronic inflammatory phases of several autoimmune diseases. p38 transduces signals through downstream effectors, including mitogen-activated protein kinase-activated protein kinases (MKs). Genetic deletion and phosphorylation studies indicated that MK2 participates in p38-dependent modulation of production of inflammatory cytokines. The catalysis and function of the p38 $\alpha$ :MK2 signaling complex have been recently described. We report here the purification, crystallization and 3.1 Å structure of the inactive p38 $\alpha$ :MK2 complex. The interactions between the two kinases involve mainly the previously identified p38 docking groove (residues E160 and E161), and MK2 docking domain peptide. The formation of the complex positions MK2 S272 (one of the residues that need to be phosphorylated for maximal activation of MK2) near the ATP-binding site of p38 $\alpha$ , suggesting that this is indeed a biological complex and not a crystallization artifact. Together with the already available biochemical data, this structure may help in understanding the complex formation and function at the molecular level.

**T-P091 Generation of Atomic Coordinates from Time-resolved X-ray Diffraction Data.** George N. Phillips, Jr., Elena J. Levin, Roman Aranda, IV, Dept. of Biochemistry, Univ. of Wisconsin-Madison, Wisconsin 53706.

New methods of refinement of time-resolved crystallography have been used to follow the dissociation of carbon monoxide from the heme pocket of sperm whale myoglobin and its mutants and to quantify the resultant conformational changes.

Electron density maps were previously created at various time points and used to describe amino acid side-chain and carbon monoxide movements. In this work, specially designed implementations of difference refinements were employed to generate atomic coordinates at each time point in order to create an explicit, quantitative representation of the photo-dissociation process. After photolysis the carbon monoxide moves to various docking sites, causing rearrangements in the heme pocket residues whose coordinate changes can be plotted as a function of time. These include rotations of the heme pocket phenylalanine, concomitant movement of the distal histidine, and proximal displacement of the heme iron. The degree of relaxation toward the intermediate and deoxy states could then be probed by analysis of the coordinate movements in the time-resolved models, revealing a non-linear progression to the unbound state and return to the bound state over time.

We acknowledge Philip Anfinrud and Friedrich Schotte for generating the experimental data and training grants NIH 5 T32 GM08349, NIH T32 GM07215 for support.

**T-P092 Crystal Structure of Human NMPRTase, a Novel Target for Anti-cancer Therapy.** Javed A. Khan, Xiao Ta, Liang Tong, Dept. of Biological Sciences, Columbia Univ., New York, NY.

Nicotinamide adenine dinucleotide (NAD) is involved in many important biochemical processes, and NAD turnover constitutes an important metabolic process in most cells. Nicotinamide phosphoribosyltransferase (NMPRTase) is a key enzyme of the salvage pathway for NAD biosynthesis and catalyzes the condensation of nicotinamide with 5-phosphoribosyl-1-pyrophosphate to yield nicotinamide mononucleotide (NMN). NMPRTase is an attractive target for developing novel anticancer drugs, as cancer cells have a high rate of NAD turnover. Inhibition of NMPRTase could lead to a decrease of NAD levels in tumor cells and ultimately apoptosis of these cells. Recent studies also suggest that NMPRTase, when secreted, could activate the insulin receptor. We have determined the crystal structure of human NMPRTase, alone and in complex with the NMN product or a potent inhibitor. The structural information provides a molecular basis for understanding the substrate specificity and the inhibition mechanism of this enzyme.

**T-P093 Auto-Rickshaw: An Automated Crystal Structure Determination as an Efficient Tool to Validate an X-Ray Diffraction Experiment.** M.S. Weiss, V. Parthasarathy, V. Lamzin, P.A. Tucker, S. Panjekar. EMBL Hamburg Outstation, c/o DESY, Notkestr. 85, D-22603 Hamburg, Germany.

The EMBL-Hamburg automated crystal structure determination platform (aka Auto-Rickshaw) combines various macromolecular crystallographic software packages with several decision-making steps. Auto-Rickshaw is able to automatically determine macromolecular crystal structures as soon X-ray data are collected and processed. A large number of structure solution paths are encoded in the system and the optimal path through the system is selected by the computer-coded decision-makers as the structure solution evolves. The primary aim of the pipeline is to validate the crystallographic experiment at the synchrotron site while the crystal is still at or near the beam line. Thus, the system has been optimized for speed, so that typically within a few minutes the answer is provided as to whether the collected data are of sufficient quality to allow successful structure determination.

The platform is installed on a 16-processor Linux cluster and the web-server is accessible for Hamburg beamline users and EMBL staff. An overview of the pipeline with its design, functionality, some examples and the way this platform is used as a feedback system for X-ray data collection or validation of X-ray experiment, will be discussed.

**T-P094 The Liganding of Glycolipid Transfer Protein is Controlled by Glycolipid Acyl Structure.** Lucy Malinina<sup>1#</sup>, Margarita L. Malakhova<sup>2#</sup>, Alex T. Kanack<sup>2</sup>, Ruben Abagyan<sup>3</sup>, Rhoderick E. Brown<sup>2\*</sup>, Dinshaw J. Patel<sup>1</sup>, <sup>1</sup>Structural Biology Program, Memorial Sloan-Kettering Cancer Center, New York, NY 10021, <sup>2</sup>Hormel Inst., Univ. of Minnesota, Austin, MN 55912, <sup>3</sup>Dept. of Molecular Biology, The Scripps Research Inst., La Jolla, CA, 92037.

Glycosphingolipids (GSLs) play major roles in cellular growth and development. Mammalian glycolipid transfer proteins (GLTPs) are potential regulators of cell processes mediated by GSLs and display a unique architecture among lipid binding/transfer proteins. We determined crystal structures of human GLTP bound to GSLs of diverse acyl chain length, unsaturation and sugar composition. Structural comparisons show a highly conserved anchoring of galactosyl- and lactosyl-amide headgroups by the GLTP recognition center. By contrast, acyl chain structure dictates partitioning between sphingosine-

in and sphingosine-out ligand-binding modes. In the sphingosine-out mode, the sphingosine chain is directed outwards and enters the hydrophobic tunnel of a partner complex, whereas the sphingosine-in mode is achieved through encapsulation of both ceramide chains within a hydrophobic tunnel of a single GLTP molecule. The structural insights, combined with computed interaction propensity distributions, suggest a concerted sequence of events mediated by GLTP conformational changes during GSL transfer to/from membranes or presentation/transfer to other proteins.

**T-P095 Diffraction Image Ranking and Data Collection Strategy.** J.W. Pflugrath, T.J. Niemeyer, Angela R. Criswell, Robert Bolotovskiy, Rigaku Americas, Corp., 9009 New Trails Drive, The Woodlands, TX 77381.

While the minimum requirements for a diffraction data set are completeness in the unique Miller indexes to a given resolution, many other factors play a role in achieving good statistics and good redundancy required for optimal phasing and crystal structure refinement. Two synergistic programs, dtranker and dtmultistrategy have been developed which fulfill the role of an experienced crystallographer in evaluating diffraction images and determining the best data collection strategy. These programs allow for screening and automated diffraction data collection from crystalline samples in both manual and robotic experimental setups. Many aspects of optimizing the diffraction data collection experiment with 2D detectors are dealt with, including choice of crystal, exposure time, rotation width per image, axes to scan, scan setting angles, multiple scans, rotation ranges, potential collisions, multiple detector positions, spot overlap, and tolerance for completeness. These new programs are now available in the d\*TREK suite. d\*TREK is flexible, customizable, device-independent software and toolkit which collects and processes single crystal X-ray diffraction images from two-dimensional position sensitive detectors such as IP and CCD detectors.

**T-P096 Structural insights into the Mechanism of Recognition by Ubiquitin Specific Protease 7.** Vivian Chan<sup>1,2,3</sup>, Yi Sheng<sup>2</sup>, Feroz Sarkari<sup>1</sup>, Melissa Holowaty<sup>1</sup>, A. D. M. Edwards, Cheryl H. Arrowsmith<sup>2,3</sup>, Lori Frappier<sup>1</sup>, <sup>1</sup>Dept. of Medical Genetics and Microbiology, Univ. of Toronto, 1 King College Circle, Toronto, Ontario Canada M5S 1A8. <sup>2</sup>Ontario Cancer Inst., Dept. of Medical Biophysics, 610 University Ave. Toronto, Ontario Canada M5G 2M9. <sup>3</sup>Banting and Best Dep. of Medical Research, Univ. of Toronto, 100 College St., Toronto, Ontario Canada M5G 1L5.

The deubiquitinating enzyme, Ubiquitin Specific Protease (USP) 7, is a key regulator of both p53 and mdm2 and is targeted by the EBNA1 protein of Epstein-Barr virus. The crystal structures of the N-terminal domain of USP7 alone and bound to EBNA1, p53 and mdm2 peptides were determined. We show that USP7 binds two closely spaced 4-residue sites in both p53 and MDM2, falling between p53 residues 359-367 and MDM2 residues 147-159 as well as one 4-residue site in EBNA1, encompassing residues 444-447. These peptides all bind to the same surface of USP7 elucidating the competitive nature of the interactions. Structural and mutational analysis indicated a preference for a P/AxxS motif in peptides that bind USP7 whereby contacts made by Ser are critical. The data provide a structural framework for understanding the mechanism of substrate recognition by USP7 and regulation of the p53/mdm2 pathway.

**T-P097 Finding the Best Composite Model from Multiple Sources.** Dusan Turk<sup>1</sup>, M. Chruszcz<sup>2</sup>, M. Cymborowski<sup>2</sup>, W. Minor<sup>2</sup>, Z. Otwinowski<sup>3</sup>, <sup>1</sup>Jozef Stefan Inst., Ljubljana, Slovenia, <sup>2</sup>Univ. of Virginia, Charlottesville, VA, <sup>3</sup>Univ. of Texas, Dallas, TX.

Molecular models generated by automated chain tracing are sensitive to resolution of maps, their contouring level, software and even to grid spacings used, which means that the generated models resulting from single runs are different. The observation is that a single model may not be the best everywhere especially when only medium resolutions phases are available. Therefore it makes sense to generate an ensemble of models, superimpose them and select fragments, which define the best trace and merge them into the unique, composite model.

For this purpose a procedure has been developed in MAIN 2006, which can generate the best trace from a variety of molecular models. First all models are superimposed using crystal symmetry operators. Superimposed residues are assigned into clusters, which build overlapping chain traces. These get secondary structures assigned. The best helix and beta strand traces are found by choosing the smaller number of fragments, which build the longest secondary structure segment. All other connectivities between the clusters in the secondary structure region are then discarded. In the next step the connecting segments between the ends of secondary structure elements and the chain termini are being found. Cross connections between the connecting segments are removed considering the chain directionality and reduction of cross segment connections. (Each knot may have up to two outgoing branches.) The trace of connecting segments is then optimized by a search procedure, which finds the best trace of overlapping fragments in the region. The resulting unique trace through the residue clusters is then converted into a single chain trace, energetically minimized and used for further model building.

For software see "<http://www-bmb.ijs.si/>".

**T-P098 Structure-based Development of Variola H1 Phosphatase Inhibitors.** D.S. Waugh, J. Phan, J.E. Tropea, Macromolecular Crystallography Laboratory, Center for Cancer Research, National Cancer Inst. at Frederick, Frederick, MD 21702.

Smallpox was officially eradicated more than 20 years ago but there remains a serious concern that undeclared stocks of the variola major virus may still exist and could be used as a bioterrorist weapon. Although there is a vaccine, it is not without risks and serious side effects. Consequently, there is an urgent need for effective antiviral drugs. In addition to providing potential therapy for infected people, the availability of antiviral drugs could decrease the risks associated with the smallpox vaccine by providing a treatment for vaccine-associated complications. Essential viral enzymes have frequently proven to be good targets for antiviral drugs. The dual specificity protein phosphatase (H1) encoded by the smallpox virus is essential for viral replication. We have determined the crystal structure of this enzyme, the first of any protein encoded by the variola major virus, at a resolution of 1.8 Å, thereby creating an opportunity for structure-based development and optimization of inhibitors. *In silico* screening methods have led to the identification of several small molecules that inhibit variola H1 phosphatase with IC50 values in the low micromolar range.

**T-P099 High Transition State Affinity by TrpRS Coincides with an Unstable Protein Conformation.** C.W. Carter, Jr., Violetta Weinreb, Maryna Kapustina, Dept of Biochem. Biophys., CB 7260, UNC Chapel Hill, Chapel Hill, NC.

Pre-transition state (PreTS) tryptophanyl-tRNA synthetase crystal structures are almost indistinguishable (RMSD ~0.65 Å) with that of

a complex with adenosine-5' tetraphosphate (AQP). AQP has high affinity characteristic of a transition state analog inhibitor, and its  $\gamma$ - and  $\delta$ - phosphates mimic the PPi leaving group, binding more intimately to active-site lysine and serine residues than in the PreTS state ATP complex. Free, unliganded molecular dynamics simulations of both relax to other structures within 1 ns. The unliganded PreTS state reverts *backward* along the reaction path to the Open, while the AQP structure progresses *forward* to the Products conformation. The two, quite similar structures therefore lie on opposite sides of a steeply sloping conformational free-energy maximum, characteristic of a transition state. In free simulations with  $Mg^{++}ATP$  (without Trp)  $Mg^{++}-O$  distances change from  $\sim 2.5$  Å to within  $\sim 1.9$  Å, releasing two active-site lysine residues from their interactions with the phosphate oxygen atoms, coordinately with interdomain relaxation to the *Product* state. Two kinds of restraints preserve the high energy, PreTS conformation, which is also stable in free, fully-liganded trajectories. Either the centers of mass of the two domains or the  $Mg^{++}-O$  distances can be restrained to their unstable, crystallographically observed values. Thus, the high energy  $Mg^{++}$  coordination and conformational state are jointly imposed by catalytically productive interactions of active-site lysines with the PPi leaving group (1). Supported by NIGMS.

I. Kapustina M, Carter CW, Jr. Computational Studies of Tryptophanyl-tRNA Synthetase Ligand Binding and Conformational Stability. *Journal of Molecular Biology* 2006; In Press.

**T-P100 Structure of Homolog of F420-0: $\gamma$ -Glutamyl Ligase from *Archaeoglobus fulgidus* Reveals a Novel Fold.** B. Nocek<sup>1</sup>, E. Evdokimova<sup>2</sup>, M. Kudritska<sup>2</sup>, A. Savchenko<sup>2</sup>, A. Edwards<sup>2</sup>, A. Joachimiak<sup>1</sup>,<sup>1</sup>Midwest Center for Structural Genomics, Biosciences, Argonne National Laboratory, Argonne, IL 60439, <sup>2</sup>Banting and Best Dept. of Med. Res., Univ. of Toronto, Toronto, ON, Canada.

Coenzyme F420 (8-hydroxy-5-deazaflavin) is a group of redox-active cofactors playing a crucial role in biosynthesis of diverse metabolic reactions in methanarchaea and some eubacteria. The biosynthesis of this coenzyme has been studied unveiling six-step pathway. The fifth step of the F420 biosynthesis, the GTP-dependent addition of two L-Glu to the L-lactyl phosphodiester of 7,8-didemethyl-8-hydroxy-5-deazariboflavine is catalyzed by F420-0: $\gamma$ -glutamyl ligase (CofE). CofE is a 54kD homodimeric protein showing no sequence similarity to any previously characterized protein. Here we report first crystal structure of CofE from *A. fulgidus* determined using the SAD method and refined to 2.5 Å resolution. The protein structure has mixed alpha/beta fold with monomer organized into two domains. The structural similarity search using DALI server indicates that the structure of CofE homolog represents a novel fold. The structural analysis of this enzyme will be presented.

This work was supported by the grants from the NIH (GM62414 and GM074942) and the U.S. Department of Energy, OBER under Contract W-31-109-ENG-38.

**T-P101 The Use of Shape and Pharmacophore in High Throughput Crystallography Refinements and Lead Hopping: An Application Study.** Samuel Toba, Zeljko Dzakula, Daniel Bernard, Jon Sutter, Al Maynard. Accelrys Inc, San Diego, CA.

We report here shape and pharmacophore hypotheses derived from protein binding sites. The hypotheses generated augment the electron density information in the search for bound ligand as part of the crystal refinement process. The hypotheses can further be applied for lead-hopping to discover novel molecules. Our use of shape, pharmacophore, and excluded volumes features protocol provides one step approach to reduce false positives in ligand search and helps identify novel leads from virtual screening of databases.

**T-P102 Structural Basis for Activation of OSR1 (Oxidative Stress Responsive 1) Kinase by C-terminal Regulatory Domain.** S.J. Lee, M.H. Cobb, E.I. Goldsmith, Dept. of Biochemistry, The Univ. of Texas Southwestern Medical Center at Dallas, Dallas, TX.

Ste20p kinases function as adaptors to MAP kinase signaling pathways, and in other contexts. Human OSR1 (Oxidative Stress Responsive 1) belongs to the GCK-VI subfamily of Ste20p protein kinases and is homologous to SPAK (Ste20/SPS1-related, praline alanine-rich kinase), *Drosophila* Fray. OSR1 has a conserved Ste20p-like serine/threonine kinase domain at its N terminus with C-terminal region of poorly understood function. Two putative regulatory domains are located at the c-terminus, PF1 and PF2 domains. This domain is present only in the four GCK-VI members of the Ste20p family. The PF1 C-terminal regulatory domain is required for a catalytic activity of this OSR1 kinase. Following the extensive constructs trials for expression and solubility, one kinase domain and kinase with PF1 regulatory domain turned out to be soluble. After the initial crystallization trial with kinase domain only, needles were obtained. Further study of kinase domain alone and a kinase-PF1 construct will provide a structural basis of kinase activation by non-catalytic domain in Ste20p family.

**T-P103 Using a High-throughput Pipeline to Quickly Scan Multiple NMR Structures and Solve a Difficult Molecular Replacement Problem.** Francisco Hernandez-Guzman, Pre-sales, Accelrys, 10188 Telesis Ct. Suite 100, San Diego, CA 92122.

With the advent of the structural genomics era, and the availability of a large number of structures in public databases such as the Protein Data Bank, solution by molecular replacement (MR) has become the most popular and practical method for solving new structures in macromolecular X-ray crystallography. Unfortunately, the success rate of the MR method is directly proportional to the structural homology between the model and the unknown structure; in many cases this means exploring the MR space with a large number of search models. In this study, initial attempts at solving the crystal structure of a small domain from a large multi-domain protein using the MR method with homologous crystal structures, failed to yield the correct solution. A more exhaustive MR search, using the high-throughput pipeline HT-XMR to quickly scan multiple conformers of a homologous NMR structure, successfully retrieved the correct MR solution. As expected, the refined structure has a similar fold to the search models, but with enough structural differences to make this structure difficult to solve with current MR programs, including those using maximum likelihood methods.

**T-P104 Crystal Structures of Nucleotide and Non-Nucleotide Bound FtsZ from *Bacillus subtilis*.** Scott Lovell\*, Zachary Halloran\*, Kathryn Hjerrild#, Dean Sheridan#, Alex Burgin#, Lance Stewart#, deCODE Biostructures, \*Woodridge, IL 60517, #Bainbridge Island, WA 98110.

The tubulin homolog FtsZ, polymerizes in a reversible GTP dependent manner at the site of cell division and disassembles once cell division is complete.<sup>[1]</sup> We have determined the crystal structures of FtsZ from *Bacillus subtilis* in both non-nucleotide and nucleotide bound states. A primitive orthorhombic crystal form was observed that contained non-crystallographic dimers in the asymmetric unit and GDP in the nucleotide binding pocket of each subunit. The GDP was acquired from the expression host and could be displaced in one subunit after soaking the crystals in the presence of a non-hydrolyzable form of GTP (GTP- $\gamma$ -S). C-centered orthorhombic and primitive tetragonal forms were also observed when grown in the presence of lithium sulfate. These crystal forms contain a monomer in the asymmetric unit

and no nucleotide bound. However, sulfate molecules, that apparently displaced the GDP present in the expressed protein prior to crystallization, were observed in the nucleotide-binding pocket. These sulfate ions adopt positions within the nucleotide-binding pocket that would normally be occupied by the phosphate groups of GTP or GDP and serve as mimics for nucleotide binding.

[1] Romberg, L. and Levin, P.A., *Annu. Rev. Microbiol.* 2003, **57**, 125-154.

**T-P105 Rapid and Automated Substructure Determination.** Hongliang Xu, Charles M. Weeks, Herbert A. Hauptman, Hauptman-Woodward Medical Research Inst. & Dept. of Structural Biology, SUNY at Buffalo, 700 Ellicott St., Buffalo, NY 14203.

Direct methods of phase determination have played important role in determining heavy-atom substructure from difference amplitudes of native-derivative crystal pairs or anomalous scattering crystals. The minimal principle based *Shake-and-Bake* procedure is one of the most successful direct methods for heavy-atom substructure determination. The computer program *SnB*, which implements *Shake-and-Bake* procedure and is part of the protein structure determination package *BnP*, has recently been optimized for rapid and automated substructure determination. Specifically, *SnB* has drastically increased cost effectiveness via the implementation of (1) newly developed statistical minimal function, (2) optimal FFT grid size, (3) dynamic figure-of-merits for automatic solution detection and false solution rejection, and (4) effective strategies for difficult structures. With these recent improvements, the 160 Se substructure of KPHMT, originally solved by *SnB* after 8 CPU days on an SGI Origin 2000 server, now can be determined within 2 CPU days on an SGI R10000 machine.

This research was supported by NIH grants EB002057 and GM072023.

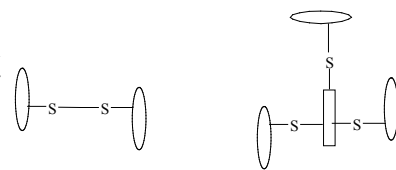
**T-P106 Crystallization Studies of Metnase, a SET/Transposase Protein.** Kristie D. Goodwin, Masahiko Oshige, Suk-Hee Lee, Millie M. Georgiadis, Dept. of Biochemistry and Molecular Biology, Indiana Univ. School of Medicine, 635 Barnhill Drive, Indianapolis, IN 46202.

Metnase is a histone methylase that stimulates foreign DNA integration and enhances nonhomologous end-joining repair. The protein consists of a SET domain and a transposase/nuclease domain that uniquely incorporate histone modification, DNA repair and integration activities; thus, Metnase is an example of a eukaryotic transposase that has normal cellular functions. Furthermore, the gene that encodes Metnase is located in a region of frequent chromosomal abnormalities in several cancers including non-Hodgkin's lymphoma, hereditary prostate cancer and breast cancer. The transposase domain has no sequence homology to any protein of known structure. Preliminary studies on Metnase include tryptic digestion to determine structural domains within the protein resulting in identification of a C-terminal domain that retains endonuclease activity. This domain has been expressed in *E. coli* and purified. We have obtained crystals of the C-terminal domain in the presence of oligonucleotide and are currently pursuing experimental phasing techniques to solve the structure.

**T-P107 Assembly Directed by Novel Functional Ligands with Transition Metals.** Shaohua Gou, Haibin Zhu, and Huaze Dong, State Key Laboratory of Coordination Chemistry, Nanjing Univ., Nanjing, 210093, P. R. China.

A variety of well-defined supramolecular arrays and coordination

polymers with diverse structural motifs have been realized by using a number of sulfur-containing organic ligands as building blocks. These functional ligands are composed of 4-(2', 3' or 4')-pyridine-2-mercaptopyrimidine, which have also been connected via the sulfur atom with alkyl chains or aromatic chains as shown below.



Different transition metals with square, tetrahedral and octahedral coordination geometries have been applied to construct new architecture through coordination bonding. Crystal structures of a number of compounds have been determined by single crystal X-ray diffraction, in which non-covalent interactions such as coordination bonds, hydrogen bonding, and aromatic  $\pi$ - $\pi$  stacking are studied.

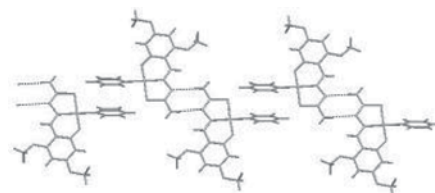
This research is supported by the National Natural Science Foundation of China (Project 20271026). H. Zhu is grateful to Jiangsu Province Personnel Department for a postdoctoral research grant.

**T-P108 The Interactions Between a Peptide Sex Pheromone Receptor PrgX to Two Antagonists: cCF10 and iCF10.** Ke Shi<sup>1</sup>, C. Kent Brown<sup>1</sup>, Zuyi Gu<sup>1</sup>, Briana K. Kozlowicz<sup>2</sup>, Gary M. Dunny<sup>2</sup>, Douglas H. Ohlendorf<sup>1</sup>, Cathleen A. Earhart<sup>1</sup>, <sup>1</sup>Dept. of Biochemistry, Molecular Biology, and Biophysics and <sup>2</sup>Dept. of Microbiology, Univ. of Minnesota, Minneapolis, MN55455.

PrgX, a key player in controlling conjugation induced by the peptide pheromone cCF10 in *Enterococcus faecalis*, is the cytoplasmic receptor for the cCF10 peptide pheromone and has been shown to bind to two sequences in the intergenic region of pCF10 between *prgX* and *prgQ* (the *prgQ* operon encodes the conjugative transfer functions of pCF10). iCF10 is a plasmid-encoded peptide competitor of cCF10. We proposed that PrgX functions as a tetramer in vivo from our PrgX crystal structures. The structure of the pheromone-PrgX complex reveals that pheromone binds in the cleft of the central dimerization domain, causes the C-terminal regulatory domain rotates about 120° and thus disrupts the PrgX tetramer. Amino acids 304-317 are mobile and invisible in either the PrgX or PrgX/cCF10 structures. The iCF10 binds in the pheromone-binding pocket the same way as cCF10 and the C-terminal domain in PrgX/iCF10 complex keeps the same conformation as in uncomplexed PrgX. The C-terminal amino acids interacting with iCF10 stabilizing this "native conformation" of PrgX and the PrgX tetramer and thus enhancing PrgX repression of the *prgQ* operon.

**T-P109 Exploring the Non Covalent Assembly Capabilities of Thiosemicarbazones and Their Coordination Compounds.** P. X. García-Reynaldos, J. Valdés-Martínez, S. Hernández-Ortega, Inst. de Química, Univ. Nacional Autónoma de México, México DF, 04510, México.

Crystal engineering, synthesis and building of functional crystals, uses reliable interactions on constructing reproducible supramolecular motifs. Among these,  $\pi$ - $\pi$  interactions and hydrogen-bonding have been studied, nevertheless its use in designing coordination compounds, is little extended. Thiosemicarbazones have interesting structural and biological properties; as ligands they form chelating rings that we hypothesized may present H-bonding interactions similar to those observed in 2-amino-



pyridines. We will present a systematic study of the intermolecular H-bonds formed by coordinated thiosemicarbazones as well as the joint use of  $\pi$ - $\pi$  interactions, through the introduction of pyridine ligands, to organize in predictable way neutral square planar Ni (II) complexes into extended networks.

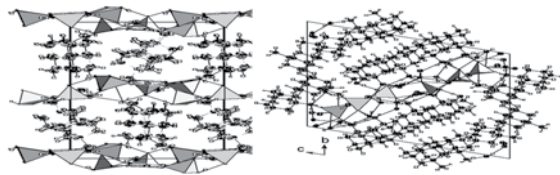
**T-P110 Structure of STM3548 Cytoplasmic Protein from *Salmonella typhimurium*.** M.E. Cuff, Ry. Wu, T. Petrova, A. Joachimiak, Midwest Center for Structural Genomics and Structural Biology Center, Biosciences, Argonne National Laboratory, 9700 South Cass Ave., Bldg 202, Argonne, IL 60439.

Cytoplasmic protein DUF1355 from *S. typhimurium* forms a striking hexamer exhibiting D3 noncrystallographic symmetry. The monomer is a globular  $\alpha/\beta$  fold with a 5-stranded parallel  $\beta$ -sheet at its core and a  $\beta$ -hairpin. Near the N-terminus is a 23 residue  $\beta$ -hairpin that reaches across the hexamer and H-bonds with the hairpin of the monomer diagonally across from it, forming a 4-stranded anti-parallel  $\beta$ -sheet. Three of these sheets form a triangular center to the hexamer, which may be described as two layers of trimers. Structural homologs can be found to the globular region of DUF1355, but not including the extended hairpin. A SeMet derivative of the 253 amino acid protein was crystallized in space group P2<sub>1</sub>2<sub>1</sub>2 (a=183.0Å, b=79.5Å, c=115.75Å). The structure was solved with two wavelength MAD data. Structure solution, phasing, and density modification were facilitated with autoSHARP and the model was refined at 2.3Å with Refmac. Sequence, structural comparisons and relationships to members of the glutamine aminotransferase family will be presented.

This work was supported by the grants from the NIH (GM62414 and GM074942) and the U.S. Department of Energy, OBER under Contract W-31-109-ENG-38.

**T-P111 Systematic Synthesis and Studies of Hydrogen Bonding Networks Built with 1,3,5-benzene-trisphosphonic Acid and 1-Adamantane amine.** Deyuan Kong, Jerzy Zoń, Abraham Clearfield\*, Dept. of Chemistry, Texas A&M Univ., College Station, TX, 77842, Inst. of Organic Chemistry, Biochemistry and Biotechnology, Wrocław Univ. of Technology, Poland.

The phosphonic acid benzene-1,3,5-tris(phosphonic acid), was reacted with 1-adamantane amine in different molar ratio to give out different hydrogen bonded complexes. The deprotonation of the ligand trigger the formation of self-complementary layered hydrogen bonding architectures.



Thanks for the financial support from the Department of Energy, Basic Sciences Division through grant no. DE-FG03-00ER 15806.

1. (a) Reiter, S. A.; Assmann, B.; Nogai, S. D.; Mitzel, N. W.; Schmidbaur, H. *Helv. Chim. Acta*, 2002, 85, 1140. (b) Mehring, M. *Eur. J. Inorg. Chem.*, 2004, 3240.
2. Mehring, M.; Schürmann, M.; Ludwig, R. *Chem. Eur. J.* 2003, 9, 837.
3. Kong, D. Y.; Zoń, J.; Clearfield, A. *Cryst. Growth & Design*. 2005, 5, 1767.

**T-P112 A Comparison of Pt and Br Phasing for Structure Determination.**<sup>‡</sup> B.D. Santarsiero<sup>\*,</sup> K. Ratia<sup>\*,</sup> K.S. Saikatendu<sup>§</sup>, N. Barretto<sup>†</sup>, S.C. Baker<sup>†</sup>, R.C. Stevens<sup>§</sup>, A.D. Mesecar<sup>\*,</sup> \*Center for Pharmaceutical Biotechnology and Dept. of Medicinal Chemistry and Pharmacognosy, Univ. of Illinois at Chicago, Chicago, IL, <sup>§</sup>Depts. of Cell and Molecular Biology, The Scripps Research Inst., <sup>†</sup>Dept. of Microbiology and Immunology, Loyola Univ., Chicago Stritch School of Medicine.

We have determined the structure of PL<sub>pro</sub>, a SARS coronavirus papain-like protease, to a resolution of 1.85Å. The native enzyme, with 313 residues, crystallizes in space group C2 with three chains related by non-crystallographic symmetry. We obtained two heavy atom derivatives using Pt and Br. The Pt derivative was collected at one wavelength, and the Br derivative was collected at two different wavelengths. All three data sets, and a native data set, were used for initial phasing using SOLVE. Six Pt atoms but no Br atoms were found. HYSS finds five Pt atoms or six Br atoms from their respective data sets. The Br data is at the highest resolution, and we used one of the data sets for building and refinement of the structure; nine Br atoms are included in the final model. This affords an opportunity to compare the phasing power of Pt vs. Br. We also compare the different results in phasing using SOLVE, HYSS, and other phasing programs.

<sup>‡</sup>We acknowledge support by a Public Health Service research grant P01 AI060915, and the National Institutes of Health, NIAID Contract HHSN 266200400058C. Diffraction intensities were collected at the Southeast Regional Collaborative Access Team (SER-CAT, 22-ID), Advanced Photon Source (APS), and use of the APS is supported by the U. S. Department of Energy, Office of Basic Energy Sciences, under Contract No. W-31-109-Eng-38.

**T-P113 Hydrophobic Hydration – Information from Solution of Small Molecules as a Source of Structural Models for Macromolecular Crystallography.** Janusz Lipkowski<sup>a</sup>, Konstantin Udachin<sup>b</sup>, Dariusz Świerczyński<sup>a</sup>, Jerzy Ostyk-Narbutt<sup>c</sup>, <sup>a</sup>Inst. Phys. Chem., Polish Acad. Sci., Warszawa, Poland, klatrat@ichf.edu.pl, <sup>b</sup>Stacie Inst. Mol. Sci., NRC Ottawa, Canada, <sup>c</sup>Inst. Radiation Chem. and Techn., Warszawa, Poland.

In the present paper an up-to-date review of hydrophobic hydrates will be given, some new, yet unpublished, experimental data will be presented as well.

As known from literature, complex cavities may be formed *via* different deformations of arrangement of water molecules: either by combination of dodecahedra to form Jeffrey-type complex cavities or by incorporating foreign species. Strong ionic environment exerts significant deforming influence as well. Thus, the resulting structural pattern is a combination of hydrophobic hydration, ionic strength and foreign species incorporated into the framework.

The illustrations will be based on recent, partly unpublished X-ray structures of hydrates of macrocyclic compounds (crowns, calixarenes) and their intermolecular complexes, coordination complexes and fatty acids. Statistics on water coordination number in these compounds will be presented as well.

The importance of the structural patterns to stabilize selected structures has been experimentally demonstrated, e.g. in extraction studies in the water/organic systems, proton or ionic conductivities in the systems and redox equilibria, with water aggregates serving as proton or electron sponges.

**T-P114 Structure of a Novel Acyltransferase.** R. Bott<sup>1</sup>, M. Saldajeno<sup>1</sup>, G. Ganshaw<sup>1</sup>, M. Cervin<sup>1</sup>, Gregg Whited<sup>1</sup>, W Weyler<sup>1</sup>, R. Sala<sup>1</sup>, M. Soltis<sup>2</sup>, M. Irimpan<sup>2</sup>, <sup>1</sup>Genencor International a Div. of Danisco, Palo Alto CA, <sup>2</sup>SSRL, Stanford Univ., Stanford, CA.

We have determined the three dimensional structure of a unique acyltransferase that catalyzes acyl transfer reactions in water. Unlike hydrolases that perform alcoholysis under anhydrous conditions, this acyltransferase, isolated from *Mycobacterium smegmatis* (MsAcT), demonstrated alcoholysis even in substantially aqueous media. MsAcT crystallizes as an octamer in the tetragonal space group P4. The molecule was determined using selenomet MAD phasing and has been refined to a working R-factor of 17.5% and  $R_{\text{free}}$  of 19.6%. A structural-homology search performed with MsAcT using the program DALI (Holm and Sander, 1995), which is based on a distance criterion and does not use sequence information for the comparison, showed five closely related proteins all belonging to the SGNH hydrolase class of enzymes. The structure of MsAcT provides additional insight into the structural basis of its ability to perform acyl transfer in aqueous media.

Holm, L. and Sander C. (1995) Dali: A network tool for protein structure comparisons, *Trends Biochem. Sci.* 478-480.

**T-P115 Subtle Crystal Environmental Influence on Pseudo-Jahn-Teller Effect Expression.** Larry R. Falvello, Inmaculada Escorihuela, Rosa M. Llusar,<sup>a</sup> Tatiana Soler<sup>b</sup>, Milagros Tomás, Dept. of Inorganic Chemistry and I.C.M.A., Univ. of Zaragoza - C.S.I.C., Plaza San Francisco s/n E-50009 Zaragoza, Spain, <sup>a</sup>Dept. de Ciències Experimentals, Univ. Jaume I, Campus de Riu Sec, P.O. Box 224, Castelló, Spain, <sup>b</sup>Servicios Técnicos de Investigación, Facultad de Ciencias, Univ. de Alicante, 03080 Alicante, Spain.

A parametric study has been conducted on crystals with two independent pseudo-Jahn-Teller active monocations,  $[\text{Cu}(\text{NO}_3)(\text{bipy})_2]^+$  (bipy = 2,2'-bipyridyl), crystallized with a large dianion,  $[\text{Pt}(\text{C}_6\text{F}_5)_4]^{2-}$ . In crystals with one molecule of acetone in the asymmetric unit, one of the independent cations is dynamic at all temperatures studied, while the other has static distortion at low temperature and suffers increasing amounts of disorder as the temperature is raised. When this system is crystallized with one molecule of  $\text{CH}_2\text{Cl}_2$  instead of acetone, the Jahn-Teller behavior changes although the gross aspects of the crystal structure -- unit cell, space group, molecular arrangement -- remain essentially the same. In the  $\text{CH}_2\text{Cl}_2$ -containing crystals both of the cation sites have a component of static behavior at low temperature. This represents a change in expression of the JT effect that could not be achieved at any attainable temperature for the acetone solvate.

**T-P116 The Crystal Structure of the Trp Repressor Binding Protein TwqN from *B. subtilis*.** Y. Kim, P. Quartey and A. Joachimiak, Midwest Center for Structural Genomics and Structural Biology Center, Biosciences, Argonne National Laboratory, 9700 South Cass Ave., Bldg 202, Argonne, IL 60439.

The Trp repressor binding protein TwqN from *B. subtilis* belongs to the family of flavodoxin-like proteins, also known as the NADPH-dependent FMN reductases, as indicated by sequence analysis. However, its biological function remains to be determined. Since SeMet derivative crystals couldn't be obtained, the heavy atom derivative crystals were prepared by soaking the native crystals in relatively high concentration of  $\text{PtCl}_4$  for less than half an hour. The structure was determined to 1.7 Å by SAD phasing and utilizing Pt anomalous scattering. The TwqN is an  $\alpha/\beta$  fold, a five stranded parallel  $\beta$ -sheet is flanked by three  $\alpha$ -helices in one side and four in

the other, strikingly similar to previously determined flavoproteins such as Ylr011wp, *S. cerevisiae* NADPH-dependent FMN reductase (ITOI), and a monomeric flavoprotein azobenzene reductase from *B. subtilis* (1NNI). The crystal structure of TwqN assembles into a tetramer unique among flavodoxin-like proteins. In the crystal structure none of four protomers binds FMN. Structural analysis is reported.

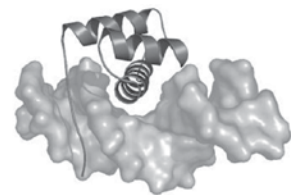
This work was supported by the grants from the NIH (GM62414 and GM074942) and the U.S. Department of Energy, OBER under Contract W-31-109-ENG-38.

**T-P117 Self-recognition Patterns of Oxalurate in its Alkali and Alkaline Earth Salts. Different Ribbon Topologies and Polytypes.** Milagros Tomás, José Ignacio Peñacoba, Larry R. Falvello, Tatiana Soler, Dept. of Inorganic Chemistry, Univ. of Zaragoza, and Aragón Materials Science Inst., Univ. of Zaragoza - C.S.I.C., Plaza San Francisco s/n, E-50009 Zaragoza, Spain, and Servicios Técnicos de Investigación, Facultad de Ciencias Fase II, 03690 San Vicente de Raspeig, Alicante, Spain, milagros@unizar.es.

Oxalurate is a product of the mutagenic oxidation of DNA, and is formed depending on the conditions under which the oxidation takes place -- such as the presence of  $\text{Mg}(2+)$  or  $\text{Ca}(2+)$ . Oxalurate is a versatile polyfunctional ligand in coordination chemistry, and presents a rich variety of topologies for metal coordination and for non-covalent interactions with its environment. The oxalurate aqua complexes of Mn(II), Ni(II) and Cu(II) form regularly shaped supramolecular structures, despite the lack of symmetry in the ligand itself. The crystal structures of some oxalurate salts will be presented, displaying different aggregates and packing assemblies of these aggregates. A system which forms two distinct polytypes will also be described.

**T-P118 Crystal Structure of the DNA-bound Pdx-1 Homeodomain Complex.** A. Longo\*, G. Guanga, R. Rose. Dept. of Molecular and Structural Biochemistry, NCSU, Raleigh, NC 27695, \*also CCS-CSM, ORNL, Oak Ridge, TN 37831.

Pancreas duodenal homeobox-1 (Pdx-1) is a homeodomain (HD) protein belonging to the ParaHOX family, essential for pancreatic endocrine and exocrine islet cell development and maintenance of adult islet beta cell function<sup>[1]</sup>. Mutations in the human *pdx-1* gene lead to a form of Type II diabetes, termed maturity-onset diabetes of the young (MODY-4)<sup>[2]</sup>. We determined the crystal structure of the 60 amino acids of the HD bound to the target DNA. Data were collected on frozen crystals at the SER-CAT beamline at the APS. The structure was solved at 2.5 Å resolution by molecular replacement using the Antennapedia HD structure<sup>[3]</sup> as a search model. The data were refined to an R-free of 28.7% and R-factor of 23.9%. Comparison of the Pdx-1 HD structure to other HOX-HD/DNA complex structures indicates a conserved overall structure. The N-terminal arm of the Pdx1 is clearly visible in the structure, providing a detailed view of all interactions between Pdx1 and the DNA. Analysis of the R197H mutant, the only mutation in MODY-4 located in the HD, indicates that the residue is involved in DNA binding.



[1] Melloul, D., Ann N Y Acad Sci, 2004 (1014):28.

[2] MacFarlane et al. *J. Clin Invest.* 2000 (5):717.

[3] Fraenkel E, Pabo CO., *Nat Struct Biol.* 1998 (8):692.

**T-P119 Unique Bimetallic Cu/Cd Complex with Crystal Structure Dependent on Temperature.** O.V. Nesterova,<sup>1</sup> S.R. Petrusenko,<sup>1</sup> V.N. Kokozay<sup>1</sup>, O.V. Shishkin<sup>2</sup>, <sup>1</sup>Chemistry Dept., National Taras Shevchenko Univ., Volodymyrska Str. 64, Kyiv 01033, Ukraine, <sup>2</sup>STC “Inst. for Single Crystals”, National Academy of Sciences of Ukraine, Lenina ave. 60, Kharkov 61001, Ukraine.

Synthesis of multicomponent materials by self-assembly of molecular species into covalently or noncovalently joined aggregates is one of the most useful approaches to obtain new functional materials. The reaction of copper powder, cadmium oxide and ammonia acetate in methanol solution of ethylenediamine (en) affords the complex  $\{[\text{Cu}(\text{en})_2][\text{Cd}_2(\text{OAc})_6]\}_n$  I (red crystals), the crystal structure of which consists of the unique 1D ladder-like anions  $[\text{Cd}_2(\text{OAc})_6]_n^{2-}$  and cations  $[\text{Cu}(\text{en})_2]^{2+}$ . After heating these crystals up to 150°C, the crystal structure is transformed so that a new type of polymeric chains  $[\text{Cu}(\text{en})_2\text{Cd}_2(\text{OAc})_6]_n$  II (dark violet crystals) are formed. The coordination geometry of the Cu(II) atom in I is square planar [closest axial contacts Cu...O of 3.084(2) Å] while in II it is elongated octahedral with the axial Cu–O bond distances of 2.744(10) Å.

This work was supported in part by the INTAS (Project 03-51-4532).

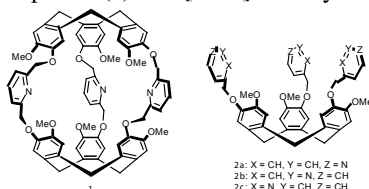
**T-P120 Structural Studies on a 23S rRNA Modifying Enzyme from *E. coli*.** J. Sivaraman<sup>1</sup>, S. Sunita<sup>1</sup>, H. Zhenxing<sup>1</sup>, J. Swaathi<sup>1</sup>, M. Cygler<sup>2</sup>, A. Matte<sup>2</sup>, <sup>1</sup>Dept. of Biological Sciences, National Univ. of Singapore, 14 Science Dr., Singapore 117543, <sup>2</sup>Biotechnology Research Inst., National Research Council, Canada, 6100 Royalmount Ave., Montréal Québec Canada H4P 2R2.

Pseudouridylation is one of the most abundant post transcriptional modifications found in RNA. The conversion of Uridine (U) to Pseudouridine ( $\Psi$ ) is carried out by enzymes called  $\Psi$  synthases.  $\Psi$  has been identified as the fifth nucleoside and is found in all three domains of life namely, prokaryotes, archae and eukaryotes. The  $\Psi$ s in the 23S rRNA of the Large subunit of the ribosome are clustered in or around the Peptidyl Transferase Centre (PTC), which is the site of peptide bond formation. Mutations in genes encoding  $\Psi$  synthases in prokaryotes as well as lower and higher eukaryotes have dramatic effects on the growth of the organism and in some cases are also lethal.

Here, our focus is on structural studies of the  $\Psi$  synthase that modifies U2604 of 23S rRNA, namely, RluF. The catalytic module of RluF was crystallized and after selenomethionyl substitution, a complete Multiwavelength Anomalous Dispersion (MAD) data set was collected and the structure was refined to a final resolution of 2.6Å. The crystal packing revealed a dimeric structure of RluF. It was also observed to form dimers in solution, based on Dynamic Light Scattering as well as Gel filtration experiments. We have also done limited proteolysis, mass spectrometry and N terminal sequencing to reveal the distinct domain architecture of this enzyme.

**T-P121 Pyridyl-functionalized Cavitanes and Capsules.** S.D. Drake, K.T. Holman, Georgetown Univ., Washington, DC.

Molecular cavitanes and capsules will exhibit recognition and self-assembly properties that are influenced by their specific endo- and/or exo-functionalization. In this context, the structures of synthesized pyridyl-substituted cryptophane capsules (1) and [1.1.1]-orthocyclophane cavitanes (2) will be presented. Capsule molecules that are endo-*N*-functionalized are being explored for their behavior toward anion binding (when protonated),



cation binding, and as organocatalysts, whereas the pyridyl-substituted [1.1.1]-orthocyclophanes are being explored as ligands for coordination driven self-assembly of both discrete and infinite structures. Progress on these fronts will be presented.

**T-P122 Structure of Mouse Apolipoprotein A-I Binding Protein.** I.A. Shumilin, K.N. Jha, H. Zheng, M. Chruszcz, M. Cymbrowski, J.C. Herr, W. Minor, Univ. of Virginia, Charlottesville, VA.

Apolipoprotein A-I binding protein (AI-BP) specifically binds to apolipoprotein A-I, the major component of high-density lipoprotein particles. Despite the widespread presence of the AI-BP homologs in various organisms, its function remains unknown. SeMet-substituted mouse AI-BP missing N-terminal signal peptide and containing C-terminal His-tag was expressed in *E. coli* and used for the crystallization and structure determination. The crystals belong to space group C2 with cell dimensions  $a = 104.9$  Å,  $b = 125.7$  Å,  $c = 163.6$  Å,  $\beta = 106.6^\circ$  and diffract to 2.5 Å. The asymmetric unit contains six subunits of 265 residue protein organized in three dimers and includes 48 SeMet residues in total. 36 Se atoms were found and used for SAD phasing. 12 remaining SeMet are located on the 27 residue long N-terminal segments that are disordered in all subunits. The model was refined to  $R = 19.7\%$  and  $R(\text{free}) = 21.9\%$ . A cluster of residues conserved among AI-BP homologs is likely to constitute an active site indicating that these proteins function as enzymes. The series of complex structures with various ligands supporting this hypothesis will be presented.

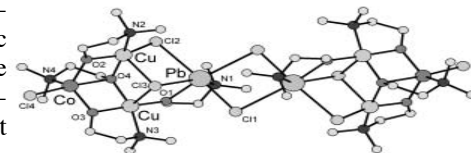
**T-P123 A Unique Heterotrimetallic  $\text{Cu}_4\text{Co}_2\text{Pb}_2$  Complex with the 2-(dimethylamino)ethanol Ligand.** D.S. Nesterov,<sup>1</sup> V.N. Kokozay,<sup>1</sup> B.W. Skelton<sup>2</sup>, <sup>1</sup>Chemistry Dept., National Taras Shevchenko Univ., Volodymyrska Str. 64, Kyiv 01033, Ukraine, <sup>2</sup>Chemistry, Univ. of Western Australia, Crawley, Western Australia.

The synthetic strategy<sup>1</sup>, based on the self-assembly of building blocks, generated *in situ*, into crystalline materials, has been successfully applied for the preparation of a novel octanuclear coordination compound  $[\text{Cu}^{\text{II}}_2\text{Co}^{\text{II}}\text{Pb}^{\text{II}}\text{Cl}_4(\text{L})_4]_2$  (HL = 2-(dimethylamino)ethanol). It was obtained by reaction of copper powder with cobalt chloride, lead chloride and an acetonitrile solution of 2-(dimethylamino)ethanol in air.

The complex exhibits a centrosymmetric molecule with the inversion centre situated at the mid-point of the central  $\text{Pb}_2\text{Cl}_2$  unit. The hexacoordinate Pb presents a very distorted coordination geometry with Pb–O(N, Cl) distances in the range 2.303(4)–3.1988(18) Å. The Cu atoms adopt distorted square pyramidal geometries. The Co atom has a trigonal bipyramidal environment. The compound crystallizes in the monoclinic system with space group  $P2_1/c$  and the cell dimensions:  $a = 19.7380(10)$ ,  $b = 10.9365(9)$ ,  $c = 13.908(2)$  Å,  $\angle\beta = 97.549(2)^\circ$ ,  $Z = 2$ ,  $V = 2976.2(5)$  Å<sup>3</sup>.

This work was supported in part by the INTAS (Project 03-51-4532).

[1]. D.S. Nesterov, V.G. Makhankova, V.N. Kokozay and B.W. Skelton, *Inorg. Chim. Acta*, 2005, 358, 4519.



**T-P124 The Crystal Structure of IFS: A Novel Endogenous Inhibitor of the Secreted Streptococcal NAD-glycohydrolase.** Craig L. Smith, Jerry S. Pinkner, Joydeep Ghosh, Michael A. Meehl, Michael G. Caparon, Scott J. Hultgren, Molecular Microbiology, Washington Univ., St. Louis, MO.

The *Streptococcus pyogenes* NAD-glycohydrolase (SPN) is a toxic enzyme that is introduced into infected host cells by the Cytolysin-Mediated Translocation (CMT) pathway. However, how *S. pyogenes* protects itself from the self-toxicity of SPN had been unknown. A small protein of 161 amino acids, IFS is localized in the cytoplasmic compartment. Previous experiments showed that IFS forms a stable complex with SPN at a 1:1 molar ratio and inhibits SPN's NAD glycohydrolase activity by acting as a competitive inhibitor of its  $\beta$ -NAD<sup>+</sup> substrate (Meehl et al., in press). In order to better understand the molecular determinants of IFS inhibition, we determined the crystal structure of IFS. The polypeptide, expressed with carboxyl-terminal c-myc and his tags, crystallizes in the trigonal space group P3121 with unit cell dimensions a=b=107.95 c=146.93. Diffraction data were phased using the multiwavelength anomalous dispersion (MAD) method. Refinement is currently in progress. Currently, the Rwork = 31% and Rfree = 26% at a resolution of 2.5 Å using all available data. IFS is an  $\alpha$ -helical protein that looks like the letter "P" with a helical "meander" N-terminal domain and a long C-terminal tail extend from the N-terminal domain. Future analysis includes determine residues critical for binding to SPN.

**T-P125 Reinecke Anion as a Building Block in Designing of Heterometallic Cr(III) Complexes.** D. Shevchenko<sup>1</sup>, V. Nikitina<sup>1</sup>, V. Kozoyaz<sup>1</sup>, V. Dyakonenko<sup>2</sup>, O. Shishkin<sup>2</sup>, <sup>1</sup>Kyiv National Taras Shevchenko Univ., Volodymyrska St 64, Kyiv, 01033 Ukraine, <sup>2</sup>STC "Inst. for Single Crystals", National Academy of Sciences of Ukraine, 60 Lenin Ave, Kharkiv, 61001 Ukraine.

The search for new metal-containing building blocks is of current interest in molecular magnetism and in crystal engineering. It is well known that the thiocyanato anion acts as a bridge between either identical or different metal ions. Nevertheless, the thiocyanato complexes have rarely been used in assembling heterometallic architectures. A very appealing complex in this respect is the anion of the Reinecke salt, [Cr(NCS)<sub>4</sub>(NH<sub>3</sub>)<sub>2</sub>]<sup>-</sup>, which can interact with the second metal ion through the sulphur atom. Moreover, the family of such type building blocks can be extended by replacing the NH<sub>3</sub> ligands from the Reinecke anion with organic molecules that can act as bridges. The series of the Cu(II)/Cr(III) heterometallic complexes have been prepared by the direct synthesis from the following systems: Cu<sup>0</sup>-NH<sub>4</sub>[Cr(NCS)<sub>4</sub>(NH<sub>3</sub>)<sub>2</sub>]<sub>2</sub>·H<sub>2</sub>O-L-solvent (L = ethylenediamine or its derivatives). It was found that the nuclearity of complexes (2, 3, 5, polymeric), which was determined by means of X-ray measurements, depends on a reagent ratio and a solvent.

This work was supported in part by INTAS Grant 03-51-4532.

**T-P126 SP0731 from *Streptococcus pneumoniae* is a Member of the VOC Superfamily.** N.E.C. Duke, H. Li, F. Collart, A. Joachimiak, Structural Biology Center and Midwest Center for Structural Genomics, Biosciences, Argonne National Laboratory, 9700 South Cass Ave., Bldg 202, Argonne, IL 60439.

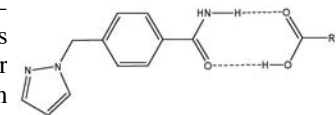
The vicinal oxygen chelate (VOC) superfamily is composed of structurally related proteins containing paired (βbeta-αalpha-βbeta-βbeta), motifs. SP0731, a conserved small protein from *S. pneumoniae*, also belongs to this superfamily. A SeMet derivative of the 115 amino acid protein was crystallized in space group P65 (a=97.62 Å, b=97.62 Å,

c=55.15 Å). The structure was solved using SAD data collected at the 19BM beamline of the Structural Biology Center. Structure solution, phasing, and density modification were facilitated with the HKL2000\_PH suite, and the model was refined to 2.3 Å using Refmac. Comparisons with other known protein structures in the PDB proves that structural genomics projects have now located several members of this family, though the structural homologies are not evident at the sequence level. Comparisons of these structures to known VOC superfamily representatives will be presented, along with similarities and differences in possible functional sites.

This work was supported by the grants from the National Institute of Health (GM62414 and GM074942) and the U.S. Department of Energy, Office of Biological and Environmental Research under Contract W-31-109-ENG-38.

**T-P127 Giving Pyrazole a Helping Hand in the Competition Against the Amide.** Benjamin Scott, Christer Aakeroy, John Desper, Chemistry, Kansas State Univ., Manhattan, KS 66506.

Previous work has shown predictable co-crystal formation between a pyrazole-benzamide ligand and carboxylic acids. In these cases, the pyrazole nitrogen is not able to compete with the amide due to its poor binding ability (based on electrostatic potential) resulting in co-crystals consisting of an acid:amide dimer via O-H···O and N-H···O hydrogen bonds (Scheme 1).



In order to synthesise ternary co-crystals, it is essential to have two different 'active' binding sites available for hydrogen bonding, making it necessary for the pyrazole nitrogen to have the ability to compete with the amide functionality for the carboxylic acid. To improve the acceptor ability (based on electrostatic potential) of the pyrazole nitrogen, methyl substituents have been added to the heterocycle (Scheme 2).

The design and synthesis of the new supramolecular reagent and the subsequent formation of co-crystals with carboxylic acids will be presented.

C. B. Aakeroy, J. Desper, B. M. T. Scott, *Chem. Commun.* 2006, ASAP, DOI:10.1039/b517118k

**T-P128 Crystal Structure of a New Type of Bacteriophytochrome.** Xiaojing Yang, Emina A. Stojković, Jane Kuk, Keith Moffat, Dept. of Biochemistry and Molecular Biology, The Univ. of Chicago, Chicago, IL 60637.

Phytochromes are bilinproteins found across bacterial, fungal and plant kingdoms. Most phytochromes direct photosensory responses by switching between two photo-interconvertible forms, Pr and Pfr, which absorb red and far-red light, respectively. We have determined the crystal structure of the chromophore binding domain from a new type of bacteriophytochrome RpBphP3 from *R. palustris*. RpBphP3 displays different photochemistry that converts between the red and near-red light absorbing forms, Pr and Pnr, respectively. RpBphP3 was crystallized with its chromophore (biliverdin, BV) assembled, and the structure was solved by molecular replacement based on the structure of the chromophore binding domain from *D. radiodurans* phytochrome (Wagner et al. 2005).

We thank BioCARS for access to beamline 14 BM-C at the APS. Supported by NIH RO1 GM36452 to KM.

**T-P129 Design, Synthesis and Characterization of Polymerizable Terminal Diacetylene Salts.** Zhong Li, Frank W. Fowler, Joseph W. Lauher, Dept. of Chemistry, State Univ. of New York, Stony Brook, NY, 11794.

**Polydiacetylenes (PDAs)** have attracted great interest due to their potential uses as advanced materials. PDAs are commonly prepared by 1,4 polymerization of **diacetylene** monomers in the solid state. Recently, we have reported the first single-crystal-to-single-crystal polymerization of a terminal **diacetylene**. Herein, we developed a general crystal engineering approach of controlling the packing of cationic guest molecules guided by the crucial hydrogen bonds between anionic host molecules. As an application, we have prepared a series of new terminal **diacetylene** monomers, including aryl terminal **diacetylenes**. They were successfully arranged via host-guest chemistry in patterns suitable for solid state 1,4 polymerization. The heat-induced polymerization of these **diacetylenes** has been carefully followed using X-ray diffraction.

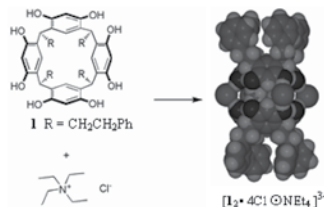
**T-P130 Scaffolding Protein Islet-brain 1 Homodimerization.** Michael Gajhede<sup>1</sup>, Sylvie Guenat<sup>2</sup>, Imran Dar<sup>1</sup>, Jette S. Kastrop<sup>1</sup>, Christophe Bonny<sup>2</sup>, Ole Kristensen<sup>1</sup>, <sup>1</sup>Biostructural Research, Dept. of Medicinal Chemistry, The Danish Univ. of Pharmaceutical Sciences, Universitetsparken 2, DK-2100 Copenhagen, Denmark, <sup>2</sup>Unit of Molecular Genetics, University Hospital of Lausanne (CHUV), Falaises 1, 1011 Lausanne, Switzerland.

Islet-brain 1 (IB1 or JIP-1) is a scaffold protein that interacts with components of the JNK signal-transduction pathway. IB1 is expressed at high levels in neurons and in pancreatic  $\beta$ -cells, where it controls expression of insulin-secretory components and secretion. We have shown that IB1 homodimerizes through a novel and unique set of SH3-SH3 interactions<sup>[1]</sup>. X-ray crystallography studies show that the dimer interface covers a region usually engaged in PxxP-mediated ligand recognition, even though the IB1 SH3 domain lacks this motif. The highly stable IB1 homodimer can be significantly destabilized *in vitro* by three point-mutations directed against key residues involved in dimerization. Taken together with *in-vivo* results this indicates that IB1 homodimerization through its SH3 domain has pleiotropic effects including regulation of the insulin secretion process.

[1] Kristensen, O., Guenat, S., Dar, I., Allaman-Pillet, N., Abderrahmani, A., Feraoussi, M., Roduit, R., Maurer, F., Beckmann, J. S., Kastrop, J. S., Gajhede, M., & Bonny, C. (2006). *EMBO J.* **25**, 785-97.

**T-P131 On Molecular Capsules Obtained from Calix[4]resorcinarene.** O. Ugono, K. T. Holman,\* Dept. of Chemistry, Georgetown Univ., Washington, DC, oou@georgetown

Self-assembled molecular capsules have been the subject of much recent research related to their ability to act as hosts for suitable guests. One theme of our research is directed at the assembly of molecular capsules, nano containers of sorts, from calix[4]resorcinarenes and other components. Co-crystallization of 1 and tetraethyl ammonium chloride yielded a chloride mediated capsule with an encapsulated alkyl ammonium cation. The capsule is held together by 8 OH...Cl<sup>-</sup> intermolecular hydrogen bonds. Complexes of 1 and other alkyl ammonium salts have been obtained. Alcohols have been shown to assist in the construction of similar molecular capsules, wherein calix[4]resorcinarene units are held in place by hydrogen bonds between the respective compo-



nents. An array of similar containers and other interesting structures have been obtained by the co-crystallization of alcohols and resorcinarenes such as 1. The solid state structures and solution studies of these capsules will be presented.

**T-P132 An Integrated High-throughput Approach to Study Proteomes of Infectious Agents: A Case Study of the Severe Acute Respiratory Syndrome Coronavirus.** Saikatendu Kumar, Jeremiah Joseph, Vanitha Subramanian, Benjamin Neuman, Michael Buchmeier, Raymond Stevens, Peter Kuhn, Depts. of Cell Biology and Molecular Biology, The Scripps Research Institute, 10550 N. Torrey Pines Rd, La Jolla, CA 92122.

We have developed a biology-driven, high-throughput approach to study emerging infectious agents like the Severe Acute Respiratory Syndrome coronavirus (SARS-CoV). The 28 mature proteins encoded by the ~29kb viral RNA genome have been subjected to a miniaturized crystallomics pipeline. We have successfully obtained soluble high-yield expression of 20 proteins (71%) in *E. coli* and one in baculovirus system. 13 structures have been determined by a combined global effort, covering ~21% of the proteome. The structure of a conserved domain of nsp3 (nsp3b) has shown it to be a macro domain phosphatase specific for Appr-1<sup>o</sup>-P, pointing to its role in RNA maturation pathway. The structure of nsp10 revealed a new fold with two novel zinc fingers. The structure of the nsp(7/8)<sub>8</sub> supercomplex along with the those of nsp9 and nsp10 are beginning to provide important details on the supramolecular organization of the SARS replicase complex and its role in viral genome replication. This study was supported by NIAID/NIH Contract #HHSN266200400058C "Functional & Structural Proteomics of the SARS-CoV".

**T-P133 Supramolecular Design of Photoactive Coordination Assemblies: Synthesis, Materials Characterization, and Reactivity.** Ivan G. Georgiev, Leonard R. MacGillivray, Univ. of Iowa, Iowa City, Iowa, 305 Chemistry Bldg., 52242.

A synthetic strategy based on the emergence of the fields of coordination and supramolecular chemistry has lead to the formation of metal-organic assemblies that exhibit reactivity in the solid-state. In this study, our attention focuses upon the construction of a series of metal-organic assemblies that direct the [2+2] photodimerization of olefins in the solid state. Such assemblies enable a means to combine the properties of metals with organic solid-state reactivity.

As a starting point, we synthesized dinuclear Zn(II) complexes based on ditopic Schiff-base ligands. The complexes directs photodimerization, of *trans*-1,2-bis(4-pyridyl)ethylene, in the cationic assembly [Zn<sub>2</sub>L<sub>2</sub>(OH)(4,4-bpe)<sub>2</sub>]<sup>2+</sup> (LH=2,6-bis[N-(2-pyridylethyl)formimidoyl]-4-methylphenol), by way of coordination bonds.

We will also show that the solid-state reactivity is maintained within derivatives of the complexes, which have been synthesized by attaching functional groups to the peripheries and arms of the Schiff-base ligands. We also demonstrate that such reactivity can proceed *via* single-crystal-to-single-crystal reactions and lead to materials that exhibit changes in fluorescence.

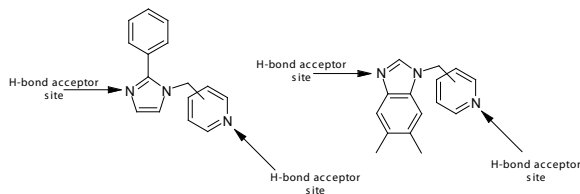
A photoreactive assembly with a cavity that hosts molecules and anions as guests will also be described.

**T-P134 The Crystal Structure of BCL-XL in Complex with Full-length BAD.** Kwang-Hoon Lee, Ji-Hye Baek, Byung-Ha Oh, Pohang Univ. of Science & Technology, Namgu Hyojadong San 31, Pohang, Korea.

The BCL-2 family of intracellular proteins is the central regulator of apoptosis. We overproduced a complex between an antiapoptotic member BCL-XL (residues 1-196) and a proapoptotic member BAD (residues 43-204). Here, the 2.3 Å ring; crystal structure of BCL-XL: BAD complex shows that BAD is totally disordered except for 27 amino acids occupying the extended BH3-binding groove of BCL-XL. The structure indicates that BAD is a natively unstructured protein, but becomes partly structured upon binding to the proapoptotic partner proteins, in a sharp contrast with another BH3-only protein BID, which adopts an  $\alpha$ -helical fold. The snapshot of the structure of BCL-XL disabled by BAD-binding in conjunction with the  $\sim$ 40 nM dissociation constant between the two proteins supports that BAD exerts the proapoptotic activity by displacing other proapoptotic proteins responsible for mitochondrial dysfunction. The structure also shows that Ser155 of BAD is completely buried in the binding groove of BCL-XL, which explains why the survival factor-mediated phosphorylation of this residue inactivates BAD and protects cells from apoptotic stimuli.

**T-P135 Ditopic Ligands in A World Where Discrimination is Desirable: Studies in Organic Cocrystal Syntheses.** Christer B Aakeröy, John Desper, Michelle Smith, Dept. of Chemistry, Kansas State Univ., Manhattan, Kansas 66502.

A series of ditopic ligands have been synthesized equipped with two different hydrogen bond acceptor sites. These two sites are subtle in their differences, being geometrically similar, but electrostatically



very different. In order to answer the question as to whether it is possible for a hydrogen bond donor such as a carboxylic acid or an oxime to be able to distinguish between, and hence discriminate against, one binding site over the other, cocrystallization experiments, X-ray crystallography, and a series of electrostatic surface potential calculations have been performed and are employed as tools in the study of these supramolecular reagents.

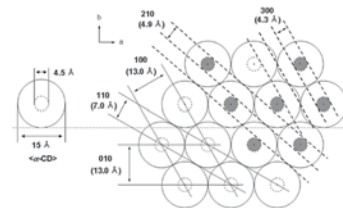
**T-P136 Structure of the Catalytic Domain of Human Protein Kinase C-beta II Complexed with a Bisindolylmaleimide Inhibitor.** Neil Grodsky, Ying Li, Djamel Bouzida, Robert Love, Jordan Jensen, Beverly Nodes, Jim Nonomiya, Stephan Grant, Pfizer Global Research & Development, San Diego, CA 92121.

The conventional protein kinase C isoform, PKC $\beta$ II, is a signaling kinase activated during the hyperglycemic state that has been identified as a therapeutic target for the treatment of microvascular-related diabetic complications. In this report, we describe the protein crystal structure of the catalytic kinase domain of PKC $\beta$ II complexed with an ATP-competitive inhibitor, 2-methyl-1*H*-indol-3-yl-BIM-1, at 2.6 Å resolution. The kinase domain of PKC $\beta$ II was cleaved and purified from full-length PKC $\beta$ II expressed in baculovirus-infected insect cells. The overall kinase domain structure followed the classical bilobal fold and was in its fully activated conformation with three well-defined phosphor-

ylated residues: Thr-500, Thr-641, and Ser-660. Different from the crystal structures of other PKC-isoforms, the PKC $\beta$ II catalytic domain had a novel  $\alpha$ -helix in the turn motif located near the ATP-binding site. The bound inhibitor adopted a nonplanar conformation within the ATP binding site. This PKC $\beta$ II-inhibitor complex represents the first structural description of any conventional PKC kinase domain and may serve as a template for the rational design of conventional PKC inhibitors.

**T-P137 Crystalline Structure and Morphology of Inclusion Complexes of  $\alpha$ -Cyclodextrin with Poly( $\epsilon$ -caprolactone) Having Various Architectures.** Seung-Yeop Kwak, Jae Woo Chung, School of Materials Science and Engineering, Seoul National Univ., Sillim-dong, Gwanak-gu, Seoul, Korea.

Inclusion complexes (ICs) of  $\alpha$ -cyclodextrin ( $\alpha$ -CD) with poly( $\epsilon$ -caprolactone) (PCL) templates having various architectures such as hyperbranched PCL (HPCL), star-shaped PCL (SPCL), diblocked PCL (PPG-PCL), and linear PCL (LPCL) were formed by the van der Waals and hydrophobic interaction. Then, ICs were retreated by polar solvent. Crystalline structure and morphology of ICs were investigated by WXR and FE-SEM, respectively. Characteristic diffraction peaks of all ICs were observed at  $2\theta = 7.20^\circ$  (100),  $12.70^\circ$  (110),  $19.70^\circ$  (210), and  $22.30^\circ$  (300). These indicate that all ICs have hexagonal unit cell and channel-type crystalline structure.



In FE-SEM images, the ICs of  $\alpha$ -CD with HPCL and PPG-PCL showed needle-like or sheet-like shape, while ICs of  $\alpha$ -CD with SPCL and LPCL showed disordered aggregation.

These may be ascribed by microphase separation of the ICs of  $\alpha$ -CD with HPCL and PPG-PCL, because they consist of solved PCL and unsolved complex parts in polar solvent. However, ICs formed by SPCL and LPCL have only an unsolved complex part in polar solvent, and then microphase separation may not be arisen. Therefore, architecture of template plays an important role to determine the morphology of the IC.

**T-P138 Structural and Biochemical Characterization of an Archaeal XPB: A Helicase Adapted For Damaged DNA Unwinding.** Li Fan, Andrew Arvai, Priscilla K. Cooper, Shigenori Iwai, Fumio Hanaoka, John A. Tainer, Dept. of Molecular Biology, The Scripps Research Institute, La Jolla, CA 92037.

The human xeroderma pigmentosum group B (XPB) helicase is essential for transcription, nucleotide excision repair, and TFIIH functional assembly. Here we determined crystal structures of an *Archaeoglobus fulgidus* XPB homolog (AfXPB) that characterize two RecA-like XPB helicase domains and discover a DNA damage recognition domain (DRD), a unique RED motif, a flexible thumb motif (ThM), and implied conformational changes within a conserved functional core. RED motif mutations dramatically reduce helicase activity, and the DRD and ThM, which flank the RED motif, appear structurally as well as functionally analogous to the MutS mismatch recognition and DNA polymerase thumb domains. Substrate specificity is altered by DNA damage, such that AfXPB unwinds dsDNA with 3' extensions but not blunt-ended dsDNA, unless it contains a lesion, as shown for CPD or (6-4) photoproducts. Together these results provide an unexpected mechanism of DNA unwinding with implications for XPB damage verification in nucleotide excision repair.

**T-P139 Crystal Structure of the 2:1 Adduct of 1,2-Benzenediol and Hexamethylenetetramine.** Kadsada Sala<sup>1</sup>, Kenneth J. Haller<sup>1</sup>, Seik Weng Ng<sup>2</sup>, <sup>1</sup>School of Chemistry, Suranaree Univ. of Technology, Nakhon Ratchasima 30000 Thailand, <sup>2</sup>Institute of Postgraduate Studies, Univ. of Malaya, Kuala Lumpur 50603 Malaysia.

The cocrystal product of an aqueous solution of 1,2-benzenediol (catechol) and hexamethylenetetramine (HMT) has been characterized by single crystal X-ray diffraction. The crystal structure consists of a zigzag arrangement of HMT along the *c* direction, with adjacent molecules connected by strong O–H···N hydrogen bonds from two catechol molecules. Each catechol molecule is hydrogen bonded to two HMT molecules, and each HMT molecule is hydrogen bonded to four catechol molecules. Thus, pairs of catechol molecules connect adjacent HMT molecules along the chain. Only weak interactions are observed between the chains in the *a* and *b* directions.

Crystal Data:  $2C_6H_6O_2 \cdot C_6H_{12}N_4$ ,  $M_r = 360.41$ , monoclinic,  $C2/c$ ,  $a = 23.5925(7)$ ,  $b = 6.8339(2)$ ,  $c = 13.1856(3)$  Å,  $\beta = 123.136(2)^\circ$ ,  $V = 1780.2(1)$  Å<sup>3</sup>,  $Z = 4$ ,  $D_{calc} = 1.345$  Mg m<sup>-3</sup>,  $T = 200$  K,  $m = 0.097$  mm<sup>-1</sup>, 2264 refl, 1956 refl  $> 2\sigma(I)$ ,  $R = 0.053$ ,  $\rho_{max} = 0.39$  e Å<sup>-3</sup>.

**T-P140 Crystal Structure of the HP1-EMSY Complex Reveals a New Mode of HP1 Binding.** Rui-Ming Xu, Ying Huang, Michael P. Myers, W.M. Keck Structural Biology Laboratory, Cold Spring Harbor Laboratory, Cold Spring Harbor, NY 11724.

Heterochromatin protein-1 (HP1) plays an essential role in both the assembly of higher order chromatin structure and epigenetic inheritance. The C-terminal chromo shadow domain (CSD) of HP1 is responsible for homodimerization and interaction with a number of chromatin-associated non-histone proteins including EMSY, which is a BRCA2-interacting protein that has been implicated in the development of breast and ovarian cancer. We have determined the crystal structure of the HP1b CSD in complex with the N-terminal domain of EMSY at 1.8 Å resolution. Surprisingly, the structure reveals that EMSY is bound by two HP1 CSD homodimers, and the binding sequences differ from the consensus HP1 binding motif PXVXL. This structural information expands our understanding of HP1 binding specificity and provides insights into interactions between HP1 homodimers that are likely to be important for heterochromatin formation.

**T-P141 Packing Interactions of 2,3,7,8,12,13,17,18-Octaethylporphyrinato(picrato)iron(III).** Ratchadaporn Puntharod, Kenneth J. Haller, School of Chemistry, Inst. of Science, Suranaree Univ. of Technology, Nakhon Ratchasima 30000 Thailand.

The X-ray structure of 2,3,7,8,12,13,17,18-octaethylporphyrinato(picrato)iron(III), [Fe(OEP)(picrate)], is reported. The compound crystallizes in the monoclinic space group  $C2/c$  with eight molecules per unit cell, thus one full molecule in the asymmetric unit. The five-coordinate Fe(III) atom is significantly displaced above the 4N-coordination plane towards the axially coordinated picrate ligand. The Fe–O distance and the Fe–O–C angle to the axial ligand are 1.935(4) Å and 125.9(4)°, respectively, both larger than the expected values, perhaps due to steric interactions between the 2,6 nitro substituents on the picrate and the plane of the porphyrin core. The nitro groups rotate relative to the picrate ligand such that they are parallel to, and in contact with the face of the porphyrin plane.

Crystal Data:  $C_{44}H_{46}FeN_7O_7$ ,  $M_r = 816.71$ , monoclinic  $C2/c$ ,  $a = 26.400(2)$ ,  $b = 13.781(2)$ ,  $c = 25.413(2)$  Å,  $\beta = 119.96(1)^\circ$ ,  $V = 8010.2(2)$  Å<sup>3</sup>,  $Z = 8$ ,  $D_{Calc} = 1.354$  Mg m<sup>-3</sup>,  $T = 298$  K,  $\mu_{Mo} = 0.44$  mm<sup>-1</sup>.

**T-P142 The Structure Determination of a Crp/Fnr Protein from 1.9-Å SAD Data Collected at the Structural Biology Center 19ID Beamline.** F.J. Rotella, R.G. Zhang, R. Mulligan, S. Moy, A. Joachimiak, Biosciences Div., Argonne National Laboratory, Argonne, IL 60439.

A transcriptional regulator protein, Crp/Fnr family, from *Porphyromonas gingivalis*, was expressed, purified and crystallized as a project of the Midwest Center for Structural Genomics. The experiment facilities of the insertion-device beamline of the Structural Biology Center (Sector 19 at the Advanced Photon Source) were used to acquire single-wavelength anomalous diffraction (SAD) data. The data were collected at the peak wavelength of the Se K-edge employing inverse-beam geometry for the tetragonal sample ( $P4_12_1$ ,  $a = 76.723$  Å,  $c = 86.320$  Å,  $Z = 8$ ,  $MW = 26.3$  kDa). X-ray diffraction from the sample was observed to a resolution of 1.9 Å. Images were processed and the structure was solved using HKL2000. The structure consists of two domains: an hTh DNA-binding domain and a cAMP domain (PDB ID: 2gau). Additional details of data collection and structure solution, refinement and analysis will be presented.

This work was supported by the National Institutes of Health Grant GM62414 and the U. S. Department of Energy, Office of Biological and Environmental Research, under Contract W-31-109-ENG-38.

**T-P143 Using Small Ditopic Molecules and Metal Chelates as Building Blocks to Construct Extended Metal-Containing Supramolecular Solid-State Architectures.** N. Judaš, Dubravka Matković-Čalogović, Laboratory of General and Inorganic Chemistry, Dept. of Chemistry, Faculty of Science, Univ. of Zagreb, Horvatovac 102a, HR-10 000 Zagreb, Croatia.

Complexes of Cu<sup>II</sup>, Co<sup>II</sup> and Ni<sup>II</sup> with  $\beta$ -diketonate ligands acetylacetonone,  $\alpha$ -benzylacetylacetonone, benzoylacetonone and dibenzoylmethane exhibit a planar structure with a coordinatively unsaturated metal center. Such properties make the complexes suitable for the exploration of weak interactions that steer molecular self-assembly in solids. In particular, the ability of such molecules to form adducts through binding additional ligands provides for the synthesis of extended metal-containing motifs. The assembly and organization of molecules in such a motif is regulated by weak interactions (e.g. hydrogen bonds). Ditopic ligands that would bind to the central metal ion of the starting  $\beta$ -diketonate complex “hub”, while participating in intermolecular hydrogen bonding are expected to affect the morphology of the crystals at the macroscopic level and steer the self-assembly into the ribbon-like and two-dimensional architectures at the molecular level. Several crystal and molecular structures that illustrate such possibilities will be presented, together with a strategy to affect the crystal growth and resulting morphology of Cu<sup>II</sup> complexes.

**T-P144 Structure of Human Protein Tyrosine Phosphatase Receptor Type O (PTPRO) with Bound Phosphate Ions in the Active Site.** Desigan Kumaran, Subramanyam Swaminathan, Biology Dept., Brookhaven National Laboratory, Upton, NY 11973

Receptor-type tyrosine-protein phosphatase O isoform (PTPRO) is selected as one of the protein structure initiative II (PSI-II) target by NYSGRG (www.nysgrg.org). PTPRO is a tumor suppressor candidate and dephosphorylates tyrosine phosphate. It encodes as a single intracellular catalytic domain with a characteristic signature motif (H/V)C(5X)R(S/T). Here, we report the crystal structure of PTPRO, the first structure of this family from *Homo sapiens* at 2.2 Å resolution. PTPRO associates as a homo-dimer in the crystal structure via a NCS two-fold. Two phosphate ions were located in the active site. One of the phosphate ions is bound in the cleft formed by the p-loop resi-

dues and interacts with the active site residues Cys225, Arg231 and Asp191. Interestingly, another phosphate ion was located at a distance of 8 Å from the first phosphate ion and interacts with the C-terminal his-tag of a symmetry related molecule. The binding environment of phosphate ion with the his-tag mimics the substrate binding. The correlation between the structure and function will be presented.

Acknowledgements: Research was supported by the National Institutes of Health (GM62529) under Prime Contract No. DEAC02-98CH10886 with the Brookhaven National Laboratory.

**T-P145 Hydrothermal Synthesis and Structural Characterization of an Open-framework Arsenic Vanadate:  $\text{As}_2\text{V}_{10}\text{O}_{26}$ .** Samroeng Krachodnok, Kenneth J. Haller, School of Chemistry, Inst. of Science, Suranaree Univ. of Technology, Nakhon Ratchasima 30000 Thailand.

An open framework arsenic vanadate:  $\text{As}_2\text{V}_{10}\text{O}_{26}$  system has been synthesized under hydrothermal reaction conditions and its structure characterized by single crystal X-ray diffraction. The structure is composed of  $\text{V}_{10}\text{O}_{26}$  clusters, interconnected into a three-dimensional porous open-framework network by sharing the O atoms of  $\text{AsO}_4$  tetrahedra. The oxovanadium cluster consists of two  $\text{V}_5\text{O}_9$  pentamers linked together and to the four As atoms by eight  $\mu_3\text{-O}$  atoms. The resulting framework has cavities about the  $-43\text{m}$  sites. The minimum size of these cavities is defined by the  $\mu_3\text{-O}$  atoms which are 17.5 Å apart across the cavity. The cavities are interconnected by hexagonal channels with a mean diameter of 11.8 Å extending along the [111] direction of the unit cell.

Crystal data: cubic, space group  $I-43m$ ,  $a = 16.274(2)$  Å,  $V = 4310.1(9)$  Å<sup>3</sup>,  $Mr = 1075.2$ ,  $Z = 4$ ,  $T = 298(2)$  K,  $\lambda(\text{Mo K}\alpha) = 0.71073$  Å.

**T-P146 Crystal Structure of Thiamine Monophosphate Kinase (thiL).** Subramaniam Eswaramoorthy, Subramanyam Swaminathan, Biology Dept., Brookhaven National Laboratory, Upton, NY.

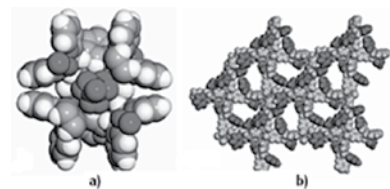
Thiamine monophosphate kinase is an enzyme that phosphorylates thiamine monophosphate. The enzyme thiL from *Aquifex aeolicus* was selected as a target by NYSGRC ([www.nysgrc.org](http://www.nysgrc.org)) and its crystal structure has been determined by the multiwavelength anomalous dispersion method (MAD). This representative structure of thiL family exists as a dimer. Each monomer has two domains, an  $\alpha\beta$ -domain comprising an anti-parallel  $\beta$ -sheet and  $\alpha$ -helices, and a small domain with an  $\alpha$  and  $\beta$  layers. The  $\alpha$  and  $\beta$  layers of two protomers come together and form an  $\alpha\beta\beta\alpha$  sandwich. A deep cavity is formed between the  $\alpha\beta$ -domain and the  $\alpha\beta\beta\alpha$  sandwich. A pyrophosphate molecule with a partial occupancy of one phosphate is located in a minor cleft further from this groove. The side chains of Glu58 has dual conformation with one of them competing with the partially occupied phosphate. As can be seen in the HSSP database more than 200 proteins with sequence identity >30% may be modeled using this structure. Fold of this protein resembles aminoimidazole ribonucleotide synthase (PurM). Details of the structure and active site will be discussed.

Acknowledgement: Research was supported by a National Institutes of Health grant (GM62529) to the NYSGXRC under DOE Prime Contract No. DEAC02-98CH10886 to Brookhaven National Laboratory.

**T-P147 Self-assembled Metal-organic Frameworks Based on Polyfunctional Ligands Derived from the Organic Solid State.** D.-K. Bučar, T.D. Hamilton, L.R. MacGillivray, Dept. of Chemistry, Univ. of Iowa, Iowa City, IA 52242.

Our focus on the design of functional material has led to the creation

of a series of polyfunctional ligands following a design strategy in which linear templates direct stereospecific and regiospecific [2+2]-photodimerizations in the solid state. To prepare the ligands *rctt*-1,2-bis(2-pyridyl)-3,4-bis(3-pyridyl)cyclobutane (2,3-tpcb) and *rctt*-1,3-bis(2-pyridyl)-2,4-bis(4-pyridyl)cyclobutane (2,4-tpcb-ht), linear templates (4,6-diphenylethyl-resorcinol and catechol) were used as a means to direct a [2+2]-photodimerization of *trans*-1-(2-pyridyl)-2-(3-pyridyl)ethylene and *trans*-1-(2-pyridyl)-2-(4-pyridyl)ethylene in the solid-state. The ligands self-assemble with Cu(II) and Zn(II) ions into complex three-dimensional structures that are held together coordination bonds.



In this contribution, we present a chiral tetrahedral host for a polyatomic anionic guest (*i.e.* perchlorate) in which the Cu(II) ions occupy four vertices (Fig. 1a) and the 2,3-tpcb ligands occupy each of the four faces of a tetrahedron. Furthermore, we show that Cu(II) and Zn(II) ions in a reaction with 2,4-tpcb-ht gives one- and two-dimensional metal-organic frameworks with walls decorated by 2-pyridyl groups suitable for hydrogen bonding with guest species (Fig. 1b).

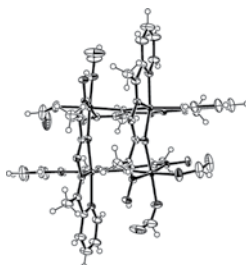
**T-P148 Crystal Structure of APPL1 BAR-PH Domain.** Guangyu Zhu<sup>1</sup>, Simon Terzyan<sup>1</sup>, Joseph S. Brunzelle<sup>2</sup>, and Xuejun C. Zhang<sup>1</sup>, <sup>1</sup>Crystallogr. Res. Prog, Oklahoma Medical Research Foundation, Oklahoma City, OK USA, <sup>2</sup>Life Sciences Collaborative Access Team, Argonne National Labs, Argonne, IL

APPL1 is an 80-kDa adaptor protein directly interacting with antiapoptotic kinase AKT2 and tumor suppressor DCC. Recently, it is found that APPL1 also acts as an effector of small GTPase Rab5 which is a master regulator of early endocytosis. APPL1 binds with Rab5 using both its N-terminal BAR and PH domains, and this interaction is essential for conveying extracellular signals from plasma membrane to nucleus. A sequence analysis shows that the BAR domain of APPL1 shares no detectable sequence-homology (<15% identity) with any protein structure in PDB. To understand the structural mechanism of APPL1-Rab5 interaction, we determined the crystal structures of both BAR domain alone and BAR-PH super-motif of APPL1 at a resolution of 1.8 Å and 2.8 Å, respectively. The crystal form of BAR domain is orthorhombic (space group  $P2_12_12_1$ ) with cell dimensions of  $a = 52.7$ ,  $b = 129.0$ , and  $c = 36.7$  Å; and the crystal of BAR-PH belongs to the same space group with cell dimensions of  $a = 103.6$ ,  $b = 105.5$ , and  $c = 36.3$  Å. The crystal structures were solved using Single Anomalous Dispersion (SAD) and molecular replacement methods, respectively. Our results suggest a novel binding mode between a BAR-PH super-motif and small GTPases.

**T-P149 Structural Versatility of 3d-metal Complexes with a Polydentate Oxime-containing Schiff Base Ligand.** Y.S. Moroz, I.O. Fritsky, Dept. of Chemistry, Kiev National Taras Shevchenko Univ., Kiev, Ukraine.

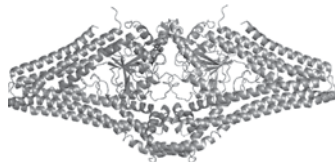
A series of 3d-metal complexes with novel polyfunctional Schiff base ligand (2E)-2-hydroxyimino-N'-(1-(2-Pyridyl)ethylidene)propanohydrazone (POP) containing several donor functions (oximic, hydrazide, hydrazone and pyridine cycle) has been synthesized and characterized by a variety of spectral methods; three complexes of different composition:  $[\text{Zn}(\text{POP})\text{Cl}_2]\cdot\text{H}_2\text{O}$  (1),  $[\text{Co}(\text{POP}-\text{H})_2]\text{NO}_3$  (2) and  $[\text{Ni}_4(\text{POP}-\text{H})_4(\text{HCOO})_4]\cdot 9\text{H}_2\text{O}$  (3) were studied by X-ray single crystal analysis. In all the complexes 1-3 the primary coordination of the ligand is realized in a tridentate mode via the pyridine and azomethine

nitrogen atoms and the amide oxygen. In 1 the ligand is neutral, while in 2 and 3 it is monodeprotonated on account of ionization of the amide group. The later in 2 and 3 even being deprotonated was found to be O-coordinated. In 1, the Zn:POP ratio is 1:1, and two additional sites in the coordination sphere are occupied by the chloride ions giving rise to the coordination number 5 (trigonal bipyramide). In 2 two POP ligands form the octahedral coordination of the central ion. In both 2 and 3 the coordinated ligands still contain vacant donor atoms and potential chelating units which can be utilized in synthesis of polynuclear assemblies of high nuclearity. This approach has been realized in synthesis of tetranuclear complex 3 (Figure) when 1:1 Ni:POP ratio and calculated quantities of alkali and a co-ligand formate was used. In 3 the ligand forms an additional 5-membered chelate ring on account of the oxime nitrogen and amide oxygen atoms, thus the latter bridges two metal ions. Four ligand anions are disposed in such a way that they form a grid tetranuclear molecule.



**T-P150 Bynamin, a Bacterial Dynammin-like Protein.** Harry Low, Jan Löwe. MRC Laboratory of Molecular Biology, Cambridge, CB2 2QH, UK.

Dynammins form a superfamily of large mechano-chemical GTPases that include the classical dynamins and dynamin-like proteins (DLPs). Found in core cellular processes such as endocytosis, plastid division and cytokinesis, their presence spans the Eukaryota. Sequence similarity searches have tentatively shown many bacteria to have large GTPases with domain architecture akin to DLPs. This includes a GTPase, middle and GTPase effector domain. Here, we present the first complete crystal structure of a DLP, from a cyanobacteria, in both nucleotide free and GDP associated conformation, and show that it shares biochemical characteristics with eukaryotic DLPs.

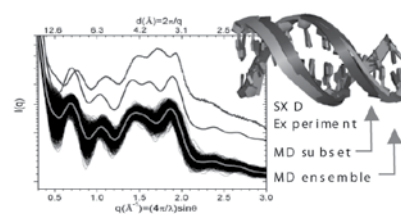


Our discovery that bacteria have DLPs is compounded further by its functional characterisation *in vivo*. Immunofluorescent studies show this DLP to be recruited to the future site of cell division and remarkably, to form a circumferential cytokinetic ring. Such a ring is strikingly reminiscent of the role of eukaryotic dynamin in plastid division and cytokinesis. Given the endosymbiotic origins of chloroplasts, our findings in a cyanobacteria question the evolutionary origins of the dynamin superfamily and has implications for key cellular processes such as endocytosis. Due to the similarity of our bacterial DLP to eukaryotic dynamin, we utilise the name 'bynamin' to describe this novel class of proteins.

**T-P151 Testing the Reliability of the Self-complementary Noncovalent Interactions: Supramolecular Implications and Supramolecular Design.** Catalina Ruiz-Pérez, Lab. de Rayos X y Materiales Moleculares, Dept. de Física Fundamental II, Univ. de La Laguna, La Laguna (Tenerife), Spain, caruiz@ull.es.

Noncovalent interactions play a special role in supramolecular chemistry, which has been defined by Lehn <sup>[1]</sup> as "chemistry beyond the molecule". Noncovalently assisted synthetic procedures are used to assemble various types of supramolecular species. These syntheses rely on the stabilization provided by noncovalent interactions between recognition sites incorporated within precursors. As a recognition motif utilized to guide the synthesis, various types of noncovalent inter-

actions can be used. These are, specifically, hydrogen bonds (Hbonds), stacking interactions, electrostatic interactions, hydrophobic interactions, charge-transfer interactions, and metal coordination <sup>[2]</sup>.



Unconventional polymers composed of covalent and noncovalent bonds differ dramatically from standard, conventional polymers with just covalent bonds. They possess novel physical, optical, electrochemical, photochemical, biological, and catalytic properties.

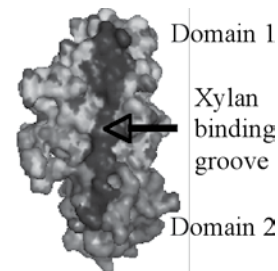
Targeted synthesis of macro- and supramolecular structures of various sizes, shapes, and functionality has now become possible. Supramolecular chemistry offers incredible applications in various fields such as medical chemistry (drug delivery systems), host-guest chemistry, catalysis and molecular electronics.

- [1] Lehn J.-M., *Angew. Chem., Int. Ed. Engl.*, 1988, 27, 89, *ibid.* 1990, 29, 1304.  
 [2] Lehn J.-M., Atwood J. L., Davies J. E. D., MacNicol D. D., Vögtle F., *Comprehensive Supramolecular Chemistry*, Eds. Pergamon, Oxford, 1996.

**T-P152 Crystal Structure and Biochemical Activity of Zea m 1 (EXPB1) : Implications for the Mechanism of Cell Wall Loosening by Beta Expansins.** Neela Yennawar<sup>1</sup>, Lian-Chao Li<sup>2</sup>, Hemant Yennawar<sup>3</sup>, Akira Tabuchi<sup>2</sup>, Daniel J. Cosgrove<sup>2</sup>, <sup>1</sup>Huck Institute of the Life Sciences, <sup>2</sup>Dept. of Biology, <sup>3</sup>Dept. of Biochemistry and Molecular Biology, Penn State Univ., University Park, PA 16802.

Zea m 1 is a member of the beta-expansin subfamily known as group-1 grass pollen allergens. It has wall-loosening activity with grass cell walls. We have determined its crystal structure by X-ray crystallography to 2.75Å resolution. It has two domains. Domain 1 has substantial structural similarity to the catalytic domain of an endoglucanase (Humicola EGV) from family GH45. However, tests for hydrolytic activity against various wall polysaccharides proved negative.

Domain 2 of Zea m 1 is an immunoglobulin-like beta sandwich, structurally similar to Phl p 2, a group-2 grass pollen allergen. Domains 1 and 2 have aromatic and polar residues that form a 55 Å long shallow binding groove for potential polysaccharide binding running the length of the protein. The residues along the groove are conserved in beta-expansins. Our biochemical studies have shown that Zea m1 binds to maize cell walls, where the binding is to an arabinoxylan and cellulose. We have modeled a glucuronoarabinoxylan in the putative sugar binding groove and hypothesized a mechanism for the cell wall-loosening action of beta-expansins.



**T-P153 A Relation Between Photochromism and Structure in the Three Crystal Forms of a Salicylideneaniline Derivative.** Y. Ohashi, K. Johmoto, H. Uekusa, Tokyo Inst. of Technology, Tokyo 152-8551, Japan.

Reversible color change by photoirradiation has been well known as photochromism which has been attracted as a variety of application. The crystals of salicylideneaniline derivatives, some of which show photochromism, have been extensively studied. We reported that the photochromism is caused by the structural change from enol to *trans*-keto form in the crystal, analyzing the structure at the unstable photo-

colored state.<sup>1)</sup> Recently we found that one of the derivative, N-3,5-di-tert-butylsalicylideneaniline-3-carboxyaniline, was crystallized in three forms, a, b and c-forms. When the crystals were irradiated with the mercury lamp, the  $\alpha$ -form changed the color from colorless to red and the  $\beta$ -form did from light yellow to red, whereas the  $\gamma$ -form with orange color showed no change. The lifetime of the colored species for the  $\alpha$ - and  $\beta$ -forms were estimated 17 and 780 min, respectively. Not only the structures of the three forms before the irradiation but also the structure of the colored  $\alpha$ -form was successfully analyzed. The structures clearly explained the different photochromic properties among the three crystal forms.

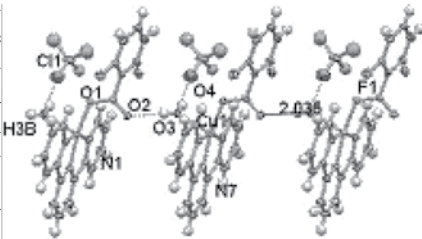
1) J. Harada, H. Uekusa and Y. Ohashi, *J. Am. Chem. Soc.*, 121, 5809-5810 (1999)

**T-P154 Structural Studies of the Methionine Biosynthesis Enzyme Homoserine Transsuccinylase from *Escherichia coli*.** S.M. Noble<sup>1</sup>, T.L. Born<sup>2</sup>, D.P. Huddler<sup>1</sup>, <sup>1</sup>Div. of Experimental Therapeutics, Walter Reed Army Inst. of Research, Silver Spring, MD 20910, <sup>2</sup>Dept. of Chemistry and Biochemistry, George Mason Univ., Manassas, VA 20110.

The biosynthesis of methionine is critical for cell growth and viability in microorganisms and plants. Unlike mammals which acquire methionine from their diet, microorganisms and plants synthesize methionine, making enzymes along the methionine biosynthesis pathway attractive antimicrobial targets. In *E.coli* and other bacteria, the first unique step in methionine biosynthesis is catalyzed by homoserine transsuccinylase (HTS). Steady-state kinetic experiments have revealed that HTS exhibits a ping-pong mechanism in transferring succinyl from succinyl-CoA to a catalytic nucleophile before subsequent transfer to homoserine. We initially crystallized HTS by free interface diffusion using the TOPAZ system (Fluidigm, Corp); however micro-liter scale crystallization by vapor diffusion produced crystals that diffracted to 8Å. We are currently collecting data on a new crystal form resulting from optimization of previous conditions.

**T-P155 Building Hydrogen-bonded Frameworks of Copper (II) Complexes, via Interactions Between Carboxyl Ligands and Coordinated Water Molecules.** Sergio Martínez-Vargas, Simón Hernández-Ortega, Rubén A. Toscano, Jesús Valdés-Martínez, Inst. de Química, UNAM. Circuito Exterior s/n, Cd. Universitaria 04510 Coyoacán, México D.F., jvaldes@servidor.unam.mx

We will present the predictable use of coordinated water molecules to assemble [Cu (N,N,N) (CA)H<sub>2</sub>O] tectones into hydrogen bonded networks. Where (N,N,N) represents the tridentate amines terpyridine and 4-phenylterpyridine, and CA represents ligands containing a carboxylic group. The tridentate amines allows us to control the usually non-controllable geometry around the Cu atom<sup>[1]</sup>. The CA has two functions, one to coordinate, as monodentate ligand, in an equatorial position to the metal ion and second to act as hydrogen bond acceptors to the coordinated water molecules. In this way, we use the very good H-bonding properties of water molecules under controlled conditions to build up infinite hydrogen bonded 1-D chains.



[1] C.B. Aakeröy, A.M. Beatty, J.Desper, M. O'Shea and J.Valdés-Martínez *Dalton Trans.*, 2003, 3956.

**T-P156 Ultra Fast Framing X-ray Detector for Time-Resolved Synchrotron Experiments.** R.D. Durst, M. Benning, D. Khazins, B. Becker, Y. Diawara, S. Medved, V. Sedov, G. Waechter, Bruker AXS, Madison, WI 53711.

A new fast photon-counting X-ray imaging detector capable of frame rates of up to 1 million frames per second is described. This detector is capable of studying fast kinetic processes such as chemical reactions, phase transitions, photo-excited processes, etc. with unprecedented time resolution. The principle of operation of the detector is described and examples of microsecond-resolution data are presented.

**T-P157 Radiation-induced Damage of Explosives at Ambient and High Pressure.** Hubertus Giefers, Michael Pravica, Malcolm Nicol, High Pressure Science and Engineering Center, Dept. of Physics, Univ. of Nevada Las Vegas, Las Vegas, NV 89154.

We have investigated radiation-induced decomposition of PETN (pentaerythritol tetranitrate) and TATB (triamino trinitrobenzene) in a diamond anvil cell at ambient temperature and at variable pressures using white synchrotron x-ray radiation from the 16 BM-D beamline at the Advanced Photon Source. We present evidence of a dramatic slowing of the decomposition rate of TATB when pressurized to 5.9 GPa. The measurements were highly reproducible and allowed us to obtain decomposition rates and the order parameters of the reactions.

**T-P158 Adaptation of a Commercial Optical CMOS Image Sensor for Direct-Detection Fast X-ray Imaging.** L.W. Marschand<sup>2</sup>, X. Jiao<sup>1</sup>, M. Sprung<sup>1</sup>, B. Tieman<sup>1</sup>, A.R. Sandy<sup>1</sup> L.B. Lurio<sup>2</sup>, <sup>1</sup>The Advanced Photon Source, Argonne National Laboratory, Argonne, IL 60439, <sup>2</sup>Dept. of Physics, Northern Illinois Univ., DeKalb, IL 60115.

We have adapted a commercial CMOS optical image sensor for use as a fast x-ray detector. The sensor was used in a mode where the x-rays impinge directly on the sensor. We will report on a number of characterization measurements: the overall efficiency for absorption of X-rays, the analog-digital-unit response per photon as a function of gain, and the root-mean-square noise in the dark current of the detector. In addition, we will present the first use of the camera for small-angle X-ray scattering and X-ray photon correlation spectroscopy measurements.

**T-P160 Wavelength-shifting Fiber Scintillation Neutron Detectors for POWGEN3 & VULCAN at SNS.** Jason Hodges, Lowell Crow, Luke Heroux, Bruce Hannan, Spallation Neutron Source, Oak Ridge National Laboratory Oak Ridge, TN 37830.

We have constructed & tested the initial production wavelength-shifting (WLS) fiber scintillation neutron detector module for the Spallation Neutron Source POWGEN3 & VULCAN diffractometers. The design is based on a successful prototype<sup>[1]</sup>. These diffractometers require neutron detector systems with large, narrow pixels (about 5mm x 50 mm), good efficiency up to 0.5 eV, and array areas of > 10 m<sup>2</sup>. The detector uses a <sup>6</sup>LiF/ZnS:Ag scintillation screen for neutron conversion. The scintillation light is collected using a two-layer grid of 308 ★ 152 WLS plastic optical fibers (area is ~0.3 m<sup>2</sup>). The vertical (V) fiber ends, encoding 5 mm wide horizontal (H) pixels, are mapped to an array of 20 photomultiplier tubes (PMTs) in a <sup>2</sup>C<sub>n</sub> coincidence pattern. Each horizontal fiber, mirrored at one end, conducts light to a PMT; bundling of these fibers defines the vertical pixels. The detector operates in coded coincidence, requiring signals from 1 V & 2 H PMTs. The PMT output is converted to digital signals using fast

comparators, and the neutron identification and position encoding are processed digitally. The detector module has been successfully tested at the High Flux Isotope Reactor.

[1] M. L. Crow *et al.*, Nucl. Instr. Meth. A 529 (2004) 287.

**T-P162 Functional Studies of Membrane Proteins.** Maria Nyblom<sup>1</sup>, Euan Gordon<sup>2</sup>, Richard Neutze<sup>1</sup>, <sup>1</sup>Molecular Biotechnology, Chalmers Univ. of Technology, Gothenburg, Sweden, <sup>2</sup>AstraZeneca, Mölndal, Sweden.

In order to fully understand the function of integral membrane proteins several approaches have to be considered. X-ray crystallography gives a snapshot of how proteins behave in different environments and this method often give a clear picture of what is going on.

However working with overproduction of membrane proteins in heterologous systems complementary information of the actual activity of the protein produced is needed in order to give the whole picture and estimate the success of the production.

The methodology depends of what sort of protein is under investigation, and if the objective is to find out the function or the activity. Various techniques such as semi *in vivo* assays, used when the water permeability of membrane protein AQP1 was determined by comparing wild-type red cells and AQP1-deficient red cells, and *in vitro* assays measuring the water permeability of purified, reconstituted membrane proteins, will be described. The advantages and drawbacks of different assay systems will be discussed.

**T-P164 Dimeric Structural Significance for Ligand Binding in Putative Peptidyl-tRNA Hydrolase from *Pyrococcus horikoshii* OT3.** K. Shimizu, Y. Fujimoto, M. Sugahara, N. Kunishima, RIKEN Harima Inst., RIKEN Spring-8 Center, Sayo-cho, Sayo-gun, Hyogo, 679-5148, Japan.

In the biosynthesis process of the protein translation, peptidyl-tRNA molecules may happen to dissociate from the ribosome before mRNAs readout do not reach the stop codon. Peptidyl-tRNA hydrolases (Pths) catalyze removal of peptidyl moiety from peptidyl-tRNA molecule and the resultant free tRNA and peptide will reuse for the protein translation. So far, we have determined two crystal forms of putative Pths from *Pyrococcus horikoshii* OT3 (*Ph*Pths): (1) form 1 at 1.2 Å resolution,  $P4_22_2$  and (2) form 2 at 1.9 Å resolution,  $P4_22$ . *Ph*Pths protomer are composed of an  $\alpha/\beta$  fold with a four-stranded antiparallel  $\beta$ -sheet in its core surrounded by two  $\alpha$ -helices on each side. Both forms show a biologically dimer and the asymmetric unit of forms 1 and 2 includes 1 and 2 molecules, respectively. We will present the structural difference between two forms and furthermore discuss the dimeric structural significance for the recognition of the substrate, tRNA in *Ph*Pths dimer.



Fig. 1 Ribbon diagram of the crystal structure, *Ph*Pths protomer.

The present study is supported by "National Project on Protein Structural and Functional Analyses" funded by MEXT of Japan.

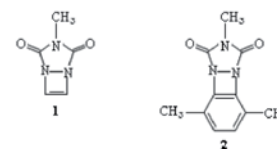
**T-P166 Structural Studies on *Helicobacter pylori* Apoflavodoxin Contributes to Investigate Conformational Changes in Flavodoxins Induced by FMN Binding.** M. Martínez-Júlvez, M. Bueno, N. Cremades, J. Sancho, J. Hermoso, Dept. de Bioquímica y Biología Molecular y Celular, Fac. de Ciencias y BIFI, Univ. de Zaragoza, España, Grupo de Cristalografía Macromolecular y Bi-

ología Estructural, Inst. Química-Física Rocasolano. C.S.I.C -Madrid, España.

In this work, we present the structure of apoflavodoxin from *Helicobacter pylori* solved by X-ray diffraction at 2.1 Å. The active form, holoflavodoxin, contains a no covalently bound FMN that receives electrons from the piruvate oxidoreductase complex during the metabolism of the pathogen. The  $\alpha/\beta$  folding of the structure of the apo form shows high similarity to that of holoprotein when both structures are superimposed. Nevertheless, some differences are detected in the FMN binding regions. Some details of this structure in these regions and crystallisation conditions reveal important clues to investigate the mechanism of protein/flavin recognition. Our conclusions are that apoflavodoxins display, regardless of the presence of an aromatic residue in the binding loop, a closed isoalloxazine pocket, together with a native phosphate site that carries whatever available anion is present in solution. The high flexibility of one of the isoalloxazine loops (55-58) might facilitate that FMN binding begins there.

**T-P167 Comparative Crystal Structures and Aromaticity Studies of a Diazetine and a Benzodiazetine.** Kenneth L. Martin<sup>1</sup>, Gary W. Breton<sup>1</sup>, Edwin D. Stevens<sup>2</sup>, <sup>1</sup>Dept. of Chemistry, Berry College, Mt. Berry, GA, <sup>2</sup>Dept. of Chemistry, Univ. of New Orleans, New Orleans, LA.

The compounds 1 and 2 (referred to as "diazetine" and "benzodiazetine", respectively) were synthesized as part of an investigation in the nature of aromaticity of cyclic molecules bearing two nitrogen atoms and  $4n+2$  electrons which could be in the  $\pi$  system. X-ray diffraction data sets were collected at 150 K using a Bruker SMART 1-K CCD single crystal diffractometer and Mo-K $\alpha$  radiation. For 1, 14927 reflections were measured, the space group was found to be  $P2_1/m$  with the following unit cell parameters:  $a = 3.7770(1)$  Å,  $b = 9.4807(2)$  Å,  $c = 8.2024(2)$  Å,  $\beta = 98.348(1)^\circ$ ,  $Z = 2$ . The refinement led to  $R(F) = 0.0318$  for the strongest 1615 reflns [ $F_o > 4\sigma(F_o)$ ]. For 2, 15598 reflections were measured, the space group was found to be  $P2_12_12_1$  with the following unit cell parameters:  $a = 7.3068(7)$  Å,  $b = 9.8265(0)$  Å,  $c = 15.0873(14)$  Å,  $Z = 4$ . The refinement led to  $R(F) = 0.0435$  for the strongest 1329 reflns. The experimental structure of 2 suggests that there is some localization of the  $\pi$  system of the benzene portion of the molecule. However, NICS calculations (RHF/6-311+G\*\*) show that the 4-member rings of both 1 and 2 are nonaromatic, and the aromaticity of the 6-member ring of 2 is virtually the same as in C<sub>6</sub>H<sub>6</sub>.



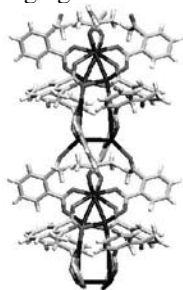
**T-P168 Collection of Diffraction Data from Crystals grown in TOPAZ® Crystallization Chips.** John Tainer<sup>3</sup>, Andrew P. May<sup>1</sup>, James M. Holton<sup>2</sup>, Ken Frankel<sup>2</sup>, Hany Nassef<sup>1</sup>, <sup>1</sup>Fluidigm Corporation, South San Francisco, CA 94080, <sup>2</sup>Advanced Light Source, Lawrence Berkeley National Laboratory, Berkeley, California 94720, <sup>3</sup>The Skaggs Inst. for Chemical Biology, The Scripps Research Inst., La Jolla, CA 92037.

Fluidigm® Corporation has developed and commercialized the TOPAZ® system for protein crystallization. Crystallization in TOPAZ chips is effected through microfluidic free-interface diffusion (FID). Current commercially available TOPAZ microfluidic chips provide the means to screen for crystallization conditions in sub-nanoliter volumes. As part of the ongoing development of the TOPAZ system, Fluidigm has also developed chips that allow users to grow crystals of sufficient size for diffraction data collection. Data can be collected from crystals extracted from the chips, and also directly from

sections of the chip without extraction. Mounting devices compatible with standard cryovials have been developed to allow sections from the chip to be cryo-cooled directly in liquid nitrogen or in a cryostream. X-ray diffraction data can be collected directly from the cooled crystals. Data from diffraction experiments, collected in collaboration with researchers at the ALS, will be presented from crystals located within the chips and will be compared with data collected from equivalent crystals extracted from the chip.

**T-P169 Structural Diversity in Silver Coordination Chemistry.** Manju Rajeswaran, David R. Whitcomb, Eastman Kodak Company, Research & Development, Rochester, NY 14450.

The solid-state coordination environment of silver has been considered to be a classic case of being limited to two or three ligands. Over the last few decades, this view has been changing as it has become clear that the silver ion is capable of more structural diversity than previously thought, particularly with the detection of argentophilic bonding interactions. We report here a variety of recently resolved solid-state structures of silver complexes having a diversity, which requires that the silver coordination sphere include 3-6 ligands, in line with contemporary literature reports. We have observed complexes containing bonding motifs, such as chelated silver, including an unusual organic Ag-Cl or Ag-Br bond, silver carboxylate dimers containing the shortest Ag-Ag bond reported to date, and polymeric repeating units of asymmetrically constructed S-Ag-N and N-Ag-N links. In all cases, the coordination capability is similar to many other transition metals. Specific examples of the structural diversity observed within silver coordination chemistry will be the subject of this talk.



**T-P170 Remote Access Modes for Data Collection at IMCA-CAT.** Lisa J. Keefe, Kevin Battaile, J. Lewis Muir, Anne Mulichak, IMCA-CAT, Univ. of Chicago, Sector 17, Advanced Photon Source, Argonne National Laboratory, Argonne, IL 60439.

The Industrial Macromolecular Crystallography Association Collaborative Access Team (IMCA-CAT), located at sector 17 of the Advanced Photon Source, operates two beamlines for high-throughput macromolecular crystallography data collection. The two beamlines, an insertion device beamline and a bending magnet beamline, each are equipped with a Rigaku ACTOR robot. Integrated with the robotics are automation protocols for several modes of user access. The ACTOR robotics system, with a sample capacity of 60 crystals on the ID beamline and 180 crystals on the BM beamline, enables rapid sample mounting, autocentering, screening, tracking, sorting and ranking, immediately followed by data collection. Alert notification mechanisms provide for status communication to the user during unattended data collection. Experiments can be performed either via the conventional on-site access to the beamlines or via secure remote modes for unattended mail-in data collection, including remote monitoring and remote access. The automated procedures can be tailored to readily accommodate the spectrum of demands of pharmaceutical and structural genomics researchers.

**T-P171 Experimental and Theoretical Charge Density Study of Estrone.** E.A. Zhurova, C.F. Matta, N. Wu, V.V. Zhurov, A.A. Pinkerton, Dept. of Chem., Univ. of Toledo, Toledo, OH, Dept. of Chem., Dalhousie Univ., Halifax, Nova Scotia, Canada, Dept. of Biochem., Case Western Reserve Univ., Cleveland, OH.

The electron density and the electrostatic potential (ESP) distributions of estrone have been determined using X-ray diffraction analysis and compared with theoretical calculations in the solid and gas phases. X-ray diffraction measurements were performed with a Rigaku Rapid rotating anode diffractometer at 20 K. The electron density in the estrone crystal (orthorhombic phase II) has been described with the Hansen-Coppens multipole model, which allowed extensive topological analysis and calculation of the ESP. An interesting locally stabilizing hydrogen-hydrogen bond path is found in the experimental and all three calculated densities and represents the first characterization of such bonding in a steroid molecule. It is estimated that this interaction contributes between 8 and 11 kcal/mol of *local* stabilization to estrone. The aromaticity of ring A is discussed and quantified since it is crucial to biological activity. Chemical bonding, the O(1)...O(2) distance necessary for estrogenic activity, and the electrostatic potential (ESP) features are also discussed.

**T-P172 Remote Data Collection for Single-Crystal and Powder Diffraction.** Joerg Kaercher, Michael Ruf, Bruker AXS Inc., Madison, WI.

Many synchrotrons and other X-ray laboratories offer remote data collection services today. Remote data collection has advantages for these facilities and for the crystallographers. Local staff is already familiar with the instrumentation and safety regulations, whereas visiting scientists first need to be trained. Remote access increases the efficiency of the facilities and leads to higher throughput. The crystallographers in addition save time and money on travel.

Bruker's client/server based software architecture is well suited for remote data collection. The server part, called Bruker Instrument Service (BIS), is installed at the X-ray laboratory to control the equipment. BIS communicates with its client applications over a network, e.g. the Internet. At the other end of the connection, the client software sets up the experiment and analyzes the data collected by BIS. Three client software packages currently exist: APEX2 for small molecule applications, PROTEUM2 for protein applications, and PILOT for Phase ID applications.

The client software packages use a relational database for storing sample related data. This database can be installed on the same computer as the client software or on a separate computer. Multiple clients can share the same database. Conventional mass storage devices, e.g. a network attached RAID, hold the diffraction data.

**T-P173 Cost, Space, Time: What are the Limits for Publishable Structures?** Lee M. Daniels, Ronald E. Benson, Joseph D. Ferrara, Katsunari Sasaki, Rigaku Americas Corp., 9009 New Trails Dr., The Woodlands, TX, 77381.

Access to modern single-crystal diffraction experiments continues to be limited to those with the significant funding, laboratory facilities, training and time (or personnel) required for the techniques. Most of us would also hope to produce publishable material from such experiments. So what are the lower limits for cost, space, time and training that might enable access to the technique to a larger pool of scientists?

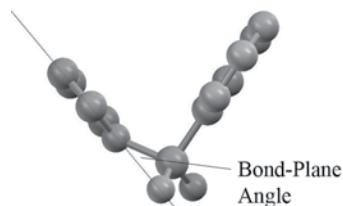
The accepted paradigm for single-crystal experiments might need to

be suspended to reach some of these goals. In terms of cost and space, what can we do without and still produce acceptable results? In terms of time and training, how much automation can be implemented?

A side benefit of an affordable, minimal system for single-crystal diffraction is the ability to include the technique in undergraduate teaching situations. The new Rigaku SCXmini benchtop crystallography system will be described as a possible answer to these problems. Several examples of published or publishable structures from such a system are included as examples.

**T-P174 SGX-CAT: An Automated Synchrotron Beamline Dedicated to Mail-in Crystallography.** David W. Smith, Stephen R. Wasserman, John W. Koss, Laura L. Morisco, Kevin L. D'Amico, SGX Pharmaceuticals, Inc., Advanced Photon Source, Argonne National Laboratory, IL 60439.

SGX Pharmaceuticals, Inc. developed and operates SGX-CAT, a beamline at the Advanced Photon Source whose sole mode of operation is mail-in crystallography. All samples, whether from the company, corporate partners, or general users, are assessed and collected by a staff of five based locally at the synchrotron. The beamline operations are linked to an Oracle database that tracks the crystals, their collection status, and the quality of the data from them. The initial descriptions of the crystals, including their provenance and likely properties, are entered into the database, either directly or through an electronic spreadsheet. Samples are identified by 1-D and 2-D barcodes that link the information in the database to the physical samples. Screening and collection utilize several automated processes, including generation of protocols for data collection, centering of loops, removal of surface ice, scoring of crystal quality, processing of data, and updating of the database. For most crystals, quality is evaluated and data are generated without a human examining a single diffraction image from the crystal. The high degree of automation permits the staff to operate and maintain the beamline while providing the crystallographic information. In 2005, 9000 crystals were screened and 4200 datasets were collected using these processes.



**T-P175 Bond-plane Angle in Pyrrole Systems as an Indicator of the Degree of Aromaticity.** David A. Grossie, P.G. Seybold, Daniel M. Ketcha, Dept. of Chemistry, Wright State Univ., Dayton, Ohio 45435.

The structures of many 1-benzenesulfonyl pyrroles have been determined in the examination of the regioselectivity of Friedel-Crafts acylations of the pyrrole. In the analysis of the 1-benzenesulfonyl and 1-tosylpyrrole structures, interesting variations in the geometry of the pyrrole nitrogen atom have been noted. The angle between N-S bond and the mean plane of the pyrrole ring varies from 0 to 27.5 degrees in the structures examined, indicating a change in the hybridization in the nitrogen atom. If a condition of aromaticity demands  $sp^2$  hybridized atoms, then this change in the bond-plane angle may be a useful indicator of the degree of aromaticity.

**T-P176 The Beauty of Not Being There: Integrating Interactive Screening with Offline Data Collection.** James M. Holton<sup>1,2</sup>, George Meigs<sup>2</sup>, <sup>1</sup>Univ. of California San Francisco, <sup>2</sup>Lawrence Berkeley National Laboratory, Berkeley, CA.

At ALS 8.3.1 we are focusing on maintaining the advantages of screening crystals on-site and eliminating the need for users to stay up all night. Going home to sleep while your data are collected is already a common method of “remote” data collection, but it is impractical on beamlines bright enough to destroy the sample in half an hour. The obvious solution is to queue up data collection runs for many samples and change them out with a robot. However, the problem of automatically placing the crystal into the beam is a difficult one, and even the best crystal identification algorithms might not put the crystal where the user wants it.

Instead of solving the problem of finding the crystal in the loop, we have circumvented it. Users center their crystal as usual as they screen them. However, they now have the option to postpone data collection until after they go home. Digital photos of the centered sample are taken before the robot dismounts it. Early the next morning, the sample is re-mounted and these photos are used to reliably re-center the sample to within a few microns and a few degrees of where it was when the photos were taken. Data collection then commences as specified while the user sleeps.

This work is supported by the member of the ALS 8.3.1 Participating Research Team: University of California San Francisco, University of California Berkeley, Plexxikon Inc, The Alberta Synchrotron Institute and the MD Anderson Cancer Research Institute.

**T-P177 Energy of Intermolecular Interactions from Charge Density Data in Molecular Crystals.** Mikhail Yu. Antipin<sup>1,2</sup>, Konstantin A. Lyssenko<sup>2</sup>. <sup>1</sup>New Mexico Highlands Univ., Las Vegas, NM 87701, <sup>2</sup>Inst. of Organoelement Compounds, Russian Academy of Sciences, Moscow, Russia.

Charge density distribution in several organic crystals was described from multipole refinement of precise X-ray diffraction experiments. Several characteristics of intermolecular interactions, such as intermolecular hydrogen bonds, specific contacts with halogen atoms and stacking interactions have been considered in terms of their energy. It was found that energies of intermolecular interactions are in a good agreement with data obtained by quantum calculations. Individual impacts of intermolecular interactions helped to estimate from diffractive data energy of crystal structure that was found to be in good correspondence with experimental data on sublimation energy.

**T-P178 Fast Vitrifying of Solutions Using Protein Crystal Cryopreservation: Effects of Cryoprotectant Concentration and Cooling Rates.** Matt Warkentin<sup>a</sup>, Viatcheslav Berejnov<sup>a</sup>, N.S. Hussein<sup>b</sup>, O.A. Alsaied<sup>d</sup>, R.E. Thorne<sup>a</sup>, <sup>a</sup>Physics Dept., Cornell Univ., <sup>b</sup>Applied & Engineering Physics Dept., Cornell Univ., <sup>c</sup>Weill Cornell Medical College, Doha, Qatar.

Successful flash cooling of protein crystals requires inhibition of crystalline ice formation both inside the crystal and in the liquid surrounding it. This is usually accomplished by adding cryoprotectants to the growth or harvest solutions. Excessive cryoprotectant concentrations may cause the crystal damage and degrade diffraction quality. We have measured the phase boundary between amorphous ice and crystalline ice produced by flash cooling from  $T=295$  K to  $T=77$  K in liquid nitrogen as a function of both cryoprotectant concentration and liquid volume from  $\sim$ nL to 20  $\mu$ L<sup>(1)</sup>. Fourteen common cryoprotectants were used: glycerol, methanol, isopropanol, sucrose, xylitol, dextrose, trehalose, ethylene glycol, PEG 200, PEG 2 000, PEG 20 000, DMSO, MPD, and NaCl. For most of the studied cryoprotectants, the critical concentration required to obtain amorphous ice decreases strongly with volume in the range from  $\sim$ 5  $\mu$ L to  $\sim$ 0.1  $\mu$ L, typically by a factor of two. By combining measurements of the critical concentration versus volume with cooling time versus volume for glycerol, we

obtain the critical CPA concentration versus cooling rate during flash cooling. Our results provide a basis for more rational design of cryo-protective protocols, and should yield insight into the physics of glass formation in aqueous mixtures.

This work was supported by the NIH (R01 GM65981).

[1] V. Berejnov, N. S. Hussein, O. A. Alsaied and R. E. Thorne, *J. Appl. Cryst.* (2006) (in press).

**T-P179 Single Crystal ESEEM Spectroscopic and Computational Chemical Analysis of Coupled  $^{17}\text{O}$  in Copper-Doped Enriched Tutton Salt.** M.J. Colaneri, J. Vitali, J. Peisach, Dept. of Chemistry & Physics, SUNY at Old Westbury, Old Westbury, NY 11568, Dept. of Physics, Cleveland State Univ., Cleveland, OH 44114 and Dept. of Physiology & Biophysics, Albert Einstein College of Medicine, Bronx, NY 10461

Electron Spin-Echo Envelope Modulation (ESEEM) spectroscopic studies and quantum mechanical calculations were performed on  $\text{Cu}^{2+}$ -doped  $^{17}\text{O}$ -enriched potassium zinc sulfate hexahydrate (tutton salt) crystals in order to measure the  $^{17}\text{O}$  hyperfine and quadrupole coupling tensors from  $\text{H}_2^{17}\text{O}$  weakly bound to copper. This analysis extends our earlier ESEEM results on tutton crystal samples. The obtained  $^{17}\text{O}$  hyperfine tensor can be modeled to arise from a combination of classical dipole-dipole components, producing a significantly rhombic form. The measured  $^{17}\text{O}$  quadrupole tensor is in the range of nuclear quadrupole interactions reported in studies of  $^{17}\text{O}$ -water salt hydrates. Chemical computations were carried out with the Gaussian 03 suite using various model chemistries. Theoretical coupling tensors derived from these models will be compared to those experimentally determined. The analysis of small coupling interactions from distant  $\text{H}_2^{17}\text{O}$  have important implications in studies of copper enzymes where substrates have been proposed to displace weakly bound water in the active site.

**T-P181  $\text{Ln}_2[\text{O}_2\text{C}-(\text{CH}_2)_3-\text{CO}_2]_3(\text{H}_2\text{O})_z \cdot m\text{H}_2\text{O}$  Framework Structures Features.** G. Punte<sup>1</sup>, G. Echeverría<sup>1,2</sup>, C.G. Pozzi<sup>1</sup>, E.V. Brusau<sup>3</sup>, G.E. Narda<sup>3</sup>, J.A. Ellena<sup>4</sup>, <sup>1</sup>LANADI e IFLP, Dept. de Física, Fac. de Cs. Exactas, <sup>2</sup>Fac. de Ingeniería, UNLP, Argentina, <sup>3</sup>Area de Química General e Inorgánica "Dr. G. F. Puelles", Fac. de Química, Bioquímica y Farmacia, UNSL, Argentina, <sup>4</sup>Inst. de Física São Carlos, Univ. de São Paulo, SP, Brazil.

Frameworks characteristics of three lanthanide glutarates (*glut*) synthesized from aqueous solutions are discussed. Two of them,  $[\text{Nd}_2(\text{glut})_3(\text{H}_2\text{O})_2] \cdot 4\text{H}_2\text{O}$  (I) and  $[\text{Nd}_2(\text{glut})_3(\text{H}_2\text{O})_4] 10\text{H}_2\text{O}$  (II), were produce at room temperature, while the third one,  $[\text{La}_2(\text{glut})_3(\text{H}_2\text{O})_3] \cdot 2\text{H}_2\text{O}$ , was obtained at 313K (Benmerad *et al.*, 2004). The three compounds crystallize in different space groups, contain unlike number of hydration waters and have dissimilar number of waters coordinated to Ln, but their 3D structures can be described as 1D networks build from O bridged Ln(III) cations and linked by *glut* anions in a way that channels, running parallel to the 1D network are developed. I is built from Nd(III) cations coordinated to nine O,  $\text{NdO}_8(\text{H}_2\text{O})$ , and shows to be similar to others already reported in the literature. II presents a novel framework structure with tenfold coordinated Nd(III) atoms,  $\text{NdO}_8(\text{H}_2\text{O})_2$ . III shows two independent La atoms, which are nine- and tenfold coordinated, leading to  $\text{LaO}_7(\text{H}_2\text{O})_2$  and  $\text{LaO}_9(\text{H}_2\text{O})$  polyhedra, respectively.

Benmerad *et al.*, *Acta Cryst.* (2004). C60, m119-m122.

**T-P183 Histidine Controlled Two-dimensional Assembly of Zinc Phosphite Four-Ring Units.** Xianhui Bu, Lan Chen, Dept. of Chemistry and Biochemistry, California State Univ., Long Beach, 1250 Bellflower Blvd., Long Beach, CA 90840.

Despite numerous examples of metal-organic frameworks in which metal centers or clusters are joined together by bi- or polydentate ligands into extended structures, biologically important amino acids, histidine in particular, are rarely known to serve as bridging ligands for the construction of open-framework architecture. Here we report hydrothermal self-assembly between neutral zwitterionic histidine molecules and inorganic secondary building units (i.e.,  $(\text{Zn}-\text{O}-\text{P}-\text{O})_2$  four-rings) into a crystalline solid containing infinite two-dimensional arrays. We demonstrate that the acid-base and coordination chemistry of histidine can be controlled to promote the formation of open architecture with bridging histidine ligands instead of the commonly observed metal-chelates with chelating histidine ligands. Crystallographic data for  $\text{Zn}(\text{HPO}_3)(\text{dl}-\text{C}_6\text{H}_9\text{N}_3\text{O}_2)(\text{H}_2\text{O})_{1/2}$ , C2/c,  $a = 15.1307(3)\text{\AA}$ ,  $b = 8.4230(2)\text{\AA}$ ,  $c = 16.6322(4)\text{\AA}$ ,  $\beta = 100.420(1)^\circ$ ,  $V = 2084.75(8)\text{\AA}^3$ ,  $Z = 8$ .

We thank the support of this work by the donors of the Petroleum Research Fund (administered by the ACS) (Grant Number: 41382-GB10) and the National Institutes of Health (Grant Number: 2 S06 GM063119-05).

**T-P185 A Search for Isostructural "Bridge-flipped" Isomers.** W.H. Ojala<sup>1</sup>, J.M. Spude<sup>1</sup>, T.M. Arola<sup>1</sup>, M.K. Kuspa<sup>1</sup>, Y. Moua<sup>1</sup>, H.M. Sexe<sup>1</sup>, B.L. Sanders<sup>1</sup>, N. Herrera<sup>1</sup>, J.M. Smieja<sup>1</sup>, C.R. Ojala<sup>2</sup>, <sup>1</sup>Dept. of Chemistry, Univ. of St. Thomas, St. Paul, MN, <sup>2</sup>Dept. of Chemistry, Normandale Community College, Bloomington, MN.

We designate as "bridge-flipped" isomers those pairs of molecules related by reversal of a bridge of atoms connecting two major parts of the individual molecules. This kind of isomerism is found among the benzylideneanilines ( $\text{Ar}-\text{CH}=\text{N}-\text{Ar}'$  vs.  $\text{Ar}-\text{N}=\text{CH}-\text{Ar}'$ ) and the phenylhydrazones ( $\text{Ar}-\text{CH}=\text{N}-\text{NH}-\text{Ar}'$  vs.  $\text{Ar}-\text{NH}=\text{N}-\text{CH}-\text{Ar}'$ ) ( $\text{Ar} = \text{aryl}$ ). We are examining compounds of both types to identify isostructural pairs of bridge-flipped isomers for co-crystallization experiments. Published structures of isomeric pairs are numerous, but isostructural examples are rare. We describe here the influence of structural features that might encourage isostructuralism if they were to operate similarly on both isomers, including disorder, similarity in conformation (in particular, planarity) and similarity in such intermolecular influences on packing as hydrogen bonding and Lewis acid-base interactions. In practice we have found some of these to be occasionally structure-differentiating, and we have obtained isostructural pairs in their absence.

Acknowledgment is made to the Donors of the American Chemical Society Petroleum Research Fund for support of this research.

**T-P187 Structural Characterization of Two Variants of the Green Fluorescent Protein.** J.D. Pédelacq, S. Cabantous, T.C. Terwilliger, G.S. Waldo, Los Alamos National Laboratory, Los Alamos, NM 87545.

Current enhanced versions of GFP fold well and are brightly fluorescent only when expressed alone or when fused to very well-folded proteins (1,2). Starting with the traditional folding reporter GFP (FR-GFP), we applied a directed evolution approach for engineering a superfolder GFP (SF-GFP) variant that folds well even when fused to poorly folded proteins (3). We applied a wide array of biophysical techniques to characterize the folding robustness of SF-GFP and several single-point mutants derived from SF-GFP. SF-GFP fusion fluorescence is unaffected by fusion partner misfolding and is directly proportional to total expression. Complete, highly redundant data sets

were collected for FR-GFP and SF-GFP to a resolution of 2.5 Å and 1.45 Å, respectively. These studies provide a structural explanation for why the mutations Y39N and S30R confer substantial improvement to SF-GFP folding robustness. SF-GFP should have widespread utility as a less-perturbing fluorescent protein tag for protein localization and trafficking experiments and provides the basis for new fluorescent protein derivatives.

- [1] Pédelacq J. D. *et al.* (2002) *Nat. Biotechnology* 20, 927-932  
 [2] Pédelacq J. D. *et al.* (2005) *Protein Science* 14, 2562-2573  
 [3] Pédelacq J. D. *et al.* (2006) *Nat. Biotechnology* 24, 79-88

**T-P189 Crystal structure of modular stator subunit E of archaeal H<sup>+</sup>-ATPase from *Pyrococcus horikoshii* OT3.** Neratur K. Lokanath, Chizu Kuroishi, Mitsuaki Sugahara, Naoki Kunishima, Advanced Protein Crystallography Research Group, RIKEN SPring-8 Center, Harima Inst., Hyogo, Japan.

H<sup>+</sup>-ATPase is an important multi-subunit complex which acts to produce ATP using the electrochemical proton potential across various biological membranes. Archaeal H<sup>+</sup>-ATPase (A-ATPase) is composed of an A<sub>1</sub> region that hydrolyzes ATP and an integral membrane part A<sub>0</sub> that conducts protons. The subunit E is a component of A<sub>0</sub> peripheral stalk(s) that couples A<sub>1</sub> and A<sub>0</sub> parts of the A-ATPase. Here we determined the first crystal structure of the subunit E of A-ATPase from *Pyrococcus horikoshii* OT3 at atomic resolution. The protomer structure of the subunit E indicates a novel fold. The quaternary structure of subunit E revealed a dimer consisting of two identical protomers, which might be important for the function of stator. On the basis of the modular architecture of stator subunits, it is suggested that both top and bottom sides of the subunit E and H dimer are possible binding site with the subunits A/B and H. The EH complex was characterized using circular dichroism spectroscopy which indicates a tight interaction between the subunits E and H. We propose that A-ATPase EH complex forms one of the peripheral stator as formed by the subunit b in F-ATPase.

This research work was supported by 'National Project on Protein Structural and Functional Analysis' funded by the MEXT of Japan.

**T-P191 Surface Modulated Motion Switch: The Capture-and-Release of Iron-Sulfur Protein in the Cytochrome *bc*<sub>1</sub> Complex D.** Xia<sup>1</sup>, L. Esser<sup>1</sup>, C. Yu<sup>2</sup>, <sup>1</sup>Lab of Cell Biology, National Cancer Inst., NIH, Bethesda MD 20892, <sup>2</sup>Dept. of Biochemistry & Molecular Biology, Oklahoma State Univ., Stillwater, OK 74078.

Most proton pumps are membrane channels, but the cyt *bc*<sub>1</sub> complex (*bc*<sub>1</sub>) uses a different mechanism by shuttling protons across the membrane and couples the process to electron transfer. The motion of the iron-sulfur-protein subunit (ISP) between two redox sites is a key component of the mechanism for the bifurcated electron transport originating at the quinol oxidation (Q<sub>o</sub>) site. However, it is not the motion alone but its control that prevents both electrons of a quinol from entering the favorable chain via the ISP. The analysis of eight structures of mitochondrial *bc*<sub>1</sub> with bound Q<sub>o</sub> site inhibitors of different types revealed that the presence of inhibitors causes changes in the position of the cd1 helix of the cyt *b* subunit. As the cd1 forms a major part of the ISP binding crater, any positional shift of this helix modulates the ability of cyt *b* to bind ISP. The analyses suggest a mechanism for reversal of the ISP fixation when the shape complementarity is significantly reduced following a positional reorientation of the reaction product quinone. The importance of the shape complementarity in this mechanism was confirmed by functional studies of *bc*<sub>1</sub> mutants.

**T-P193 On Understanding Solution Conditions that Maximize Protein Complex Formation.** P.S. Horanyi, B. Dillard, Z.-J. Liu, J.P. Rose, B.C. Wang, Dept. of Biochemistry and Molecular Biology, Univ. of Georgia, Athens, GA 30602.

Structure determination of protein complexes represents an increasing area of interest in structural biology. However, protein complexes are much more difficult to crystallize than single proteins, since the purified protein complex, when set-up in crystallization trials, routinely yields crystals of the individual proteins alone. This is due, in part, to the lack of understanding the solution conditions that promote stable interactions of the proteins in complex over interactions that promote self aggregation of the individual protein components.

Using the Amplified Luminescence Proximity Homogeneous Assay (ALPHA), we have developed a method to assess protein-protein interactions in solution that can be used to identify conditions that promote protein complex formation.

Initial tests using the T7 RNA polymerase - T7 lysozyme complex showed that we can differentiate between solution conditions that promote single complex formation (which may lead to crystallization of the complex) and those conditions that promote non-specific complex formation (that will not lead to crystallization due to the presence of multiple complex types in solution).

Work supported by NIGMS (GM062407), the Georgia Research Alliance, The UGA Research Foundation and PerkinElmer Life and Analytical Sciences.

**T-P195 Crystallization of Reaction Centre from *Rhodobacter Sphaeroides* in Bicontinuous Lipid Systems.** A. Wöhri, P. Wadsten, A. Snijder, S. Engström, R. Neutze, Dept. of Chemical and Biological Engineering, Chalmers Univ. of Technology, Gothenburg, Sweden.

Plants and some bacteria can convert light into chemical energy (photosynthesis). One such bacterium is *Rhodobacter sphaeroides* where the light driven reaction takes place in the membrane bound protein reaction centre (RC). Since the protein is normally surrounded by membrane bilayers, RC has been crystallized using the lipidic cubic phase (LCP) and a new crystal form (type I) was obtained using monoolein (MO) as the bilayered host. At room temperature MO forms a lamellar crystalline phase (L<sub>α</sub>) and changes its phase behaviour with its water content. Depending on the hydration level a lamellar liquid phase (L<sub>α'</sub>), cubic phases (*Ia3d* and *Pn3m*) or a liquid phase (L<sub>3</sub>) will form.

In this work we show the crystallization of RC from *R. sphaeroides* (2.1 Å) using jeffamine as a precipitant, which leads to phase transition to a liquid phase (L<sub>3</sub>). This phase has an inner structure in resemblance with the LCP with less curved lipid bilayers and larger aqueous pores, which makes it a better host for membrane proteins with larger hydrophilic domains such as RC. Since the L<sub>3</sub> phase is a liquid, one can take the advantage of performing a vapour diffusion experiment and one will be more confident in using this new method compared to the LCP.



**T-P197 Room to Move. Crystallizing Membrane Proteins in Swollen Lipidic Mesophases.** V. Cherezov<sup>1</sup>, J. Clogston<sup>1</sup>, M.Z. Papiz<sup>2</sup>, M. Caffrey<sup>1,3</sup>, <sup>1</sup>Dept. of Chemistry, The Ohio State Univ., Columbus, OH, USA; <sup>2</sup>CCLRC Daresbury Lab., Daresbury, Warrington, UK; <sup>3</sup>College of Science, Univ. of Limerick, Limerick, Ireland.

The cubic phase or *in meso* crystallization method is responsible for almost 40 solved integral membrane protein structures. Most of these are small and compact proteins. A model for how crystals form by the

*in meso* method has been proposed. In light of this model, we speculated that a more hydrated and open mesophase of reduced interfacial curvature would facilitate crystallization of bigger and bulkier proteins. The proposal was explored in the current study by performing crystallization in the presence of additives that swell the cubic phase. The additive concentrations inducing swelling, as quantified by small-angle X-ray diffraction, coincided with a ‘crystallization window’ in which two, very different membrane proteins produced crystals. That the swollen mesophase can grow structure-grade crystals was proven with one of these, the light-harvesting II complex. Packing density in the *in meso*-grown crystals was dramatically higher accounting for their enhanced diffracting power. These results present a rational case for including mesophase-swelling additives in screens for *in meso* trials, which will broaden the range of membrane proteins yielding to structure determination.

**T-P199 Microscale Self-interaction Chromatography for Rapid Determination of Membrane Protein Virial Coefficients.** P.J. Loll<sup>1</sup>, W.W. Wilson<sup>2</sup>, C.S. Henry<sup>3</sup>, <sup>1</sup>Drexel Univ. College of Medicine, Philadelphia PA; <sup>2</sup>Mississippi State Univ., Mississippi State, MS, <sup>3</sup>Colorado State Univ., Fort Collins, CO.

Our knowledge of the 3-D structures of membrane proteins lags far behind our understanding of soluble proteins, in large part due to the difficulties associated with preparing membrane protein crystals. Direct measurement of the interaction forces that control crystal lattice formation will help rationalize the search for crystallization conditions and overcome some of these difficulties. However, until now such measurements were too laborious and consumed too much material to be of any practical use. We are developing a rapid, high-throughput method utilizing self-interaction chromatography that will these measurements to be made using only microgram quantities of protein. The strength of attractive or repulsive protein-protein interactions is inferred from the second virial coefficient, which is derived quantitatively from shifts in chromatographic retention times. Recent progress will be presented.

This work is supported by NIH grant R21 GM075816.

**T-P201 Activation and Inhibition of the Multidrug ABC Transporter MsbA.** Christopher L. Reyes, Geoffrey Chang, Dept. of Molecular Biology, The Scripps Research Inst., 10550 N. Torrey Pines Rd. CB105, La Jolla, CA, 92137, clreyes@scripps.edu.

ATP binding cassette transporters transport a wide variety of substrate molecules across the cell membrane. MsbA, LmrA, and human MDR1 P-glycoprotein are members of the ABC transporter family that have been implicated in multidrug transport by coupling ATP binding and hydrolysis to drug efflux that results in resistance to antibiotics and chemotherapeutic drugs in the treatment of infections and cancers. We report two X-ray structure of MsbA: *i*) in complex with transition state mimic ADP·Vi and the human immunomodulatory substrate Ra lipopolysaccharide, and *ii*) in complex with a clinical multidrug resistant MDR) modulator. MsbA undergoes a rigid-body torque of its two transmembrane domains coupled to ATP hydrolysis. Lipid “flip-flop” from the inner to the outer membrane leaflet is driven on the membrane exposed surface of MsbA suggesting two possible transport pathways. The structure of MsbA with the MDR inhibitor reveals an unexpected binding site that decouples ATP hydrolysis from substrate binding and closes the transmembrane translocation pathways. Taken together, these structures help to elucidate the molecular basis for transport and transport inhibition for this class of ABC transporters.

**T-P203 Crystal Structures of Anabaena Sensory Rhodopsin and its Soluble Transducer.** L. Vogeley, H. Luecke, Dept. of Molecular Biology and Biochemistry, Univ. of California Irvine, Irvine, CA 92697.

Anabaena sensory rhodopsin (ASR) is a membrane-embedded light receptor of the cyanobacterium *Anabaena sp.* and is thought to be involved in the regulation of the assembly/composition of the phycobilisomes responsible for light harvesting in cyanobacterial photosynthesis. It is co-transcribed with a soluble 14 kDa protein – its putative transducer ASRT.

The structure of Anabaena sensory rhodopsin was solved by molecular replacement and shows an unusually hydrophilic cytoplasmic side for rhodopsins with an almost complete hydrogen-bonded network connecting the chromophore to the cytoplasmic surface of the protein where the transducer would have to bind.

The transducer ASRT forms tetramers in solution. The (as of yet incomplete) structure of the tetramer was solved in three different space groups using SIRAS phasing with an iodide derivative from a KI quick soak as well as by molecular replacement. The tetramer of ASRT bears a mild resemblance to the G-beta protein monomer which is involved in eukaryotic rhodopsin signaling. Differences between the different ASRT structures and disordered regions indicate a rigid and a somewhat disordered face for the tetramer. The latter could be involved in signal transduction.

The ASR-ASRT interaction is currently under further investigation.

**T-P205 Domain Flexibility and Catalysis in the Complex II Superfamily.** Thomas M. Tomasiak<sup>1,2,6</sup>, Elena Maklashina<sup>7,8</sup>, Kristian Kaufmann<sup>5,6</sup>, Eric Dawson<sup>3,4,6</sup>, Jens Meiler<sup>1,3,5,6</sup>, Gary Cecchini<sup>7,8</sup>, Tina M. Iverson<sup>1,2,3,4,6</sup>, <sup>1</sup>Dept. of Pharmacology, <sup>2</sup>Vanderbilt Inst. for Chemical Biology, <sup>3</sup>Center for Structural Biology, <sup>4</sup>Dept. of Biochemistry, <sup>5</sup>Dept. of Chemistry, <sup>6</sup>Vanderbilt Univ., Nashville, TN, <sup>7</sup>Molecular Biology Div., VA Medical Center, San Francisco, CA, <sup>8</sup>Dept. of Biochemistry and Biophysics, UCSF, San Francisco, CA.

The catalytic subunits of integral membrane Complex II enzymes have a conserved fold comprising two domains: an FAD-binding domain and a capping domain. The capping domain covers the active site with multiple residues within hydrogen bonding distance of substrate. Of note is Thr 244, which has not been assigned a direct catalytic role, yet when substituted to Ala reduces catalytic activity by 97%. To establish the basis for this loss of activity, the structure of a T244A variant in the *Escherichia coli* Complex II homolog Quinol: Fumarate Reductase (QFR) was determined to 3.65Å resolution. In this structure, the capping domain significantly rotates to expose the active site to solvent. This domain shift combined with interface stability calculations suggests that the hydrogen bond between Thr 244 and substrate is critical for inducing capping domain closure and correct orientation of catalytic residues upon substrate binding.

**T-P207 Structure Determination of Colicin I Receptor Alone and in Complex with Colicin IA: Transport of Large Proteins Across Bacterial Outer Membranes.** Susan K. Buchanan<sup>1</sup>, Sylvestre Grizot<sup>1</sup>, Maruf Ali<sup>1</sup>, and Lothar Esser<sup>2</sup>, <sup>1</sup>Laboratory of Molecular Biology, National Institute of Diabetes and Digestive and Kidney Diseases, <sup>2</sup>Laboratory of Cell Biology, National Cancer Inst., National Institutes of Health, Bethesda, MD 20892.

We use X-ray crystallography to study the structures and functions of integral membrane proteins in the outer membranes of bacteria. Bacteria require iron for survival, and they express transport systems

dedicated to iron acquisition. Iron complexes are transported across the bacterial outer membrane using a transmembrane beta barrel protein coupled to an inner membrane protein (TonB) and proton motive force. We have been studying the questions of ligand specificity at the extracellular side of the transporter, and TonB recognition at the periplasmic side of the receptor. Exactly how these small molecules are transported through the barrel is not yet understood, despite the availability of several high resolution crystal structures. These same beta barrel proteins also serve as receptors / transporters for colicins, which are large proteins with bacteriocidal activity. This poster will describe the differences between binding small molecules and large proteins to the same receptors, and will discuss how TonB and energy may be involved in the transport process(es). The knowledge gained from studying these systems may facilitate vaccine and drug design against Gram-negative bacterial pathogens.

**T-P209 Regulation of a Cyclic Nucleotide Binding Regulated Ion Channel.** Gina M Clayton, Joao Morais Cabral, Yale Univ., New Haven, CT.

The cyclic nucleotide regulated ion channels, include the HCN (eukaryote hyper-polarisation activated, cyclic nucleotide-dependent) the CNG (cyclic nucleotide gated) channels and a recently recognized family of bacterial cAMP regulated channels. All of these channels are tetrameric, with 6 transmembrane helices (TMs) in each monomer. TMs 5 and 6 form the ion conduction pore whose activity is regulated by a C-terminal cytoplasmic Cyclic Nucleotide Binding Domain (CNBD). The structural basis for channel gating, i.e. opening and closing of the channel pore, and CNBD-mediated regulation, is still unclear. We have solved X-ray structures of a potassium channel's CNBD from the bacterium *M. luti* with and without nucleotide ligands. Comparison of these two structures demonstrates conformational changes in the ligand pocket, the C-terminal helix and the dimer interface, and we suggest a model for gating. Current work is focused on testing this model by studying full-length channels, in different functional states, with a variety of methods, including 2D and 3D crystallography. Here we present our preliminary 2D results.

**T-P211 Factors Influencing Recombinant Transmembrane Protein Expression.** G. Mazock, V. Madhavan, C. Jeffery, Laboratory for Molecular Biology, Univ. of Illinois at Chicago, Chicago, IL.

Approximately 30% of known proteins are predicted to be transmembrane proteins. These proteins play key roles in important cellular activities, including ion transport, multi-drug resistance, biofilm formation, and host-pathogen interactions. The misfolding or improper activity of transmembrane proteins can lead to genetic diseases. The majority of pharmaceuticals in use target transmembrane proteins. However, there are far fewer structures known for transmembrane proteins than there are of soluble enzymes because the presence of the hydrophobic membrane-embedded domains result in difficulties in protein expression, purification, and crystallization. Our project addresses the first bottleneck in working with these proteins: expressing sufficient levels of protein for structural studies. We selected eighty-seven transmembrane proteins from the opportunistic bacterial pathogen *Pseudomonas aeruginosa*. These proteins featured at least two predicted alpha-helical regions and a wide variety of predicted functions. Relative protein expression levels were determined under a variety of culture growth conditions to address whether transmembrane protein expression levels correlate with physical features of the protein (such as the number of transmembrane helices) and/or growth conditions.

**T-P213 Efforts in the Crystallization and Structure Determination of a Ternary Complex of Human Urokinase and its Receptor.** Qing Huai, Yongdong Li, Cai Yuan, Chuanbing Bian, Liqing Chen, Mingdong Huang., Div. of Haemostasis and Thrombosis, Beth Israel Deaconess Medical Center, 330 Brookline Ave, Boston, MA 02215.

Urokinase plasminogen activator (uPA) and its cellular receptor (uPAR) have received extensive study as one of the two primary endogenous systems that mediate plasminogen activation. The uPA binds to uPAR at high affinity ( $K_d$  of 0.1–1nM), thus localizing the generation of plasmin from plasminogen onto pericellular regions of a variety of cells. uPA-uPAR binding is also involved in other general cellular functions and in subsequent diverse pathophysiological processes such as tissue remodeling, arteriosclerosis, tumorigenesis, and tumor metastasis. uPAR is heavily glycosylated and tends to oligomerize, posing difficulty for structural study. Here we report the crystal structure of soluble uPAR complexed with the urokinase amino terminal fragment and an anti-receptor antibody at 1.9Å (Huai, et al., Science 2006; 311:659). suPAR is composed of three consecutive domains that form a concave shape with a diameter of about 52 Å and a height of 27 Å. At the center of teacup and surrounded by three suPAR domain is a cone shape cavity with wide opening (25 Å) and large depth (14 Å). All three domains of uPAR and two domains of uPA work in cooperation yielding high affinity uPA-uPAR binding. The structure provides insight into the flexibility of urokinase receptor that enables its interaction with a wide variety of ligands and a basis for design de novo uPA-uPAR antagonists that will be important for anti-tumor metastasis therapy.

**T-P215 Crystal Structure of the Coiled-coil N-terminal Fragment of NudEL.** Derewenda U., Kim M.H., Cooper D. Derewenda Z., Dept. of Mol. Physiology and Biological Physics, Univ. of Virginia, Charlottesville, VA 22936.

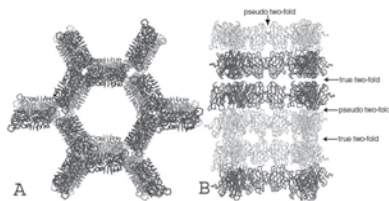
NudEL is a 39kDa protein that implicated in diverse cellular functions ranging from nucleokinesis in fungi, through kinetochore biology and mitotic cell division in eukaryotes, to cerebral cortex development in man. NudEL assembles with Lis1 and dynein/dynactin complexes. A number of human genetic disorders (i.e. lissencephaly, microcephaly dyslexia and schizophrenia) have been linked to mutations in genes coding for proteins active in these pathways.

As most coiled-coils, the structure was crystallographer's proverbial nightmare. Crystals were non-isomorphous and diffracted poorly, with different spaces groups and unit cells. The structure was finally solved with MAD data collected at SER-CAT to 2.1Å resolution, using SOLVE/RESOLVE suite for phasing.

The density maps revealed a fascinating homotetrameric molecule that, to our knowledge, is the longest coiled-coil structure to be structurally characterized at high-resolution. The parallel homodimer, which occupies the asymmetric unit, is 230Å long, while the tetramer is 350Å long with a diameter of only about 25Å. Every step of the analysis including crystallization, data collection, phasing, model building and refinement proved to be a challenge for this difficult structure.

**T-P217 Perils of Pseudosymmetry Combined with Meroheral Twinning.** J.P. Schuermann, A.J. Rodriguez, A.B. Taylor, P.J. Hart, Univ. of Texas Health Science Center at San Antonio, TX.

The structure determination of a human copper-zinc superoxide dismutase (SOD1) mutant that causes amyotrophic lateral sclerosis (ALS) was complicated by a combination of nearly perfect hemihedral twinning and pseudosymmetry. Twinning was suspected when refinement stalled at R and R-free values of 0.25 and 0.29 in space group C22<sub>1</sub>. The shape of the cumulative intensity distribution plot appeared to support this suspicion. The diffraction data were reprocessed in space group P3 and uploaded to the Merohedral Crystal Twinning Server, which returned a twin fraction ( $\alpha$ ) of 0.47 for each of the 3 possible twin laws. Brute force molecular replacement was performed in all 18 possible space groups (6/mmm, 6/m, 3m1, 31m). Four candidates (P622, P6, P321, P312) returned reasonable statistics and crystal packing. In each of these space groups, the packing consists of a six-fold “honeycomb” looking down the *c* axis (Figure 1A). The correct space group was eventually determined to be P321 (and not P312) with the help of a native Patterson. Mature SOD1 is an enormously stable homodimer with two metal ions and a disulfide bond within each subunit. In this case, the asymmetric unit contains four pathogenic SOD1 subunits. Two associate to form a canonical SOD1 homodimer, but the remaining two lack metal ions and the disulfide bond. Metal- and disulfide-free SOD1 is known to be monomeric. These dimers and “pseudodimers” pack in alternating bilayers and generate two sets of pseudo-two-fold axes (Figure 1B). The structural differences between these forms of this pathogenic SOD1 mutant have profound implications for both SOD1 maturation and the etiology of SOD1-linked ALS. These differences, and the insight derived from them, would have been completely missed had the twinning issues not been detected and handled properly.



**T-P219 A Preliminary Model of Major Vault Protein.** Daniel H. Anderson<sup>1</sup>, Valerie A. Kickhoefer<sup>2</sup>, Stuart A. Sievers<sup>3</sup>, Leonard H. Rome<sup>2</sup>, David Eisenberg<sup>1,2</sup>, <sup>1</sup>HHMI at UCLA, <sup>2</sup>Dept. of Biol. Chem. at UCLA Medical School, <sup>3</sup>Dept. of Chem. and Biochem, UCLA.

Vaults are the largest known ribonucleoprotein structures. The vault is 405Åx405Åx680Å and is among the largest objects to have crystallized. The vault capsule is built from 96 copies of the 95.8kDa major vault protein, with 24- and 48-fold symmetry. Although the resolution is only about 9Å, the symmetry-averaged electron density could be parsed to build a model. Atom placement was not possible at this resolution, but it was possible to deduce what structural elements could result in each region of density. Sequence analysis assisted model-building. A preliminary model was built mostly by a “stream-pool” algorithm. A “stream” of density connected to its context at its ends could be assigned helical structure. A flat “pool” of density could be assigned 2-, 3-, or 4-strand beta-sheets, depending on whether its connections were on the same or opposite edges of the “pool.” A perfect chain trace would contain 873 residues with correctly assigned sequence. This first model (the “connectivity diagram”) contains 668 residues, mostly poly-alanine. Although the model contains obvious flaws, it does indicate zones of structure stabilization, and is an important step towards the goal of engineering the vault nanocapsule.

**T-P221 Determination of ytrI Architecture.** D. Borek<sup>1</sup>, J. Osipiuk<sup>2</sup>, R. Wu<sup>2</sup>, S.F. Moy<sup>2</sup>, A. Joachimiak<sup>2</sup> & Z. Otwinowski<sup>1</sup>, <sup>1</sup>UT Southwestern, Dallas, TX, <sup>2</sup>SBC-ANL, Argonne, IL.

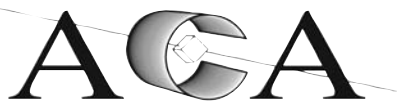
ytrI is a structural protein specific for endospore-forming bacteria from *Bacillus* genus. It is implicated in maintaining spore integrity at the late stages of sporulation process. We solved the structure of ytrI soluble domain. The crystals we obtained diffracted anisotropically in the range 2.8-3.0 Å. Data analysis indicated six molecules in ASU with the solvent content ~70%. Heavy atom positions were found, but were poorly ordered due to only a single Se-site located on the protein surface. Initial NCS averaging was not successful as the protein forms only quasi-symmetric high order oligomeric assemblies. Due to unique pseudo-symmetry, the consequences of phase errors were not uniformly distributed, with two molecules having a particularly poor electron density. The solution of the structure integrated phasing and model building with an unusual procedure involving steps that increased bias, followed by returning to earlier phases to remove it.

The crystal structure consists of parallel fibers that are likely to be physiologically relevant. Interactions between flexible coil-coiled segments and alpha-beta core of the fiber are observed. The structure provides insight into the so far poorly understood group of the membrane-anchored, structural proteins.

**T-P223 Quick Solution of Difficult Structures is not Necessarily an Oxymoron.** W. Minor<sup>1</sup>, M. Cymborowski<sup>1</sup>, M. Chruszcz<sup>1</sup>, Z. Otwinowski<sup>2</sup>, D. Borek<sup>2</sup>, <sup>1</sup>Univ. of Virginia, Charlottesville, VA, <sup>2</sup>UT Southwestern Medical Center, Dallas, TX.

The term difficult structure is very subjective and is quite often related to the time difference between the start of the project and PDB deposition. However, in many cases, the process of discovering what makes the structure resistant takes a long time, and when it is revealed, the structure is solved relatively fast. When an appropriate treatment of a particular problem can be coded in the structure solution system, a similar problem encountered next time does not pose a serious difficulty. For that reason, the frequently used term ‘high-hanging fruit’ is constantly redefined. We can define a difficult structure as one that has pathologies that are not easily recognizable by current methods or an experimenter’s experience.

We have developed an expert system HKL-2000\_ph, for semi-automatic or automatic analysis of X-ray diffraction data, which has been successfully used for more than 120 new structure determinations. The current system is oriented towards very fast structure solution, in order to provide feedback during the diffraction experiment. The typical end result is an interpretable electron density map with a partially built structure. The system recognizes sample or data pathologies, sets the optimal data collection strategy, and identifies and corrects for many experimental set-up errors. The most important corrections include, but are not limited to: absorption correction, spindle axis misalignment, uneven speed of spindle axis rotation, and vibration of the cryogenic loop with the frozen crystal during data collection. Examples of various pathologies and their successful (and sometimes unsuccessful) treatment will be presented and discussed.



# 2006 Annual Meeting

## July 22 - 27 Honolulu, Hawaii

### Organization

**Program Chair:** Judith Kelly

**Local Chairs:** Karl Seff, Charles Simmons

**Program Committee:** Simon Billinge  
Bryan Chakoumakos  
Aina Cohen

Lachlan Cranswick  
Chad Haynes  
Charles Kissinger

Thomas Koetzle  
Jeanette A. Krause  
Paul Langan

Craig Ogata  
Allen Oliver  
Volker S. Urban

### Sponsors

American Chemical Society-PRF  
Blake Industries, Inc.  
Bristol-Myers Squibb Pharmaceutical  
Research Institute  
Bruker AXS, Inc.  
Canadian Light Source  
Charles Supper Company, Inc.

Genentech  
GlaxoSmithKline  
Hampton Research  
ICDD  
IUCr  
Merck Research Laboratories  
NIAID/NIH

NIST  
Nextal/Qiagen, Inc.  
Pfizer Global R&D, La Jolla  
Rigaku Americas Corp.  
Schering-Plough Research Inst.  
Wyeth Research

### Exhibitors

Accelrys  
Area Detector Systems Corp.  
Art Robbins Instruments  
Axygen Biosciences  
Blake Industries Inc.  
Bruker AXS, Inc.  
CCP4  
Cryo Industries of America Inc.  
Crystal Logic, Inc.  
Emerald Biosystems  
Fluidigm Corp.  
FMP Products  
Formulatrix, Inc.

GE Healthcare Bio-Sciences  
Genomic Solutions  
Hampton Research  
Incoatec GmbH  
IUCr  
Jena Bioscience GmbH  
Korima Inc.  
Malvern Instruments  
MARResearch  
MarUSA, Inc.  
Mitegen, LLC  
Molecular Dimensions Inc.  
Open Eye Scientific Software

Oxford Cryosystems  
Oxford Diffraction Ltd.  
PANalytical  
Perkin Elmer Life & Analytical  
Sciences  
QIAGEN, Inc.  
RCSB Protein Data Bank  
Rigaku Americas Corp.  
SER-CAT  
TriTek Corp.  
TTP LabTech  
Wyatt Technology Corp.  
Xenocs S.A.

### Corporate Members

ActiveSight  
Area Detector Systems Corp.  
Art Robbins Instruments  
ATPS, Inc.  
Axxora, LLC  
Axygen Biosciences  
Biblioteca Universitaria  
Bibliothek Technische Hochschule  
Blake Industries, Inc.  
Bruker AXS, Inc.  
Cambridge Cryst Data Center  
Charles Supper Company, Inc.  
Corning, Inc.

Cryo Industries of America, Inc.  
Crystal Logic, Inc.  
Douglas Instruments Ltd.  
Emerald Biosystems  
Fluidigm Corp.  
Genomic Solutions  
Gilson, Inc.  
Hampton Research  
Jena Bioscience GmbH  
Korima, Inc.  
Malvern Instruments  
Mar USA, Inc.  
MARResearch GmbH

Mitegen LLC  
Molecular Dimensions, Inc.  
Neuro Probe, Inc.  
Oxford Cryosystems  
Oxford Diffraction Ltd.  
RCSB Protein Data Bank  
Rigaku Americas, Corp.  
Select Biosciences Ltd.  
Taylor & Francis  
TriTek Corp.  
Viscotek Corp.  
Wyatt Technology Corp.  
Xenocs S.A.

Meeting Registration Desk  
Opening Reception & Exhibit Show

7:30am-7:30pm  
7:30pm - Name tag required for entry

Ballroom Foyer  
Ballroom

## WK.01 Methods in Neutron Protein Crystallography

Kohala P. Langan,  
P. Adams, Presiding

- 08:30-08:45 Introduction and Welcome
- 08:45-09:05 An Introduction to Neutron Protein crystallography. Benno Schoenborn
- 09:05-09:30 Protein Deuteration. Leighton Coates
- 09:30-9:50 Protein Crystal Preparation. Nobuo Niimura
- 09:50-10:15 Available Neutron Beam Lines. Bob Bau
- 10:15-10:30 Cryotechniques. Flora Meilleur
- 10:30-11:00 Coffee Break
- 11:00-11:30 Refinement using SHELX. Leighton Coates
- 11:30-12:30 Refinement using CNS-solve. Paul Langan, Marat Mustyakimov
- 12:30-01:30 Lunch Break
- 01:30-02:15 Refinement using CNS-solve. Paul Langan, Marat Mustyakimov
- 02:15-03:00 Refinement using PHENIX. Paul Adams, Pavel Afonine
- 03:00-03:30 Coffee Break
- 03:30-04:45 Refinement using PHENIX. Paul Adams, Pavel Afonine
- 04:45-05:00 Summing Up

## WK.02 Management of Synchrotron Image Data: imgCIF File System and Beyond

Oahu Herbert Bernstein,  
Robert Sweet, Presiding

- 08:30-08:50 Definition of the problem. Objectives of workshop. R. Sweet
- 08:50-09:10 The structure and flexibility of imgCIF, available supporting software and mechanisms for making changes to both accepted mechanism for updating. H. Bernstein
- 09:10-09:30 Introduction of participants.
- 09:30-10:00 Coffee Break
- 10:00-12:30 Speakers
- What is the problem should we be solving? G. Bricogne
  - Issues for equipment vendors. C. Nielsen
  - Issues for data-red'n software developers. W. Minor, J. Pflugrath
  - Issues for beam-line software developers.
  - Issues for other software developers. A. Ashton
  - Issues for data archivists. J. Westbrook
  - Issues for CIF wonks. B. McMahon
  - Issues for relative to HDF and XML.
- 12:30-01:30 Lunch Break
- 01:30-03:00 Working groups meet for discussion and conclusions
- 03:00-03:30 Coffee Break
- 03:30-04:30 Discussion
- 04:30-05:00 Plans for future

## WK.03 An Introduction to Grazing Incidence Small Angle Scattering with X-rays and Neutrons

Kona Jin Wang,  
Randall Winans, Presiding

- 08:30-09:15 GISAXS of Liquid-liquid Interfaces. Thomas Russell
- 09:15-10:00 Practical Aspects of GISAXS. Byeongdu Lee
- 10:00-10:30 Coffee Break
- 10:30-11:15 Grazing Incidence Small-Angle X-ray Scattering and Diffuse Scattering and Diffuse Scattering from Interfaces. Sunil Sinha
- 11:15-12:00 Grazing Incidence Small Angle Neutron Scattering Techniques and Applications to Bilayer Membranes. David Worcester

# Sunday, July 23

Council Meeting Room	Waimea Canyon	Rigaku Lunch	Oahu/Waialua	12:05	SAS SIG Meeting	Kohala/Kona	12:00
Speaker Ready Room	Ewa 7:30am-5:30pm	Powder Diff. SIG Meeting	Honolulu/Kahuku	12:00	Poster Session S	Ballroom	5:30-7:30pm
Interview Room	Puna	Neutron Scattering SIG	Niihau	12:00	YS-SIG Mixer	Diamond	8:30pm
Guest Get-together	Koko Crater 9:00am	Meeting			<i>Sponsored in part by Nextal (pre-purchased ticket required)</i>		
Exhibit Show	Ballroom 10am-7:30pm	Industrial SIG Meeting	Lanai	12:00	Braker Luau (invitation only)	Head Lawn	

## Morning Sessions

### Opening Ceremony and Welcome

08:00am Lanai  
Robert Bau, ACA President, Presiding

### 01.01 New Structures

Lanai S. Ginell,  
D. Garboczi, Presiding

08:20-08:40 01.01.01  
Catch the Precious Moments of Reduction of Disulfide by FeS Cluster: Structures of Ferredoxin:Thioredoxin Reductase at Different Intermediate States. Shaodong Dai.

08:40-09:00 01.01.02  
Enzyme Flexibility is the Key to Cyclizing a Linear Tetrapyrrole. Heidi L. Schubert, John D. Phillips, Christopher P. Hill.

09:00-09:20 01.01.03  
The Mechanism of Double-Stranded RNA Processing by Ribonuclease III: How Dicer Dices. Xinhua Ji, Jianhua Gan, Joseph Tropea, Brian Austin, Donald Court, David Waugh.

09:20-09:40 01.01.04  
First Structure of a Monofunctional Proline Dehydrogenase Involved in Reactive Oxygen Species Generation. Tommi White, Navasona Krishnan, Donald Becker, John Tanner.

09:40-10:00 01.01.05  
Structural Insights into the Function of the Thiamin Biosynthetic Enzyme Thi4 From *Saccharomyces cerevisiae*. C.T. Jurgenson, A. Chatterjee, T.P. Begley, S.E. Ealick.

10:00-10:40 Coffee Break.

10:40-11:00 01.01.06  
Crystal Structures of Catalytic Complexes of the Oxidative DNA/RNA Repair Enzyme AlkB. Bomina Yu, John F. Hunt.

11:00-11:20 01.01.07  
Crystal Structures of the PhoQ Sensor Domain Suggest a Novel Mechanism for Signal Transduction Across Cell Membranes. Uhn Soo Cho, Martin W. Bader, Maria F. Amaya, Margaret E. Daley, Rachel E. Klevit, Samuel I. Miller, Wenqing Xu.

11:20-11:40 01.01.08  
Is There a Preponderance of Novel Folds in the SARS Coronavirus Proteome? Jeremiah Joseph, Saikatendu Kumar, Vanitha Subramanian, Benjamin Neuman, Michael Buchmeier, Raymond Stevens, Peter Kuhn.

11:40-12:00 01.01.09  
Domain-swapped Structure of an Antiviral Protein Griffithsin. Alexander Wlodawer, Natasza Ziolkowska, Charles Zhu, Toshiyuki Mori, Kenneth Palmer, Barry R. O'Keefe.

### 01.07 International Macromolecular Crystallographic Advances

Honolulu/Kahuku B. Duax, Presiding

08:30-08:50 01.07.01  
Three-dimensional Structure of a Ferritin from the Hyperthermophilic Archaeon and Anaerobe *Pyrococcus furiosus*. Pedro Matias, Jadwiga Tatur, Maria Carrondo, Wilfred Hagen.

08:50-09:10 01.07.02  
Plant L-Asparaginase and its Relation to Human and Bacterial Cousins. Mariusz Jaskolski, Karolina Michalska, Grzegorz Bujacz.

09:10-09:30 01.07.03  
Crystal Structure of the Human FOXK1a/DNA Complex and its Implications on the Diverse Binding Specificity of Winged Helix/forkhead Proteins. Chwan-Deng Hsiao, Kuang-Lei Tsai, Cheng-Yang Huang, Chia-Hao Chang, Yuh-Ju Sun, Woei-Jer Chuang.

09:30-09:50 01.07.04  
The Crystal Structure of YaeQ from *Xanthomonas axonopodis* pv. *Citri*. J.A.R.G. Barbosa, C.R. Guzzo, R.A.P. Nagem, L.M.P. Galvão-Botton, C.S. Farah.

09:50-09:55 T-P162  
Functional Studies of Membrane Proteins. Maria Nyblom, E. Gordon, R. Neutze.

09:55-10:30 Coffee Break.

10:30-10:50 01.07.05  
Structural Basis of Plant Disease Resistance in Flax against Flax Rust. Bostjan Kobe, Ching-I Wang, Gregor Guncar, Trazel Teh, Ann-Maree Catanzariti, Jeffrey G. Ellis, Peter N. Dodds.

10:50-11:10 01.07.06  
When Crystal Structure Does Not Seem to Depict Physiologically Relevant Conformation - A Novel Calmodulin Conformation in Calmodulin and Calcineurin-peptide Complex. Zongchao Jia, Qilu Ye, Xin Li, Andrew Wong, Qun Wei.

11:10-11:30 01.07.07  
A Edium-scale, High-efficiency and Low-cost Platform for Structural Genomics Studies. Xiao-Dong Su.

11:30-11:50 01.07.08  
Structural Insights Into SARS Coronavirus Proteins. Zihao Rao.

11:50-11:55 T-P164  
Dimeric Structural Significance for Ligand Binding in Putative Peptidyl-tRNA Hydrolase from *Pyrococcus horikoshii* OT3. K. Shimizu, Y. Fujimoto, M. Sugahara, N. Kunishima.

11:55-12:00 T-P166  
Structural Studies on *Helicobacter pylori* Apoflavodoxin Contributes to Investigate Conformational Changes in Flavodoxins Induced by FMN Binding. Marta Martínez-Júlvez, Marta Bueno, Nunilo Cremades, Javier Sancho, Juan Hermoso.

### 09.01 Grazing Incidence Methods for Nanoscience and Biotechnology

Kohala/Kona J. Wang,  
R. Winans Presiding

09:00-09:30 09.01.01  
Developing A Dedicated Grazing-Incidence Small-Angle X-ray Scattering Beamline at the APS. Xuefa Li, Michael Sprung, Suresh Narayanan, Alec Sandy, Dong Ryeol Lee, Jin Wang.

09:30-10:00 09.01.02  
Self-assembly and Cross-linking of Nanoparticles at Liquid-liquid Interfaces. Thomas Russell.

10:00-10:30 Coffee Break.

10:30-11:00 09.01.03  
Internal and Interface Structure in Diblock Copolymer Brushes. M.D. Foster B. Akgun G. Ugur W.J. Brittain X. Li D.R. Lee J. Wang.

check the schedule carefully - morning sessions begin at different times

Morning Sessions

11:00-11:30 09.01.04  
GISAXS Studies of Gold and Platinum Nanoparticles Formed by Atomic Cluster Deposition. Stefan Vajda, Randall Winans, Gregory Ballentine, Jeffrey Elam, Byeongdu Lee, Michael Pellin, Soenke Seifert, George Tikhonov, Nancy Tomczyk.

11:30-12:00 09.01.05  
Spin Echo Resolved Grazing Incidence Neutron Scattering. Suzanne G. E. te Velthuis, Péter Falus, Gian P. Felcher, Alexei Vorobiev, János Major, Helmut Dosch, Peter Müller-Buschbaum.

**13.01 Crystalline Materials for Storage and Containment**  
Niihau A. Beatty,  
C. Jensen, Presiding

08:30-09:00 13.01.01  
Investigation of the Microstructure of Ti-Doped Sodium Aluminum Hydride. Martin Sulic, Craig Jensen, Lance Culnane, Bjorn Hauback, Hendrick Brinks, Mark Pitt, Ian Robertson.

09:00-09:30 13.01.02  
Probing Structure and Bonding in Hydrogen-Storage Materials by Combined Neutron-Scattering Techniques and First-Principles Calculations. Terrence J. Udovic.

09:30-10:00 13.01.03  
Diffraction Studies of Complex Al-based Hydrides for Hydrogen Storage. Yumiko Nakamura, Magnus H. Sorby, Anita Fossdal, Didier Blanchard, Hendrik W. Brinks, Craig M. Jensen, Bjorn C. Hauback.

10:00-10:30 Coffee Break.

10:30-11:00 13.01.04  
Characterization of Phase Compositions and Structures for Metal Hydrides Used in Hydrogen Storage. Robert Bowman, James Kulleck, Son-Jong Hwang, Mike Hartman, Terry Udovic, John Rush.

11:00-11:30 13.01.05  
Crystal Structure and Reaction Mechanism of Complex Metal Hydrides Studied by *in-situ* Synchrotron and Neutron Techniques. Yan Gao, Job Rijssenbeek.

11:30-12:00 13.01.06  
Crystal Structures of and Charge Density Distributions in Perovskite-type Hydrides as a New Series of Hydrogen Storage Materials. K. Ikeda, S. Kato, Y. Nakamori, S. Orimo.

**13.02 Whole-Molecule Disorder**  
Oahu/Waialua P. Mueller, Presiding

08:30-09:10 13.02.01  
About Whole-Molecule Disorder. Håkon Hope.

09:10-09:50 13.02.02  
The Use of Advanced Refinement Techniques to Model Whole Molecule Disorder: Examples of Applications in Chemical Crystallography. Charles Campana.

09:50-10:10 13.02.03  
Searching for WMD. Peter Mueller.

10:10-10:30 Coffee Break.

10:30-10:50 13.02.04  
Penta-*Tert*-Butyl-Corannulene vs. Corannulene: Structure, Disorder, and Reactivity. Yulia Sevryugina, Edward A. Jackson, Lawrence T. Scott, Marina A. Petrukhina.

10:50-11:05 13.02.05  
Disordered Structures: Identification and Interpretation. Peter Zavalij.

11:05-11:20 13.02.06  
Solid-State Compound Formation Between Stereoisomers: 2,3-Tetralindiol. Carolyn P. Brock, Sean Parkin, Brian O. Patrick.

11:20-11:35 13.02.07  
Whole-Molecule Disorder in Adenine Salts and Substituted Adenine Derivatives. John Desper, Christer Aakeroy, Michelle Smith, Goran Wennerberg.

11:35-11:50 13.02.08  
Examples of Crystal Structures with Whole Molecule Disorder. Gary Enright, John Ripmeester.

11:50-12:05 13.02.09  
Disorder may be a Misnomer. Brahma D. Sharma.

Afternoon Sessions

**SP.01 Undergraduate Research Showcase**  
Niihau M. Olmstead,  
K. Kantardjieff, Presiding

01:30-01:35 Opening Remarks.  
M. Olmstead, K. Kantardjieff.

01:35-02:20 SP.01.01  
Sustaining Crystallography in the 21st Century: Crystallography Education Policies for the Physical and Life Sciences. Katherine Kantardjieff.

02:20-03:00 SP.01.02  
The STaRBURSTT - CIC - Teaching Initiative. Paul Szalay, Marcus Bond, Ray Butcher, Guy Crundwell, Greg Ferrence, Katherine Kantardjieff, Laura Ramirez, Tom Higgins, Matthias Zeller, Allen Hunter.

03:00-03:30 Coffee Break.

03:30-04:00 SP.01.03  
The Good, the Bad, and the Ugly: Balancing Interactions that Drive the Formation of Co-Crystals. Meg E. Fasulo, Christer B. Aakeroy, John Desper.

04:00-04:30 SP.01.04  
A Systematic Approach for the Selection of Automated Docking Programs for Screening and Structure-Based Inhibitor Design. Kazuo Katagiri, Jiarong Xia, Kimberly Stieglitz.

04:30 Closing Remarks. M. Olmstead and K. Kantardjieff.

Afternoon Sessions

**AW.01 Buerger Award Structural Biology from All Angles**

Lanai J. Flippen-Anderson, Presiding

*Acknowledgement is made to Blake Industries and Merck Research Laboratories for partial support of this session.*

01:30-01:45 Award Presentation to Helen M. Berman. Bob Bau, ACA President. Introduction, Judith Flippen-Anderson.

01:45-02:30 AW.01.01  
A Personal Journey through Structure Space. Helen M. Berman.

02:30-03:00 AW.01.02  
An Anthropological Review of the Development of mmCIF. Paula Fitzgerald, John Westbrook.

03:00-03:30 Coffee Break.

03:30-04:00 AW.01.03  
Drug-Nucleic Acid Structures: Thirty Years On. Stephen Neidle.

04:00-04:30 AW.01.04  
Collagen Crystallography: From Early Fiber Diffraction to High-resolution Structures. Jordi Bella.

04:30-05:00 AW.01.05  
Electron Cryomicroscopy of Macromolecular Assembly at Subnanometer Resolution. Wah Chiu.

05:00-05:30 AW.01.06  
Fragment Based Drug Discovery for Oncology Targets. Stephen Burley.

**10.01 Applications of Crystal Growth and Low-Temperature Techniques**

Kohala/Kona A. Sargeant,  
R.C. Haltiwanger, Presiding

01:30-01:40 Introductory Comments.  
Amy A. Sarjeant, R. Curtis Haltiwanger.

01:40-02:00 10.01.01  
Methods for Containing Radioactive Materials for Diffraction Analysis. Donna Smith.

02:00-02:20 10.01.02  
[Ni(H<sub>2</sub>O)<sub>6</sub>](NO<sub>3</sub>)<sub>2</sub>·(15-crown-5)·2H<sub>2</sub>O: An Uncommon Polymorphic System. M. A. Sieglar, X. Hao, S. Parkin, C. P. Brock.

02:20-02:40 10.01.03  
Crystal Structure of  $\alpha$ -Nitro-*trans*-stilbene. Carly S. Anderson, Gary W. Breton, Edwin D. Stevens, Kenneth L. Martin.

02:40-03:00 10.01.04  
[Fe(TPFP)(1-meIm)(NO)], A Tale of One Crystal, Three Cells, and Too Many Data Collections. Multiple Temperature Studies to Resolve Disorder and Twinning. Bruce C. Noll, Nathan J. Silvernail, W. Robert Scheidt.

03:00-03:30 Coffee Break.

03:30-04:00 10.01.05  
Experiences with Scaling and Absorption Corrections. George M. Sheldrick.

04:00-04:20 10.01.06  
Chemical Bonding in Pentaerythritol at Very Low Temperature or at High Pressure: An Experimental and Theoretical Study. Alan Pinkerton, Elizabeth Zhurova, Vladimir Tsirelson, Adam Stash, Vladimir Zhurov.

04:20-04:40 10.01.07  
Small Molecule Crystallography with Undergraduate Researchers. Allison J. Dobson, Adam Donnelly, Bridgette Massey, Shae Vaughn, Kennon Deal, Lindsey Spedding.

04:40-05:00 10.01.08  
Preparing Manuscripts for Acta Crystallographica C and E with Programs *publCIF* and *modiCIFer*. Ilia A. Guzei.

**13.03 PDF Analysis of Industrially Relevant Materials**

Honolulu/Kahuku I. Swainson, Presiding

01:45-02:10 13.03.01  
Total Scattering: The Key to the Local and Medium Range Structure of Complex Materials. Thomas Proffen.

02:10-02:35 13.03.02  
Structural Disorder in the Negative Thermal Expansion Material ZrW<sub>2</sub>O<sub>8</sub> and Quartz-based Piezoelectrics: An RMC Analysis of Total Scattering Data. David Keen, Matt Tucker, Martin Dove, Andrew Goodwin, Stephen Wells, John Evans, Julien Haines, Olivier Cambon.

02:35-03:00 13.03.03  
Diffraction studies of Nanocrystalline Diamond and SiC in Real and Reciprocal Spaces. Bogdan Palosz.

03:00-03:30 Coffee Break.

03:35-04:00 13.03.04  
Internal Strain Measurements using PDF Analysis. Bjorn Clausen, Thomas Proffen, Ersan Üstündag.

04:00-04:25 13.03.05  
Collective Properties from RMC Analysis of Total Scattering Data: Excitations, Modulations and Some Limitations. Andrew Goodwin, Martin Dove, Elizabeth Cope, Matthew Tucker, David Keen.

04:25-04:50 13.03.06  
Uncovering Structural Features Related to the Material Properties by the PDF Method. Wojtek Dmowski, Karen E. Swider-Lyons, Takeshi Egami.

# Monday, July 24

Council Meeting Room	Waimea Canyon	Topaz Industrial Development Team	Poster Session M	Ballroom	5:30-7:30pm
Speaker Ready Room	Ewa 7:30am-5:30pm	Spallation Source Meeting Lanai 12:00	MarUSA Party (ticket required)	Diamond Head Lawn	7:30pm
Interview Room	Puna	Fiber Diff. SIG Meeting Kohala/Kona 12:00	Mentee/Mentor Dinner (ticket required)	Pacific Beach Hotel Marlin Room	8:00pm
Exhibit Show	Ballroom 10am-7:30pm	General Interest Meeting Oahu/Waialua 12:00			
Synchrotron SIG Meeting	Honolulu/Kahuku 12:00	IUCr Commission on Journals Koko Crater 12:00			
		Small Molecule SIG Meeting Niihau 12:00			

## Morning Sessions

### TR.01 Transactions Symposium: The Future of Neutron Crystallography: Smaller Crystals, Larger (Macro) Molecules

Lanai R. Bau, T. Koetzle, Presiding

*Acknowledgement is made to the American Chemical Society-PRF for partial support of this symposium.*

08:35-08:40 Opening Remarks. Robert Bau and Thomas Koetzle, Chairs.

08:40-09:20 TR.01.01 Capabilities of Single-crystal Neutron Diffraction: A Summary and a Discussion of Future Potential. Robert Bau.

09:20-10:00 TR.01.02 Single Crystal Diffraction at Pulsed Neutron Sources: Present and Future Capabilities. Arthur Schultz.

10:00-10:20 Coffee Break.

10:20-11:00 TR.01.03 Beyond the Folding Structure of Biomolecules. Structural Chemistry and Molecular Recognition in Biomolecules Evolved at J-PARC. Nobuo Niimura.

11:00-11:40 TR.01.04 LMX: Large Molecule Neutron Diffractometer for Supramolecular Chemistry and Biological Structure. Lee Brammer.

11:40-12:00 TR.01.05 Protein Crystallography with Spallation Neutrons. Leighton Coates, Paul Langan, Benno Schoenborn.

12:00-01:30 Lunch Break. Session continues at 01:30pm

### 04.01 Structural Biology in Industry

Honolulu/Kahuku P. Fitzgerald, H. Klei, Presiding

08:30-09:00 04.01.01 Nature's Sometimes Indifference to Stoichiometry in Assembling Crystal Structures - Hypersalts. Jack Gougoutas, John DiMarco, Michael Galella, Mary Malley.

09:00-09:30 04.01.02 Differing Protein Conformations Used in the Design of VEGFR2 Kinase Inhibitors. Michele McTigue, Steve Bender, Robert Kania, Michael Niesman, Cynthia Palmer, Christopher Pinko, David Rewolinski, John Wickersham.

09:30-10:00 04.01.03 Targeting the HCV RNA Polymerase: Study of Two Types of Non Nucleoside Analogs that Inhibit HCV Polymerase by Binding In-and-Outside of the Catalytic Site. Nanhua Yao, Todd Appleby, Shunqi Yan, Yili Ding.

10:00-10:30 Coffee Break.

10:30-11:00 04.01.04 Crystal Structures of DPP-IV Exhibit Flexible Accommodation of Peptidase-selective Inhibitors. Kenton Longenecker.

11:00-11:30 04.01.05 Automated Validation of Ligand Fitness Using "Difference of Difference" Analysis. Brian Kelley, James Nettles.

11:30-12:00 04.01.06 Molecular Recognition of RNA by Neomycin and a Restricted Neomycin Derivative. Qiang Zhao, Fang Zhao, Kenneth Blount, Qing Han, Yitzhak Tor, Thomas Hermann.

### 09.02 Bio-Macromolecular Assemblies

Kohala/Kona H. Tsuruta, V. Urban, Presiding

08:00-08:40 09.02.01 Structural Studies of Macromolecular Complexes in Solution by Small-angle X-ray and Neutron Scattering. Dmitri Svergun.

08:40-09:00 09.02.02 X-ray Diffraction "Fingerprints" of Biomolecular Structure and Dynamics in Solution. David Tiede, Xiaobing Zuo, Andrew Goshe.

09:00-09:30 09.02.03 Visualizing Protein-Protein and Protein-Nucleic Acid Interactions by Small-angle Scattering. William Heller.

09:30-10:00 09.02.04 Virus Particle Maturation Followed by SAX. Jack Johnson, Kelly Lee, Hiro Tsuruta.

10:00-10:30 Coffee Break.

10:30-11:10 09.02.05 The Role of SAXS in the Study of Non-crystalline Biological Systems. Michel H. J. Koch.

11:10-11:40 09.02.06 Nanotubular Structures of Microtubule-Spermine and Microtubule-Lipid Complexes. Youli Li, D.J. Needleman, U. Raviv, M.A. Ojeda-Lopez, H.P. Miller, L. Wilson, C.R. Safinya.

11:40-12:00 09.02.07 The Center for Structural Molecular Biology at Oak Ridge National Laboratory. Volker Urban, William Heller, Gary Lynn, George Wignall, Kevin Weiss, Dean Myles.

### 13.05 Difficult Organic/Organometallic Structures

Niihau L. Daniels, Presiding

10:30-10:50 13.05.01 Synthetic Small-molecule Models of Peptides and Nucleic Acids - The Definitive Not-so-small Molecules. Lee M. Daniels, Ivan Huc, Jean-Michel Leger.

10:50-11:10 13.05.02 A Nitrosyl Heme Thiolate Product from a Heterogeneous Reaction. Douglas R. Powell, Nan Xu, Lin Cheng, George B. Richter-Addo.

11:10-11:30 13.05.03 Crystal Structures and Solid Forms of 6-OH Buspirone. Qi Gao, Dedong Wu, Garry McGeorge, W. Larry Parker.

11:30-11:50 13.05.04 Enhanced Resolution PDF from Home Lab Based X-ray Scattering. Alex Yokochi, Larry Marple.

check the schedule carefully - morning sessions begin at different times

## Afternoon Sessions

**TR.01 Transactions Symposium:  
The Future of Neutron Cry-  
stallography: Smaller Crystals,  
Larger (Macro) Molecules**Lanaï P. Langan,  
A. Podjarny, Presiding*Acknowledgement is made to the American  
Chemical Society-PRF for partial support of  
this symposium.*01:30-02:10 TR.01.06  
Neutron Diffraction from Cyclodextrin Hy-  
drates to Photosystem II. Wolfram Saenger.02:10-02:40 TR.01.07  
Complementary 2.2Å Neutron and 0.8Å X-  
Ray Diffraction Studies Reveal a Catalytic  
Proton Pathway in Fully Deuterated Human  
Aldose Reductase. Alberto Podjarny, Andre  
Mitschler, Mathew Blakeley, Federico Ruiz,  
Steve Ginell, Michael Haertlein, Isabelle  
Hazemann, Flora Meilleur, Andrzej Joachi-  
miak, Dean Myles.02:40-03:10 TR.01.08  
Location of Active-site Hydrogen Atoms in  
D-Xylose Isomerase. Gerard Bunick, Amy  
Katz, Xinmin Li, Jenny Glusker, H. L. Car-  
rell, B. Leif Hanson, Paul Langan, Leighton  
Coates, Benno Schoenborn.

03:10-03:40 Coffee Break.

03:40-04:00 TR.01.09  
Neutron Diffraction Structure of *E. coli* Di-  
hydrofolate Reductase in Complex with the  
Chemotherapeutic Methotrexate at 2.2Å  
Resolution. Chris Dealwis, Brad Ben-  
nett, Paul Langan, Leighton Coates, Marat  
Mustyamikov, Benno Schoenborn, Eliza-  
beth Howell.04:00-04:20 TR.01.10  
Smaller Crystals, Larger Proteins: Deuteri-  
um Labeling for Neutron Crystallography.  
Dean Myles, Kevin Weiss, Dale Pelletier.04:20-04:40 TR.01.11  
New Possibilities for the Determination of  
Macromolecular Structure from Selected  
H/D Derivative Crystals Utilizing Neutron  
Data Alone. David A. Langs, Herbert A.  
Hauptman, Hongliang Xu.

04:40-04:50 Closing Remarks.

**05.01 Non-Ambient  
Crystallography**

Kohala/Kona O. Degtyareva, Presiding

01:30-01:55 05.01.01  
Phase Diagram of Nitrogen at High Pres-  
sures and Temperatures. Eugene Gregory-  
anz, Chrysteale Sanloup, Alexander Goncha-  
rov, Russell Hemley, Ho-kwang Mao.01:55-02:20 05.01.02  
Crystal Structure of High-pressure Phases  
in Simple Metals: View from the Reciprocal  
Space. Valentina Degtyareva.02:20-02:40 05.01.03  
High Pressure Phases of CaCO<sub>3</sub>, S and H  
Obtained by USPEX. Colin W. Glass, Ar-  
tem R. Oganov.02:40-03:00 05.01.04  
Crystal Structure, Equation of State and  
Pressure-Induced Phase/Distortional  
Transition(s) in B<sub>4</sub>C: *In-situ* Synchrotron  
XRD and Raman Study to 60 GPa. Mur-  
li Manghnani, George Amulele, Jilian Zhu,  
Pzremek Dera, Yuchang Wang, Mariappan  
Sekar.

03:00-03:30 Coffee Break.

03:30-03:55 05.01.05  
Reactivity of Xe with Silica at High Pres-  
sures and Temperatures. Chrysteale Sanloup,  
Burkhard Schmidt, Eva Chamorro Perez,  
Albert Jambon, Eugene Gregoryanz, Mo-  
hamed Mezouar.03:55-04:20 05.01.06  
Structure and Stability of Low-Z Ion-  
ic Solids at High Pressure. Amy Lazicki,  
Choong-Shik Yoo, Warren Pickett, Richard  
Scalettar.04:20-04:40 05.01.07  
The Molecular Structure of RDX at High  
Pressure. Wayne Pearson, Suhithi Peiris.04:40-05:00 05.01.08  
Advanced Processing of High-Pressure Data  
from CCD Detector System. Michael Ruf.**13.06 Structural Genomics  
Big and Small**Honolulu/Kahuka G. DeTitta,  
A. Deacon, Presiding01:30-02:00 13.06.01  
the Joint Center for Structural Genomics: A  
Multitiered approach to Structural Genom-  
ics. Ian Wilson.02:00-02:20 13.06.02  
Expression, Purification and Crystallization  
Methods Developed at the MCSG Adopt-  
able to a Structural Biology Laboratory.  
Min Zhou, Youngchang Kim, Pearl Quartey,  
Hui Li, Ruying Wu, Cathy Hatzos, Lour  
Volkart, Grazyna Joachimiak, Mark Donnel-  
ly, Andrzej Joachimiak.02:20-02:40 13.06.03  
High Throughput Optimization of Initial  
Crystallization Conditions. Joseph Luft,  
Stacey Gulde, Angela Lauricella, Meriem  
Said, Jennifer Smith, Max Thayer, Christi-  
na Veatch, Jennifer Wolfley, Michael Mal-  
kowski, George DeTitta.02:40-03:00 13.06.04  
Biological Crystallization Resource: Facil-  
itating Knowledge-Based Biological Mac-  
romolecule Crystallization. Chunmin Li,  
Kevin Kirkwood, Brayer Gary.

03:00-03:30 Coffee Break.

03:30-04:00 13.06.05  
Structural Genomics Experimental Pipe-  
lines - Insights from the First Five Years.  
Olga Kirillova, Marek Grabowski, Heping  
Zheng, Zbyszek Otwinowski, Wlodek Mi-  
nor.04:00-04:20 13.06.06  
Probability-based Cryo Condition Optimi-  
zation Procedure for High Throughput X-  
ray Crystallography. Minmin Yu, Evan  
Bursey, Thirumuruhan Radhakannan, Li-  
Wei Hung.04:20-04:40 13.06.07  
Robotic Crystal Harvesting: The Final Fron-  
tier in Automated High Throughput Cryst-  
tallography. Bernhard Rupp, Peter Carmen,  
Jace Walsh, Echo Miller, Robert Viola.04:40-05:00 13.06.08  
The Role of Follow-Up Studies at the Cen-  
ter for Eukaryotic Structural Genomics. Ja-  
son McCoy, Abolfazl Arabshahi, Eduard  
Bitto, Craig Bingman, Frank Ruzicka, Perry  
Frey, George Phillips.

Afternoon Sessions

10.02 Natural Products and Drugs

Niihau

X. Wang, Presiding

01:30-01:55 10.02.01

Effect of Blocking Groups on the Conformation and Intermolecular Interactions of Andrographolide. Carl Schwalbe, Chris Bache, Dan Rathbone, Sreenivasa Sagineedu, Srinivasa Jada, Johnson Stanslas, Malcolm Stevens.

01:55-02:20 10.02.02

Combined Vibrational Circular Dichroism and X-ray Powder Diffraction to Establish Absolute Stereochemistry and Structures Small Molecules. Gregory Stephenson, Krishna Chavali.

02:20-02:35 10.02.03

Electron Density Distribution in Crystals of Pharmacophores. Tatiana Timofeeva, Andrey Yakovenko, Tiffany Kinnibrugh, Mikhail Antipin, Long Robert.

02:35-02:50 10.02.04

A New Biological Insight for the Organic Compounds  $C_6H_{12}O_5$ . Hamilton Napolitano, Ademir Camargo, Jahyr Theodoro, Marcelo Castilho, Javier Ellena.

02:50-03:05 10.02.05

The Structure of Natural Gas Hydrates. Konstantin Udachin, Hailong Lu, John Ripmeester.

03:05-03:30 Coffee Break.

03:30-03:55 10.02.06

Hydrothermal Crystallization of Organic Molecular Solids: Applications to Pharmaceuticals, Co-crystal Engineering and Neutron Diffraction Studies. Ian D. Williams, Fanny L-Y. Shek, Samuel M-F. Lo, Herman H-Y. Sung.

03:55-04:10 10.02.07

Sesquiterpene Lactones Isolated from Plants of the Venezuelan Andes. Graciela Diaz de Delgado, Julia Bruno C., Valentina Cote, Juan Manuel Amaro-Luis, Jose Miguel Delgado.

04:10-04:25 10.02.08

Carbon-Ether Supramolecular Building Block in 25,26-Oxidofriedel-1,3-dione. Kenneth Haller, Auphatham Phothikanith.

04:25-04:40 10.02.09

The X-ray Structure of Novel Tetrazolo[1,5-a]-1,3,5-triazine and 1,3,5-triazine Derivatives. Ekaterina Mironova, Dmitry Krivolapov, Igor Litvinov, Vladimir Baharev, Alexander Gidaspov.

04:40-05:05 10.02.10

Taxol - Single Crystal Structures and Solid State Behavior of Six Forms. John DiMarco, Jack Gougoutas.

2006 Margaret C. Etter Student Lecturer Awards

Each Special Interest Group (SIG) within the ACA has the opportunity to select one student to receive an award and to present a lecture in one of the sessions organized by that SIG. Selections are based upon submitted abstracts and are independent of whether the student presenter originally requested an oral or poster presentation. Award winners are determined by the elected officers of the SIGs. Students who are selected receive a monetary award of \$250 and a certificate.

Congratulations to this year's winners:

Biological Macromolecules SIG	Simon Jenni, Swiss Federal Institute of Technology (Switzerland)	01.03.04
Materials Science SIG	Sayon Kumalah, Georgetown Univ.	13.12.06
Neutron Scattering SIG	Peng Wang, Univ. of Cincinnati	13.11.05
Powder Diffraction SIG	Katherine Page, Univ. of California at Santa Barbara	13.13.06
Small Angle Scattering SIG	Ryan Justice, Air Force Research Lab, Univ. of Cincinnati	T-P001 (session 09.03)
Small Molecule SIG	Yulia Sevryugina, State Univ. of New York at Albany	13.02.04
Synchrotron Radiation SIG	Jean Jankoncic, Brookhaven National Laboratory	11.01.05

# Tuesday, July 25

Council Meeting Room	Waimea Canyon	Mat'ls Sci. SIG Meeting	Lanai	12:00	Poster Session T	Ballroom	5:30-7:30pm
Speaker Ready Room	Ewa 7:30am-5:30pm	BioMac SIG Meeting	Honoulu/Kohuku	12:00	Rigaku Fun Run	Entrance of	7:45pm
Interview Room	Puna	Young Scientist SIG Meeting	Oahu/Waialu	12:00		Sheraton Hotel	
Exhibit Show	Ballroom 10am-7:30pm	Service Cr SIG Meeting	Kohala/Kona	12:00			

## Morning Sessions

### AW.02 Warren Award The Development of Neutron Reflectometry and its Applications to Magnetism, Soft Matter, and Biology

Lanai

Applications in Soft Matter.  
S. Satija, Presiding

08:15-09:00 AW.02.01

Investigating the Structures of Thin Films and Multilayered Materials by Neutron Reflectometry. Charles F. Majkrzak.

09:00-09:30 AW.02.02

Ordering and Orienting Block Copolymer Nanostructures: The Influence of Ions. Thomas P. Russell.

09:30-10:00 AW.02.03

Neutron Reflectometry Investigation of Interfacial Structure in Tethered Polymer Systems. Mark D. Foster.

10:00-10:30 Coffee Break.

Applications in Biology.  
D. McGillivray, Presiding

10:30-11:00 AW.02.04

pH-dependent Conformational Changes and Insertion of Diphtheria Toxin Adsorbed to Lipid Membranes by Neutron and X-ray Reflection. Michael Kent, Hyun Yim, Sushil Satija, Ivan Kuzmenko.

11:00-11:30 AW.02.05

Neutron Reflectometry from Biological Thin Films at the NIST Center for Neutron Research: Past, Present and Future. Susan Krueger.

11:30-12:00 AW.02.06

Bio-Membranes: X-ray and Neutron Scattering Studies. Jaroslaw Majewski, Chad Miller, Tonya Kuhl.

12:00-01:30 Lunch Break.

Session continues at 01:30

### 01.06 Proteins Involved in Host Immune System and Pathogen Interactions

Honolulu/Kahuku

E. Collins,  
P. Sun, Presiding

*Acknowledgement is made to GlaxoSmith-Kline, Pfizer Global R&D La Jolla and Qia-gen, Inc.*

08:30-09:00 01.06.01

Structural Basis of Lipid Antigen Presentation by CD1. I.A. Wilson, D.M. Zajonc, D. Wu, G. Painter, V. Kumar, M. Kronenberg, D.B. Moody, C.-H. Wong, L. Teyton.

09:00-09:30 01.06.02

The Molecular Structure of the Toll-like Receptor 3 Ligand-binding Domain. David Davies, Jessica Bell, Istvan Botos, Pamela Hall, Janine Askins, Jossi Shiloach, David Segal.

09:30-10:00 01.06.03

Structure and Bi-functionality of Dscam Headpiece: One Stone For Two Birds. Jiahui Wang.

10:00-10:30 Coffee Break.

10:30-11:00 01.06.04

TB Drug Discovery: Addressing Issues of Persistence and Resistance. James Sacchettini.

11:00-11:15 01.06.05

Crystal Structure of a Complete Ternary Complex Between a TCR, Superantigen, and Peptide/MHC Molecule. Hongmin Li, Limin Wang, Yiwei Zhao, Zhong Li, Yi Guo, Walid Mourad.

11:15-11:30 01.06.06

Structure of Tracheal Cytotoxin in Complex with a Heterodimeric Pattern-recognition Receptor. Chung-I Chang, Yogarany Chelliah, Dominika Borek, Dominique Mengin-Lecreulx, Johann Deisenhofer.

11:30-11:45 01.06.07

Closing the Lid on the Mono-ADP-ribosylating Reaction Mechanism by Bacterial Toxins. Rene Jorgensen, Xu Wang, Xiaobo Liu, A. Rod Merrill.

11:45-12:00 01.06.08

Crystal Structure of m157, A Viral Antigen that Directly Engages Ly49 Natural Killer (NK) Cell Receptors. Z.S. Juo, E.J. Adams, L.L. Lainer, K.C. Garcia.

### 09.03 Polymer Science and Technology

Kohala/Kona

D. Londono,  
V. Urban, Presiding

08:20-09:00 09.03.01

Structure Evolution and Gradients in Oriented Polymer Parts Studied by Scattering Methods Using Synchrotron Radiation. Norbert Stribeck, Stephan Volkher Roth, Peter Bösecke, Christian Schroer, Armando Almendarez Camarillo, Marion Kuhlmann, Ulrich Nöchel.

09:00-09:30 09.03.02

Deformation Mechanisms of Polyethylene via *in-situ* X-ray Scattering. Brian Landes, Theresa Hermel-Davidock, A. Willem de Groot, Mehmet Demirors, Rajen Patel, Tracy Peltier, Danny King, Steven Landes.

09:30-10:00 09.03.03

*in-situ* Studies of Strain-induced Crystallisation of Poly (lactic acid) During Fast Uniaxial Deformation. Arumugam Mahendrasingham, David Blundell, Mark Parton, Watson Fuller, Theyencheri Narayanan.

10:00-10:30 Coffee Break.

10:30-11:10 09.03.04

Electric Field Induced Effects on the Microdomains in Concentrated Block Copolymer Solutions. Alexander Boker.

11:10-11:40 09.03.05

Phase Behavior of Nanoparticle/Diblock Copolymers. P. Thiyagarajan, Chieh-Tsung Lo, Byeongdu Lee. Randall E. Winans.

11:40-12:10 09.03.06

Dynamic Responses in Nanocomposite Hydrogels. Elena Loizou, Paul Butler, Lionel Porcar, Gudrun Schmidt.

12:10-12:30 T-P001

Simplified Models for Hierarchical Structures Based on Disks Rods, and Tubes. Ryan S. Justice, Jan Ilavsky, Dale W. Schaefer.

Morning Sessions

**13.07 Remote Data Collection**

Oahu/Waialua

G. Ferrence,  
R. Sweet, Presiding

08:00-08:30 13.07.01

STaRBURSTT - CIC: CyberEnabled Instrumentation Access. Allen Hunter, Paul Szalay, Matthias Zeller, Marcus Bond, Ray Butcher, Guy Crundwell, Greg Ferrence, Katherine Kantardjieff, Laura Ramirez, Tom Higgins.

08:30-09:00 13.07.02

Remote Monitoring and Access to Instruments and Data. The CIMA Crystallography Portal. John C. Huffman, Donald F. McMullen, Kianosh L. Huffman.

09:00-09:30 13.07.03

Protein Crystallography in the 21st Century. S. Michael Soltis, PX Group.

09:30-10:00 13.07.04

DNA & e-HTPX: High Throughput and Remote Access PX. Graeme Winter.

09:30-10:00 13.07.05

Routine Crystal Reorientation. Sandor Brockhauser, Florent Cipriani, Sean McSweeney, Raimond Ravelli, The DNA Collaboration ([www.dna.ac.uk](http://www.dna.ac.uk)).

10:00-10:30 Coffee Break.

10:30-10:55 13.07.06

Methods, Hardware, and Software for High-Throughput and Remote Data Collection in Macromolecular Crystallography: The Brookhaven Experience. D.K. Schneider, H. Robinson, A. Heroux, A. Soares, A. Saxena, J. Skinner, R. Bruono, M. Cowan, H. Bosshard, R.M. Sweet.

10:55-11:20 13.07.07

Automatic Beamline Operation at SPring-8 RIKEN Structural Genomics Beamlines. Masaki Yamamoto, Go Ueno, Raita Hirose, Kazuya Hasegawa, Nobuo Okazaki, Takashi Kumasaka.

11:20-11:45 13.07.08

The SER-CAT Remote User Participation Program. John Rose, Zhongmin Jin, Jim Fait, Victor Babson, John Chrzas, Bi-Cheng Wang.

11:20-11:45 13.07.09

From Sample to Structure: Automation at SER-CAT. James Fait, John Chrzas, John Gonczy, Andy Howard, Zhongmin Jin, John P. Rose, B. C. Wang.

11:45-11:50 T-P170

Remote Access Modes for Data Collection at IMCA-CAT. Lisa J. Keefe, Kevin Battaille, J. Lewis Muir, Anne Mulichak.

11:50-11:55 T-P172

Remote Data Collection for Single-Crystal and Powder Diffraction. Joerg Kaercher, Michael Ruf.

11:55-12:00 T-P174

SGX-CAT: An Automated Synchrotron Beamline Dedicated to Mail-in Crystallography. David W. Smith, Stephen R. Wasserman, John W. Koss, Laura L. Morisco, Kevin L. D'Amico.

Afternoon Sessions

**AW.02 Warren Award  
The Development of Neutron  
Reflectometry and its Appli-  
cations to Magnetism, Soft  
Matter, and Biology**

Lanai

Applications in Magnetism.  
J. Ankner, Presiding

01:30-02:00 AW.02.07

Polarized Neutron Reflectivity for the Analysis of Nanomagnetic Systems. Hartmut Zabel, Katharina Theis-Broehl, Boris P. Toperverg.

02:00-02:30 AW.02.08

Origin of Positive and Negative Exchange Bias in Co/FeF<sub>2</sub>. M.R. Fitzsimmons, B.J. Kirby, S. Roy, Zhi-Pan Li, Igor V. Roshchin, S.K. Sinha, Ivan K. Schuller.

02:30-03:00 AW.02.09

Magnetic Behavior of Rare Earth Thin Films and Superlattices. Philippe Mangin, Karine Dumesnil, Catherine Dufour.

03:00-03:30 Coffee Break.

**03:30-03:35 Presentation of Warren Award to Charles Majkrzak. Robert Bau, ACA President.**

Theory, Instrumentation and Future Directions. L. Passell, Presiding

03:35-04:05 AW.02.10

Elements of Neutron Specular Reflection Phase-Inversion. N.F. Berk.

04:05-04:35 AW.02.11

Echoes from Nanostructured Films. Roger Pynn.

04:35-05:05 AW.02.12

Off-Specular Grazing Incidence Scattering from Surfaces: Theory and Applications. Sunil Sinha.

Afternoon Sessions

**01.02 Computational Methods**

Honolulu/Kahuku R. Grosse-Kunstleve,  
T. Terwilliger, Presiding

- 01:30-02:00 01.02.01  
Protein Structure as a Blurred Snapshot -  
Dynamic Information from a Static Experiment.  
Ethan Merritt.
- 02:00-02:30 01.02.02  
Explorations in Conformational Space: Re-  
vealing Inaccuracy and Heterogeneity in  
Crystal Structures. Nicholas Furnham, Tom  
Blundell.
- 02:30-03:00 01.02.03  
Adapting BnP for Different Computing En-  
vironments. Charles Weeks, Stephen Potter,  
Naimesh Shah, Hongliang Xu, Mark Green,  
Russ Miller, Lakshminarasimhulu Pasupula-  
ti, William Furey.
- 03:00-03:30 Coffee Break.
- 03:30-04:00 01.02.04  
Automated Refinement for Protein Crystal-  
lography. Min Yao, Yong Zhou, Isao Tana-  
ka.
- 04:00-04:30 01.02.05  
Enhancing the Capabilities of ARP/wARP.  
Serge X. Cohen, Krista Joosten, Marouane  
Ben Jelloul, Victor Lamzin, Anastassis  
Perrakis.
- 04:30-05:00 01.02.06  
Automated Structure Refinement in PHE-  
NIX: Recent Advances and New Algo-  
rithms. Pavel Afonine, Ralf Grosse-Kunst-  
leve, Peter Zwart, Paul Adams.

**10.03 Supramolecular  
Chemistry: From Assembly to  
Structure and Function**

Niihau C. Aakeröy, Presiding

- Intermolecular Forces, Crystal  
Growth, and Polymorphism
- 01:30-02:10 10.03.01  
Can Co-crystals be Assembled Employing  
a Specific Hydrogen-Bonded Motif? Joel  
Bernstein.
- 02:10-02:30 10.03.02  
The Influence of Disorder on Polymor-  
phism. A.G. Beasley, T.R. Welberry, D.J.  
Goossens.
- 02:30-03:00 10.03.03  
Space Group Frequencies of Hydrogen  
Bonded Networks. Joseph Lauher.
- 03:00-03:30 Coffee Break.
- 03:30-03:50 10.03.04  
Synergy of Intermolecular Forces in Self-  
Assembly of Propargylic Alcohols. Michal  
Sabat, Marilise Hyacinth, Lin Pu.
- 03:50-04:10 10.03.05  
Crystallographic Perspective of Pharmaceu-  
tical Co-crystals: Intermolecular Hydrogen  
Bonding Modes between Heterocyclic Ni-  
trogen Compounds and Carboxylic Acids.  
Dedong Wu, James Osborn, Craig Collins,  
Jean Surian.
- 04:10-04:30 10.03.06  
Cocrystallization Tendencies of Hexamethy-  
lenetetramine. Kraig Wheeler, Philias Daka.
- 04:30-05:00 10.03.07  
Design and Synthesis of Co-crystals using  
Molecular Sense and Supramolecular Sensi-  
bility. Christer Aakeröy.

Session continues on Wednesday, July 26.

**12.01 Topics of Interest to  
the Young Scientist**

Oahu/Waialua P. Hornayi, Presiding

- 01:45-01:50 Opening Remarks.  
Peter Horanyi.
- 01:50-02:30 "I Got The Job! Morpho-  
genesis into an Assistant Professor at a Re-  
search University/Institute". Carrie Wilmot.
- 02:30-03:00 The ACA: Past and Pres-  
ent. Robert Bau.
- 03:00-03:30 Coffee Break.
- 03:30-03:50 Subverting the Dominant  
Paradigm, or Life as a Service Macromolec-  
ular Crystallographer. Leif Hanson.
- 03:50-04:10 From Both Sides Now -  
What Impresses Search Committees. Doug  
Ohlendorf.
- 04:10-04:50 Nextal Story: How Ideas  
Crystallized in a Business. Jean-Pascal Viola.
- 04:50-05:00 Closing Remarks.  
Anna Gardberg, YS-SIG Chair-elect.

# Wednesday, July 26

Council Meeting Room	Waimea Canyon	Exhibit Show	Ballroom	10:00am-4:00pm	<b>Awards Banquet</b>	
Speaker Ready Room	Ewa 7:30am-5:30pm	Canadian Div. Meeting	Kohala/Kona	12:00	Cash bar 6:30pm	Royal Hawaiian Hotel
Interview Room	Puna	<b>ACA All Member Business Meeting</b>			Dinner 7:30pm	Monarch Room
			<b>Kohala/Kona</b>	<b>5:00pm</b>	(pre-purchased ticket required)	

## 10.03 Supramolecular Chemistry: From Assembly to Structure and Function

Niihau C. Aakeröy, Presiding

### Directed Assembly of Organic and Hybrid Architectures

08:30-09:10 10.03.08  
A Way from Static to Dynamic Micropores in Crystalline Coordination Polymers. Susumu Kitagawa.

09:10-09:40 10.03.09  
Polyhedral Clusters and Networks with Host-type Ligands. Michael Hardie, Christopher Sumby.

09:40-10:00 10.03.10  
Design and Serendipity in the Construction of a Non-centrosymmetric Network Through  $\pi$ - $\pi$  Interactions. Jesús Valdés-Martínez, J.M. Serrano-Becerra, S. Hernández-Ortega, D. Morales-Morales.

10:00-10:30 Coffee Break.

10:30-11:10 10.03.11  
Synthetic Crystallography of Metal Complexes. Guy Orpen.

11:10-11:40 10.03.12  
Design, Synthesis and Application of N-based Ligands for Coordination and Hydrogen Bonded Networks. Eric Bosch.

11:40-12:00 10.03.13  
Closed-Shell Interactions in Ag(I) Complexes: The Utility of the Metal-Ligand Mismatch. Hilary A. Jenkins, Darren D.W. Mercer, Stephen A. Beaton.

12:00-01:30 Lunch Break.  
Session continues after lunch.

## 13.08 Complementary Methods to Macromolecular Crystallography

Lanai J.E. Johnson  
A. McPherson, Presiding

09:00-09:20 13.08.01  
Atomic Force Microscopy in Structural Biology. Alexander McPherson.

09:20-09:40 13.08.02  
Molecular Envelope Determination and *ab initio* Phasing. Quan Hao.

09:40-10:00 13.08.03  
Time-resolved Crystallographic Studies of a Cooperative Dimeric Hemoglobin. William Royer, James Knapp, Reinhard Pahl, Vukica Srajer.

10:00-10:30 Coffee Break.

## Morning Sessions

10:30-10:50 13.0.804  
Diffraction Microscopy a New Tool for Structural Biologists. Andrew Stewart, Enju Lima, H. Miao, X-J. Huang, D. Shapiro, P. Thibault, V. Elser, C. Jacobsen, J. Kirz, D. Sayre.

10:50-11:10 13.08.05  
Determining the Phospholipid Packing within a Lipoprotein Particle Using Diffuse Scattering from Crystals and SAXS. Clare Peters-Libeu, Yvonne Newhouse, Karl Weisgraber.

11:10-11:30 13.08.06  
Biophysical Characterization of alpha to beta Transition in Collagen Binding Domain. Joshua Sakon, Sagaya Leena Philominathan, Osamu Matsushita.

11:30-11:50 13.08.07  
Biophysical Analysis of Virus Particles and their Maturation: Insights into Elegantly Programmed Nanomachines. John Johnson.

11:50-12:00 Closing Remarks.

## 13.09 Time-dependent Investigations

Honolulu/Kahuku X. Wang, Presiding

08:30-08:55 13.09.01  
The Spallation Neutron Source: On Time. I.S. Anderson.

08:55-09:20 13.09.02  
High Flux Neutron Diffractometers on Reactor Sources for Real-time Crystallography. Alan W. Hewat.

09:20-09:40 13.09.03  
Time Resolved Neutron Diffraction Studies of the Hydrogen Storage Material Li<sub>3</sub>N. Ashfia Huq, James Richardson, Evan Maxey, Dhanesh Chandra, Wen-Ming Chien.

09:40-10:05 13.09.04  
Time-resolved Studies at the Wide Angle Neutron Diffractometer. Jaime Fernandez-Baca, Yoshinobu Ishii.

10:05-10:30 Coffee Break.

10:30-10:55 13.09.05  
Center for Nanophase Materials Sciences. Linda Horton.

10:55-11:20 13.09.06  
*in-situ* Synchrotron X-ray Studies of Creep Damage in CuZn-alloys. Anke Pyzalla, A.I. Cerceau Neta, B. Camin, A. Kottar, H. Kaminski, T. Buslaps, M. Di Michiel, W. Reimers.

11:20-11:40 13.09.07  
Simultaneous *in-situ* Neutron Diffraction

Measurement of Rapid Transient Temperature and Stress Fields. Z. Feng, W. Woo, X.-L. Wang, D.W. Brown, B. Clausen, K. An, C. Hubbard, H. Choo, S.A. David.

11:40-12:00 13.09.08  
*in-situ* Time-resolved Study of Nanocrystallization in ZR-based Bulk Metallic Glass. Xun-Li Wang, Ling Yang, Alexandru D. Stoica, Jon Almer.

## 13.10 Canadian Light Source

Kohala/Kona J. Britten,  
L. Howell, Presiding

*Support for this session provided by the Canadian Light Source*

08:30-08:40 Introduction.

08:40-09:05 13.10.01  
The Canadian Macromolecular Crystallography Facility 08ID-1 Beamline at the Canadian Light Source. Louis Delbaere, Pawel Grochulski, Ingvar Blomqvist, Lata Prasad, Jennifer Puttick, Julien Cotelesage.

09:05-09:30 13.10.02  
Beamline and Infrastructure for High-Throughput Protein Crystallography at the Canadian Light Source. Ernst Bergmann, N. Strynadka, L. Delbaere, P. Grochulski, R. Berg, M. Fodje, E. Hallin.

09:30-09:45 13.10.03  
Structure of MRSA Resistance Determinant PBP2a in Complex With an Efficient beta-lactam. Andrew Lovering, Franck Danel, Malcolm Page, Natalie Strynadka.

09:45-10:00 13.10.04  
Toward the Design of Aminoglycoside Kinase Inhibitors. Desiree Fong, Bing Xiong, Jiyoung Hwang, Albert Berghuis.

10:00-10:30 Coffee Break.

10:30-10:45 13.10.05  
Structural Studies of BTB Domains from Transcription Factors and their Complexes with Corepressors. Alexandru Ghetu, Gilbert Prive.

10:45-11:10 13.10.07  
SAXS of Biological Macromolecules and the Canadian Light Source. Brian Shilton.

11:10-11:35 13.10.08  
Materials under Extreme Conditions: Their Crystalline Structures by X-Ray Diffraction with the Use of Synchrotron Radiation. Serge Desgreniers

11:35-12:00 13.10.09  
The Brockhouse X-Ray Diffraction and Scattering Sector for Materials Science. Stefan Kycia.

check the schedule carefully - morning sessions begin at different times

Afternoon Sessions

**AW.03 Etter Early Career Award Session**

Honolulu/Kahuku A. Gardberg, A.R. Pearson, Presiding

01:30-01:40 Presentation of Etter Award to Carrie Wilmot.

01:40-02:40 AW.03.01 X-rays, Action, Camera! The Joys and Heartaches of Making Movies of Redox Enzymes in Motion. Carrie Wilmot.

02:40-03:00 AW.03.02 Effect of Hydrophobic Mutations on Proton Transfer and Active Site Structure in Human Carbonic Anhydrase II. S. Zoe Fisher, Deepa Bhatt, Chingkuang Tu, Mavis Agbandje-McKenna, David N. Silverman, Robert McKenna.

03:00-03:30 Coffee Break.

03:30-03:50 AW.03.03 Structural Studies in Rieske Dioxxygenase Electron Transport. Eric Brown, Dan Ferraro, Chi-Li Yu, David Gibson, S. Ramaswamy.

03:50-04:10 AW.03.04 Structures of Wild Type E. coli Adenylosuccinate Lyase and a Mutant-substrate Complex Provide New Insights Into the Enzymatic Mechanism. May Tsai, Patrick Yip, Jason Koo, Mark L. Segall, Roberta F. Colman, P. Lynne Howell.

04:10-04:30 AW.03.05 X-ray Structural, Thermodynamic and Laser T-jump Kinetic Studies of Villin. Thang Chiu, Jan Kubelka, James Hoffrichter, William Eaton, David Davies.

**01.03 Large Macromolecular Assemblies**

Lanai T. Earnest, B. Wimberly, Presiding

01:30-02:00 01.03.01 Structures of the Bacterial Ribosome at 3.5 Å Resolution: Apo-Ribosome and Complexes with Translocation Inhibitors. Maria A. Borovinskaya, Jamie H.D. Cate.

02:00-02:30 01.03.02 Mechanism of RNA synthesis: Understanding Nucleotide Addition and Selectivity in Multi-subunit RNA Polymerases. David Bushnell, Dong Wang, Craig Kaplan, Ken Westover, Roger Kornberg.

02:30-03:00 01.03.03 Conformational Variability in Eukaryotic Transcription Complexes Revealed by Cryo-Electron Microscopy Studies. Patricia Grob, Seth Kostek, Sacha DeCarlo, Robert Tjian, Pawel Penczek, Eva Nogales.

03:00-03:30 Coffee Break.

03:30-03:55 01.03.04 Architecture of a Fungal Fatty Acid Synthase: a 2.6 MDa Molecular Assembly Line. Simon Jenni, Marc Leibundgut, Timm Maier, Nenad Ban.

03:55-04:20 01.03.05 The Domain Architecture of Mammalian Fatty Acid Synthase at 4.5 Å Resolution. Timm Maier, Simon Jenni, Nenad Ban.

04:20-05:00 01.03.06 3D Coherent Diffraction Microscopy and Its Applications in Structural Biology. Jianwei (John) Miao.

**10.03 Supramolecular Chemistry: From Assembly to Structure and Function**

Niihau C. Aakeröy, Presiding

**Function and Reactivity of 'Engineered' Materials**

01:30-02:10 10.03.14 Direct Crystallographic Observation of Chemical Transformations within a Self-Assembled Cages. Makoto Fujita.

02:10-02:40 10.03.15 Designer Container-Molecule Materials. K. Travis Holman, Scott T. Mough, Onome Ugono, Stephen D. Drake.

02:40-03:00 10.03.16 From Covalent Synthesis to Supramolecular Assembly: Investigating Cavitand-based Host-guest Architectures. Nate Schultheiss, Christer Aakeroy, John Desper.

03:00-03:30 Coffee Break.

03:30-03:50 10.03.17 Stacking of Semiconductor Molecules Enforced Through Hydrogen Bonding. Anatoliy N. Sokolov, Leonard R. MacGillivray.

03:50-04:20 10.03.18 Challenges in the Drug Form Selection. Z. Jane Li.

04:20-04:50 10.03.19 Application of Crystallographic Information to Pharmaceutical Problems. Matthew Peterson.

**13.11 Combined Techniques in Materials Science**

Oahu/Waialua P. Fenter, A. Sandy, Presiding

01:30-02:00 13.11.01 Combined Scattering Techniques for the Characterization of Polymer Crystallization. Bart Goderis.

02:00-02:30 13.11.02 Probing Nanoscale Structure and Dynamics in Polymer Nanocomposites by SAXS and XPCS. Aravinda Raghavan, Sarah Lewis, Amitabh Bansal, Linda Schadler, Lawrence Lurio, Suresh Narayanan, Pappannan Thiagarajan.

02:30-03:00 13.11.03 Combined XRD and Raman Combinatorial Screening System. Bob He, Chris Framp-ton, Juergen Sawatzki.

03:00-03:25 Coffee Break.

03:25-03:45 13.11.04 Factors Affecting the Self Assembly of Amyloid Peptides. Sai Venkatesh Pingali, Yan Liang, Peng Liu, Seth W. Childers, Kun Lu, Liang Guo, David G. Lynn, Pappannan Thiagarajan.

03:45-04:05 13.11.05 Characterization of Epoxy-Silane Films by Combined Scattering Techniques. Peng Wang, Dale Schaefer.

04:05-04:35 13.11.06 Fluctuation X-ray Microscopy - A Novel Approach for Characterization of Medium-range Order in Noncrystalline Systems. Lixin Fan, D. J. Paterson, I. McNulty, M. M. J. Treacy, D. Kumar, P. Du, U. Wiesner, J. M. Gibson.

04:35-05:05 13.11.07 Combination of Three-beam Diffraction and Resonant Scattering for Study of Orbital Ordering in Microcrystal of LaMnO<sub>3</sub>. Qun Shen, Kenneth D. Finkelstein, Roberto Colella.

05:05-05:30 13.11.08 X-ray Imaging of Electro-deposited Microparticles by Near-Field Coherent Diffraction. Martin de Jonge, Xianghui Xiao, Yong Chu, Qun Shen.

**ACA ALL MEMBER BUSINESS MEETING**  
Kohala/Kona 5:00PM

**01.04 Membrane Protein Structures**

Lanai S. Buchanan, P. Loll, Presiding

08:30-08:50 01.04.01  
Structural Mechanism of Plant Aquaporin Gating. Susanna Tornroth-Horsefield, Yi Wang, Kristina Hedfalk, Urban Johanson, Per Kjellbom, Richard Neutze.

08:50-09:10 01.04.02  
Structure of the Outer Membrane Cobalamin Transporter BtuB Complexed with TonB. David Shultis, Michael Purdy, Christian Banchs, Michael Wiener.

09:10-09:25 01.04.03  
Membrane Protein Crystallization in Bicontinuous Lipid Systems. Pia Wadsten, Annemarie Wöhri, Arjan Snijder, Richard Neutze, Sven Engström.

09:25-09:40 01.04.04  
Crystal Structure of TonB in Complex with FhuA, *E. coli* Outer Membrane Receptor. Marc Allaire, Natalia Moiseeva, Peter Pawelek, Nathalie Croteau, Christopher Ng-Thow-Hing, Cezar M. Khursigara, James Coulton.

09:40-10:00 01.04.05  
Structural Studies of an ABC Transporter. Heather Pinkett, Allen Lee, Douglas Rees.

10:00-10:30 Coffee Break.

10:30-10:50 01.04.06  
Crystal Structure of Particulate Methane Monooxygenase. Raquel L. Lieberman, Amy C. Rosenzweig.

10:50-11:05 01.04.07  
Structures of a Cyanobacterial Photoreceptor and its Soluble Transducer. Hartmut Luecke, Lutz Vogeley.

11:05-11:20 01.04.08  
Experiments Toward Crystallization of Transhydrogenase. C. David Stout, Mutsuo Yamaguchi, Holly Heaslet, Mark Yeager.

11:20-11:40 01.04.09  
The 2.0 Å Structure of a Bacterial Cytochrome c Oxidase: Evidence for the Conservation of Lipid Binding Sites. Ling Qin, Carrie Hiser, Xi Zhang, Anne Mulichak, R. Michael Garavito, Shelagh Ferguson-Miller.

11:40-12:00 01.04.10  
The bc1 Complex from *Rhodobacter Sphaeroides* at 2.85 Å Resolution. Lothar Esser, Maria Elberry, Chang-An Yu, Linda Yu, Di Xia.

**Morning Sessions**

**11.01 Radiation Damage and Macromolecular Crystallography**  
Honolulu/Kahuku A. Gonzalez, Presiding

08:30-08:40 Introduction.

08:40-09:10 11.01.01  
Thermal Imaging Applied to Cryocrystallography: Cryocooling and Beam Heating. Edward Snell, Henry Bellamy, Gerd Rosenbaum, Mark van der Woerd, Michael Kazmierczak.

09:10-09:35 11.01.02  
Helium Temperature Mitigation of Radiation Damage. Leif Hanson, Unmesh Chinte, Binal Shah, John Ruble, Keith Brister, Constance Schall, B.-C. Wang, Alan Pinkerton.

09:35-10:00 11.01.03  
Effects of Absorbed Dose on X-ray Radiation Damage in Protein Crystals at Cryogenic Temperatures. Jan Kmetko, Naji Hussein, Matthew Naides, Yevgeniy Kalinin, Robert Thorne.

10:00-10:30 Coffee Break.

10:30-10:55 11.01.04  
Radiation Damage of Protein Crystal in Various X-ray Energies. Nobutaka Shimizu, Kazuya Hasegawa, Go Ueno, Masaki Yamamoto.

10:55-11:20 11.01.05  
Anomalous Diffraction at Ultra High Energy for Protein Crystallography. Jean Jakoncic, Marco di Michiel, Zhong Zhong, Veijo Honkimaki, Peter David Siddons, Yves Jouanneau, Vivian Stojanoff.

11:20-11:55 11.01.06  
Computational Removal of Radiation-induced Changes. Zbyszek Otwinowski, Dominika Borek, Marcin Cymborowski, Wladek Minor.

**13.12 Metal-Organic Hybrids Crystal Engineering**  
Niihau C. Cahill, Presiding

*Acknowledgement is made to Bruker AXS, Inc. for partial support of this session.*

09:00-09:30 13.12.01  
Hybrid Materials from the F Elements. Christopher Cahill, Lauren Borkowski, Daniel De Lill.

09:30-10:00 13.12.02  
Heterometallic Metal-Organic Frameworks: Metalloligands vs. Organic Ligands. Seth Cohen, Sara Halper, Drew Murphy.

10:00-10:30 Coffee Break.

10:30-11:00 13.12.03  
The Use of Pi-Bonded Organometallic Quinonoid Complexes in the Construction of Self-Assembled Metal-Organic Hybrid Materials. Dwight Sweigart, Seung Uk Son, Jeffrey Reingold, Sang Bok Kim, Gene Carpenter.

11:00-11:30 13.12.04  
Hybrid Materials Based on Chalcogenide Tetrahedral Clusters and Functional Organic Molecules. Pingyun Feng, Nanfeng Zheng, Xianhui Bu.

11:30-12:00 13.12.05  
Tunable Inorganic-Organic Hybrid Nanostructures by Crystal Engineering. Jing Li, Xiaoying Huang, Wooseok Ki.

12:00-12:15 13.12.06  
Metal-Organometallic Frameworks Derived from Facially Metalated Arylcarboxylates. Sayon Kumalah, K. Travis Holman.

**13.13 Pair Distribution Function Analysis and Small Angle Scattering**  
Oahu/Waialua T. Proffen, Presiding

08:30-09:00 13.13.01  
Nanometer Range Local Atomic Structure Probed by the PDF Method. Takeshi Egami.

09:00-09:30 13.13.02  
The Probability Distribution Function in Small-angle Scattering. Rex Hjelm.

09:30-10:00 13.13.03  
Structure of CdSe/ZnS Core/Shell Nanoparticles. Reinhard Neder.

10:00-10:30 Coffee Break.

10:30-11:00 13.13.04  
Investigating the Structure of Proteins in Solution by Small-angle Scattering. Lise Arleth.

11:00-11:30 13.13.05  
Pair Distribution Function Analysis: The Dependence of Entropic PDF's Upon Non-Uniform Priors. R.J. Papoular.

11:30-11:45 13.13.06  
Pair Distribution Function Analysis of Nanosystems. Katharine Page, Ram Seshadri, Anthony K. Cheetham.

11:45-12:00 13.13.07  
The Whole Particle Structural Analysis on TiO<sub>2</sub> and Ge<sub>2</sub>Sb<sub>2</sub>Te<sub>5</sub> Nanoparticles. S. Shamoto, K. Kodama, S. Iikubo, T. Taguchi, Th. Proffen, N. Yamada.

Afternoon Sessions

**01.05 Difficult Structures**

Honolulu/Kahuku C. Carter,  
T. Izard, Presiding

01:30-02:05 01.05.01  
How to Make the Structure Difficult. Zbigniew Dauter.

02:05-02:35 01.05.02  
On-going Developments Aimed at Improving the Success Rate of Challenging Projects. Gerard Bricogne.

02:35-03:00 01.05.03  
Conformational Complexity of Complement Component C3. Bert Janssen, Eric Huizinga, Hans Raaijmakers, Anja Roos, Mohamed Daha, Kristina Nilsson-Ekdahl, Bo Nilsson, Piet Gros.

03:00-03:30 Coffee Break.

03:30-04:05 01.05.04  
Molecular Machines, Tropical Pathogens and Difficult Structures. Wim Hol, Junpeng Deng, Jan Abendroth, Konstantin Korotkov, Marissa Yanez, Dan Mitchell, Claudia Roach, Brian Krumm, Stewart Turley.

04:05-04:35 01.05.05  
Rational Approaches in Structure Determination of Membrane Proteins. Poul Nissen, Anne-Marie L. Jensen, Claus Olesen, Thomas L. Sørensen, Jesper V. Møller.

04:35-05:00 01.05.06  
Overcoming Severe Diffraction Anisotropy in Crystallographic Refinement. Michael Sawaya, Michael Strong, David Eisenberg.

**09.04 Membranes and Membrane Proteins**

Kohala/Kona T. Salditt,  
R. Winter, Presiding

01:30-02:00 09.04.01  
Structure and Fluidity of Solid-supported Membranes. Bert Nickel, Christian Reich, Joachim Rädler.

02:00-02:30 09.04.02  
Using Neutron Spectroscopy to Study Collective Dynamics of Biological and Model Membrane Systems. Maikel Rheinstadter, Wolfgang Haussler, Tilo Seydel, Tim Salditt.

02:30-03:00 09.04.03  
Salt Screening of Lipid Membrane Interactions Measured by Small-Angle X-ray Scattering. Horia Petrache.

03:00-03:30 Coffee Break.

03:30-04:00 09.04.04  
Structural and Functional Properties of Glycosphingolipid-containing Mixture as a Model Raft. Mitsuhiro Hirai.

04:00-04:30 09.04.05  
Investigation of Membranes and Membrane Proteins Dynamics from Molecular Dynamics Simulations. Connection to Inelastic Scattering Techniques. Mounir Tarek, Bernard Maigret, Christophe Chipot, Francois Dehez, Werner Treptow.

04:30-04:45 09.04.06  
The Kinetics and Mechanisms of Pressure-Jump Induced Phase Transitions in Lyotropic Lipid Systems. Roland Winter.

04:45-05:00 09.04.07  
Perspectives in the Structure and Collective Dynamics of Multi-component Membranes. Tim Salditt.

**13.14 Cool Structures**

Oahu/Waialua B. Barnett, Presiding

01:30-02:00 13.14.01  
The High-Resolution Structure of a Processive Exopolyphosphatase with a Novel Regulatory GTPase fold. David Sanders, Johnjeff Alvarado, Anita Ghosh, Miriam Hasson.

02:00-02:30 13.14.02  
Conformational Microheterogeneity Shapes the Photochemical Response of the Bacterial Photoreceptor PYP. Pierre-Damien Coureux, Zi Peng Fan, Ulrich K. Genick.

02:30-03:00 13.14.03  
What Does George Lucas Know About Crystallography? Patrick Carroll.

03:00-03:30 Coffee Break.

03:30-04:00 13.14.04  
Low-Melting Organic Salts: Phase Transitions, Twinning, and Disorder. Victor Young, Wesley Henderson, Stefano Passerini, Paul Trulove. Hugh C. DeLong

04:00-04:30 13.14.05  
Chemical Reaction in a Single Crystal: Monitoring Structural Changes in a Multi-Step Oxidation Process by Single Crystal X-ray Crystallography. Xiaoping Wang, Qinliang Zhao, Rongmin Yu, Carlos A. Murillo, F. Albert Cotton.

04:30-05:00 13.14.06  
Surprising New Results Concerning the Endohedral Fullerene Structures of C<sub>80</sub>, C<sub>82</sub>, C<sub>84</sub>, C<sub>86</sub>, and C<sub>88</sub>. Marilyn M. Olmstead, Christine M. Beavers, Alan L. Balch, Harry C. Dorn.

**13.15 Science at X-Ray and Neutron Facilities Around the Pacific Rim**

Lanai P. Stephens, Presiding

02:00-02:10 Introductory Remarks.

02:10-02:30 13.15.01  
The High Resolution X-ray Structure of Taka-amylase; The Crystal Grown in Microgravity Environment. Akifumi Higashiura, Hiroaki Tanaka, Koji Inaka, Masaru Sato, Shigeru Sugiyama, Sachiko Takahashi, Mari Yamanaka, Mamoru Suzuki, Tetsuo Tanaka, Atsushi Nakagawa.

02:30-02:50 13.15.02  
Synthesis and Thermodecomposition Study of Zn(tda)H<sub>2</sub>O. Ming-Chen Wu, Chi-Shen Lee, Hwo Shuenn Sheu.

02:50-03:10 13.15.03  
Small-Angle Scattering with a Focus on Biomolecular Structure in Australia. Jill Trewhella.

03:10-03:30 Coffee Break.

03:30-03:50 13.15.04  
A New Macromolecular Crystallography Beam Line at the Stanford Synchrotron Radiation Laboratory Designed for the Analysis of Very Small Crystals. Daniel Harrington, Andy Ringwall, Jean-Charles Castagna, Armin Busse, James Safranek, Aina Cohen, Thomas Rabedeau.

03:50-04:10 13.15.05  
IBARAKI Biological Crystal Diffractometer in J-PARC (BIX-P1) - General View. Ichiro Tanaka, Nobuo Niimura, Tomoji Ozeki, Takashi Ohhara, Kazuo Kurihara, Katsuhiko Kusaka, Kazuya Aizawa, Yukio Morii, Matsutoshi Arai, Kazuhiro Ebata.

04:10-04:30 13.15.06  
Glycosphingolipid-facilitated Membrane Insertion and Internalization of Cobra Cardiotoxin: Crystal Structure of the Cardiotoxin/sulfatide Complex. Jyung-Hung Liu, Chia-Hui Wang, Shao-Chen Lee, Wen-guey Wu, Chwan-Deng Hsiao.

04:30-04:50 13.15.07  
Cephalosporin Acylase: A Protein with Two Chemistries. Jin kwang Kim, In Seok Yang, Hye Jung Shin, Ki Joon Cho, Eui Kyung Ryu, Sun Hwa Kim, Sung Soo Park, Kyung Hyun Kim.

**ACA 2007 Meeting  
Salt Lake City Planning Session  
04:00pm Niihau Room**

## Posters beginning with S:

- should be assembled before 5:00pm on Sunday
- should be removed before 7:30pm on Monday
- author should be present Sunday, 5:30-7:30pm

S-P001

Crystal Structure of RecF Exhibits Structural Conservation with Rad50: Implications for DNA Recognition and Formation of Presynaptic Complexes. Sergey Korolev, Nodar Makharashvili, Olga Koroleva.

S-P003

Distribution of Water Around Amino Acid Side Chains: Statistical and Computational Analysis. R.H. Lai, K.A. Kantardjieff.

S-P005

Crystal Structures of Chicken Muscle Lactate Dehydrogenase. L. Grant, E.R. Greiner, J.M. Warfel, N. Polder, G. Watanabe, C. Smith, B. Rupp, X. Ouyang, S.R. Herron, C.R. Meyer, C. Srinivasan, K.A. Kantardjieff.

S-P007

Structural Comparison of the Binding Mode of a Thioxolone Ester Product to Classic Sulfonamide Inhibitors in Carbonic Anhydrase II. Caroli Genis, S. Zoe Fisher, Lakshmanan Govindasamy, Mavis Agbandje-McKenna, Jared N. Orwenyo, Brian Tripp, Robert McKenna.

S-P009

Determination of Sialic Acid Binding Region of Adeno-Associated Virus 5. Michael DiMattia, Lakshmanan Govindasamy, Britteny Whitaker, Robert McKenna, Sergei Zolotukhin, Nicholas Muzyczka, Mavis Agbandje-McKenna.

S-P011

Structure of Adeno-Associated Virus 1 to 8.6 Å Resolution by Cryo-Electron Microscopy. Edward Miller, Brittney Gurda-Whitaker, Lakshmanan Govindasamy, Xiaodong Yan, Robert McKenna, Sergei Zolotukhin, Nicholas Muzyczka, Timothy Baker, Mavis Agbandje-McKenna.

S-P013

Differential Recognition of the Type-I and Type-II H-Antigen Acceptors by the Human ABO(H) Blood Group A and B Glycosyltransferases. James Letts, Natisha Rose, Ying Fang, Svetlana Borisova, Nina Seto, Monica Palcic, Stephen Evans.

S-P015

The W.M. Keck Foundation Center for Molecular Structure: A Core Facility of CSUPERB and Core Node of the STaBURSTT-CyberDiffraction Consortium. Xiang Ouyang, Katherine Kantardjieff.

## Posters beginning with M:

- should be assembled before 5:00pm on Sunday
- should be removed before 7:30pm on Monday
- author should be present Monday, 5:30-7:30pm

S-P017

Novel Iron-Sulfur Cluster in *Pseudomonas aeruginosa* Adenosine Phosphosulfate Reductase. Justin Chartron, Kate Carroll, Hong Gao, Huiyi Chen, Julie Leary, Carolyn Bertozzi, C. David Stout.

S-P019

Cyber-Tutorials for Undergraduate Crystallographic Education. Gregory Ferrence, Elizabeth Tabler.

S-P021

Quokka: The Small-angle Neutron Scattering Instrument at OPAL. E.P. Gilbert.

S-P025

Vector Resolution of a Focusing SANS Instrument. Kenneth Littrell.

S-P027

Neutron Diffraction and X-ray Charge Density Studies of Tetraacetylene. Paula Piccoli, Elizabeth Zhurova, Juergen Eckert, Alan Pinkerton, Thomas Koetzle, Arthur Schultz, Dusan Hadzi.

S-P029

Variable Low-Temperature Data Collection and Hierarchical Refinement to Study an Order-Disorder Phase Transition. Weenawan Somphon, Kenneth J. Haller, A. David Rae.

S-P031

High-Energy X-ray Diffraction PDF Study of a Novel Class of Supermicroporous Alumina/Silica/Manganese Materials. Lev N. Zakharov, Boris G. Shpeizer, Abraham Clearfield, Asel Sartbaeva, Simon Billinge.

S-P033

Identification of a Novel *Escherichia coli* O157:H7 Heme Oxygenase ChuS and Its Structural Similarity to ChuX. Michael Suits, Gour Pal, Zongchao Jia.

S-P035

Achieving Successful Discovery Through Effective Lab Management. M. Rabiathul Thanuja, J. Jabarullahan.

S-P039

Cyclization of N(4)-R Thiosemicarbazones Derived from 2-formyl and 2-acetylpyridine (R = alkyl or aryl). Fábio Nascimento, Cláudia Rodrigues, Leticia Teixeira, Alzir Batista, Heloisa Beraldo, Javier Ellena.

## Posters beginning with T:

- should be assembled before 5:00pm on Tuesday
- should be removed before 3:30pm on Wednesday
- author should be present Tuesday, 5:30-7:30pm

S-P043

Crystallization Studies of the MgO-ZrO<sub>2</sub>-WO<sub>3</sub> System. Amy Gindhart, Cora Lind.

S-P045

Crystal Structures of [M(H<sub>2</sub>O)<sub>6</sub>](BF<sub>4</sub>)<sub>2</sub>, M = Mg, Mn, Fe, Co, Ni, and Zn. James Kaduk.

S-P051

Phasing and Modeling of Large Structures with Se-SAD - Crystal Structure of Deblocking Aminopeptidase. Andrzej Joachimiak, Changsoo Chang, Ruiying Wu, James Abdullah, Marcin Cymborowski, Wladek Minor.

S-P053

Controlled-temperature Diffraction Measurements on Samples in Glass Capillaries. Brian Litteer, Martijn Fransen, Richard Glazer.

S-P057

Structural Basis for O<sub>2</sub> Activation In Extradiol Ring Cleaving Dioxygenases. E.G. Kovalova, J.D. Lipscomb.

S-P059

Crystal Structure of the Catalytic Core Domain of a Novel Histone Demethylase. Xia Hong, Zhongzhou Chen, Jangye Zang, Johnathan Whetstone, Yang Shi, Gongyi Zhang.

S-P061

Protein Crystallization Optimization Techniques and Cryoprotectant Selection at Ontario Center for Structural Proteomics. X. Xu, T. Skarina, E. Evdokimova, M. Kudritska, J. Gu, H. Zheng, O. Kagan, O. Onoprienko, O. Egorova, A.M. Edwards, A. Savchenko.

S-P063

Probing Protein Mechanisms of Antibiotic Resistance Factors using Potential Transition State Mimics in Structural Studies. Oliver Baettig, Anish Sharma, Albert Berghuis.

S-P065

Structures of Human Deoxycytidine Kinase in Complex with L-nucleoside Analogs Give Insight into the Enzyme's Non-enantioselective Catalytic Activity. Elisabetta Sabini, Saugata Hazra, Arnon Lavie.

S-P067

CMP-Induced Structural Changes in a Multifunctional Sialyltransferase from *Pasteurella multocida*. Lisheng Ni, Mingchi Sun,

Harshal Chokhawala, Xi Chen, Andrew Fisher.

S-P069

Thioesterase Domain of Human Fatty Acid Synthase: Structural Insights into Chain-length Selectivity. Charles Pemble, Steve Kridel, Todd Lowther.

S-P071

Crystal Structure of Human Urokinase Complexed with a Cyclic Peptidyl Inhibitor, Upain-1. Mingdong Huang, Gengxiang Zhao, Cai Yuan, Chuanbing Bian, Troels Wind, Peter Andreasen, Xiaoming Ye, Zixian Huang.

S-P073

Crystallographic Studies of HTLV-1 Protease. Mi Li, Alla Gustchina, Gary Laco, Jan Rozycki, Alexandratos Jerry, Mariusz Jaskolski, Alexander Wlodawer.

S-P075

Towards Crystals of Proteorhodopsin. Pontus Gourdon, Ronnie Berntsson, Nicklas Bonander, Arjan Snijder, Richard Neutze.

S-P077

Dioxygen Activation in *Hansenula polymorpha* Amine Oxidase. Bryan Johnson, Arwen Pearson, Judith Klinman, Carrie Wilmot.

S-P079

Complete Reaction Cycle of a Cocaine Catalytic Antibody at Atomic Resolution. Xueyong Zhu, Tobin Dickerson, Claude Rogers, Gunnar Kaufmann, Jenny Mee, Kathleen McKenzie, Kim Janda, Ian Wilson.

S-P081

Substrate Recognition and Catalysis in Thimet Oligopeptidase. Nicholas Noinaj, David Rodgers.

S-P083

Extended CIF Validation Software. Georgi Todorov, Kostadin Z. Mitev, Herbert J. Bernstein.

S-P085

Structure of Ras-like GTPase Cdc42 bound to a GTP analogue GMPPCP. Matt Phillips, Guillermo Calero, Richard Cerione.

S-P087

Evaluation of Target Residues for Crystallization by Surface Entropy Reduction. David Cooper, Tomasz Boczek, Katarzyna Grelewski, Malgorzata Pinkowska, Michal Zawadzki, Lukasz Goldschmidt, David Eisenberg, Zygmunt Derewenda.

S-P089

Cytochrome *ba3* Oxidase in Nanoscale Lipid Bilayers: A Roadmap to Crystallization. V. Mitch Luna, James Fee, C. David Stout.

S-P091

Investigating the Catalytic Mechanism of Golgi alpha-mannosidase II: A Possible Target for Cancer Chemotherapy. Niket Shah, Douglas A. Kuntz, David R. Rose.

S-P093

Towards a Better Understanding of Exopolysaccharide Export in Gram-Negative Bacteria. Carrie-Lynn Keiski, Patrick Yip, Lori L. Burrows, P. Lynne Howell.

S-P095

Structural Studies of the Prion Replicative Interface. Christopher Kimberlin, Anne Belton, Gil Abalos, J. Cruite, Anthony Williamson, Erica Ollmann Saphire.

S-P097

Mechanism of Hexamerization of gpU, the Tail Terminator Protein from Bacteriophage Lambda. Lisa Pell, A. Liu, L. Edmonds, L. Donaldson, P. L. Howell, A. R. Davidson.

S-P099

Structure and Function of Adenylate Forming Enzymes: A ~140° C-terminus Domain Rotation. Albert Reger, Jill Carney, Andrew Gulick.

S-P101

Enolase and Its Role in Accumulation of Cholesteryl Esters. Ramin Radfar, Jason Holliday.

S-P103

An Innovative Method to Produce Human Telomerase Reverse Transcriptase (hTERT). Edward Wu, Stephen Hughes.

S-P105

Crystal Structure of Nudix Family Proteins BT0354 and EF2700. Changsoo Chang, Erika Duggan, James Abdullah, Andrzej Joachimiak.

S-P107

New Approaches to High Throughput Crystallization Based on Contact Line Pinning. Yevgeniy Kalinin, Viatcheslav Berejnov, Robert Thorne.

S-P109

New Methods to Prepare Iodine Derivatives by Vaporizing Iodine Labeling (VIL) and Hydrogen Peroxide VIL (HYPER-VIL). Hideyuki Miyatake, Tomokazu Hasegawa, Akihito Yamano.

S-P111

Towards the Structural Basis for Bacterial Two-Partner Secretion. Hye-Jeong Yeo, Katarzyna Walkiewicz, Michal Szymanski, Takeshi Yokoyama, Joseph St. Geme.

S-P113

Structure-Based Fragment Screening using High Throughput Crystallography. Robin Rosenfeld, John Badger, Paul Collins, Daniel Bensen, Les Tari, Russ Athay, Duncan McRee.

S-P117

Fingerprint and Structural Analyses in a Putative Short Chain Oxidoreductase Enzyme. Robert Huether, Bi-Cheng Wang, James Zhi-Jie Liv, Vladimir Pletnev, Timothy Umland, Qilong Mao, Leah Gambino, William Duax.

S-P119

NrdF1, an Additional Ribonucleotide Reductase Small Subunit from *M. tuberculosis* with a More Protected Tyrosyl Radical. Jemaine Davis, Harvey Rubin.

S-P123

Structure of A Novel Acetylcitrulline Deacetylase from *Xanthomonas campestris*. Dashuang Shi, Xiaolin Yu, Lauren Roth, Mendel Tuchman, Norma Allewell.

S-P125

Structural and Biophysical Characterization of Two hEphB4 Complexes: Insights into Modulating Protein-Protein Interactions. Jill Chrencik, Alexei Brooun, Michael Recht, Michelle Kraus, Anand Kolatkar, Hans Widmer, Peter Kuhn.

S-P127

Complexed Crystal Structure of Primosomal Protein PriB Reveals a Novel Single-stranded DNA Binding Mode. Cheng-Yang Huang, Che-Hsiung Hsu, Yuh-Ju Sun, Huey-Nan Wu, Chwan-Deng Hsiao.

S-P129

Crystal Structure of Human Apolipoprotein A-I: Insights into its Protective Effect Against Cardiovascular Diseases. Abdul Ajees Abdul Salam, Anantharamaiah G.M., Mishra Vinod. K., Mahmood Hussain M., Krishna Murthy H.M.

S-P131

Crystal Structures of Free Textilinin-1 and its Complex with the Catalytic Domain of Human Plasmin. Emma-Karin Millers, Geoff Birrell, Paul Masci, Martin Lavin, John de Jersey, Luke Guddat.

S-P133

Crystal Structure of HP0242, a Hypotheti-

cal Protein from *Helicobacter pylori* with a Novel Fold. Jia-Yin Tsai, Bo-Tsang Chen, Hui-Chun Cheng, Hsin-Yi Chen, Nai-Wan Hsaio, Ping-Chiang Lyu, Yuh-Ju Sun.

S-P135

Kinetic and Structural Properties of Triose-phosphate Isomerase from *Helicobacter pylori*. Chen-Hsi Chu, Yi-Ju Lai, Yuh-Ju Sun.

S-P137

Crystal Structures of  $\Delta^1$ -pyrroline-2-carboxylate Reductase from *Pseudomonas*. Masaru Goto, Hisashi Muramatsu, Hisaaki Mihara, Tatsuo Kurihara, Nobuyoshi Esaki, Rie Omi, Ikuko Miyahara, Ken Hirotsu.

S-P139

Structural Basis for the Dehalogenation of Fluoroacetate by Fluoroacetate Dehalogenase. Rie Omi, Keiji Jitsumori, Tatsuo Kurihara, Nobuyoshi Esaki, Ikuko Miyahara, Ken Hirotsu.

S-P141

Structural Analysis of ROM Mutants Using Crystallographic and NMR Techniques. Evi Struble, Danielle Barbazon, Jane Ladner, John Marino.

S-P143

Crystal Structure of Shikimate Dehydrogenase from *Aquifex Aeolicus*. J. Gan, P. Prabhakaran, Y. Li, Y. Gu, M. Andrykovitch, H. Yan, X. Ji.

S-P145

Structures of 5-methylthioribose Kinase Phased by ADP-2Ho: Catalytic Mechanism and Drug Design. Shao-Yang Ku, Patrick Yip, Kenneth Cornell, Michael Riscoe, Lynne Howell.

S-P147

Crystal Structure of Penicillin Binding Protein 4 (dacB) from *E. coli*, Both in the Native Form and Covalently Linked to Various Antibiotics. Sam-Yong Park, Hiroyuki Kishida, Satoru Unzai, R. H. Jeremy Tame.

S-P149

Crystal Structure of Methionyl-tRNA Formyltransferase from *Clostridium thermocellum*. Hua Yang, Irina Kataeva, Hao Xu, Min Zhao, Jessie Chang, Zhi-Jie Liu, John Rose, Bi-Cheng Wang.

S-P151

The Reaction of PMM/PGM from *P. aeruginosa*: Structural Insights Into a Simple Processive Enzyme. Andrew Schramm, Catherine Regni, Lesa Beamer.

S-P153

Structural and Biochemical Studies of Carnitine Acyltransferases. Yu-Shan Hsiao, Gerwald Jögl, Liang Tong.

S-P155

Structure of the Type IV Pilus Scaffold Protein PilF from *P. aeruginosa*. Jason Koo, Shao-Yang Ku, Lili Sampaleanu, Lori L. Burrows, P. Lynne Howell.

S-P157

Crystal Structure of Quinolinate Synthase, an Enzyme Involved in the *de novo* NAD Biosynthesis. Erika V. Soriano, Ethan C. Settembre, Tadhg P. Begley, SΔΔΔΔteven E. Ealick.

S-P159

Crystal Structures of the Nitric Oxide Complexes of Horse Heart Myoglobin. Daniel Copeland, Alexei Soares, Ann West, George Richter-Addo.

S-P161

Sec15 interacts with Rab11 via a Novel Domain and Affects Rab11 Localization *in Vivo*. Shuya Wu, Sunil Mehta, Franck Pichaud, Hugo Bellen, Florante Quiocho.

S-P163

Discovery of the HCV NS3/4A Protease Inhibitor SCH503034. Key Steps in Structure-based Optimization. Andrew J. Prongay, Z. Guo, J. Pichardo, N. Yao, T. Fischmann, J. Myers Jr., P.C. Weber, B. Malcolm, B.M. Beyer, R. Ingram, R. Zhang, A. Arasappan, F. Bennett, S.L. Bogen, K. Chen, E. Jao, R.G. Lovey, S. Venkatraman, F.G. Njoroge, V. Madison.

S-P165

Structural Studies and Comparison of the Crystal Structures of Human Apo- and Holo-Cellular Retinoic Acid Binding Protein (CRABP) II. Soheila Vaezeslami, Erika Mathes, Chrysoula Vasileiou, Babak Borhan, James H. Geiger.

S-P167

Crystal Structure of D-Ribulose 5-Phosphate 3-Epimerase in Complex with D-Xylitol 5-Phosphate. Alexander Fedorov, Elena Fedorov, Julie Akana, John Gerlt, Steve Almo.

S-P169

Substrate-assisted in Oxygen Activation by Cytochrome P450 158A2: A New Mechanism of Proton Transfer. Bin Zhao, F. Peter Guengerich, Markus Voehler, Michael Waterman.

S-P171

Binding of the Substrate Analog Azide to the Active Site of Human Manganese Superoxide Dismutase. John Domsic, Patrick Quint, Lakshmanan Govindasamy, Chingkuang Tu, David Silverman, Robert McKenna.

S-P173

Structure and Catalytic Mechanism of S-adenosylmethionine Synthetase. Fusao Takusagawa, Junichi Komoto, Taro Yamada, George Markham.

S-P175

Structural Basis of Why a Thermophilic Acylphosphatase is a Poor Enzyme at Lower Temperatures. Kam-Bo Wong, Sonia Y. Lam, Rachel C. Y. Yeung.

S-P177

Effect of Solution Stirring on Protein Crystallization. Ryota Murai, Shinya Nakata, Masafumi Kashii, Hiroaki Adachi, Kazufumi Takano, Hiroyoshi Matsumura, Satoshi Murakami, Tsuyoshi Inoue, Yusuke Mori, Takatomo Sasaki.

S-P179

Protein Crystal Processing Using Ultraviolet Laser Irradiation. Kazufumi Takano, Hiroshi Kitano, Hiroaki Adachi, Masafumi Kashii, Hiroyoshi Matsumura, Satoshi Murakami, Tsuyoshi Inoue, Yusuke Mori, Masaaki Doi, Takatomo Sasaki.

S-P181

Structural Studies on a NADP<sup>+</sup>/H Dependent Oxidoreductase Contributes to Investigate Coenzyme Specificity. Milagros Medina, Marta Martínez-Júlvez, José Ramón Peregrina, Juan Hermoso.

S-P183

Structures of AlkA:DNA Complexes in Search Mode. Duane A. Lehtinen, Thomas Hollis.

S-P185

The Refined Structure of Hypothetical Protein PF0725 from *P. furiosus* Confirms its function as a CoA Binding Protein. Min Zhao, Jessie Chang, Jeff Habel, Hao Xu, Lirong Chen, Shu-Huey Chang, Michael W. W. Adams, Zhi-Jie Liu, John P. Rose, Bi-Cheng Wang.

S-P187

Crystal Structure of the Ternary Complex of Allantoate-amidohydrolase with its Substrate and a Ligand: A Crucial Enzyme of Purine Catabolism from *E. coli* K12. Rakhi Agarwal, Subramanyam Swaminathan.

S-P189

Structural Analysis of *E. coli*  $\beta$ -sliding Clamp 148-152 Ala Mutant and its Role in DNA Polymerase V-dependent Translesion DNA Synthesis. Vivian Cody, Jim Pace, Edward Snell, Mark Sutton, Laurie Sanders, Sarah Ponticelli, Jill Duzen, Robert Maul.

S-P191

The Structural Biology Center User Program at the Advanced Photon Source, Argonne National Laboratory. Stephan L. Ginnell, Randy W. Alkire, Changsoo Chang, Marianne E. Cuff, Norma E. C. Duke, Youngchang Kim, Krzysztof Lazarski, Jurek Osipiuk, Gerd Rosenbaum, Frank J. Rotella, Rongguang Zhang, Andrzej Joachimiak.

S-P193

Antibody Complex of a Cockroach Allergen Bla g 2. Alla Gustchina, Mi Li, Sabina Wünschmann, Martin D. Chapman, Anna Pomés, Alexander Wlodawer.

S-P195

Crystal Structure of PurO from *Methanobacterium thermoautotrophicum*. You-Na Kang, Robert H. White, Steven E. Ealick.

S-P197

MD Reveals the Binding Conformation of HIV Protease with the MAC4A Binding Domain of GAG. Philip Martin, Ladislau Kovari.

S-P199

Phasing in the Home Laboratory. Joseph Ferrara, Cheng Yang, Robert Bolotovsky, James Pflugrath.

S-P201

Searching for Silver Bullets: An Alternative Strategy for Crystallizing Macromolecules. Bob Cudney, Alexander McPherson.

S-P203

Is the Protein Folding Problem Solvable? The Structure of Tetrameric IMPase from *T. maritima* Shows Unusual Protein Plasticity. Boguslaw Stec, Kimberly A. Stieglitz, Mary F. Roberts.

S-P205

Playing LEGO with BRCT-repeats, FHA-domains and C/EBP Transcription Factors. Maria Miller.

S-P207

Microfluidic Chips for Parallelized Analytical Crystallization. Andrew May, David Cohen, Suzanne Weaver, Yong Yi, Kevin Farrell.

S-P209

Optimization of Crystallization Condition in Gel-Tube Method. Hiroaki Tanaka, Mari Yamanaka, Koji Inaka, Masaru Sato, Sachiko Takahashi, Shigeru Sugiyama, Satoshi Sano, Moritoshi Motohara, Tomoyuki Kobayashi, Tetsuo Tanaka.

S-P211

Structural and Biochemical Analysis of Active Site Mutants in *B. subtilis* SecA. Dorothy Kim, John F. Hunt.

S-P213

The Refined Crystal Structures of Flock House Virus and Virus-like-particles Reveal Structural Features Important to the Virus Maturation and Assembly. Zhongguo Chen, Vijay Reddy, John E. Johnson.

S-P215

New Tools for Protein Crystal Retrieval and Handling. Robert Thorne, Guanhan Chew, Matthew Sochor.

S-P217

The CombiClover 384™ Plate: A Novel High-Density Plate for Protein Crystallization. Hidong Kim, Craig Sterling, Lance Stewart.

S-P219

Global Protein Surface Survey: A Comprehensive Survey of Protein Surface Features. T. Andrew Binkowski, Andrzej Joachimiak.

S-P221

What Makes MAP2Ks Dual Specificity Kinases? John Humphreys, Seung-Jae Lee, Prashanti Madhavapeddi, Tianjun Zhou, Elizabeth Goldsmith.

S-P223

Helium-cooled X-ray Diffraction Studies Enhance the Visibility of a Proton Pathway in Human-Aldose Reductase. Andre Mitschler, Steve Ginell, Alexandra Cousido, Tatiana Petrova, Volodia Lunin, Isabelle Hazemann, Michael Van Zandt, Andrzej Joachimiak, Alberto Podjarny.

M-P002

IBARAKI Biological Crystal Diffractometer in J-PARC (BIX-P1), Optimization of Design Parameters. K. Kusaka, T. Ohhara, I. Tanaka, N. Niimura, T. Ozeki, K. Kurihara, K. Aizawa, Y. Morii, M. Arai, K. Ebata, Y. Takano.

M-P004

Crystallization Phase Diagram of Several Proteins. Yuki Ohnishi, Yoichiro Kobayashi, Masahiro Yamashita, Toshinobu Ebata, Ichiro Tanaka, Nobuo Niimura.

M-P006

Crystallization of a Large Single Crystal of  $\beta$ -lactoglobulin for Neutron Protein Crystallography. Daichi Yagi, Yuki Ohnishi, Ichiro Tanaka, Nobuo Niimura.

M-P008

Neutron Diffraction from Cubic Insulin at pD6 and 7. Takuya Ishikawa, Yuki Ohnishi, Ichiro Tanaka, Toshiyuki Chatake, Kazuo Kurihara, Taro Tamada, Ryota Kuroki, Nobuo Niimura.

M-P010

Flash Cooling and Preliminary Low Temperature Neutron Diffraction Studies of the Crenarchaeal Aeropyrum Pernix Flap Endonuclease-1 (FEN-1). Stephen Tomanicek, Binal Shah, Constance Schall, Timothy Mueser, Leif Hanson.

M-P012

CyBi@-HTPC Work station for Protein Crystallization. Automation of Protein Crystallization in Sitting Drop. Harris Grevelis, Isabelle Broutin Fabien Bonheure

M-P014

A Data Processing Software for Neutron (Quasi-)Laue Diffraction. Zhong Ren.

M-P016

New Possibilities Offered by Current Progress in Neutron Macromolecule Crystallography. Flora Meilleur.

M-P018

Increasing Crystallization Trials Productivity through Imaging Automation. Pierre Le Magueres, Eric Hnath, Jian Xu.

M-P020

Automated Ligand Refinement with a Combined Force Field and Shape Potential. Stanislaw Wlodek, A. G. Skillman, A. Nicholls.

M-P022

Description of Software for the Planning, Execution, and Refinement of Crystallization Experiments including Remote Submission and Viewing. Paige Vinson.

M-P024

Software for Efficient Co-crystal Structure Determination. John Badger, Paul Collins, Robin Rosenfeld, Bradley Smith, Russ Athay, Duncan McRee.

M-P028

Structural Flexibility of *E. coli* Peptide Deformylase Deduced from Multiple Independent Crystal Lattices. Nandini Sharma, Paula M. D. Fitzgerald.

M-P030

Crystal Structure of Proline-rich Tyrosine Kinase 2. Kam Y. J. Zhang, Abhinav Kumar, Yoshihisa Suzuki, Ben Powell, Brandi P. Grondona, Heike Krupka, James Tsai, Chao Zhang, Gideon Bollag.

M-P032

Novel Binding Site for Protein Kinase Inhibitors. Radha Akella, Xiaoshan Min, Elizabeth Goldsmith.

M-P034

Crystal Structure of the Human Rhinovirus RNA Polymerase. Todd Appleby, Hartmut Luecke, Jae Hoon Shim, Jim Wu, Wayne Cheney, Lutz Vogeley, Zhi Hong, Nanhua Yao.

M-P036

Advances in Crystallographic Hardware and Software for Structural Biology. Cary Bauer, Matthew Benning, David Khazins, Vladislav Sedov, Sergei Medved.

M-P038

Design, Synthesis and X-ray Structure of Protein-Ligand Complexes: Important Insight into Selectivity of  $\beta$ -secretase Inhibitors. Lin Hong, Arun Ghosh, Azhar Hussain, Hui Lei, Chun-Feng Liu, Thippeswamy Devasamudram, Geoffrey Bilcer, Gerald Koelsch, Jordan Tang.

M-P040

Structural Basis of Apramycin Recognition of the Ribosomal Decoding A Site. Qiang Zhao, Qing Han, Sarah Fish, Klaus Simonson, Dionisios Vourloumis, Jamie Froelich, Dan Wall, Thomas Hermann.

M-P042

The Crystal Structure of the Chimeric Cry1A.105 Insecticidal Protein at 3.0 Å Resolution. Timothy Rydel, Eric Sturman, Thomas Lee, Natalia Bogdanova, Thomas Malvar.

M-P044

Electrostatic Potential of Aminoacyl-tRNA Synthetase Navigates tRNA on its Pathway to the Binding Site. Mark Safro, Dmitry Tworowski, Anna Feldman.

M-P046

Crystal Structure of Mouse Cleavage Stimulation Factor 77 (CstF-77). Yun Bai, Thierry Auperin, James Manley, Liang Tong.

M-P048

Processing Conformation of MAP kinases. Elizabeth Goldsmith, Tianjun Zhou, John Humphreys, Radha Akella.

M-P050

Small Angle X-ray Scattering with the NanoSTAR on Biological Macromolecules. Kurt Erlacher.

M-P052

The 40 Residues that Control Folding, Co-factor Binding, Catalysis, Oligomerization and Function of 13000 Short Chain Oxidoreductase Enzymes. W.L. Duax, R. Huether, V. Pletnev, C.M. Weeks, T. Umland, Q. Mao, L. Gambino.

M-P054

A Structural Genomics Analysis of Histidine Kinase Sensor Domains. J. Cheung, W.A. Hendrickson.

M-P056

*In situ* Extension as a Protocol for Identifying Novel Alpha-Amylase Inhibitors. Gary Brayer, Chunmin Li, Anjuman Begum, Stephen Withers.

M-P058

An Automated Image Collection System for Crystallization Experiments using SBS Standard Microplates. Erik Brostromer, Jie Nan, Xiao-Dong Su.

M-P060

A Laboratory Information Management System for High Throughput Laboratory Environment. Jie Nan, Xiao-Dong Su.

M-P062

The Joint Center for Structural Genomics: A Multi-tiered Approach to Structural Genomics. Marc Elsliger, A. Deacon, A. Godzik, S.A. Lesley, K. O. Hodgson, J. Wooley, K. Wuthrich, I. A. Wilson.

M-P064

Improved Success Rate of Molecular Replacement. Lukasz Jaroszewski, Robert Schwarzenbacher, Adam Godzik.

M-P066

Generation of Expression Clones Using High-Throughput Technologies for Protein Structure Determination and Drug Discovery. Shiu Moy, YoungChang Kim, Changsoo Chang, Jerzy Osipiuk, Rongguang Zhang, Hui Li, Ruiying Wu, Frank Collart, Andrzej Joachimiak.

M-P068

Structure of *B. subtilis* NrdI - An Auxiliary Protein of Class Ib Ribonucleotide Reductase has Flavodoxin Fold and Binds FMN. Ruiying Wu, RongGuang Zhang, Shiu F. Moy, Andrzej Joachimiak.

M-P070

Structure of Toprim Domain-containing Protein from *Bacillus stearothermophilus*. Pavlina Rezacova, Dominika Borek, Shiu Moy, Andrzej Joachimiak, Zbyszek Otwinowski.

M-P072

CrystalMation: Capacity, Reproducibility and Efficiency of a Fully Integrated Automatic High-Throughput Crystallization Platform. Jian Xu, David Robbins, Rollan Mosko, Matt Lundy, Tom Vorndran, Mandel Mickley, Michael Willis.

M-P074

Structural Investigations of the Hydrophobic Core of the FAD Dependent Thymidylate Synthase. Irimpan Mathews, Heath Klock, Eileen Ambing, Scott Lesley, Ashley Deacon.

M-P076

Structural and Biochemical Studies of the Tryptophan 2,3-dioxygenase Reveal the Molecular Detail of Tryptophan Oxidation. Farhad Forouhar, Ross Anderson, Chris Mowat, Sergey M. Vorobiev, Mariam Abashidze, Seetharaman Jayaraman, Chiara Bruckmann, Gaetano T. Montelione, Steve Chapman, Liang Tong.

M-P078

Optimization of Protein Crystallization Screens at the Ontario Centre for Structural Proteomics. Tatiana Skarina, Elena Evdokimova, Linda Xu, Alexander Ignatchenko, Aled Edwards, Alexei Savchenko.

M-P080

Identification of Small Molecule Ligands for Structural Genomics Targets and their Application in Crystallization Trials. Elena Evdokimova, T. Skarina, M. Kudritska, L. Xu, O. Egorova, M. Pennycook-Brown, A. Ezerzsky, A. Edwards, A. Yakunin, A. Savchenko.

M-P082

The Undiscovered Bourne: The Helsinki Low-volume Medium-throughput Crystallisation Facility. Adrian Goldman, Pirkko Heikinheimo, Seija Mäki, Veli-Pekka Jaakola, Lari Lehtiö, Heidi Repo.

M-P084

A Nearly-Automated High-Throughput Method for Identifying Well-Expressed Soluble Protein Variants. Evan Bursey, Thomas Terwilliger, Li-Wei Hung.

M-P088

Biosynthesized Magnetic  $(Zn_{x3}Fe_{1-x})Fe_2O_4$  Nanoparticles. C.J. Rawn, L.W. Yeary, J.-W. Moon, B.C. Chakoumakos, M.E. Madden, T.J. Phelps, L.J. Love.

M-P090

Synthesis and Structure of an Aluminophosphate Built From 3-rings. Hemant P. Yennawar, David E.W. Vaughan, Anthony J. Perrotta.

M-P094

Using the TEM and X-ray Diffraction to Study Structure and Morphology of the Perovskite Nanoparticles. Vong Vo, Tien Hung Luu, Steffen Schulze, Michael Hiettschold.

M-P096

On Diamond Nucleation Sites and Relativistic Rehybridization in Pyramidalizing Reactions. Boris Udovic.

M-P098

Anomalous Scattering of HgSe Nanoclusters in Zeolites using Synchrotron X-ray Radiation. M. Castro-Colin, A. M. Milinda, S. C. Moss, W. Donner, E. Anokhina.

M-P100

Structural Phase Transitions Coupled with Magnetic Order in the Geometrically Frustrated Triangular Lattice Antiferromagnet  $\text{CuFeO}_2$ . Qingzhen Huang, F. Ye, Y. Ren, J. A. Fernandez-Baca, Pengcheng Dai, J. W. Lynn, T. Kimura.

M-P102

Synthesis and Characterization of Quaternary Chalcogenide  $\text{In}_2\text{Sn}_4\text{Bi}_3\text{Se}_8$ . Ming-Fang Wang, Chi-Shen Lee, Chia-Jyi Liub.

M-P104

Chemical Disorder in As-Te Glasses Studied by Pulsed Neutron and High-Energy X-ray Diffraction. Eugene Bychkov, Mariana Milochova.

M-P106

Exploring Local Distortion Modes via Single-crystal Diffuse Scattering. Branton J. Campbell, Harold T. Stokes.

M-P108

Molecular Motion and Macroscopic Actuation in Liquid Crystal Elastomers. Jeffrey Deschamps, John Konnert, Christopher Spillmann, Jawad Naciri, Banahalli Ratna.

M-P110

Teaching Crystallography in a Materials Science Program. Marueen M. Julian.

M-P112

High-Pressure Diffraction Study of the  $\text{A}_2\text{M}_3\text{O}_{12}$  family. Stacy Gates, Cora Lind.

M-P114

Crystal Structure of Solid  $\text{SiH}_4$  at High Pressure. Olga Degtyareva, Xiaojia Chen, Viktor V. Struzhkin, Ho-kwang Mao, Russell J. Hemley.

M-P116

Pressure Dependence of Tolerance Factor of  $\text{Sr}_{0.7}\text{Ca}_{0.3}\text{MnO}_3$ . Ryoji Kiyonagi, Omar Chmaissem, Bogdan Dabrowski, James Jorgensen, James Richardson, Joseh Fieramosca.

M-P118

Pressure-induced FE to AFE Phase Transition of PZT95/5-2Nb: A Neutron Diffraction and Dielectric Study. Bruno Morosin, Maxim Avdeev, James Jorgensen, Simine Short, Eugene Venturini, Pin Yang, George Samara.

M-P120

Solid state Structure of 1,2,3-selenadiazole Derivatives. Nigam Rath, A. Marx, V. Manivannan, S. Saravanan, S. Muthusubramanian.

M-P122

Crystal Structure of Carbonic anhydrase Complexed with Bicarbonate from *Pyrococcus horikoshii*  $\text{OT}_3$ . Jeyaraman Jeyakanthan, Chizu Kuroishi, Seiki Kuramitsu, Shigeyuki Yokoyama, Yoshitugu Shiro.

M-P124

Crystal Structure of  $\beta$  Hemolysin: Mechanism of Sphingomyelin Cleavage. Medora Huseby, Ke Shi, Cathleen Earhart, Douglas Ohlendorf.

M-P126

Aerolysin Binding to a GPI Anchor Core Glycan: High-Resolution Structure of Proaerolysin in Complex with the Receptor Component Mannose-6-phosphate. Cory Brooks, Svetlana Borisova, Thomas Buckley, Stephen Evans.

M-P128

Crystal Structure of Staphylococcal Enterotoxin I in Complex with a Human MHC II Molecule. Rongjin Guan, Marisa Fernandez, Emilio Malchiodi, Roy Mariuzza.

M-P130

Solution of Protein Crystallographic Structures by High Pressure Cryocooling and Noble Gas Phasing. Chae Un Kim, Quan Hao, Sol M. Gruner.

M-P132

A Prediction System for Protein Crystallization Conditions. Koji Inaka, Shigeru Sugiyama, Fujiko Shibata, Yoshiko Kobayashi, Kaoru Sugimori, Michiyo Takeuchi, Jose Martin Ciloy, Masato Kitajima.

M-P134

Gene Composer: A Tool for Designing and Optimizing Protein Constructs for X-ray Crystallography. Mark Mixon, John Walchli, Kai Post, Peter Nollert, Lance Stewart, Alex Burgin.

M-P136

Biophysical Characterization of Collagenase S1 domain. Cynthia Sides, Sagaya T. Leena Philominathan, Osamu Matsushita, Joshua Sakon.

M-P138

X-ray Structures of Methylamine Dehydrogenase Reaction Intermediates. Teresa De la Mora, Arwen R. Pearson, Kevin T. Watts, Ed Hoeffner, Carrie Wilmot.

M-P140

Crystal Structure of AAV8 and Structural Implications of Acidification. Hyun-Joo Nam, Michael Lane, Brittney Gurda-Whitaker, Robert McKenna, Sergei Zolotukhin, Nicholas Muzyczka, Mavis Agbandje-McKenna.

M-P142

X-ray Structure of AAV5, A Gene Therapy Vector for Cystic Fibrosis. Lakshmanan Govindasamy, M. DiMattia, H. Levy, B. Gurda-Whitaker, JA Chiorini, R. McKenna, N. Muzyczka, S. Zolotukhin, M. Agbandje-McKenna.

M-P144

Biophysical and Structural Characterization of Adaptor-related Protein Complex 4. Lauren Parker, Helen Kent, Phil Evans.

M-P146

A New Crystal Form of the 70S Ribosome Functional Complex. Andrei Korostelev, Sergei Trakhanov, Martin Laurberg, Albion Baucom, Laura Lancaster, Haruichi Asahara, William Scott, Harry Noller.

M-P148

Structure of an Electron Transfer Complex Between Plant Ferredoxin and Sulfite Reductase. Genji Kurisu, Masato Nakayama, Masami Kusunoki, Toshiharu Hase.

M-P150

Structural Basis of Phosphorylation-independent Desensitization of Gq-coupled Receptors. Aruna Shankaranarayanan, Valerie Tesmer, Takeharu Kawano, Tohru Kozasa, John Tesmer.

M-P152

The  $\beta$ -lactam Sensor of *Staphylococcus aureus* and its Role in Triggering Antibiotic Resistance. Mark Wilke, Tanya Hills, Hong-Zhong Zhang, Henry Chambers, Natalie Strynadka.

M-P154

Novel Cu<sup>2+</sup> Binding Site in C<sub>2</sub>A Domain of Synaptotagmin I. Fei Guo, Dakshinamurthy Rajalingam, Thallapuram Krishnaswamy S. Kumar, Joshua Sakon.

M-P156

NeXus with Binary XML - Efficient Support of Binary Data in the XML Implementation of the NeXus File Format. Georgi Darakev, Vassil Litchev, Kostadin Z. Mitev, Herbert J. Bernstein.

M-P158

MX at Diamond. Jose Brandao-Neto, Louise Johnson, Elizabeth Duke, Gwynndaf Evans, Armin Wagner, Alan Grant, Geoff Preece, Richard Wooliscroft, Alun Ashton, Mic Harding.

M-P160

The SSRL Macromolecular Crystallography Facility. Aina Cohen, Pete Dunten, Ana Gonzalez, Dan Harrington, Irimpan Mathews, Michael Soltis, representing the entire SMB group.

M-P162

Synthesis and Characterization of Novel 2D Organic - Inorganic Hybrid Cobalt and Nickel Vanadates. Kittipong Chainok, Kenneth J. Haller, Herman, H. -Y. Sung, Ian D. Williams.

M-P164

Tb<sub>3</sub>N@C<sub>84</sub> -- A Non-IPR isomer of C<sub>84</sub>. Christine Beavers, Marilyn Olmstead, Alan Balch, Harry Dorn.

M-P166

Crystallographic Studies of Pyruvate-formate lyase Activase. Jessica Vey, Meng Li, Jian Yang, Joan Broderick, Catherine Drennan.

M-P168

Structural Biology of the Type II Secretion System from *Vibrio cholerae*. Jan Abendroth, Allison Kreger, Paul Murphy, Maria Sandkvist, Wim Hol.

M-P170

Quantum Mechanics Studies on 2-Mercaptothiazoline Polymorphs. Rogério Salloum, Javier Ellena.

M-P172

Degree-of-freedom-based Methods for Phasing Centrosymmetric Structures from X-ray Diffraction Data. Alexander Smith, Nick Sahinidis.

M-P174

Evaluation of the Different Choice Method of Absorption Correction Used in the Struc-

tural Determination in Complex with Heavy Metals. Sauli Santos-Jr, Javier Ellena.

M-P176

X-ray Crystallography at the University of the West Indies (UWI), Jamaica: Structures of Novel Metal Complexes and the H-Bonding Interactions Featured in Them. Marvadeen Singh-Wilmot.

M-P178

Co-crystal of Bacteriophage T4 RNase H with a Fork DNA Substrate: Insight into Lagging Strand RNA Primer Removal from Okazaki Fragments. Juliette Devos, Charles Jones, Nancy Nossal, Timothy Mueser.

M-P180

Manganese Protoporphyrin-IX Reconstituted Myoglobin and its Complexes with Various Ligands. Zaki Zahran, Lilian Chooback, Daniel Copeland, Ann West, George Richter-Addo.

M-P182

Structure of the Bi-functional ATP Sulfurylase/APS kinase from *Aquifex aeolicus*, a Chemolithotrophic thermophile. Zhihao Yu.

M-P184

Crystal Structure of the Ligand-bound Saccharopine Reductase from *Saccharomyces cerevisiae*. Babak Andi, Paul F. Cook, Ann H. West.

M-P186

Crystal Structure of Conserved Hypothetical Protein Rv0390 from *Mycobacterium tuberculosis*. Thirumuruhan Radhakannan, Evan Bursey, Minmin Yu, Brent Segelke, Tim Lakin, Chang-Yub Kim, S.T. Anthony Kaviratne, Theresa L. Woodruff, Tom Terwilliger, Li-Wei Hung.

M-P188

Structural Differences Between *E. coli* and *A. thaliana* MTA Nucleosidase Explain Divergence in Substrate Specificity. Karen K.W. Siu, J. E. Lee, J. Sufirin, B. Moffatt, P. L. Howell.

M-P190

X-ray Crystallographic Study of CBL3-interacting Protein, C38 from *Arabidopsis thaliana*. Eun Young Park, Seung-Ick Oh, Jeong Sheop Shin, Kyung-Nam Kim, Hyun Kyu Song.

M-P192

Structural and Knetic Analysis of Mutants of an Active Site Base in a Non-heme Extradiol Dioxygenase. Rebecca Hoefl, Stephanie Groce, John Lipscomb, Douglas Ohlendorf.

M-P194

Crystal Structure of NH<sub>3</sub>-dependent NAD<sup>+</sup> Synthetase from *Bacillus anthracis*. Heather McDonald, Champion Deivanayagam, Larry DeLucas, Irina Protassevitch, Pam Pruett, Wayne Brouillette, Christie Brouillette.

M-P196

Crystal Structures of Multi-drug Resistant HIV-I Protease Mutants Define a New Target for Protease Inhibitor Design. Ravikiran Yedidi, George Proteasa, Jorge Martinez, John Vickrey, Philip Martin, Ladislau Kovari.

M-P198

Crystal Structure of a Putative pduO-type ATP: cobalamin Adenosyltransferase from *Mycobacterium tuberculosis*. Jin Ho Moon, Anthony Kaviratne, Minmin Yu, Evan H. Bursey, Li-Wei Hung, Timothy P. Lakin, Brent W. Segelke, Thomas C. Terwilliger, Chang-Yub Kim.

M-P200

Structural Basis of Serpin Inhibitory Mechanism. Soon-Hee Sul, Elizabeth Goldsmith.

M-P202

Crystal Structure of IMP Dehydrogenase from *Bacillus anthracis*. Rongguang Zhang, Ruiying Wu, Lour Volkart, Grazyna Joachimiak, Piotr Gornicki, Andrzej Joachimiak.

M-P204

Modulation of Axial Methionine Coordination in Type-1 Copper Sites. Iain MacPherson, Iain MacPherson, Michael Murphy.

M-P206

Structural Constraints on Protein Autoprocessings through an N-O or N-S Acyl Shift. Yixin Sun, Yeming Wang, Hwai-Chen Guo.

M-P208

Crystal Structure of Thermophilic Cytochrome P450 from *Picrophilus torridus*. Winny Ho, Huiying Li, Clinton Nishida, Paul Ortiz de Montellano, Thomas Poulos.

M-P210

Crystal Structure of the Aerobic FMN-Dependent Azoreductase (AzoA) From *Enterococcus faecalis*. Zhi-Jie Liu, Huizhong Chen, Lirong Chen, S.L. Hopper, C.E. Cerniglia, Neil Shah, John Rose, Bi-Cheng Wang.

M-P212

Crystal Structure of MC159 Reveals Molecular Mechanism of DISC Assembly and FLIP Inhibition. Jin Kuk Yang, Liwei Wang, Lixin Zheng, Fengyi Wan, Misonara Ahmed, Michael Lenardo, Hao Wu.

M-P214

Crystal Structure of the BTB Domains from LRF and Kaiso: Implications for the Protein-protein Interaction Properties of BTB Transcription Factors. Peter J. Stogios, Lu Chen, Gilbert G. Prive.

M-P216

Asymmetric Hexameric Assembly of the Archaeal Secretion ATPase. Atsushi Yamagata, John Tainer.

M-P218

WRN Exonuclease Structure and Molecular Mechanism Imply an Editing Role in DNA End Processing. John Perry, Steve Yannone, Lauren Holden, Chiharu Hitomi, Aroumougame Asaithamby, Seungil Han, Priscilla Cooper, David Chen, John Tainer.

M-P220

Structure of a Highly Active Insect Epsilon-class Glutathione S-transferase from a DDT-resistant Strain of the Malaria Vector *Anopheles gambiae*. Yujun Wang, Jing Zhou, Janet Hemingway, Hilary Ranson, Edward Meehan, Liqing Chen.

M-P222

Crystal Structure of Trehalose-6-phosphate Phosphatase Related Protein. Narasimharao Krishnamurthy, Subramanyam Swaminathan.

M-P224

Nerve Agent Processing by Human Carboxylesterase I. Christopher Fleming, Carol Edwards, Douglas Cerasoli, Philip Potter, Matthew Redinbo.

M-P226

Crystal Structure of Molybdopterin-Guanine Biosynthesis Protein B (Mob B). Damodharan Lakshminarasimhan, Eswaramoorthy Subramaniam, Kumaran Desigan, Swaminathan Subramanyam.

M-P228

Structural Basis for PYK2 Adhesion Targeting in Osteoclast Activation. Rongbao Li, Yimin Wang, Senthil Ranganathan, Zhican Qu, Xu Feng, Wen-Cheng Xiong.

T-P001

Simplified Models for Hierarchical Structures Based on Disks Rods, and Tubes. Ryan S. Justice, Jan Ilavsky, Dale W. Schaefer.

T-P002

Robotic Crystallization and Precipitation Point Proximity. Shahzad Majeed, Tongqing Zhou, Peter D. Kwong.

T-P003

Bilayer Membranes and the Formation of Unilamellar Vesicles. Thomas M. Weiss.

T-P004

Functional Diversity from a Simple Protein Fold. Marvin Hackert, Jeffrey Almrud, William Johnson, Chris Whitman.

T-P005

Low Temperature Mixed Lipid Phase: Understanding Bicelle Formation. Paul Butler, Divya Singh, Lionel Porcar, Ursula Perez-Salas, William Hamilton, Gary Lynn.

T-P006

JAXA-GCF Project: High-Performance Protein Crystallization in Space. Masaru Sato, Hiroaki Tanaka, Koji Inaka, Shinichi Shinozaki, Ari Yamanaka, Mitsuyasu Kato, Chie Saito, Tai Nakamura, Tomoyuki Kobayashi, Tetsuo Tanaka.

T-P007

Model-Independent Imaging of Interfacial Structures at the Mineral-Water Interface. Paul Fenter, Changyong Park, Zhan Zhang, Jeffrey Catalano, Michael Bedzyk, Kathryn Nagy, Neil Sturchio, David Wesolowski.

T-P008

Function-biased Choice of Additives for Optimization of Protein Crystallization. Maksymilian Chruszcz, M.D. Zimmerman, K. Koclega, J. Raynor, J.J. Petkowski, M. Cymborowski, X. Xu, T. Skarina, E. Evdokimova, A. Savchenko, A. Edwards, Z. Otwinowski, W. Minor.

T-P009

*Ab initio* Structure Determination from Pair Distribution Function. Pavol Juhas, Phillip M. Duxbury, Simon J. L. Billinge.

T-P010

The Inactivation of HAV 3C Protease by Peptide-based Ketone Inhibitors via an Unusual Episulfide Ring. Jiang Yin, Maia Cherny, Ernst Bergmann, Jianmin Zhang, Hanna Petersen, John Vederas, Michael James.

T-P011

Neutron Structure of  $[Zn_2[L-Sala)_2(H_2O)_2] \cdot 2H_2O$ . Wim T. Klooster, Garry J. McIntyre, J. J. Vittal.

T-P012

Dual-wavelength X-ray Generation From one Machine to Facilitate Protein Structure Determination. Kurt L. Krause, John Cutfield, Sue Cutfield, Catherine Day, Peter Mace, Calum Smits, Sigurd Wilbanks.

T-P013

Mail-in Crystallography Program at Brookhaven National Laboratory's NSLS: Update on our Operation. Annie Héroux, Alexei S. Soares, Robert M. Sweet, Howard H. Robinson.

T-P014

Microcrystallography at MacCHESS. Richard Gillilan, Mike Cook, Sterling Cornaby, Tom Szebenyi, Don Bilderback.

T-P015

Crystallography in Fiction: The Sequel. Frank Fronczek.

T-P016

Practical Application of Absorption Anisotropy Correction at Long Wavelengths. Kanagalaghatta Rajashankar, Igor Kourinov.

T-P017

Metal Induced alpha to beta Transitions in Collagen Binding Domain. Sagaya T. Leena Philominathan, Osamu Matsushita, Joshua Sakon.

T-P018

Preliminary Protein Crystallization Using the Honeybee Crystallization Robot. Milya Davlieva, Hamid Khoja, Anne Stone, Joseph Longtin, Ulrich Strych, Sanka Tennakoon, Kurt Krause.

T-P019

Citrate-dependent and Heparan Sulfate-mediated Cell Surface Retention of Cobra Cardiotoxin. Chun-Jung Chen, Hong-Hsiang Guan, Shao-Chen Lee, Wen-guey Wu.

T-P020

Effects of Mutations on a Pre-decarboxylation Reaction Intermediate Analogue-Pyruvate Dehydrogenase E1 Component Complex. Palaniappa Arjunan, Krishnamoorthy Chandrasekhar, Natalia Nemeria, Frank Jordan, William Furey.

T-P021

The Implication of the Sequence of Disulfides Breaking in the Reductive Unfolding Pathways of Ribonuclease A. Jun Wang, Igor Kourinov, Steve Ealick.

T-P022

How a New Chemical Compatibility Test Facilitates Proteins Crystallization. Jean-Pascal Viola, Christian Houde, Steve Tetreault.

T-P023

Accurate Single Crystal X-ray Charge Density Quality Data Collected at ChemMat-CARS, Advanced Photon Source (APS). Yu-Sheng Chen, T. Graber, P.J. Viccaro, Ras-

mus Poulsen, Henrik Clausen, Bo Iversen.

## T-P024

Novel Cell-free Expression System for Synthesis of Proteins used in Structural Analyses. Jean Pascal Viola, Frank Schäfer, Uritza von Groll, Annette Zacharias, Steve Tetreault, Christian Houde.

## T-P025

Upgrade of NSLS X25 Macromolecular Crystallography Beamline. L.E. Berman, J. Skaritka, T. Tanabe, G. Rakowsky, D. Harder, S. Ramamoorthy, E. Zitvogel, I. Pinayev, T. Shaftan, P. Montanez, A. Lenhard, S. LaMarra, S. Hulbert, D. Lynch, M. Becker, W. Nolan, A. Saxena, D. Schneider, R. Sweet, G. Rosenbaum

## T-P026

Structure of a Ubiquitin Specific Protease 8 (UPS8) - E3 Ligase NRDP1 Complex. J.R. Walker, G. Avvakumov, S. Xue, F. Mackenzie, E.M. Newman, S. Dhe-Paganon.

## T-P027

Cryogenic Automounters at the NSLS Facilitate Efficient Use of Undulator Beam Lines For Macromolecular Crystallography. A.M. Saxena, D.K. Schneider, A. Soares, H. Robinson, M. Carlucci-Dayton, J. Skinner, R. Buono, G. Shea-McCarthy, W. Nolan, R.M. Sweet.

## T-P028

Structure of a General Anesthetic Binding Site on PKC. S. Shanmugasundararaj, J. Das, K.W. Miller.

## T-P029

Potential of an Energy Recovery Linac (ERL) X-ray Source for Structural Studies. Doletha Szebenyi.

## T-P030

Structural Insights into the Evolution of Drug Resistance in HIV-1 Protease. Holly Heaslet, Victoria Kutilek, Garrett Morris, Ying-Chuan Lin, John H. Elder, Bruce E. Torbett, C. David Stout.

## T-P031

Development of a Real Time Timing-Shutter Performance Monitor for Protein Crystallography. Randy Alkire, Michael Molitsky, F. J. Rotella, N.E.C. Duke, John Lee, Tim Madden, Patrick De Lurgio.

## T-P032

Structures of Human  $\alpha$ -Phosphomannomutase 1 Reveal the Basis of Glycoprotein Syndrome Type 1a. Nicholas R. Silvaggi, Debra Dunaway-Mariano, Karen N. Allen.

## T-P033

BioCARS: A Facility for Macromolecular Crystallography at the Advanced Photon Source. Robert Henning, Vukica Srajer, Reinhard Pahl, Tim Graber, Spencer Anderson, Shengyang Ruan, Ning Lei, Harry Tong, Keith Moffat.

## T-P034

Crystal Structure of the Platelet Integrin GPIIb/IIIa: A Target for Allo-, Auto-, and Drug-dependent Antibodies Associated with Immune Thrombocytopenia. Tsan Xiao, Bing-Hao Luo, Timothy A. Springer.

## T-P035

Time-resolved Crystallography and Optical Studies of Single Crystals at BioCARS: Present Capabilities and Future Directions. Reinhard Pahl, Vukica Srajer, Keith Moffat.

## T-P036

Crystal Structure of the C-terminal RNase III Domain of Human Dicer. Daijiro Takeshita, Shuhei Zenno, Woo Cheol Lee, Koji Nagata, Kaoru Saigo, Masaru Tanokura.

## T-P037

Automated Data Collection at the IMCA-CAT Advanced Photon Source User Facility. Anne Mulichak, Kevin P. Battaile, J. Lewis Muir, Lisa J. Keefe.

## T-P038

Crystallographic Studies of Phosphoenolpyruvate Carboxykinase. Julien Cotelesage, Louis T. J. Delbaere, Hughes Goldie, J. Gregory Zeikus, Lata Prasad, Maris Laivenieks.

## T-P039

GM/CA: An NIH-Funded Dual Canted Undulator Sector for Protein Crystallography at the APS. Ward Smith, Robert Fischetti, Janet Smith, Derek Yoder, Rich Benn, Sergey Stepanov, Shenglan Xu, Alex Urakhchin, Oleg Makarov, Satish Devarapalli.

## T-P040

Structure of CHIP, a Novel Chaperone-Associated Ubiquitin Ligase. Zhen Xu, Karl Ian Devlin, Saurav Misra.

## T-P041

Testing the Compact Light Source: A Miniature Synchrotron Light Source for the Homelab. Ronald Ruth, Jeffrey Rifkin, Rodrick Loewen.

## T-P042

Some Strategies to Get the Best MAD/SAD Data from Synchrotron Beamlines. Xiaoping Dai, Ian Wilson.

## T-P043

High Throughput Protein Crystallography at the NIGMS East Coast Structural Biology Facility. Anubhav Jain, Jean Jakoncic, Marc Allaire, Alec Berntson, Kun Qian, Fabiano Yokaichiya, Vivian Stojanoff.

## T-P044

Structural Studies of MosA, a Dihydrodipicolinate Synthase from *Sinorhizobium meliloti*. Kurt Nienaber, Chris Phenix, David Palmer, Louis Delbaere.

## T-P045

NorthEastern Collaborative Access Team (NE-CAT) Beam Lines at the Advanced Photon Source. Craig Ogata, S. Ealick, M. Capel, I. Kourinov, E. Lynch, R. Kanagalaghatta, N. Sukumar, J. Unik, J. Wang, X. Yang.

## T-P046

Structural Analysis of an *E. coli* Phosphoenolpyruvate Carboxykinase (PCK) Complex with Carbon Dioxide. Jennifer Puttick, Hughes Goldie, Louis T. J. Delbaere.

## T-P047

A New Method for Flash Cooling Protein Crystals. Matt Warkentin, Viatcheslav Berejnov, Robert Thorne.

## T-P048

The Crystal Structure of Cytochrome P460 from *N. europaea* Reveals a Novel Cytochrome Fold and Crosslinked Heme. Arwen Pearson, Brad Elmore, Cheng Yang, Alan Hooper, Carrie Wilmot.

## T-P049

A State-of-the-art Undulator Beamline for Time-resolved Laue and Monochromatic Crystallography at BioCARS. Timothy Graber, F. Westferro, M. Meron, P.J. Viccaro, R.W. Henning, V. Srajer, R. Pahl, S. Anderson, P. Anfinrud, K. Moffat.

## T-P050

Structural Basis for Inhibition of Translation by the Tumor Suppressor, Pcd4. Nicole LaRonde-LeBlanc, Arti Santhanam, Nancy Colburn, Alexander Wlodawer.

## T-P051

Next-generation Automation for Biological Crystallography X-ray Data Collection. Thomas Earnest, Carl Cork, Jim O'Neill.

## T-P052

Mms2/Ubc13 with Covalently Bound Ubiquitin: Structural Basis of Linkage-specific Ubiquitin Chain Formation. Michael Edkins, Candice Carlile, Kamila Gomez, Cecile Pickart, Cynthia Wolberger.

T-P054

Structure of GTP Dependent Phosphoenolpyruvate Carboxykinase (PCK) from *Corynebacterium glutamicum*. Lata Prasad, Sanjukta Aich, Fumie Imabayashi, Louis Delbaere.

T-P055

The SIBYLS beamline (ALS 12.3.1) at the Advanced Light Source: A Valuable Resource for Both SAXS and Protein Crystallography. Scott Classen, Ken Frankel, Greg Hura, John Tainer, Susan Tsutakawa.

T-P056

Crystal Structure of a LDLR/RAP Complex: Insights into Ligand Binding and Intracellular Trafficking of the LDLR Family Proteins. Natalia Beglova, Carl Fisher, Stephen C. Blacklow.

T-P057

Structural Basis of Human Hookworm Host Interactions and Vaccine Development. Oluwatoyin Asojo.

T-P058

Crystal Structure of Mouse Nicotinamide Phosphoribosyltransferase. Tao Wang, Xiangbin Zhang, Cynthia Wolberger.

T-P059

Unusual Features of a Rare  $V\lambda_x$  Antibody Fab Fragment that Neutralizes the Ebola Virus. Jeffrey E. Lee, Mary Kate Hart, Erica Ollmann Saphire.

T-P060

Crystal Structures of ColE7 in complex DNA/ $Zn^{2+}$  and Im7/ $Ni^{2+}$  Show How a Transition Metal Ion Bound ColE7 Binds and Cleaves DNA. Lyudmila Doudeva, Huang Hsinchin, Hsia Kuo - Chiang, Shi Zhonghao, Li Chia - Lung, Chen Yongliang, Cheng Yi - Sheng, Yuan Hanna.

T-P061

Alternative Intermolecular Contacts of the VP5\* Antigen Domain Underlie the Two- to Three-Fold Reorganization of the Rotavirus Spike Protein. Joshua Yoder, Philip Dornitzer.

T-P062

Kinetic and Structural Properties of Inorganic Pyrophosphatase from *Helicobacter pylori*. Yuh-Ju Sun, Ti-Chun Chao, Jia-Yin Tsai, Haimei Huang, Chung-Yu Huang.

T-P063

Structure Determination of Two Extracellular Ig-like Domains of Human Myeloid Cell Inhibitory Receptor Siglec-5. Marina Zhuravleva, Peter Sun.

T-P064

Structural Basis for Sequence-Dependent DNA Cleavage by the Non-Specific Endonuclease. Wei-Jen Yang, Yi-Ting Wang, Lucy G. Doudeva, Chia-Lung Li, Hanna S. Yuan.

T-P065

Structural Basis for Recognition of a Mutated Human Melanoma Antigen by an Anti-Tumor T Cell Receptor. Lu Deng, Ries Langley, Suzanne Topalianb, Roy Mariuzza.

T-P066

Crystal Structures of the Biotin Protein Ligase and Biotin Carboxyl Carrier Protein from *Pyrococcus horikoshii* OT3: Stages of Biotin Activation and Biotinylation. Bagautdin Bagautdinov, Naoki Kunishima.

T-P067

Architecture and Affinity Maturation of Shark New Antigen Receptors. Robyn Stanfield, Helen Dooley, Martin Flajnik, Ian Wilson.

T-P068

Crystal Structure of SO1698 Protein from *Shewanella oneidensis*, a Putative Aspartic Endopeptidase. Jerzy Osipiuk, Rory Mulligan, Monireh Bargassa, Frank Collart, Andrzej Joachimiak.

T-P070

Crystal Structure of the Human TRPV2 Channel Ankyrin Repeat Domain. Clare McCleverty, Eric Koesma, Ardem Patapoutian, Scott Lesley, Andreas Kreuzsch.

T-P071

Structural Work On Potential Drug Targets From Tropical Parasites. Tracy Arakaki, Margaret Holmes, Isolde Le Trong, Jonathan Caruthers, George DeTitta, Fred Buckner, Wesley Van Voorhis, Christophe LMJ Verlinde, Wim GJ Hol, Ethan A. Merritt.

T-P072

Ternary Substrate Complex Structures of DNA Polymerase  $\beta$  with Mutagenic DNA Intermediates: Active Site Constraints for Mismatch Extension. Vinod Batra, William Beard, Lars Pedersen, Samuel Wilson.

T-P073

Recognition of Human Epithelial Cells by Moraxella Pathogens. Rebecca Connors, Darryl Hill, Richard Sessions, Tony Clarke, Tim Joseph-Horne, Mumtaz Virji, R. Leo Brady.

T-P074

Structural Determination of Yeast CPSF-100 and Direct Biochemical Evidence for Endoribonuclease Activity of CPSF-73. Co-

rey Mandel, Hailong Zhang, Syuzo Kaneko, Damara Gerbauer, Vasupradha Vethantham, Manley James, Liang Tong.

T-P075

The Secret of Broadly Neutralizing Anti-HIV-1 Antibody b12. Tongqing Zhou, Ling Xu, Barna Dey, Shi-Hua Xiang, Dennis R. Burton, Joseph G. Sodroski, Richard T. Wyatt, Gary J. Nabel, Peter D. Kwong.

T-P076

Crystal Structure of a *S. aureus* Pathogenicity Island Protein, EAR. Ramachandriah Gosu, Christopher (Kent) Brown, Zu-Yi Gu, Patrick Schlievert, Cathleen Earhart, Douglas Ohlendorf.

T-P077

Analysis of the Crystal Structure of the Major House Dust Mite Allergen Der p 1. Kåre Meno, Peter B. Thorsted, Henrik Ipsen, Ole Kristensen, Jørgen N. Larsen, Michael D. Spangfort, Michael Gajhede, Kaare Lund.

T-P078

Structural Studies on Two Doxygenases in the Prokaryotic Tryptophan-based Quinolinate Biosynthetic Pathway. Yang Zhang, Keri L. Colabroy, Seong A. Kang, Shridhar Bale, Tathagata Mukherjee, Brian R. Crane, Tadhg P. Begley, Steven E. Ealick.

T-P079

Crystal Structure of the Trimeric Complex of Interleukin-13, IL-13 Receptor  $\alpha 1$  and the Binding Domain of the Inhibitory Antibody Fab13.2. Kevin Parris John Dumas Marion Kasaian Amy Tam Lioudmila Tchistiakov Tan Xiang-Yang Kimberly Marquette James Wilhelm Laura Lin Lidia Mosyak

T-P080

Crystallization of Partially Trypsinized *E. coli* PEP Carboxykinase. Kent Klemmer, Hughes Goldie, Lata Prasad, Louis Delbaere.

T-P081

Crystal structure of Imidazolonepropionase from *Agrobacterium tumefaciens* at 1.87 Å Resolution. Rajiv Tyagi, Desigan Kumaran, Subramanyam Swaminathan.

T-P082

Crystallization and Preliminary X-ray Analysis of the Laccase from *Coriopsis gallica*. Eugenio De la Mora, Alvaro Resines, Brenda Valderrama, Eduardo Horjales, Enrique Rudiño-Piñera.

T-P083

Crystal Structure of Hypothetical Protein TM1727 of *Thermotoga maritima*. Mahen-

dra Madegowda, Eswaramoorthy Subramaniam, Seetharaman Jayaraman, Swaminathan Subramanyam.

T-P084

Crystal Structure of Metastasis-associated Protein S100A4 in the Calcium-Bound Form. Puja Pathuri, Hartmut Luecke.

T-P085

Towards Data Management for PX Structure Determination Within CCP4. Peter Briggs, Wanjuan Yang.

T-P086

The Crystal Structure of a Birnavirus RNA Polymerase Reveals a Distinct Active Site Topology and a Novel Protein-priming Domain. Junhua Pan, Vikram Vakharia, Yizhi Jane Tao.

T-P087

Complete Automation of Molecular Replacement. Fei Long, A.A. Vagin, N.N. Murshudov.

T-P088

Crystal Structure of the Hypothetical Protein Xcc0516 from *Xanthomonas campestris*: a Novel Quaternary Structure Assembled by Five Four-Helix Bundles. Li-ying Lin.

T-P089

Computational Studies at the Micromolecule/Macromolecule Interface. William Gleason, Eric Johnson, Derek Straka, Jane Shvelidze, Caroline Nibbe, David Macdonald, Jack Anderson.

T-P090

Purification, Crystallization and Structure Solution of the Complex Between p38 $\alpha$  and its Substrate MK2. Giovanna Scapin, Sangita B. Patel, James Thompson, Joseph W. Becker, Julie DeMartino, Dennis Zaller, Steve O'Keefe.

T-P091

Generation of Atomic Coordinates from Time-resolved X-ray Diffraction Data. George Phillips, Elena Levin, Roman Aranda.

T-P092

Crystal Structure of Human NMPRTase, a Novel Target for Anti-cancer Therapy. Javed Khan, Xiao Tao, Liang Tong.

T-P093

Auto-Rickshaw: An Automated Crystal Structure Determination as an Efficient Tool to Validate an X-ray Diffraction Experiment. Manfred Weiss, Venkataram Parthasarathy, Victor Lamzin, Paul Tucker, Santosh Panjikar.

T-P094

The Liganding of Glycolipid Transfer Protein is Controlled by Glycolipid Acyl Structure. Lucy Malinina, Margarita L. Malakhova, Alex T. Kanack, Ruben Abagyan, Rhoderick E. Brown, Dinshaw J. Patel.

T-P095

Diffraction Image Ranking and Data Collection Strategy. J. W. Pflugrath, T. J. Niemeyer, Angela Criswell, Robert Bolotovskiy.

T-P097

Finding the Best Composite Model from Multiple Sources. Dusan Turk, Maksymilian Chruszcz, Marcin Cymborowski, Zbyszek Otwinowski, Wladek Minor.

T-P098

Structure-Based Development of Variola H1 Phosphatase Inhibitors. David Waugh, Jason Phan, Joseph Tropea.

T-P099

High Transition State Affinity by TrpRS Coincides with an Unstable Protein Conformation. Charles Carter, Maryna Kapustina, Violetta Weinreb.

T-P100

Structure of Homolog of F420-0: $\gamma$ -Glutamyl Ligase from *Archaeoglobus fulgidus* Reveals a Novel Fold. Bogi Nocek, Elena Evdokimova, Maryna Kudriska, Alex Savchenko, Aled Edwards, Andrzej Joachimiak.

T-P101

The Use of Shape and Pharmacophore in High Throughput Crystallography Refinements and Lead Hopping: An Application Study. Samuel Toba, Dipesh Risal, Jon Sutter, Daniel Berard, Zeljko Dzakula.

T-P102

Structural Basis for Activation of OSR1 (Oxidative Stress Responsive 1) Kinase by C-terminal Regulatory Domain. Seung-Jae Lee, Elizabeth Goldsmith, Melanie Cobb.

T-P103

Using a High-throughput Pipeline to Quickly Scan Multiple NMR Structures and Solve a Difficult Molecular Replacement Problem. Francisco Hernandez-Guzman.

T-P104

Crystal Structures of Nucleotide and Non-Nucleotide Bound FtsZ from *Bacillus subtilis*. Scott Lovell, Zachary Halloran, Kathryn Hjerrild, Dean Sheridan, Alex Burgin, Lance Stewart.

T-P105

Adapting P for Different Computing Environments. Charles Weeks, Stephen Potter,

Naimesh Shah, Hongliang Xu, Mark Green, Russ Miller, Lakshminarasimhulu Pasupulati, William Furey.

T-P106

Crystallization Studies of Metnase, a SET/Transposase Protein. Kristie Goodwin, Masahiko Oshige, Suk-Hee Lee, Millie Georgiadis.

T-P107

Assembly Directed by Novel Functional Ligands With Transition Metals. Shaohua Gou, Haibin Zhu, Huaze Dong.

T-P108

The Interactions Between a Peptide Sex Pheromone Receptor PrgX to Two Antagonists: cCF10 and iCF10. Ke Shi, Kent Brown, Zuyi Gu, Briana Kozlowicz, Gary Dunny, Douglas Ohlendorf, Cathleen Earhart.

T-P109

Exploring the Non Covalent Assembly Capabilities of Thiosemicarbazone and their Coordination Compounds. Paula X. Garcia-Reynaldos, J. Valdes-Martinez, S. Hernandez-Ortega.

T-P110

Structure of STM3548 Cytoplasmic Protein from *Salmonella typhimurium*. Marianne E. Cuff, Ruiying Wu, Tatiana Petrova, Andrzej Joachimiak.

T-P111

Systematic Synthesis and Studies of Hydrogen Bonding Networks Built with 1,3,5-benzene-trisphosphonic Acid and 1-Adamantane amine. Deyuan Kong, Abraham Clearfield, Jerzy Zon.

T-P112

A Comparison of Pt and Br Phasing for Structure Determination. Bernard Santarsiero, Kiira Ratia, Kumar Saikatendu, Naina Barretto, Susan Baker, Raymond Stevens, Andrew Mesecar.

T-P113

Hydrophobic Hydration - Information from Solvation of Small Molecules as a Source of Structural Models for Macromolecular Crystallography. Janusz Lipkowski, Konstantin Udachin, Dariusz Swierczynski, Jerzy Ostyk-Narbutt.

T-P114

Structure of a Novel Acyltransferase. Richard Bott, Mae Saldajeno, Grant Ganshaw, Maggie Cervin, Gregg Whited, Walter Weyler, Raphael Sala, Michael Soltis, Mathews Irimpan.

T-P115

Subtle Crystal Environmental Influence on Pseudo-Jahn-Teller Effect Expression. Larry R. Falvello, Inmaculada Escorihuela, Rosa M. Llusar, Tatiana Soler, Milagros Tomás.

T-P116

The Crystal Structure of the Trp Receptor Binding Protein TwqN from *B. subtilis*. Youngchang Kim, Pearl Quartey, Andrzej Joachimiak.

T-P117

Self-Recognition Patterns of Oxalurate in Its Alkali and Alkaline Earth Salts. Different Ribbon Topologies and Polytypes. Milagros Tomás, José Ignacio Peñacoba, Larry R. Falvello, Tatiana Soler.

T-P118

Crystal Structure of the DNA-Bound Pdx-1 Homeodomain Complex. Antonella Longo, Gerald Guanga, Robert Rose.

T-P119

Unique Bimetallic Cu/Cd Complex with Crystal Structure Dependent on Temperature. Oksana Nesterova, Svitlana Petrusenko, Vladimir Kokozay, Oleg Shishkin.

T-P120

Structural Studies on a 23S rRNA Modifying Enzyme from *E. coli*. J. Sivaraman, S. Sunita, H. Zhenxing, J. Swaathi, M. Cygler, A. Matte.

T-P121

Pyridyl-Functionalized Cavitands and Capsules. Stephen D. Drake, K. Travis Holman.

T-P122

Structure of Mouse Apolipoprotein A-I Binding Protein. I.A. Shumilin, K.N. Jha, H. Zheng, M. Chruszcz, M. Cymborowski, J.C. Herr, W. Minor.

T-P123

A Unique Heterotrimetallic  $\text{Cu}_4\text{Co}_2\text{Pb}_2$  Complex with the 2-(dimethylamino)ethanol Ligand. Dmytro Nesterov, Vladimir Kokozay, Brian Skelton.

T-P124

The Crystal Structure of IFS: A Novel Endogenous Inhibitor of the Secreted Streptococcal NAD-glycohydrolase. Craig Smith, Jerry Pinkner, Joydeep Ghosh, Mike Meehl, Mike Caparon, Scott Hultgren.

T-P125

Reinecke Anion as a Building Block in Designing of Heterometallic Cr(III) Complexes. Denys Shevchenko, Vitalina Nikitina, Vladimir Kokozay, Viktoriya Dyakonenko, Oleg Shishkin.

T-P126

SP0731 from *Streptococcus pneumoniae* is a Member of the VOC Superfamily. Norma Duke, Hui Li, Frank Collart, Andrzej Joachimiak.

T-P127

Giving Pyrazole a Helping Hand in the Competition Against the Amide. Benjamin Scott, Christer Aakeroy, John Desper.

T-P128

Crystal Structure of a New Type of Bacterial Phytochrome. Xiaojing Yang, Emina Stojkovic, Jane Kuk, Keith Moffat.

T-P129

Design, Synthesis and Characterization of Polymerizable Terminal Diacetylene Salts. Zhong Li, Frank Fowler, Joseph Lauher.

T-P130

Scaffolding Protein Islet-brain 1 Homodimerization. Michael Gajhede, Ole Kristensen, Jette Sandholm Kastrup, Imran Dar, Silvie Guenat, Christophe Bonny.

T-P131

On Molecular Capsules Obtained From Calix[4]resorcinarene. Onome Ugono, K. Travis Holman.

T-P132

An Integrated High-throughput Approach to Study Proteomes of Infectious Agents: A Case Study of the Severe Acute Respiratory Syndrome Coronavirus. Saikatendu Kumar, Jeremiah Joseph, Vanitha Subramanian, Benjamin Neuman, Michael Buchmeier, Raymond Stevens, Peter Kuhn.

T-P133

Supramolecular Design of Photoactive Coordination Assemblies: Synthesis, Materials Characterization, and Reactivity. Ivan Georgiev, Leonard MacGillivray.

T-P134

The Crystal Structure of BCL-XL in Complex with Full-length BAD. Byung-Ha Oh, Kwang-Hoon Lee, Ji-Hye Baek.

T-P135

Ditopic Ligands in a World Where Discrimination is Desirable: Studies in Organic Co-crystal Syntheses. Michelle Smith, Christer Aakeroy, John Desper.

T-P136

Structure of the Catalytic Domain of Human Protein Kinase C- $\beta$  II Complexed with a Bisindolylmaleimide Inhibitor. Neil Grodsky, Ying Li, Djamal Bouzida, Robert Love, Jordan Jensen, Beverly Nodes, Jim Nonomi-

ya, Stephan Grant.

T-P137

Crystalline Structure and Morphology of Inclusion Complexes of  $\alpha$ -Cyclodextrin with Poly( $\epsilon$ -caprolactone)s Having Various Architectures. Seung-Yeop Kwak, Jae Woo Chung.

T-P138

Structural and Biochemical Characterization of an Archaeal XPB: A Helicase Adapted for Damaged DNA Unwinding. Li Fan, Andrew Arvai, Priscilla Cooper, Shigenori Iwai, Fumio Hanaoka, John Tainer.

T-P139

Crystal Structure of the 2:1 Adduct of 1,2-Benzenediol and Hexamethylenetetramine. Kadsada Sala, Kenneth Haller, Seik Weng Ng.

T-P140

Crystal Structure of the HP1-EMSY Complex Reveals a New Mode of HP1 Binding. Rui-Ming Xu, Ying Huang, Michael P. Myers.

T-P141

Packing Interactions of 2,3,7,8,12,13,17,18-Octaethylporphyrinato(picrato)iron(III). Ratchadaporn Puntharod, Kenneth Haller.

T-P142

The Structure Determination of a Crp/Fnr Protein from 1.9-Å SAD Data Collected at the Structural Biology Center 19ID Beamline. Frank Rotella, Rongguang Zhang, Rory Mulligan, Shiu Moy, Andrzej Joachimiak.

T-P143

Using Small Ditopic Molecules and Metal Chelates as Building Blocks to Construct Extended Metal-containing Supramolecular Solid-state Architectures. Nenad Judas, Du-bravka Matkovic-Calogovic.

T-P144

Structure of Human Protein Tyrosine Phosphatase Receptor Type O (PTPRO) with Bound Phosphate Ions in the Active Site. Desigan Kumaran, Subramanyam Swaminathan.

T-P145

Hydrothermal Synthesis and Structural Characterization of an Open-framework Arsenic Vanadate:  $\text{As}_2\text{V}_{10}\text{O}_{26}$ . Samroeng Kra-chodnok, Kenneth Haller.

T-P146

Crystal Structure of Thiamine Monophosphate Kinase (thiL). Eswaramoorthy Subramaniam, Swaminathan Subramanyam.

- T-P147  
Self-assembled Metal-organic Frameworks Based on Polyfunctional Ligands Derived from the Organic Solid State. Dejan-Kresimir Bucar, Tamara D. Hamilton, Leonard R. MacGillivray.
- T-P148  
Crystal Structure of APPL1 BAR-PH Domain. Guangyu Zhu, Simon Terzyan, Joseph Brunzelle, Xuejun Zhang.
- T-P149  
Structural Versatility of 3d-metal Complexes with a Polydentate Oxime-containing Schiff Base Ligand. Yura Moroz, Igor Fritsky.
- T-P150  
Bynamin, a Bacterial Dynammin-like Protein. Harry Low, Jan Lowe.
- T-P151  
Testing the Reliability of the Self-complementary Non-covalent Interactions: Supramolecular Implications and Supramolecular Design. Catalina Ruiz-Pérez.
- T-P152  
Crystal Structure and Biochemical Activity of Zea m 1 (EXPB1) - Implications for the Mechanism of Cell Wall Loosening by Beta Expansins. Neela Yennawar, Lian-Chao Li, Hemant Yennawar, Akira Tabuchi, Daniel Cosgrove.
- T-P153  
A Relation Between Photochromism and Structure in the Three Crystal Forms of a Salicylideneaniline Derivative. Yuji Ohashi, Kohei Johmoto, Hidehiro Uekusa.
- T-P154  
Structural Studies of the Methionine Biosynthesis Enzyme Homoserine Transsuccinylase from *Escherichia Coli*. Schroeder M. Noble Timothy L. Born Donald P. Huddler
- T-P155  
Building Hydrogen-bonded Frameworks of Copper (II) Complexes, via Interactions Between Carboxyl Ligands and Coordinated Water Molecules. Sergio Martinez Vargas, Simón Hernández-Ortega, Rubén A. Toscano, Jesús Valdés-Martínez.
- T-P156  
Ultra Fast Framing X-ray Detector for Time-resolved Synchrotron Experiments. R. Durst, M. Benning, D. Khazins, B. Becker, Y. Diawara, S. Medved, V. Sedov, G. Wachter.
- T-P157  
Radiation-induced Decomposition of Explosives at Ambient and High Pressure. Michael Pravica, Hubertus Giefers, Malcolm Nicol.
- T-P158  
Adaptation of a Commercial Optical CMOS Image Sensor for Direct-Detection Fast X-Ray Imaging. Alec Sandy, Lyle Marschand, Xuesong Jiao, Michael Sprung, Brian Tietman, Laurence Lurio.
- T-P160  
Wavelength-Shifting Fiber Scintillation Neutron Detectors for POWGEN3 & VULCAN at SNS. Jason Hodges, Lowell Crow, Luke Heroux, Bruce Hannan.
- T-P162  
Functional Studies of Membrane Proteins. Maria Nyblom, Euan Gordon, Richard Neutze.
- T-P164  
Dimeric Structural Significance for Ligand Binding in Putative Peptidyl-tRNA Hydroxylase from *Pyrococcus horikoshii* OT3. K. Shimizu, Y. Fujimoto, M. Sugahara, N. Kunishima.
- T-P166  
Structural Studies on *Helicobacter pylori* Apoflavodoxin Contributes to Investigate Conformational Changes in Flavodoxins Induced by FMN Binding. Marta Martínez-Júlvez, Marta Bueno, Nunilo Cremades, Javier Sancho, Juan Hermoso.
- T-P167  
Comparative Crystal Structures and Aromaticity Studies of a Diazetidine and a Benzodiazetidine. Kenneth L. Martin, Gary W. Bretton, Edwin D. Stevens.
- T-P168  
Collection of Diffraction Data from Crystals Grown in TOPAZ® Crystallization Chips. John Tainer, Andrew May, James Holton, Ken Frankel, Hany Nassef.
- T-P169  
Structural Diversity in Silver Coordination Chemistry. Manju Rajeswaran, David Whitcomb.
- T-P170  
Remote Access Modes for Data Collection at IMCA-CAT. Lisa J. Keefe, Kevin Battaille, J. Lewis Muir, Anne Mulichak.
- T-P171  
Experimental and Theoretical Charge Density Study of Estrone. Elizabeth Zhurova, Cherif Matta, Nan Wu, Vladimir Zhurov, Alan Pinkerton.
- T-P172  
Remote Data Collection for Single-Crystal and Powder Diffraction. Joerg Kaercher, Michael Ruf.
- T-P173  
Cost, Space, Time: What are the Limits for Publishable Structures? Lee Daniels, Ronald Benson, Joseph Ferrara, Katsunari Sasaki.
- T-P174  
SGX-CAT: An Automated Synchrotron Beamline Dedicated to Mail-in Crystallography. David W. Smith, Stephen R. Wasserman, John W. Koss, Laura L. Morisco, Kevin L. D'Amico.
- T-P175  
Bond-Plane Angle in Pyrrole Systems as an Indicator of the Degree of Aromaticity. David Grossie, Paul Seybold, Daniel Ketcha.
- T-P176  
The Beauty of Not Being There: Integrating Interactive Screening with Offline Data Collection. James Holton, George Meigs.
- T-P177  
Energy of Intermolecular Interactions from Charge Density Data in Molecular Crystals. Mikhail Antipin, Konstantin Lyssenko.
- T-P178  
Fast Vitrifying of Solutions Using Protein Crystal Cryopreservation: Effects of Cryoprotectant Concentration and Cooling Rates. Matt Warkentin, Viatcheslav Berenov, N.S. Hussein, O.A. Alsaied, Robert Thorne.
- T-P179  
Single Crystal ESEEM Spectroscopic and Computational Chemical Analysis of Coupled <sup>17</sup>O in Copper-Doped Enriched Tutton Salt. Michael Colaneri, Jacqueline Vitali, Jack Peisach.
- T-P181  
Ln<sub>2</sub>[O<sub>2</sub>C-(CH<sub>2</sub>)<sub>3</sub>-CO<sub>2</sub>]<sub>3</sub>(H<sub>2</sub>O)<sub>z</sub>.mH<sub>2</sub>O Framework Structures Features. G. Punte, G. Echeverria, C.G. Pozzi, E.V. Brusau, G.E. Narada, J.A. Ellena.
- T-P183  
Histidine Controlled Two-Dimensional Assembly of Zinc Phosphite Four-Ring Units. Xianhui Bu, Lan Chen.
- T-P185  
A Search for Isostructural "Bridge-Flipped: Isomers. W.H. Ojala, J.M. Spude, T.M. Arola, M.K. Kuspa, Y. Moua, H.M. Sexe, B.L. Sanders, N. Herrera, J.M. Smieja, C.R. Ojala.

T-P187

Structural Characterization of Two Variants of the Green Fluorescent Protein. Jean-Denis Pedelacq, Stephanie Cabantous, Thomas C. Terwilliger, Geoffrey S. Waldo.

T-P189

Crystal Structure of Modular Stator Subunit E of Archaeal H<sup>+</sup>-ATPase from *Pyrococcus horikoshii* OT3. Neratur K. Lokanath, Chizu Kuroishi, Matsuaki Sugahara, Naoki Kunishima.

T-P191

Surface Modulated Motion Switch: The Capture-and-Release of Iron-Sulfur Protein in the Cytochrome bc<sub>1</sub> Complex. Di Xia, Lothar Esser, Chang-An Yu.

T-P193

On Understanding Solution Conditions that Maximize Protein Complex Formation. Peter Horanyi, Bret Dillard, Liu Zhi-Jie, Rose John, Wang Bi Cheng.

T-P195

Crystallization of Reaction Centre from *Rhodobacter sphaeroides* in Bicontinuous Lipid Systems. Annemarie Wöhri, Pia Wadsten, Arjan Snijder, Sven Engström, Richard Neutze.

T-P197

Room to Move. Crystallizing Membrane Proteins in Swollen Lipidic Mesophases. Vadim Cherezov, Jeffrey Clogston, Miroslav Z. Papiz, Martin Caffrey.

T-P199

Microscale Self-Interaction Chromatography for Rapid Determination of Membrane Protein Virial Coefficients. Patrick J. Loll, William W. Wilson, Charles S. Henry.

T-P201

Activation and Inhibition of the Multidrug ABC Transporter MsbA. Christopher L. Reyes, Geoffrey Chang.

T-P203

Crystal Structures of Anabaena Sensory Rhodopsin and its Soluble Transducer. Lutz Vogeley, Hartmut Luecke.

T-P205

Domain Flexibility and Catalysis in the Complex II Superfamily. Thomas Tomasiak, Elena Maklashina, Kristian Kaufmann, Eric Dawson, Jens Meiler, Gary Cecchini, Tina Iverson.

T-P207

Structure Determination of the Colicin I Receptor Alone and in Complex with Colicin IA: Transport of Large Proteins Across Bacterial Outer Membranes. Susan Buchanan, Sylvestre Grizot, Maruf Ali, Lothar Esser.

T-P209

Regulation of a Cyclic Nucleotide Binding Regulated Ion Channel. Gina Clayton, Joao Morais Cabral.

T-P211

Factors Influencing Recombinant Transmembrane Protein Expression. Gloria Mazoock, Vidya Madhavan, Constance Jeffery.

T-P213

Efforts in the Crystallization and Structure Determination of a Ternary Complex of Human Urokinase and its Receptor. Qing Huai, Yongdong Li, Cai Yuan, Chuanbing Bian, Liqing Chen, Mingdong Huang.

T-P215

Crystal Structure of the Coiled-coil N-terminal Fragment of NudEL. Urszula Derewenda, Myung Hee Kim, David Cooper, Zygmunt Derewenda.

T-P217

Perils of Pseudosymmetry Combined with Merohedral Twinning. Jonathan Schuermann, Angela Rodriguez, Alex Taylor, P. John Hart.

T-P219

A Preliminary Model of Major Vault Protein. Daniel Anderson, Valerie Kickhoefer, Stuart Sievers, Leonard Rome, David Eisenberg.

T-P221

Determination of ytrI Architecture. Dominika Borek, Jerzy Osipiuk, Ruiying Wu, Shiu F. Moy, Andrzej Joachimiak, Zbyszek Otwinowski.

T-P223

Quick Solution of Difficult Structures is not Necessarily an Oxymoron. Wladek Minor, Marcin Cymborowski, Maksymilian Chruszcz, Zbyszek Otwinowski, Dominika Borek.

## POSTER PRIZES

### Pauling Prize

Awarded to not more than six of the best student poster presentations including the one poster from a Canadian Lab.

### IUCr Prize

The Executive Committee is pleased to continue the series of IUCr awards to be presented at meetings of the regional affiliates and national crystallographic associations.

### Journal of Chemical Crystallography Prize

The best student poster presentation in the area of chemical crystallography or small molecule structure determination and analysis.

### RSCB Protein Data Bank Prize

To recognize a student poster presentation involving macromolecular crystallography.

### Oxford Cryosystems Prize

Awarded to any poster describing work in low temperature crystallography.

### Journal Crystal Growth & Design Prize

Awarded to the best poster submitted to the Small Molecule Symposium "Supramolecular Chemistry: From Assembly to Structure and Function".

### AIP Undergraduate Research Prize

Presentation must describe research with a significant crystallographic component, students must demonstrate a command of the science, and must have completed the majority of the work being presented.

## Vendors and Booth Numbers

Accelrys .....	#209
Area Detector Systems Corp.....	#301
Art Robbins Instruments .....	#308
Axygen Biosciences.....	#406
Blake Industries Inc.....	#200
Bruker AXS, Inc.....	#500
CCP4 .....	#601
CRYO Industries of America Inc...#206	
Crystal Logic, Inc.....	#108
Emerald Biosystems .....	#506
Fluidigm Corp.....	#312
FMP Products.....	#511
Formulatrix, Inc.....	#513
GE Healthcare Bio-Sciences .....	#508
Genomic Solutions .....	#400
Hampton Research .....	#213
Incoatec GmbH .....	#404
IUCr.....	#607
Jena Bioscience GmbH .....	#100
Korima Inc.....	#202
Malvern Instruments.....	#407
MARRESEARCH.....	#210
MarUSA, Inc.....	#410
Mitegen, LLC .....	#409
Molecular Dimensions Inc.....	#101
Open Eye Scientific Software .....	#102
Oxford Cryosystems .....	#413
Oxford Diffraction Ltd.....	#501
PANalytical.....	#411
Perkin Elmer Life and Analytical Sciences.....	#204
QIAGEN, Inc.....	#305
RCSB Protein Data Bank.....	#603
Rigaku.....	#300
SER-CAT .....	#609
TriTek Corp.....	#103
TTP LabTech .....	#105
Wyatt Technology Corp.....	#512
Xenocs S.A.....	#509

## Show Hours and Dates

Saturday, July 22	7:30pm - 10:30pm
Sunday, July 23	10:00am-7:30pm
Monday, July 24	10:00am-7:30pm
Tuesday, July 25	10:00am-7:30pm
Wednesday, July 26	10:00am-4:00pm

